Sedimentary provenance analysis of Cretaceous Basins in the Andes-Amazon Equatorial Margin System and its relation to paleogeography and tectonics)

Mariana de Assunção Rodrigues

THÈSE

En vue de l'obtention du
DOCTORAT DE L'UNIVERSITÉ DE TOULOUSE

Délivré par l'Université Toulouse 3 - Paul Sabatier

Cotutelle internationale: Université de Brasilia

Présentée et soutenue par

Mariana DE ASSUNCAO RODRIGUES

Le 18 décembre 2023

Analyse de la provenance sédimentaire des bassins du Crétacé du système Andes-Amazonie-Marge équatoriale et des relations avec la paléogéographie et la tectonique

Ecole doctorale : **SDU2E - Sciences de l'Univers, de l'Environnement et de l'Espace**

Spécialité : **Sciences de la Terre et des Planètes Solides**

Unité de recherche :
GET - Geosciences Environnement Toulouse

Thèse dirigée par
Martin RODDAZ et Roberto VENTURA SANTOS

Jury

M. Christian GORINI, Rapporteur
M. Jean-Michel LAFON, Rapporteur
Mme Cécile GAUTHERON, Examinatrice
M. Jérôme VIERS, Examinateur
M. Martin RODDAZ, Directeur de thèse
M. Roberto VENTURA SANTOS, Co-directeur de thèse

Universidade de Brasília
Instituto de Geociências
Programa de Pós-graduação em Geologia

Análise da proveniência de sedimentos das bacias cretáceas do sistema Andes-Amazônia-Margem Equatorial e sua relação com a paleogeografia e tectônica

Analyse de la provenance sédimentaire des bassins du Crétacé du système Andes-Amazonie-Marge équatoriale et de des relations avec la paléogéographie et la tectonique

Sedimentary provenance analysis of Cretaceous Basins in the Andes-Amazon Equatorial Margin System and its relation to paleogeography and tectonics

MARIANA DE ASSUNÇÃO RODRIGUES

Tese de Doutorado Nº

Orientador: Prof. Dr. Roberto Ventura Santos
Co-orientador: Prof. Dr. Martin Roddaz

Brasília, dezembro 2023

Universidade de Brasília
Instituto de Geociências
Programa de Pós-graduação em Geologia

Análise da proveniência de sedimentos das bacias cretáceas do sistema Andes-Amazônia-Margem Equatorial e sua relação com a paleogeografia e tectônica

Analyse de la provenance sédimentaire des bassins du Crétacé du système Andes-Amazonie-Marge équatoriale et de des relations avec la paléogéographie et la tectonique

Sedimentary provenance analysis of Cretaceous Basins in the Andes-Amazon Equatorial Margin System and its relation to paleogeography and tectonics

MARIANA DE ASSUNÇÃO RODRIGUES

Tese apresentada ao Programa de Pós-Graduação em Geologia – Instituto de Geociências – IG da Universidade de Brasília – UnB como requisito parcial obrigatório para a obtenção do título de Doutor em Geologia.

Área de concentração: Geologia Regional

Orientador: Prof. Dr. Roberto Ventura Santos

Co-orientador: Prof. Dr. Martin Roddaz

Comissão Examinadora:

Prof. Dr. Christian Gorini (Sorbonne Université);
Prof. Dr. Jean-Michel Lafon (Universidade Federal do Pará - UFPA)
Prof.ª Dr.ª Natalia Hauser (IG/Universidade de Brasília - UnB);
Prof.ª Dr.ª Cécile Gautheron (Université Grenoble Alpes);
Prof. Dr. Jérôme Viers (Université Toulouse III – Paul Sabatier);

de Assunção Rodrigues, Mariana
dR696a Análise da proveniência de sedimentos das bacias cretaceas do sistema Andes-Amazônia-Margem Equatorial e sua relação com a paleogeografia e tectônica / Mariana de Assunção Rodrigues; orientador Roberto Ventura Santos; co-orientador Martin Roddaz. -- Brasília, 2023.
421 p.

Tese(Doutorado em Geologia) -- Universidade de Brasília, 2023.

1. Geologia. 2. Paleogeografia. 3. Cretaceo. 4. Plataforma Sul Americana. 5. Proveniência Sedimentar. I. Ventura Santos, Roberto, orient. II. Roddaz, Martin, co-orient. III. Título.

AGRADECIMENTOS

O presente trabalho foi realizado com apoio da Coordenação de Aperfeiçoamento de Pessoal de Nível Superior-Brasil (CAPES) – Código de Financiamento 001” e também recebeu suporte do programa CAPES-COFECUB Te 924/18 “Paléo-Amazone: evolution Néogéne de l’Amazonie Brésilienne”, o qual me deu a oportunidade de ficar 18 meses no GET (Toulouse)

Cette thèse a été financée en partie par la Coordenação de Aperfeiçoamento de Pessoal de Nível Superior - Brasil (CAPES) - Finance Code 001". Cette thèse a également été soutenue par le programme CAPES-COFECUB Te 924/18 "Paléo-Amazone : évolution Néogéne de l'Amazonie Brésilienne" qui m'a permis de séjourner 18 mois au GET (Toulouse).

This study was financed in part by the Coordenação de Aperfeiçoamento de Pessoal de Nível Superior - Brasil (CAPES) - Finance Code 001”. This Phd has also been supported by the CAPES-COFECUB program Te 924/18 “Paléo-Amazone: evolution Néogéne de l’Amazonie Brésilienne” which allows me to stay 18 months at the GET (Toulouse).

Quatro anos (e alguns meses), alguns campos, várias amostras, muitas análises, uma pandemia global, uma perda incomensuravelmente dolorida, dois países (três, contando o Peru), três idiomas (as vezes simultâneos), um amor (*oui* 😊), muita discussão construtiva (com e sem lágrimas), dois artigos, um manuscrito, uma defesa e MUITO aprendizado. Ufa, este foi o resumo do caminho que percorri ao longo desse tempo de doutorado. Para chegar até aqui, muita gente me ajudou, me acolheu e me incentivou. Obrigada Deus, por colocá-las no meu caminho e por me guiar e me dar forças durante todo o trajeto.

Gostaria de agradecer imensamente aos professores Martin Roddaz e Roberto Ventura Santos, pela oportunidade de trabalhar e aprender, pela compreensão demonstrada em várias situações difíceis, pelas puxadas de orelha e pelo incentivo ao longo de toda orientação. Agradeço também ao apoio do professor Elton Dantas, que esteve presente em todas as fases do doutorado, discutindo, sugerindo, ajudando e incentivando, sentirei falta de ouvir sua voz ao

longe no corredor enquanto trabalho. Foi uma honra ter realizado este projeto com vocês.

Agradeço aos professores do Programa de Pós-Graduação em Geologia da UnB que contribuíram de diversas formas durante as disciplinas e cursos realizados; obrigada pelo compartilhamento de conhecimento. Ao pessoal do Laboratório de Geocronogia da UnB, gostaria de agradecer pelo espaço concedido para a realização dos trabalhos de preparação das amostras e análises. Vivi boa parte desses quatro anos no laboratório de geocronologia da UnB, la foi minha segunda casa. Obrigada Vanessa, Sr. Gilvan e Felipo, que sempre foram muito simpáticos e atenciosos comigo. Agradeço imensamente ao professor Guilherme Gonçalves, que me ensinou a utilizar o Iolite e esteve sempre disposto a ajudar no tratamento dos dados, obrigada por toda ajuda e pelo compartilhamento de figurinhas e podcasts. Aos professores Gustavo e Tiago, agradeço por cederem um espaço na sala para eu ter uma mesa de trabalho. Tenho que agradecer a Jeane, pelo tratamento dos dados de Sm-Nd e pela ajuda com a metodologia, a Letícia, por me ajudar com trâmites burocráticos e pelos docinhos que salvavam meu dia após o almoço.

Ao pessoal do “Sucupira” (Artur, Carol, João, Seba, Tarcísio, Matheus, Alanielson...), que alegravam os fins de tarde silenciosos da UnB, agradeço às risadas e mesmo as ressacas, aos “Destemidos do Araripe,” (Gabriel, que agora virou Breton e André, vulgo Foguinho), e Michele, que dividiu a vivência toulousaine (desde a burocracia até os pints no Black Lion) durante um ano e meio. Obrigada pelas discussões, pelas trocas de informações e inquietudes, pelo apoio do carregamento de amostras (pepinos, abacaxis, malas...), pelos dias de trabalho no lab e de lazer na cidade.

Au personnel du GET, je tiens à remercier Carine Baritaud pour son accueil chaleureux et son attention constante, Françoise Maube pour sa sympathie lors de l'utilisation du MEB, Fabienne de Parseval pour m'avoir laissé de l'espace dans l'Atelier des Roches pour réaliser les montages des zircons et pour avoir essayé de m'aider à gérer l'allergie psychosomatique causée par le stress de la thèse. Merci à Mathieu Leisen pour son aide lors des analyses effectuées sur Element et pour son soutien lors de la rédaction du deuxième article. Merci à mes collègues de la salle S09, Ibrahim et Thai, et à la délégation brésilienne de l'OMP (Rômulo, David, Lia, Daniel, Maurício et Sly) qui m'ont aidé

avec des informations académiques, bureaucratiques, politiques (merci pour le covoiturage pour voter aux élections présidentielles) et de la vie quotidienne.

Gostaria de agradecer aos amigos do Brasil, em especial à Ana, Amanda, Mirella, Fernanda Bretas, Fernanda Furlan, André, Carlinha, Alexandre, Paty e Harry que viveram comigo momentos dramáticos e alegrias repentinas durante esses quatro anos e aos amigos que fiz na França, brasileiros e franceses, que me acolheram, partilharam suas experiências e contribuíram com meu crescimento pessoal, merci beaucoup.

Agradeço à minha família, minha mãe que me deu apoio ao longo da vida e em mais esta jornada, entendendo que sempre levarei mais uma rocha para "guardar" em sua casa; ao meu pai (*in memoriam*) por estar ao meu lado sempre, mesmo agora em outro plano; ao Gilmar e Giselly por estarem presentes nos momentos tristes e felizes dos últimos tempos e por terem me dado um sobrinho lindo durante este período e ao Felipeto que no auge de sua adolescência, me traz indagações desafiadoras sobre a vida. Agradeço também a Família Dalton (Naninha, Dona Cleusa, Guilherme e Kika), que me acolheram e me fizeram sentir em casa nos momentos finais desta caminhada. Je voudrais également remercier la famille Rochard pour m'avoir encouragé et pour toutes les vougies allumées pour Saint Antoine.

Mon Nico, merci d'être venu à un moment si peu prétentieux mais si important. Merci pour tout le soutien émotionnel que tu m'as apporté tout au long de la rédaction de la thèse, pour ta patience (et tes chocolats) dans les jours les plus stressants (surtout après des réunions tendues) et aussi pour le partage des moments de bonheur et des victoires ! Je t'aime !

RESUMO

O Cretáceo é caracterizado por grandes mudanças paleogeográficas, geodinâmicas e climáticas, incluindo a formação de novos oceanos, como o Oceano Atlântico equatorial, a fragmentação contínua do Gondwana e períodos de efeito estufa. Todas essas mudanças estão potencialmente contidas nos registros sedimentares das bacias. O sistema Andes-Amazônia-Margem Equatorial é um vasto sistema sedimentar cuja evolução geodinâmica e paleoambiental está registrada nas bacias foreland do retroarco amazônico, nas bacias intracratônicas brasileiras e nas da margem equatorial. Na parte ocidental (região andina), estudos recentes sugerem que o início da orogenia andina ocorreu durante o Cretáceo Superior, mas o desenvolvimento dos sistemas de drenagem e a origem dos sedimentos depositados durante o Cretáceo ainda são pouco conhecidos. O Cretáceo Inferior é registrado nas bacias intracratônicas e equatoriais brasileiras e testemunha as fases de rifteamento da crosta após a quebra de Gondwana. A Bacia do Araripe, nordeste do Brasil, é um bom exemplo dessas bacias, pois contém um registro sedimentar completo e particularmente bem estudado. No entanto, a origem dos sedimentos dos vários estágios tectônicos da formação da bacia e a origem cretácea das incursões marinhas que a afetaram ainda não foram determinadas. O objetivo desta tese é propor uma reconstrução paleogeográfica do sistema Margem Andes-Amazônia-Equatorial durante o Cretáceo e analisar as mudanças geodinâmicas e tectônicas que o afetaram. Para isso, usamos métodos de proveniência, em especial a geoquímica de elementos principais e traços, a composição isotópica de Sm e Nd e idades U-Pb em zircões. Os resultados obtidos nos permitiram identificar as zonas de origem da Bacia do Araripe durante as fases pré, sin e pós-rifte e, assim, obter uma melhor compreensão da configuração paleogeográfica da região nordeste do Brasil no início do Cretáceo. Os sedimentos da Bacia do Araripe provêm principalmente dos terrenos paleoproterozoicos (2,3-1,6 Ga) da Província Borborema e dos plútons graníticos do ciclo Brasiliano (720-541Ma). A bacia tem uma história sedimentar ligada às fases de ruptura do Atlântico Sul e Equatorial. Durante a fase pré-rifte (~152-135 Ma), a bacia fazia parte da depressão afro-brasileira e recebia sedimentos do N-NW. Durante a fase de rifte (~135-125Ma), houve uma mudança na fonte devido

à ruptura continental e à formação do Atlântico Sul, com um influxo de sedimentos da parte oriental da província da Borborema. Durante a fase pós-rifte (121-113 Ma), a bacia deixou de ser alimentada pela parte oriental e as incursões marinhas dominaram o ambiente de sedimentação. Finalmente, durante a fase pós-rifte II (113-100 Ma), foi observada uma última mudança nas fontes, com fontes para o NE refletindo o momento final da fragmentação de Gondwana. Um estudo da proveniência dos sedimentos das bacias da Amazônia ocidental (Acre e Madre de Dios) indica que as fontes são cratônicas, originadas principalmente dos terrenos Ventuari-Tapajós (2,0 - 1,82 Ga) e Rio Negro - Juruena (1,82 - 1,54 Ga). Esses resultados indicam que uma vasta rede de drenagem intracontinental ("Sanozama") surgiu em resposta à elevação do Arco do Purus e das regiões cratônicas do Brasil e das Guianas durante a abertura do Oceano Atlântico equatorial. A integração dos resultados obtidos, compilados com dados da literatura, possibilitou a proposta de quatro mapas paleogeográficos da parte norte da plataforma sul-americana. Eles destacam como os mecanismos geodinâmicos ligados à abertura dos oceanos Atlântico Sul e equatorial controlaram e moldaram a paleogeografia dessa região.

Palavras-chave: Proveniência, datação U-Pb em zircões, isotopia Sm-Nd, Amazônia, Margem Equatorial, Cretáceo, Oceano Atlântico equatorial, Sanozama, Araripe, Acre, Madre de Dios.

RÉSUMÉ

Le Crétacé est caractérisé par d'importants changements paléogéographiques, géodynamiques et climatiques, incluant notamment la formation de nouveaux océans dont l'Océan Atlantique équatorial, la fragmentation continue du Gondwana et des périodes à effet de serre. Tous ces changements sont potentiellement contenus dans les enregistrements sédimentaires des bassins. Le système Andes-Amazonie-Marge équatoriale est un vaste système sédimentaire dont l'évolution géodynamique et paléoenvironnementale est enregistrée dans les bassins d'avant-pays retroarc amazonien, les bassins intracratoniques brésiliens et ceux de la marge équatoriale. Dans la partie occidentale (région andine), des études récentes suggèrent que le début de l'orogenèse andine s'est produit au cours du Crétacé supérieur, mais le développement des systèmes de drainage et la source des sédiments déposés au cours du Crétacé restent encore peu connus. Le Crétacé inférieur est enregistré dans des bassins brésiliens intracratoniques et équatoriaux et témoigne des phases de rifting crustal suivant la fragmentation du Gondwana. Le bassin d'Araripe, nord-est du Brésil, est un bon exemple de ces bassins puis qu'il contient un registre sédimentaire complet et particulièrement bien étudié. Cependant, l'origine des sédiments issus des différentes étapes tectoniques de la formation de bassin ainsi que la provenance crétacée des incursions marines l'ayant affecté restent à préciser. Cette thèse vise à proposer une reconstruction paléogéographique du système Andes-Amazonie-Marge équatoriale pendant le Crétacé et à analyser les changements géodynamiques et tectoniques qu'ont affecté. Pour ce faire, nous avons utilisé les méthodes de la provenance et en particulier la géochimie des éléments majeurs et traces, la composition isotopique en Sm et Nd, les âges U-Pb sur zircons. Les résultats obtenus ont permis d'identifier les zones sources du bassin d'Araripe pendent les phases pré, syn et post-rift et ainsi de mieux comprendre la configuration paléogéographique de la région nord-est du Brésil au début du Crétacé. Les sédiments du bassin d'Araripe proviennent principalement des terrains Paléoprotérozoïque (2,3–1,6 Ga) de la province de Borborema et des plutons granitiques du cycle Brasiliano (720–541Ma). Le bassin possède une histoire sédimentaire liée aux phases de rupture de l'Atlantique Sud et équatorial. Pendant la phase pré-rift (~152-135

Ma), le bassin faisait partie de la dépression Afro-Brésilienne et recevait des sédiments en provenance du N-NO. Lors la phase rift (~135-125Ma), il y a eu un changement de source due à rupture continentale et à la formation de l'Atlantique Sud, avec un apport de sédiments en provenance de la partie orientale de la province de Borborema. Pendant la phase post-rift (121–113 Ma), le bassin a cessé d'être alimenté par la partie orientale et les incursions marines ont dominé l'environnement de sédimentation. Enfin, au cours de la phase post-rift II (113–100 Ma) un dernier changement de sources a été observée, avec des sources au NE qui reflètent le moment final de la fragmentation du Gondwana. L'étude de la provenance des sédiments des bassins de l'Amazonie occidentale (Acre et Madre de Dios) indique que les sources sont cratoniques, provenant principalement des terrains Ventuari-Tapajos (2,0 - 1,82 Ga) et Rio Negro - Juruena (1,82 - 1,54 Ga). Ces résultats indiquent qu'un vaste réseau de drainage intracontinental (« Sanozama ») qu'a émergé en réponse au soulèvement de l'Arche de Purus et des régions cratoniques du Brésil et des Guyanes pendant l'ouverture de l'océan Atlantique équatorial. L'intégration des résultats obtenue compilée avec les données de la littérature a permis de proposer quatre cartes paléogéographiques de la partie septentrionale de la plate-forme sud-américaine. Ils mettent en évidence comment les mécanismes géodynamiques liées à l'ouverture des océans atlantiques sud et équatoriaux ont contrôlé et façonné la paléogéographie de cette région.

Mots-clés : Provenance, datations U-Pb sur zircons, isotopie Sm-Nd, Amazonie, marge équatoriale, Crétacé, océan atlantique équatorial, Sanozama, Araripe, Acre, Madre de Dios.

ABSTRACT

The Cretaceous is characterized by major paleogeographic, geodynamic, and climatic changes, including the formation of new oceans such as the equatorial Atlantic Ocean, the continued fragmentation of Gondwana, and greenhouse effect periods. All these changes are potentially contained in the sedimentary records of the basins. The Andes-Amazonia-Equatorial Margin system is a vast sedimentary system whose geodynamic and palaeoenvironmental evolution is recorded in the Amazonian retroarc foreland basins, the Brazilian intracratonic basins, and those of the equatorial margin. In the western part (Andean region), recent studies suggest that the onset of the Andean orogeny occurred during the Late Cretaceous, but the development of drainage systems and the source of sediments deposited during the Cretaceous are still poorly understood. The Lower Cretaceous is recorded in Brazilian intracratonic and equatorial basins and bears witness to crustal rifting phases following Gondwana's break-up. The Araripe Basin (Brazilian northeast) is a good example of these basins since it contains a complete and particularly well-studied sedimentary record. However, the origin of the sediments from the various tectonic stages of basin formation and the Cretaceous origin of the marine incursions that affected it remain to be determined. The aim of this thesis is to propose a palaeogeographic reconstruction of the Andes-Amazonia-Equatorial Margin system during the Cretaceous and to analyze the geodynamic and tectonic changes that affected it. To do this, we used provenance methods, in particular major and trace element geochemistry, Sm and Nd isotopic composition, and U-Pb ages on zircons. The results obtained have enabled us to identify the source zones of the Araripe Basin during the pre-, syn- and post-rift phases and thus to gain a better understanding of the palaeogeographic configuration of the north-eastern region of Brazil at the beginning of the Cretaceous. The sediments in the Araripe basin come mainly from the Palaeoproterozoic (2.3-1.6 Ga) terrains of the Borborema province and the granitic plutons of the Brasiliano cycle (720-541Ma). The basin has a sedimentary history linked to the South Atlantic and equatorial break-up phases. During the pre-rift phase (~152-135 Ma), the basin was part of the Afro-Brazilian depression and received sediments from the N-NW. During the rift phase (~135-125Ma), there was a change in source due to continental break-up and the

formation of the South Atlantic, with an influx of sediments from the eastern part of the Borborema province. During the post-rift phase (121-113 Ma), the basin ceased to be fed by the eastern part and marine incursions dominated the sedimentation environment. Finally, during the post-rift II phase (113-100 Ma) a last change in sources was observed, with sources to the NE reflecting the final moment of the fragmentation of Gondwana. A study of the provenance of sediments from the basins of western Amazonia (Acre and Madre de Dios) indicates that the sources are cratonic, originating mainly from the Ventuari-Tapajos (2.0 - 1.82 Ga) and Rio Negro - Juruena (1.82 - 1.54 Ga) terrains. These results indicate that a vast intracontinental drainage network ('Sanozama') emerged in response to the uplift of the Purus Arch and the cratonic regions of Brazil and the Guianas during the opening of the equatorial Atlantic Ocean. The integration of the results obtained compiled with data from the literature has made it possible to propose four palaeogeographic maps of the northern part of the South American platform. They highlight how geodynamic mechanisms linked to the opening of the South Atlantic and equatorial oceans controlled and shaped the paleogeography of this region.

Keywords: Provenance, U-Pb dating on zircons, Sm-Nd isotopy, Amazonia, Equatorial Margin, Cretaceous, Equatorial Atlantic Ocean, Sanozama, Araripe, Acre, Madre de Dios.

LISTA DE ILUSTRAÇÕES

Figura 1: Reconstrução do continente Pangea antes de sua fragmentação com a localização das zonas de estudo. A quebra do continente ocorreu em três fases, separadas por cerca de 60 Ma (linhas vermelhas distinguem a primeira fase; linhas verdes a segunda e linhas azuis a terceira). Projeção de Hammer, modificado de Moulin et al. (2010) **16**

Figura 2: Quatro segmentos identificados durante a separação da América do Sul e da África e zonas de estudo localizadas nos retângulos negros. Modificado de Moulin et al. (2010) **17**

Figura 3: Localização das bacias sedimentares Sub Andinas na plataforma Sul Americana. Modificado de (Albert et al. 2018) **23**

Figura 4: A: Localização das bacias formadas a partir do riftiamento regional. B: Condicionantes tectônicos das bacias interiores da Região Nordeste Oriental. C: Provável paleogeografia das bacias interiores. Modificado de Machado Junior et al. (1990). **29**

Figura 5: Reconstrução paleogeográfica feita por Arai (2014) baseada nos paleomapas de Scotese (2014a) mostrando as ocorrências da Ecozona Subtlisphaera (círculos vermelhos), de palinofloras marinas (círculos amarelos) do seaway e a localização das bacias sedimentares interiores. Retirado de Arai (2014). A- Morocco; B – Senegal; C - Bacia Maracaibo; D – Bacia São Luís; E – Bacia do Ceará; F – Bacia Potiguar; G - Bacia Parnaíba; H - Bacia do Araripe; I - Bacia Almada; J – Bacia Sergipe; M - Bacia Pelotas; L - Río Fosiles, Provincia de Santa Cruz, Argentina. **31**

Figura 6: Reconstrução paleogeográfica modificada de (Scotese 2014) mostrando a configuração do Aptiano antes da deposição evaporítica e a disposição das bacias sedimentares representadas por letras: D – Bacias São Luís e Parnaíba; A – Bacia Barreirinhas; B – Bacia Ceará, Formação Mundaú; C- Bacia Potiguar; E – Bacia Araripe, Formação Rio da Batateira. Retirado de (Arai, 2016). **34**

Figura 7: Reconstrução paleogeográfica do nordeste brasileiro durante o Aptiano baseada em Assine et al. (2016). As setas amarelas e verdes representam as principais rotas sedimentares. As setas azuis estão relacionadas as ingressões marinhas. Retirado de Custódio et al. (2017). **35**

Figura 8: Reconstrução paleogeográfica durante a incursão marinha no Aptiano Superior. A reconstrução foi baseada no modelo cinemático de Heine et al 2013 e Richetti et al 2018. Modificado *de (Godot Souza et al. 2022)*. PeSZ: Zona de Cisalhamento Pernambuco; PaSZ: Zona de Cisalhamento Parnaíba. **36**

Figura 9: Exemplos de reconstruções paleogeográficas mundiais durante o Cretáceo. Retirado de Scotese, 1991 e Scotese, 2014. **38**

Figura 10: Detalhe do afloramento onde foi coletada a amostra ACRE 29. **53**

Figura 11: Afloramentos ao longo do rio Moa – Acre - Brasil. A esquerda: coleta da amostra ACRE 33. A direita: coleta da amostra ACRE 17 **53**

Figura 12: Equipe de campo na região de Mazuko – Madre de Dios – Peru. **54**

Figura 13: Vista panorâmica do afloramento da Formação Chonta, zona subandina peruana. **54**

Figura 14: Afloramento Formação Chonta, zona subandina – Peru. Coleta da Amostra MD 2019 03. **54**

Figura 15: Processo de concentração de amostras para transporte. Zona Subandina, Peru. **55**

Figura 16: Equipe de campo, Araripe – Brasil. **55**

Figura 17: Vista panorâmica do afloramento, no qual encontra-se o contato entre a Formação Araripina e Exu, Bacia do Araripe – Brasil. **55**

Figura 18: Vista panorâmica do afloramento Mãozinha, Bacia do Araripe, Brasil. **56**

Figura 19: A esquerda: Moinho de disco; A direita: Separador magnético isodinâmico Frantz, tipo barreira magnética. Retirado de www.legga.unb.br **57**

Figura 20: Montagem de mount (esquerda); MEV FEI Quanta^{TM} 450 do LEGGA-IG-UnB (Retirado de de www.legga.unb.br) **57**

Figura 21: MEV Tescan Veja 4 LMU localizado no GET – Toulouse (Retirado de www.get.omp.eu) e imagem panorâmica da amostra M2AR 1-3. **58**

Figura 22: Neptune XT^{TM} MC-ICP-MS localizado no LEGGA-UnB - Brasília (Retirado de www.legga.unb.br) **63**

Figura 23: ThermoScientific Element HR-ICPMS localizado no GET – Toulouse. **64**

Fig. 24: Pre-drift reconstruction of South America e Africa showing the Andean belt, Archean/Proterozoic cratons, and Brasiliano/Pan-African provinces of western Gondwana. (b) Tectonic compartmentation of Borborema Province with the division into Northern, Central, and Southern subprovinces. (c) The schematic map of the Borborema Province shows the Northern and Southern subprovinces subdivision. Map based on Neves (2015); Brito Neves and Passarelli (2020), Brito Neves and Campos Neto (2016), Matos et al (2021), Van Schumus et al (2011), Ferreira et al. (1998), and Godot Souza et al. (2022). **76**

Fig. 25: The Geologic map of the Araripe Basin shows the stratigraphic record of the rift and post-rift stages (modified from Assine, 2007 and Fambini et al. 2020). **83**

Fig. 26: Stratigraphic chart of the Araripe Basin (taken from Assine 2007) showing the samples analyzed in this study (in black color) and by Godot Souza et al. 2022 (in red). Loc. and Geoch. refer to Location and Major and trace element analysis respectively. **86**

Fig. 27: Selected trace element ratios (Eu/Eu*, Th /Cr; Th/Sc and, Al/Si see text for details) of analyzed samples (green points -Rift stage; blue points – Post-rift I stage; yellow points – Post-rift II stage. The horizontal **101**

bars for the Eu/Eu*, Th/Cr, and Th/Sc, ratios correspond to 5% (i.e., the Eu concentration analytical error, see supplementary material), 15% (i.e., the sum of the Cr and Th concentration analytical errors), and 25% (i.e., the sum of the Th and Sc concentration analytical errors) Pink and blue rectangles indicate the values range for basic and felsic sediments, respectively (Cullers, 2000).

Fig. 28: HREE/LREE vs. MREE/MREE* diagram. HREE/LREE and MREE/MREE* values are calculated following (Martin et al., 2010), where HREE = Tm + Yb + Lu, LREE = La + Pr + Nd, MREE = Gd + Tb + Dy (all PAAS normalized), and MREE* = the average of HREE+LREE. The MREE bulge and “bell-shaped” REE profiles correspond to REE patterns observed in fish teeth, Fe-Mn oxides, organic matter, and pore waters, while “HREE-enriched” profiles correspond to modern seawater (Huck et al., 2016; Moiroud et al., 2016). These end-members reflect the REE contents of marine sediments influenced by seawater or authigenic phases, while “flat” REE patterns are characteristic of continental clays (see Huck et al., 2016; Moiroud et al., 2016 for a review). **104**

Fig. 29: Stratigraphic variation of the Nd isotope composition (expressed as ƐNd(0) for the blue points, and ƐNd(T) for the yellow points). The lengths of the horizontal bar for the Sr-Nd isotopic compositions correspond to 2σ analytical errors (see Table 4) **107**

Fig. 30: Stage evolution of the U-Pb zircon age distribution of the Araripe Basin with the age probability (black line) and age histogram (bars). **110**

Fig. 31: A) Non-matrix metric multi-dimensional scaling (MDS) plot (Vermeesch, 2013) based on the U-Pb age distributions of detrital zircons in the analyzed samples using the Kolmogorov–Smirnov test. Closest and second closest neighbors are linked by solid and dashed lines, respectively; B) Shepard plot of the U-Pb data showing the transformation from dissimilarity to distances and disparities. **116**

Fig. 32 Schematic paleogeographic maps based on sample provenance interpretations. Each time step corresponds to one of the tectonic **122**

stages that affected the Araripe Basin between the late Jurassic and the Cenomanian. The paleogeographic reconstruction is based on the kinematic model of Heine et al. (2013), and the paleogeographic maps from Godot Souza et al. (2022), and Matos et al. (2021). The Borborema Province sub-divisions and their references are listed in Figure 1. The Capianga Lake geometry (Map A) and the highland location in Map B were based on Kuchle et al. (2011). The paleoflow directions were based on data from Fambrini et al (2019), Assine (1994, 2007), Custodio et al (2017), Godot Souza et al. (2022), and this study

Fig. 33: Geological map of the Andes and Amazon basins modified from the CPRM tectonic map of South America **163**

Fig. 34: Comparative chronostratigraphic diagrams showing stratigraphic nomenclature, age, and lithology for (A) the Subandean Amazonian Basins and (B) Peruvian and Brazilian Amazonian Basins. The chronostratigraphic diagram (A) was constructed based on (Calderon, 2017; Hermoza et al., 2006; Louterbach et al., 2014; Louterbach et al., 2018; Martinez et al., 1999; Roddaz et al., 2010). The chronostratigraphic diagram (B) is based on (Calderon, 2017; Caputo, 2014; Caputo & Soares, 2016; Cunha, 2007; Hurtado et al., 2018; Wanderley Filho et al., 2007). **167**

Fig. 35: Map of the northern part of South America illustrating the major tectonic provinces and the ages of their more recent metamorphic events. Modified and adapted from (Chew et al., 2008; Chew et al., 2007; Cordani et al., 2000; Miškovic et al., 2009; Naipauer et al., 2015; Oliveros et al., 2012; Ramos, 2018; Sempere et al., 2002; Spikings et al., 2016). Modified from Hurtado et al. (2018). Nd isotopes may be used as a provenance tool because they are not easily fractionated by sedimentary or post-depositional processes (Konieczna et al., 2015; Mahoney, 2005; McLennan et al., 1990). Cratonic-derived river sediments have εNd(0) values between -14.5 and -20, while Andean-derived sediments have εNd(0) values >-13.8 (Figueiredo et al., 2009; Horbe et al., 2013; Roddaz et al., 2005). This difference in the Nd **171**

isotopes recorded in fine-grained sediments has been used to decipher the provenance and reconstruct the paleodrainage systems in Western Amazonia (e. g. Roddaz et al., 2005; Louterbach et al., 2018; Hurtado et al., 2018).

Fig. 36 Major and selected trace element contents of analyzed samples normalized to PAAS (Pourmand et al., 2012; Taylor & McLennan, 1985). From left to right on the diagram, these include the major elements (SiO2, TiO2, Al2O3, Fe2O3, MnO, MgO, CaO, Na2O, K2O, and P2O5), LILE (Rb, Cs, Ba, Sr, Th, and U), HFSE (Y, Zr, Nb, Hf), and TTE (Sc, Cr, Co, V, and Ni). (A) Acre Basin, (B) Madre de Dios Basin. **186**

Fig. 37: Rare earth element (REE) contents of studied samples normalized to PAAS. (Pourmand et al., 2012; Taylor and McLennan, 1985). (A) Acre Basin, (B) Madre de Dios Basin. **190**

Fig. 38 Stratigraphic variation of Nd isotope composition (expressed as ƐNd(0) / TDM (0) for the blue points, and ƐNd(T) / TDM (T) for the red points) and selected trace element ratios (Th/Sc and Eu/Eu*, see text for details) of analyzed samples A - Acre Basin; B - Madre de Dios Basin. The lengths of the horizontal bar for the Sm-Nd isotopic compositions correspond to 2σ analytical errors (see Table 3). Dashed lines in ƐNd show the Amazonian recent rivers ƐNd values. Purple and orange symbols indicate the values of Th/Sc and Eu/Eu*, respectively. The $Ɛ_{Nd}$ (T) values of Acre Basin samples were calculated based on the stratigraphic interpretation from Cunha (2007), and the palynology ages analyzed in this study and by Haag (2019). For AC49, 42B, 38, 37, 33, 30A, 27A, 22A, and 20A2 we used 90Ma, and for 16 and 15A, 70Ma. The $Ɛ_{Nd}$ (T) values of Made de Dios Basin samples were calculated based on the stratigraphic ages of Louterbach et al. (2018) (75Ma). **196**

Fig. 39: Stratigraphic evolution of Acre U-Pb ages on zircon grains. The detrital age distribution presents the Kernel Density Estimations (KDE) (black line), which were calculated following (Vermeesch, 2012) in the Python-based DetritalPy program (Sharman et al., 2018) and age **198**

histogram (bars). N.G.: Number of grains; R.P.: Relative Percentage (Table 5).

Fig. 40: Stratigraphic evolution of Madre de Dios U-Pb ages on zircon grains. The detrital age distribution presents the Kernel Density Estimations (KDE) (black line), which were calculated following (Vermeesch, 2012) in the Python-based DetritalPy program (Sharman et al., 2018) and age histogram (bars). N.G.: Number of grains; R.P.: Relative Percentage (Table 5). **203**

Fig. 41: REE patterns observed in fish teeth, Fe-Mn oxides, organic matter, and pore waters, while “HREE-enriched” profiles correspond to modern seawater (Huck et al., 2016; Moiroud et al., 2016). These end-members reflect the REE contents of marine sediments influenced by seawater or authigenic phases, while “flat” REE patterns are characteristic of continental clays (see Huck et al., 2016; Moiroud et al., 2016 for a review). **205**

Fig. 42: A) Non-metric multi-dimensional scaling (MDS) plot (Vermeesch, 2013) based on the U-Pb age distributions of detrital zircons in the analyzed samples using the Kolmogorov-Smirnov test. Closest and second closest neighbors are linked by solid and dashed lines, respectively; B) Shepard plot of the U-Pb data showing the transformation from dissimilarity to distances and disparities. Groups 1, 2, and 3 indicate samples with a similar detrital zircon age population (see discussion in the text). **209**

Fig. 43: Schematic paleogeographic maps summarizing the Cenomanian to Maastrichtian paleogeographic evolution of Western Amazonia. See text for details. The paleogeographic maps were built based on (Hurtado et al., 2018; Roddaz et al., 2010). The position of the Purus Arch is based on Caputo and Soares, (2016) and Hurtado et al. (2018). The position of Coastal Batholith, Precambrian basement, and Geologic terranes is based on (Chew et al., 2008; Chew et al., 2007; Chew et al., 2016; Cordani et al., 2000; Hurtado et al., 2018). The sedimentary input directions are based on Chavez et al. (2022); Erlich **213**

et al. (2018); George et al., (2019); Hurtado et al. (2018); Louterbach et al. (2018); Moreno et al. (2020); Roddaz et al. (2021) and U-Pb detrital zircon ages of this study. Are: Arequipa Basin; MDn: North of Madre de Dios Basin; MDs: south of Madre de Dios Basin; Ac: Acre Basin; Uc: Ucayali Basin; Hua: Huallaga Basin; Ba: Bagua Basin; San/ Santiago Basin; Mar: Marañón Basin; Or: Oriente Basin; M: Madaglena Basin and L: Llanos Basin.

Figura 44 :Reconstrução paleogeográfica proposta para o início do riftiamento entre a América do sul e a África (Jurássico Superior-Neocomiano), baseada no modelo cinemático de Heine et al (2013) e nos dados discutidos ao longo do texto. SLC: Craton São Luís; SFC: Craton São Francisco, CC: Craton do Congo; BPB: Província Borborema; DeR: Plataforma Demerara; MarB: Bacia do Marajó; PotB: Bacia Potiguar; RTJ: Bacia Recôncavo-Tucano-Jatobá; SA-G: Bacia Sergipe-Alagoas-Gabon. **262**

Figura 45 : Reconstrução paleogeográfica proposta para Aptiano, baseada no modelo cinemático de Heine et al (2013) e nos dados discutidos ao longo do texto. SLC: Craton São Luís; SFC: Craton São Francisco, CC: Craton do Congo; BPB: Província Borborema; DeR: Plataforma Demerara; MarB: Bacia do Marajó; PotB: Bacia Potiguar; RTJ: Bacia Recôncavo-Tucano-Jatobá. O retângulo laranja representa as reconstruções paleogeográficas discutidas no capítulo 3 e as setas em azul correspondem as hipóteses da direção de incursão marina discutidas no texto. **266**

Figura 46 : Reconstrução paleogeográfica proposta para o Albiano-Cenomaniano, baseada no modelo cinemático de Heine et al (2013) e nos dados discutidos ao longo do texto. SLC: Craton São Luís; SFC: Craton São Francisco, CC: Craton do Congo; BPB: Província Borborema; DeR: Plataforma Demerara; Mar: Bacia do Marajó; Pot: Bacia Potiguar; RTJ: Bacia Recôncavo-Tucano-Jatobá; Ben: Bacia do Benin; Cd'I-G: Bacia de Côte d'Ivoire – Gana; G-S: Bacia Guianas-Suriname; FAm: Bacia Foz do Amazonas; P-M: Bacia Parnaíba- **274**

Maranhão; Bar: Bacia Barreiras; Ce: Bacia do Ceará; Mg: Bacia Madaglena; Lh: Bacia Lhanos; Or: Bacia Oriente; Mr: Bacia Marañon; Hu: Bacia Huallaga; Uc: Bacia Ucayali; Ac: Bacia do Acre; MD: Bacia de Madre de Dios (n-norte, s-sul); Are: Bacia de Arequipa.

LISTA DE TABELAS

Tabela 1: Origem de drenagens durante períodos de soerguimento e fragmentação da parte norte da Plataforma Sul Americana. Retirado de (Potter 1997). **22**

Tabela 2:Tabela de incertezas para os elementos medidos em ICP-MS. **58**

Tabela 3 Relação de amostras das bacias de Madre de Dios (MD) e Acre realizadas no laboratório LEGGA-IG-UnB e os equipamentos utilizados. **62**

Tab. 4: Borborema Province sub-division with general information about rock types, U-Pb ages, and Sm-Nd isotopic compositions. **79**

Tab. 5: Label, formation, age, and location for the analyzed samples in this study and in Souza et al., 2021 (in red). **87**

Tab. 6: Major and trace element concentrations of sedimentary rocks analyzed in this study. D.L.: Detection Limit. **96**

Tab. 7: Sm-Nd systematics of analyzed sedimentary rocks from Araripe Basin. **106**

Tab. 8: Numbers and percentages (%) of U–Pb ages **109**

Tab. 9: Label, formation, age, and localization for the analyzed samples of Madre de Dios and Acre basins. Madre de Dios basin: Ages are from Louterbach (2014) and Louterbach et al. (2018) Acre basin: Ages are from Cunha (2007) (*) and Haag (2019) (**) Brito et al. (1994) (***). **172**

Tab. 10: Paleontological content of the sedimentary rocks analyzed in this work. **175**

Tab. 11: Major and trace element concentrations of sedimentary rocks analyzed in this study. D.L.: Detection Limit. **182**

Tab. 12: Sm-Nd systematics of analyzed sedimentary rocks. Madre de Dios basin: Ages are from Louterbach (2014) and Louterbach et al. (2018). The ƐNd (T) values of Made de Dios Basin samples were calculated based on the stratigraphic ages of Louterbach et al. (2018) (75Ma). For all the samples we used 75Ma. Acre basin: Ages are from Cunha (2007) (*) and Haag (2019) (**) Brito et al. (1994) (***). The ƐNd **192**

(T) values of Acre Basin samples were calculated based on the stratigraphic interpretation from Cunha (2007), and the palynology ages analyzed in this study and by Haag (2019). For ACRE 49, ACRE 42B, ACRE 38, ACRE 37, ACRE 33, ACRE 30A, ACRE 27A, ACRE 22A, and ACRE 20A2 we used 90Ma, and for ACRE 16 and ACRE 15A 70Ma.

Tab. 13: Numbers and percentages (%) of U–Pb ages representing known and distinct geochronological events in probable source regions on the Amazonia craton and the central Andes. Temporal ranges of events according to Bahlburg et al. (2009), Chew et al. (2008), and Calderon et al. (2017). n is the number of samples analyzed for the time interval. **199**

SUMÁRIO

1 INTRODUÇÃO / INTRODUCTION 2

Présentation 2

1.1 Apresentação 9

1.1. Arcabouço Teórico 15

1.1.1. Evolução geodinâmica do Cretáceo na parte norte da Plataforma Sul Americana 15
1.1.2. Atividade magmática e abertura do Atlântico Sul e Equatorial 15
1.1.3. As incursões marinhas e abertura do Atlântico Sul 18
1.1.4. Soerguimento dos Andes e o comportamento das drenagens na parte norte da plataforma sul-americana 20

1.2. Bacias sedimentares Cretáceas - Sistema Andes-Amazônia e bacias interiores 23

1.2.1. Bacias sedimentares Andes-Amazônia 23
1.2.2. Bacia do Araripe 26

1.3. Reconstrução paleogeográfica 36

1.4. Objetivos 40

1.4.1. Objetivo Geral 40
1.4.2. Objetivos específicos 40

Referências bibliográficas 41

2 MATERIAIS E MÉTODOS / MATÉRIEL ET MÉTHODES 52

2.1 Pesquisa bibliográfica e trabalhos de campo 52

2.2 Preparação de amostras 56

2.3 Análises laboratoriais 58

2.3.1 Geoquímica dos elementos maiores, traços e terras raras 58
2.3.2 Composição isotópica de Sm-Nd 60
2.3.3 Datação U-Pb em zircão detritico 61

REFERÊNCIAS 66

3 INFLUENCE DES PROCESSUS DE RIFTING ET DE POST RIFTING SUR LA PARTIE CONTINENTALE NORD DE L'AMERIQUE DU SUD : EXEMPLE DE L'ETUDE DE L'EVOLUTION MESOZOÏQUE DU BASSIN ARARIPE A PARTIR DE LA PROVENANCE SEDIMENTAIRE 69

Résumé 69

3.1 The provenance of the late Jurassic to Cenomanian sedimentary succession of the Araripe Basin (NE Brazil) and implication for the geodynamic evolution of Western Gondwana 72

3.2 Introduction 74

3.3 Geological settings and sampling 77

3.3.1 Geological setting 77

The potential sources: the Borborema Province and the Paranaiba Basin 77

The sink: the Araripe Basin 82

Sampling and stratigraphic constraints 85

3.4 Analytical procedures 90

3.4.1 Major and trace element concentrations 90

3.4.2 Sm-Nd isotope composition 90

3.4.3 U-Pb ages and trace element concentrations in zircons 91

3.5 Results 93

3.5.1 Major elements, Large-Ion Lithophile Elements (LILE), High Field Strength Elements (HFSE), and Trace Transition Elements (TTE) 93

3.5.2 Rare Earth Elements (REE) 102

3.5.3 Sm-Nd isotopes 105

3.5.4 U-Pb detrital zircon 108

3.6 Discussion 111

3.6.1 Provenance interpretations 114

3.6.2 Paleogeographic implications 119

3.7 Conclusion 124

References 126

4 EVOLUTION CRETACEE DE LA PARTIE OCCIDENTALE DU SYSTEME ANDES AMAZONIE MARGE EQUATORIALE : RECONSTITUTION DU PALEO RESEAU DE DRAINAGE A PARTIR DE LA PROVENANCE SEDIMENTAIRE DES SEDIMENTS DES BASSINS ANDO MAZONIENS ... 156

Résumé 156

NEW INSIGHTS INTO THE CRETACEOUS EVOLUTION OF THE WESTERN AMAZONIAN PALEODRAINAGE SYSTEM 158

4.1 Introduction 160

4.2 Geological settings and sampling 162

4.2.1 Cretaceous stratigraphy of western Amazonian basins 162

4.2.2 Potential sources 169

4.3 Sampling and stratigraphic constraints 171

4.4 Materials and methods 179

4.4.1 Major and trace element concentrations 179
4.4.2 Sm-Nd isotope composition 179

4.5 Results ... 180
4.5.1 Major elements, Large-Ion Lithophile Elements (LILE), High Field Strength Elements (HFSE), and Trace Transition Elements (TTE) 180
4.5.1.1 Acre ... 187
4.5.1.2 Madre de Dios ... 187
4.5.2 Rare Earth Elements (REE) 188
4.5.2.1 Acre ... 188
4.5.2.2 Madre de Dios ... 191
4.5.3 Sm-Nd isotopes 191

4.6 U-Pb detrital zircon ... 197

4.7 Discussion ... 203
4.7.1 Influence of geochemical characteristics in the provenance sedimentary interpretation. 203
4.7.2 Interpretation of provenance 206
4.7.3 Implications for the paleogeographic evolution of Cretaceous Andes-Amazonian drainage 211

4.8 Conclusions ... 218

References ... 219

5 5. DISCUSSÃO/ DISCUSSION ... 259

5.1 Paleogeografia da Plataforma Sul Americana Setentrional durante o Cretáceo ... 260

5.2 Cretáceo inferior: Fragmentação do Gondwana e as deposições durante o Neocomiano, Aptiano e Albiano. ... 261
5.2.1 Incursões Marinhas no nordeste brasileiro 265

5.3 Albiano – Cenomaniano (110 – 101 Ma): Formação do Oceano Atlântico Equatorial e os reflexos geodinâmicos no Escudo do Brasil e Guianas e NW África. ... 269

5.4 Turoniano – Maastrichtiano (89 – 66 Ma): Clímax da drenagem intercontinental e as deposições na Amazônia Ocidental. ... 275

Referências ... 280

6 CONCLUSÃO E PERSPECTIVAS / CONCLUSION ET PERSPECTIVES 292

Referências ... 297

ANEXOS/ ANNEXÉS ... 298

CAPÍTULO 1

INTRODUÇÃO

INTRODUCTION GÉNÉRALE

1 INTRODUÇÃO / INTRODUCTION

Présentation

La paléogéographie est la représentation des anciennes géographies de la Terre au cours des temps géologiques. La reconstitution des géographies anciennes passe par des analyses sédimentologiques (caractérisation des faciès, pétrographie, analyse des paléocourants) (e.g. Assine 1994 ; Custódio et al. 2017 ; Fellin et al. 2023), des études de positionnement cinématique et de paléomagnétisme (e.g. Moulin et al. 2010 ; Heine et al. 2013), des datations isotopiques (e.g. Hurtado et al. 2018 ; Liu et al. 2018 ; Godot Souza et al. 2022), de la géochimie (éléments majeurs, traces et terres rares (RTE) (e.g. Mourlot et al. 2018 ; Roddaz et al. 2021), des études paléoclimatologiques (Frakes 1990; Wang *et al.* 2014)*, ainsi que des études liés à la paléontologie et à la palynologie* (Arai 2014; Rodrigues *et al.* 2020)*. Cependant, la qualité et la quantité des données disponibles, ainsi que les résolutions temporelles et spatiales, représentent certaines limites pour les reconstructions paléogéographiques*. *Dans le cas de la géochronologie U-Pb dans le zircon détritique, les grains qui ont subi des recristallisations successives, qui ont des structures internes difficiles à dater (métamisation) ou qui présentent une altération chimique peuvent présenter des données incompatibles ou erronées (Corfu et al. 2003 ; Howard et al. 2009), ce qui rend difficile l'identification des zones d'origine et des anciens reliefs.*

Lors de l'étude de la formation et de la configuration des bassins sédimentaires dans un contexte géographique, l'analyse de la provenance des sédiments siliciclastiques est un bon outil pour la reconstruction paléogéographique, car elle permet de comprendre la relation entre la zone

source et les lieux de dépôt au cours des changements géodynamiques et tectoniques (Morton et Hallsworth 1994 ; Weltje et von Eynatten 2004 ; Cawood et al. 2012 ; Nie et al. 2012 ; Zhu et al. 2020).

Le système Andes-Amazonie-marge équatoriale est un grand complexe sédimentaire qui a fait l'objet de plusieurs études récentes sur son évolution (van Soelen *et al.* 2017a; Albert *et al.* 2018; Hurtado *et al.* 2018; Louterbach *et al.* 2018; Bajolet *et al.* 2022; Fellin *et al.* 2023)*. Ce système est situé dans la partie nord de la plate-forme sud-américaine et comprend plusieurs bassins sédimentaires dont l'histoire est liée aux mouvements tectoniques survenus au cours du Mésozoïque et du Cénozoïque* (Hurtado *et al.* 2018; Louterbach *et al.* 2018; Horbe *et al.* 2019; Bajolet *et al.* 2022; Chavez *et al.* 2022; Fellin *et al.* 2023)*. Au Crétacé, des changements géodynamiques et climatiques ont affecté l'évolution paléoenvironnementale et géographique de ce système, dont les traces sont visibles dans les bassins andino-amazoniens, les bassins intracratoniques brésiliens, ainsi que les bassins de la marge équatoriale (Fig.1).*

La marge occidentale de l'Amérique du Sud a subi des mouvements tectoniques associés à des processus de subduction qui ont produit des changements significatifs dans la croûte continentale (Catuneanu 2004; Ramos and Folguera 2009; Maloney et al. 2013; Schellart 2017). Des études récentes ont montré que le début de l'érosion des Andes qui est interprétée comme correspondant au début du soulèvement des Andes (Hurtado *et al.* 2018; Louterbach *et al.* 2018) *a été enregistré dans l'enregistrement sédimentaire Maastrichtien (~69-66 Ma) des bassins Ando-Amazoniens péruviens. Cependant, la genèse et l'évolution de ce système avant le Maastrichtien et*

durant le Crétacé restent mal comprises. L'existence d'éventuels pulses orogéniques en provenance des Andes ne peut être totalement exclue. Les travaux récemment publiés se sont concentrés sur la partie proximale péruvienne des bassins Ando-Amazoniens (Erlich *et al.* 2018; Hurtado *et al.* 2018) *et la partie brésilienne de ces bassins (bassin de l'Acre) reste peu étudiée. Etudier cette zone d'un point de vue de la provenance sédimentaire est fondamental si on veut essayer de comprendre l'evolution régionale du système Andes-Amazonien-Marge Équatoriale et notamment la transition entre les bassins andins et cratoniques du système et les relations entre les Andes naissantes et le bassin amazonien sensu lato.*

Au cours du Crétacé inférieur, un processus de divergence s'est produit dans l'Atlantique Sud, lié à la montée d'un panache mantellique qui a débuté il y a environ 138 Ma (Stewart *et al.* 1996)*. La propagation de ce panache a été à l'origine du développement d'un « rifting » vers le nord, permettant la sédimentation dans des bassins syn-rift intracontinentaux* (Basile *et al.* 2005)*. À partir du Barrémien, les bassins d'Araripe et de Foz do Amazonas ont commencé à se former (Brandão et Feijó 1994 ; Baudin et Berthou 1996). Plusieurs incursions marines sont observées durant cette période (Arai, 2006, 2014, 2016), mais malgré des études sédimentaires détaillant la présence de ces incursions et leur faciès* (Assine 1994; Milani and Thomaz-Filho 2000; Arai 2006)*, la localisation des zones sources et les détails sur le remplissage de ces bassins restent controversés.*

Les bassins sédimentaires de la marge équatoriale du Brésil sont liés à l'ouverture et à l'hyperextension de l'océan Atlantique équatorial (Albien-

Cénomanien) (Mohriak *et al.* 2013)*. Cette période est également connue pour l'élévation relative du niveau de la mer caractérisée par des transgressions cénomaniennes-turoniennes et des événements anoxiques (OAE 2 et OAE3)* (Schlanger and Jenkyns 1976; Takashima *et al.* 2007; Jenkyns 2010; Gomes *et al.* 2016)*. Le changement climatique causé par l'augmentation de l'activité volcanique et méthanogène peut accélérer le cycle hydrologique et augmenter l'altération, encourageant la production et l'export de sédiments dans les océans et les lacs* (Jenkyns 2010)*. L'étude de la provenance des sédiments du bassin d'Araripe peut apporter des précisions sur la localisation des sources alimentant le bassin durant le Crétacé et ainsi sur la présence d'éventuelle barrière qui pourrait empêcher les ingressions marines et sur l'impact des processus post ritfs sur la partie continentale de la partie nord de l'Amérique du Sud.*

Le paléo réseau de drainage mésozoïque amazonien a subi plusieurs modifications en réponse à des processus géodynamiques (Potter 1997; Rodríguez Tribaldos et al. 2017; Bajolet et al. 2022). Trois facteurs clés ont conduit à la rupture et à la réorganisation de ce paléo réseau : les soulèvements crustaux, le rifting et les rifts avertés (Potter 1997)*. Potter (1997) suggère qu'au cours du Jurassique et du Crétacé, les mers intérieures au pied des Andes étaient connectées au Paléo-Pacifique avec des zones sources alimentant ces bassins localisés à l'est et au nord. Si on compare avec la configuration actuelle du réseau de drainage amazonien, le paléo réseau de drainage crétacé était inversé, prenant sa source dans le craton brésilien pour aller se jeter dans les mers intérieures localisées au pied des Andes crétacées. Par commodité, nous appellerons ce réseau de drainage inverse crétacé « Sanozama ». Cependant, d'après Potter (1997) au début du Crétacé supérieur, la paléo-pente s'est*

inversée et les anciens fleuves Colorado et Negro ont commencé à se jeter dans l'Atlantique. Des études plus récentes montrent que les rivières andines-amazoniennes ont développé un drainage vers l'ouest au moins à la fin du Maastrichtien et au début du Paléocène (Hurtado et al. 2018 ; Louterbach et al. 2018). Avant le Maastrichtien, le réseau de drainage amazonien avait pour principale source la craton amazonien (Hurtado et al. 2018 ; Louterbach et al. 2018), qui était une zone en soulèvement en réponse certainement à des processus géodynamiques résultant de l'ouverture de l'océan Atlantique équatorial.

Néanmoins, plusieurs questions restent en suspens concernant l'évolution crétacée du système Andes-Amazonie-marge équatoriale. En particulier, les informations sur la provenance des sédiments peuvent contribuer à la reconstruction paléogéographique de cette période, puisque des questions telles que : "Y a-t-il eu une influence du soulèvement andin sur le dépôt des bassins de la marge équatoriale de l'Atlantique pendant le Crétacé ?" et/ou "Quelles sont les sources des bassins intracratoniques brésiliens et leur relation avec l'ouverture de l'Atlantique Equatorial ?" pourraient trouver une réponse. En outre, le timing de la date du drainage « Sanozama » et le passage à un drainage d'origine andine n'est pas bien établi.

Dans cette optique, cette thèse vise à réaliser une reconstruction paléogéographique du système Andes-Amazonie-Océan Atlantique pendant le Crétacé, en utilisant la provenance des sédiments clastiques piégés dans les bassins amazoniens. Cette étude apportera de nouvelles données qui pourraient permettre une meilleure compréhension des effets de l'hyperextension de l'océan

Atlantique équatorial, ainsi que du développement de l'orogenèse la partie septentrionale de la plate-forme sud-américaine.

Ce chapitre introductif (chapitre 1) traite de l'importance de cette recherche, discute du cadre théorique qui guide cette étude et énumère les objectifs intermédiaires afin de proposer une reconstruction paléogéographique pendant le Crétacé dans la partie septentrionale de la plate-forme sud-américaine.

Le chapitre 2 détaille la méthodologie utilisée au cours de cette thèse.

Le chapitre 3 traite de l'influence du rifting et des processus post rift sur la partie continentale de la marge équatoriale brésilienne, ainsi que des changements géodynamiques qui se sont produits sur le continent pendant la rupture du Gondwana et la formation des océans Atlantique Sud et Équatorial, à partir de l'étude de la provenance des sédiments mésozoïques du bassin d'Araripe. Ce chapitre se présente sous la forme d'un manuscrit en cours de soumission à Tectonics intitulé « The provenance of the late Jurassic to Cenomanian sedimentary succession of the Araripe Basin (NE Brazil) and implication for the geodynamic evolution of Western Gondwana ».

Le chapitre 4 traite de l'effet du soulèvement du craton Amazonien sur le système de drainage crétacé de la partie occidentale de l'Amazonie à partir de la provenance des sédiments piégés dans la partir sud du bassin de Madre de Dios (Pérou) et de l'Acre (Brésil). Ce chapitre fait l'objet d'un article publié à Sedimentary Geology "New insights into the Cretaceous evolution of the Western Amazonian palaeodrainage system" (https://doi.org/10.1016/j.sedgeo.2023.106434). Ce manuscrit apporte de

nouvelles contraintes temporelles sur l'établissement et l'évolution du paleo réseau de drainage « Sanozama ».

Le chapitre 5 présente une discussion sur la paléogéographie de la partie nord de la plate-forme sud-américaine et sur la façon dont les données obtenues dans les bassins étudiés contribuent à la compréhension des mécanismes tectoniques et géodynamiques qui se sont produits pendant le Crétacé.

Enfin, le chapitre 6 présente les conclusions et les perspectives générales de la thèse et les annexes présentent les données supplémentaires utilisées tout au long de la rédaction de la thèse et des manuscrits soumis à des revues scientifiques.

1.1 Apresentação

A paleogeografia é a representação das superfícies da Terra ao longo do tempo geológico. A reconstrução de antigas geografias envolve análises sedimentológicas (caracterização de fáceis, petrografia, análise de paleocorrentes) (Assine 1994; Custódio *et al.* 2017; Fellin *et al.* 2023); estudo do posicionamento cinemático e de paleomagnetismo (Moulin *et al.* 2010; Heine *et al.* 2013); datações isotópicas (Hurtado *et al.* 2018; Liu *et al.* 2018; Godot Souza *et al.* 2022), geoquímica (elementos maiores, traços e elementos terras raras (ETR) (Mourlot *et al.* 2018; Roddaz *et al.* 2021), estudos paleoclimatológicos (Frakes 1990; Wang *et al.* 2014) além de estudos ligados à paleontologia e palinologia (Arai 2014; Rodrigues *et al.* 2020). Entretanto, a qualidade e a quantidade de dados disponíveis, além de resoluções temporais e espaciais representam alguns limites para a reconstruções paleogeográficas. No caso da geocronologia U-Pb em zircão detrítico, grãos que sofreram sucessivos eventos de recristalização, que possuem estruturas internas de difícil datação (metamitização) ou que possuam alguma alteração química podem apresentar dados incompatíveis ou equivocados (Corfu *et al.* 2003; Howard *et al.* 2009), dificultando a identificação de áreas fontes e de antigos padrões de relevo. Dados de mapeamentos e projeções espaciais não atualizadas dificultam as interpretações e novas reconstruções de antigas geografias (Tang *et al.* 2022).

Ao estudar a formação e configuração de bacias sedimentares no contexto geográfico, a análise da proveniência de sedimentos siliciclásticos se mostra como uma ferramenta de reconstrução paleogeográfica, pois possibilita compreender a relação existente entre a área fonte e os locais de deposição durante as mudanças geodinâmicas e tectônicas (Morton and Hallsworth 1994;

Weltje and von Eynatten 2004; Cawood *et al.* 2012; Nie *et al.* 2012; Zhu *et al.* 2020).

O sistema Andes-Amazonia-Margem Equatorial é um grande complexo sedimentar que tem sido objeto de vários estudos recentes sobre sua evolução (van Soelen *et al.* 2017b; Albert *et al.* 2018; Hurtado *et al.* 2018; Louterbach *et al.* 2018; Bajolet *et al.* 2022; Fellin *et al.* 2023). Este sistema encontra-se na parte norte da Plataforma Sul Americana e inclui diversas bacias sedimentares com histórias relacionadas a movimentos tectônicos durante o Mesozóico e o Cenozóico (Hurtado *et al.* 2018; Louterbach *et al.* 2018; Horbe *et al.* 2019; Bajolet *et al.* 2022; Chavez *et al.* 2022; Fellin *et al.* 2023). No Cretáceo ocorreram mudanças geodinâmicas e climáticas que afetaram a evolução paleoambiental e geográfica deste sistema, cujo registro pode ser recuperado em bacias Andino-Amazônicas, bacias intracratônicas brasileiras, bem como nas bacias da margem equatorial (Fig.1).

A margem ocidental da América do Sul sofreu movimentos tectônicos associados a processos de subducção que produziram mudanças expressivas na crosta continental (Catuneanu 2004; Ramos and Folguera 2009; Maloney *et al.* 2013; Schellart 2017). Estudos recentes têm mostrado que o início da erosão dos Andes, correspondente ao início do seu soerguimento (Hurtado *et al.* 2018; Louterbach *et al.* 2018), encontra-se registrado nos estratos sedimentares Maastrichtianos (~69-66 Ma) das bacias Ando-amazônicas peruanas. Entretanto, a gênese e evolução deste sistema antes do Maastrichtiano e durante o Cretáceo permanece mal compreendida. A existência de possíveis pulsos orogênicos não pode ser totalmente excluída. Trabalhos recentes se concentram sobre a parte proximal peruana das bacias Ando-Amazônicas (Erlich

et al. 2018; Hurtado *et al.* 2018). A parte brasileira dessas bacias (Bacia do Acre) resta pouco estudada. Estudar esta zona do ponto de vista da proveniência sedimentar é fundamental para se compreender a evolução regional do sistema Andes-Amazônia-Margem Equatorial e, notadamente, a transição entre as bacias andinas e cratonicas deste sistema, bem como a relação entre o nascimento dos Andes e da bacia amazônica propriamente dita.

Durante o Cretáceo Inferior houve um processo divergente no Atlântico Sul relacionado à ascensão de pluma mantélica, a aproximadamente 138 Ma (Stewart *et al.* 1996). A propagação dessa pluma foi responsável pelo desenvolvimento de um sistemas de riftes em direção a norte, possibilitando a sedimentação em bacias *syn-ritf* intracontinentais (Basile *et al.* 2005). A partir do Barremiano (129 – 121 Ma), as bacias do Araripe e a Foz do Amazonas começam a se formar (Brandão and Feijó 1994; Baudin and Berthou 1996). Diversas incursões marinhas são observadas neste período (Arai, 2006, 2014, 2016) como demonstram os estudos sedimentares detalhando a presença dessas incursões e suas fácies características (Arai, 2006; Assine, 1994; Milani and Thomaz-Filho, 2000). Entretanto, a localização das áreas fontes e detalhes sobre preenchimento dessas bacias permanecem controversos.

As bacias sedimentares da margem equatorial do Brasil possuem conexão com a abertura e hiperextensão do Oceano Atlântico Equatorial (Albiano-Cenomaniano) (Mohriak *et al.* 2013). Este período também é conhecido pelo relativo aumento no nível do mar caracterizado pelas transgressões cenomano-turonianas e pelos eventos anóxicos (OAE 2 e OAE3) (Schlanger and Jenkyns 1976; Takashima *et al.* 2007; Jenkyns 2010; Gomes *et al.* 2016) As mudanças climáticas causadas pelo aumento de atividades vulcânicas podem

acelerar o ciclo hidrológico e aumentar o intemperismo, fomentando a produção e descarga de sedimentos em oceanos e lagos (Jenkyns 2010). O estudo da proveniência dos sedimentos da Bacia do Araripe pode trazer informações mais precisas sobre a localização das fontes que alimentaram a bacia durante o Cretáceo, além de informar sobre a presença de eventual barreira às incursões marinhas e sobre o impacto dos processos pós *rift* na área continental da parte norte da América do Sul.

A paleo rede de drenagens na amazônica mesozóica sofreu muitas modificações em resposta aos processos geodinâmicos (Potter 1997; Rodríguez Tribaldos *et al.* 2017; Bajolet *et al.* 2022). Três fatores chaves proporcionam a ruptura e reorganização desta paleo rede: soerguimentos crustais; rifteamentos e *rifts* abortados (Potter 1997). Potter (1997) sugere que durante o Jurássico e o Cretáceo mares interiores estavam conectados ao paleo Pacífico e fontes sedimentares de bacias estavam localizadas a leste e a norte. Comparada à configuração atual das redes de drenagens amazônicas, a paleo rede de drenagem cretácea possuía sentido contrário, transportando sedimentos vindos do craton brasileiro em direção aos mares interiores localizados nos pés dos andes cretáceos. Por comodidade, nós chamamos esta rede de drenagem cretácea inversa como “Sanozama”. No entanto, conforme Potter (1997), no início do Cretáceo Superior o paleo declive inverteu-se e os antigos rios Colorado e Negro começaram a fluir para o Atlântico. Estudos mais recentes demonstram que os rios Andino-Amazônicos desenvolveram drenagem em direção ao oeste pelo menos no final do Maastrichtiano e início do Paleoceno (Hurtado *et al.* 2018; Louterbach *et al.* 2018). Antes do Maastrichtiano, a rede de drenagem amazônica tinha como principal fonte o craton amazônico (Hurtado *et al.* 2018;

Louterbach *et al.* 2018), que era uma zona que foi soerguida em função dos processos geodinâmicos resultantes da abertura do Oceano Atlântico Equatorial.

Contudo, várias questões continuam em aberto em relação à evolução cretácea do sistema Andes-Amazônia-Margem Equatorial, principalmente em relação às mudanças nas fontes de sedimentos. Em particular, as informações sobre a proveniência dos sedimentos podem contribuir para a reconstituição paleogeográfica deste período, diante de perguntas como: “Quais são as fontes das bacias intracratônicas brasileiras e a suas relações com a abertura do Atlântico Equatorial?”. Além do mais, o momento do fim da drenagem “Sanozama” e a passagem para uma drenagem de origem andina não é bem estabelecida.

Nesta perspectiva, essa tese se propõe a realizar uma reconstrução paleogeográfica do sistema Andes-Amazônia-Oceano Atlântico durante o Cretáceo, utilizando a proveniência dos sedimentos detríticos coletados nas bacias amazônicas. Este estudo traz novos dados que permitem compreender os reflexos da hiperextensão do Oceano Atlântico Equatorial, bem como o desenvolvimento do orógeno andino na parte norte da Plataforma Sul Americana.

O presente capítulo introdutório (Capítulo 1) aborda a importância desta pesquisa, discursa sobre o arcabouço teórico que norteia o estudo e lista os objetivos para propor uma reconstrução paleogeográfica durante o Cretáceo na parte norte da Plataforma Sul Americana.

O Capítulo 2 detalha da metodologia empregada durante esta tese.

O Capítulo 3 trata da influência do rifteamento e dos processos pós *rift* sobre a parte continental da margem equatorial brasileira. A partir do estudo da

proveniência dos sedimentos da Bacia do Araripe, aborda ainda as mudanças geodinâmicas produzidas no continente durante a ruptura do Gondwana e a formação dos oceanos Atlântico do Sul e Equatorial. Este capítulo se apresenta sob forma de um manuscrito a ser submetido à revista Tectonics intitulado: “Provenance of the late Jurassic to Cenomanian sedimentary succession of the Araripe Basin (NE Brazil) and implication for the geodynamic evolution of Western Gondwana”.

O Capítulo 4 trata das relações entre o craton amazônico e o sistema de drenagem cretácea da parte ocidental da Amazonia a partir da proveniência de sedimentos oriundos da parte sul das bacias de Madre de Dios (Peru) e do Acre (Brasil). Este capítulo foi objeto de um artigo publicado na *Sedimentary Geology* intitulado “New insights into the Cretaceous evolution of the Western Amazonian paleodrainage system” (https://doi.org/10.1016/j.sedgeo.2023.106434). O artigo apresenta e discute as restrições temporais sobre o estabelecimento e a evolução da rede de paleo-rede de drenagem “Sanozama”.

O Capítulo 5 apresenta uma discussão sobre a paleogeografia da parte norte da Plataforma Sul Americana e como os dados obtidos nas bacias estudadas contribuem para o entendimento dos mecanismos tectônicos e geodinâmicos ocorridos durante o Cretáceo.

Por fim, no Capítulo 6 serão apresentadas as conclusões e perspectivas gerais da tese. Apresenta ainda os anexos e dados suplementares utilizados ao longo da escrita da tese e dos manuscritos submetidos aos periódicos científicos.

1.1. Arcabouço Teórico

1.1.1. Evolução geodinâmica do Cretáceo na parte norte da Plataforma Sul Americana

O Período Cretáceo abrange cerca de 80 milhões de anos e evidencia mudanças importantes na configuração geodinâmica e climática da Terra. Atividades magmáticas e eventos vulcânicos desencadearam a fragmentação do Gondwana e abertura do Atlântico Sul e Equatorial; mudanças climáticas significantes são marcadas por eventos anóxicos e o início da orogenia dos Andes contribui para a reconfiguração da paleogeografia da Plataforma Sul Americana (Hill 1991; Weissert 2000; Sahabi *et al.* 2004; Jenkyns 2010; Moulin and Aslanian 2010; Moulin *et al.* 2010; Robinson *et al.* 2017). Os reflexos dessas mudanças podem ser observados ao longo da plataforma, como por exemplo, no sistema sedimentar Andes-Amazônia-Oceano Atlântico.

1.1.2. Atividade magmática e abertura do Atlântico Sul e Equatorial

A fragmentação do supercontinente Pangea iniciou-se no final do Triássico e se desenvolveu em três fases. A primeira separou os continentes Gondwana e Laurentia (Sahabi *et al.* 2004) a partir de atividade vulcânica da Província Magmática Atlântica Central por volta de 200 Ma (Moulin *et al.* 2010) e referências nele contidas). Durante o Jurássico superior o vulcanismo Karoo funcionou como mecanismo para o desmembramento de três mega blocos, Laurussia; África e América do Sul; Índia, Antártica e Austrália (Eagles and König 2008; Moulin *et al.* 2010) (Figura 1). A segunda fase de fragmentação ocorreu durante o Cretáceo Inferior, entre ~133 e 120Ma. A configuração dos três grandes blocos mudou a configuração paleogeográfica, e novos oceanos

começaram a se formar (Moulin *et al.* 2010). Houve a separação entre a América do Norte, Groelândia e Europa, e posteriormente entre Antártica, Índia e Austrália. Durante este período também aconteceu a abertura do Oceano Atlântico Sul. A última fase de desmembramento ocorreu ao longo do Cenozoico fazendo com que a configuração das zonas continentais ficassem dispostas tal qual temos acesso em tempos mais recentes (Moulin *et al.* 2010).

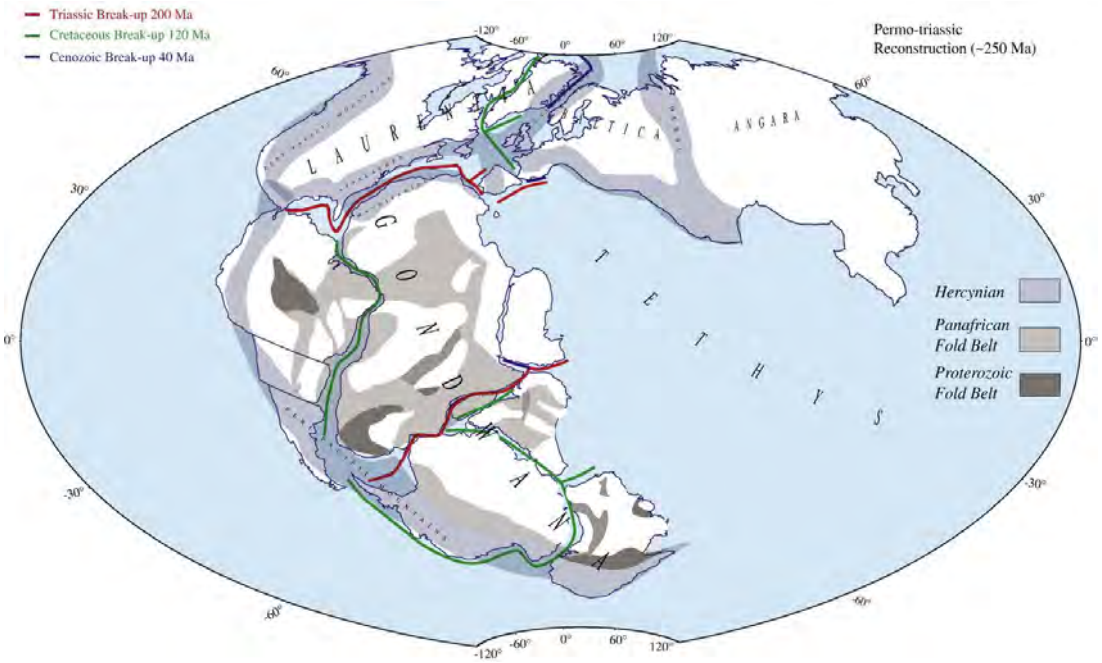

Figura 1: Reconstrução do continente Pangea antes de sua fragmentação com a localização das zonas de estudo. A quebra do continente ocorreu em três fases, separadas por cerca de 60 Ma (linhas vermelhas distinguem a primeira fase; linhas verdes a segunda e linhas azuis a terceira). Projeção de Hammer, modificado de Moulin et al. (2010)

Quatro segmentos podem ser identificados durante a separação da América do Sul e da África: segmento Equatorial; Central; Austral e Falkland (Moulin *et al.*, 2010, 2005) (Figura 2). No segmento Equatorial é possível observar zonas de fraturas relacionadas ao início do espalhamento do fundo oceânico é datado do início do Albiano Superior (Moulin *et al.* 2010). O segmento central é caracterizado por uma evolução tectono-sedimentar que parte de uma fase *rift* e evolui para fases *sags* (Chaboureau *et al.* 2013). Este compartimento é ainda caracterizado pela presença de uma extensa bacia evaporítica

desenvolvida no Aptiano (Moulin *et al.* 2010; Mohriak *et al.* 2013). O espalhamento do assoalho oceânico nesta região se inicia no Barremiano, durante um período de quiescência magmática do Cretáceo Inferior. A parte Austral está limitada entre as zonas de fratura Rio Grande e a Falkland-Agulhas.

A força motriz relacionada ao afinamento e ruptura da crosta continental, está contida na ação de *hotspots* e no espalhamento de vulcanismo basáltico (Hill 1991). A abertura do Atlântico Sul, por exemplo, está intimamente ligada ao espalhamento basáltico do evento Parana-Etendeka (Marzoli *et al.* 1999) e a pelo menos duas plumas mantélicas principais, Santa Helena e Tristão da Cunha, que parecem ter sido influentes no enfraquecimento da litosfera continental ao longo do desenvolvimento Atlântico Sul (Moulin *et al.* 2010).

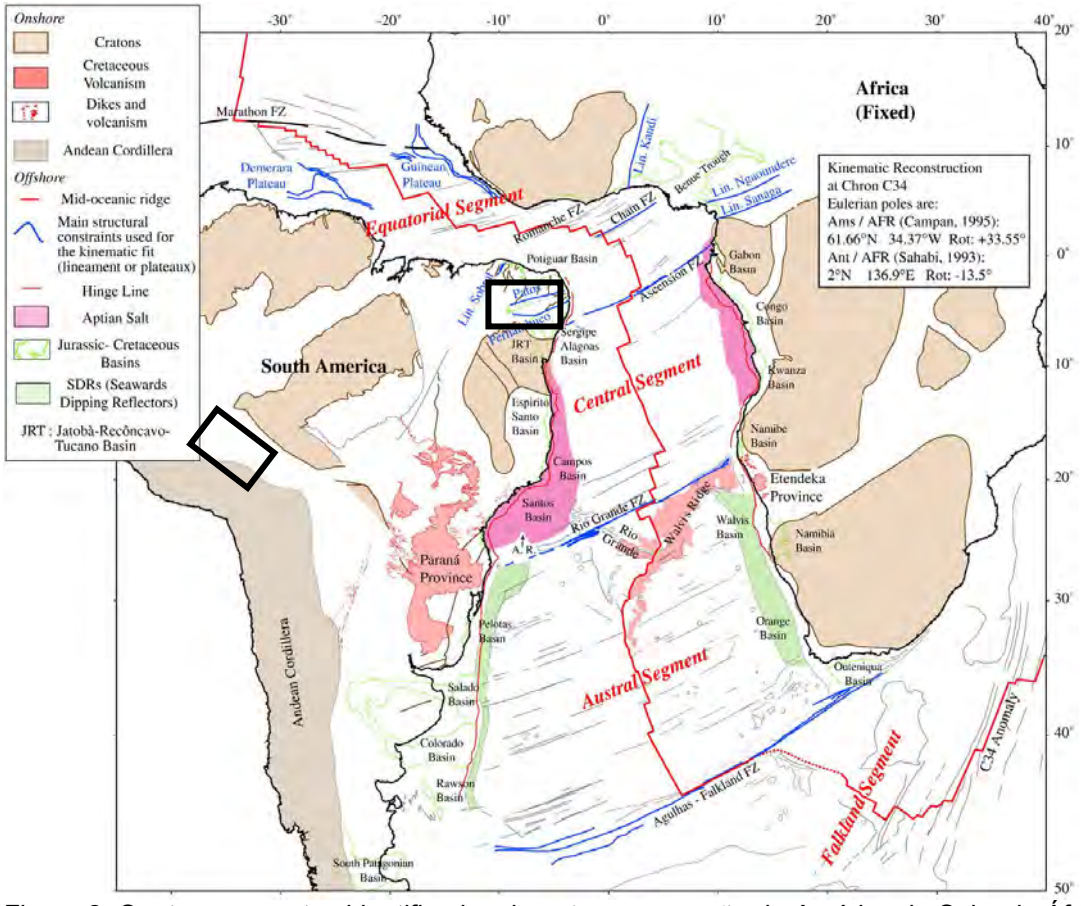

Figura 2: Quatro segmentos identificados durante a separação da América do Sul e da África e zonas de estudo localizadas nos retângulos negros. Modificado de Moulin et al. (2010)

Eventos Anóxicos Oceânicos (OAE) tem sido relacionados ao crescimento abrupto da temperatura induzido por um rápido influxo de CO_2 na atmosfera, cuja fonte está associada a eventos vulcanogênicos e/ou metanogênicos (Jenkyns 2010). Nesta situação, os oceanos tornam-se cada vez mais ácidos, resultado da dissolução de CO_2 e SO_2. O excesso de deposição de matéria orgânica, reflexo do aquecimento e do efeito estufa, coincide com uma crise na biocalcificação de alguns organismos marinhos como em recifes produtores. O colapso desse ecossistema marinho influenciou o fluxo de carbono que nos sedimentos pode ser identificado por meio do enriquecimento do $\delta^{13}C$ observado em carbonatos (Mello *et al.* 1989; Koutsoukos *et al.* 1990; Weissert 2000; Jenkyns 2010; Robinson *et al.* 2017). Nove OAEs são reconhecidos com significância global, dentre os quais três são mais extensos: T-OAE (Jurássico Inferior) (Jenkyns 1980), OAE1a (Aptiano Inferior ou Evento Selli) (Coccioni *et al.* 1992) e OAE2 (Cenomaniano-Turoniano ou Evento Bonarelli) (Jenkyns 2010).

Na plataforma Sul-Americana alguns registros de OAE foram descritos, principalmente durante o Cretáceo. Esses eventos estão relacionados à perturbação no ciclo do carbono devido ao rápido aquecimento global e a abertura do oceano Atlântico, que por sua vez apresentava eventos vulcanogênicos e a dissociação de hidratos de metano e metano termogênicos (Arai 1988; Mello *et al.* 1989; Koutsoukos *et al.* 1990; Jenkyns 2010; Dot *et al.* 2015; Robinson *et al.* 2017; Tedeschi *et al.* 2017).

1.1.3. As incursões marinhas e abertura do Atlântico Sul

A inundação de um continente pela água dos oceanos é denominada incursão marinha. Também chamada de transgressão, esses eventos ocorrem normalmente como resultado do aumento do nível do mar e de uma subsidência

tectônica (Bloom and Lovejoy 2011). Durante o Cretáceo houve um aumento significativo do nível do mar, fato que provocou importantes modificações na produtividade orgânica dos oceanos e na distribuição dos sedimentos ao longo das margens continentais e nas bacias interiores (Haq *et al.* 1987).

Na plataforma Sul-Americana as incursões marinhas deixaram registros nas bacias Andino-Amazônicas, as quais apresentam ciclos transgressivos com deposição sedimentar desde o Albiano até o Campaniano. (Baby *et al.* 1999; Cunha 2007; Hurtado *et al.* 2018; Louterbach *et al.* 2018; Zamora and Gil 2018). Dentre as incursões destaca-se a deposição da Formação Chonta de idade Cenomanina-Turoniana (Louterbach *et al.* 2018), que marca a última transgressão e o início de um período regressivo com uma superfície máxima de inundação (Wine *et al.* 2001). Nas bacias da margem equatorial, os primeiros registros de ingressões marinhas ocorreram no Aptiano Superior (Assine 1994) e estão representados em sedimentos da Bacia do Parnaíba e São Luís (Formação Codó); Bacia do Ceará (Membro Trairi da Formação Paracuru) e Bacia Potiguar (Camadas Ponta do Tubarão da Formação Alagamar) (Bagni 2010). Na Bacia do Araripe os registros cretáceos marinhos são registrados no Aptiano (Goldberg *et al*. 2019) restringem-se ao Albiano Inferior (Formação Santana) (Assine 1994).

No interior do Brasil, a ingressão marinha ocorreu entre o Aptiano e Albiano, tendo se estendido localmente ao Cenomaniano. Limitada à Bacia do Parnaíba e às áreas vizinhas do Nordeste Oriental, como a Bacia do Araripe, há também registros dessa ingressão na Bacia Franciscana (Almeida e Carneiro 2016). As incursões marinhas durante o Cretáceo apresentam depósitos sedimentares importantes para o entendimento do sistema paleoclimático e

geográfico da Plataforma Sul Americana, que, ainda são pouco documentados e carecem de informações temporais e espaciais mais precisas (Bloom e Lovejoy 2011). Discussões sobre as incursões marinhas e a deposição da bacia do Araripe, por exemplo, bem como a abertura do Atlântico Sul, foram feitas ao longo das últimas décadas (Assine 1994; Arai 2014, 2016; Assine *et al.* 2016; Custódio *et al.* 2017). Há, no entanto, uma carência de estudos sobre reconstituição paleogeográfica que integrem com dados das áreas fontes, dados sedimentares e paleontológicos.

1.1.4. Soerguimento dos Andes e o comportamento das drenagens na parte norte da plataforma sul-americana

Os Andes se originaram num complexo cenário geotectônico, no qual os processos geodinâmicos condicionaram as características de suas principais morfoestruturas (Potter 1997; Ramos and Folguera 2009). De norte a sul os Andes estão divididos em: Andes Setentrionais, cuja formação possui relação com a interação entre as placas do Caribe, Cocos, Nazca e Panamá e com os processos de acreção dos fragmentos de crosta oceânica e dos arcos insulares durante o Mesozóico e Cenozoico (Ramos and Folguera 2009); Andes Centrais, com extensão entre o Norte do Peru e a Argentina, em que o desenvolvimento se deu como reflexo da subducção da Placa de Nazca sob o Continente Sul-Americano; e Andes Austrais ou Meridionais, interpretado como resultado da interação entre as placas Nazca, Antártica, Scotia e Sul-Americana (Ramos and Folguera 2009).

A organização da drenagem na América do Sul durante o Cretáceo está relacionada a um controle tectônico e às mudanças geodinâmicas e/ou climática desse período. Duas situações principais moldam o sistema fluvial: a separação

do continente africano e o soerguimento da cordilheira andina (Potter 1997). Durante a maior parte do Fanerozóico as margens da América do Sul estiveram bordejadas pelo paleo-oceano Pacífico e o arranjo das drenagens, de forma direta ou indireta, estava condicionado a bacias pericratônicas que se estabeleciam ao longo da margem oeste (Potter, 1997). Na região mais a leste, a organização fluvial tinha influência de orógenos associados à períodos de convergência mais antigos (ver processos de fusão e fissão da plataforma em Schobbenhaus e Brito Neves, 2003).

Durante o processo de abertura do Oceano Atlântico, a tectônica formadora de bacias sedimentares teve contribuição vulcanogênica importante e se instalou em locais da margem oriental privilegiando estruturas mais antigas, como as estruturas brasilianas (Schobbenhaus and Brito Neves 2003). No Brasil, a evolução das drenagens tende a se ajustar em locais onde estão preservadas estruturas brasilianas, sotopostas após as fases de sedimentação (Schobbenhaus and Brito Neves 2003). De forma semelhante, na região mais ocidental da plataforma Sul-Americana, o sistema de drenagem ajustou-se a componentes tectônicos. Duas importantes bacias sedimentares (Amazonas e Solimões) se desenvolveram sob um *rift* neo-Paleozóico (Potter 1997). A Tabela 1 exemplifica como algumas das principais drenagens da parte norte da Plataforma Sul-Americana se comportaram durante o desenvolvimento de *uplifts* e riftes. No entanto, ainda carecem discussões sobre a evolução das drenagens na porção ocidental da Amazônia durante o período Cretáceo.

Tabela 1: Origem de drenagens durante períodos de soerguimento e fragmentação da parte norte da Plataforma Sul Americana. Retirado de (Potter 1997).

Nome	Soerguimentos	Embasamento	Associações vulcânicas	Desenvolvimento de drenagem	Idade	Riftes
Guiana/Guinea	Monte Roraima/ Gran Sabana (1000-3000 m)	Meso e paleo proterozoico/ (Super Grupo Roraima)	Diques relacionados a separação	Graben Takutu	Cretáceo	Takutu/ Foz do Amazonas
NE Brasil/Nigéria	Borborema (400-1000 m)	Neo e meso proterozoico/ Arqueano	Intrusões alcalinas mais velhos que 12 Ma	Bacia Potiguar; Rio São Francisco/ Benue Rifte;	?	Recôncavo Tucano – Jatobá
Mantiqueira/ Angola	Serras da Mantiqueira e do Mar (1000-2000m)	Neo e meso proterozoico/ Arqueano	Diques e intrusões alcalinas (45-130Ma) Vulcanismo terciário e kimberlitos	Bacia Paraíba (?) e outra bacia terciária coincidente com o graben Trindade do Rio Paraíba.	?	Taubaté

1.2. Bacias sedimentares Cretáceas - Sistema Andes-Amazônia e bacias interiores

1.2.1. Bacias sedimentares Andes-Amazônia

A parte oeste da Plataforma Sul-Americana possui bacias sedimentares que refletem as variações da paleogeografia e da geodinâmica durante o Cretáceo. As mudanças geodinâmicas neste cenário estão associadas ao desmembramento do Gondwana e à convergência entre a placa Nazca e Sul Americana localizadas em sua margem ocidental. Entre a região central andina e o interior da plataforma, as bacias sedimentares Oriente/Marañon, Ucayali, Acre, Huallaga e Madre de Dios mostram uma complexa evolução estrutural e deformacional, sendo alvo de discussões de vários autores durante os últimos tempos (Figura 3) (Wine *et al.* 2001; Hermoza *et al.* 2005; Roddaz *et al.* 2005; Baby *et al.* 2013; Erlich *et al.* 2018; Louterbach *et al.* 2018; Zamora and Gil 2018).

Figura 3: Localização das bacias sedimentares Sub Andinas na plataforma Sul Americana. Modificado de (Albert et al. 2018)

A Bacia Oriente é parte do sistema sedimentar amazônico e possui registro sedimentar desde o Paleozoico até o Recente (Christophoul *et al.* 2002). Ela é limitada a norte pela bacia Putumayo, situada em domínios colombianos e ao sul pela bacia Marañon, localizada no norte do Peru. Três megasequências podem ser observadas desde o Carbonífero até o Quaternário (Baby *et al.* 1999). Durante o Cretáceo os depósitos correspondentes ao Albiano-Campaniano apresentam sequências cíclicas de arenitos, pelitos e folhelhos ricos em matéria orgânica (Baby *et al.* 1999). As fontes desses sedimentos, sobretudo durante o final do Cretáceo, são localizadas no craton amazônico (Ruiz *et al.* 2007).

A bacia Marañon pode ser considerada uma extensão da bacia Oriente (ou o contrário) e Putumayo, localizadas no Equador e Colômbia. Ela está situada a norte das bacias Ucayali e Acre e compreende uma sucessão sedimentar que se inicia no Mesozóico (Zamora and Gil 2018). Ao longo do Cretáceo sedimentos clásticos fluviais e marinhos foram depositados controlados por mudanças eustáticas e um longo período de quiescência tectônica pode ser observado entre o período Cretáceo e o Oligoceno. Durante esse período houve uma pequena inversão estrutural, porém com poucos registros estudados (Zamora and Gil 2018).

A bacia Ucayali encontra-se entre a bacia Marañon e a bacia do Acre. Ela está limitada pelo Arco de Contaya e pela estrutura Moa-Divisor que possui um *trend* com direção NNW-SSE. A deposição sedimentar desaparece progressivamente ao sul em direção ao Arco Fitzcarrald (Hermoza *et al.* 2006; Lopez-Gamundi and Lopez-Gamundi 2018). Durante o Cretáceo a sedimentação ocorreu durante ciclos transgressivos regressivos, que depositaram seções sedimentares fluviais e marginais com contribuição carbonática sobre estruturas paleozóicas. Dentre as seções depositadas, a Formação Chonta de idade Cenomanina-Turoniana (Louterbach *et al.*

2018) indica a última transgressão e o início de um período regressivo com uma superfície máxima de inundação. Após este período houve a deposição de um complexo arenítico-quartzítico, a Formação Vivian, que marca o final do Cretáceo e o início dos pulsos orogênicos andinos (Martinez *et al.* 1999).

A bacia de Huallaga encontra-se entre a frente do sistema de dobramentos da Zona Sub Andina e Chazuta. Esta última, separa a bacia Marañon e a Cordilheira Oriental. (Hurtado *et al*. 2018) Uma inconformidade erosional separa as rochas do Cretáceo das rochas sedimentares jurássicas, representada por depósitos fluvial-deltaicos com arenitos ricos em quartzo intercalados com folhelhos e siltitos de idade Aptiana-Albiana. (Wine *et al.* 2001; Hurtado *et al.* 2018). Durante a última metade do Albiano há registros de um ambiente marinho raso (Sanchez F. *et al.* 1997; Hurtado *et al.* 2018). Depósitos cenomanianos foram formados em ambientes fluvio-deltáicos e apresentam arenitos com intercalações de folhelhos e siltitos. O Cretáceo tardio é caracterizado por folhelhos marinhos, margas, pelitos e calcários da Formação Chonta sobrepostos por arenitos fluvio costeiros ricos em quartzo da Formação Vivian. Rochas dessa unidade gradam lateralmente para folhelhos negros marinhos da Formação Cachiyacu, marcando o final do Maastrichtiano. (Sanchez F. *et al.* 1997; Hurtado *et al.* 2018).

A bacia Madre de Dios está situada ao sul do Peru e a leste dos Andes Centrais, na Zona Sub Andina. Tectonicamente é limitada ao sul pelo dobramento Azulmayo, e a norte e nordeste pelo Escudo Brasileiro. A norte, o Arco de Fitzcarrald limita sua extensão (Louterbach et al., 2018). Rochas metamórficas pré-cambrianas e cambrianas, além de metassedimentos e rochas ígneas paleozóicas formam o embasamento desta bacia. Próximo à cordilheira oriental, a bacia é constituída por seções sedimentares heterogêneas desde o Paleozoico tardio até o Cenozoico

(Louterbach *et al.* 2018). Na região subandina, as rochas do Cretáceo Inferior foram completamente encobertas por uma discordância regional, deixando visível apenas estratos sedimentares a partir do final do Campaniano, quando ocorreu a deposição de sedimentos em um ambiente marinho raso. Folhelhos avermelhados e horizontes paleo pedológicos indicam uma evolução para um ambiente mais costeiro. Acima dessas rochas, o ambiente muda para marinho raso, passando gradualmente para um ambiente dominado por maré e dunas (Louterbach et al., 2018). Durante o Maastrichtiano superior depósitos costeiros começam a se instalar com *inputs* continentais. É possível se identificar a presença de deformação causadas por falhas normais *syn*-sedimentares (Louterbach et al., 2018).

A bacia do Acre é a componente brasileira do sistema sub andino e está limitada a leste pelo Arco de Iquitos, o qual a separa da Bacia Solimões. Ela se estende até a bacia Ucayali a oeste, à bacia Marañon a noroeste e a bacia Madre de Dios a sul, completando o domínio do *retroforeland* sub andino (Cunha 2007; Haag 2019). Conforme Oliveira (1994), esta bacia possui uma complexa evolução de eventos compressivos e distensivos desde o Paleozoico até os tempos recentes. Entre o Albiano e o Cenomaniano houve uma quiescência tectônica, registrada nos sedimentos da Formação Moa. Ela é formada essencialmente por arenitos e possui uma superfície máxima de inundação caracterizada por folhelhos negros Cenomaniano-Turonianos. Acima dessa deposição observa-se os pelitos marinhos e arenitos finos da Formação Rio Azul sotopostos abruptamente pelos arenitos fluviais da Formação Divisor (Cunha 2007).

1.2.2. Bacia do Araripe

Dentre os tipos de bacias cretáceas, as bacias interiores, localizadas na parte norte da Plataforma Sul Americana possuem histórias evolutivas associadas

diretamente aos eventos geodinâmicos do período. A bacia do Araripe está localizada no Nordeste do Brasil entre os lineamentos Patos e Pernambuco, que correspondem a duas zonas de cisalhamento pré-cambrianas que sofreram reativação durante o Mesozoico (Brito Neves et al., *in* Cordani et al., 2000). A evolução dessa bacia está intimamente relacionada aos eventos geodinâmicos do Cretáceo resultantes da ruptura do Gondwana e abertura do oceano Atlântico Sul (Assine 1992, 2007; Darros de Matos 1999).

Dentre os estudos já realizados na bacia, diversas tentativas de reconstrução paleogeográficas foram feitas ao longo do século XX e XXI. Ghignome (1972) fez um ensaio sobre a paleogeografia do nordeste brasileiro caracterizando as áreas sedimentares da região em seis Sequências que indicavam as grandes fases de deposição, erosão e condições geotectônicas como um todo e para ele, o Período Cretáceo estaria contido nas Sequência IV e V. Petri (1987) elaborou trinta e seis mapas paleogeográficos cobrindo os registros cretáceos nas bacias sedimentares. Esse autor abordou ainda os vários aspectos da evolução dessas bacias: o episódio de rifteamento; as primeiras evidências sobre os mares marginais e epicontinentais com a presença de evaporitos; a abertura do mar entre o Albiano e Cenomaniano; as transgressões entre o Turoniano – Santoniano e as relações transitoriais *onlap - offlap* no Campaniano-Maastrichtiano, bem como a evolução das bacias interiores, não marinhas. Para Petri (1987) a Bacia do Araripe encontrava-se entre o Andar Alagoas e o Cenomaniano, e era evidenciada pela presença de evaporitos (áreas de mar restrito e raso), e depósitos em zonas de subsidência extensional.

Machado Junior et al., (1990) fizeram reconstruções paleoambientais nas bacias interiores do Nordeste brasileiro e apresentaram mapas que compreendem os andares Dom João, Rio da Serra/Aratu, Alagoas e Albo-Cenomaniano. Na

interpretação dos autores, a intensa movimentação tectônica, fruto da ativação mesozoica, dividiu a parte oriental da região nordeste em vários riftes controlados por falhas pré-cambrianas, os quais foram alimentados por redes de drenagens, a norte, associados à primeira fase de abertura e formação do Atlântico na região equatorial e a sudeste, alinhada com a formação do Atlântico Sul. Neste contexto, a Bacia do Araripe começou a se formar, assim como outras bacias interiores, as quais possuem semelhança litológica em função do regime tectônico e dos processos climáticos e sedimentares (Figura 4).

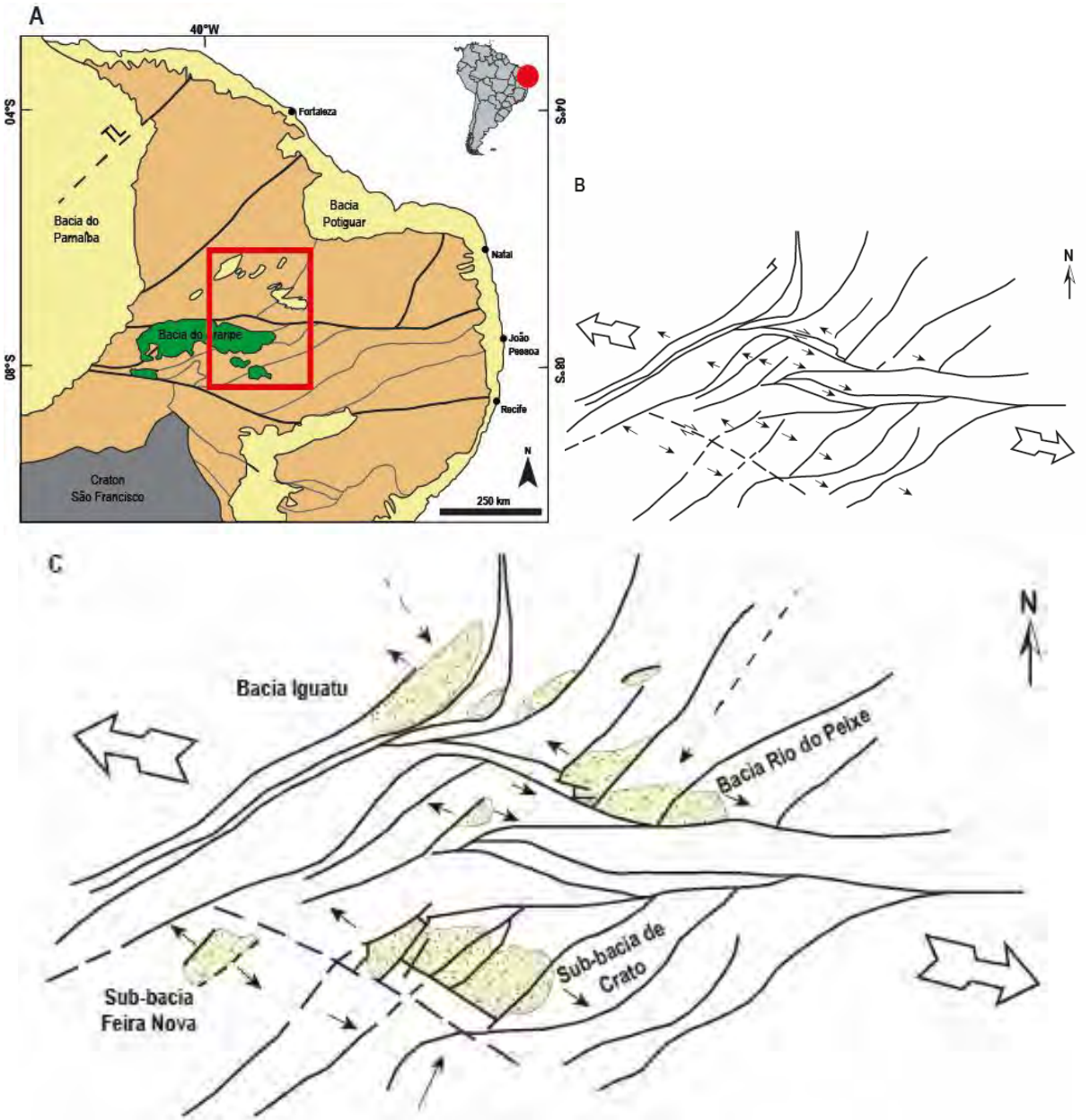

Figura 4: A: Localização das bacias formadas a partir do riftiamento regional. B: Condicionantes tectônicos das bacias interiores da Região Nordeste Oriental. C: Provável paleogeografia das bacias interiores. Modificado de Machado Junior et al. (1990).

Assine (1994) fez uma compilação de dados de paleocorrentes e analisou como elas refletiam a variação do aporte sedimentar e a modificação das áreas-fonte ao longo do tempo geológico. Por meio dessas análises foi possível interpretar movimentações tectônicas e assim esboçar contextos paleogeográficos. Ele dividiu o registro sedimentar da bacia do Araripe em quatro sequências estratigráficas, as quais apresentaram padrões de paleocorrentes fluviais definidos e distintos, refletindo um registro sedimentar fragmentário. As unidades juro-neocomianas, por exemplo,

mostram que a paleo drenagem continental fluía para sul em direção a Bacia do Recôncavo-Tucano. No entanto, durante o período Aptiano-Albiano subsequente, observou-se um padrão inverso, com um fluxo de sul-sudeste para norte-nordeste, que foi associado a uma transgressão marinha temporária na Bacia. Em uma fase mais tardia, durante a sequência Albiano-Cenomaniana, a mudança na rota da drenagem continental foi interpretada como resultado do soerguimento da Região Nordeste do Brasil a partir do Albiano médio (Fig.09).

No entanto, contrapondo esta hipótese, reconstruções paleogeográficas posteriores sugeriram outras direções para a ocorrência das ingressões marinhas. Arai (2014) abordou a paleogeografia do Atlântico Sul no Aptiano/Albiano pela perspectiva paleontológica. Para ele, a sedimentação marinha ocorrida na margem continental brasileira teve influência de fontes provenientes de norte, por meio do *seaway* que cortava a região nordeste do Brasil. A influência das águas vindas de Tethys seria dominante nesta região e estaria relacionado a deposição de unidades das bacias de São Luís e Parnaíba (Formação Codó); Araripe (Formação Santana); Tucano (Formação Marizal), Sergipe (Formação Riachuelo) e Camamu (Formação Algodões). A evidência do mar de Tethys estaria ligado a presença de organismos marinhos característicos deste ambiente. No mapa de reconstrução paleogeográfica Arai (2014) mostra que as águas proeminentes do Atlântico Central percorrem o *seaway* conectando as bacias interiores do nordeste do Brasil (Figura 5).

Figura 5: Reconstrução paleogeográfica feita por Arai (2014) baseada nos paleomapas de Scotese (2014a) mostrando as ocorrências da Ecozona Subtlisphaera (círculos vermelhos), de palinofloras marinas (círculos amarelos) do seaway e a localização das bacias sedimentares interiores. Retirado de Arai (2014). A- Morocco; B – Senegal; C - Bacia Maracaibo; D – Bacia São Luís; E – Bacia do Ceará; F – Bacia Potiguar; G - Bacia Parnaíba; H - Bacia do Araripe; I - Bacia Almada; J – Bacia Sergipe; M - Bacia Pelotas; L - Río Fosiles, Provincia de Santa Cruz, Argentina.

No mesmo sentido, Prado et al. (2015) desenvolveram uma interpretação paleoambiental através da concentração de fósseis de macroinvertebrados da Formação Santana, sugerindo que a transgressão marinha do Aptiano/Albiano teve origem a oeste e contribuição sedimentar da Bacia do Parnaíba. O estudo levou em consideração a identificação de moluscos marinhos no Membro Romualdo da Bacia do Araripe, que possuem idades equivalentes aos encontrados em unidades das bacias do Parnaíba e Sergipe-Alagoas. Os autores sugerem uma conexão marinha entre essas bacias e a região do Araripe durante o Cretáceo Inferior.

Alimentando a discussão, Assine et al. (2014) descreverem os sistemas deposicionais do Andar Alagoas da Bacia do Araripe e sugerem cenários

paleogeográficos diferentes, bem como regimes tectônicos distintos, para essas unidades estratigráficas. Os autores sugerem que a sucessão estratigráfica do Andar Alagoas apresenta um contexto paleogeográfico semelhante a outras bacias sedimentares da região (Sergipe/Alagoas; Parnaíba, Ceará e Potiguar). Porém, como a bacia encontra-se distante dos oceanos originados da ruptura de Gondwana, as características sedimentares seriam de ambientes marginais a continentais. Embora o Andar Alagoas mostre empilhamento estratigráfico similar ao da Bacia do Parnaíba, Assine et al (2014) discordam da interpretação feita por Arai (2014). A arquitetura estratigráfica e as direções de paleocorrentes fluviais indicam que as fontes sedimentares se localizavam a noroeste e desta maneira, as ingressões marinhas ocorreriam no sentido diferente ao da drenagem continental. Os autores chegaram à conclusão de que a entrada do mar na Bacia do Araripe no Aptiano Superior foi de sudeste para nordeste (Assine et al 2014).

Na mesma linha argumentativa, Assine et al. (2016) sugerem que a abertura do oceano Atlântico Sul se deu em direção a norte, baseados em trabalhos de reconhecimento do espalhamento do assoalho oceânico. Além disso, haja vista o modelo adotado por Arai (2014), os autores sugerem que deveria haver uma integração de dados de diferentes áreas da geologia para uma reconstrução paleogeográfica e não somente dados paleontológicos. Assine et al. (2016) asseveram que três bacias hidrográficas podem ser sugeridas no cenário pelogeográfico da região: as bacias Parnaíba e Potiguar seriam separadas entre si e distintas do sistema de formação da bacia do Araripe, cuja relação estaria mais próxima às bacias Tucano e Jatobá, três direções principais de ingressão marinha, desta forma, estariam ligadas ao interior do nordeste brasileiro durante o Aptiano. (Figura 6)

Arai (2016) fez a réplica aos comentários de Assine et al. (2016) enfatizando que modelos geológicos que não levam em consideração as evidências paleontológicas estão fadados ao fracasso. Ele rejeitou a existência de drenagens que dividiriam a bacia do Araripe e Parnaíba no momento da sedimentação das formações Codó (Bacia do Parnaíba) e Santana (Bacia do Araripe), pois ambas teriam similaridades de conteúdos fósseis. Se houvesse esta divisão hidrológica existiria uma barreira biogeográfica inibindo o desenvolvimento de biotas semelhantes. Outro ponto criticado foi relacionado às medidas de paleocorrentes que indicariam fluxos vindos de sul e sudeste durante o Aptiano. Segundo o autor, a Formação Rio da Batateira e Marizal não estariam depositadas em um sistema fluvial, mas no começo de transgressão marinha. Desta forma, as estratificações cruzadas indicariam paleocorrentes originadas através de inundação de marés (Figura 7).

Figura 6: Reconstrução paleogeográfica modificada de (Scotese 2014) mostrando a configuração do Aptiano antes da deposição evaporítica e a disposição das bacias sedimentares representadas por letras: D – Bacias São Luís e Parnaíba; A – Bacia Barreirinhas; B – Bacia Ceará, Formação Mundaú; C- Bacia Potiguar; E – Bacia Araripe, Formação Rio da Batateira. Retirado de (Arai, 2016).

Custódio et al., (2017) discutiram elementos paleogeográficos da Bacia do Araripe ao abordar o ciclo transgressivo-regressivo da Formação Romualdo. A partir da correlação de diversas seções dessa formação, os autores sugerem que o ciclo transgressivo-regressivo possui mergulho deposicional com direção a sudeste e fontes localizadas ao norte da bacia. Os dados estratigráficos e sedimentológicos sugerem que uma drenagem dividiu as bacias do Araripe e Potiguar e seguiu rigidamente o Lineamento Patos, corroborando com as assertivas de Assine et al.

(2016). As informações provenientes da arquitetura sedimentar da Formação Romualdo e as paleocorrentes se relacionam com a interpretação que aponta para áreas fonte ao norte e os mergulhos deposicionais em direção ao sul da bacia (Figura 8). Sendo assim, Custódio et al. (2017) concordam com as proposições de Assine (1994); Assine et al. (2014, 2016) e vão na direção oposta as interpretações propostas por Arai (2014, 2016).

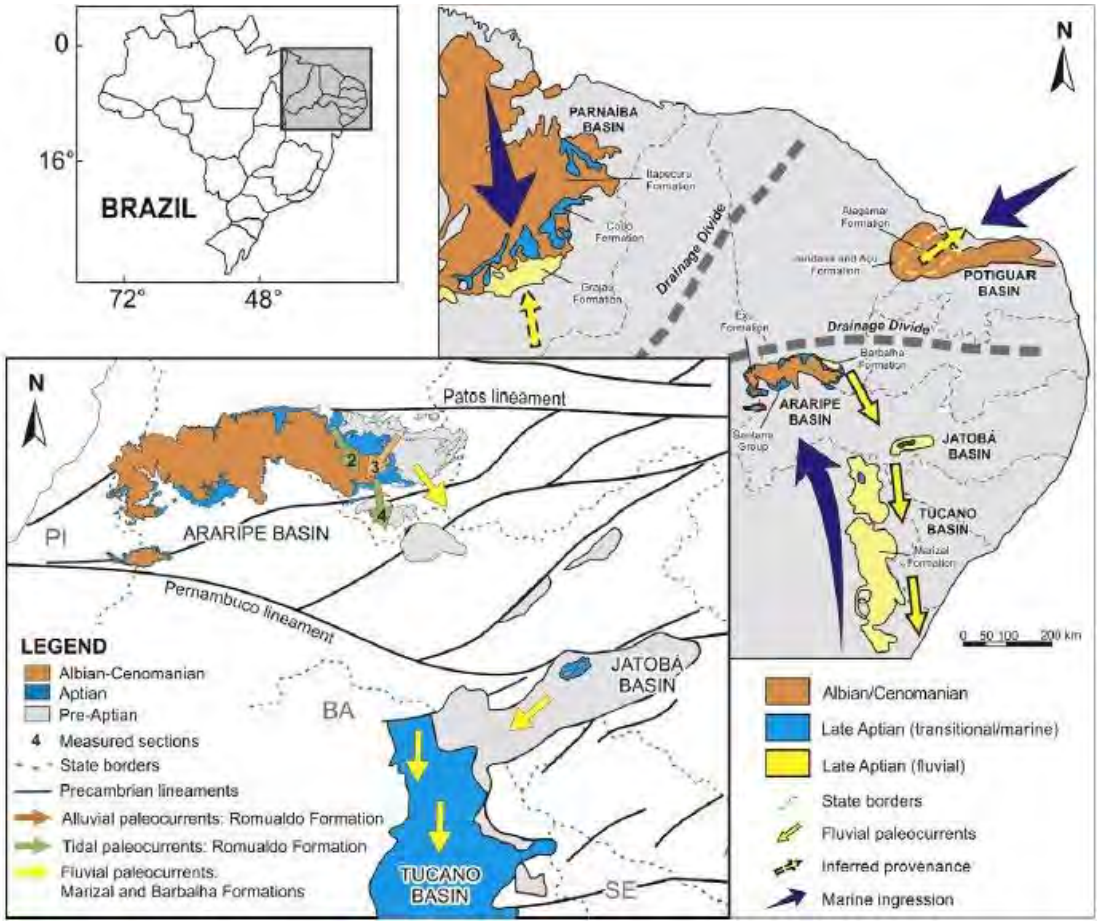

Figura 7: Reconstrução paleogeográfica do nordeste brasileiro durante o Aptiano baseada em Assine et al. (2016). As setas amarelas e verdes representam as principais rotas sedimentares. As setas azuis estão relacionadas as ingressões marinhas. Retirado de Custódio et al. (2017).

Estudos recentes realizados na bacia do Araripe buscaram identificar a proveniência de sedimentos e a direção da ingressão marinha (Godot Souza et al. 2022). Esses autores sugerem que durante o Jurássico Superior a fonte dos sedimentos da Bacia do Araripe era proveniente de rochas Paleozoicas da Bacia do Parnaíba. Durante o Aptiano houve uma diminuição de sedimentos vindos da porção

oeste e fontes oriundas da bacia dos terrenos Proterozoicos da Província Borborema a noroeste. Uma depressão instalou-se na região entre as Bacia do Araripe e Potiguar no final do Aptiano e proporcionou a entrada marítima do Proto-Oceano Atlântico Equatorial (*Figura 8*).

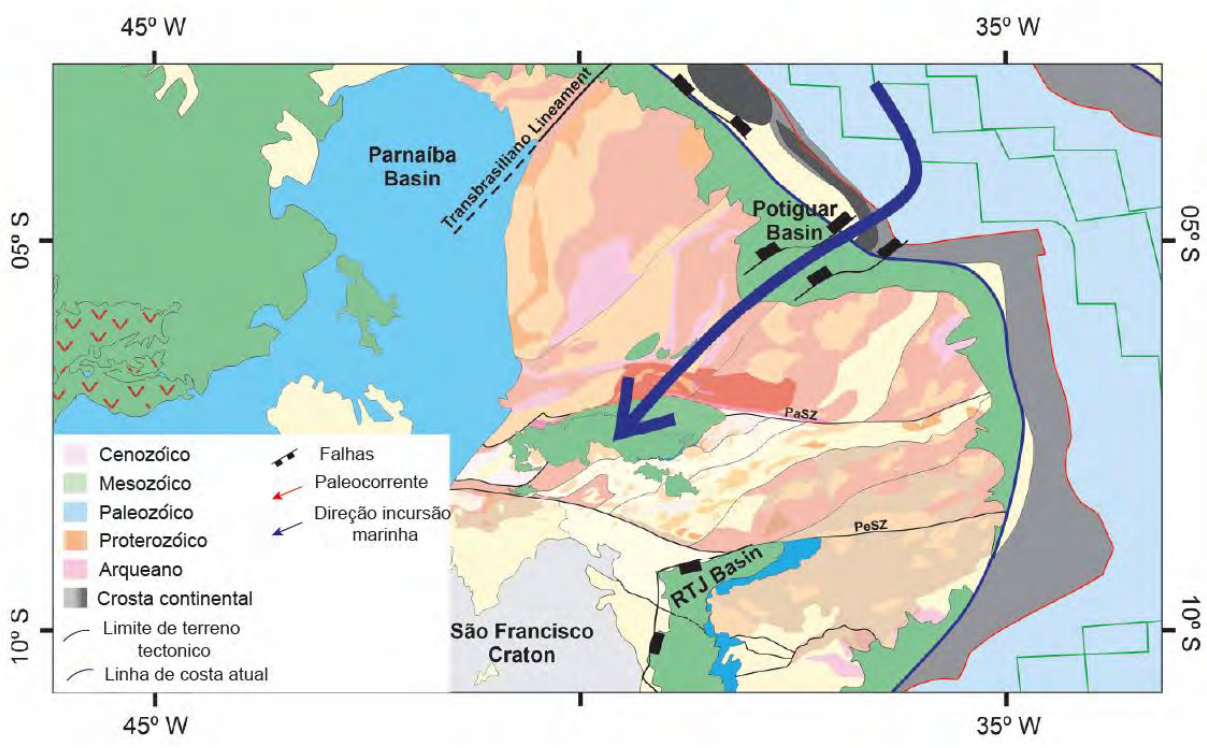

Figura 8: Reconstrução paleogeográfica durante a incursão marinha no Aptiano Superior. A reconstrução foi baseada no modelo cinemático de Heine et al 2013 e Richetti et al 2018. Modificado *de (Godot Souza et al. 2022)*. PeSZ: Zona de Cisalhamento Pernambuco; PaSZ: Zona de Cisalhamento Parnaíba.

1.3. Reconstrução paleogeográfica

A paleogeografia é a representação das superfícies antigas da Terra por meio dos tempos geológicos (Markwick 2019). Consiste basicamente na datação de rochas, caracterização dos ambientes e posicionamento das áreas estudadas no contexto paleolatitudinal e paleolongitudinal (Ziegler et al. 1985). Através deste estudo é possível entender como era a interação entre os processos climáticos, geomorfológicos e tectônicos e como eles se refletiam em superfície (Pohl *et al.* 2019). Desde a primeira metade do século XX, estudos sobre a paleogeografia foram

desenvolvidos, principalmente para atender a exploração petrolífera (e. g. Adams, 1943). Nos anos de 1980 e 1990, diversos projetos e trabalhos tinham como objetivo fazer projeções paleogeográficas a fim de dar luz à diversas interpretações (Barron 1987; Scotese *et al.* 1988; Machado Junior *et al.* 1990; Scotese 1991; Assine 1994).

Adams (1943) abordou a importância das reconstituições paleogeográficas para o entendimento dos depósitos de petróleo. Para ele, os métodos paleogeográficos são os mais efetivos para os estudos de bacias sedimentares, pois apontam para as diferenças de subsidência, as variações de sedimentação e a proveniência estratigráfica dos depósitos petrolíferos. Entre as décadas de 1970 e 1980, projetos de reconstituições e criações de modelos mundiais paleogeográficos foram desenvolvidos por pesquisadores como (Barron 1987), já a luz da teoria de tectônica de placas. Mapas base sobre a paleogeografia do Cretáceo foram produzidos com dados oceânicos e continentais provenientes de estudos geológicos e geofísicos. A trajetória da deriva continental e as linhas de paleolatitude obtidas através da média da posição paleomagnética dos polos deram suporte para a compreensão de reconfiguração das feições cretáceas globais em diferentes idades. Scotese, desde a década de 1970 vem desenvolvendo trabalhos sobre reconstituições tectônicas, paleogeográficas e paleoclimáticas. (Scotese *et al.* 1988) apresentaram nove mapas de reconstrução tectônica com isócronas magnéticas sobre as bacias oceânicas do Cretáceo e Cenozóico; (Scotese 1991 e Scotese 2014) fazem a reconstituição da fragmentação do Pangea e a evolução dos oceanos durante o Cretáceo inferior (Aptiano) e superior (Cenomaniano e Maastrichtiano) (Figura 9). Por meio desses modelos é possível entender a configuração geométrica, tectônica e paleoclimática das regiões globais ao longo do período Cretáceo. Mapas

regionalizados, no entanto, podem dar informações com mais acurácia sobre todos os elementos que constitui uma interpretação paleogeográfica.

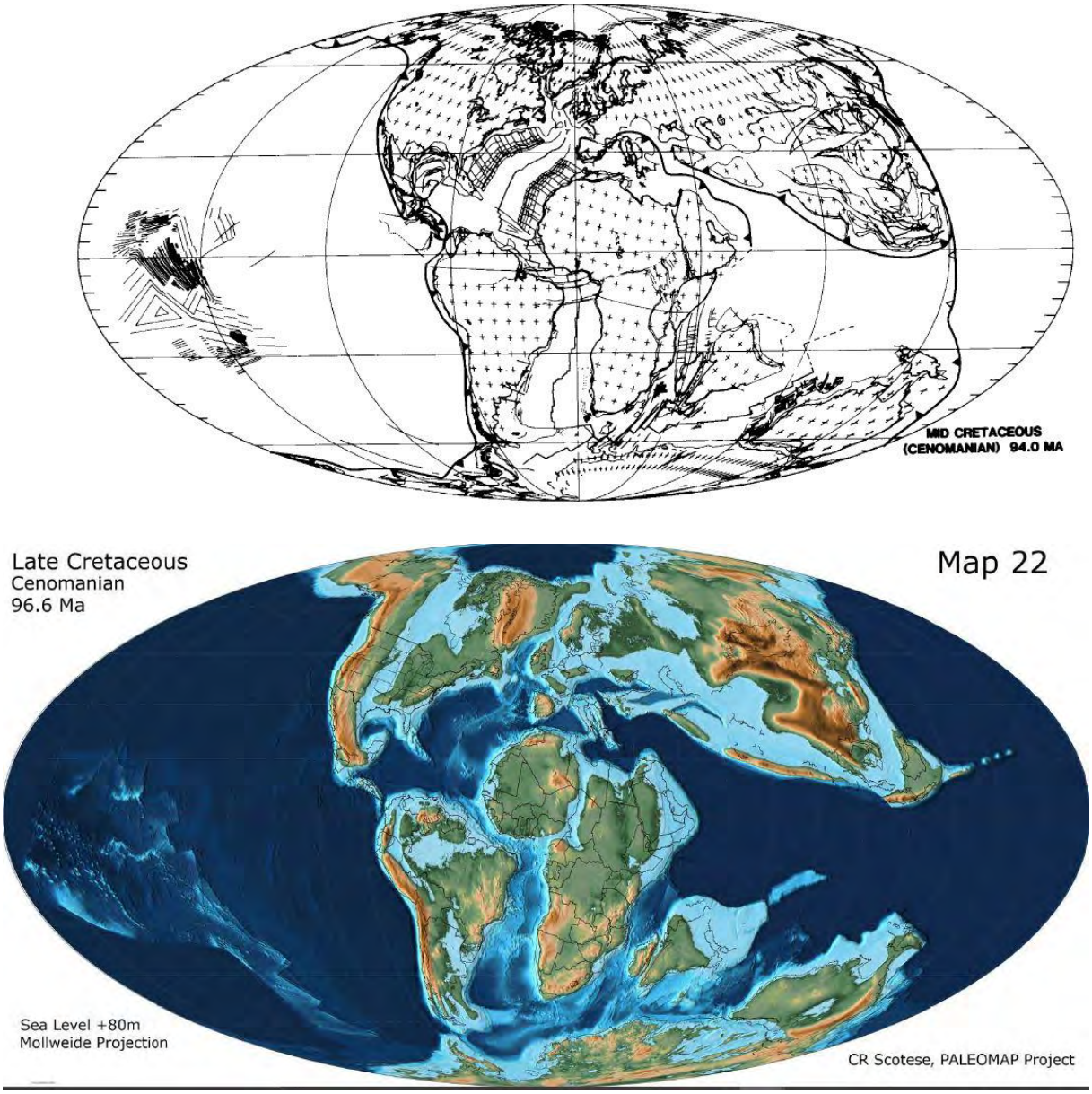

Figura 9: Exemplos de reconstruções paleogeográficas mundiais durante o Cretáceo. Retirado de Scotese, 1991 e Scotese, 2014.

Neste contexto, o Período Cretáceo foi contemplado com uma série de estudos e reconstituições. As reconstruções tectônicas, climáticas e geomorfológicas, com o auxílio da paleontologia, foram relevantes para o desenvolvimento de modelos globais paleogeográficos. Trabalhos no continente africano permitiram uma reconstituição paleogeográfica que aborda o Período Cretáceo (Simoes *et al.* 2010). Outros

trabalhos, realizados na China e no segmento central do Atlântico Sul (Chaboureau *et al.* 2013; Li *et al.* 2018) também utilizam técnicas analíticas modernas para reconstruir paleogeograficamente áreas cretáceas e podem ser exemplos de metodologias de análise. Na plataforma Sul-Americana, diversos estudos têm examinado o período Cretáceo com o objetivo de formular interpretações sobre condições paleogeográficas (e.g. Riccardi 1987; Macellari 1988). No Brasil, investigações de reconstruções paleogeográficas possuem um caráter mais localizado (e.g. Assine 1994). Contudo, é evidente a necessidade de desenvolver estudos mais abrangentes que permitam uma reconstrução mais completa da paleogeografia do Cretáceo na Plataforma Sul Americana.

1.4. Objetivos

1.4.1. Objetivo Geral

Contribuir para o entendimento do sistema sedimentar Andes-Amazônia-Margem Equatorial por meio do estudo da proveniência dos sedimentos das bacias Cretáceas andinas (Madre de Dios e Acre) e da porção leste da América do Sul (bacia do Araripe).

1.4.2. Objetivos específicos

- Identificar áreas fontes de sedimentos e sua relação com a configuração tectônica durante o período Cretáceo (abertura do Oceano Atlântico Equatorial e Sul e o soerguimento dos Andes).
- Investigar a direção dos aportes sedimentares das bacias do Acre e Madre de Dios e sua relação com o sistema de drenagens desenvolvido na região Amazônica durante o Cretáceo Superior.
- Compreender como a readequação do sistema de drenagens durante as diferentes fases de sedimentação da bacia do Araripe refletem as mudanças geodinâmicas da parte nordeste da plataforma sul americana durante a abertura do Oceano Atlântico Sul e Equatorial.
- Reconstruir os ambientes paleogeográficos relacionando os dados obtidos desde o Neocomiano (~145 Ma) até o final do Maastrichtiano (66 Ma) na parte norte da Plataforma Sul Americana.

Referências bibliográficas

Adams, J.E. 1943. Paleogeography and Petroleum Exploration. *SEPM Journal of Sedimentary Research*, **Vol. 13**, https://doi.org/10.1306/D42691B1-2B26-11D7-8648000102C1865D.

Agence Nationale de la Recherche. 2016. TOPOAFRICA: Evolution of the African topography over the last 250My from the sedimentary record to mantle dynamics. *Top Africa from the sedimentary record to mantle dynamics*https://topoafrica.univ-rennes1.fr/.

Albert, J.S., Val, P. and Hoorn, C. 2018. The changing course of the Amazon River in the Neogene: center stage for Neotropical diversification. *Neotropical Ichthyology*, **16**, e180033, https://doi.org/10.1590/1982-0224-20180033.

Almeida, F.F.M. de and Carneiro, C.D.R. 2016. Inundações Marinhas Fanerozóicas no Brasil e Recursos Minerais Associados. *In*: *Geologia Do Continente Sul-Americano: Evolução Da Obra de Fernando Flávio Marques de Almeida*.

Arai, M. 1988. Geochemical Reconnaissance of the Mid-Cretaceous Anoxic Event in the Santos Basin, Brazil. *Revista Brasileira de Geociencias*, **18**, 273–282.

Arai, M. 2006. Revisão Estratigráfica do Cretáceo Inferioe das Bacias Interiores do Nordeste do Brasil. *Geociências*, **25**, 7–15.

Arai, M. 2014. Aptian/Albian (Early Cretaceous) paleogeography of the South Atlantic: a paleontological perspective. *Brazilian Journal of Geology*, **44**, 339–350, https://doi.org/10.5327/Z2317-4889201400020012.

Arai, M. 2016. Reply to the comments of Assine et al. (Comments on paper by M. Arai ‘Aptian/Albian (Early Cretaceous) paleogeography of the South Atlantic: a paleontological perspective’). *Brazilian Journal of Geology*, **46**, 9–13, https://doi.org/10.1590/2317-4889201620150046B.

Assine, M.L. 1992. Análise estratigráfica da Bacia do Araripe, Nordeste do Brasil. *Revista Brasileira de Geociências*, **22**, 289–300, https://doi.org/10.25249/0375-7536.1992289300.

Assine, M.L. 1994. PALEOCORRENTES E PALEOGEOGRAFIA NA BACIA DO ARARIPE, NORDESTE DO BRASIL. *Revista Brasileira de Geociências*, **24**, 223–232, https://doi.org/10.25249/0375-7536.1994223232.

Assine, M.L. 2007. Bacia do Araripe. *Boletim de Geociências Petrobras*, **15**, 371–389.

Assine, M.L., Neumann, H., Varejão, F.G. and Mescolotti, P.C. 2014. Sequências deposicionais do Andar Alagoas da Bacia do Araripe, Nordeste do Brasil. 26.

Assine, M.L., Quaglio, F., Warren, L.V. and Simões, M.G. 2016. Comments on paper by M. Arai ‘Aptian/Albian (Early Cretaceous) paleogeography of the South Atlantic: a paleontological perspective’. *Brazilian Journal of Geology*, **46**, 3–7, https://doi.org/10.1590/2317-4889201620150046A.

Baby, P., Rivadeneira, M., Christophoul, F. and Barragan, R. 1999. Style and timing of deformation in the Oriente Basin of Ecuador. 6.

Baby, P., Rivadeneira, M., Barragán, R. and Christophoul, F. 2013. Thick-skinned tectonics in the Oriente foreland basin of Ecuador. *Geological Society, London, Special Publications*, **377**, 59–76, https://doi.org/10.1144/SP377.1.

Bagni, F.L. 2010. Correlação Estratigráfica e Considerações Paleogeográficas da Transgressão Marinha Aptiana nas Bacias da Margem Equatorial Brasileira. 103.

Bahia, R.B.C., Martins-Neto, M.A., Barbosa, M.S.C. and Pedreira, A.J. 2007. Análise da evolução tectonossedimentar da Bacia dos Parecis através de métodos potenciais. *Revista Brasileira de Geociências*, **37**, 639–649, https://doi.org/10.25249/0375-7536.2007374639649.

Bajolet, F., Chardon, D., Rouby, D., Dall'Asta, M., Loparev, A., Couëffe, R. and Roig, J.-Y. 2022. The sediment routing systems of Northern South America since 250 Ma. *Earth-Science Reviews*, **232**, 104139, https://doi.org/10.1016/j.earscirev.2022.104139.

Barron, E.J. 1987. Cretaceous plate tectonic reconstructions. *Palaeogeography, Palaeoclimatology, Palaeoecology*, **59**, 3–29, https://doi.org/10.1016/0031-0182(87)90071-X.

Basile, C., Mascle, J. and Guiraud, R. 2005. Phanerozoic geological evolution of the Equatorial Atlantic domain. *Journal of African Earth Sciences*, **43**, 275–282, https://doi.org/10.1016/j.jafrearsci.2005.07.011.

Baudin, F. and Berthou, P.-Y. 1996. Envoronnements de dépôt de la matière organique des sediments Aptiens-Albiens du bassin d'Araripe (NE du Brèsil). *BCREDP*, **20**.

Bloom, D.D. and Lovejoy, N.R. 2011. The Biogeography of Marine Incursions in South America. *In*: Albert, J. (ed.) *Historical Biogeography of Neotropical Freshwater Fishes*. 137–144., https://doi.org/10.1525/california/9780520268685.003.0008.

Brandão, J.A.S.L. and Feijó, F.J. 1994. Bacia da Foz do Amazonas. *Boletim de Geociências Petrobras*, **8**, 91–99.

Catuneanu, O. 2004. Retroarc foreland systems—evolution through time. *Journal of African Earth Sciences*, **38**, 225–242, https://doi.org/10.1016/j.jafrearsci.2004.01.004.

Cawood, P.A., Hawkesworth, C.J. and Dhuime, B. 2012. Detrital zircon record and tectonic setting. *Geology*, **40**, 875–878, https://doi.org/10.1130/G32945.1.

Chaboureau, A.-C., Guillocheau, F., Robin, C., Rohais, S., Moulin, M. and Aslanian, D. 2013. Paleogeographic evolution of the central segment of the South Atlantic during Early Cretaceous times: Paleotopographic and geodynamic implications. *Tectonophysics*, **604**, 191–223, https://doi.org/10.1016/j.tecto.2012.08.025.

Chavez, C., Roddaz, M., Dantas, E.L., Santos, R.V. and Alván, A.A. 2022. Provenance of the Middle Jurassic-Cretaceous sedimentary rocks of the Arequipa Basin (South Peru) and implications for the geodynamic evolution of the Central Andes. *Gondwana Research*, **101**, 59–76, https://doi.org/10.1016/j.gr.2021.07.018.

Christophoul, F., Baby, P. and Dávila, C. 2002. Stratigraphic responses to a major tectonic event in a foreland basin: the Ecuadorian Oriente Basin from Eocene to Oligocene times. *Tectonophysics*, **345**, 281–298, https://doi.org/10.1016/S0040-1951(01)00217-7.

Coccioni, R., Erba, E. and Premoli-Silva, I. 1992. Barremian-Aptian calcareous plankton biostratigraphy from the Gorgo Cerbara section (Marche, central Italy) and implications for plankton evolution. *Cretaceous Research*, **13**, 517–537, https://doi.org/10.1016/0195-6671(92)90015-I.

Cordani, U.G., Milani, E.J., Thomaz-Filho, A. and Campos, D.A. 2000. *Tectonic Evolution of South America*.

Corfu, F., Hanchar, J.M., Hoskin, P.W.O. and Kinny, P. 2003. Atlas of Zircon Textures. *Reviews in Mineralogy and Geochemistry*, **53**, 469–500, https://doi.org/10.2113/0530469.

Cunha, P.R. da C. 2007. Bacia do Acre. *Boletim de Geociências Petrobras*, **15**, 207–215.

Custódio, M.A., Quaglio, F., Warren, L.V., Simões, M.G., Fürsich, F.T., Perinotto, J.A.J. and Assine, M.L. 2017. The transgressive-regressive cycle of the Romualdo Formation (Araripe Basin): Sedimentary archive of the Early Cretaceous marine ingression in the interior of Northeast Brazil. *Sedimentary Geology*, **359**, 1–15, https://doi.org/10.1016/j.sedgeo.2017.07.010.

Darros de Matos, R.M. 1999. History of the northeast Brazilian rift system: kinematic implications for the break-up between Brazil and West Africa. *Geological Society, London, Special Publications*, **153**, 55–73, https://doi.org/10.1144/GSL.SP.1999.153.01.04.

Dot, J.A.M., Baamonde, J.M., Reyes, D. and Whilchy, R. 2015. The Cogollo Group and the oceanic anoxic events 1a and 1b, Maracaibo basin, Venezuela. *Brazilian Journal of Geology*, **45**, 41–61, https://doi.org/10.1590/2317-4889201530192.

Eagles, G. and König, M. 2008. A model of plate kinematics in Gondwana breakup. *Geophysical Journal International*, **173**, 703–717, https://doi.org/10.1111/j.1365-246X.2008.03753.x.

Erlich, R.N., Fallon, J. and O'Sullivan, P. 2018. Stratigraphy and LA-ICP-MS Zircon U-PB Provenance of middle Permian to Maastrichtian Sandstones from Outcrop and Subsurface Control in the Sub-Andean Basins of Peru. *In*: *Petroleum Basins and Hydrocarbon Potential of the Andes of Peru and Bolivia*. 179–226., https://doi.org/10.1306/13622121M1173769.

Fellin, M.G., Zattin, M., et al. 2023. New detrital petrographic and thermochronologic constraints on the Late Cretaceous–Neogene erosional history of the equatorial margin of Brazil: Implications for the surface evolution of a complex rift margin. *Basin Research*, bre.12808, https://doi.org/10.1111/bre.12808.

Frakes, L.A. 1990. Paleogeography and Paleoclimatology. *In*: Ginsburg, R. N. and Beaudoin, B. (eds) *Cretaceous Resources, Events and Rhythms*. 197–202., https://doi.org/10.1007/978-94-015-6861-6_10.

Godot Souza, J.F., Isozaki, Y., et al. 2022. Provenance analysis of the Araripe intracontinental basin, northeast Brazil – Routes for proto-Atlantic marine incursions in northwest Gondwana. *Sedimentary Geology*, **440**, 106243, https://doi.org/10.1016/j.sedgeo.2022.106243.

Goldberg, K., Premaor, E, Barbola, T., Souza, P.A. 2019. Aptian marine ingression in the Araripe Basin: Implications for paleogeographic reconstruction and evaporite accumulation. *Marine and Petroleum Geology*, **107**, 217-221, https://doi.org/10.1016/j.marpetgeo.2019.05.011

Gomes, M.L., Hurtgen, M.T. and Sageman, B.B. 2016. Biogeochemical sulfur cycling during Cretaceous oceanic anoxic events: A comparison of OAE1a and OAE2. *Paleoceanography*, **31**, 233–251, https://doi.org/10.1002/2015PA002869.

Haag, N.A. 2019. *Palinostratigrafia Do Meso-Cenozoico Da Bacia Do Acre (Amazônia Sul Ocidental, Brasil)*. Tese de doutoramento, Universidade de Coimbra.

Haq, B.U., Hardenbol, J. and Vail, P.R. 1987. Chronology of Fluctuating Sea Levels Since the Triassic. *Science*, **235**, 1156–1167, https://doi.org/10.1126/science.235.4793.1156.

Heine, C., Zoethout, J. and Müller, R.D. 2013. Kinematics of the South Atlantic rift. *Solid Earth*, **4**, 215–253, https://doi.org/10.5194/se-4-215-2013.

Hermoza, W., Brusset, S., Baby, P., Gil, W., Roddaz, M., Guerrero, N. and Bolaños, R. 2005. The Huallaga foreland basin evolution: Thrust propagation in a deltaic environment, northern Peruvian Andes. *Journal of South American Earth Sciences*, **19**, 21–34, https://doi.org/10.1016/j.jsames.2004.06.005.

Hermoza, W., Baby, P., Espurt, N., Martinez, E. and Bolaños, R. 2006. The Ucayali Subandean Basin: A Complex Fold And Thrust Belt And Inverted System. *In*: *9th Simposio Bolivariano - Exploracion Petrolera En Las Cuencas Subandinas*, https://doi.org/10.3997/2214-4609-pdb.111.08.

Hill, R.I. 1991. Starting plumes and continental break-up. *Earth and Planetary Science Letters*, **104**, 398–416, https://doi.org/10.1016/0012-821X(91)90218-7.

Horbe, A.M.C., Roddaz, M., Gomes, L.B., Castro, R.T., Dantas, E.L. and do Carmo, D.A. 2019. Provenance of the Neogene sediments from the Solimões Formation (Solimões and Acre Basins), Brazil. *Journal of South American Earth Sciences*, **93**, 232–241, https://doi.org/10.1016/j.jsames.2019.05.004.

Howard, K.E., Hand, M., Barovich, K.M., Reid, A., Wade, B.P. and Belousova, E.A. 2009. Detrital zircon ages: Improving interpretation via Nd and Hf isotopic data. *Chemical Geology*, **262**, 277–292, https://doi.org/10.1016/j.chemgeo.2009.01.029.

Hurtado, C., Roddaz, M., Santos, R.V., Baby, P., Antoine, P.-O. and Dantas, E.L. 2018. Cretaceous-early Paleocene drainage shift of Amazonian rivers driven by Equatorial Atlantic Ocean opening and Andean uplift as deduced from the provenance of northern Peruvian sedimentary rocks (Huallaga basin). *Gondwana Research*, **63**, 152–168, https://doi.org/10.1016/j.gr.2018.05.012.

Jenkyns, H.C. 1980. Cretaceous anoxic events: from continents to oceans. *Journal of the Geological Society*, **137**, 171–188, https://doi.org/10.1144/gsjgs.137.2.0171.

Jenkyns, H.C. 2010. Geochemistry of oceanic anoxic events: REVIEW. *Geochemistry, Geophysics, Geosystems*, **11**, n/a-n/a, https://doi.org/10.1029/2009GC002788.

Koutsoukos, E.A.M., Leary, P.N. and Hart, M.B. 1990. Latest Cenomanian—earliest Turonian low-oxygen tolerant benthonic foraminifera: a case-study from the Sergipe basin (N.E. Brazil) and the western Anglo-Paris basin (southern England). *Palaeogeography, Palaeoclimatology, Palaeoecology*, **77**, 145–177, https://doi.org/10.1016/0031-0182(90)90130-Y.

Li, Y., He, D., Li, D., Lu, R., Fan, C., Sun, Y. and Huang, H. 2018. Sedimentary provenance constraints on the Jurassic to Cretaceous paleogeography of Sichuan Basin, SW China. *Gondwana Research*, **60**, 15–33, https://doi.org/10.1016/j.gr.2018.03.015.

Liu, X., Li, S., et al. 2018. Detrital zircon U-Pb geochronology and provenance of the Sanxiatian Formation (Huade Group) in the North China Craton: Implications for the breakup of the Columbia supercontinent. *Precambrian Research*, **310**, 305–319, https://doi.org/10.1016/j.precamres.2018.02.006.

Lopez-Gamundi, O. and Lopez-Gamundi, C. 2018. Exhumation of a Proximal Foredeep and Associated Wedge-Top Basin Evidenced by Porosity versus Depth Trends: The Upper Cretaceous Vivian Sandstones in Northwestern Marañón and Santiago Basins (Peru). *In*: *Petroleum Basins and Hydrocarbon Potential of the Andes of Peru and Bolivia*. 251–270., https://doi.org/10.1306/13622123M1173531.

Louterbach, M., Roddaz, M., et al. 2018. Provenance record of late Maastrichtian-late Palaeocene Andean Mountain building in the Amazonian retroarc foreland basin (Madre de Dios basin, Peru). *Terra Nova*, **30**, 17–23, https://doi.org/10.1111/ter.12303.

Macellari, C.E. 1988. Cretaceous paleogeography and depositional cycles of western South America. *Journal of South American Earth Sciences*, **1**, 373–418, https://doi.org/10.1016/0895-9811(88)90024-7.

Machado Junior, D. de L., Dehira, L.K., Carneiro, C.D.R. and Almeida, F.F.M. de. 1990. Reconstruções Paleoambientais do Juto-Cretáceo no Nordeste Oriental Brasileiro. *Revista Brasileira de Geociencias*, **19**, 470–485.

Maloney, K.T., Clarke, G.L., Klepeis, K.A. and Quevedo, L. 2013. The Late Jurassic to present evolution of the Andean margin: Drivers and the geological record. *Tectonics*, **32**, 1049–1065, https://doi.org/10.1002/tect.20067.

Markwick, P.J. 2019. Palaeogeography in exploration. *Geological Magazine*, **156**, 366–407, https://doi.org/10.1017/S0016756818000468.

Martinez, E., Fernandez, J., Calderon, Y. and Galdos, C. 1999. *Ucayali/Ene Basin, Peru, Hydrocarbon Evaluation*.

Marzoli, A., Melluso, L., et al. 1999. Geochronology and petrology of Cretaceous basaltic magmatism in the Kwanza basin (western Angola), and relationships with the ParanaÁ -Etendeka continental ¯ood basalt province. *Journal of Geodynamics*, 16.

Mello, M.R., Koutsoukos, E.A.M., Hart, M.B., Brassell, S.C. and Maxwell, J.R. 1989. Late cretaceous anoxic events in the Brazilian continental margin. *Organic Geochemistry*, **14**, 529–542, https://doi.org/10.1016/0146-6380(89)90033-8.

Milani, E.J. and Thomaz-Filho, A. 2000. Sedimentary Basins of South America. *In*: *Tectonic Evolution of South America*. 389–449.

Mohriak, W.U., Danforth, A., Post, P.J., Brown, D.E., Tari, G.C., Nemčok, M. and Sinha, S.T. 2013. Conjugate divergent margins: an introduction. *Geological Society, London, Special Publications*, **369**, 1–10, https://doi.org/10.1144/SP369.26.

Morton, A.C. and Hallsworth, C. 1994. Identifying provenance-specific features of detrital heavy mineral assemblages in sandstones. *Sedimentary Geology*, **90**, 241–256, https://doi.org/10.1016/0037-0738(94)90041-8.

Moulin, M. and Aslanian, D. 2010. Corrigendum to “A new starting point for the South and Equatorial Atlantic Ocean” [Earth Science Reviews 98 (2010), 1–37]. *Earth-Science Reviews*, **103**, 197–198, https://doi.org/10.1016/j.earscirev.2010.10.001.

Moulin, M., Aslanian, D., et al. 2005. Geological constraints on the evolution of the Angolan margin based on reflection and refraction seismic data (ZaïAngo project). *Geophysical Journal International*, **162**, 793–810, https://doi.org/10.1111/j.1365-246X.2005.02668.x.

Moulin, M., Aslanian, D. and Unternehr, P. 2010. A new starting point for the South and Equatorial Atlantic Ocean. *Earth-Science Reviews*, **98**, 1–37, https://doi.org/10.1016/j.earscirev.2009.08.001.

Mourlot, Y., Roddaz, M., et al. 2018. Geochemical Evidence for Large-Scale Drainage Reorganization in Northwest Africa During the Cretaceous. *Geochemistry,*

Geophysics, Geosystems, **19**, 1690–1712, https://doi.org/10.1029/2018GC007448.

Nie, J., Horton, B.K., et al. 2012. Integrated provenance analysis of a convergent retroarc foreland system: U–Pb ages, heavy minerals, Nd isotopes, and sandstone compositions of the Middle Magdalena Valley basin, northern Andes, Colombia. *Earth-Science Reviews*, **110**, 111–126, https://doi.org/10.1016/j.earscirev.2011.11.002.

Oliveira, C.M.M. 1994. *Estilos Estruturais e Evolução Tectônica Da Bacia Do Acre*. Dissertação de mestrado, Universidade Federal de Ouro Preto.

Petri, S. 1987. Cretaceous paleogeographic maps of Brazil. *Palaeogeography, Palaeoclimatology, Palaeoecology*, **59**, 117–168, https://doi.org/10.1016/0031-0182(87)90077-0.

Pohl, A., Laugié, M., et al. 2019. Quantifying the paleogeographic driver of Cretaceous carbonate platform development using paleoecological niche modeling. *Palaeogeography, Palaeoclimatology, Palaeoecology*, **514**, 222–232, https://doi.org/10.1016/j.palaeo.2018.10.017.

Potter, P.E. 1997. The Mesozoic and Cenozoic paleodrainage of South America: a natural history. *Journal of South American Earth Sciences*, **10**, 331–344, https://doi.org/10.1016/S0895-9811(97)00031-X.

Prado, L.A.C.D., Pereira, P.A., Sales, A.M.F. and Barreto, A.M.F. 2015. Taphonomic and paleoenvironmental considerations for the concentrations of macroinvertibrate fossils in the Romualdo Member, Santana Formation, Late Aptian – Early Albian, Araripe Basin, Araripina, NE, Brazil. *Journal of South American Earth Sciences*, **62**, 218–228, https://doi.org/10.1016/j.jsames.2015.06.005.

Ramos, V.A. and Folguera, A. 2009. Andean flat-slab subduction through time. *Geological Society, London, Special Publications*, **327**, 31–54, https://doi.org/10.1144/SP327.3.

Riccardi, A.C. 1987. Cretaceous paleogeography of southern South America. *Palaeogeography, Palaeoclimatology, Palaeoecology*, **59**, 169–195, https://doi.org/10.1016/0031-0182(87)90078-2.

Robinson, S.A., Heimhofer, U., Hesselbo, S.P. and Petrizzo, M.R. 2017. Mesozoic climates and oceans – a tribute to Hugh Jenkyns and Helmut Weissert. *Sedimentology*, **64**, 1–15, https://doi.org/10.1111/sed.12349.

Roddaz, M., Viers, J., Brusset, S., Baby, P. and Hérail, G. 2005. Sediment provenances and drainage evolution of the Neogene Amazonian foreland basin. *Earth and Planetary Science Letters*, **239**, 57–78, https://doi.org/10.1016/j.epsl.2005.08.007.

Roddaz, M., Dera, G., et al. 2021. Provenance constraints on the Cretaceous-Paleocene erosional history of the Guiana Shield as determined from the geochemistry of clay-size fraction of sediments from the Arapaima-1 well

(Guyana-Suriname basin). *Marine Geology*, **434**, 106433, https://doi.org/10.1016/j.margeo.2021.106433.

Rodrigues, M.G., Matos, S.A., Varejão, F.G., Fürsich, F.T., Warren, L.V., Assine, M.L. and Simões, M.G. 2020. Short-lived “Bakevelliid-Sea” in the Aptian Romualdo Formation, Araripe Basin, northeastern Brazil. *Cretaceous Research*, **115**, 104555, https://doi.org/10.1016/j.cretres.2020.104555.

Rodríguez Tribaldos, V., White, N.J., Roberts, G.G. and Hoggard, M.J. 2017. Spatial and temporal uplift history of South America from calibrated drainage analysis: SOUTH AMERICAN DRAINAGE. *Geochemistry, Geophysics, Geosystems*, **18**, 2321–2353, https://doi.org/10.1002/2017GC006909.

Rubert, R.R., Mizusaki, A.M.P., Martinelli, A.G. and Urban, C. 2017. Paleoenvironmental reconstruction and evolution of an Upper Cretaceous lacustrine-fluvial-deltaic sequence in the Parecis Basin, Brazil. *Journal of South American Earth Sciences*, **80**, 512–528, https://doi.org/10.1016/j.jsames.2017.10.013.

Ruiz, G.M.H., Seward, D. and Winkler, W. 2007. Chapter 36 Evolution of the Amazon Basin in Ecuador with Special Reference to Hinterland Tectonics: Data from Zircon Fission-Track and Heavy Mineral Analysis. *In*: *Developments in Sedimentology*. 907–934., https://doi.org/10.1016/S0070-4571(07)58036-2.

Sahabi, M., Aslanian, D. and Olivet, J.-L. 2004. Un nouveau point de départ pour l’histoire de l’Atlantique central. *Comptes Rendus Geoscience*, **336**, 1041–1052, https://doi.org/10.1016/j.crte.2004.03.017.

Sanchez F., A., Chira F., J. and Valencia M., M. 1997. *Geología de Los Cuadrángulos de Tarapoto, Papa Playa, Utcurarca y Yanayacu: Hojas 13-k, 13-l, 14-k, 14-l.* **94**.

Schellart, W.P. 2017. Andean mountain building and magmatic arc migration driven by subduction-induced whole mantle flow. *Nature Communications*, **8**, 2010, https://doi.org/10.1038/s41467-017-01847-z.

Schlanger, S.O. and Jenkyns, H.C. 1976. Cretaceous Oceanic Anovic Events: Causes and Consequences. *Geologie en Mijnbouw*, **55**, 179–184.

Schobbenhaus, C. and Brito Neves, B.B. 2003. A Geologia do Brasil no Contexto da Plataforma Sul-Americana. *In*: *Geologia, Tectônica e Recursos Minerais Do Brasil*.

Scotese, C.R. 1991. Jurassic and cretaceous plate tectonic reconstructions. *Palaeogeography, Palaeoclimatology, Palaeoecology*, **87**, 493–501, https://doi.org/10.1016/0031-0182(91)90145-H.

Scotese, C.R. 2014. Atlas of Late Cretaceous Maps, PALEOMAP Atlas for ArcGIS, volume 2, The Cretaceous, Maps 16 – 22, Mollweide Projection, PALEOMAP Project, Evanston, IL., https://doi.org/10.13140/2.1.4691.3284.

Scotese, C.R., Gahagan, L.M. and Larson, R.L. 1988. Plate tectonic reconstructions of the Cretaceous and Cenozoic ocean basins. *Tectonophysics*, **155**, 27–48, https://doi.org/10.1016/0040-1951(88)90259-4.

Simoes, M., Braun, J. and Bonnet, S. 2010. Continental-scale erosion and transport laws: A new approach to quantitatively investigate macroscale landscapes and associated sediment fluxes over the geological past. *Geochemistry Geophysics Geosystems*, **11**, Q09001, https://doi.org/10.1029/2010GC003121.

Stewart, K., Turner, S., Hawkesworth, C.J., Kirstein, L. and Mantovani, M. 1996. 40Ar-39Ar geochronology in the Paraná continental flood basalt province. *Earth and Planetary Science Letters*, **143**, 95–109.

Takashima, R., Coccioni, R., Nishi, H. and Hayashi, K. 2007. Mid-Cretaceous Oceanic Anoxic Events recorded in SE France and central Italy. 3.

Tang, M., Ren, Q., et al. 2022. Digital paleogeographic reconstruction of the eastern Tethyan tectonic domain from the Middle Permian to the Middle Triassic. *Geosystems and Geoenvironment*, 100127, https://doi.org/10.1016/j.geogeo.2022.100127.

Tedeschi, L.R., Jenkyns, H.C., Robinson, S.A., Sanjinés, A.E.S., Viviers, M.C., Quintaes, C.M.S.P. and Vazquez, J.C. 2017. New age constraints on Aptian evaporites and carbonates from the South Atlantic: Implications for Oceanic Anoxic Event 1a. *Geology*, **45**, 543–546, https://doi.org/10.1130/G38886.1.

van Soelen, E.E., Kim, J.-H., et al. 2017a. A 30 Ma history of the Amazon River inferred from terrigenous sediments and organic matter on the Ceará Rise. *Earth and Planetary Science Letters*, **474**, 40–48, https://doi.org/10.1016/j.epsl.2017.06.025.

van Soelen, E.E., Kim, J.-H., et al. 2017b. A 30 Ma history of the Amazon River inferred from terrigenous sediments and organic matter on the Ceará Rise. *Earth and Planetary Science Letters*, **474**, 40–48, https://doi.org/10.1016/j.epsl.2017.06.025.

Wang, L., Liu, C., Gao, X. and Zhang, H. 2014. Provenance and paleogeography of the Late Cretaceous Mengyejing Formation, Simao Basin, southeastern Tibetan Plateau: Whole-rock geochemistry, U–Pb geochronology, and Hf isotopic constraints. *Sedimentary Geology*, **304**, 44–58, https://doi.org/10.1016/j.sedgeo.2014.02.003.

Weissert, H. 2000. Deciphering methane's fingerprint. *Nature*, **406**, 356–357.

Weltje, G.J. and von Eynatten, H. 2004. Quantitative provenance analysis of sediments: review and outlook. *Sedimentary Geology*, **171**, 1–11, https://doi.org/10.1016/j.sedgeo.2004.05.007.

Wine, G., Vetrici, D. and Arcuri, J. 2001. *The Huallaga Basin and Adjacent Area*. Proyecto de Asistencia para La Reglamentación del Sector Energético del Perú.

Zamora, G. and Gil, W. 2018. The Marañón Basin: Tectonic Evolution and Paleogeography. *In*: *Petroleum Basins and Hydrocarbon Potential of the Andes of Peru and Bolivia*. 121–144., https://doi.org/10.1306/13622119M1173768.

Zhu, X., Shen, C., Zhou, R., Xu, J., Zhao, J., Wang, L. and Ge, X. 2020. Paleogene sediment provenance and paleogeographic reconstruction of the South Yellow Sea Basin, East China: Constraints from detrital zircon U Pb geochronology and heavy mineral assemblages. *Palaeogeography, Palaeoclimatology, Palaeoecology*, **553**, 109776, https://doi.org/10.1016/j.palaeo.2020.109776.

Ziegler, A.M., Rowley, D.B., Lottes, A.L., Sahagian, D.L., Hulver, M.L. and Gierlowski, T.C. 1985. Paleogeographic Interpretation: With an Example From the Mid-Cretaceous. *Annual Review of Earth and Planetary Sciences*, **13**, 385–428, https://doi.org/10.1146/annurev.ea.13.050185.002125.

CAPÍTULO 2

MATERIAIS E MÉTODOS

MATERIEL ET METHODES

2 MATERIAIS E MÉTODOS / MATÉRIEL ET MÉTHODES

Ce chapitre présente le matériel et la méthodologie d'analyse utilisés au cours de cette thèse. J'ai choisi de ne pas présenter de résumé en français de chaque méthode utilisée car ces résumés se trouvent en anglais dans les chapitres 3 et 4 (article en cours de soumission à Tectonics et article publié à Sedimentary Geology)

Dentro da pesquisa, este projeto consta com abordagens metodológicas diferentes e complementares:

2.1 Pesquisa bibliográfica e trabalhos de campo

Realizou-se uma revisão detalhada sobre as bacias alvo de estudo (Bacias Andinas e Acre e Bacia do Araripe), além de estudos sobre proveniência de sedimentos siliciclásticos. Uma análise detalhada do contexto geológico, geotectônico e paleoclimático do Cretáceo a nível mundial e regional mostrou-se relevante para a delimitação da problemática a ser analisada e discutida. Nesta perspectiva, foram levantados trabalhos acadêmicos diversos, como artigos científicos, dissertações, teses, relatórios técnicos, mapas e resumos de eventos científicos em anais.

O trabalho de campo contou com três fases, realizadas em setembro de 2018 por um grupo de pesquisadores da UnB na Bacia do Acre (Figura 10 e Figura 11); agosto de 2019 cujo foco foi a coleta de amostras da Bacia de Madre de Dios, na zona Sub Andina do Peru (Figura 12,Figura 13, Figura 14 eFigura 15) e em outubro de 2020, o qual teve como objetivo o reconhecimento e amostragem das variadas formações constituintes da Bacia do Araripe (Figura 16,Figura 17 eFigura 18). Fez-se reconhecimento *in loco* do objeto de estudo, identificou-se os litotipos da área e procedeu-se a coleta das amostras para análises em laboratório.

Figura 10: Detalhe do afloramento onde foi coletada a amostra ACRE 29.

Figura 11: Afloramentos ao longo do rio Moa – Acre - Brasil. A esquerda: coleta da amostra ACRE 33. A direita: coleta da amostra ACRE 17

Figura 12: Equipe de campo na região de Mazuko – Madre de Dios – Peru.

Figura 13: Vista panorâmica do afloramento da Formação Chonta, zona subandina peruana.

Figura 14: Afloramento Formação Chonta, zona subandina – Peru. Coleta da Amostra MD 2019 03.

Figura 15: Processo de concentração de amostras para transporte. Zona Subandina, Peru.

Figura 16: Equipe de campo, Araripe – Brasil.

Figura 17: Vista panorâmica do afloramento, no qual encontra-se o contato entre a Formação Araripina e Exu, Bacia do Araripe – Brasil.

Figura 18: Vista panorâmica do afloramento Mãozinha, Bacia do Araripe, Brasil.

2.2 Preparação de amostras

O tratamento das amostras aconteceu no setor de preparação de amostras do Laboratório de Estudos Geodinâmicos e Geocronológicos e Ambientais do Instituto de Geociências da Universidade de Brasília (LEGGA-IG-UnB). Para análises isotópicas de Sm e Nd as amostras foram britadas e pulverizadas à uma granulometria maior que 250 *mesh* em moinho de panela de tungstênio e armazenadas em tubos plásticos.

Para as análises U-Pb em zircão detrítico no LA-ICP-MS, as amostras foram britadas e pulverizadas a fim de desagregar as partículas. Após este procedimento foram peneiradas seguindo a metodologia utilizada por Morton (in Zuffa, 1985) e levadas para separação gravimétrica por meio de bateia manual. Os componentes magnéticos foram separados usando imã de mão e separador magnético do tipo Frantz, utilizando corrente de 1.0 e 1.6 Å (Figura 19).

Figura 19: A esquerda: Moinho de disco; A direita: Separador magnético isodinâmico Frantz, tipo barreira magnética. Retirado de www.legga.unb.br

Após a concentração mineral, os grãos de zircão foram selecionados aleatoriamente e montados em resina epoxy com *mounts* de aproximadamente 150 cristais por amostra na fração areia. Os *mounts* foram desgastados e polidos a 1 µm, para exposição do seu interior e passaram por imageamento. As amostras das bacias de Madre de Dios de do Acre foram imageadas com Microscópio Eletrônico de Varredura (MEV) FEI Quanta^{TM} 450 gerando imagens de contraste com detector de elétrons retroespalhados (BSE), a 10 nA 20kV e distância de operação de 13.8 mm no Laboratório de Estudos Geodinâmicos e Geocronológicos e Ambientais do Instituto de Geociências da Universidade de Brasília (LEGGA-IG-UnB) (Figura 20). As amostras provenientes da bacia do Araripe foram imageadas com MEV Tescan Veja 4 equipado com um sistema EDS Bruker de 30 mm^2 a 10kV com corrente de 3 10nA no Laboratório de Géosciences Environnement Toulouse (GET) (Figura 21).

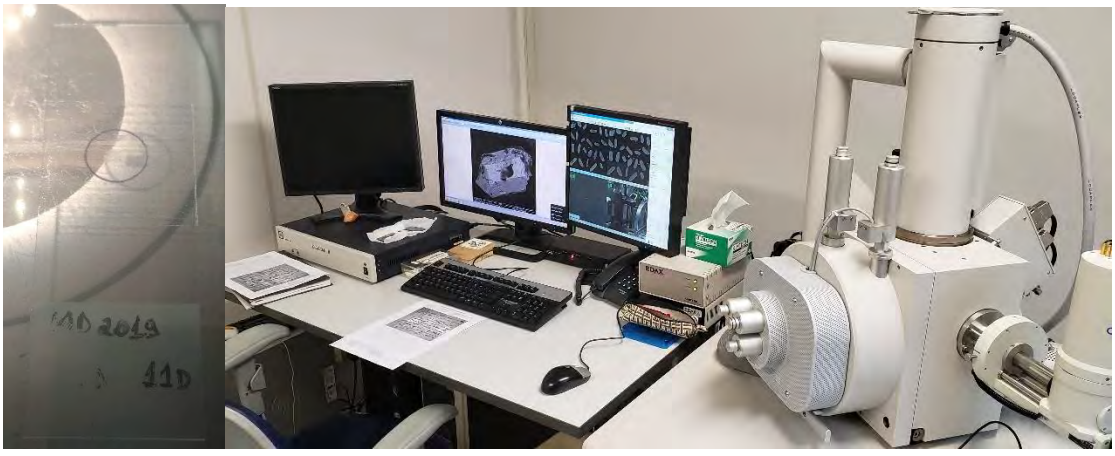

Figura 20: Montagem de mount (esquerda); MEV FEI Quanta^{TM} 450 do LEGGA-IG-UnB (Retirado de de www.legga.unb.br)

Figura 21: MEV Tescan Veja 4 LMU localizado no GET – Toulouse (Retirado de www.get.omp.eu) e imagem panorâmica da amostra M2AR 1-3.

2.3 Análises laboratoriais

2.3.1 Geoquímica dos elementos maiores, traços e terras raras

As análises químicas foram feitas no Service d'Analyse des Roches et Mineraux (SARM, INSU facility, Vandoeuvre-Les-Nancy, France). Os elementos maiores, traços e terras raras foram medidos por ICP-OES (Na, Mg, K, Ca, Sc, Ti, Mn, Fe, Al, Si e P) e ICP-MS (Rb, Cs, Ba, Sr, Th, U, Y, Zr, Nb, Hf, Cr, V, Co, Cu, Ni, Zn, La, Ce, Pr, Nd, Sm, Eu, Gd, Tb, Dy, Ho, Er, Tm, Yb, Lu e Ta) após fusão alcalina. Os detalhes analíticos estão disponíveis em http://helium.crpg.cnrs-nancy.fr/SARM/ e em (Carignan *et al.* 2001). As incertezas são menores que 5% para elemento medidos por ICP-OES e menores que 10% para elementos medidos por ICP-MS (Tab. 2.1).

Tabela 2:Tabela de incertezas para os elementos medidos em ICP-MS.

	ICP-MS iCapQ e ICP-OES iCap6500 (Sc somente)							
	Incertezas em termos de conteúdos							
	>100µg/g	**>50 µg/g**	**>10 µg/g**	**>1 µg/g**	**>0.5 µg/g**	**>0.1 µg/g**	**>0.01 µg/g**	**D.L. µg/g**
As		<5%	<15%	<20%		**		0.50
Ba		<5%	<15%	**				5.5
Be		<5%	<15%			<20%	**	0.05
Bi			<5%	<10%		<20%	**	0.045
Cd		<10%	<15%			<20%	**	0.02
Co		<5%	<10%	<20%		**		0.08
Cr			<5%	<10%		**		0.50
Cs			<5%	<15%		<20%	**	0.02

Cu		<8%	<20%	**				2.0
Ga			<5%	<10%		<20%	**	0.02
Ge		<5%		<10%		<20%	**	0.04
Hf			<5%	<10%		<15%	**	0.03
In		<5%		<15%		<20%	**	0.03
Mo		<5%	<15%	<20%		**		0.50
Nb		<5%		<10%		<20%	**	0.015
Ni			<5%	**				2.0
Pb		<10%		<20%		**		0.45
Rb		<5%	<15%	<20%		**		0.15
Sb			<5%	<10%		<20%	**	0.06
Sc	<5%	<10%		<15%	**			0.6
Sn		<5%	<15%	<20%		**		0.30
Sr		<5%	<10%	<20%		**		0.70
Ta		<5%		<10%		<20%	**	0.004
Th		<5%		<10%		<20%	**	0.015
U		<5%	<10%	<15%		<20%	**	0.01
V		<5%	<10%	<15%		**		0.85
W		<5%	<10%	<20%		**		0.80
Y		<5%		<15%		<20%	**	0.02
Zn		<10%	<20%	**				7.0
Zr		<5%	<15%	**				1.50
La			<5%	<15%		<20%	**	0.02
Ce		<5%	<10%	<15%		<20%	**	0.03
Pr		<5%	<10%			<20%	**	0.004
Nd		<5%	<15%			<20%	**	0.016
Sm			<5%	<15%		<20%	**	0.005
Eu				<5%		<10%	**	0.002
Gd			<5%	<10%		<20%	**	0.005
Tb		<5%	<10%	<15%		<20%	**	0.001
Dy			<5%	<10%		<15%	**	0.004
Ho		<5%		<10%		<20%	**	0.001
Er				<5%		<10%	**	0.002
Tm		<5%		<10%		<20%	**	0.001
Yb		<5%	<10%	<15%		<20%	**	0.002
Lu			<5%	<10%		<20%	**	0.001

	ICP-OES iCap6500							
	Incertezas em termos de conteúdos							
	>10 %	**>5 %**	**>1 %**	**>0.5 %**	**>0.1 %**	**>0.05 %**	**>0.01 %**	**D.L. %**
SiO2	<2%			<10%	<20%	**		0.05
Al2O3	<2%	<10%	<15%		<20%	**		0.04
Fe2O3	<2%		<10%	<15%		<20%	**	0.015
MnO			<5%	<15%		<20%	**	0.015
MgO		<2%	<10%	<15%		<20%	**	0.03
CaO	<2%	<5%		<15%		<25%	**	0.03
Na2O		<5%	<10%	<15%		<25%	**	0.02
K2O		<5%	<10%	<20%		<25%	**	0.03
TiO2		<5%	<10%	<20%		<25%	**	0.02
P2O5			<5%	<15%	**			0.10

**A incerteza da medida é calculada para 200mg da amostra preparada.
D.L.: Limite de detecção.

Fizemos análises de elementos traços em zircão nas amostras da Bacia do Araripe com as mesmas condições analíticas explicadas na seção 2.3.3. Utilizou-se o padrão Nist SEM 610 (Jochum *et al*., 2011). O Si (conteúdo estequiométrico 15.38% em zircão) foi empregado como um padrão interno para a determinação da concentração dos elementos traços nos grãos de zircão.

2.3.2 Composição isotópica de Sm-Nd

As razões isotópicas dos elementos foram medidas por meio de espectrômetro de massa por ionização termal (ID-TIMS) seguindo a metodologia descrita por Goia and Pimentel (2000). Primeiramente as amostras foram pesadas em balanças de precisão contendo 100 g. Em seguida, foi feita a digestão ácida em estufa (HF:HNO_3 aproximadamente 8:1) em cápsulas *Savillex* por aproximadamente dois dias. Depois da primeira digestão, a solução foi evaporada e novamente atacada com os mesmos ácidos por cerca de quatro dias. Após nova evaporação, o resíduo foi solubilizado em HCl 2.5 N. A concentração dos isótopos de Sm e Nd para análise foi feita em 2 etapas, na coluna primária separou-se e concentrou-se os elementos terras raras (REE) e na coluna secundária concentrou-se em frações distintas, os elementos Sm e Nd. A extração dos elementos lantanídeos é realizada por meio de colunas de troca iônica confeccionadas em quartzo, usando resina BIO-RAD AG-50W-X8. A retirada de Sm e Nd foi feita em colunas de Teflon empacotadas com resina eichcrom LN-Spec.

As frações de Sm e Nd foram depositadas em arranjos duplos de filamentos de Re e analisadas na forma metálica, em modo estático, utilizando o espectrômetro de massa termal (TIMS) multicoletor da marca *Thermo Scientific*, modelo *Triton Plus*. Os dados foram normalizados e a acurácia e precisão foi determinada com repetidas análises do padrão BHVO-2. Durante as análises de Nd foram efetuadas normalizações utilizando as razões naturais de $^{146}Nd/^{144}Nd$ (0,7219). As incertezas

para as razões $^{147}Sm/^{144}Nd$ e $^{143}Nd/^{144}Nd$ foram menores do que ± 0.1% (2σ) e ± 0.000006% (2σ) (6 ppm), respectivamente (Weis et al., 2005). Foi utilizada a constante de decaimento (λ) 6.54 x 10^{-12} (DePaolo 1981a). Os brancos de Nd foram <100pg e os valores de T_{DM} foram calculados utilizando o modelo do manto empobrecido proposto por DePaolo (1981).

As razões $^{143}Nd/^{144}Nd_{sample}$ e $^{147}Sm/^{144}Nd_{samples}$ foram expressas em épsilon e refletem o desvio de fracionamento em partes de $^{147}Sm/^{144}Nd$ do *Chondrict Uniform Reservior* (CHUR), definida por

$$\varepsilon Nd\ (t) = [(^{143}Nd/^{144}Nd)_{sample}\ (t) / (^{143}Nd / {}^{144}Nd)_{CHUR}\ (t) -1] \times 10^4$$

cujo t indica o tempo em que εNd é calculado. Aqui, nenhuma correção de tempo foi aplicada (t=0), e o $^{143}Nd / {}^{144}Nd_{CHUR}\ (0) = 0.512638$ (Jacobsen and Wasserburg 1980).

As idades TDM e TDM* foram calculadas seguindo (DePaolo 1981b; DePaolo *et al.* 1991; Augustsson and Bahlburg 2008).

$$T_{DM} = \ln [(^{143}Nd/^{144}Nd_{\ sample,\ today} - {}^{143}Nd/^{144}Nd)_{\ DM,\ today}) / (^{147}Sm/^{144}Nd_{sample,\ today} - {}^{147}Sm/^{144}Nd_{DM,\ today}) + 1] / \lambda;$$

$$T_{DM^*} = \ln [(^{143}Nd/^{144}Nd_{\ sample,Ts} - {}^{143}Nd/^{144}Nd)_{DM,\ Ts}) / (^{147}Sm/^{144}Nd_{crust,\ Ts} - {}^{147}Sm/^{144}Nd_{DM,\ Ts}) + 1] / \lambda + Ts;$$

onde Ts é estimado pela idade estratigráfica. O $^{147}Sm/^{144}Nd_{crust}$ foi calculado assumindo que o $^{147}Sm/^{144}Nd_{crust,\ today} = 0.11$ (Albarède and Brouxel 1987). O modelo de (Goldstein *et al.* 1984) foi usado, cujo λ (^{147}Sm) = 6.54 x $10^{-12}a^{-1}$, $^{143}Nd/^{144}Nd_{DM,\ today}$ = 0.51315, $^{147}Sm/^{144}Nd_{DM,\ today} = 0.217$, $^{143}Nd / {}^{144}Nd)_{CHUR} = 0.512638$, e $^{147}Sm/^{144}Nd_{CHUR,\ today} = 0.1967$.

2.3.3 Datação U-Pb em zircão detritico

A análise isotópica de U-Pb em grãos de zircão detríticos das bacias de Madre de Dios e do Acre foram realizadas no LEGGA-IG-UnB (Tab. 2.2).

Tabela 3 Relação de amostras das bacias de Madre de Dios (MD) e Acre realizadas no laboratório LEGGA-IG-UnB e os equipamentos utilizados.

Amostra	Denominação do laboratório	Metodologia
MD234	LAB 2083 LAB 3684	LA-ICP-MS Netune
MD-2019-4A	LABXR0019	ElementRX-ICPMS
MD-2019-12A	LABXT002	LA-ICP-MS Netune
MD-2019-11D	LABXT003	LA-ICP-MS Netune
MD-2019-10	LABXT 001 LABXTXR 001-1	LA-ICP-MS Netune ElementRX-ICPMS
MD-2019-13	LABXT_0005	LA-ICP-MS Netune
MD238	LAB 1662	LA-ICP-MS Netune
MD239	*	LA-ICP-MS Netune
MD176	*	LA-ICP-MS Netune
ACRE 49	LAB3841Final	LA-ICP-MS Netune
ACRE 39	LAB4018	LA-ICP-MS Netune
ACRE 33	LAB4013 LABXR4014	LA-ICP-MS Netune ElementRX-ICPMS
ACRE 29	LAB4015	LA-ICP-MS Netune
ACRE 27A	LAB4014 LABXR4013	LA-ICP-MS Netune ElementRX-ICPMS
ACRE 27B	LABXR021_I_II	ElementRX-ICPMS
ACRE 15	LABXR-4012 LAB-4012	ElementRX-ICPMS LA-ICP-MS Netune

* Publicado em Louterbach et al. 2018

As amostras analisadas no espectrômetro de massa *Thermo-Fisher,* modelo *Neptune,* do tipo MC-ICP-MS acoplado a um sistema de ablação a laser (LA) *ESI/New Wave Research*, modelo UP-213 tipo Nd:YAG seguiram a ablação com *spot* individual de 25 µm ajustado a uma fluência de 3.0 – 3.5 J cm^2, frequência de 10Hz e duração de 40 s. O branco foi determinado por 20 s antes de cada ablação. As massas 206, 232 e 238 foram medidas em detectores do tipo *Faraday* as massas 202, 204, 207 e

208 em detectores do tipo MIC. O espectrômetro de massa *Thermo Finnigan Element* XT acoplado a um sistema de ablação a laser Iridia Excimer (ArF) de 193 nm, foi ajustado para melhorar a sensibilidade, minimizando a produção de óxido antes de cada sessão analítica. Cada massa (202, 204, 206-208, 232, 238) foi medida usando um modo de tripla detecção (SEM + Faraday) por varredura eletrostática. Cada varredura consistiu de 82 ms, resultando em mais de 800 scans por ablação. As condições do laser incluíram: diâmetro do spot de 25 µm, frequência de 20 Hz, e fluência de 2.0 J cm^{-2}. Cada análise incorporou uma aquisição de fundo com duração de 10 - 20s, seguida de 20 - 40s aquisições de dados de cada amostra. A acurácia e precisão foi estimada pela análise do zircão 91500 (Wiedenbeck *et al.* 1995), tratado como desconhecido. A estimativa das incertezas levou em consideração o excesso de variância do material de referência primário (GJ1) e a reprodutibilidade de longo prazo do material secundário (91500).

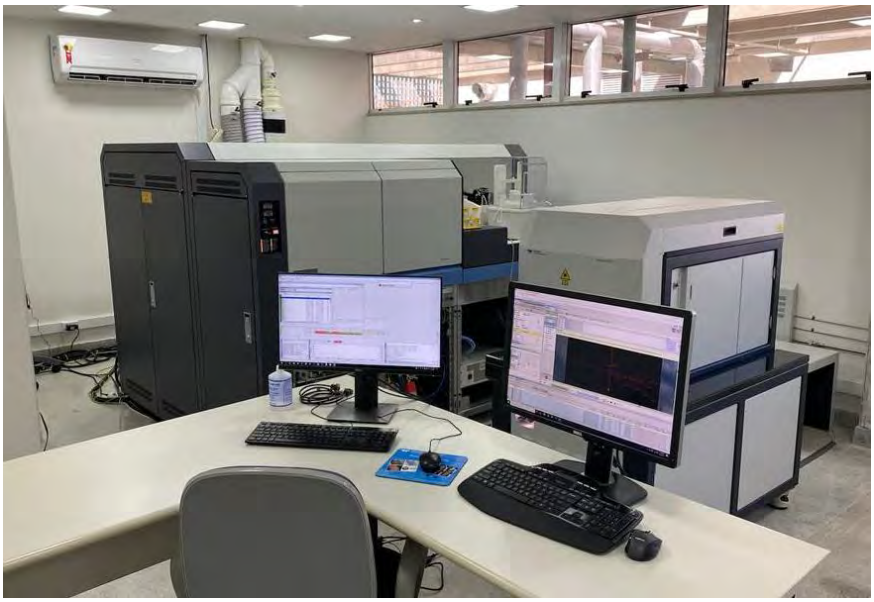

Figura 22: Neptune XT™ MC-ICP-MS localizado no LEGGA-UnB - Brasília (Retirado de www.legga.unb.br)

Todas as amostras da Bacia do Araripe foram analisadas no laboratório de ICPMS do GET com o espectrômetro de massa *ThermoScientific Element* HR-ICPMS acoplado com um laser emtosecond (ESI – New Wave NWRfemto) (Figura 23). Antes

de cada seção analítica o ICP-MS foi ajustado pela ablação de um material de referência (NIST SRM 610, (Jochum *et al.* 2011), para garantir níveis aceitáveis de sensibilidade, estabilidade, óxido e fracionamento (U/Th). As condições analíticas foram: tamanho do spot de 30 µm, frequência de 8 Hz, e fluência de ~ 2J/cm^2. O grão GJ-1 (Jackson *et al.* 2004a) foi usado como padrão primário. A acurácia e reprodutibilidade das análises foram checadas repetidas vezes com os seguintes materiais de referência: (91500, (Wiedenbeck *et al.* 2004); Plesovice, (Sláma *et al.* 2008); AUS-7, (Kennedy *et al.* 2014); Maniitsoq, (Marsh *et al.* 2019).

Figura 23: ThermoScientific Element HR-ICPMS localizado no GET – Toulouse.

Os dados brutos foram tratados *off-line* e corrigidos para branco, discriminação de massas e fracionamento induzido pelo laser (LIEF) utilizando o software *Iolite* v.4.0 (Paton *et al.* 2011) e *VizualAge* (Petrus and Kamber 2012) usando modelagem exponencial para correção LIEF e pela normalização ao zircão GJ-1 (Jackson *et al.* 2004b; Horstwood *et al.* 2016). As incertezas nas razões e idades são expressas em 2 sigma. Diagramas concórdia e histogramas de densidade (KDE) e foram calculados utilizando o *software Isoplot* 4.15 (Ludwig 2012).

As razões $^{206}Pb/^{238}U$ foram utilizadas para idade efetiva dos grãos de zircões de <1,5 Ga enquanto as razões $^{207}Pb/^{206}Pb$ foram usadas para grãos com idades >1,5 Ga (Spencer *et al.* 2016). Grãos com discordância >10% não foram considerados por causa de sua baixa representação estatística (Vermeesch 2004). As idades U-Pb em grãos de zircão foram representadas por meio de diagramas de estimação de densidade (KDE) (Vermeesch 2013) e para investigar a diferença entre as elas foi implementada a técnica estatística de escalonamento multidimensional (MDS) sem matriz métrica (Vermeesch 2013). O MDS é um superconjunto de componentes que por meio de uma tabela de diferenças entres as amostras gera um “mapa” de pontos, no qual as amostras semelhantes se agrupam e aquelas não semelhantes ficam afastadas (Vermeesch 2018). Seguimos as recomendações propostas por Vermeesch (2018) e utilizamos o teste Kolmogorov–Smirnov para produzir os mapas MDS de comparação entre as amostras.

REFERÊNCIAS

Albarède, F. and Brouxel, M. 1987. The Sm/Nd secular evolution of the continental crust and the depleted mantle. *Earth and Planetary Science Letters*, **82**, 25–35, https://doi.org/10.1016/0012-821X(87)90104-X.

Augustsson, C. and Bahlburg, H. 2008. Provenance of late Palaeozoic metasediments of the Patagonian proto-Pacific margin (southernmost Chile and Argentina). *International Journal of Earth Sciences*, **97**, 71–88, https://doi.org/10.1007/s00531-006-0158-7.

Bühn, B., Pimentel, M.M., Matteini, M. and Dantas, E.L. 2009. High spatial resolution analysis of Pb and U isotopes for geochronology by laser ablation multi-collector inductively coupled plasma mass spectrometry (LA-MC-ICP-MS). *Anais da Academia Brasileira de Ciências*, **81**, 99–114, https://doi.org/10.1590/S0001-37652009000100011.

Carignan, J., Hild, P., Mevelle, G., Morel, J. and Yeghicheyan, D. 2001. Routine Analyses of Trace Elements in Geological Samples using Flow Injection and Low Pressure On-Line Liquid Chromatography Coupled to ICP-MS: A Study of Geochemical Reference Materials BR, DR-N, UB-N, AN-G and GH. *Geostandards and Geoanalytical Research*, **25**, 187–198, https://doi.org/10.1111/j.1751-908X.2001.tb00595.x.

DePaolo, D.J. 1981a. Trace element and isotopic effects of combined wallrock assimilation and fractional crystallization. *Earth and Planetary Science Letters*, **53**, 189–202, https://doi.org/10.1016/0012-821X(81)90153-9.

DePaolo, D.J., Linn, A.M. and Schubert, G. 1991. The continental crustal age distribution: Methods of determining mantle separation ages from Sm-Nd isotopic data and application to the southwestern United States. *Journal of Geophysical Research*, **96**, 2071, https://doi.org/10.1029/90JB02219.

Goia, S.M.C.L. and Pimentel, M.M. 2000. The Sm-Nd isotopic method in the geochronology laboratory of the University of Brasília. *Anais da Academia Brasileira de Ciências*, **72**, 219–245, https://doi.org/10.1590/S0001-37652000000200009.

Goldstein, S.L., O'Nions, R.K. and Hamilton, P.J. 1984. A Sm-Nd isotopic study of atmospheric dusts and particulates from major river systems. *Earth and Planetary Science Letters*, **70**, 221–236, https://doi.org/10.1016/0012-821X(84)90007-4.

Horstwood, M.S.A., Kosler, J., et al. 2016. Community-Derived Standards for LA-ICP-MS U-(Th-)Pb Geochronology - Uncertaintu Propagation, Age Interpretation and Data Reporting. *Geostandards and Geoanalytical Research*, **40**, 311–332.

Jackson, S.E., Pearson, N.J., Griffin, W.L. and Belousova, E.A. 2004a. The application of laser ablation-inductively coupled plasma-mass spectrometry to in situ U–Pb zircon geochronology. *Chemical Geology*, **211**, 47–69, https://doi.org/10.1016/j.chemgeo.2004.06.017.

Jackson, S.E., Pearson, N.J., Griffin, W.L. and Belousova, E.A. 2004b. The application of laser ablation-inductively coupled plasma-mass spectrometry to in situ U–Pb

zircon geochronology. *Chemical Geology*, **211**, 47–69, https://doi.org/10.1016/j.chemgeo.2004.06.017.

Jacobsen, S.B. and Wasserburg, G.J. 1980. Sm-Nd isotopic evolution of chondrites. *Earth and Planetary Science Letters*, **50**, 139–155, https://doi.org/10.1016/0012-821X(80)90125-9.

Jochum, K.P., Weis, U., et al. 2011. Determination of Reference Values for NIST SRM 610-617 Glasses Following ISO Guidelines. *Geostandards and Geoanalytical Research*, **35**, 397–429, https://doi.org/10.1111/j.1751-908X.2011.00120.x.

Kennedy, A.K., Wotzlaw, J.-F., Schaltegger, U., Crowley, J.L. and Schmitz, M. 2014. EOCENE ZIRCON REFERENCE MATERIAL FOR MICROANALYSIS OF U-Th-Pb ISOTOPES AND TRACE ELEMENTS. *The Canadian Mineralogist*, **52**, 409–421, https://doi.org/10.3749/canmin.52.3.409.

Ludwig, K.R. 2012. *Isoplot 3.75 A Geochronological Toolkit for Microsoft Excel*. User's Manual.

Marsh, J.H., Jørgensen, T.R.C., Petrus, J.A., Hamilton, M.A. and Mole, D.R. 2019. U-Pb, trace element, and hafnium isotope composition of the Maniitsoq zircon: A potential new Archean zircon reference material. *In*: *Abstracts* – Goldschmidt.

Paton, C., Hellstrom, J., Paul, B., Woodhead, J. and Hergt, J. 2011. Iolite: Freeware for the visualisation and processing of mass spectrometric data. *Journal of Analytical Atomic Spectrometry*, **26**, 2508, https://doi.org/10.1039/c1ja10172b.

Petrus, J.A. and Kamber, B.S. 2012. VizualAge: A Novel Approach to Laser Ablation ICP-MS U-Pb Geochronology Data Reduction. *Geostandards and Geoanalytical Research*, **36**, 247–270.

Sláma, J., Košler, J., et al. 2008. Plešovice zircon — A new natural reference material for U–Pb and Hf isotopic microanalysis. *Chemical Geology*, **249**, 1–35, https://doi.org/10.1016/j.chemgeo.2007.11.005.

Spencer, C.J., Kirkland, C.L. and Taylor, R.J.M. 2016. Strategies towards statistically robust interpretations of in situ U–Pb zircon geochronology. *Geoscience Frontiers*, **7**, 581–589, https://doi.org/10.1016/j.gsf.2015.11.006.

Vermeesch, P. 2004. How many grains are needed for a provenance study? *Earth and Planetary Science Letters*, **224**, 441–451, https://doi.org/10.1016/j.epsl.2004.05.037.

Vermeesch, P. 2013. Multi-sample comparison of detrital age distributions. *Chemical Geology*, **341**, 140–146, https://doi.org/10.1016/j.chemgeo.2013.01.010.

Vermeesch, P. 2018. Dissimilarity measures in detrital geochronology. *Earth-Science Reviews*, **178**, 310–321, https://doi.org/10.1016/j.earscirev.2017.11.027.

Wiedenbeck, M., Allé, P., et al. 1995. Three Natural Zircon Standards for U-TH-PB, LU-HF, Trace Element and REE Analyses. *Geostandards and Geoanalytical Research*, **19**, 1–23, https://doi.org/10.1111/j.1751-908X.1995.tb00147.x.

Wiedenbeck, M., Hanchar, J.M., et al. 2004. Further Characterisation of the 91500 Zircon Crystal. *Geostandards and Geoanalytical Research*, **28**, 9–39, https://doi.org/10.1111/j.1751-908X.2004.tb01041.x.

Zuffa, G.G. (ed.). 1985. *Provenance of Arenites*, https://doi.org/10.1007/978-94-017-2809-6.

CAPÍTULO 3

INFLUENCE DES PROCESSUS DE RIFTING ET DE POST RIFTING SUR LA PARTIE CONTINENTALE NORD DE L'AMERIQUE DU SUD : EXEMPLE DE L'ETUDE DE L'EVOLUTION DU BASSIN ARARIPE A PARTIR DE LA PROVENANCE SEDIMENTAIRE.

PROVENANCE OF THE LATE JURASSIC TO CENOMANIAN SEDIMENTARY SUCCESSION OF THE ARARIPE BASIN (NE BRAZIL) AND IMPLICATION FOR THE GEODYNAMIC EVOLUTION OF WESTERN GONDWANA

Rodrigues, A. R., Roddaz, M., Santos, R. V., Dantas, E. Leisen, M. 2023. Provenance of the late Jurassic to Cenomanian sedimentary succession of the Araripe Basin (NE Brazil) and implication for the geodynamic evolution of Western Gondwana. (soumis – Tectonics)

3 INFLUENCE DES PROCESSUS DE RIFTING ET DE POST RIFTING SUR LA PARTIE CONTINENTALE NORD DE L'AMERIQUE DU SUD : EXEMPLE DE L'ETUDE DE L'EVOLUTION DU BASSIN ARARIPE A PARTIR DE LA PROVENANCE SEDIMENTAIRE

Les résultats de ce chapitre sont exprimés sous la forme d'un article intitulé «Provenance of the Late Jurassic to Cenomanian Sedimentary succession of the Araripe Basin (NE Brazil) and implications for the geodynamic evolution of Western Gonswana » qui est, lors de la soumission de ce manuscrit, en phase des dernières corrections pour être soumis à Tectonics. L'objectif de ce chapitre est de comprendre comment la réorganisation du système de drainage au cours des différentes phases de sédimentation du bassin de l'Araripe reflète les changements géodynamiques de la partie nord-est de la plate-forme sud-américaine pendant de l'ouverture de l'océan Atlantique Sud et Equatorial.

Résumé

Le processus de fragmentation du Gondwana occidental au Jurassique et au Crétacé modifie la géodynamique régionale et le paléodrainage de la partie nord de l'Amérique du Sud. Avant la fragmentation, un bassin rift s'est formé sur une grande partie de la région centrale et septentrionale du Gondwana, connue sous le nom de dépression afro-brésilienne. La localisation du rifting entre l'Amérique du Sud et l'Afrique a été contrôlée par des héritages structuraux protérozoïques et, le bassin rift avorté de l'Araripe, dans (nord-est du Brésil), en est un exemple puisque les séquences sédimentaires (rifts à post rifts) qui le composent ont potentiellement enregistrées l'histoire complète du démembrement du Gondwana. Alors que des études antérieures se sont concentrées sur les incursions paléogéographiques aptiennes-albiennes des eaux peu profondes, peu d'attention a été accordée à l'évolution des sources alimentant la bassin Araripe pendant les phases de rift et de post-rift. La compréhension de l'évolution du paléodrainage est cruciale pour

déterminer les sources de sédiments et le lien entre les changements topographiques et l'évolution géodynamique de la partie septentrionale de l'Amérique du Sud pendant la fragmentation du Gondwana. Cette étude examine la provenance des roches sédimentaires dans le bassin de l'Araripe, en utilisant un ensemble de données multi-proxy comprenant les concentrations en éléments majeurs et traces, la composition isotopique Sm-Nd et les âges U-Pb des zircons détritiques. Les analyses des valeurs d'εNd(0) (-12,3 à -23,7) et des âges TDM (1,68 à 2,55 Ga) suggèrent une source crustale ancienne. La présence d'âges U-Pb des zircons du Rhyacien à l'Orosirien (2,3 à 1,8 Ga) et de l'Édiacarien (0,63 à 0,58 Ga) indique en outre la contribution dominante de la province de Borborema influencée par le cycle Brasiliano (650 à 520 Ma), comme le révèlent les grains de zircon discordants ; La faible contribution des zircons toniens aux distributions des âges U-Pb indique des sources provenant des terrains situés au Nord-Nord Ouest du plateau de Borborema pendant la phase de début du rift. Le pourcentage important de grains de zircon d'âge Toniens (0,9-1,0 Ga) pendant la phase du rift suggère une source dominante située dans les terrains orientaux avec la présence et un sommet topographique pendant le point culminant du rift, qui a potentiellement séparé les bassins de l'Araripe et du Sergipe-Alagoas. Au cours de la phase post-rift I (groupe de Santana), la diminution des âges des zircons du Stenien-Tonien (1,2 - 0,72 Ga) suggère un changement dans les zones sources, avec des directions de paléodrainage provenant de la province septentrionale de Borborema, similaires à la phase de début du rift. Enfin, les échantillons du stade post-rift II présentent des contributions dominantes d'âges U-Pb paléoprotérozoïques et néoprotérozoïques liés au soulèvement albien à cénomanien du plateau de Borborema, ce qui suggère des sources proximales. Ces résultats contribuent à une meilleure compréhension de l'histoire géologique et de la dynamique de la provenance dans le bassin de l'Araripe, au nord-est du Brésil, et soulignent le rôle important joué

par le soulèvement continental post-rift dans le paléodrainage de la partie septentrionale de l'Amérique du Sud.

3.1 The provenance of the late Jurassic to Cenomanian sedimentary succession of the Araripe Basin (NE Brazil) and implication for the geodynamic evolution of Western Gondwana

Mariana de Assunção Rodrigues [a,b,*], Roberto Ventura Santos[a], Martin Roddaz [b], Elton Luiz Dantas [a], Mathieu Leisen [b]

[a] Universidade de Brasília, Darcy Ribeiro Campus, Asa Norte 70910-900 Brasília, DF, Brazil

[b] Géosciences-Environnement Toulouse, Université de Toulouse; UPS (SVT-OMP); 14 Avenue Édouard Belin, F-31400 Toulouse, France

*Corresponding author,

E-mail address: marianarodrigues.geologia@gmail.com (M. A. Rodrigues).

Abstract

The Jurassic-Cretaceous Western Gondwana break-up process changes the continental geodynamics as reflected in the paleodrainage organization. Before the fragmentation, a rift basin initially formed across a significant stretch along the central and northern Gondwana region, known as the Afro-Brazilian Depression. The separation of South America and Africa was controlled by preexisting Proterozoic structures and by the development of new depositional sites, such as the Araripe Basin in Northeast Brazil. This basin represents an aborted rift that accumulated sin-rift and post-rift sequences. While previous studies have focused on the paleogeographic Aptian-Albian shallow-marine incursions, little attention has been given to its paleodrainage evolution during the rift and post-rift stages. Understanding the

paleodrainage evolution is crucial for determining sediment sources and how topographic changes relate to the geodynamic development of the northern part of South America during the fragmentation of Gondwana. To add new constraints, this study investigates the provenance of sedimentary rocks in the Araripe Basin using a multi-proxy dataset comprising major and trace element concentrations, Sm-Nd isotopic composition, and detrital zircon U-Pb ages. The analyses of εNd(0) values (-12.3 to -23.7) and TDM ages (1.68 to 2.55 Ga) suggest an ancient crustal source. The presence of Rhyacian to Orosirian (2.3 – 1.8 Ga) and Ediacaran (0.63 – 0.58 Ga) U-Pb zircon ages further indicates the dominant contribution of the Borborema Province influenced by the Brasiliano cycle (650 – 520 Ma), as revealed by discordant zircon grains. A minor contribution of Tonian zircons to the U-Pb age distributions indicates sources from N-NW Borborema terrains during the early stages of rift evolution. The significant number of Cariris Velhos (0.9-1.0 Ga) zircon grains during the rift stage suggests a dominant source in the eastern terranes and a topographic high during the rift climax, which potentially separated the Araripe and Sergipe-Alagoas basins. During the post-rift I stage (Santana Group), the decrease of Stenian-Tonian (1.2 – 0.72 Ga) zircon suggests a change in the source areas, with paleodrainage coming from northern Borborema Province, similar to the rift beginning stage. Finally, the samples of the post-rift II stage exhibit dominant contributions of Paleoproterozoic and Neoproterozoic U-Pb ages related to the Albian to Cenomanian uplift of the Borborema plateau, suggesting proximal sources located in the NE direction. These findings contribute to a better understanding of the geological history and provenance dynamics in the Araripe Basin, NE Brazil, and highlight the significant role played by the post-rift continental uplift to the paleodrainage of the northern part of South America.

3.2 Introduction

The geodynamic cycles also referred to as the Wilson Cycle (Wilson 1969), have been responsible for the dispersal and subsequent reassembly of continents throughout Earth's history. This complex movement of continents repeats throughout geological times and recorded in crustal rocks since 3.0 Ga (Bleeker 2003; Van Kranendonk *et al.* 2010; Shirey and Richardson 2011). Uplift and spreading processes during the embryonic to mature stages of the ocean basins' life cycle (Wilson 1969), the interplay between driving forces, resisting factors, and crustal weakening operation contribute to the formation of a diverse range of rifts (Brune *et al.* 2023). The best example of these processes is the Pangea fragmentation.

The Pangea fragmentation began at the end of the Triassic and was developed into three phases during the Jurassic and Cretaceous (Moulin *et al.* 2010; Heine *et al.* 2013). Three mega blocks were formed after an Early Jurassic disruption led by geodynamics, kinematic, and plate tectonic changes in Western Gondwana (Matos 1999; Sahabi *et al.* 2004; Eagles and König 2008; Moulin *et al.* 2010; Heine *et al.* 2013). Before the Cretaceous breakup, an early rift basin developed in the central and northern Gondwana within the so-called Afro-Brazilian Depression (Assine 2007; Kuchle *et al.* 2011; Scherer *et al.* 2014; Guzmán-González *et al.* 2020). The rifting between South America and Africa was diachronic and controlled by preexisting Proterozoic structures (Matos 1992). In the Borborema Province (Northeast Brazil, Fig., 1), the Mesozoic sedimentary record of the rift basin (i.e. Araripe, Rio dos Peixes, Potiguar) provides important constraints on the geodynamic and tectonic processes that controlled the dislocation of Western Gondwana. However, the evolution of these rift basins was aborted during the opening of the South and Equatorial Atlantic Oceans, believed to have happened between 90 and 135 Ma (Hall *et al.* 2018 Heine *et al.* 2013; Dummann *et al.* 2023). The Araripe Basin is an example an aborted rift basins that

formed along the trend Cariri-Potiguar (Matos 1992; Camacho and Sousa 2017) (Fig. 1).

Deciphering the long-term evolution of paleodrainages is important to understand how topographic changes are related to the geodynamic evolution of large continental areas, such as the northern part of South America during the Gondwana fragmentation. This kind of approach requires integration of continental-scale scenarios, such as the Amazon and Araripe basins. The meso-Cenozoic sedimentary record of the Amazon Basin was addressed by different studies (Basu *et al.* 1990; Roddaz *et al.* 2005, 2012, 2021; Figueiredo *et al.* 2009; Hoorn *et al.* 2017; van Soelen *et al.* 2017; Horbe *et al.* 2019; Rodrigues *et al.* 2023). In contrast, most paleogeographic scenarios of the Araripe Basin focus on the existence and provenance of the Aptian-Albian shallow marine incursions that affected the evolution of the basin (Machado Junior *et al.* 1990; Assine 1994; Arai 2014, 2016; Custódio *et al.* 2017; Godot Souza *et al.* 2022). No study has addressed the paleodrainage scenario during the rift stage and after the continental break-up. This basin is located on the Precambrian terranes of the Transversal Zone in the Borborema Province (Assine 2007; Fambrini *et al.* 2020a; Brito Neves *et al.* 2023) (Fig. 24) and has a unique record of pre-rift to post-rift sediments.

In this study, we present new whole-rock and zircon geochemistry, Sm-Nd isotopic composition, and U-Pb detrital zircon ages to characterize the sedimentary provenance during the tectonic stages of the Araripe Basin. Our data extend and complement the first provenance dataset published by (Godot Souza *et al.* 2022) and will help to better understand and reconstruct the paleogeographic scenario during the evolution of the Araripe Basin. We further integrate the Araripe and Western Amazon paleodrainage scenario to address the topographic changes related to the geodynamic

development of the northern part of South America during the fragmentation of Gondwana.

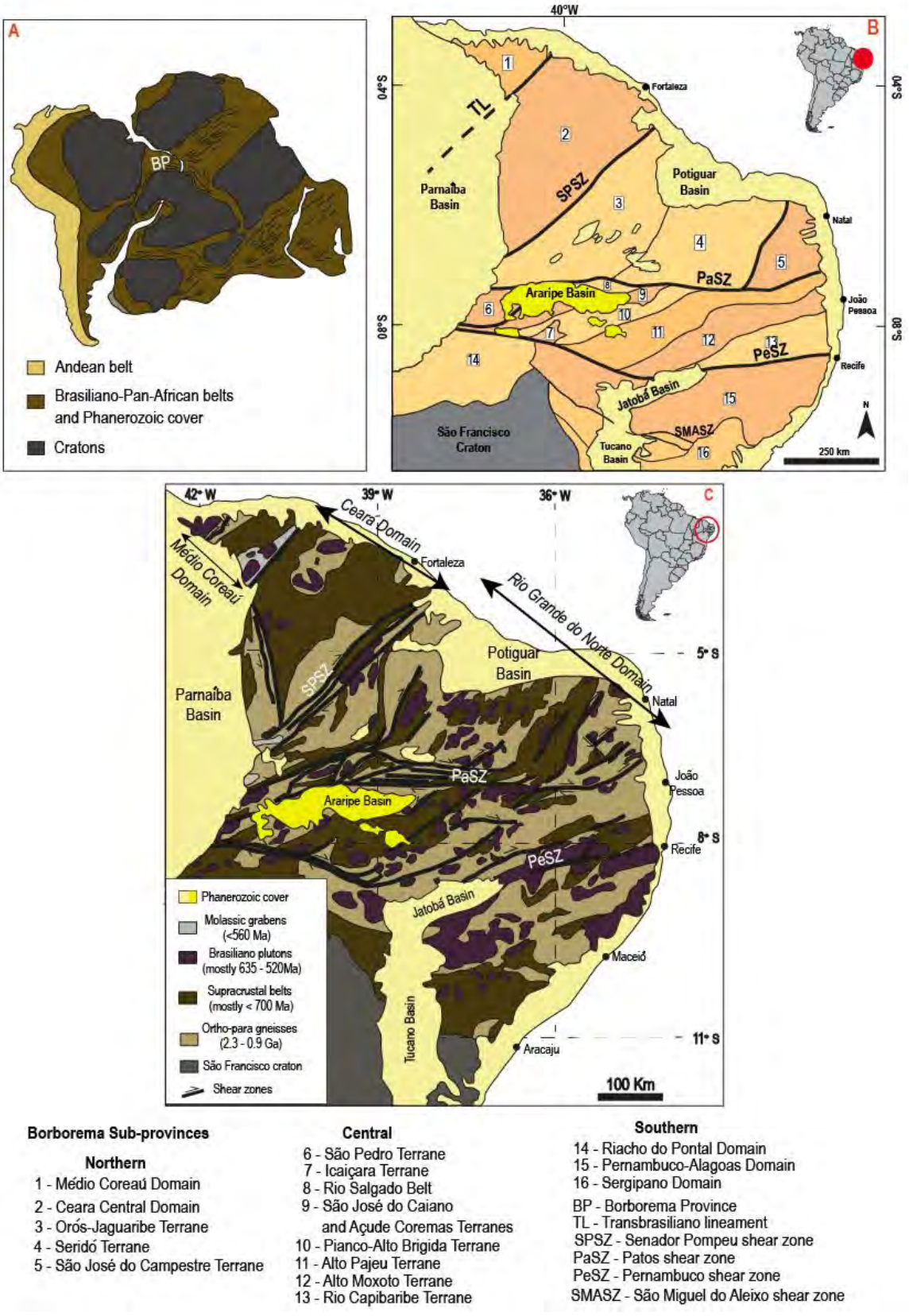

Fig. 24: Pre-drift reconstruction of South America e Africa showing the Andean belt, Archean/Proterozoic cratons, and Brasiliano/Pan-African provinces of western Gondwana. (b) Tectonic compartmentation of

Borborema Province with the division into Northern, Central, and Southern subprovinces. (c) The schematic map of the Borborema Province shows the Northern and Southern subprovinces subdivision. Map based on Neves (2015); Brito Neves and Passarelli (2020), Brito Neves and Campos Neto (2016), Matos et al (2021), Van Schumus et al (2011), Ferreira et al. (1998), and Godot Souza et al. (2022).

3.3 Geological settings and sampling

3.3.1 Geological setting

The potential sources: the Borborema Province and the Paranaiba Basin

The Borborema Province (Almeida *et al.* 1981) is located in the northeast part of the South American Platform and represents a mosaic of tectonic blocks with Paleoproterozoic basement and scattered Archean nuclei, Meso to Neoproterozoic supracrustal rocks, and large intrusions of granitic rocks emplaced during the Neoproterozoic Brasiliano orogen, from 650 to 520 Ma (Brito Neves *et al.* 2000; van Schmus *et al.* 2008; Van Schmus *et al.* 2011; Cruz *et al.* 2014) (Fig. 24). This complex orogenic system resulted from the breakup of a Paleoproterozoic supercontinent during the late Mesoproterozoic to early Neoproterozoic (van Schmus *et al.* 2008; Guimarães *et al.* 2016). The Borborema Province is situated between the West Africa-São Luis craton to the north, and late Neoproterozoic terranes to the west (Brasiliano/Pan African). It is limited to the south by the São Francisco – Congo Craton (Fig. 24) (Pimentel and Fuck 1992; Brito Neves *et al.* 2000; Guimarães *et al.* 2016). On the African side (between Togo and Gabon), there are structural and tectonic continuations of the Borborema Province, including domains of the Trans-Saharan, Nigerian, and Oubanguides Central Africa mobile belts (Brito Neves *et al.* 2000).

In the northeast part of the South America Platform, the Phanerozoic Parnaíba basin represents a cratonic basin, formed during the post-collisional stages of the Brasiliano Pan-Africano event (Vaz *et al.* 2007; Assis *et al.* 2019). Three large transgressive-regressive depositional sequences were identified: the Silurian Serra Grande, the Devonian Canindé, and the Permo-Triassic Balsas Group (Góes and Feijó 1994; Góes 1995; Vaz *et al.* 2007; Hollanda *et al.* 2014) highlight two other depositional

sequences: the Jurassic Pastos Bons Formation and the Cretaceous Corda, Grajaú, Codó, and Itapecuru formations. Detrital U-Pb zircon age from the first three sequences indicate contributions from Rhyacian-Orosirian (2.3 – 2.05 Ga), Stenian-Tonian (1.2 – 0.72 Ga), and Ediacaran (635 – 541 Ma) sources, probably originated from the southern and central parts of the Borborema Province (Hollanda *et al.* 2014). During the Triassic-Jurassic (Mosquito Formation) and Cretaceous (Sardinha Formation), several magmatic events affected the Parnaíba basin (Heilbron *et al.* 2018; Klöcking *et al.* 2018; Miloski *et al.* 2019). Basaltic dykes, sills, and other mafic magmatic bodies occurred interlayered with and intruded in thick sedimentary succession (Miloski *et al.* 2019).

Tab. 4: Borborema Province sub-division with general information about rock types, U-Pb ages, and Sm-Nd isotopic compositions.

Borborema Province *Northern sub-province*					
Domain/Terrane	**Type of rocks**	**Age (Ga)**	**eNd (0)**	**T_{DM} (Ga)**	**References**
Médio Coreaú Domain	Orthogneiss, migmatites (Granja Complex); Paragneiss (Martinopole Group); Volcano-sedimentary rocks; Granitoids	2.35 – 2.27 (Granja Complex) 0.77 (Martinopole Group) 0.56 – 0.52 (granitoids)		2.38 – 2.61	Santos et al 2008 a; Fetter et al 2000 ; Araujo et al 2012
Ceará Central Domain	Granitoids (Tamboril-Santa Suiteria Complex); Metasedimentary rocks (Ceará Group)	0.65 – 0.61 (granitoids) 1.8 - 0.74 (detrital zircon)	-21.48 to -19.09 (granitoids) -25.79 to +2.12 (metasediments)	2.19 – 2.69 (granitoids) 1.95 - 2.4 (metasediments)	Costa et al 2013 Arthaud et al 2015
Orós-Jaguaribe Terrane	Metasedimentary and metavolcanic rocks; orthogneiss	1.9 – 0.65	-	-	Parente and Arthaud 1995; Arthaud et al 2008
Seridó Terrane	Orthogneiss; metasupracrustal rocks;	2.4 – 1.74	-37.51 to -28.69	3.20 – 2.5	Hollanda et al 2011

São José do Campestre Terrane	Granitoids and metasupracrustal rocks	3.45 – 2.70	-6.18 to +3.36	4.1 – 3.2	Dantas et al 2013 ; Dantas et al 2004
Central sub-province					
São Pedro Terrane	Orthognaisses (TTG, granites, granodiorite) "Granjeiro Complex"	3.3 - 2.5	-22.64 to –43.78	2.29 to 3.48	Archanjo et al 2021;
	Metavulcano-sedimentary rocks (Ipueirinha Group)	Archean and Neoproterozoic	-5.2 to -27.3	1.13 to 3.16	
	Orthogneisses; granites and supracrustal rocks (metamorphic rocks) "Ouricuri and Bodocó"	2.0 – 2.3	-6.67 to -29	1.3 to 2.4	Brito Neves et al. (2022)
Açude Coremas Terrane	Orthogneisses; granites ("Itaporanga"); Brasiliano granites	2.0 – 2.1	-6.3 to -28.38	1.17 to 2.92	Brito Neves and Passarelli 2020
	Metamudstones (Unidade Bom Jesus)	0.61			
São José do Caiana	Orthogneisses; Paragneisses granites; Brasiliano granites; Metasedimentary rocks	2.1 – 2.2	-14.98 to -29.38	1.8 to 2.7	Neves and Passarelli 2020; Kozuch, 2003; Scherer et al, 2014
Icaiçara Terrane	Ortho-paragneisses "Complexo Parnamirim" and "Barro Complex"; Migmatites; metasedimentary rocks	2.0 – 2.1 0.99 – 0.95	-8.95 to -28.46	1.3 to 2.3	Neves and Passarelli 2020;

Piancó-Alto Brígida Terrane	Metasedimentary, metavolcanic, and metaplutonic rocks; Granitoids	1.0 – 0.64	-43.6 to -2.0	1.08 – 2.5	Brito Neves et al., 2005; Van Schmus et al 2011
Alto Pajeú Terrrane	Ortho and paragneiss; mylonite; granitoids; metasedimentary, metavolcanic, and metaplutonic rocks	2.1 to 0.64	-32.8 to -6.4	1.04 - 3.09	Rodrigues and Neves, 2008 ; Santos et al 2010 ; Brito Neves et al., 2005 ; Van Schmus et al 2011
Alto Moxotó Terrane	Ortho and paragneiss (Sertânia Complex); Amphibolite; granites	2.1 – 2.3 (orthogneiss) 2.2 – 1.9 (detrital zircons)	-25.0 to -16.7	2.2 – 2.5	Santos, 2004 ; Rodrigo and Neves, 2008; Brito Neves et al 2001; Brito Neves et al., 2005 ; Van Schmus et al 2011
Rio Capibaribe Terrane	Metasedimentary rocks; Orthogneiss; tonalites		-23.2 to -5.3	2.2 – 1.3	Brito Neves et al ., 2005 ; Van Schmus et al 2011
Southern sub-province					
Riacho do Pontal Domain	Granites; Schist; Gneiss	3.0 – 0.92	-15.1 to -7.9	1.43 – 1.60	Brito Neves et al 2015 ; Van Schmus et al 2011
Pernambuco-Alagoas Domain	Ortho and paragneiss; Granitois	2.6 – 0.87	-38.3 to -8.00	1.37 – 3.59	Cruz et al 2014
Sergipano Domain	Metasedimentary and metavolcanic rocks; granitoids; orthogneiss and migmatites	2.83 (orthogneiss) Neoproterozoic plutons	-	-	D'el Rey Silva 1995; Silva Risa et al 2020

The sink: the Araripe Basin

The Araripe Basin is more than 9000 km² and is one of the largest basins located in northeast Brazil. It was formed during the break-up of Gondwana and the opening of the South Atlantic Ocean (Assine 1992; Matos 1992; Maisey 2000; Assine 2007; Fambrini *et al.* 2020a). The Araripe Basin comprises five sedimentary sequences, starting with the Paleozoic Sequence formed by the Cariri Formation, followed by the Jurassic first Rift Pulse Sequence formed by the Brejo Santo and Missão Velha Formation (Fig. 25). The climax Rift Sequence is characterized by the upper part of the Jurassic Missão Velha Formation and the Barriasian to Barremian Abaiara Formation. The post-rift Sequence begins with the deposition of the Aptian-Albian Barbalha, Crato, and Romualdo formations and ends with the Albian-Cenomanian Araripina and Exu formations (Assine 1992, 2007; Fambrini *et al.* 2013, 2015, 2019, 2020b; Assine *et al.* 2016) (Fig. 25).

The Cariri Formation (Beurlen 1962) outcrops on the eastern side of the Araripe Basin and it is formed by fluvial coarse-grained sandstones and conglomerates (Assine 1992, 2007; Silvestre *et al.* 2017; Fambrini *et al.* 2020b). The age of this formation is under dispute (Caputo and Crowell 1985; Assine 1992, 2007; Coimbra *et al.* 2002; Fambrini *et al.* 2020b), but a recent study suggests an Ordovician age (Cerri *et al.* 2022). The Cariri Formation is sourced from Neoproterozoic, Cambrian, and Paleoproterozoic rocks from the Transversal and Southern zones of the Borborema Province (Cerri *et al.* 2022).

The mudstones of the Brejo Santo Formation were deposited during the late Jurassic extensional events that affected the northern Gondwana, with the pre-rift sequence (Garcia and Wilbert 1995; Ponte and Ponte Filho 1996; Assine 2007; Fambrini *et al.* 2013, 2020a; Vieira Melo and Carvalho 2018). The Tithonian

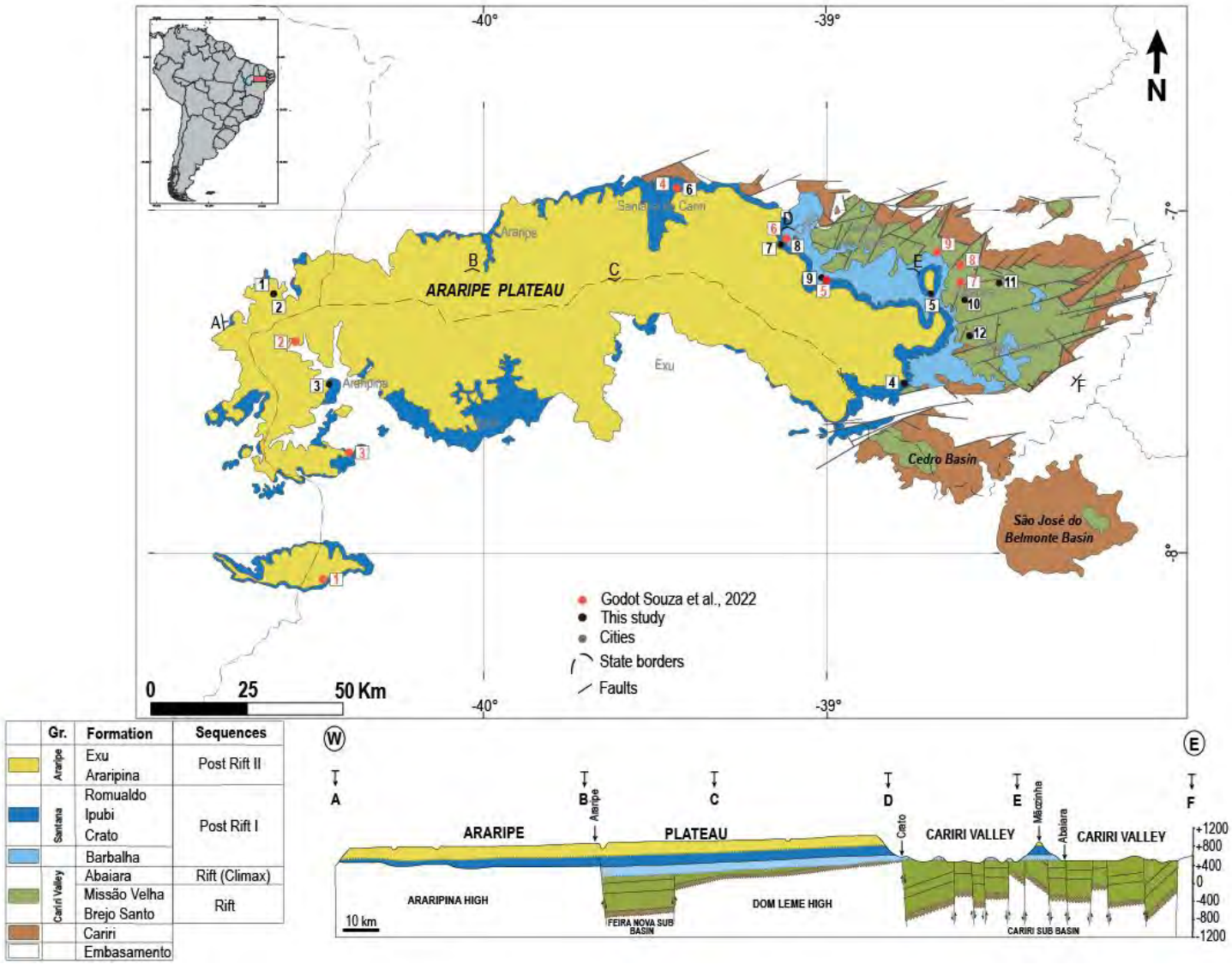

Fig. 25: The Geologic map of the Araripe Basin shows the stratigraphic record of the rift and post-rift stages (modified from Assine, 2007 and Fambini et al. 2020). Number in the map refers to samples from this study (black) and Godot Souza et al (2022) (red).

Missão Velha Formation consists of fluvial sandstones and present fossil wood fragments (*Dadoxilon benders* (Brito 1987) (Assine 2007; Scherer *et al.* 2014; Fambrini *et al.* 2020b) and paleocurrents toward the SE. The Neocomian Abaiara Formation was deposited during the climax rift stage of the Araripe Basin (Assine 2007; Scherer *et al.* 2014; Fambrini *et al.* 2020b). It is composed of deltaic and fluvial deposits with dispersed paleo flows (Scherer *et al.* 2014) and SSW paleocurrent directions (Assine 1994, 2007). The presence of syn-depositional growth normal faults indicates an active extensional tectonics during the sedimentation (Scherer *et al.* 2014).

The post-rift sequence of the Araripe basin is represented by the fluvial, lacustrine, and transitional marine Aptian-Albian Santana Group ("Post-rift I") formed by the Barbalha, Crato, Ipubi, and Romualdo formations (Neumann *et al.* 2003; Assine 2007) and the Albian-Cenomanian Chapada Group ("Post-rift II") formed by the Araripina and the Exu Formations (Assine 1992, 2007; Assine *et al.* 2014; Fambrini *et al.* 2020b) (Fig. 2). The basal Barbalha Formation, is characterized by fining upward sandstone with mudstone intervals sequences (Assine 1992) with a black shale interval with limestones termed Fundão Member (Rios Netto *et al.* 2012a), or Batateiras layer (Hashimoto *et al.* 1987; Assine *et al.* 2014). Palynological analyses in the black shale layer indicate late Aptian ages (Lima and Perinotto 1984; Hashimoto *et al.* 1987; Barbosa *et al.* 2006; Rios Netto *et al.* 2012b). The basal fluvial paleocurrents measured by (Assine 1994) present SE direction. The Crato Formation is characterized by micritic laminated limestones interlayered with calciferous shales (Assine 2007; Fambrini *et al.* 2020b). The rich fossiliferous association suggests lacustrine paleoenvironment (Assine *et al.* 2014) during the late Aptian (Lima 1978; Assine 2007). Evaporitic sedimentary rocks of the Ipubi Formation succeeded the sedimentary rocks of the Crato Formation (Assine *et al.* 2014). The fossiliferous rich

conglomerates, fine-coarse sandstones, shales, and limestones of the Romualdo Formation were deposited in a shallow marine environment (Assine *et al.* 2014; Custódio *et al.* 2017). Paleocurrents measured in tidal-influenced sandstones indicate NNW-SSE paleocurrent directions (Custódio *et al.* 2017). The age of the Romualdo Formation is early to middle Aptian or early Albian and based on microfossils (Coimbra *et al.* 2002; Heimhofer and Hochuli 2010), whereas, palynological data indicate a late Aptian age (Rios Netto *et al.* 2012b). The last post-rift sequence starts with the Araripina Formation, which overlays the Romualdo Formation in the eastern part of the basin and rests directly on the basement in the western part (Assine 2007; Fambrini *et al.* 2020b). It is formed by fine to coarse-grained sandstones deposited in a lagoon paleoenvironment (Assine 2007). Palynological associations suggest a mid-Albian age (Lima 1978). The Albian-Cenomanian Exu Formation is characterized by fluvial sandstones (Assine 2007) with paleo flows to the west interpreted to have come from the eastern Borborema Province (Assine 2007).

Sampling and stratigraphic constraints

In total, we collected thirty-nine samples from the Cretaceous sedimentary rock successions cropping out in the Araripe basin (Fig. 26 and details in the supplementary dataset). Eleven of these samples were analyzed for zircon U-Pb dating and zircon trace elements. To improve the statistical quality of our interpretations, we used the U-Pb zircon ages published in by Godot Souza et al. (2022) (Fig. 25,Fig. 26; Tab. 5). Nineteen samples were measured for their bulk major and trace element concentrations and nine for their Sm-Nd isotopic composition. The locations of the analyzed samples can be found in Fig. 25 and Tab. 5.

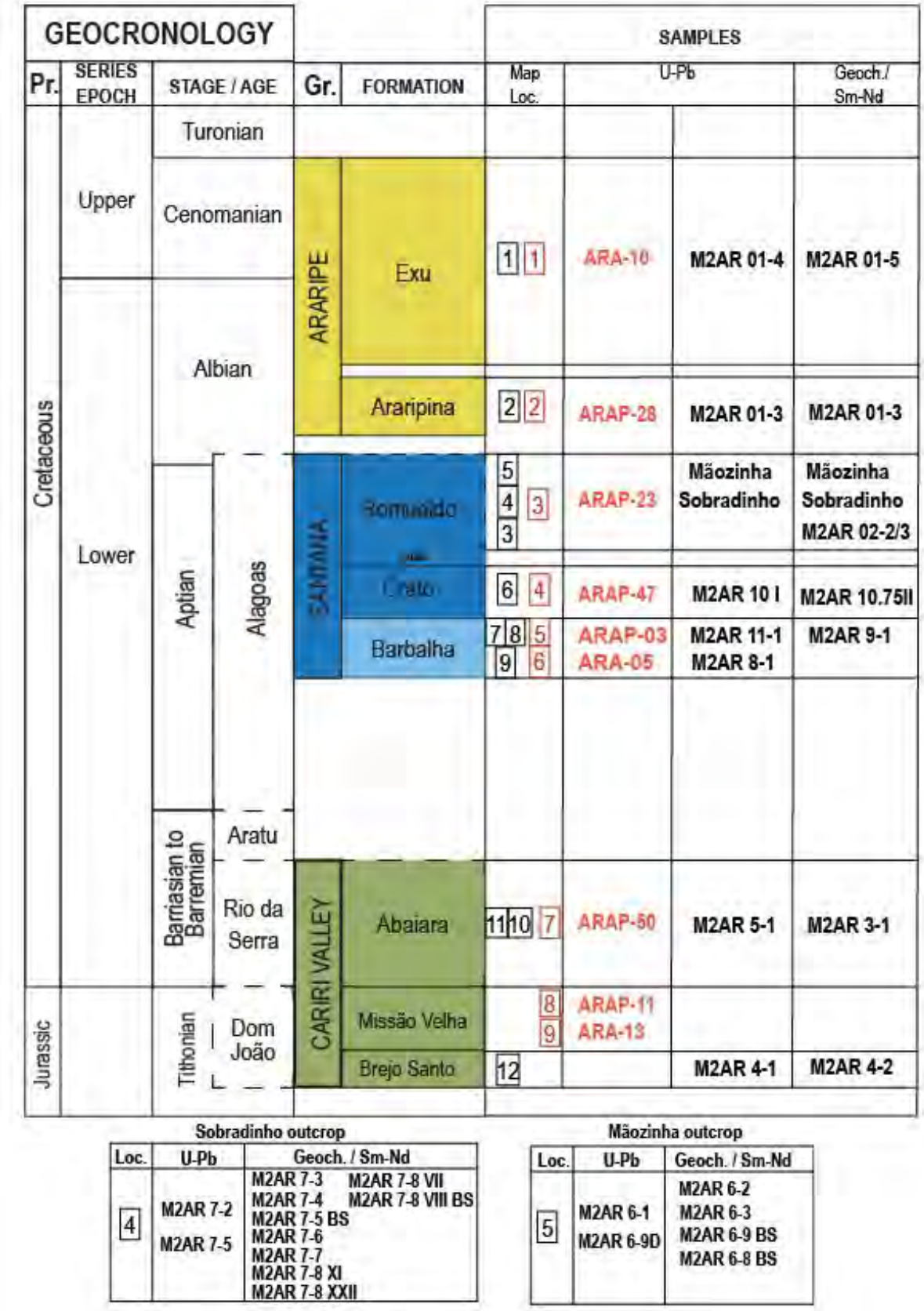

Fig. 26: Stratigraphic chart of the Araripe Basin (taken from Assine 2007) showing the samples analyzed in this study (in black color) and by Godot Souza et al. 2022 (in red). Loc. and Geoch. refer to Location and Major and trace element analysis respectively.

Tab. 5: Label, formation, age, and location for the analyzed samples in this study and in Souza et al., 2021 (in red).

Sample	Formation	Age	Longitude (W)	Latitude (S)
M2AR 01.4	Exu	Albian-Cenomanian	-40.652910°	-7.365121°
M2AR 01.5	Exu	Albian-Cenomanian	-40.652910°	-7.365121°
ARA-10	Exu	Albian-Cenomanian	-40.535697°	-8.044150°
M2AR 01.3	Araripina	Albian	-40.652910°	-7.365121°
M2AR 01.3	Araripina	Albian	-40.652910°	-7.365121°
ARAP-28	Araripina	Albian	-40.592849°	-7.492190°
M2AR 06.1	Romualdo	Aptian	-39.099406°	-7.362347°
M2AR 06.2	Romualdo	Aptian	-39.099204°	-7.362335°
M2AR 06.3	Romualdo	Aptian	-39.098932°	-7.361896°
M2AR 06.8 BS	Romualdo	Aptian	-39.098829°	-7.360865°
M2AR 06.9 BS (E2)	Romualdo	Aptian	-39.098551°	-7.358631°
M2AR 06.9 D	Romualdo	Aptian	-39.098551°	-7.358631°
M2AR 07.2	Romualdo	Aptian	-39.163729°	-7.574154°
M2AR 07.3	Romualdo	Aptian	-39.163636°	-7.573472°
M2AR 07.4	Romualdo	Aptian	-39.163521°	-7.572447°
M2AR 07.5	Romualdo	Aptian	-39.163554°	-7.572288°
M2AR 07.5 BS	Romualdo	Aptian	-39.163554°	-7.572288°
M2AR 07.6	Romualdo	Aptian	-39.163529°	-7.571304°
M2AR 07.7	Romualdo	Aptian	-39.163529°	-7.571304°
M2AR 07.8 VII	Romualdo	Aptian	-39.163105°	-7.571637°
M2AR 07.8 VIII BS	Romualdo	Aptian	-39.163105°	-7.571637°
M2AR 07.8 XI	Romualdo	Aptian	-39.163105°	-7.571637°
M2AR 07.8 XXII	Romualdo	Aptian	-39.163105°	-7.571637°
M2AR 02.2 Equin	Romualdo	Aptian	-40.523850°	-7.579407°
M2AR 02.3	Romualdo	Aptian	-40.523850°	-7.579407°
ARAP-23	Romualdo	Aptian	-40.472122°	-7.743015°
M2AR 10.0 I	Crato	Aptian	-39.697751°	-7.116543°
M2AR 10.75 II	Crato	Aptian	-39.697751°	-7.116543°
ARAP-47	Crato	Aptian	-39.697587°	-7.115617°
M2AR 11.1	Barbalha/Crato	Aptian	-39.453280°	-7.248347°
M2AR 09.1	Barbalha intermediario	Aptian	-39.441840°	-7.233942°
M2AR 08.1	Barbalha base	Aptian	-39.356768°	-7.327129°
ARAP-03	Barbalha	Aptian	-39.341421°	-7.334172°
ARA-05	Barbalha	Aptian	-39.441184°	-7.233616°
M2AR 05.1	Abaiara	Berriasian-Hauterivian	-38.936652°	-7.339516°
ARAP-50	Abaiara	Berriasian-Hauterivian	-39.024444°	-7.339457°

ARAP-11	Missão Velha	Jurassic	-39.024850°	-7.298578°
ARA-13	Missão Velha	Jurassic	-39.079448°	-7.267781°
M2AR 04.1	Brejo Santo	Jurassic	-39.006662°	-7.464279°
M2AR 04.2	Brejo Santo	Jurassic	-39.006662°	-7.464279°

Two samples (M2AR 4-2; M2AR 4-1) were collected in sandstone and siltstone levels of the beginning rift sequence of the Brejo Santo Formation, exposed to the Transnordestina railway, near Brejo Santo city (Fig. 25 and Tab. 5). The M2AR 4-2 was collected for major and trace elements concentrations and Sm-Nd isotopes analyses, and the M2AR 4-1 was collected for U-Pb age analyses. The M2AR 5-1 and M2AR 3-1 samples were collected for U-Pb age analyses in the Abaiara Formation outcrop exposed in the BR-116 highway, near the Padre Cícero Village in the Milagres city (Fig. 25 and Tab. 5) and characterized the rift (climax) sequence.

Three samples were collected from the “Post-rift I” sequence Barbalha Formation. The M2AR 8-1 sample was collected in the fluvial facies of the lower Barbalha Formation at the Salamanca River valley described by (Scherer *et al.* 2015; Fambrini *et al.* 2016, 2019), and was analyzed for U-Pb ages. The M2AR 9-1 was collected in the Rio da Batateira Geosite, the eastern sector of the Crato city (Fig. 25,Fig. 26; Tab. 5) and corresponds to the Batateira Layer (Assine 2007) or Batateira Formation (Ponte and Appi 1990). This sample was analyzed for major and trace element concentrations and Sm-Nd isotopes analyses. (Godot Souza *et al.* 2022) analyzed the ARA -05 sample from the same sedimentary succession for U-Pb age (Fig. 26: Stratigraphic chart of the Araripe Basin (taken from Assine 2007) showing the samples analyzed in this study (in black color) and by Godot Souza et al. 2022 (in red). Loc. and Geoch. refer to Location and Major and trace element analysis respectively.). The M2AR 11.1 was collected in the upper part of the Barbalha Formation in the Chico da Cascata passage above the Batateira Layer (Assine 2007) and was used to know U-Pb detrital ages.

The M2AR 10I and 10.75II samples were collected in the outcrop exposed at the Três Irmãos Mine and were used for U-Pb detrital ages and major and trace element concentrations, following the description of (Godot Souza *et al.* 2022), which collected the ARAP-47 sample in the same outcrop (Fig. 26: Stratigraphic chart of the Araripe Basin (taken from Assine 2007) showing the samples analyzed in this study (in black color) and by Godot Souza et al. 2022 (in red). Loc. and Geoch. refer to Location and Major and trace element analysis respectively.). The M2AR 10I was collected in the laminated sandstones and the M2AR 10.75 II in the gray-colored shale level (see Fig. 5 in Godot Souza *et al.* 2022). Three outcrops of the “Post-rift I” Romualdo Formation were sampled. The M2AR 2-2 and M2AR2-3 samples were collected on the western side of the basin near Araripina city (Fig. 25), in the thin layers of coquinas and limestone coquinoids (Sales 2005; Prado *et al.* 2015; Fambrini *et al.* 2020b) and were used to obtain the major and trace elements concentrations information. On the eastern side of the basin, we collected seventeen samples from Mãozinha and Sobradinho outcrops (Fig. 25; Tab. 5), which were described in (Custódio *et al.* 2017). At the Sobradinho outcrop, we collected two samples for U-Pb and zircon analyses (M2AR 7-2; 7-5), and nine samples (M2AR 7-3; 7-4; 7-5BS; 7-6; 7-7; 7-8 XI; 7-8XII; 7-8 VII; 7-8 VIII BS) for major and traces elements concentrations and Sm-Nd isotopic composition. At the Mãozinha outcrop, we collected two samples for U-Pb zircon analyses (M2AR 6-1; 6-9D), and four samples (M2AR 6-2; 6-3; 6-9BS; 6-8BS) for major and traces elements concentrations and Sm-Nd isotopic composition (Fig. 26).

The “Post-rift II” sequence Araripina Formation and Exu Formation outcrops are exposed at the PI–142 road between Marcolândia and Caldeirão Grande cities on the crystalline basement (Fig. 25). We built up a log of the sedimentary section of this site

(see Fig. S1 in the supplementary dataset) and collected two samples from Araripina Formation: a coarse-grained sandstone (M2AR 1-3) for U-Pb ages analyzed in zircon grain, and a siltstone (M2AR 1-3) for major and trace element concentrations and Sm-Nd isotopes. The M2AR 1-4 and M2AR 1-5 were collected in the Exu Formation for major and trace element concentrations and Sm-Nd isotopic composition, and U-Pb zircon analyses.

3.4 Analytical procedures

3.4.1 Major and trace element concentrations

The major and trace element concentrations were measured at the Service d'Analyse des Roches et Mineraux (SARM, INSU facility, Vandoeuvre-Les-Nancy, France) by ICP-OES and ICP-MS in whole rock. Analytical details are available on http://helium.crpg.cnrs-nancy.fr/SARM/ and in (Carignan *et al.* 2001). Precision is better than 5% for elements measured by ICP-OES, and 10% for elements measured by ICP-MS (see supplementary dataset for details).

3.4.2 Sm-Nd isotope composition

The samples were processed for Sm-Nd isotopes at the Geochronos Laboratory of the Geosciences Institute of the Universidade de Brasília. Before chemical preparation, the samples were dried at 60° C for approximately 12h. Sample digestion and extraction of Sm-Nd isotopes following the procedures described in (Goia and Pimentel 2000). The isotopic ratios of both elements were measured using a Thermo Scientific TRITON Plus thermal ionization mass spectrometer. During the Nd runs, isotopic normalizations were made using the natural ratios of $^{146}Nd/^{144}Nd = 0.7219$. The accuracy of the measurements was estimated by repeated analysis of the BHVO-2 standard. Repeated analysis of the BHVO-2 standard gave a $^{143}Nd/^{144}Nd$ ratio of 0.512996 ± 0.000006 (2SD, n=10) (Weis *et al.* 2005).

The measured $^{143}Nd/^{144}Nd_{sample}$ and $^{143}Sm/^{144}Nd_{sample}$ ratios were expressed in epsilon notation and reflect the fractional deviation in parts per 104 unit from the $^{143}Sm/^{144}Nd$ from the Chondritic Uniform Reservoir (CHUR). This notation is defined as:

$$\varepsilon Nd\ (t) = [(^{143}Nd/^{144}Nd)_{sample}\ (t) / (^{143}Nd / {}^{144}Nd)_{CHUR}\ (t) -1] \times 10^4$$

where t indicates the time at which εNd is calculated. Here, no time correction was applied (t = 0), and the $^{143}Nd / {}^{144}Nd_{CHUR}\ (0) = 0.512638$ (Jacobsen and Wasserburg 1980).

The TDM and TDM* ages were calculated following (DePaolo 1981; DePaolo *et al.* 1991; Augustsson and Bahlburg 2008).

$$T_{DM} = \ln [(^{143}Nd/^{144}Nd_{\ sample,\ today} - {}^{143}Nd/^{144}Nd)_{\ DM,\ today}) / (^{147}Sm/^{144}Nd_{sample,\ today} - {}^{147}Sm/^{144}Nd_{DM,\ today}) + 1] / \lambda;$$

$$T_{DM^*} = \ln [(^{143}Nd/^{144}Nd_{\ sample,Ts} - {}^{143}Nd/^{144}Nd)_{DM,\ Ts}) / (^{147}Sm/^{144}Nd_{crust,\ Ts} - {}^{147}Sm/^{144}Nd_{DM,\ Ts}) + 1] / \lambda + Ts;$$

where Ts is the estimated stratigraphic age. The $^{147}Sm/^{144}Nd_{crust,}$ Ts was calculated assuming that the $^{147}Sm/^{144}Nd_{crust,\ today} = 0.11$ (Albarède and Brouxel 1987). The model of (Goldstein *et al.* 1984) was used, where $\lambda\ (^{147}Sm) = 6.54 \times 10^{-12}a^{-1}$, $^{143}Nd/^{144}Nd_{DM,\ today} = 0.51315$, $^{147}Sm/^{144}Nd_{DM,\ today} = 0.217$, $^{143}Nd / {}^{144}Nd)_{CHUR} = 0.512638$, and $^{147}Sm/^{144}Nd_{CHUR,\ today} = 0.1967$.

3.4.3 U-Pb ages and trace element concentrations in zircons

The samples were processed at the Geochronos Laboratory of the Geosciences Institute of the University of Brasília (Brazil). First, they were fragmented in a rock crusher, sifted, and concentrated using a pan to separate the heavy mineral fraction. A Frantz magnetic separator was used to remove the magnetic fraction. At the laboratory of Géosciences Environnement Toulouse (GET) (France), approximately 150 zircons were handpicked from each sample under a binocular microscope and

mounted in epoxy resin. The resin discs were then polished, cleaned, and carbon-coated, then, cathodoluminescence (CL) images of zircon grains were obtained using a scanning electron microscope (SEM) Tescan Vega 4 equipped with a Bruker 30mm^2 EDS system, working at 10kV with a beam current of 3 10 nA.

Traces element concentrations and U-Pb ages in zircons were measured with an Element HR-ICPMS (ThermoScientific) coupled with a femtosecond laser (ESI - New Wave NWRfemto) at the ICPMS laboratory of Géosciences Environnement Toulouse GET, Toulouse, France. Before each analysis session, the ICP-MS was tuned by ablating a NIST SRM 610 glass reference material (Jochum *et al.* 2011), to ensure acceptable levels of sensitivity, stability, oxide, and fractionation (U/Th). The analytical conditions of the LA-ICPMS system were: spot size of 30 μm, frequency of 8 Hz, and fluence of ~ 2J/cm2. The GJ-1 (Jackson *et al.* 2004) was used as the primary standard, and Nist SRM (Jochum *et al*., 2011) for trace element analysis. Si (stoichiometric content 15.38%) was employed as an internal standard to determine trace element concentration in the zircons. The accuracy and reproducibility of the analyses were checked by repeated analyses of reference materials (91500, (Wiedenbeck *et al.* 2004); Plesovice, (Sláma *et al.* 2008); AUS-7, (Kennedy *et al.* 2014); Maniitsoq, (Marsh *et al.* 2019) (see supplementary dataset for details). Data processing and correction of laser-induced fractionation (LIEF) were performed using IOLITE v4.0 software (Paton *et al.* 2011) as a time-resolved signal, and individual signal inspection was done with the assistance of VisualAge (Petrus and Kamber 2012) with exponential plus linear modeling. Our measurements of 91500 yielded weighted man $^{206}Pb/^{238}U$ ages of 1063 ± 10 Ma (2σ, *n* = 309) in agreement with the recommended age of 1062.4 ± 0.4 Ma (Wiedenbeck *et al.* 1995).

The effective U-Pb ages were $^{206}Pb/^{238}U$ ages for zircons grains with ages ≤1.5 Ga and $^{207}Pb/^{206}Pb$ ages for grains with ages >1.5 Ga (Spencer *et al.* 2016). Ages with discordance degrees >10% and samples with few zircons were not considered because of their low statistical representation (Vermeesch 2004). Detrital zircon age data are visualized and compared using kernel density estimation (KDE) diagrams (Vermeesch 2013). To investigate the difference between detrital zircon U-Pb age distributions, we implemented the non-matrix metric multi-dimensional scaling (MDS) statistical technique (Vermeesch 2013). The MDS is a "superset of principal component analysis" that, given a table of pairwise 'dissimilarities' between samples, produces a 'map' of points on which 'similar' samples cluster closely together, and 'dissimilar' samples plot far apart (Vermeesch 2018). Following the latest recommendations by (Vermeesch 2018), we use the Kolmogorov–Smirnov test to produce an MDS map comparing analyzed samples.

3.5 Results

3.5.1 Major elements, Large-Ion Lithophile Elements (LILE), High Field Strength Elements (HFSE), and Trace Transition Elements (TTE)

The major elemental concentrations (LILE, HFSE, and TTE) of the analyzed samples were normalized to the Post Archean Australian Shales (PAAS) concentration (Taylor and McClennan 1985; Pourmand *et al.* 2012) (Fig. S2 in the supplementary dataset):

On the eastern part of the Araripe Basin, the earlier rift sample M2AR 4.2 (Brejo Santo Formation) is strongly depleted in MgO, Na_2O, and K_2O, Sc, Rb, Cs, Ba, and Sr relative to PAAS. The post-rift I M2AR 9.1 (Barbalha Formation) sample is strongly enriched MnO, CaO, P_2O_5, Y, Nb, V, Co, Cu, and Ni relative to PAAS. The M2AR 10.75 II sample (Crato Formation) has enrichment in MnO, MgO, CaO, Sr, Y, and Nb. All the

post-rift I sample from the Sobradinho outcrop (Romualdo Formation) (M2AR 7.8 XXII, M2AR 7.8 XI, M2AR 7.8 VII, M2AR 7.8 VII, M2AR 7.7, 2AR 7.6, M2AR 7.5, M2AR 7.3) are depleted in Al_2O_3, Na_2O, TiO_2, Cs, K_2O (except for M2AR 7.6), P_2O_5 and Sc (except for M2AR 7.6 and 7.8 VIII); SiO_2 (except for M2AR 7.4) and Ba (excepted M2AR 7.8 VII) against PAAS. High enrichment in CaO is noted for M2AR 7.8 XI, M2AR 7.7, M2AR 7.5, M2AR 7.8 VII, and M2AR 7.8 XXII samples, while all other samples from the Sobradinho outcrop are depleted against PAAS (Tab. 6 and Fig. 27). All the post-rift I samples from Mãozinha outcrop (Romualdo Formation) (M2AR 6.9, M2AR 6.8, M2AR 6.3, M2AR 6.2) are depleted in Al_2O_3, Na_2O, TiO_2, Cs, Sr, and V against PAAS and all the samples present slight enrichment in K_2O and high enrichment in MgO and Nd against the PAAS. (Tab. 6 and Fig. 27). On the western part of the Araripe Basin, the post-rift I stage samples M2AR 2.3 and M2AR 2.2 (Romualdo Formation) samples are enriched in CaO and MnO against the PAAS. The M2AR 2.3 is also enriched in P2O5. All other elements are depleted relative to PAAS. The post-rift II M2AR 1.3 (Araripina Formation) is depleted in SiO_2, Fe_2O_3, MgO, Rb, Cs, Ba, Sr, Y, Nb, V, Co, Cu, and Ni relative to PAAS. The M2AR 1.5 sample (Exu Formation) is enriched in SiO_2, TiO, P_2O_5, Sr, Zr, Nb, Hf, and Cr relative to PAAS (Tab. 6).

The CIA (Chemical Index of Alteration) is useful to indicate the degree of source-area weathering and the paleo-weathering conditions of ancient sediments (Nesbitt and Young 1982; Fedo *et al.* 1995). It is defined as CIA = $[Al_2O_3/(Al_2O_3+CaO^*+Na_2)+K_2O)]$ x 100 (in molar proportions), in which CaO* represents the CaO content in the silicate fraction. We do not have CO_2 data for our analyses and some samples have high carbonate content (e.g. M2AR 2.2, M2AR 2.3, M2AR 7.8 VII, and M2AR 7.8 XI), thus we cannot correct for Ca in carbonates to obtain CaO*. To calculate CaO*, we have assumed the value CaO = Na_2O if CaO>Na_2O

(Bock *et al.* 1998). CIA values for unaltered plagioclase and K-feldspars typical of unaltered upper crustal rocks are approximately equal to 50,

Tab. 6: Major and trace element concentrations of sedimentary rocks analyzed in this study. D.L.: Detection Limit.

Formation	Brejo Santo	Barbalha	Crato	Romualdo	Romualdo	Romualdo	Romualdo	Romualdo	Romualdo	Romualdo	Romualdo
Sample	M2AR 04-2	M2AR 9-1	M2AR 10.75 II	M2AR 6-9 BS	M2AR 6-8 BS	M2AR 6-3	M2AR 6-2	M2AR 7-8 XXII	M2AR 7-8 XI	M2AR 7-8 VIII BS	M2AR 7-8 VII
wt%											
SiO2	58.89	5.18	35.68	51.23	48.13	66.02	63.44	42.50	14.89	44.96	4.75
Al2O3	20.60	1.60	7.49	16.43	18.04	11.94	13.06	14.12	5.15	17.16	1.52
Fe2O3	7.82	5.35	5.97	6.69	8.74	2.57	4.16	6.34	3.87	8.06	2.60
MnO	D.L.	1.32	0.41	0.06	0.06	0.03	0.02	0.11	0.30	0.05	0.26
MgO	0.51	0.65	3.38	2.72	3.32	2.35	2.54	3.14	1.53	2.66	0.65
CaO	D.L.	37.67	20.01	2.51	1.17	1.60	1.52	10.07	35.30	0.91	45.01
Na2O	0.04	0.02	0.60	0.10	0.11	0.15	0.33	0.23	0.08	0.08	0.03
K2O	1.10	0.33	1.81	3.83	3.67	3.53	4.02	3.29	1.08	3.47	0.27
TiO2	1.72	0.08	0.28	0.85	0.95	0.45	0.57	0.75	0.26	0.88	0.08
P2O5	D.L.	0.58	0.13	0.20	0.23	0.12	0.17	0.13	0.15	0.28	0.11
LOI	9.29	41.15	23.70	15.10	15.76	11.14	10.38	18.90	34.15	21.28	36.72
Total	99.98	93.93	99.47	99.71	100.17	99.90	100.21	99.56	96.75	99.80	91.98
Al/Si	0.40	0.35	0.24	0.36	0.42	0.21	0.23	0.38	0.39	0.43	0.36
CIA	95	81	71	80	82	76	74	79	81	83	83
ppm											
Sc	28.88	2.05	6.20	14.88	19.08	7.04	8.76	14.61	6.15	18.12	2.30
Rb	56.34	11.66	58.26	176.89	200.14	114.78	143.04	145.19	46.18	200.04	11.25
Cs	4.78	0.59	1.12	5.63	7.63	2.31	3.18	5.47	1.75	7.94	0.41
Ba	157.64	71.22	509.57	828.06	604.04	869.48	999.90	573.63	151.79	638.78	20176.39
Sr	27.15	227.84	251.25	101.38	100.51	135.72	187.37	151.35	239.30	73.77	725.52
Th	8.26	2.06	5.52	22.32	28.35	7.17	10.74	16.24	6.19	25.83	1.63
U	1.83	1.71	1.52	3.73	5.65	1.81	2.33	3.07	3.29	8.89	2.54
Y	26.61	31.55	48.02	28.71	40.76	18.64	20.03	28.84	13.60	32.63	7.90
Zr	252.69	21.93	122.24	193.75	162.34	275.35	338.11	159.00	62.02	111.07	20.87
Nb	23.36	26.09	51.48	55.63	74.50	21.95	30.36	43.78	19.52	66.21	9.59

Hf	6.98	0.53	3.22	5.25	4.43	6.87	8.70	4.43	1.64	3.13	0.52
Cr	171.44	12.84	31.95	87.58	122.15	73.56	44.52	86.96	46.45	103.87	10.05
V	224.68	167.79	25.58	65.88	101.97	38.86	38.48	77.33	71.00	159.70	106.56
Co	14.86	27.67	20.22	14.78	21.70	7.24	26.67	22.06	7.58	38.91	9.79
Cu	24.40	150.73	9.40	33.27	65.23	16.95	9.05	46.66	43.50	147.60	19.30
Ni	13.56	33.00	14.57	37.67	63.22	17.84	16.57	39.27	25.52	37.75	12.31
Zn	35.71	6599.50	1414.78	96.85	196.92	39.32	43.69	100.88	42.78	139.60	45.87
La	27.51	25.99	60.22	73.55	97.84	24.22	34.60	55.02	28.13	79.34	18.20
Ce	47.80	59.31	171.95	139.88	188.71	50.58	68.04	106.89	55.10	152.88	27.25
Pr	6.10	6.43	13.63	15.80	20.96	5.81	8.04	12.05	5.43	18.23	2.83
Nd	23.36	26.09	51.48	55.63	74.50	21.95	30.36	43.78	19.52	66.21	9.59
Sm	4.58	5.07	10.34	9.42	13.01	4.25	5.72	8.00	3.52	11.42	1.59
Eu	1.21	1.21	2.11	1.71	2.30	0.93	1.25	1.53	0.67	1.93	0.63
Gd	4.30	5.40	9.28	7.00	9.87	3.41	4.57	6.35	2.77	8.27	1.35
Tb	0.71	0.77	1.49	0.98	1.39	0.52	0.66	0.94	0.41	1.15	0.20
Dy	4.66	4.44	9.15	5.53	7.86	3.30	3.92	5.49	2.44	6.46	1.23
Ho	1.03	0.90	1.87	1.10	1.52	0.72	0.78	1.10	0.50	1.23	0.26
Er	2.89	2.13	4.98	2.86	3.87	2.04	2.10	2.86	1.40	3.19	0.74
Tm	0.45	0.26	0.73	0.43	0.56	0.32	0.32	0.43	0.22	0.46	0.11
Yb	2.99	1.42	4.52	2.71	3.49	2.09	2.12	2.66	1.48	2.87	0.74
Lu	0.45	0.21	0.67	0.41	0.51	0.32	0.32	0.40	0.23	0.42	0.12
Ta	1.26	0.14	0.61	1.68	1.85	1.14	1.24	1.30	0.44	1.67	0.14
Sm/Nd	0.20	0.19	0.20	0.17	0.17	0.19	0.19	0.18	0.18	0.17	0.17
Eu/Eu*	0.83	0.71	0.66	0.64	0.62	0.74	0.75	0.66	0.65	0.61	1.31
ΩCe	0.89	1.10	1.45	0.99	1.00	1.03	0.98	1.00	1.07	0.97	0.90
Cr/Th	12.64	0.39	2.19	3.92	4.31	10.27	2.69	5.35	7.50	4.02	6.15
Th/Cr	0.05	0.16	0.17	0.25	0.23	0.10	0.24	0.19	0.13	0.25	0.16
Th/Sc	0.29	1.01	0.89	1.50	1.49	1.02	1.23	1.11	1.01	1.43	0.71
Zr/Sc	11.91	11.91	11.91	13.02	8.51	39.11	11.91	10.88	10.08	6.13	9.07
LREE	1.84	1.92	4.07	4.70	6.26	1.70	2.38	3.59	1.69	5.35	0.94
HREE	3.02	1.54	4.66	2.78	3.57	2.14	2.15	2.73	1.49	2.93	0.76
MREE	2.39	2.59	4.92	3.29	4.67	1.77	2.24	3.14	1.37	3.87	0.68
MREE*	2.43	1.73	4.37	3.74	4.91	1.92	2.26	3.16	1.59	4.14	0.85

Formation	Romualdo	Romualdo	Romualdo	Romualdo	Romualdo	Romualdo	Araripina	Exu
Sample	**M2AR 7-6**	**M2AR 7-5**	**M2AR 7-4**	**M2AR 7-3**	**M2AR 2-3**	**M2AR 2-2**	**M2AR 1-3**	**M2AR 1-5**
wt%								
SiO2	50.58	13.22	68.65	57.89	1.59	3.43	56.13	76.55
Al2O3	16.72	1.14	12.64	15.96	0.53	0.87	26.44	12.00
Fe2O3	8.17	38.31	4.53	5.86	0.73	0.39	5.37	2.14
MnO	0.05	D.L.	0.03	0.03	0.32	0.23	D.L.	D.L.
MgO	3.95	0.10	2.08	2.51	0.35	0.36	0.06	0.13
CaO	0.99	7.14	0.66	0.84	53.89	54.01	D.L.	0.08
Na2O	0.16	0.09	0.39	0.16	D.L.	D.L.	D.L.	0.35
K2O	3.91	0.53	2.98	3.18	0.10	0.20	D.L.	0.21
TiO2	0.93	0.03	0.74	0.95	0.02	0.05	1.04	0.78
P2O5	0.17	D.L.	0.14	D.L.	0.26	0.11	D.L.	0.23
LOI	14.84	34.12	7.80	12.68	42.55	40.82	10.72	6.61
Total	100.48	94.68	100.64	100.06	100.33	100.46	99.76	99.07
Al/Si	0.37	0.10	0.21	0.31	0.38	0.29	0.53	0.18
CIA	80	61	77	82				93
ppm								
Sc	16.83	D.L.	11.42	16.34	1.60	0.88	17.51	10.46
Rb	189.86	13.29	105.74	132.25	5.05	9.26	3.08	7.80
Cs	6.94	0.17	3.12	4.49	0.18	0.29	0.29	0.20
Ba	551.78	201.33	493.38	407.21	54.67	120.70	114.58	458.32
Sr	147.42	146.23	93.31	82.09	168.81	135.99	52.11	468.78
Th	25.92	0.39	12.99	16.49	0.51	1.69	21.17	12.99
U	5.04	0.37	2.89	3.60	2.12	0.80	3.42	2.42
Y	30.29	1.02	26.21	24.39	5.17	4.46	5.71	25.35
Zr	144.57	25.10	336.08	271.03	6.90	14.56	483.49	355.95
Nb	65.11	1.59	31.14	34.02	3.57	4.96	6.22	170.01
Hf	3.98	0.43	8.49	7.04	0.14	0.36	11.83	9.07
Cr	95.56	2.95	102.64	80.86	11.36	6.55	256.47	129.79
V	91.03	56.21	61.62	90.34	51.04	34.27	76.66	34.13
Co	27.73	22.48	12.47	34.08	3.31	10.27	1.36	3.02

Cu	55.93	11.74	26.74	43.94	45.23	21.68	22.58	18.65
Ni	45.83	54.01	26.57	38.74	14.20	6.07	11.24	17.79
Zn	139.24	446.26	64.72	69.20	22.91	22.35	10.06	24.67
La	87.11	1.70	36.82	43.56	8.78	7.64	21.01	71.11
Ce	168.00	3.68	74.58	81.39	10.73	11.47	32.59	330.51
Pr	18.43	0.42	8.35	9.38	1.01	1.33	2.45	34.36
Nd	65.11	1.59	31.14	34.02	3.57	4.96	6.22	170.01
Sm	10.87	0.34	5.95	6.42	0.58	0.87	0.83	31.58
Eu	2.09	0.09	1.26	1.36	0.13	0.16	0.19	5.27
Gd	7.98	0.24	4.98	5.11	0.59	0.76	0.75	15.04
Tb	1.09	0.04	0.76	0.78	0.09	0.11	0.14	1.66
Dy	6.05	0.20	4.61	4.65	0.59	0.67	0.96	7.33
Ho	1.17	0.04	0.96	0.94	0.14	0.14	0.21	1.17
Er	2.98	0.10	2.65	2.60	0.44	0.40	0.63	2.82
Tm	0.43	0.02	0.41	0.39	0.07	0.06	0.10	0.40
Yb	2.67	0.10	2.70	2.58	0.54	0.38	0.79	2.66
Lu	0.40	0.02	0.42	0.40	0.09	0.06	0.12	0.41
Ta	1.72	0.07	1.11	1.48	0.04	0.10	2.18	1.35
Sm/Nd	0.17	0.21	0.19	0.19	0.16	0.17	0.13	0.19
Eu/Eu*	0.69	0.98	0.71	0.72	0.66	0.60	0.74	0.74
ΩCe	1.01	1.05	1.02	0.97	0.82	0.86	1.04	1.50
Cr/Th	2.09	7.62	7.90	2.09	0.80	1.08	22.81	7.29
Th/Cr	0.27	0.13	0.13	0.20	0.04	0.26	0.08	0.10
Th/Sc	1.54		1.14	1.01	0.32	1.92	1.21	1.24
Zr/Sc	11.91		29.43	11.91	11.91	11.91	11.91	11.91
LREE	5.52	0.12	2.48	2.81	0.39	0.44	0.88	9.54
HREE	2.76	0.10	2.76	2.63	0.55	0.40	0.76	2.71
MREE	3.68	0.12	2.54	2.59	0.31	0.37	0.46	5.73
MREE*	4.14	0.11	2.62	2.72	0.47	0.42	0.82	6.12

Note: Uncertainties for all elements are given in the supplementary material
LREE = LaPAAS + PrPAAS + NdPAAS (in ppm); MREE = GdPAAS + TbPAAS + DyPAAS (in ppm);
HREE = TmPAAS + YbPAAS + LuPAAS (in ppm); MREE* = (HREE+LREE) / 2;
CIA=[Al2O3/(Al2O3+CaO*+Na2O+K2O)] ×100 (in molar proportions); Eu/Eu* = EuN/(SmN × GdN)1/2 where XN refers to the chondrite-normalized concentration value [Condie, 1993];
ΩCe = 2 x (Cesample/CePAAS) / [(Lasample/LaPAAS) + (Prsample/PrPAAS)]

whereas higher CIA values represent higher degrees of weathering. For comparison, the CIA value of the PAAS standard, which is representative of the upper continental crust composition is equal to 67 (Taylor and McLennan 1985). The grain-size sorting effect can be evaluated using the Al/Si ratio as it can be considered a proxy for sediment grain size (Bouchez *et al.* 2011a). The sedimentary sorting effect favors heavy mineral concentrations such as zircon and quartz dilution in the coarser fraction, which could modify the trace element ratios used as provenance proxies (McLennan et al., 1993; Roddaz et al., 2014).

On the eastern part of the Araripe Basin, the calculated CIA value from the rift beginning sample (M2AR 4-2, Brejo Santo Formation) is 95, therefore it is higher than the unaltered plagioclase and K-feldspars typical of unaltered upper crustal rocks and then those of the PAAS. The calculated CIA values for the post-rift I stage (M2AR 9-1 (Barbalha Formation); M2AR 10.75II (Crato Formation); M2AR 6-9, M2AR 6-8, M2AR 6-3, 6-2 (Romualdo Formation), M2AR 7-8 XXII, 7-8 M2AR XI, M2AR 7-8 VIII, M2AR 7-8 VII, M2AR 7-6, M2AR 7-5, M2AR 7-4, M2AR 7-3 (Romualdo Formation) range from 61 to 83. On the western side, the post-rift II stage sample (M2AR 1-5 – Exu Formation) has 93 as the CIA value. However, we are unable to calculate CIA values for some following samples. M2AR 1.3 (Araripina Formation), M2AR 2.2, and M2AR 2.3 (Romualdo Formation) have concentrations below the detection limit. (Tab. 6).

The rift beginning sample M2AR 4-2 (Brejo Santo Formation) has a higher Al/Si ratio (0.40). The post-rift I stage samples (M2AR 9-1 (Barbalha Formation); M2AR 10.75II (Crato Formation); M2AR 6-9, M2AR 6-8, M2AR 6-3, 6-2 (Romualdo Formation), M2AR 7-8 XXII, 7-8 M2AR XI, M2AR 7-8 VIII, M2AR 7-8 VII, M2AR 7-6, M2AR 7-5, M2AR 7-4, M2AR 7-3 (Romualdo Formation) have Al/Si ratio between 0.10

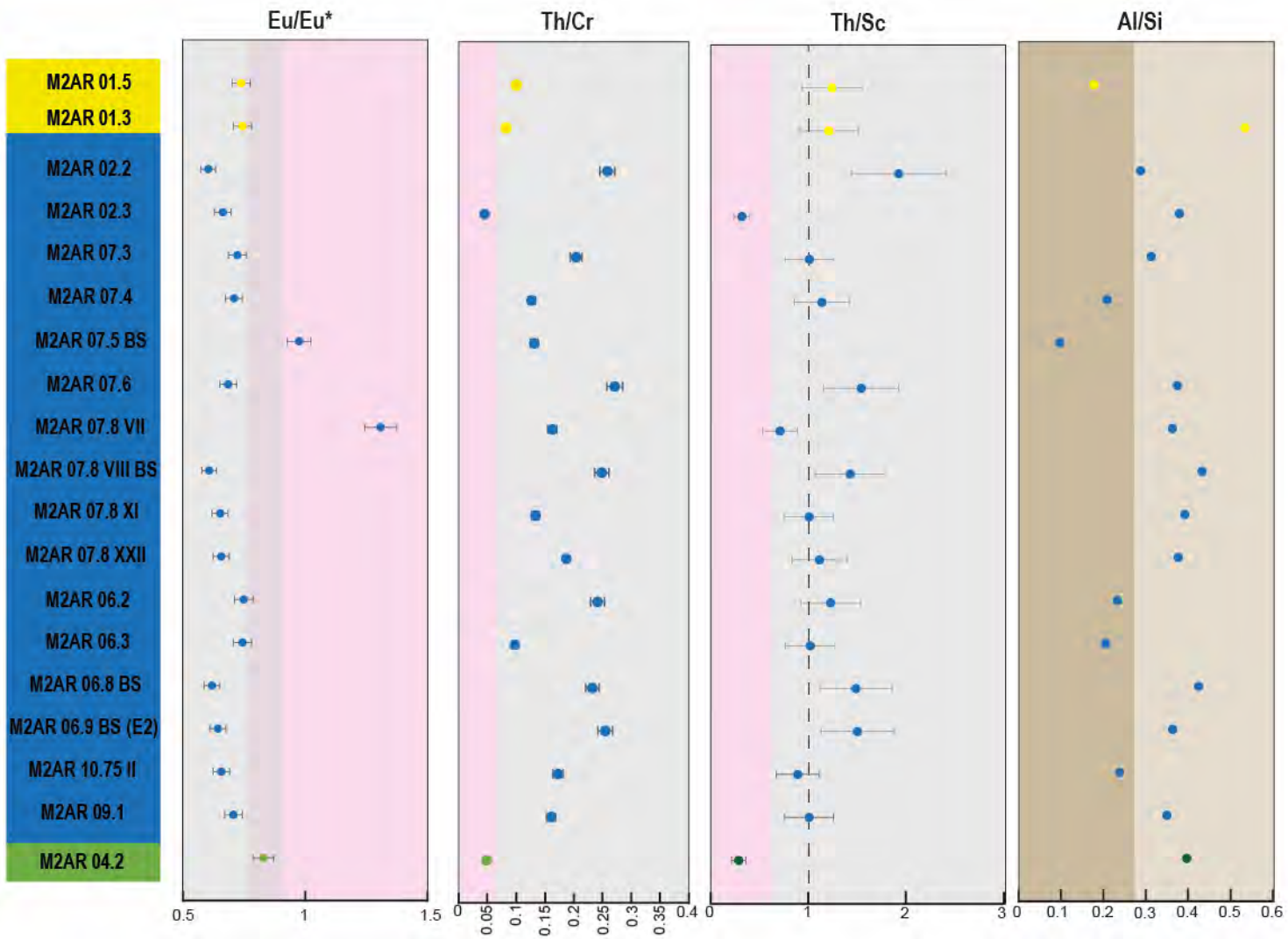

Fig. 27: Selected trace element ratios (Eu/Eu*, Th /Cr; Th/Sc and, Al/Si see text for details) of analyzed samples (green points -Rift stage; blue points – Post-rift I stage; yellow points – Post-rift II stage. The horizontal bars for the Eu/Eu*, Th/Cr, and Th/Sc, ratios correspond to 5% (i.e., the Eu concentration analytical error, see supplementary material), 15% (i.e., the sum of the Cr and Th concentration analytical errors), and 25% (i.e., the sum of the Th and Sc concentration analytical errors) Pink and blue rectangles indicate the values range for basic and felsic sediments, respectively (Cullers, 2000).

and 0.43. On the western side, the post-rift I stage samples of Romualdo Formation (M2AR 2-2 and M2AR 2-3) have 0.29 and 0.38 Al/Si ratio values, respectively. The post-rift II stage samples M2AR 1.3 (Araripina Formation) has 0.53, and M2AR 1.5 (Exu Formation) has 0.18 Al/Si ratios values.

3.5.2 Rare Earth Elements (REE)

The Eu anomaly was calculated relative to chondrites: $Eu/Eu^* = Eu_N/(Sm_N \times Gd_N)^{½}$, where N refers to the chondrite-normalized concentration value (Condie 1993). This parameter facilitates comparisons between sediments derived from basic or felsic sources (Cullers 2000a) and the PAAS (Taylor and McLennan 1985; Pourmand *et al.* 2012). For instance, low Eu/Eu* ratios (0.3 to 0.94) (Figure 27), and high Th/Sc (> 0.64) are characteristic of felsic and silicic source rocks in fine-grained sedimentary protoliths, whereas higher Eu/Eu* ratios (0.71 - 1.02) and lower Th/Sc (<0.4) of fine-grained sedimentary rocks indicate more mafic and less differentiated source rocks (Cullers, 2000; McLennan et al., 1990). The Cerium anomaly (ΩCe) normalized to PAAS is calculated following (De Baar *et al.* 1985a): $\Omega Ce = 2 \times (Ce_{sample}/Ce_{PAAS})/[(La_{sample}/La_{PAAS}) + (Pr_{sample}/Pr_{PAAS})]$, where X_{sample} is the concentration of samples and X_{PAAS} refers to the concentration of the PAAS standard.

When normalized against PAAS, most of the analyzed samples have relatively flat REE patterns, variable Eu anomalies, and slight enrichment in HREE. The exceptions are two samples: the post-rift I stage sample M2AR 2.3 (Romualdo Formation), which presents decreasing LREE, variable Eu anomalies, and increasing HREE; and the post-rift II stage sample M2AR 1.5 (Exu Formation), which presents enrichment in LREE (Fig. 28). The Ce anomalies of the rift beginning stage (M2AR 4-2 – Brejo Santo Formation) have value 0.89. The post-rift stage samples (M2AR 9-1 – Barbalha Formation; M2AR 10.75II – Crato Formation; M2AR 6-9, M2AR 6-8, M2AR 6-3, 6-2, M2AR 7-8 XXII, 7-8 M2AR XI, M2AR 7-8 VIII, M2AR 7-8 VII, M2AR 7-6, M2AR

7-5, M2AR 7-4, M2AR 7-3, and M2AR 2-3 – Romualdo Formation) display a range of values between 0.82 and 1.45, close to that of the PAAS (i.e., ΩCe = 1). The post-rift II stage sample M2AR 1-3 (Araripina Formation) has ΩCe value near to that of the PAAS (1.04) however the post-rift II sample M2AR 1-5 (Exu Formation) has ΩCe much higher than PAAS (1.50) (Tab. 6). All the analyzed values are systematically higher than those measured in authigenic smectites and seawater (Ωe < 0.50) (De Baar *et al.* 1985a) and they do not show any variation with the stratigraphic position. The Eu/Eu* ratios of the rift beginning stage analyzed sample (M2AR 4-2 – Bejo Santo Formation) has 0.80; the post-rift I stage samples (M2AR 9-1 – Barbalha Formation; M2AR 10.75II – Crato Formation; M2AR 6-9, M2AR 6-8, M2AR 6-3, 6-2, M2AR 7-8 XXII, 7-8 M2AR XI, M2AR 7-8 VIII, M2AR 7-8 VII, M2AR 7-6, M2AR 7-5, M2AR 7-4, M2AR 7-3, and M2AR 2-3 – Romualdo Formation) range between 0.60 and 1.31, and the post-rift II stage samples M2AR 1-3 (Araripina Formation) and M2AR 1-5 (Exu Formation) have 0.74 value, higher than that of the PAAS (i.e., Eu/Eu* = 0.58) (Tab. 6 and Fig. 27). The Cr/Th ratio value of the rift stage sample M2AR 4-2 (Brejo Santo Formation) is 12.6; post-rift I stage samples: M2AR 9-1 (Barbalha Formation) is 0.4; M2AR 10.75II (Crato Formation) is 2.2; M2AR 6-9, M2AR 6-8, M2AR 6-3, 6-2, M2AR 7-8 XXII, 7-8 M2AR XI, M2AR 7-8 VIII, M2AR 7-8 VII, M2AR 7-6, M2AR 7-5, M2AR 7-4, M2AR 7-3, M2AR 2-2 and M2AR 2-3 (Romualdo Formation) range from 0.8 to 10.3; and the post-rift II stage samples M2AR 1-3 (Araripina Formation) and M2AR 1-5 (Exu Formation) are 22.81 and 7.29, respectively. The Th/Sc ratio value of the rift beginning stage sample M2AR 4-2 (Brejo Santo Formation) is 0.29; the post-rift I stage samples: M2AR 9-1 (Barbalha Formation) is 1.01; M2AR 10.75II (Crato Formation) is 0.89; M2AR 6-9, M2AR 6-8, M2AR 6-3, 6-2, M2AR 7-8 XXII, 7-8 M2AR XI, M2AR 7-8 VIII, M2AR 7-8 VII, M2AR 7-6, M2AR 7-5, M2AR 7-4, M2AR 7-3, M2AR 2-2 and M2AR 2-3 (Romualdo

Formation) range from 0.32 to 1.92; and the post-rift II stage samples M2AR 1-3 (Araripina Formation) and M2AR 1-5 (Exu Formation) are 1.21 and 1.24, respectively.

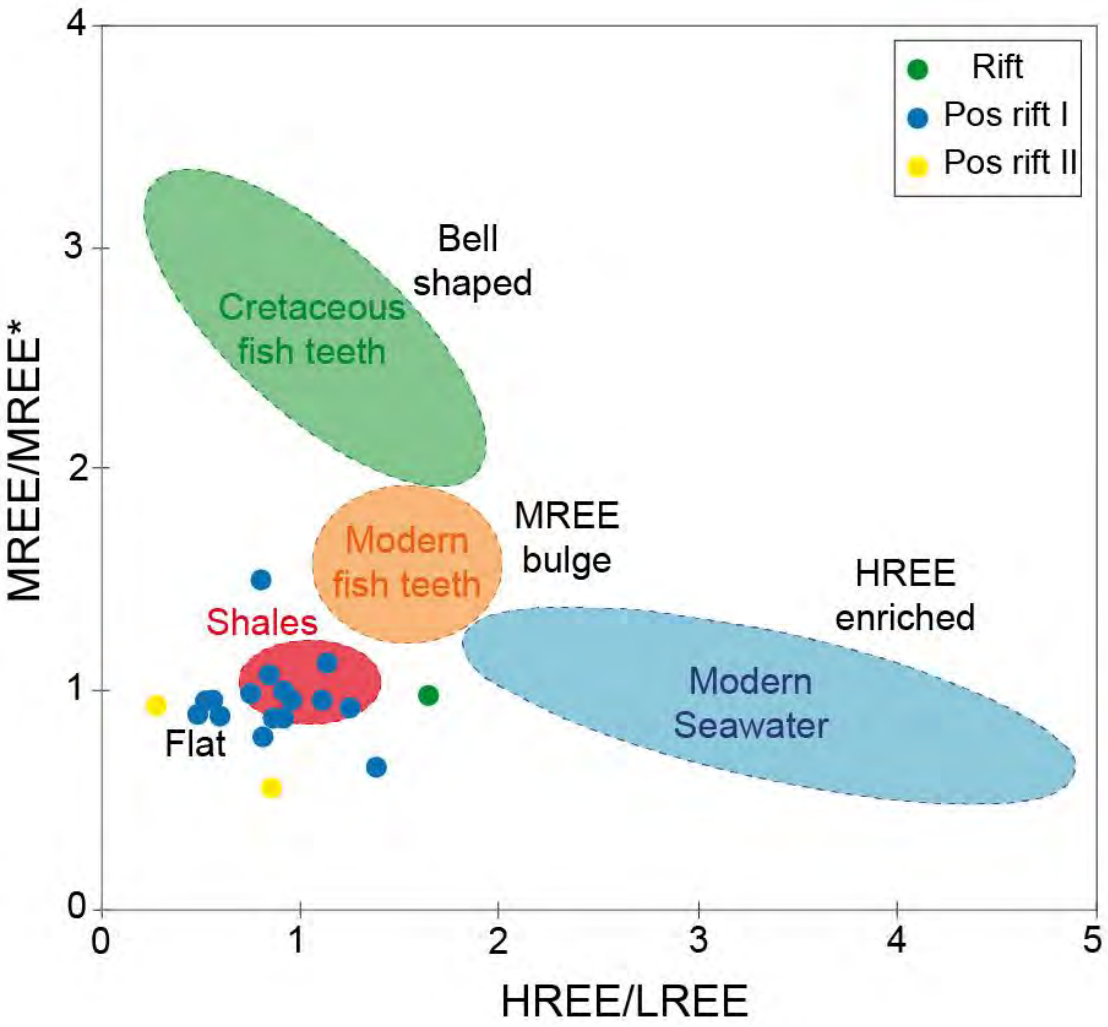

Fig. 28: HREE/LREE vs. MREE/MREE* diagram. HREE/LREE and MREE/MREE* values are calculated following (Martin et al., 2010), where HREE = Tm + Yb + Lu, LREE = La + Pr + Nd, MREE = Gd + Tb + Dy (all PAAS normalized), and MREE* = the average of HREE+LREE. The MREE bulge and "bell-shaped" REE profiles correspond to REE patterns observed in fish teeth, Fe-Mn oxides, organic matter, and pore waters, while "HREE-enriched" profiles correspond to modern seawater (Huck et al., 2016; Moiroud et al., 2016). These end-members reflect the REE contents of marine sediments influenced by seawater or authigenic phases, while "flat" REE patterns are characteristic of continental clays (see Huck et al., 2016; Moiroud et al., 2016 for a review).

3.5.3 Sm-Nd isotopes

The Sm-Nd isotope compositions of early Cretaceous sedimentary rocks of the Araripe basin are presented in Tab. 7 and Fig. 29. The analyzed sample M2AR 4-2 (Bejo Santo Formation) from the rift beginning stage has the $^{147}Sm/^{144}Nd$ isotopic composition of 0.1173, with ε_{Nd} (0) value of -12.98, and ε_{Nd} (T) value of -11.6. The $T_{DM\ (0)}$ age is 1.68 Ga, and $T_{DM\ (*)}$ age is also 1.68 Ga. For the post-rift I stage, sample M2AR 9-1 (Barbalha Formation) has a $^{147}Sm/^{144}Nd$ isotopic composition value of 0.1154, with ε_{Nd} (0) value of -12.28, ε_{Nd} (T) value of -11.1, $T_{DM\ (0)}$ age of 1.59 Ga, and $T_{DM\ (*)}$ age from 1.63 Ga. In the post-rift I stage, sample M2AR 10.75 II (Crato Formation) has a $^{147}Sm/^{144}Nd$ isotopic composition value of 0.1176, with ε_{Nd} (0) value of –23.54, ε_{Nd} (T) value of –22.4, $T_{DM\ (0)}$ age of 2.55 Ga and $T_{DM\ (*)}$ age of 2.44 Ga. The $^{147}Sm/^{144}Nd$ isotopic composition of the post-rift I stage sample from Romualdo Formation (M2AR 6-2, M2AR 7-3, M2AR 7-6, and M2AR 2-3 range from 0.0985 to 0.1123, with ε_{Nd} (0) values from -16.42 to -23.57, and ε_{Nd} (T) values ranging from -11.8 to -22.2. $T_{DM\ (0)}$ ages have between 1.71 and 2.38 Ga and $T_{DM\ (*)}$ ages from 1.67 and 2.43 Ga.

Tab. 7: Sm-Nd systematics of analyzed sedimentary rocks from Araripe Basin.
Ages and the ℰNd (T) values samples were calculated based on stratigraphic ages from Assine (2007) and Fambrini et al. (2020). For Abaiara Formation we used 140 Ma; For Barbalha Formation, 119 Ma; For Romualdo Formation, 113 Ma; For Araripina Formation, 110 and For Exu Formation, 100Ma.

	Sample	Formation	Age	Longitude (W)	Latitude (S)	Sm (ppm)	Nd (ppm)	$^{147}Sm/^{144}Nd$	$^{143}Nd/^{144}Nd$	±2σ (10^{-6})	$e_{Nd\ (0)}$	$e_{Nd\ (T)}$	TDM (Ga)	TDM* (Ga)
1	**M2AR 04.2**	**Brejo Santo**	Jurassic	-39.006662°	-7.464279°	4.611	23.760	0.1173	0.511973	±18	-12.98	-11.6	1.68	1.68
2	**M2AR 09.1**	**Barbalha**	Aptian	-39.441840°	-7.233942°	5.119	26.808	0.1154	0.512008	±16	-12.28	-11.1	1.59	1.63
3	**M2AR 10.75 II**	**Crato**	Aptian	-39.697751°	-7.116543°	9.796	50.356	0.1176	0.511431	±3	-23.54	-22.4	2.55	2.44
4	**M2AR 02.3**	**Romualdo**	Aptian	-40.523850°	-7.579407°	0.821	4.811	0.1031	0.511796	±33	-16.42	-15.1	1.71	1.91
5	**M2AR 06.2**	**Romualdo**	Aptian	-39.099204°	-7.362335°	5.957	32.205	0.1118	0.511973	±5	-12.97	-11.8	1.60	1.67
6	**M2AR 07.3**	**Romualdo**	Aptian	-39.163636°	-7.573472°	6.512	35.054	0.1123	0.511640	±6	-19.47	-18.3	2.10	2.14
7	**M2AR 07.6**	**Romualdo**	Aptian	-39.163529°	-7.571304°	11.091	68.069	0.0985	0.511430	±6	-23.57	-22.2	2.12	2.43
8	**M2AR 01.3**	**Araripina**	Albian-Cenomanian	-40.652910°	-7.365121°	0.834	6.518	0.0774	0.511422	±13	-23.72	-22.1	1.80	2.42
9	**M2AR 01.5**	**Exu**	Albian-Cenomanian	-40.652910°	-7.365121°	34.019	189.053	0.1088	0.511673	±16	-18.82	-17.7	1.98	2.09

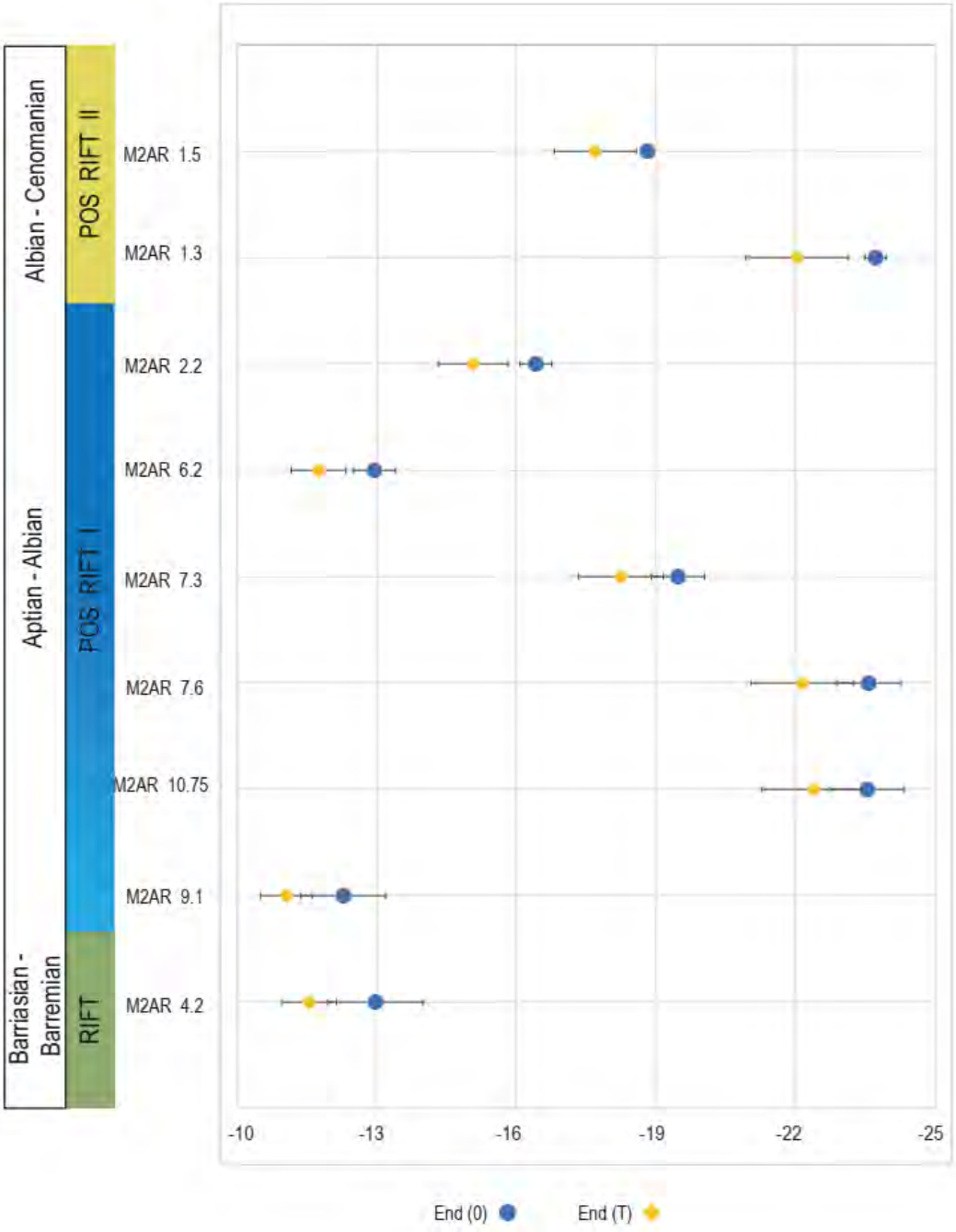

Fig. 29: Stratigraphic variation of the Nd isotope composition (expressed as ƐNd(0) for the blue points, and ƐNd(T) for the yellow points). The lengths of the horizontal bar for the Sr-Nd isotopic compositions correspond to 2σ analytical errors (see Table 4)

3.5.4 U-Pb detrital zircon

TableTab. 8 and Fig. 30 present the U-Pb zircon ages obtained across the Cretaceous successions of the Araripe Basin. The rift beginning stage analyzed sample, M2AR 4-1 (Brejo Santo Formation), presents two dominant peaks, the first indicates Cryogenian-Ediacaran (720 – 541 Ma) zircon ages (28%), and the second presents Rhyacian – Orosirian (2.3 – 1.6 Ga) U-Pb ages (25%). Subordinately, there are 18% of Stenian – Tonian (1.2 – 0.7 Ga); 13 % of Calymmian – Ectasian (1.6 – 1.2 Ga); 7% of Archean (3.6 – 2.5 Ga); 6% of Paleozoic (< 485 Ma); and 2% of Siderian (2.5 - 2.3 Ga) age zircon grains. The rift stage sample, M2AR 5-1 (Abaiara Formation), has one peak of Cryogenian-Ediacaran (720 – 541 Ma) zircon ages (35%) one of Rhyacian – Orosirian (2.3 – 1.6 Ga) (29%), and one peak of Stenian – Tonian (1.2 – 0.7 Ga) U-Pb ages (20%). There are still 10% of Paleozoic (< 541 Ma); Calymmian – Ectasian (1.6 – 1.2 Ga) grains (3%); and Archean (3.6 – 2.5 Ga) grains (2%).

The post-rift I stage samples of Barbalha Formation (M2AR 8-1 and M2AR 11-1) have two age peaks of Cryogenian-Ediacaran (720 – 541 Ma) U-Pb ages (46% and 22%, respectively) and Rhyacian – Orosirian (2.3 – 1.6 Ga) ages (21% and 24% respectively). However, the sample M2AR 11-1 presents a dominant peak of Statherian (1.8 – 1.6 Ga) (41%), which is absent in M2AR 8-1. The M2AR 8-1 has 1% of Statherian (1.8 – 1.6 Ga) and 6% of Calymmian – Ectasian (1.6 – 1.2 Ga) grains, which are absent in M2AR 11-1. The percentage of Stenian – Tonian (1.2 – 0.7 Ga) is 15 in M2AR 8-1 sample and 2 in M2AR 11-1, and Paleozoic grains (< 541 Ma) represent 7% in M2AR 8-1 and 4% in M2AR 11-1 sample. The Rhyacian – Orosirian (2.3 – 1.6 Ga) zircon ages represent 45% of the post-rift I sample M2AR 10I (Crato Formation). The Statherian (1.8 – 1.6 Ga) grains represent 32%; Cryogenian-Ediacaran (720 – 541 Ma) 8%; Siderian (1.8 – 1.6 Ga) 6%; Calymmian (1.6 – 1.4 Ga) 2% and Paleozoic grains (<541 Ma) 2%.

Tab. 8: Numbers and percentages (%) of U–Pb ages

Time (Ma)	Age	Rift beginning		Rift		Post-rift I		Post-rift II	
		number	%	number	%	number	%	number	%
145.0-100.5	Early Cretaceous					1	0.1%		
251.9-145.0	Jurassic/Triassic	1	0.5%	1	0.6%			1	0.4%
298.9-251.9	Devonian	1	0.5%						
358.9-298.9	Carboniferous	2	1.0%	1	0.6%	3	0.4%		
419.2-358.9	Devonian					1	0.1%		
443.8-419.2	Silurian	1	0.5%			2	0.3%		
485.4-443.8	Ordovician					3	0.4%	1	0.4%
541.0-485.4	Cambrian	2	1.0%	12	7.6%	17	2.2%	28	10.9%
635-541	Ediacaran	27	13.7%	31	19.5%	167	21.3%	105	41.0%
720-635	Cryogenian	16	8.1%	13	8.2%	47	6.0%	7	2.7%
1000-720	Tonian	6	3.0%	17	10.7%	31	3.9%	7	2.7%
1200-1000	Stenian	15	7.6%	17	10.7%	22	2.8%	2	0.8%
1400-1200	Ectasian	27	13.7%	4	2.5%	9	1.1%	2	0.8%
1600-1400	Calymmian	3	1.5%	1	0.6%	4	0.5%	1	0.4%
1800-1600	Statherian	9	4.6%	1	0.6%	141	18.0%	13	5.1%
2050-1800	Orosinian	34	17.3%	19	12.0%	73	9.3%	37	14.4%
2300-2050	Rhyacian	31	15.7%	29	18.2%	192	24.5%	32	12.5%
2500-2300	Siderian	5	2.5%	2	1.3%	12	1.5%	3	1.2%
2800-2500	Neoarchean	12	6.0%	10	6.3%	45	5.7%	13	5.1%
3200-2800	Mesoarchean			1	0.6%	3	0.4%	2	0.8%
3600-3200	Paleoarchean	5	2.5%			12	1.5%	2	0.8%
Total grains		**197**	100%	**159**	100%	**785**	100%	**256**	100%

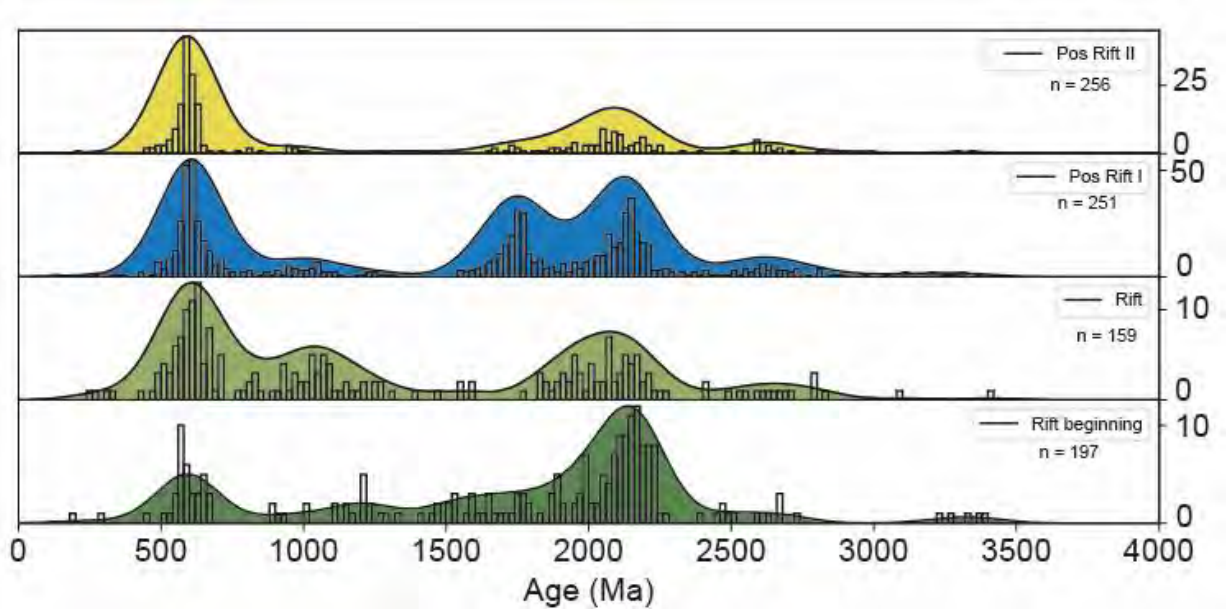

Fig. 30: Stage evolution of the U-Pb zircon age distribution of the Araripe Basin with the age probability (black line) and age histogram (bars).

The post-rift I samples of Romualdo Formation present one peak of Rhyacian – Orosirian (2.3 – 1.6 Ga) zircon ages, which represent 20 to 25%, one peak of Statherian (1.8 – 1.6 Ga) grains (7 to 26%), and one dominant peak of Cryogenian-Ediacaran (720 – 541 Ma) grains (38 to 52%). The M2AR 7-2 and M2AR 6-9 D samples have more significative Stenian – Tonian (1.2 – 0.7 Ga) grains (16% and 12%, respectively) than M2AR 7-5 (4%) and M2AR 6-1 (1%). The Paleozoic grains (<541 Ma) range between 7 and 2%, however in M2AR 6-1 samples this range of age is absent. The Archean (3.6 – 2.5 Ga) grains are present only in the samples M2AR 7-2 (6%) and M2AR 7-5 (7%).

The post-rift II stage is represented by Araripina Formation (M2AR 1-3) and the Exu Formation samples (M2AR 1-4). In the M2AR 1-3 there is a dominant peak of Cryogenian-Ediacaran (720 – 541 Ma) ages which represent 85% of the grains and subordinately, Paleozoic (<541 Ma) grains represent 15%. In the Exu Formation sample, the Statherian (1.8 - 1.6 Ga) grains represent 11%; the Rhyacian – Orosirian (2.3 – 1.6 Ga) 10%; and the dominant peak is represented by Cambrian (541 – 485

Ma) grains with 17%. Cryogenian-Ediacaran (720 – 541 Ma) grains are 10%, Stenian – Tonian (1.2 – 0.7 Ga) 4%, and Calymmian – Ectasian (1.6 – 1.2 Ga) 2%.

Even if the upper and lower intercept ages of the samples do not show realistic values, the grains with discordance ages present common characteristics in all of the analyzed samples. The rift beginning sample M2AR 4-1 (Brejo Santo Formation) and the rift sample M2AR 5-1 (Abaiara Formation) show discordant grains with upper intercepts between 2.0 and 2.4 Ga and lower intercepts around 0.48 Ga (Fig. S3 in supplementary data). The post-rift I sample M2AR 8-1 and M2AR 11-1 from Barbalha Formation have upper intercepts from 1.9 and 2.0 Ga and lower intercepts around 0.3 and 0.19 Ga, respectively (Fig. S3 in supplementary data). The M2AR 10I (Crato Formation) sample has an upper intercept of 2.1 Ga and a lower intercept of 0.3 Ga. The post-rift I samples of Romualdo Formation (M2AR 6-9D; 6-1; 7-5 and 7-2) present an upper intercept between 2.1 and 2.2 Ga and a lower intercept around 0.5 Ga, except M2AR 7-2 which have 0.4 Ga (Fig. S3 in supplementary data). The post-rift II M2AR 1-4 sample from Exu Formation has 2.3 Ga in the upper intercept and 0.48 Ga in the lower intercept (Fig. S3 in supplementary data).

3.6 Discussion

Geochemical traces like Eu anomalies expressed as Eu/Eu*, elemental ratios (Cr/Th, Th/Sc, Zr/Sc), and Sm-Nd isotopic compositions of sedimentary rock have proven to be useful tools for determining the provenance of ancient sediments (McLennan *et al.* 1993). For instance, low Eu/Eu* ratios (0.3 to 0.94), high Th/Sc (> 0.64), and low Cr/Th (< 15) of fine-grained sedimentary rocks are characteristic of felsic and silicic source rocks, whereas higher Eu/Eu* ratios (0.71 - 1.02), higher Cr/Th (> 22), and lower Th/Sc (<0.4) of fine-grained sedimentary rocks suggest more mafic and less differentiated source rocks (McLennan *et al.* 1993; Cullers 2000b). However, before determining the provenance of the analyzed sedimentary rocks, it is important

to evaluate the effects of grain-size sorting and diagenesis, on trace element ratios, and REE concentration of the analyzed sedimentary rocks.

The grain-size sorting effect can be evaluated using the Al/Si ratio as it can be considered as a proxy for sediment grain size (Bouchez *et al.* 2011a). The sedimentary sorting effect favors the concentration of quartz and heavy minerals like zircon in the coarser fraction (McLennan et al., 1993; Roddaz et al., 2014). The samples M2AR 4-2; M2AR 6.8BS; M2AR 6-9BS; M2AR 7-3; M2AR 7-6; M2AR 7.8VII; M2AR 7-8VIII; M2AR 7-8XI; M2AR 7-8 XXII; M2AR 2-2; M2AR 2-3; M2AR 1-3, and M2AR 9-1 have high Al/Si ratio (0.29 - 0.53) (Tab. 6, Fig. 27), suggesting a high concentration of fine and clay-rich sediments (Bouchez *et al.* 2011b). The samples M2AR 7-7; M2AR 6-3; M2AR 7-5BS; M2AR 7-4; M2AR 1-5; M2AR 6-2; and M2AR 10-75II have low Al/Si ratios (0.10 – 0.24), suggesting that these samples are enriched in quartz. There is no correlation of the Al/Si ratio with the REE content, Eu/Eu*, Cr/Th, Th/Sc, and ε_{Nd} (0) (see Table S1 in the supplementary dataset), which indicates that sedimentary sorting has not modified these provenances proxies.

Diagenesis can promote the remobilization of Eu under reducing conditions (MacRae *et al.* 1992). These processes can modify the REE patterns, the Eu,/Eu*, and Cr/Th ratios (Tribovillard *et al.* 1996). Compared to PAAS, authigenic smectites formed in deep-water environments are characterized by LREE depletion, HREE enrichment, and strong negative Ce anomalies (ΩCe < 0.50, De Baar *et al.* 1985). Most samples from the Araripe Basin, mainly the post-rift Isamples (M2AR 6.8BS; M2AR 6-9BS; M2AR 7-3; M2AR 7-6; M2AR 7.8VII; M2AR 7-8VIII; M2AR 7-8XI; M2AR 7-8 XXII; and M2AR 2-2;) have Ce anomalies (ΩCe) higher than 0.80 (Tab. 7) indicating that authigenic smectites were not incorporated during the early diagenetic process. These samples have flat REE patterns against PAAS corresponding to the “shales” field (Fig. 28), typical of continental clays (see Moiroud *et al.* 2016), and hence are not influenced

by authigenesis. The sample M2AR 4-2 from the rift phase, and the sample M2AR 2-3 from the post-rift I phase are enriched in HREE over LREE and plotted between the “shales” and “seawater” fields (Fig. 28). They both have ΩCe>0.80 suggesting that the formation of authigenic smectites if occurred, was a minor process. The low Eu/Eu* ratios values suggest that the diagenetic remobilization of Eu under reducing conditions was negligible in the analyzed samples.

In the rift phase, the sample M2AR 4-2 presents low Th/Sc values (0.3), low Th/Cr (0.05), and high Eu/Eu* ratios (0.8), which suggest trace elements ratios typical of “basic” source sediments (Tab. 6, Fig. 27). Whereas in the “Post-rift I” and ”Post-rift II” phases all the samples show felsic and silicic parameters. Three samples (M2AR 4-2, 7-5, and 7-8 VII) present high Eu/Eu* ratios (0.8-1.3). The positive Eu anomaly in the post-rift I phase (M2AR 7-5, and 7-8 VII) could be explained by the remobilization of Eu under reducing conditions, as suggested by geochemical and paleontological proxies onto the Romualdo Formation (i. e. Sobradinho section in (Bom *et al.* 2021) in the paleo-redox environnemental situation (Tyson and Pearson 1991; MacRae *et al.* 1992; Rivera *et al.* 2018). The low Eu/Eu* ratios values suggest that the diagenetic remobilization of Eu under reducing conditions was negligible in the rest of the analyzed samples.

The REE concentrations of the post-rift II analyzed samples (M2AR 1-3 and M2AR 1-5) against PAAS show contrasting patterns. The samples plot outside of the shale field suggesting that the REE concentrations have been perturbed by post-depositional processes (Fig. 28). The M2AR 1-5 shows a strong enrichment in HREE (Fig. 28) that could be associated with a primary phase of the pedologic process. In a study of the lateritic process in a tropical environment, (Viers and Wasserburg 2004) indicated that the Zr dispersion could elevate the HREE concentrations at the early stage of the weathering process, and the Zr could remove the REE during that phase

explaining the HREE enrichment, for the sample. Finally, the trace element signatures of concordant and discordant zircon from Araripe Basin analyzed samples show similar characteristics (Fig. S4 in supplementary data). Most grains are plotted in continental arc provenance, which suggests the majority contribution of ancient continental crust. However, some grains, generally from Ediacarian (0.63 – 0.54 Ga), Calymmian (1.6 – 1.4 Ga), and Rhyacian (2.3 - 2.0 Ga) ages, plotted in mid-ocean ridge provenance (Fig. S4 in supplementary data), which suggest some juvenile contribution.

3.6.1 Provenance interpretations

The εNd (0) values (-12.3 to -23.7) together with the T_{DM} ages (1.68 to 2.55 Ga) suggest an old crustal source for all the sedimentary rocks analyzed in the Araripe Basin (Table 4, Fig 6). Proximal terrains, as São José do Caiano and Açude Coremas (Fig. 6) have negative εNd (0) values (-6.3 and -28.38) and T_{DM} ages between 1.8 and 2.6 Ga (Brito Neves and Passarelli 2020). Distal areas, such as Médio Coreaú and Ceará Central Domains (Fig. 24) also present T_{DM} ages between 1.6 and 2.5 Ga, and negative εNd (t = 0) (between +0.5 and -25.8) (Santos *et al.* 2008; Arthaud *et al.* 2015).

The U-Pb zircon age distribution of the analyzed samples indicates multiple sediment sources. For simplification, the U-Pb zircon age distribution of each analyzed sample was grouped into the four tectonic stages that defined the tectonic evolution of the Araripe Basin during the Mesozoic: the rift beginning stage, the rift stage, the “Post-rift I” stage, and the “Post-rift II” stage. The significant presence of Rhyacian to Orosirian (2.3 – 1.8 Ga), and Ediacaran (0.63 – 0.54 Ga) ages are the common features among all tectonic stages. These zircon ages can be found elsewhere in the Borborema province (Fig. 24,Tab. 4). The detrital zircon grains with discordant values may provide additional information about the source and the influence of the Brasiliano cycle in the Borborema Province. In all stages (except in the Araripina Formation sample – M2AR 1-3), the upper intercept indicates Paleoproterozoic sources (2.2 – 1.8

Ga) and the lower intercept indicates the crystallization of Cambrian-Ordovician (489 – 460 Ma) post-orogenic granites (See supplementary dataset Fig S4).

Additional constraints can be obtained from the MDS graph (Fig. 31), which represents statistically the degree of similarity in U-Pb zircon age distribution between analyzed samples (Vermeesch 2013, 2018). In this map (Fig. 31), alike samples cluster closely together and are linked by solid and dashed lines (closest and second-closest neighbors), whereas “dissimilar” samples plot far apart. In the MDS map (Fig. 31), the rift beginning and rift samples plot apart suggesting different sources for these stages. The U-Pb age distribution of the “Post-rift I” is connected with dashed lines with those of the rift beginning and rift stages suggesting common sources. The U-Pb age distribution of the Post-rift II” stage is connected by solid lines to other U-Pb distributions suggesting similar sources.

The main peak ages (2.3 to 1.8 Ga, 33%, and 0.72 to 0.54 Ga, 22%) (Fig. 30, Tab. 8) during the beginning of the rift (Brejo Santo and Missão Velha formations – 152 -145 Ma) may be sourced by the Borborema Province. The sources of Paleoproterozoic grains could be represented by supracrustal rocks from São Pedro, São José do Caiana and Açude Coremas terranes (2.1 -2.2 Ga) placed in the Central sub-province; and, the Caicó Complex (2.15 – 2.2 Ga) and Orós-Jaguaribe Terrane (2.2 – 1.7 Ga) placed in the Northern sub-province (Parente and Arthaud 1995; Hollanda *et al.* 2011; Brito Neves and Passarelli 2020). The Cryogenian – Ediacaran (0.72 – 0.54 Ga) (22%, Tab. 8) may have been sourced by the Brasiliano (0.7 – 0.55 Ga) granitoids that are widespread in the Borborema Province (Ferreira *et al.* 1998;

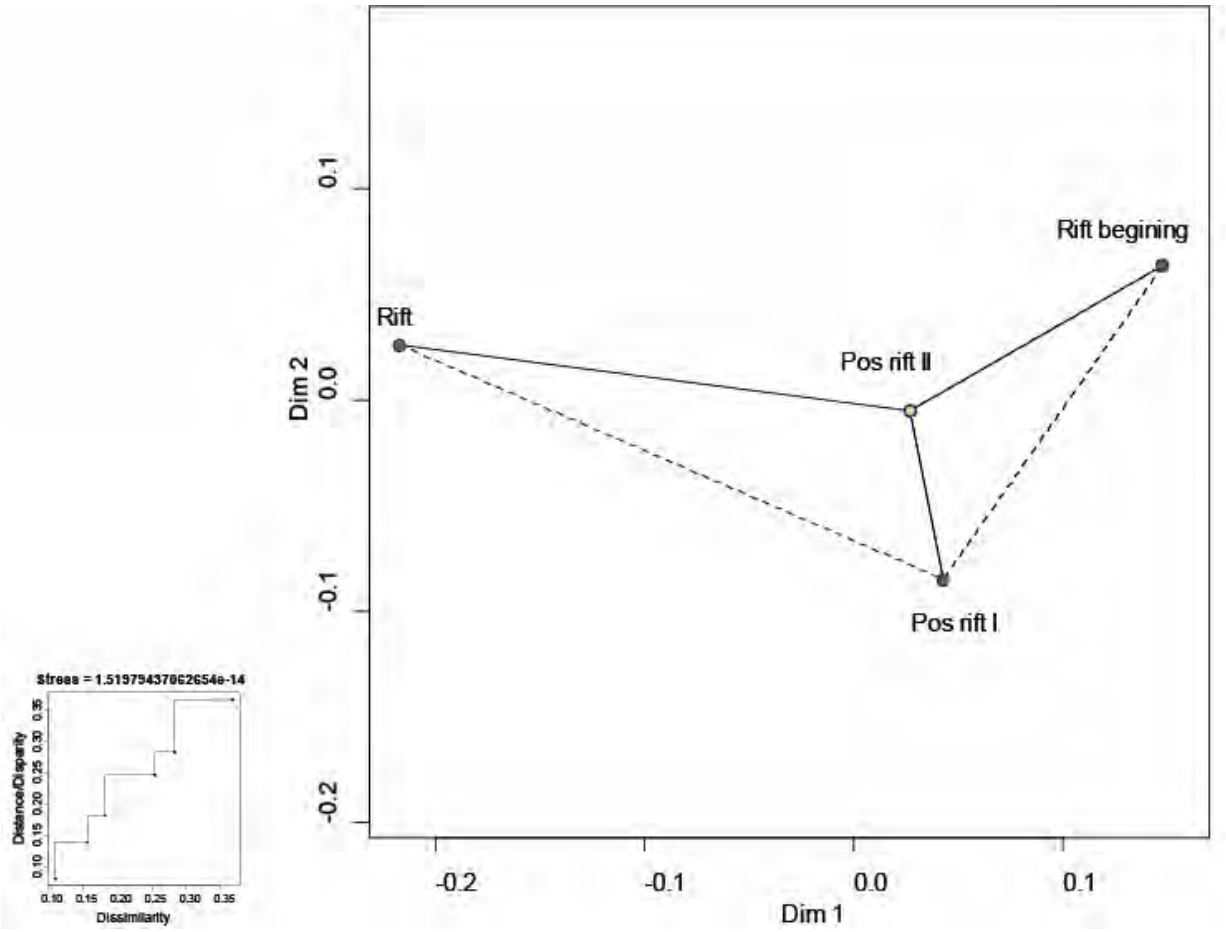

Fig. 31: A) Non-matrix metric multi-dimensional scaling (MDS) plot (Vermeesch, 2013) based on the U-Pb age distributions of detrital zircons in the analyzed samples using the Kolmogorov–Smirnov test. Closest and second closest neighbors are linked by solid and dashed lines, respectively; B) Shepard plot of the U-Pb data showing the transformation from dissimilarity to distances and disparities.

Brito Neves *et al.* 2003; Costa *et al.* 2013). The Rio Salgado belt rocks could also have been a source of recycled sediments, because they have pre brasiliano igneous intrusions (ca. 780 Ma), Ediacaran (635 – 541 Ma), and Tonian (ca. 940 Ma) detrital zircon grains (Brito Neves and Campos Neto 2016). Zircon grains younger than 450 Ma could be associated with post-orogenic granites (Teixeira 2005, Castro et al 2012), however, they may also have come from recycled sediments (Parnaíba Basin; Mauriti Formation?) given the low number of zircons of this age (< 3%, Tab. 8). In the Southern sub-province, the Riacho do Pontal Domain presents supracrustal sequences with Paleoarchean ages up to 3.5 Ga, Paleoproterozoic ages (2.2 – 2.0 Ga,); and volcano-sedimentary sequences with late Tonian to Ediacaran ages (820 – 530Ma) (Caxito *et*

al. 2017). However, the analyzed samples do not have a significant percentage of Tonian grains (3%, Tab. 8), which suggests there is no significant source from the eastern Central sub-province (Rio Gravatá and Alto-Pajeú Domain, Fig. 24,Fig. 30) and the internal zone of the Riacho do Pontal Domain, Southern sub-province (Fig. 24,Fig. 30). The paleocurrent data of the Missão Velha and Brejo Santo formations indicate S-SE paleo directions (Assine 1994, 2007; Fambrini *et al.* 2013; Godot Souza *et al.* 2022), and agree with a sedimentary provenance of the northern terranes.

The rift stage (Abaiara Formation) occurred during the Neocomian (145 - 130 Ma). The associated sedimentary rocks are characterized by a significant population of U-Pb zircon ages between 2.3 to 1.8 Ga (30%), 1.2 to 0.72 Ga (22%), and 0.72 to 0.54 Ga (28%) (Tab. 8, Fig. 30). The Paleoproterozoic grains could be sourced by supracrustal rocks from the São José do Caiana and Açude Coremas terranes (2.1 - 2.2 Ga) placed in the Central sub-province; and, the Caicó Complex (2.15 – 2.2 Ga) and Orós-Jaguaribe Terrane (2.2 – 1.7 Ga) localized the Northern sub-province, similarly to what occurred during the rift beginning stage (Fig. 32). Similarly, the Cryogenian and Ediacaran zircons (0.7 – 0.55 Ga) may have been sourced by the Brasiliano granitoids (Ferreira *et al.* 1998). The main difference between the beginning of the rift stage is the abundance of Stenian-Tonian ages (1.1 – 0.72 Ga) detrital zircon grains (Tab. 8, Fig. 30), which we interpret to indicate a variation in the source areas during the deposition of sedimentary rocks of the rift stage. The Rio Gravatá and Alto-Pajeú Domain (Brito Neves *et al.* 2005) present rocks from the Cariris Velhos cycle (970-960 Ma) with an overprint of Brasiliano granitoids with 550-510 Ma (Brito Neves *et al.* 2005). In the Internal Zone of the Riacho do Pontal Domain, it is also possible to find plutonic rocks with 1000-960 Ma (Kozuch 2003; Santos *et al.* 2010) related to the same tectonic event (Caxito *et al.* 2017). There are different interpretations of paleoflow during the deposition of sedimentary units from the rift stage. (Godot Souza *et al.* 2022)

indicated paleocurrents towards the south; (Fambrini *et al.* 2019) suggested paleoflow to the north toward the Iguatu and Rio do Peixe basins, whereas (Assine 1994, 2007) suggested paleoflows to SSW. The abundance of Stenian-Tonian (1.2 – 0.72 Ga) zircon grains (22%, Tab. 8) suggests a dominant source located in the eastern terranes (Fig. 32), which is supported by the paleocurrent direction found by (Assine 1994, 2007).

The analyzed samples of the Aptian first post-rift stage (Barbalha, Crato, and Romualdo formations) contained a significant population of U-Pb Paleoproterozoic ages, between 2.3 to 1.6 Ga (52%, Table 5) and Neoproterozoic ages (720-541 Ma) (27%, Tab. 8). This “Post-rift I” sequence does not present an important percentage of Tonian detrital zircons, which we interpret to suggest a decrease of sedimentary input from the eastern terranes of the Central sub-province (Rio Gravatá and Alto-Pajeú Domain (Fig. 24) when compared with the rift sequence. The increase of Paleoproterozoic zircon ages, mainly Statherian (1.8 – 1.6 Ga) grains, suggests a major contribution from the Northern sub-province (Statherian belts in the Ceará Domain and Alto Moxotó subdomain (Lages *et al.* 2019). Additionally, the paleoflows to the SE of the sedimentary rocks of the Barbalha Formation (Assine 1994; Fambrini *et al.* 2019, 2020b; Godot Souza *et al.* 2022) might suggest a contribution from the Orós-Jaguaribe Terrane, but also from the Ceará Domain, which has a Paleoproterozoic basement and plutonic suits (2.3 - 2.1 Ga), Neoproterozoic granites (640 – 560 Ma), and Brasilisiano molasses rocks (530 Ma) (Fetter *et al.* 2000; Arthaud *et al.* 2015), and recycled sedimentary from Parnaíba Basin (Hollanda *et al.* 2018). The Albian-Cenomanian sedimentary rocks of the second post-rift phase (“Post-rift II”, Araripina and Exu formations) are characterized by a significant increase of Cryogenian - Ediacaran U-Pb ages (720 – 541 Ma) (44%) and an important percentage of Paleoproterozoic ages (2.3 – 1.6 Ga) (32%) (Tab. 8). The Araripina Formation was

deposited in the western part of the Araripe Basin in the basement (Assine 2007; Fambrini *et al.* 2020a). The M2AR 1-3 sample has 85% of Neoproterozoic ages (720-541 Ma), which could come from proximal sources, such as São Pedro Terrane (Fig. 1, 8), where there are Brasiliano plutons (Brito Neves *et al.* 2023). The Paleoproterozoic ages (2.3 – 1.6 Ga) and the subordinary Archean ages (3.6 – 2.5 Ga) are present only in the Exu Formation sample (M2AR 1-4), and may have come also from São Pedro Terrane ("Granjeiro Complex" (Brito Neves and Passarelli 2020). However, the paleoflow of the Exu Formation indicates a direction to the W-SW (Assine 1994; Godot Souza *et al.* 2022 and this study, see supplementary material Fig. S1), which suggests a change of the sedimentary sources from NW to NE. In this scenario, the sources of the Araripina Formation may have come from proximal terranes, as discussed above, and the Exu Formation sample may have come from the eastern part of Orós Jaguaribe Terrane (Seridó – Jaguaribe domain, (Hollanda *et al.* 2011), which had a "long-lived Paleoproterozoic magmatic history" (Hollanda *et al.* 2011).

3.6.2 Paleogeographic implications

Our provenance dataset brings new constraints on the paleogeographic evolution of the Araripe Basin and to a larger extent, to the northern part of the South American platform from the Jurassic to the Cenomanian.

During the late Jurassic-Neocomian times (152 - 139 Ma), the Araripe Basin was part of the so-called Afro-Brazilian (Garcia and Wilbert 1995; Assine 2007; Kuchle *et al.* 2011) depression formed in response to early rifting caused by lithospheric stretching of the central and northern Gondwana before the break up (Assine 2007; Kuchle *et al.* 2011; Scherer *et al.* 2014; Guzmán-González *et al.* 2020). During this period, the Brejo Santo and Missão Velha formations of the Araripe Basin were deposited (Assine 2007; Fambrini *et al.* 2020b) and were part of the basal sequence (SEQ-1) that characterized the first infilling stage of the Afro-Brazilian depression (the

Dom João Stage, (Kuchle *et al.* 2011). This basal sequence (SEQ-1) is characterized by Capianga Lake lacustrine deposits (Kuchle *et al.* 2011) that extend through the Recôncavo, Tucano, Jatobá, Araripe, Sergipe, Alagoas, and Gabon basins (Fig. 9). This Afro-Brazilian depression had a depocenter in the Recôncavo-Tucano-Jatobá Basin and there is no evidence of internal structural high that could have compartmentalized the depression is found (Kuchle *et al.* 2011). Our provenance data further suggest that the source area during the early rift stage (SEQ-1) was located in the northern and northwestern terranes of the Borborema (Fig. 32, Tab. 4). This agrees with the hypothesis of Assine (1994), who suggest a source located in the basement block localized toward the north, near the Parnaíba lineament based on the occurrence of paleocurrents to the southeast in the Araripe Basin.

The rift stage is recorded in the Afro-Brazilian depression by the development of an unconformity overlying the first sedimentary sequence (SEQ-1) and by the deposition of two sedimentary sequences (SEQ-2 and SEQ-3) (Kuchle *et al.* 2011), which correspond to the deposition of the Abaiara Formation in the Araripe Basin (Assine 2007; Kuchle *et al.* 2011). In the Araripe Basin, the rift stage is marked by the increase of Tonian zircon grains (Tab. 8, Fig. 30) and the contribution of the Central Sub-province eastern terranes (Fig. 32). Additionally, the significant percentage of Cariris Velhos ages (0.9 - 1.0 Ga) (Tab. 8) suggests that the eastern terranes (Riacho do Gravatá and Alto Pajeú) constituted a topographic high during the rift climax suggesting a separation between the Araripe and Sergipe-Alagoas basins. Our findings are in agreement with the suggestions of Scherer *et al.* (2014), who proposed a regional rearrangement of the paleodrainage system at the end of the first rift stage deposition related to tectonic activity. (Fig. 32).

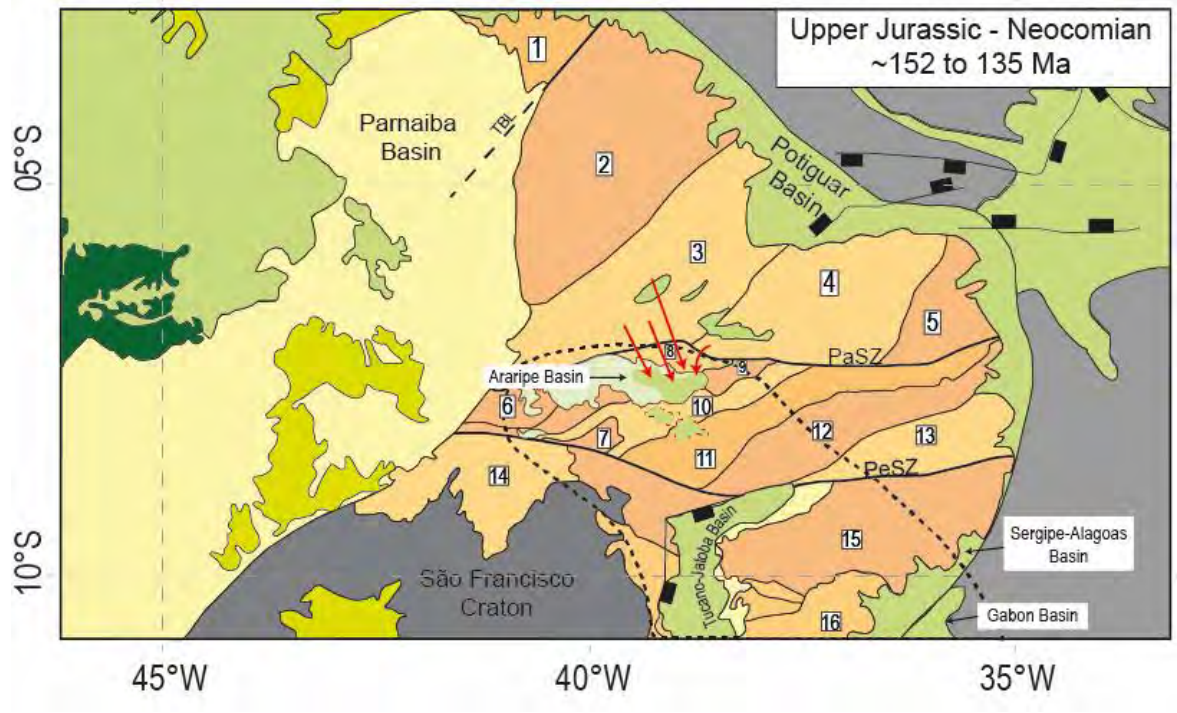
Upper Jurassic - Neocomian
~152 to 135 Ma
Parnaiba Basin
TBL
Potiguar Basin
Araripe Basin
PaSZ
PeSZ
Tucano-Jatoba Basin
Sergipe-Alagoas Basin
Gabon Basin
São Francisco Craton
05°S
10°S
45°W
40°W
35°W

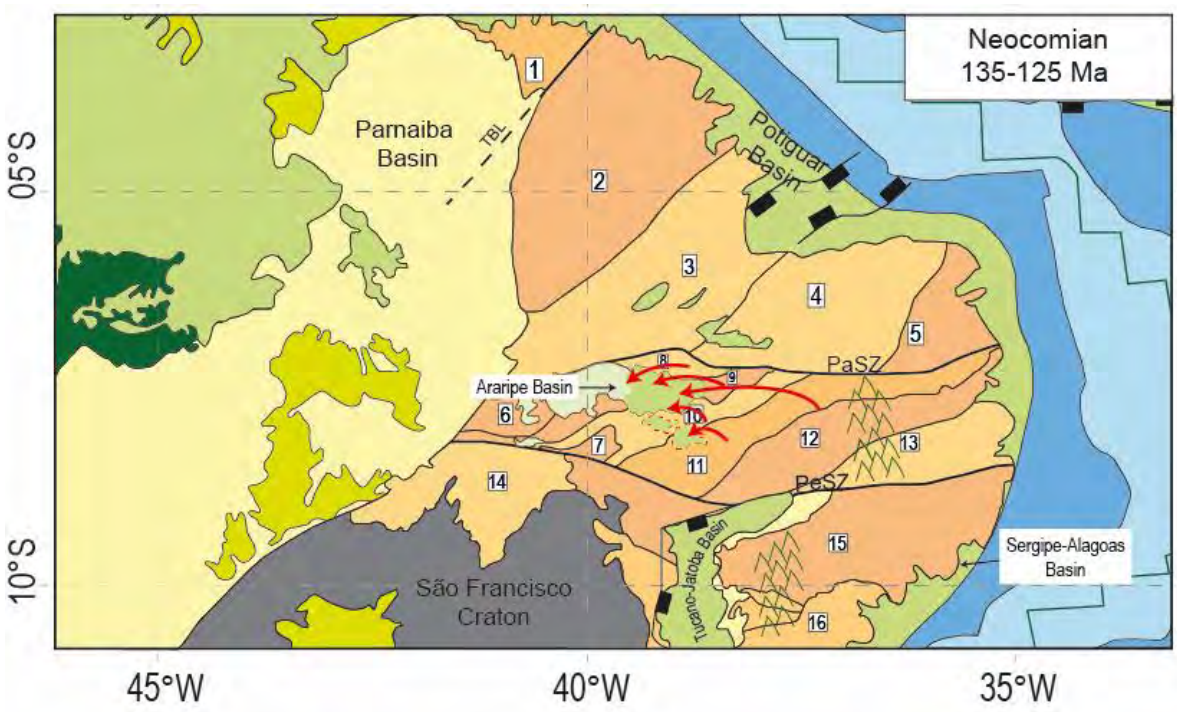
Neocomian
135-125 Ma
Parnaiba Basin
TBL
Potiguar Basin
Araripe Basin
PaSZ
PeSZ
Tucano-Jatoba Basin
Sergipe-Alagoas Basin
São Francisco Craton
05°S
10°S
45°W
40°W
35°W

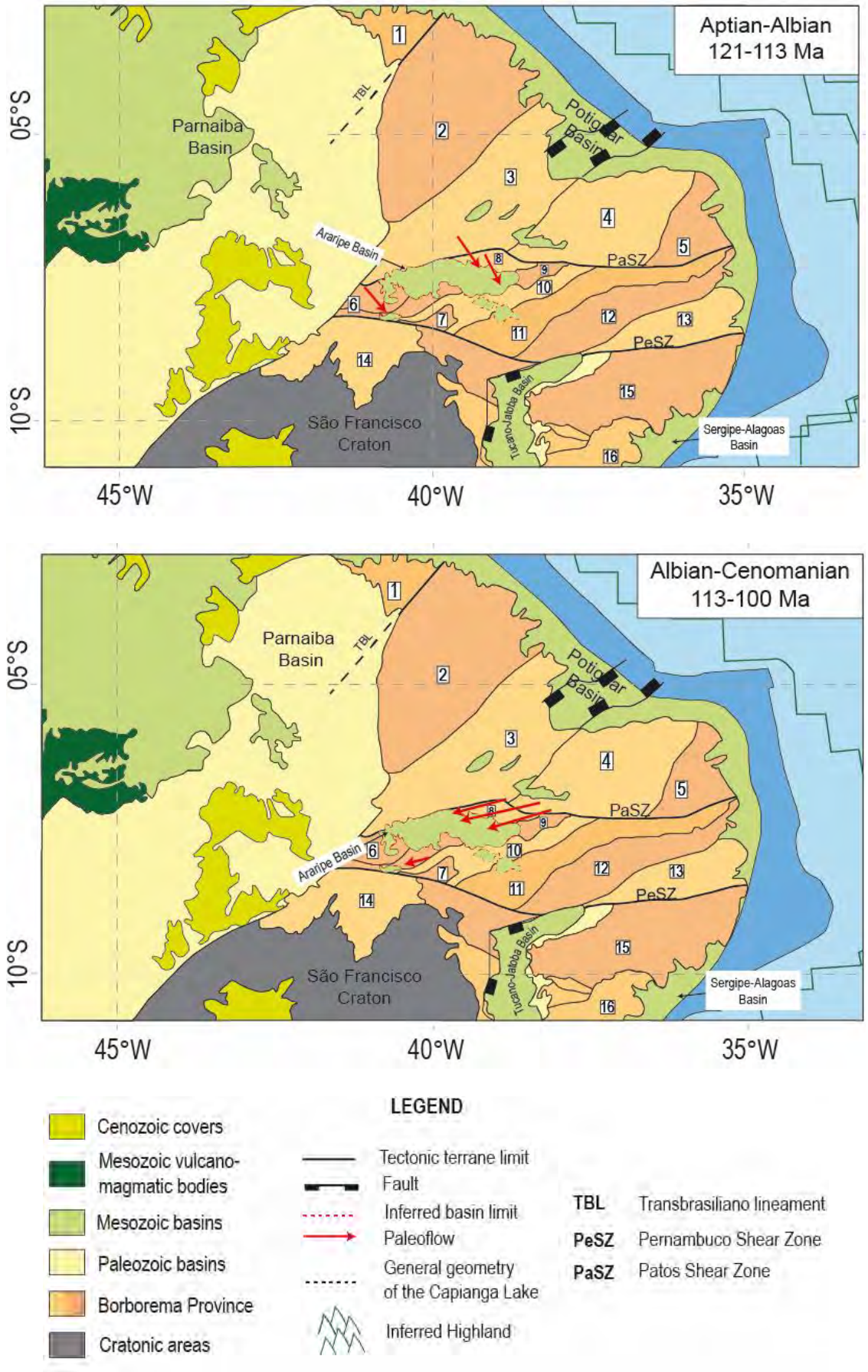

Fig. 32 Schematic paleogeographic maps based on sample provenance interpretations. Each time step corresponds to one of the tectonic stages that affected the Araripe Basin between the late Jurassic and

the Cenomanian. The paleogeographic reconstruction is based on the kinematic model of Heine et al. (2013), and the paleogeographic maps from Godot Souza et al. (2022), and Matos et al. (2021). The Borborema Province sub-divisions and their references are listed in Figure 1. The Capianga Lake geometry (Map A) and the highland location in Map B were based on Kuchle et al. (2011). The paleoflow directions were based on data from Fambrini et al (2019), Assine (1994, 2007), Custodio et al (2017), Godot Souza et al. (2022), and this study

In the early Aptian (120 Ma) the continental break-up occurred between the Brazilian northeast and the western African basins (Potiguar and Benin, Pernambuco-Paraíba and Rio Muni; Jequitinhonha-Camumu and Gabon basins) (Heine *et al.* 2013). At ca. 115 Ma, the South Atlantic and the Equatorial rifts systems broke up and started experiencing post-rift thermal subsidence (Milani *et al.* 2007; Heine *et al.* 2013). In the Araripe Basin, the Aptian post-rift successions were deposited. The basal Barbalha Formation is correlated with the Marizal Formation in the Recôncavo-Tucano-Jatobá Basin and presents similar fluvial paleoflow (N-NW to S-SE) (Assine 1994, 2007; Freitas *et al.* 2017). The Batateiras layer (Assine, 2007) is deposited in a lake under anoxic conditions and is correlated with the Trairi Layer (Ceará Basin) and Ponta do Tubarão Layer (Potiguar Basin) (Hashimoto *et al.* 1987; Assine 2007). Our data suggest a change in the source areas compared to the rift phase with contributions from N-NW to S-SE sources, similar to what is observed in the early rift stage. This interpretation is based on the decrease in Tonian U-Pb zircon ages, and the increase in Paleoproterozoic and Neoproterozoic zircon ages (Fig. 29, Tab. 8). Our data further suggest that the area in the E-NE of the Araripe Basin, which was the source for the rift stage stopped being a topographic high during the Aptian.

The Albian-Cenomanian post-rift II fluvial and alluvial Araripina and Exu formations are characterized by paleocurrent directions toward WSW (Assine 1994; Godot Souza *et al.* 2022 and this study; see supplementary Fig. S1) with probably proximal eastern sources. We ascribed this change in provenance to the Albian - Cenomanian uplift of the Borborema plateau that occurred after the Gondwana

breakup (Assine 2007; Eagles 2007; Eagles and König 2008; Matos *et al.* 2021b, a), as indicated by the increases of Archean and Neoproterozoic zircons in the sedimentary rocks of the Exu Formation. This uplift may have induced drainage reorganization at the local scale such in the Araripe Basin (this study), Potiguar Basin (Baesso *et al.* 2021), and São Luís-Grajaú Basin (Nascimento *et al.* 2007), and also at regional scale such as in Guyana (Roddaz *et al.* 2021; Girault *et al.* 2023). This drainage reorganization along the Equatorial margin was also contemporaneous with the establishment of the so-called “Sanozama” paleodrainage in western Amazonia (Rodrigues *et al.* 2023), which might suggest that the entire northern part of South America experienced major drainage reorganization in response to the post-rift uplift of the equatorial Atlantic rifting.

3.7 Conclusion

The provenance study of the sedimentary rocks of the Araripe Basin (NE Brazil) based on a multi-proxy dataset (major and trace element concentrations, Sm-Nd isotopic composition, and detrital zircon U-Pb ages) yields the following conclusions:

- The εNd (0) values (-12.3 to -23.7) together with the T_{DM} ages (1.68 to 2.55 Ga) suggest an old crustal source for the sedimentary rocks analyzed in the Araripe Basin. The presence of Rhyacian to Orosirian (2.3 – 1.8 Ga) and Ediacaran (0.63 – 0.54 Ga) U-Pb zircon ages further suggest the dominant contribution of the Borborema province influenced by the Brasiliano cycle (650 - 520 Ma), as shown by the discordant zircon grains;
- The low contribution of Tonian (~940 Ma) zircons to the U-Pb zircon age distribution, with published paleocurrent direction, suggest sources located in the northern and northwestern terranes of the Borborema Province, probably near the

Parnaíba lineament, for the Brejo Santo and Missão Velha formations deposited during the rift beginning stage;

- The increase of Stenian-Tonian (1.2 – 0.72 Ga) zircon grains in the U-Pb zircon age distribution of the Abaiara Formation suggests a dominant source located in the eastern terranes during the rift stage. The significant percentage of Cariris Velhos ages (0.9 - 1.0 Ga) further indicates that the eastern terranes (Riacho do Gravatá and Alto Pajeú) constituted a topographic high during the rift climax, which may have separated the Araripe and Sergipe-Alagoas basins;
- The decrease of Tonian U-Pb zircon ages and the increase of Paleoproterozoic and Neoproterozoic zircon ages in the U-Pb zircon age distributions of the post-rift I (Santana Group) suggest a change in the source areas with sources located in the northern terranes of the Borborema Province similar to what is observed in the rift beginning stage suggesting that the E-NE area of the Araripe Basin stopped being a topographic high during the Aptian;
- The Albian-Cenomanian post-rift II fluvial and alluvial Araripina and Exu formations are characterized by dominant contributions of Paleoproterozoic and Cryogenian - Ediacaran (720 – 541 Ma) zircon ages, which we interpret to suggest proximal sources located in the NE. We ascribed this change in provenance to the Albian to Cenomanian uplift of the Borborema plateau.

Finally, similarly to other recently published studies, our provenance data emphasize the major role played by the post-rift uplift of the Brazilian craton in shaping the late Cretaceous paleodrainage of the northern part of South America.

Acknowledgments

We are thankful to the University of Brasilia and University Toulouse III Paul Sabatier for the infrastructure and technical support. We also thank for the financial support of

the Brazilian National Council for Scientific and Technological Development (CNPq-428843/2916-6; 312941/2018-8), the Coordination for the Improvement of Higher Education Personnel – Brazil (CAPES), and the French Evaluation Committee of the University and Scientific Cooperation with Brazil (COFECUB) for funding the first author during the Ph.D. degree. This study was also supported and funded by CAPES-COFECUB program Te 924/18 “Paléo-Amazone: évolution Néogène de l’Amazonie Brésilienne.”

References

Albarède, F. and Brouxel, M. 1987. The Sm/Nd secular evolution of the continental crust and the depleted mantle. *Earth and Planetary Science Letters*, **82**, 25–35, https://doi.org/10.1016/0012-821X(87)90104-X.

Almeida, F.F.M., Hasui, Y., de Brito Neves, B.B. and Fuck, R.A. 1981. Brazilian structural provinces: An introduction. *Earth-Science Reviews*, **17**, 1–29, https://doi.org/10.1016/0012-8252(81)90003-9.

Angelim, L.A.A. and Kosin, M. 2001. *Estados Da Bahia, Pernambuco e Piaui: Escala 1:500.000*. Programa Levantamentos Geológicos Básicos do Brasil - PLGB.

Arai, M. 2014. Aptian/Albian (Early Cretaceous) paleogeography of the South Atlantic: a paleontological perspective. *Brazilian Journal of Geology*, **44**, 339–350, https://doi.org/10.5327/Z2317-4889201400020012.

Arai, M. 2016. Reply to the comments of Assine et al. (Comments on the paper by M. Arai ‘Aptian/Albian (Early Cretaceous) paleogeography of the South Atlantic: a paleontological perspective’). *Brazilian Journal of Geology*, **46**, 9–13, https://doi.org/10.1590/2317-4889201620150046B.

Arthaud, M.H., Caby, R., Fuck, R.A., Dantas, E.L. and Parente, C.V. 2008. Geology of the northern Borborema Province, NE Brazil and its correlation with Nigeria, NW Africa. *Geological Society, London, Special Publications*, **294**, 49–67, https://doi.org/10.1144/SP294.4.

Arthaud, M.H., Fuck, R.A., Dantas, E.L., Santos, T.J.S., Caby, R. and Armstrong, R. 2015. The Neoproterozoic Ceará Group, Ceará Central domain, NE Brazil: Depositional age and provenance of detrital material. New insights from U–Pb and Sm–Nd geochronology. *Journal of South American Earth Sciences*, **58**, 223–237, https://doi.org/10.1016/j.jsames.2014.09.007.

Assine, M.L. 1992. Analise estratigrafica da Bacia do Araripe, Nordeste do Brasil. *Revista Brasileira de Geociências*, **22**, 289–300, https://doi.org/10.25249/0375-7536.1992289300.

Assine, M.L. 1994. Paleocorrentes e Paleogeografia na Bacia do Araripe, Nordeste do Brasil. *Revista Brasileira de Geociências*, **24**, 223–232, https://doi.org/10.25249/0375-7536.1994223232.

Assine, M.L. 2007. Bacia do Araripe. *Boletim de Geociências da Petrobras*, **15**, 371–389.

Assine, M.L., Neumann, H., Varejão, F.G. and Mescolotti, P.C. 2014. Sequências deposicionais do Andar Alagoas da Bacia do Araripe, Nordeste do Brasil. *Boletim de Geociências da Petrobras*, **22**, 3–28.

Assine, M.L., Quaglio, F., Warren, L.V. and Simões, M.G. 2016. Comments on paper by M. Arai 'Aptian/Albian (Early Cretaceous) paleogeography of the South Atlantic: a paleontological perspective'. *Brazilian Journal of Geology*, **46**, 3–7, https://doi.org/10.1590/2317-4889201620150046A.

Assis, A.P., Porto, A.L., Schmitt, R.S., Linol, B., Medeiros, S.R., Correa Martins, F. and Silva, D.S. 2019. The Ordovician-Silurian tectono-stratigraphic evolution and paleogeography of eastern Parnaiba Basin, NE Brazil. *Journal of South American Earth Sciences*, **95**, 102241, https://doi.org/10.1016/j.jsames.2019.102241.

Augustsson, C. and Bahlburg, H. 2008. Provenance of late Palaeozoic metasediments of the Patagonian proto-Pacific margin (southernmost Chile and Argentina). *International Journal of Earth Sciences*, **97**, 71–88, https://doi.org/10.1007/s00531-006-0158-7.

Baesso, A., Remus, M.V.D., Pereira, B.R.B., Alkmim, A.R., Lana, C.C., Vignol-Lelarge, M.L. and Porcher, C.C. 2021. Insights into sedimentary provenance and the evolution of the Potiguar Basin, NE Brazil, using U–Pb ages and Lu–Hf isotopes in detrital zircons. *Marine and Petroleum Geology*, **131**, 105170, https://doi.org/10.1016/j.marpetgeo.2021.105170.

Barbosa, J.A., Hessel, M.H., Nascimento, M.C. do and Neumann, V.H. 2006. Ocorrência de Taenidium Barreti na Formação Rio da Batateira, Crétacéo da Bacia do Araripe. *Estudos Geológicos*, **16**, 50–60.

Basu, A.R., Sharma, M. and DeCelles, P.G. 1990. Nd, Sr-isotopic provenance and trace element geochemistry of Amazonian foreland basin fluvial sands, Bolivia and Peru: implications for ensialic Andean orogeny. *Earth and Planetary Science Letters*, **100**, 1–17, https://doi.org/10.1016/0012-821X(90)90172-T.

Beurlen, K. 1962. A geologia da Chapada do Araripe. *Anais da Academia Brasileira de Ciências*, **34**, 365–370.

Bleeker, W. 2003. The late Archean record: a puzzle in ca. 35 pieces. *Lithos*, **71**, 99–134, https://doi.org/10.1016/j.lithos.2003.07.003.

Bock, B., Mclennan, and Hanson. 1998. Geochemistry and provenance of the Middle Ordovician Austin Glen Member (Normanskill Formation) and the Taconian Orogeny in New England. *Sedimentology*, **45**, 635–655, https://doi.org/10.1046/j.1365-3091.1998.00168.x.

Bom, M.H.H., Ceolin, D., et al. 2021. Paleoenvironmental evolution of the Aptian Romualdo Formation, Araripe Basin, Northeastern Brazil. *Global and Planetary Change*, **203**, 103528, https://doi.org/10.1016/j.gloplacha.2021.103528.

Bouchez, J., Gaillardet, J., France-Lanord, C., Maurice, L. and Dutra-Maia, P. 2011a. Grain size control of river suspended sediment geochemistry: Clues from Amazon River depth profiles: RIVER SEDIMENTS GRAIN SIZE AND CHEMISTRY. *Geochemistry, Geophysics, Geosystems*, **12**, n/a-n/a, https://doi.org/10.1029/2010GC003380.

Bouchez, J., Gaillardet, J., France-Lanord, C., Maurice, L. and Dutra-Maia, P. 2011b. Grain size control of river suspended sediment geochemistry: Clues from Amazon River depth profiles: river sediments grain size and chemistry. *Geochemistry, Geophysics, Geosystems*, **12**, n/a-n/a, https://doi.org/10.1029/2010GC003380.

Brito, L.M. 1987. As unidades litoestratigraficas da passagem Jurassico-Cretaceo do Nordeste do Brasil. *Revista Brasileira de Geociências*, **17**, 81–85.

Brito Neves, B.B. de and Campos Neto, M.D.C. 2016. A faixa de dobramentos do Rio Salgado, norte-noroeste da Zona Transversal-Província Borborema (PB-CE). *Geologia USP. Série Científica*, **16**, 3, https://doi.org/10.11606/issn.2316-9095.v16i3p3-17.

Brito Neves, B.B. de and Passarelli, C.R. 2020. Terrenos tectonoestratigráficos dispersos do embasamento pré-Brasiliano (São José do Caiana, Açude Coremas e Icaiçara) na porção centro-oeste da Zona Transversal (Paraíba, Ceará e Pernambuco). *Geologia USP. Série Científica*, **20**, 81–105, https://doi.org/10.11606/issn.2316-9095.v20-159425.

Brito Neves, B.B. de, Santos, E.J.D. and Van Schmus, W.R. 2000. Tectonic History of the Borborema Province, Northeast Brazil. *In*: *Tectonic Evolution of South America*. 151–182.

Brito Neves, B.B. de, Passarelli, C.R., Basei, M.A.S. and Santos, E.J. dos. 2003. Idades U-Pb em zircão de alguns granitos clássicos da Província Borborema. *Geologia USP. Série Científica*, **3**, 25–38, https://doi.org/10.5327/S1519-874X2003000100003.

Brito Neves, B.B. de, Van Schmus, W.R., Kozuch, M., Santos, E.J. dos and Petronilho, L. 2005. A Zona Tectônica Teixeira Terra Nova - ZTTTN - fundamentos da geologia regional e isotópica. *Geologia USP. Série Científica*, **5**, 57–80, https://doi.org/10.5327/S1519-874X2005000100005.

Brito Neves, B.B. de, Santos, T.J.S. dos and Dantas, E.L. 2023. O Terreno Tectonoestratigráfico São Pedro: Oeste da Zona Transversal – Província Borborema. *Geologia USP. Série Científica*, **22**, 45–69, https://doi.org/10.11606/issn.2316-9095.v22-197489.

Brune, S., Kolawole, F., Olive, J.-A., Stamps, D.S., Tech, V., Buck, W.R. and Buiter, S.J.H. 2023. Geodynamics of continental rift initiation and evolution. *Nature Reviews Earth & Environment*, **4**, 235–253.

Camacho, C.R. and Sousa, F.R.F.R. de O. e. 2017. O arcabouço estrutural da Bacia Sedimentar do Araripe, Província Borborema, baseado em dados aeromagnetométricos. *Geologia USP. Série Científica*, **17**, 149, https://doi.org/10.11606/issn.2316-9095.v17-393.

Caputo, M.V. and Crowell, J.C. 1985. Migration of glacial centers across Gondwana during Paleozoic Era. *Geological Society of America Bulletin*, **96**, 1020, https://doi.org/10.1130/0016-7606(1985)96<1020:MOGCAG>2.0.CO;2.

Carignan, J., Hild, P., Mevelle, G., Morel, J. and Yeghicheyan, D. 2001. Routine Analyses of Trace Elements in Geological Samples using Flow Injection and Low Pressure On-Line Liquid Chromatography Coupled to ICP-MS: A Study of Geochemical Reference Materials BR, DR-N, UB-N, AN-G and GH. *Geostandards and Geoanalytical Research*, **25**, 187–198, https://doi.org/10.1111/j.1751-908X.2001.tb00595.x.

Caxito, F.A., Uhlein, A., Dantas, E., Stevenson, R., Egydio-Silva, M. and Salgado, S.S. 2017. The Rio Preto and Riacho do Pontal Belts. *In*: Heilbron, M., Cordani, U. G. and Alkmim, F. F. (eds) *São Francisco Craton, Eastern Brazil*. Regional Geology Reviews, 221–239., https://doi.org/10.1007/978-3-319-01715-0_12.

Cerri, R.I., Warren, L.V., Spencer, C.J., Varejão, F.G., Promenzio, P., Luvizotto, G.L. and Assine, M.L. 2022. Using detrital zircon and rutile to constrain sedimentary provenance of Early Paleozoic fluvial systems of the Araripe Basin, Western Gondwana. *Journal of South American Earth Sciences*, **116**, 103821, https://doi.org/10.1016/j.jsames.2022.103821.

Coimbra, J.C., Arai, M. and Carreño, A.L. 2002. Biostratigraphy of Lower Cretaceous microfossils from the Araripe basin, northeastern Brazil Biostratigraphie (microfossiles) du Crétacé inférieur du Bassin de Araripe, nord-est du Brésil. 12.

Condie, K.C. 1993. Chemical composition and evolution of the upper continental crust: Contrasting results from surface samples and shales. *Chemical Geology*, **104**, 1–37, https://doi.org/10.1016/0009-2541(93)90140-E.

Costa, F.G. da, Araújo, C.E.G. de, Amaral, W. da S., Vasconcelos, A.M. and Rodrigues, J.B. 2013. U-Pb (LA-ICPMS) zircon ages and Nd isotopes for granitoids of the Tamboril-Santa Quitéria Complex, Ceará Central Domain[/title]: [subtitle]implication for Neoproterozoic syncollisional magmatism in north Borborema Province. *Geologia USP. Série Científica*, **13**, 159–174, https://doi.org/10.5327/Z1519-874X2013000200009.

Cruz, R.F. da, Pimentel, M.M., Accioly, A.C. de A. and Rodrigues, J.B. 2014. Geological and isotopic characteristics of granites from the Western Pernambuco-Alagoas Domain: implications for the crustal evolution of the Neoproterozoic Borborema Province. *Brazilian Journal of Geology*, **44**, 627–652, https://doi.org/10.5327/Z23174889201400040008.

Cullers, R.L. 2000a. The geochemistry of shales, siltstones and sandstones of Pennsylvanian–Permian age, Colorado, USA: implications for provenance and

metamorphic studies. *Lithos*, **51**, 181–203, https://doi.org/10.1016/S0024-4937(99)00063-8.

Cullers, R.L. 2000b. The geochemistry of shales, siltstones and sandstones of Pennsylvanian–Permian age, Colorado, USA: implications for provenance and metamorphic studies. *Lithos*, **51**, 181–203, https://doi.org/10.1016/S0024-4937(99)00063-8.

Custódio, M.A., Quaglio, F., Warren, L.V., Simões, M.G., Fürsich, F.T., Perinotto, J.A.J. and Assine, M.L. 2017. The transgressive-regressive cycle of the Romualdo Formation (Araripe Basin): Sedimentary archive of the Early Cretaceous marine ingression in the interior of Northeast Brazil. *Sedimentary Geology*, **359**, 1–15, https://doi.org/10.1016/j.sedgeo.2017.07.010.

De Baar, H.J.W., Bacon, M.P., Brewer, P.G. and Bruland, K.W. 1985a. Rare earth elements in the Pacific and Atlantic Oceans. *Geochimica et Cosmochimica Acta*, **49**, 1943–1959, https://doi.org/10.1016/0016-7037(85)90089-4.

De Baar, H.J.W., Bacon, M.P., Brewer, P.G. and Bruland, K.W. 1985b. Rare earth elements in the Pacific and Atlantic Oceans. *Geochimica et Cosmochimica Acta*, **49**, 1943–1959, https://doi.org/10.1016/0016-7037(85)90089-4.

DePaolo, D.J. 1981. Trace element and isotopic effects of combined wallrock assimilation and fractional crystallization. *Earth and Planetary Science Letters*, **53**, 189–202, https://doi.org/10.1016/0012-821X(81)90153-9.

DePaolo, D.J., Linn, A.M. and Schubert, G. 1991. The continental crustal age distribution: Methods of determining mantle separation ages from Sm-Nd isotopic data and application to the southwestern United States. *Journal of Geophysical Research*, **96**, 2071, https://doi.org/10.1029/90JB02219.

Dummann, W., Hofmann, P., Herrle, J.O., Frank, M. and Wagner, T. 2023. The early opening of the Equatorial Atlantic gateway and the evolution of Cretaceous peak warming. *Geology*, **51**, 476–480, https://doi.org/10.1130/G50842.1.

Eagles, G. 2007. New angles on the South Atlantic opening. *Geophysical Journal International*, **168**, 353–361, https://doi.org/10.1111/j.1365-246X.2006.03206.x.

Eagles, G. and König, M. 2008. A model of plate kinematics in Gondwana breakup. *Geophysical Journal International*, **173**, 703–717, https://doi.org/10.1111/j.1365-246X.2008.03753.x.

Ebert, H. 1970. The Precambrian geology of the Borborema Belt (states of Paraíba and Rio Grande do Norte, northeastern Brazil), and the origin of its mineral resources. *Geologische Rundschau*, **59**, 1294–1326.

Fambrini, G.L. and Junior, S.T. 2010. Sedimentary facies analyses and depositional systems of Missão Velha Formation in the type area, Araripe Basin, Northeastern Brazil: Reservoir implication. 11.

Fambrini, G.L., Neumann, V.H. de M.L., Barros, C.L. de, Silva, S.M.O.A. da, Galm, P.C. and Menezes Filho, J.A.B. de. 2013. Análise estratigráfica da Formação Brejo Santo, Bacia do Araripe, Nordeste do Brasil: implicações

paleogeográficas. *Geologia USP. Série Científica*, **13**, 3–28, https://doi.org/10.5327/Z1519-874X201300040001.

Fambrini, G.L., Menezes-Filho, J.A.B., Jesuíno, P.C.L., Araújo, J.T., Durval, L.G.L. and Neumann, V.H.M.L. 2015. Sucessão Faciológica da Formação Barbalha, Bacia do Araripe, Nordeste do Brasil. *Estudos Geológicos*, **25**, 137–164, https://doi.org/10.18190/1980-8208/estudosgeologicos.v25n1p137-164.

Fambrini, G.L., Menezes-Filho, J.A.B., Jesuíno, P.C.L., Silvestre, D.D.C., Neumann, V.H.M.L. and Lemos, D.R. de. 2016. Characterization of the depositional systems of the Barbalha formation, Araripe basin, northeastern Brazil. *Comunicações Geológicas*, **103**, 51–65.

Fambrini, G.L., Silva-Filho, W.F. da, et al. 2019. Análise tectonossedimentar das fases início de rifte e clímax de rifte da Bacia do Araripe, Nordeste do Brasil. *Geologia USP. Série Científica*, **19**, 205–236, https://doi.org/10.11606/issn.2316-9095.v19-150526.

Fambrini, G.L., Silvestre, D. da C., Barreto Junior, A.M. and Silva-Filho, W.F. da. 2020a. Estratigrafia da Bacia do Araripe: estado da arte, revisão crítica e resultados novos. *Geologia USP. Série Científica*, **20**, 169–212, https://doi.org/10.11606/issn.2316-9095.v20-163467.

Fambrini, G.L., Silvestre, D. da C., Barreto Junior, A.M. and Silva-Filho, W.F. da. 2020b. Estratigrafia da Bacia do Araripe: estado da arte, revisão crítica e resultados novos. *Geologia USP. Série Científica*, **20**, 169–212, https://doi.org/10.11606/issn.2316-9095.v20-163467.

Fedo, C.M., Wayne Nesbitt, H. and Young, G.M. 1995. Unraveling the effects of potassium metasomatism in sedimentary rocks and paleosols, with implications for paleoweathering conditions and provenance. *Geology*, **23**, 921, https://doi.org/10.1130/0091-7613(1995)023<0921:UTEOPM>2.3.CO;2.

Ferreira, V.P., Sial, A.N. and Jardim de Sá, E.F. 1998. Geochemical and isotopic signatures of Proterozoic granitoids in terranes of the Borborema structural province, northeastern Brazil. *Journal of South American Earth Sciences*, **11**, 439–455, https://doi.org/10.1016/S0895-9811(98)00027-3.

Fetter, A.H., Schmus, W.R.V., Santos, T.J.S.D., Nogueira Neto, J.A. and Arthaud, M.H. 2000. U-PB AND SM-ND GEOCHRONOLOGICAL CONSTRAINTS ON THE CRUSTAL EVOLUTION AND BASEMENT ARCHITECTURE OF CEARÁ STATE, NW BORBOREMA PROVINCE, NE BRAZIL: IMPLICATIONS FOR THE EXISTENCE OF THE PALEOPROTEROZOIC SUPERCONTINENT ‘ATLANTICA’. *Revista Brasileira de Geociências*, **30**, 102–106, https://doi.org/10.25249/0375-7536.2000301102106.

Figueiredo, J., Hoorn, C., Ven, P. van der and Soares, E. 2009. Late Miocene onset of the Amazon River and the Amazon deep-sea fan: Evidence from the Foz do Amazonas Basin. *Geology*, **37**, 619–622, https://doi.org/10.1130/G25567A.1.

Freitas, B.T., Almeida, R.P., Carrera, S.C., Figueiredo, F.T., Turra, B.B., Varejão, F.G. and Assine, M.L. 2017. Aptian sedimentation in the Recôncavo-Tucano-Jatobá Rift System and its tectonic and paleogeographic significance. *Journal of South*

American Earth Sciences, **80**, 460–481, https://doi.org/10.1016/j.jsames.2017.10.001.

Gain, S.E.M., Gréau, Y., Henry, H., Belousova, E., Dainis, I., Griffin, W.L. and O'Reilly, S.Y. 2019. Mud Tank Zircon: Long-Term Evaluation of a Reference Material for U-Pb Dating, Hf-Isotope Analysis and Trace Element Analysis. *Geostandards and Geoanalytical Research*, **43**, 339–354, https://doi.org/10.1111/ggr.12265.

Garcia, A.J.V. and Wilbert, A. 1995. Paleogeographic Evolution of Mesozoic pre-rift Sequences in coastal and interior basins of Northeastern Brazil. *In*: *Pangea: Global Environments and Resources.* 123–130.

Girault, I., Basile, C., et al. 2023. Thermochronology and U–Pb dating of detrital zircons from the Demerara Plateau (French Guiana-Suriname): Implications for the provenance of the Early Cretaceous syn-rift sedimentation. *Basin Research*, **35**, 1386–1406, https://doi.org/10.1111/bre.12758.

Godot Souza, J.F., Isozaki, Y., et al. 2022. Provenance analysis of the Araripe intracontinental basin, northeast Brazil – Routes for proto-Atlantic marine incursions in northwest Gondwana. *Sedimentary Geology*, **440**, 106243, https://doi.org/10.1016/j.sedgeo.2022.106243.

Góes, A.M. 1995. *A Formação Poti (Carbonifero Inferior) da Bacia do Parnaíba*. Tese de doutoramento, Universidade de São Paulo.

Góes, A.M. and Feijó, F.J. 1994. Bacia do Parnaíba. *Boletim de Geociências da Petrobras*, **8**, 57–67.

Goia, S.M.C.L. and Pimentel, M.M. 2000. The Sm-Nd isotopic method in the geochronology laboratory of the University of Brasília. *Anais da Academia Brasileira de Ciências*, **72**, 219–245, https://doi.org/10.1590/S0001-37652000000200009.

Goldstein, S.L., O'Nions, R.K. and Hamilton, P.J. 1984. A Sm-Nd isotopic study of atmospheric dusts and particulates from major river systems. *Earth and Planetary Science Letters*, **70**, 221–236, https://doi.org/10.1016/0012-821X(84)90007-4.

Guimarães, I.P., de Fatima L. de Brito, M., de A. Lages, G., da Silva Filho, A.F., Santos, L. and Brasilino, R.G. 2016. Tonian granitic magmatism of the Borborema Province, NE Brazil: A review. *Journal of South American Earth Sciences*, **68**, 97–112, https://doi.org/10.1016/j.jsames.2015.10.009.

Guzmán-González, J., Sial, A.N., Piovesan, E.K., Oliveira, E.V. and Fambrini, G.L. 2020. Paleolimnological reconstruction of a marginal area of Jurassic Capianga Lake, Jatobá Basin, northeast Brazil. *Journal of Paleolimnology*, **63**, 113–128, https://doi.org/10.1007/s10933-019-00105-0.

Hall, S.A., Bird, D.E., McLean, D.J., Towle, P.J., Grant, J.V. and Danque, H.A. 2018. New constraints on the age of the opening of the South Atlantic basin. *Marine and Petroleum Geology*, **95**, 50–66, https://doi.org/10.1016/j.marpetgeo.2018.03.010.

Hashimoto, A.T., Appi, C.J., Soldan, A.L. and Cerqueira, J.R. 1987. O Neo-Alagoas nas Bacias do Ceara, Araripe e Potiguar (Brasil): Caracterização estratigrafica e Paleoambiental. *Revista Brasileira de Geociências*, **17**, 118–122, https://doi.org/10.25249/0375-7536.1987118122.

Heilbron, M., Guedes, E., et al. 2018. Geochemical and temporal provinciality of the magmatism of the eastern Parnaíba Basin, NE Brazil. *Geological Society, London, Special Publications*, **472**, 251–278, https://doi.org/10.1144/SP472.11.

Heimhofer, U. and Hochuli, P.-A. 2010. Early Cretaceous angiosperm pollen from a low-latitude succession (Araripe Basin, NE Brazil). *Review of Palaeobotany and Palynology*, **161**, 105–126, https://doi.org/10.1016/j.revpalbo.2010.03.010.

Heine, C., Zoethout, J. and Müller, R.D. 2013. Kinematics of the South Atlantic rift. *Solid Earth*, **4**, 215–253, https://doi.org/10.5194/se-4-215-2013.

Hollanda, M.H.B.M., Archanjo, C.J., Souza, L.C., Dunyi, L. and Armstrong, R. 2011. Long-lived Paleoproterozoic granitic magmatism in the Seridó-Jaguaribe domain, Borborema Province–NE Brazil. *Journal of South American Earth Sciences*, **32**, 287–300, https://doi.org/10.1016/j.jsames.2011.02.008.

Hollanda, M.H.B.M., Goes, A.M., Silva, D.B. and Negri, F.A. 2014. Proveniência sedimentar dos arenitos da Bacia do Parnaíba (NE do Brasil). *Boletim de Geociências da Petrobras*, **22**, 191–211.

Hollanda, M.H.B.M., Góes, A.M. and Negri, F.A. 2018. Provenance of sandstones in the Parnaíba Basin through detrital zircon geochronology. *Geological Society, London, Special Publications*, **472**, 181–197, https://doi.org/10.1144/SP472.16.

Hoorn, C., Bogotá-A, G.R., et al. 2017. The Amazon at sea: Onset and stages of the Amazon River from a marine record, with special reference to Neogene plant turnover in the drainage basin. *Global and Planetary Change*, **153**, 51–65, https://doi.org/10.1016/j.gloplacha.2017.02.005.

Horbe, A.M.C., Roddaz, M., Gomes, L.B., Castro, R.T., Dantas, E.L. and Do Carmo, D.A. 2019. Provenance of the Neogene sediments from the Solimoes formation (Solimoes and Acre basins), Brazil. *Journal of South American Earth Sciences*, **93**, 232–241.

Jackson, S.E., Pearson, N.J., Griffin, W.L. and Belousova, E.A. 2004. The application of laser ablation-inductively coupled plasma-mass spectrometry to in situ U–Pb zircon geochronology. *Chemical Geology*, **211**, 47–69, https://doi.org/10.1016/j.chemgeo.2004.06.017.

Jacobsen, S.B. and Wasserburg, G.J. 1980. Sm-Nd isotopic evolution of chondrites. *Earth and Planetary Science Letters*, **50**, 139–155, https://doi.org/10.1016/0012-821X(80)90125-9.

Jardim Sá, E.F., Macedo, M.H.E., Fuck, R.A. and Kawashita, K. 1992. Terrenos Proterozoicos na Provincia Borborema e a Margem Norte do Craton São Francisco. *Revista Brasileira de Geociências*, **22**, 742–780, https://doi.org/10.25249/0375-7536.1991472480.

Jochum, K.P., Weis, U., et al. 2011. Determination of Reference Values for NIST SRM 610-617 Glasses Following ISO Guidelines. *Geostandards and Geoanalytical Research*, **35**, 397–429, https://doi.org/10.1111/j.1751-908X.2011.00120.x.

Kennedy, A.K., Wotzlaw, J.-F., Schaltegger, U., Crowley, J.L. and Schmitz, M. 2014. EOCENE ZIRCON REFERENCE MATERIAL FOR MICROANALYSIS OF U-Th-Pb ISOTOPES AND TRACE ELEMENTS. *The Canadian Mineralogist*, **52**, 409–421, https://doi.org/10.3749/canmin.52.3.409.

Klöcking, M., White, N. and MacLennan, J. 2018. Role of basaltic magmatism within the Parnaíba cratonic basin, NE Brazil. *Geological Society, London, Special Publications*, **472**, 309–319, https://doi.org/10.1144/SP472.4.

Kozuch, M. 2003. *Isotopic and Trace Elements Geochemistry of Early Neoproterozoic Gneissic and Metavolcanic Rocks in the CaririsVelhos Orogen of the Borborema Province, Brazil, and Their Bearing on Tectonic Setting*. Ph.D. Thesis, University of Kansas.

Kuchle, J., Scherer, C.M. dos S., Born, C.C., Alvarenga, R. dos S. and Adegas, F. 2011. A contribution to regional stratigraphic correlations of the Afro-Brazilian depression – The Dom João Stage (Brotas Group and equivalent units – Late Jurassic) in Northeastern Brazilian sedimentary basins. *Journal of South American Earth Sciences*, **31**, 358–371, https://doi.org/10.1016/j.jsames.2011.02.007.

Lages, G.A., Montefalco de Lira Santos, L.C., Brasilino, R.G., Rodrigues, J.B. and Dantas, E.L. 2019. Statherian-Calymmian (ca. 1.6 Ga) magmatism in the Alto Moxotó Terrane, Borborema Province, northeast Brazil: Implications for within-plate and coeval collisional tectonics in West Gondwana. *Journal of South American Earth Sciences*, **91**, 116–130, https://doi.org/10.1016/j.jsames.2019.02.003.

Lima, M.R. de. 1978. *Palinologia Da Formação Santana (Cretaceo Do Nordeste Do Brasil)*. PhD Thesis, Univesidade de São Paulo.

Lima, M.R. de and Perinotto, J.A.J. 1984. Palinologia de sedimentos da parte superior da Formação Missão Velha, Bacia do Araripe. *Geociências*, **3**, 67–76.

Machado Junior, D. de L., Dehira, L.K., Carneiro, C. dal R. and Almeida, F.F.M. de. 1990. Reconstruções Paleoambientais do Juro-Cretaceo no Nordeste Oriental Brasileiro. *Revista Brasileira de Geociências*, **19**, 470–485.

MacRae, N.D., Nesbitt, H.W. and Kronberg, B.I. 1992. Development of a positive Eu anomaly during diagenesis. *Earth and Planetary Science Letters*, **109**, 585–591, https://doi.org/10.1016/0012-821X(92)90116-D.

Maisey, J.G. 2000. Continental break up and the distribution of fishes of Western Gondwana during the Early Cretaceous. *Cretaceous Research*, **21**, 281–314, https://doi.org/10.1006/cres.1999.0195.

Marsh, J.H., Jørgensen, T.R.C., Petrus, J.A., Hamilton, M.A. and Mole, D.R. 2019. U-Pb, trace element, and hafnium isotope composition of the Maniitsoq zircon: A potential new Archean zircon reference material. *In*: *Abstracts* – Goldschmidt.

Matos, R.M.D. de. 1999. History of the northeast Brazilian rift system: kinematic implications for the break-up between Brazil and West Africa. *Geological Society, London, Special Publications*, **153**, 55–73, https://doi.org/10.1144/GSL.SP.1999.153.01.04.

Matos, R.M.D. de, Medeiros, W.E., Jardim de Sá, E.F., Almeida, C.B. de, Norton, I. and Córdoba, V.C. 2021a. A solution to the Albian fit challenge between the South American and African plates based on key magmatic and sedimentary events late in the rifting phase in the Pernambuco and Paraíba basins. *Marine and Petroleum Geology*, **128**, 105038, https://doi.org/10.1016/j.marpetgeo.2021.105038.

Matos, R.M.D. de, Krueger, A., Norton, I. and Casey, K. 2021b. The fundamental role of the Borborema and Benin–Nigeria provinces of NE Brazil and NW Africa during the development of the South Atlantic Cretaceous Rift system. *Marine and Petroleum Geology*, **127**, 104872, https://doi.org/10.1016/j.marpetgeo.2020.104872.

Matos, R.M.D. 1992. The Northeast Brazilian Rift System. *Tectonics*, **11**, 766–791, https://doi.org/10.1029/91TC03092.

McLennan, S.M., Taylor, S.R., McCulloch, M.T. and Maynard, J.B. 1990. Geochemical and Nd□Sr isotopic composition of deep-sea turbidites: Crustal evolution and plate tectonic associations. *Geochimica et Cosmochimica Acta*, **54**, 2015–2050, https://doi.org/10.1016/0016-7037(90)90269-Q.

McLennan, S.M., Hemming, S., McDaniel, D.K. and Hanson, G.N. 1993. Geochemical approaches to sedimentation, provenance, and tectonics. *In*: *Processes Controlling the Composition of Clastic Sediments*.

Medeiros, V.C. de. 2000. *Aracaju NE: Folha SC. 24-X*.

Milani, E.J., Rangel, H.D., Bueno, G.V., Stica, J.M., Winter, W.R., Caixeta, J.M. and Neto, O. da C.P. 2007. Bacias Sedimentares Brasileiras - Cartas Estratigraficas. *Boletim de Geosciências da Petrobras*, **15**, 183–205.

Miloski, P., Mendes, J.C., Almeida, C.N. de, de Castro Valente, S. and Regina de Medeiros, S. 2019. Petrogenesis of continental flood basalts in eastern Parnaiba basin, Brazil: A singular sill occurrence with low- and high-TiO2 tholeiites. *Journal of South American Earth Sciences*, **94**, 102192, https://doi.org/10.1016/j.jsames.2019.05.008.

Moiroud, M., Pucéat, E., et al. 2016. Evolution of neodymium isotopic signature of seawater during the Late Cretaceous: Implications for intermediate and deep circulation. *Gondwana Research*, **36**, 503–522, https://doi.org/10.1016/j.gr.2015.08.005.

Moulin, M., Aslanian, D. and Unternehr, P. 2010. A new starting point for the South and Equatorial Atlantic Ocean. *Earth-Science Reviews*, **98**, 1–37, https://doi.org/10.1016/j.earscirev.2009.08.001.

Nascimento, M.D.S., Góes, A.M., Macambira, M.J.B. and Brod, J.A. 2007. Provenance of Albian sandstones in the São Luís–Grajaú Basin (northern Brazil) from the

evidence of Pb–Pb zircon ages, mineral chemistry of tourmaline, and palaeocurrent data. *Sedimentary Geology*, **201**, 21–42, https://doi.org/10.1016/j.sedgeo.2007.04.005.

Nesbitt, H.W. and Young, G.M. 1982. Early Proterozoic climates and plate motions inferred from major element chemistry of lutites. *Nature*, **299**.

Neumann, V.H., Borrego, A.G., Cabrera, L. and Dino, R. 2003. Organic matter composition and distribution through the Aptian–Albian lacustrine sequences of the Araripe Basin, northeastern Brazil. *International Journal of Coal Geology*, **54**, 21–40, https://doi.org/10.1016/S0166-5162(03)00018-1.

Neves, S.P. 2003. Proterozoic history of the Borborema province (NE Brazil): Correlations with neighboring cratons and Pan-African belts and implications for the evolution of western Gondwana: PROTEROZOIC HISTORY OF THE BORBOREMA PROVINCE. *Tectonics*, **22**, n/a-n/a, https://doi.org/10.1029/2001TC001352.

Neves, S.P., Lages, G.A., Brasilino, R.G. and Miranda, A.W.A. 2015. Paleoproterozoic accretionary and collisional processes and the build-up of the Borborema Province (NE Brazil): Geochronological and geochemical evidence from the Central Domain. *Journal of South American Earth Sciences*, **58**, 165–187, https://doi.org/10.1016/j.jsames.2014.06.009.

Parente, C.V. and Arthaud, M.H. 1995. O SISTEMA ORÓS-JAGUARIBE NO CEARÁ, NE DO BRASIL. *Revista Brasileira de Geociências*, **25**, 297–306, https://doi.org/10.25249/0375-7536.1995297306.

Paton, C., Hellstrom, J., Paul, B., Woodhead, J. and Hergt, J. 2011. Iolite: Freeware for the visualization and processing of mass spectrometric data. *Journal of Analytical Atomic Spectrometry*, **26**, 2508, https://doi.org/10.1039/c1ja10172b.

Petrus, J.A. and Kamber, B.S. 2012. VizualAge: A Novel Approach to Laser Ablation ICP-MS U-Pb Geochronology Data Reduction. *Geostandards and Geoanalytical Research*, **36**, 247–270, https://doi.org/10.1111/j.1751-908X.2012.00158.x.

Pimentel, M.M. and Fuck, R.A. 1992. Neoproterozoic crustal accretion in central Brazil. *Geology*, **20**, 375, https://doi.org/10.1130/0091-7613(1992)020<0375:NCAICB>2.3.CO;2.

Ponte, F.C. and Appi, C.J. 1990. Proposta de revisão da coluna litoestratigrafica da Bacia do Araripe. *In*: *Anais* – Congresso Brasileiro de Geologia. 211–226.

Ponte, F.C. and Ponte Filho, F.C. 1996. *Estrutura Geológica e Evolução Tectônica Da Bacia Do Araripe*.

Pourmand, A., Dauphas, N. and Ireland, T.J. 2012. A novel extraction chromatography and MC-ICP-MS technique for rapid analysis of REE, Sc, and Y: Revising CI-chondrite and Post-Archean Australian Shale (PAAS) abundances. *Chemical Geology*, **291**, 38–54, https://doi.org/10.1016/j.chemgeo.2011.08.011.

Prado, L.A.C.D., Pereira, P.A., Sales, A.M.F. and Barreto, A.M.F. 2015. Taphonomic and paleoenvironmental considerations for the concentrations of macroinvertebrate fossils in the Romualdo Member, Santana Formation, Late Aptian – Early Albian, Araripe Basin, Araripina, NE, Brazil. *Journal of South American Earth Sciences*, **62**, 218–228, https://doi.org/10.1016/j.jsames.2015.06.005.

Rios Netto, A. de M., Paula-Freitas, A.B.L., Carvalho, I. de S., Regali, M. da S.P., Borghi, L. and Freitas, F.I. de. 2012a. Formalização estratigráfica do Membro Fundão, Formação Rio da Batateira, Cretáceo Inferior da Bacia do Araripe, Nordeste do Brasil. *Revista Brasileira de Geociências*, **42**, https://doi.org/10.5327/Z0375-75362012000200005.

Rios Netto, A. de M., Regali, M. da S.P., Carvalho, I. de S. and Freitas, F.I. de. 2012b. Palinoestratigrafia do intervalo Alagoas da Bacia do Araripe, Nordeste do Brasil. *Revista Brasileira de Geociências*, **42**, https://doi.org/10.5327/Z0375-75362012000200009.

Rivera, H.A., Le Roux, J.P., Sánchez, L.K., Mariño-Martínez, J.E., Salazar, C. and Barragán, J.C. 2018. Palaeoredox conditions and sequence stratigraphy of the Cretaceous storm-dominated, mixed siliciclastic-carbonate ramp in the Eastern Cordillera Basin (Colombia): Evidence from sedimentary geochemical proxies and facies analysis. *Sedimentary Geology*, **372**, 1–24, https://doi.org/10.1016/j.sedgeo.2018.05.003.

Roddaz, M., Viers, J., Brusset, S., Baby, P. and Hérail, G. 2005. Sediment provenances and drainage evolution of the Neogene Amazonian foreland basin. *Earth and Planetary Science Letters*, **239**, 57–78, https://doi.org/10.1016/j.epsl.2005.08.007.

Roddaz, M., Christophoul, F., Burgos Zambrano, J.D., Soula, J.-C. and Baby, P. 2012. Provenance of late Oligocene to quaternary sediments of the Ecuadorian Amazonian foreland basin as inferred from major and trace element geochemistry and Nd–Sr isotopic composition. *Journal of South American Earth Sciences*, **37**, 136–153, https://doi.org/10.1016/j.jsames.2012.02.008.

Roddaz, M., Viers, J., Moreira-Turcq, P., Blondel, C., Sondag, F., Guyot, J.-L. and Moreira, L. 2014. Evidence for the control of the geochemistry of Amazonian floodplain sediments by stratification of suspended sediments in the Amazon. *Chemical Geology*, **387**, 101–110, https://doi.org/10.1016/j.chemgeo.2014.07.022.

Roddaz, M., Dera, G., et al. 2021. Provenance constraints on the Cretaceous-Paleocene erosional history of the Guiana Shield as determined from the geochemistry of clay-size fraction of sediments from the Arapaima-1 well (Guyana-Suriname basin). *Marine Geology*, **434**, 106433.

Rodrigues, M. de A., Roddaz, M., et al. 2023. New insights into the Cretaceous evolution of the Western Amazonian paleodrainage system. *Sedimentary Geology*, **453**, 106434, https://doi.org/10.1016/j.sedgeo.2023.106434.

Sahabi, M., Aslanian, D. and Olivet, J.-L. 2004. Un nouveau point de départ pour l'histoire de l'Atlantique central. *Comptes Rendus Geoscience*, **336**, 1041–1052, https://doi.org/10.1016/j.crte.2004.03.017.

Sales, A.M.F. 2005. *Análise tafonômica das ocorrências fossiliferas de macroinvertebrados do Membro Romualdo (Albiano) da Formação Santana, Bacia do Araripe, NE do Brasil: Significado estratigrafico e paleoambiental*. Tese de doutoramento, Universidade de São Paulo.

Santos, T.J.S. dos, Fetter, A.H., Neto, J.A., Hackspacher, P.C. and Van Schmus, R. 1998. Geochronology and geochemistry of the Medio Coreau Domain NW Borborema Province. *XL Congresso Brasileiro de Gologia*.

Santos, E.J., Schmus, W.R.V., Kozuch, M. and Neves, B.B. de B. 2010. The Cariris Velhos tectonic event in Northeast Brazil. *Journal of South American Earth Sciences*, **29**, 61–76, https://doi.org/10.1016/j.jsames.2009.07.003.

Santos, T.J.S., Fetter, A.H. and Neto, J.A.N. 2008. Comparisons between the northwestern Borborema Province, NE Brazil, and the southwestern Pharusian Dahomey Belt, SW Central Africa. *Geological Society, London, Special Publications*, **294**, 101–120, https://doi.org/10.1144/SP294.6.

Scherer, C.M. dos S., Jardim de Sá, E.F., Córdoba, V.C., Sousa, D. do C., Aquino, M.M. and Canelas Cardoso, F.M. 2014. Tectono-stratigraphic evolution of the Upper Jurassic–Neocomian rift succession, Araripe Basin, Northeast Brazil. *Journal of South American Earth Sciences*, **49**, 106–122, https://doi.org/10.1016/j.jsames.2013.10.007.

Scherer, C.M.S., Goldberg, K. and Bardola, T. 2015. Facies architecture and sequence stratigraphy of an early post-rift fluvial succession, Aptian Barbalha Formation, Araripe Basin, northeastern Brazil. *Sedimentary Geology*, **322**, 43–62, https://doi.org/10.1016/j.sedgeo.2015.03.010.

Shirey, S.B. and Richardson, S.H. 2011. Start of the Wilson Cycle at 3 Ga Shown by Diamonds from Subcontinental Mantle. *Science*, **333**, 434–436, https://doi.org/10.1126/science.1206275.

Silvestre, D., Fambrini, G. and Santos, A. 2017. CARACTERIZAÇÃO FACIOLÓGICA DAS FORMAÇÕES CARIRI E BREJO SANTO EM AFLORAMENTOS A NE DO MUNICÍPIO MISSÃO VELHA (CEARÁ – BRASIL). *Estudos Geológicos*, **27**, 19–33, https://doi.org/10.18190/1980-8208/estudosgeologicos.v27n1p19-33.

Sláma, J., Košler, J., et al. 2008. Plešovice zircon — A new natural reference material for U–Pb and Hf isotopic microanalysis. *Chemical Geology*, **249**, 1–35, https://doi.org/10.1016/j.chemgeo.2007.11.005.

Spencer, C.J., Kirkland, C.L. and Taylor, R.J.M. 2016. Strategies towards statistically robust interpretations of in situ U–Pb zircon geochronology. *Geoscience Frontiers*, **7**, 581–589, https://doi.org/10.1016/j.gsf.2015.11.006.

Taylor, S.R. and McClennan, S.M. 1985. *The Continental Crust: Its Composition and Evolution: An Examination of the Geochemical Record Preserved in Sedimentary Rocks*, Blackwell Scientific.

Taylor, S.R. and McLennan, S.M. 1985. *The Continental Crust: Its Composition and Evolution*. Geoscience texts.

Tribovillard, N.-P., Caulet, J.-P., Vergnaud-Grazzini, C., Moureau, N. and Tremblay, P. 1996. Lack of organic matter accumulation on the upwelling-influenced Somalia margin in a glacial-interglacial transition. *Marine Geology*, **133**, 157–182, https://doi.org/10.1016/0025-3227(96)00034-5.

Tyson, R.V. and Pearson, T.H. 1991. Modern and ancient continental shelf anoxia: an overview. *Geological Society, London, Special Publications*, **58**, 1–24, https://doi.org/10.1144/GSL.SP.1991.058.01.01.

Van Kranendonk, M.J., Hugh Smithies, R., Hickman, A.H., Wingate, M.T.D. and Bodorkos, S. 2010. Evidence for Mesoarchean (~3.2Ga) rifting of the Pilbara Craton: The missing link in an early Precambrian Wilson cycle. *Precambrian Research*, **177**, 145–161, https://doi.org/10.1016/j.precamres.2009.11.007.

van Schmus, W.R., Oliveira, E.P., da Silva Filho, A.F., Toteu, S.F., Penaye, J. and Guimarães, I.P. 2008. Proterozoic links between the Borborema Province, NE Brazil, and the Central African Fold Belt. *Geological Society, London, Special Publications*, **294**, 69–99, https://doi.org/10.1144/SP294.5.

Van Schmus, W.R., Kozuch, M. and de Brito Neves, B.B. 2011. Precambrian history of the Zona Transversal of the Borborema Province, NE Brazil: Insights from Sm–Nd and U–Pb geochronology. *Journal of South American Earth Sciences*, **31**, 227–252, https://doi.org/10.1016/j.jsames.2011.02.010.

van Soelen, E.E., Kim, J.-H., et al. 2017. A 30 Ma history of the Amazon River inferred from terrigenous sediments and organic matter on the Ceará Rise. *Earth and Planetary Science Letters*, **474**, 40–48, https://doi.org/10.1016/j.epsl.2017.06.025.

Vaz, P.T., Rezende, N. das G. de A., Wanderley Filho, J.R. and Travassos, W.A.S. 2007. Bacia do Parnaíba. *Boletim de Geociências da Petrobras*, **15**, 253–263.

Vermeesch, P. 2004. How many grains are needed for a provenance study? *Earth and Planetary Science Letters*, **224**, 441–451, https://doi.org/10.1016/j.epsl.2004.05.037.

Vermeesch, P. 2013. Multi-sample comparison of detrital age distributions. *Chemical Geology*, **341**, 140–146, https://doi.org/10.1016/j.chemgeo.2013.01.010.

Vermeesch, P. 2018. Dissimilarity measures in detrital geochronology. *Earth-Science Reviews*, **178**, 310–321, https://doi.org/10.1016/j.earscirev.2017.11.027.

Vieira Melo, B.G. and Carvalho, I.S. 2018. The Brejo Santo Formation Fauna, Neojurassic from Araripe Basin, Brazil: Paleoenvironmental Interpretations. *Anuário do Instituto de Geociências - UFRJ*, **40**, 62–74, https://doi.org/10.11137/2017_3_62_74.

Viers, J. and Wasserburg, G.J. 2004. Behavior of Sm and Nd in a lateritic soil profile. *Geochimica et Cosmochimica Acta*, **68**, 2043–2054, https://doi.org/10.1016/j.gca.2003.10.034.

Weis, D., Kieffer, B., Maerschalk, C., Pretorius, W. and Barling, J. 2005. High-precision Pb-Sr-Nd-Hf isotopic characterization of USGS BHVO-1 and BHVO-2 reference materials: Pb-Sr-Nd-Hf CHARACTERIZATION. *Geochemistry, Geophysics, Geosystems*, **6**, https://doi.org/10.1029/2004GC000852.

Wiedenbeck, M., Allé, P., et al. 1995. Three Natura Zircon Standards for U-Th-Pb, Lu-Hf, Trace Element, and REE Analyses. *Geostandards Newsletter*, **19**, 1–23.

Wiedenbeck, M., Hanchar, J.M., et al. 2004. Further Characterisation of the 91500 Zircon Crystal. *Geostandards and Geoanalytical Research*, **28**, 9–39, https://doi.org/10.1111/j.1751-908X.2004.tb01041.x.

Wilson, J.T. 1969. Static or mobile earth: The current scientific revolution. *Tectonophysics*, **7**, 600–601, https://doi.org/10.1016/0040-1951(69)90033-X.

Suporting information

The provenance of the late Jurassic to Cenomanian sedimentary succession of the Araripe Basin (NE Brazil) and implication for the geodynamic evolution of Western Gondwana

Mariana de Assunção Rodrigues [a,b,*], Roberto Ventura Santos[a], Martin Roddaz [b], Elton Luiz Dantas [a], Mathieu Leisen [b]

[a] Universidade de Brasília, Darcy Ribeiro Campus, Asa Norte 70910-900 Brasília, DF, Brazil

[b] Géosciences-Environnement Toulouse, Université de Toulouse; UPS (SVT-OMP); 14 Avenue Édouard Belin, F-31400 Toulouse, France

*Corresponding author,

E-mail address: marianarodrigues.geologia@gmail.com (M. A. Rodrigues).

Contents

Figures S1 to S5

Tables S2

Additional Supporting Information (Annexes)

Table S1

Introduction

This supporting information provides a detailed description of instrumentation, including analytical conditions and the methodology used. Furthermore, the full analytical datasets produced during the U-Pb ages analysis are available as separate tables in the annexes section.

Tab. S2: Araripe samples correlations based on correlation coefficient (R^2) for geochemical proxies used in this study based on a data matrix without outlier data. Significant correlations are represented in blue.

	εNd(0)	Eu/Eu*	ΩCe	Cr/Th	Th/Sc	Zr/Sc	LREE	HREE	MREE	MREE*	Al/Si	CIA
εNd(0)	1	0.33	-0.26	-0.14	-0.64	0.00	-0.22	-0.22	-0.15	-0.25	0.08	-0.45
Eu/Eu*		1	-0.13	0.21	-0.42	0.05	-0.34	-0.40	-0.40	-0.39	-0.19	-0.50
ΩCe			1	0.04	0.09	0.03	0.58	0.45	0.64	0.58	-0.38	0.04
Cr/Th				1	-0.08	0.58	-0.23	-0.18	-0.27	-0.23	-0.04	-0.19
Th/Sc					1	0.03	0.35	0.05	0.23	0.27	-0.08	0.64
Zr/Sc						1	-0.25	-0.07	-0.20	-0.21	-0.65	-0.08
LREE							1	0.69	0.93	0.97	0.03	0.70
HREE								1	0.88	0.85	0.05	0.55
MREE									1	0.98	-0.01	0.60
MREE*										1	0.04	0.71
Al/Si											1	0.10
CIA												1

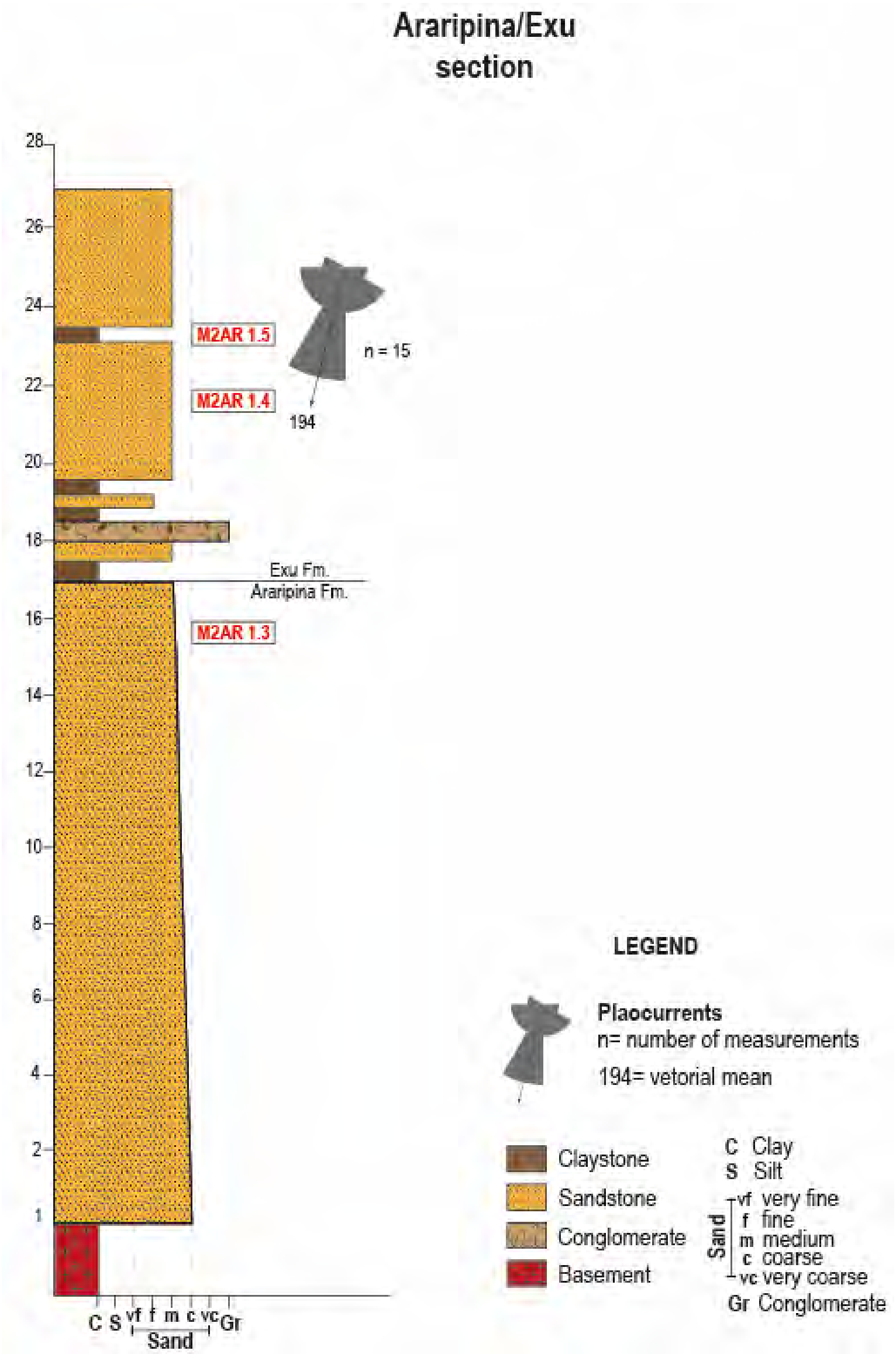

Figure S1: Araripina Exu formations outcrop with sampling locals marked and paleoflows direction.

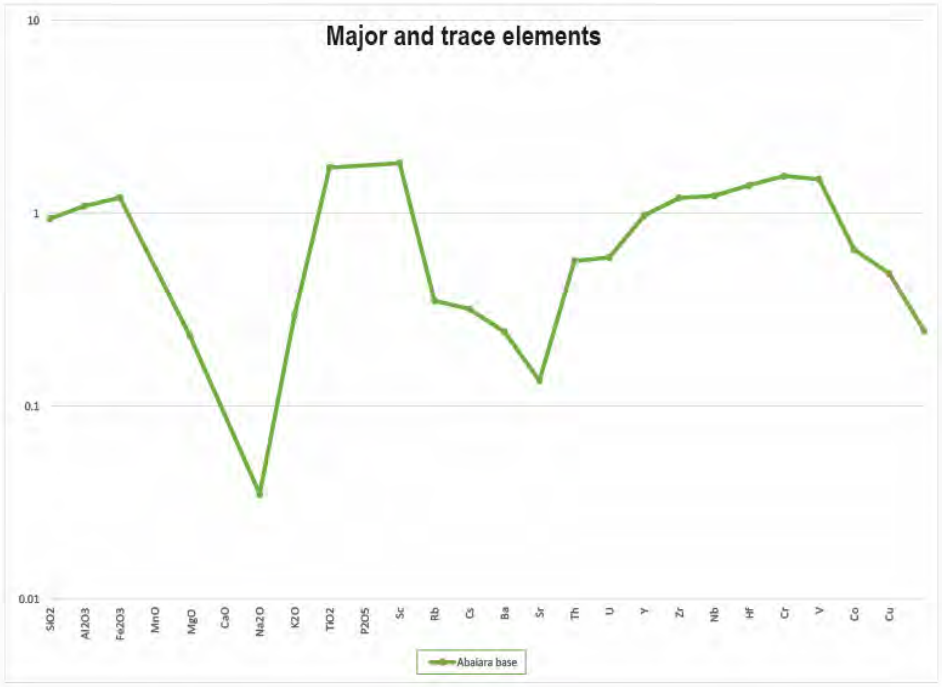

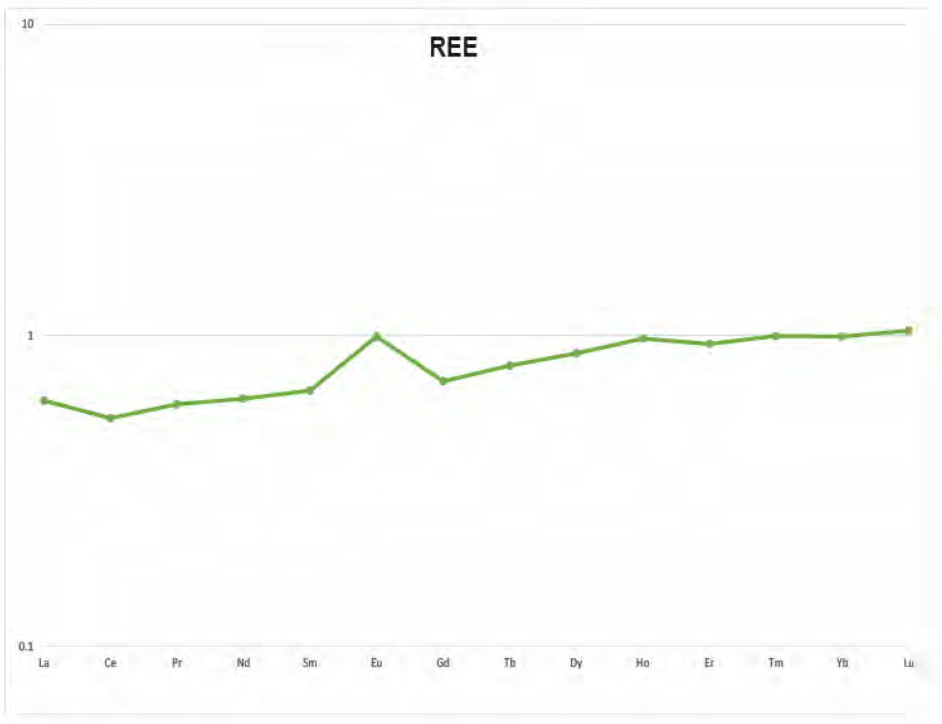

	Gr.	Formation	Sequences
	Araripe	Exu Araripina	Post Rift II
	Santana	Romualdo Ipubi Crato	Post Rift I
		Barbalha	
	Cariri Valley	Abaiara	Rift (Climax)
		Missão Velha	Rift
		Brejo Santo	
		Cariri	
		Embasamento	

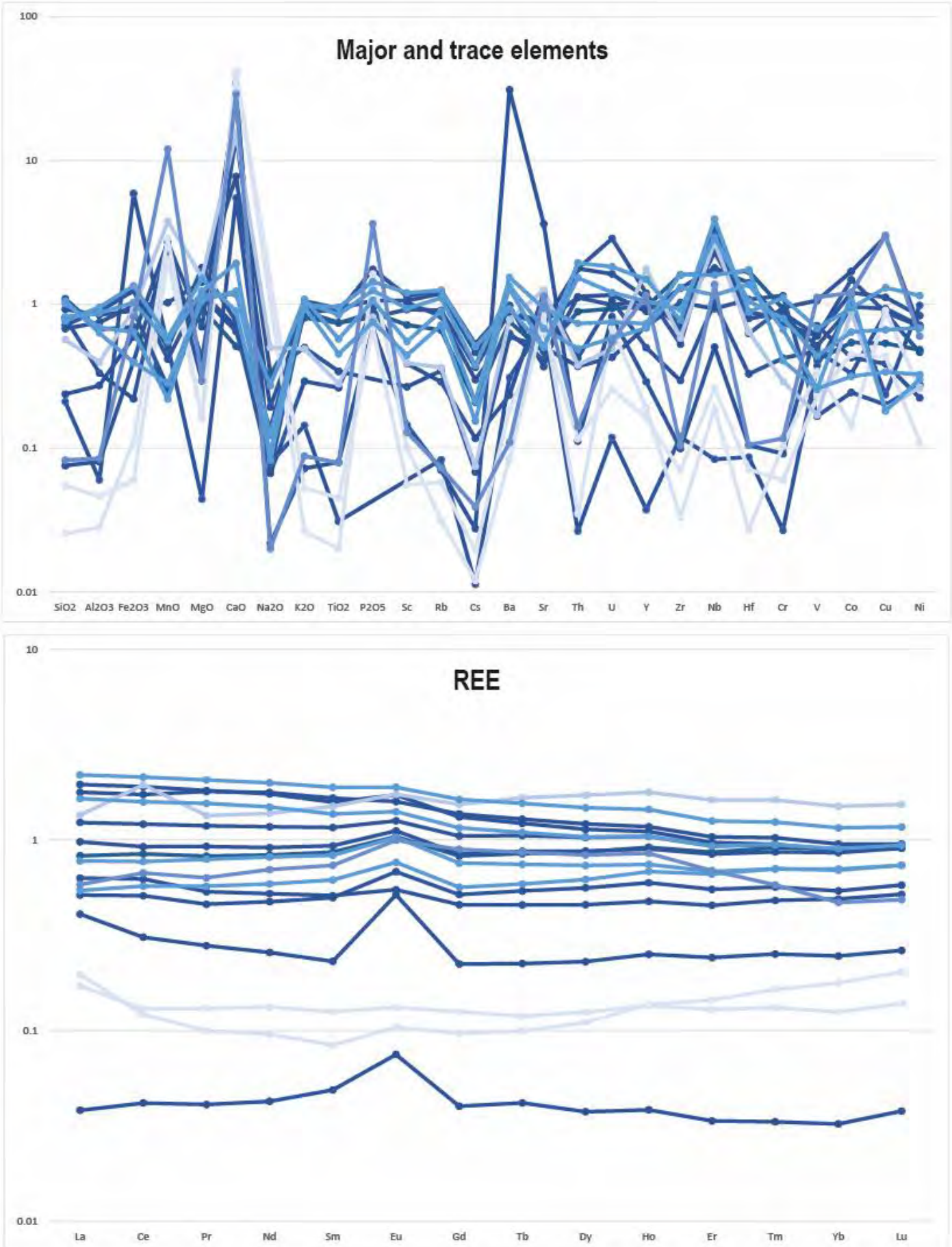

	Gr.	Formation	Sequences
	Araripe	Exu Araripina	Post Rift II
	Santana	Romualdo Ipubi Crato	Post Rift I
		Barbalha	
	Cariri Valley	Abaiara	Rift (Climax)
		Missão Velha Brejo Santo	Rift
		Cariri	
		Embasamento	

Sobradinho section

M2AR 7.3
M2AR 7.4
M2AR 7.5 bs
M2AR 7.6
M2AR 7.8 VII
M2AR 7.8 VIII bs
M2AR 7.8 XI
M2AR 7.8 XXII
M2AR 2.2 Equin
M2AR 2.3
M2AR 10.75 II
M2AR 9.1

Mãozinha section

M2AR 6.2
M2AR 6.3
M2AR 6.8
M2AR 6.9 bs

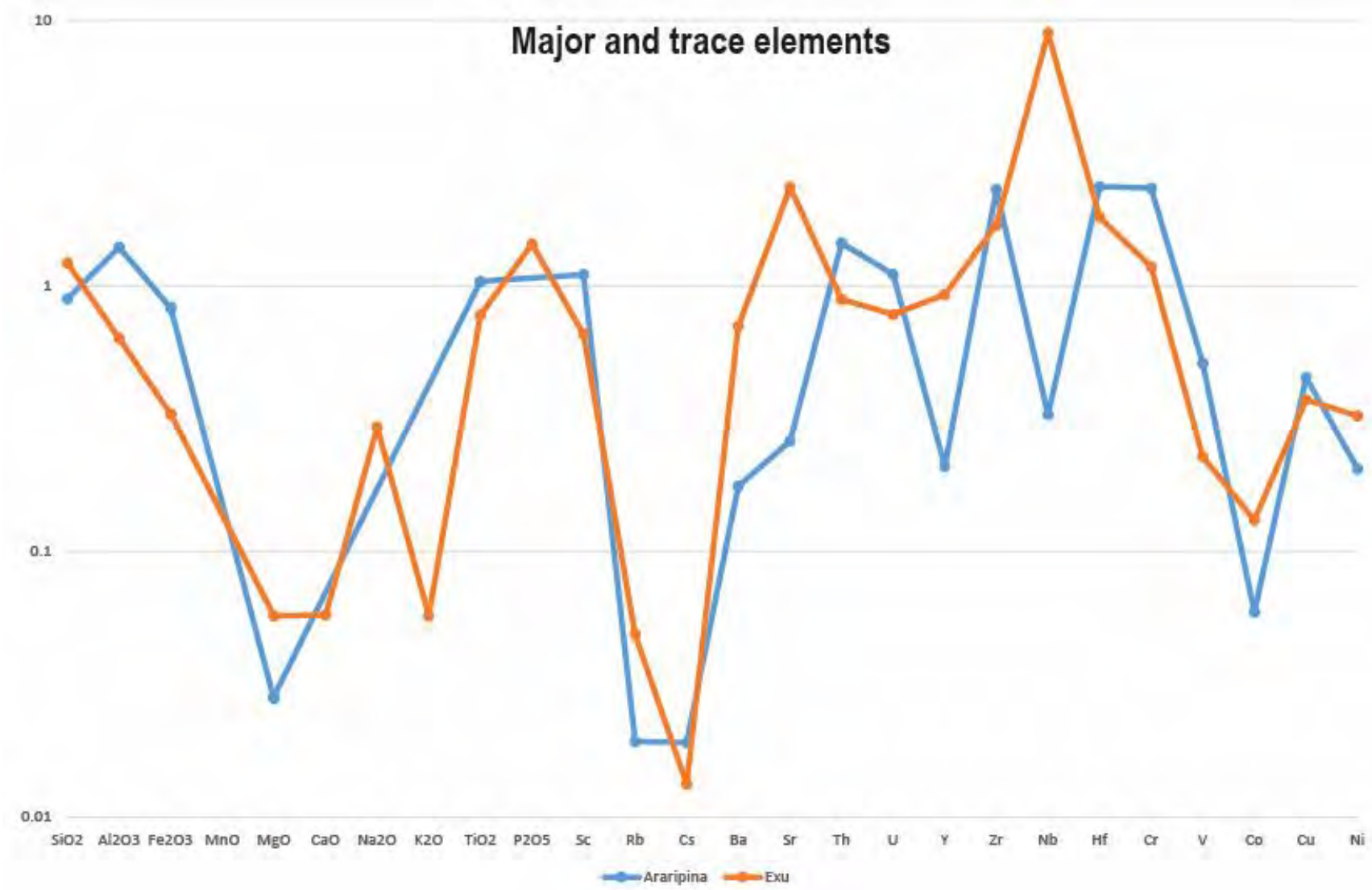
Major and trace elements
10
1
0.1
0.01
SiO2 Al2O3 Fe2O3 MnO MgO CaO Na2O K2O TiO2 P2O5 Sc Rb Cs Ba Sr Th U Y Zr Nb Hf Cr V Co Cu Ni
Araripina
Exu

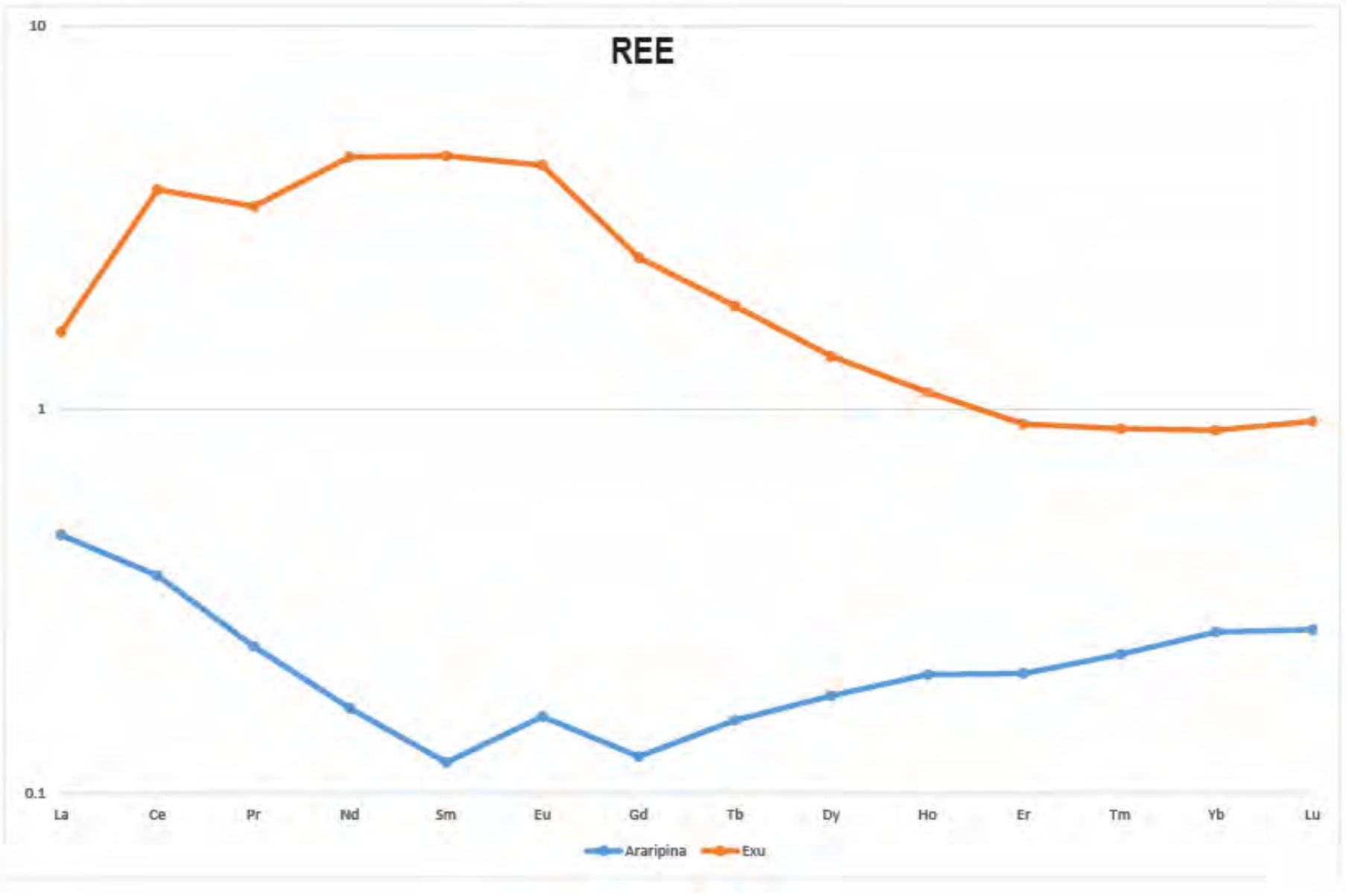
REE
10
1
0.1
La Ce Pr Nd Sm Eu Gd Tb Dy Ho Er Tm Yb Lu
Araripina
Exu

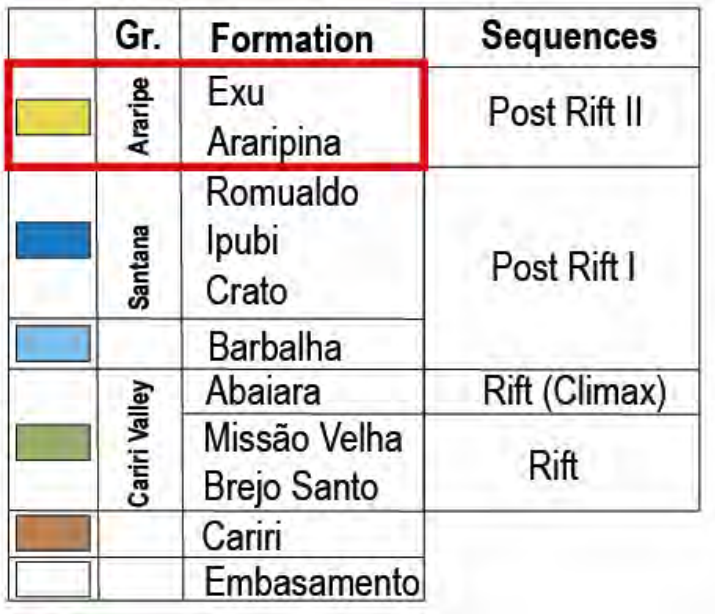

Figure S2: Major and selected trace element contents of analyzed samples normalized to PAAS (Pourmand et al., 2012; Taylor and McLennan, 1985). From left to right on the diagram, these include the major elements (SiO_2, TiO_2, Al_2O_3, Fe_2O_3, MnO, MgO, CaO, Na_2O, K_2O, and P_2O_5), LILE (Rb, Cs, Ba, Sr, Th, and U), HFSE (Y, Zr, Nb, Hf), and TTE (Sc, Cr, Co, V, and Ni). B) Rare earth element (REE) contents of studied samples normalized to PAAS. (Pourmand et al., 2012; Taylor and McLennan, 1985). A – Rift stage; B – Post-rift I stage; C – Post-rift II stage.

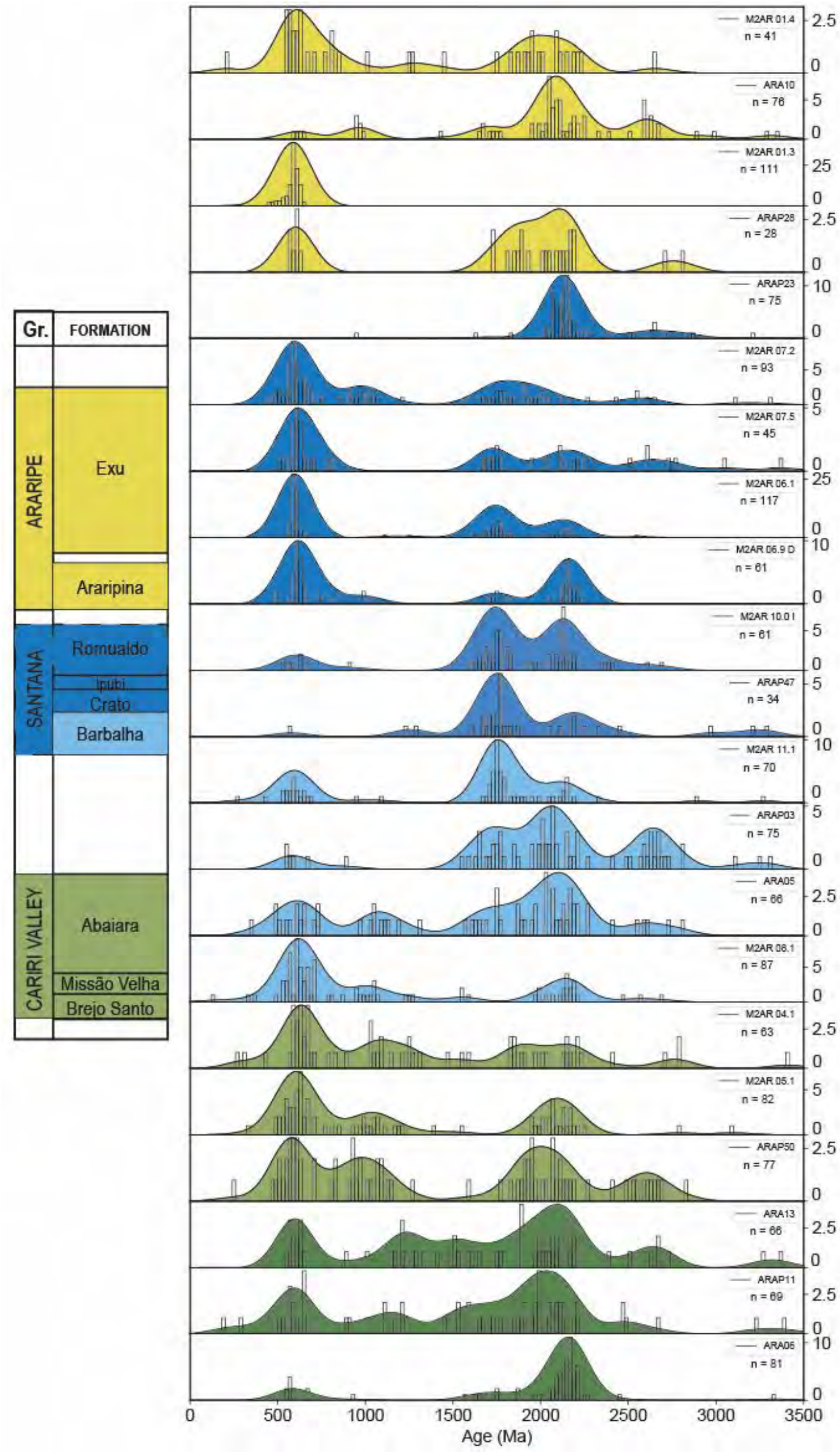

Figure S3: Stratigraphic evolution of Araripe Basin U-Pb ages on zircon grains with the age probability (black line) and age histogram (bars). The colors represent the tectonic stages: Dark green – Rift beginning; Green – Rift; Light blue and blue – Post Rift I, and Yellow – Post-Rift II.

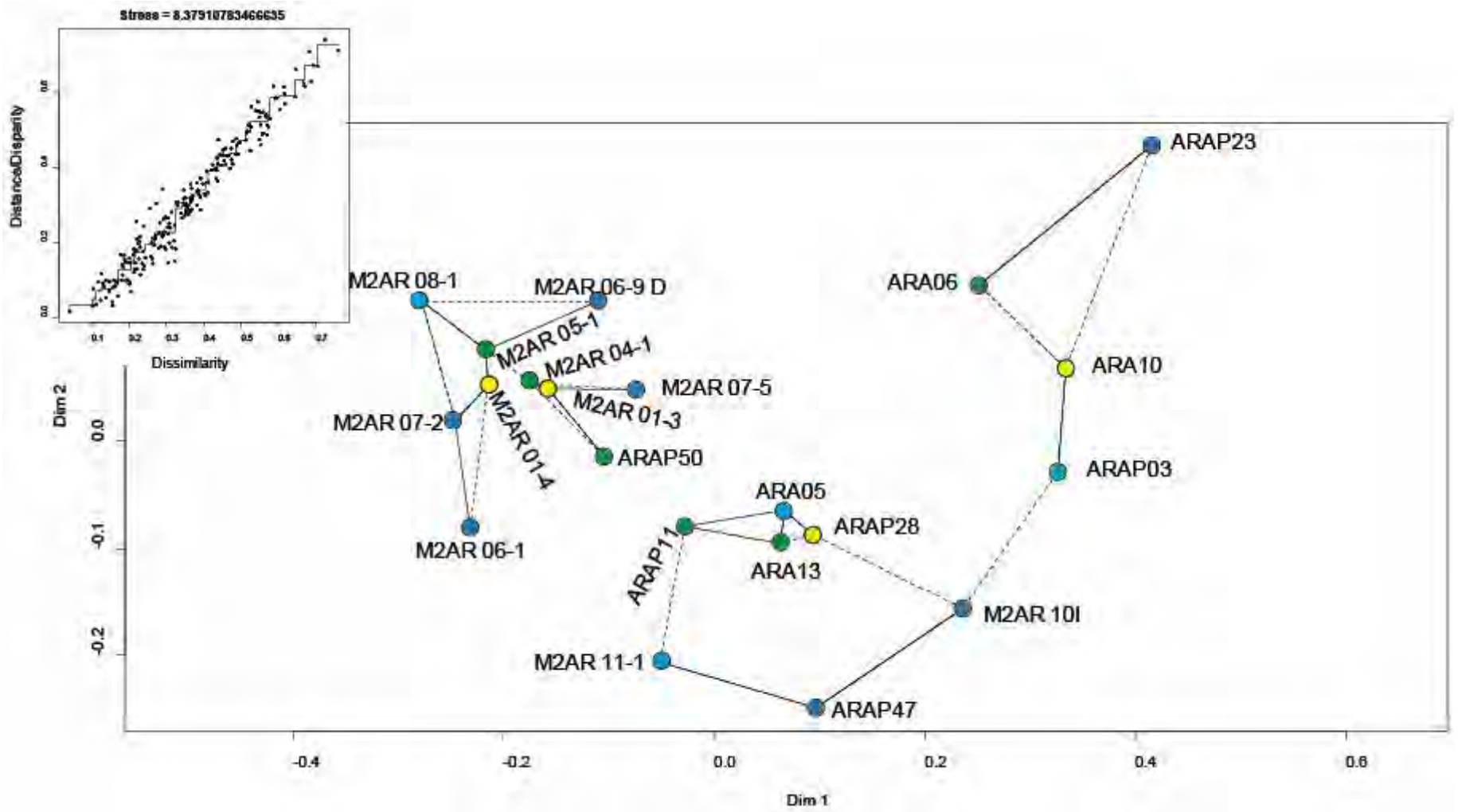

FigureS4: A) Non-matrix metric multi-dimensional scaling (MDS) plot (Vermeesch, 2013) based on the U-Pb age distributions of detrital zircons in the analyzed samples using the Kolmogorov–Smirnov test. Closest and second closest neighbors are linked by solid and dashed lines, respectively; B) Shepard plot of the U-Pb data showing the transformation from dissimilarity to distances and disparities.

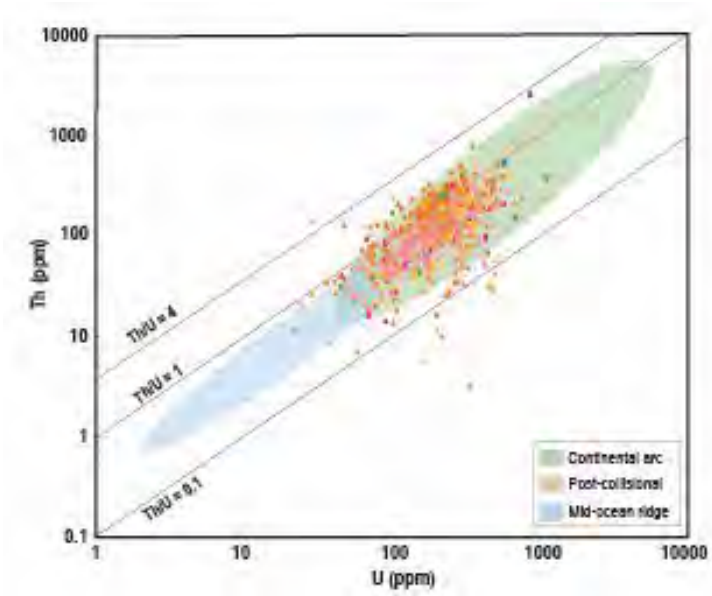

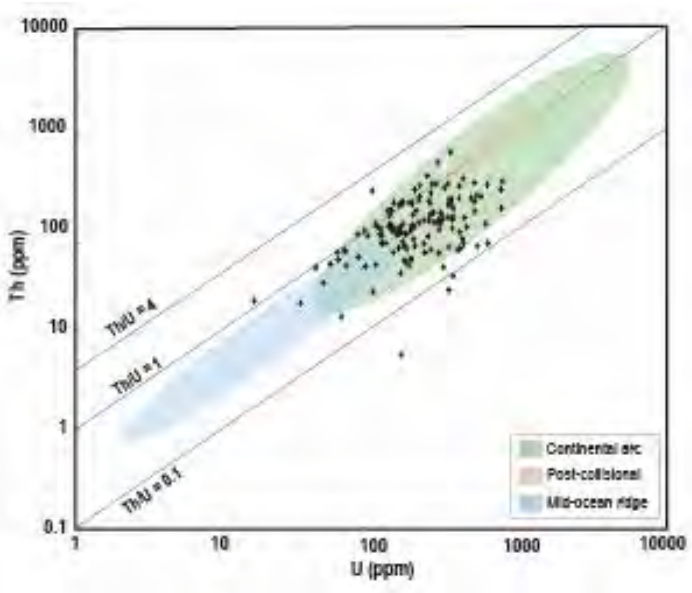

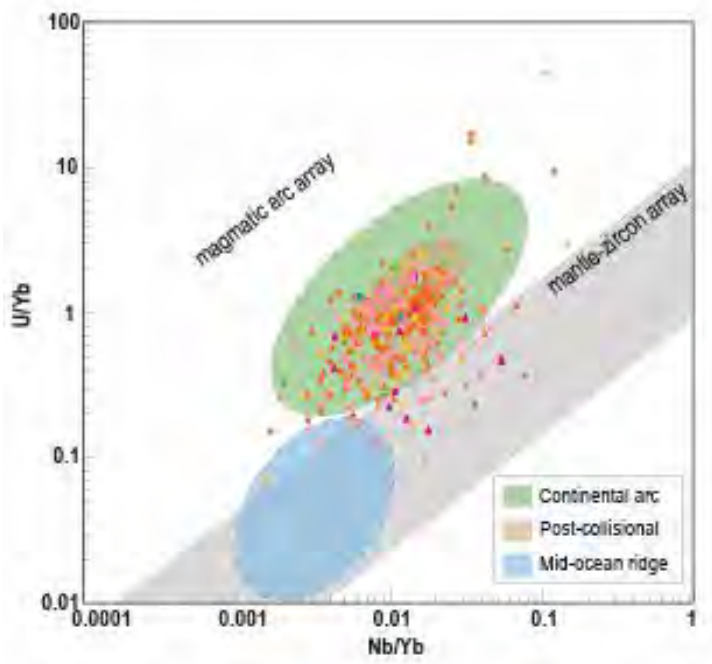

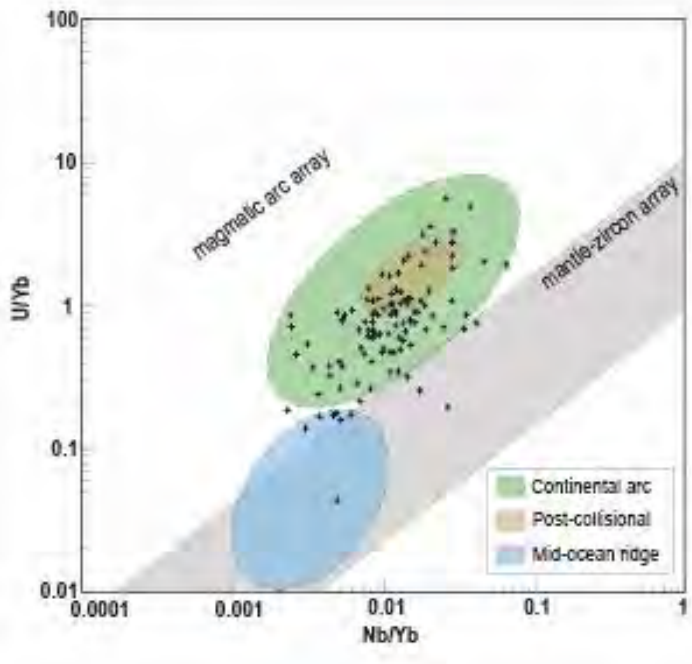

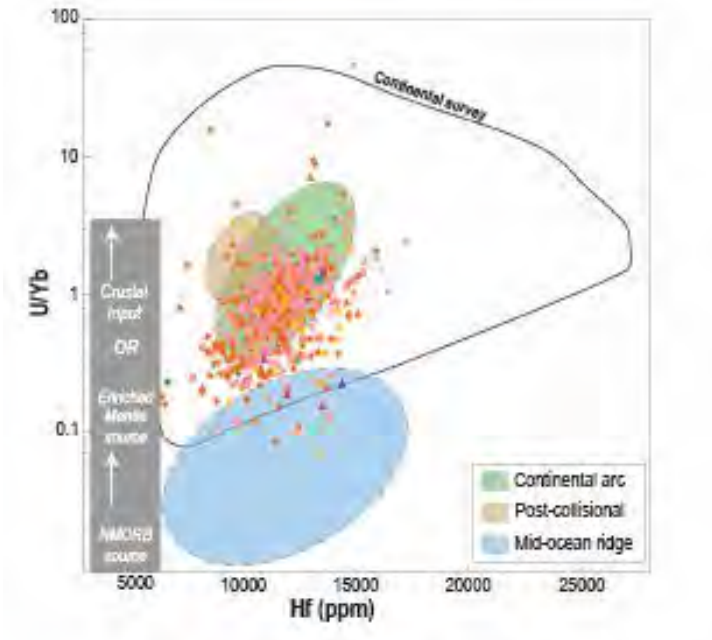

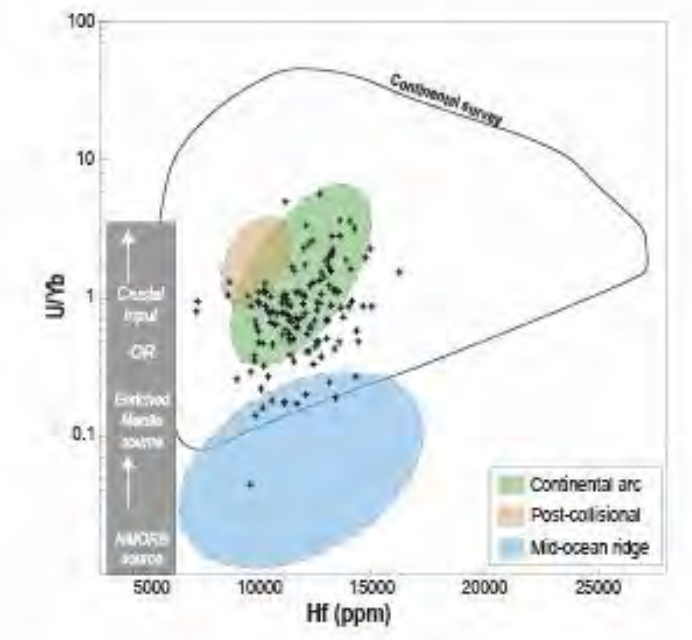

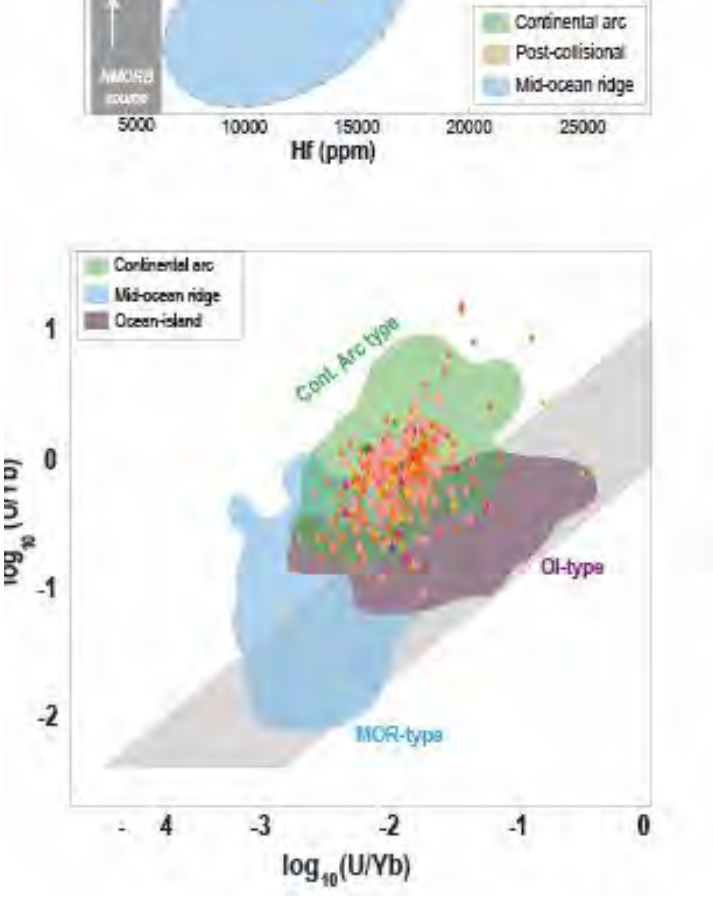

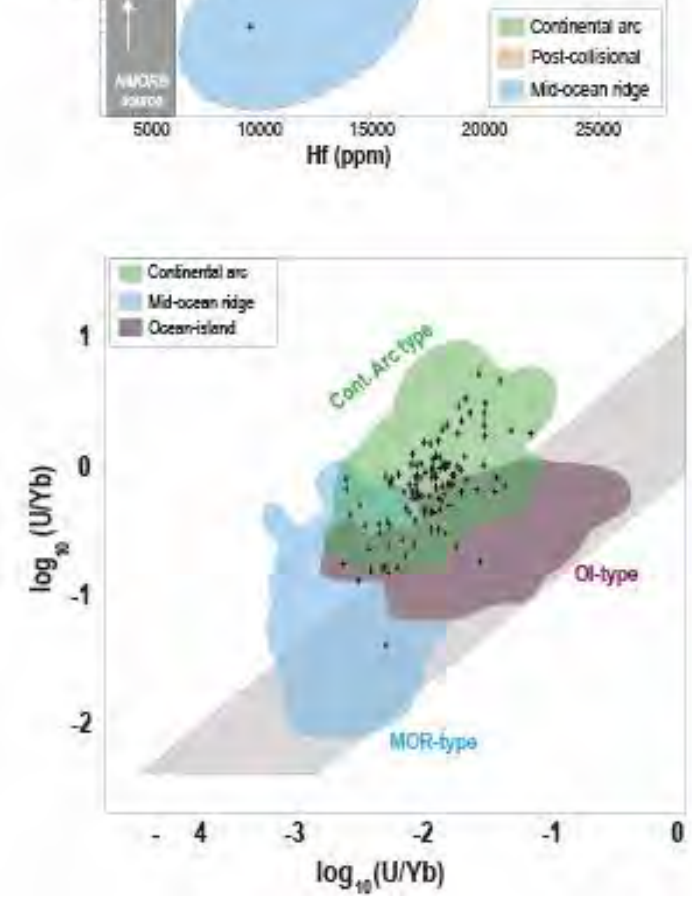

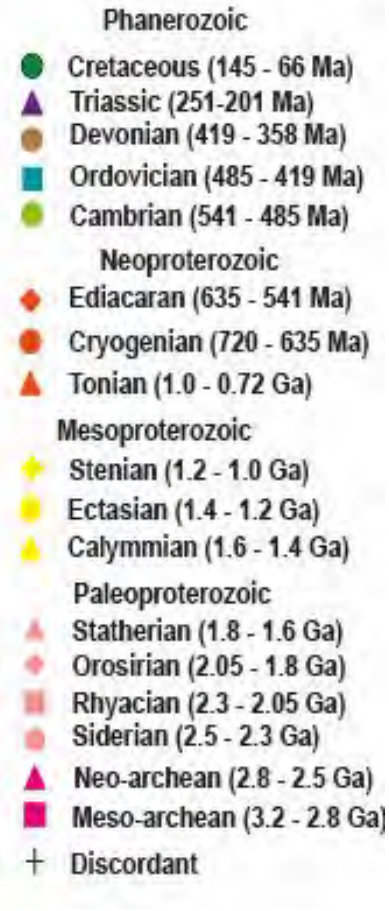

Figure S4: Selected trace element ratio diagrams from geochemistry in detrital zircon grains with proxies for crustal setting. Based on Grimes et al., 2015. A- Th vs. U diagram; B – U/Nb proxy for the tectonic magmatic source of zircon; C - U/Yb vs. Hf in zircon. The field-labeled “Continental Survey” was defined by Grimes et al. (2007)

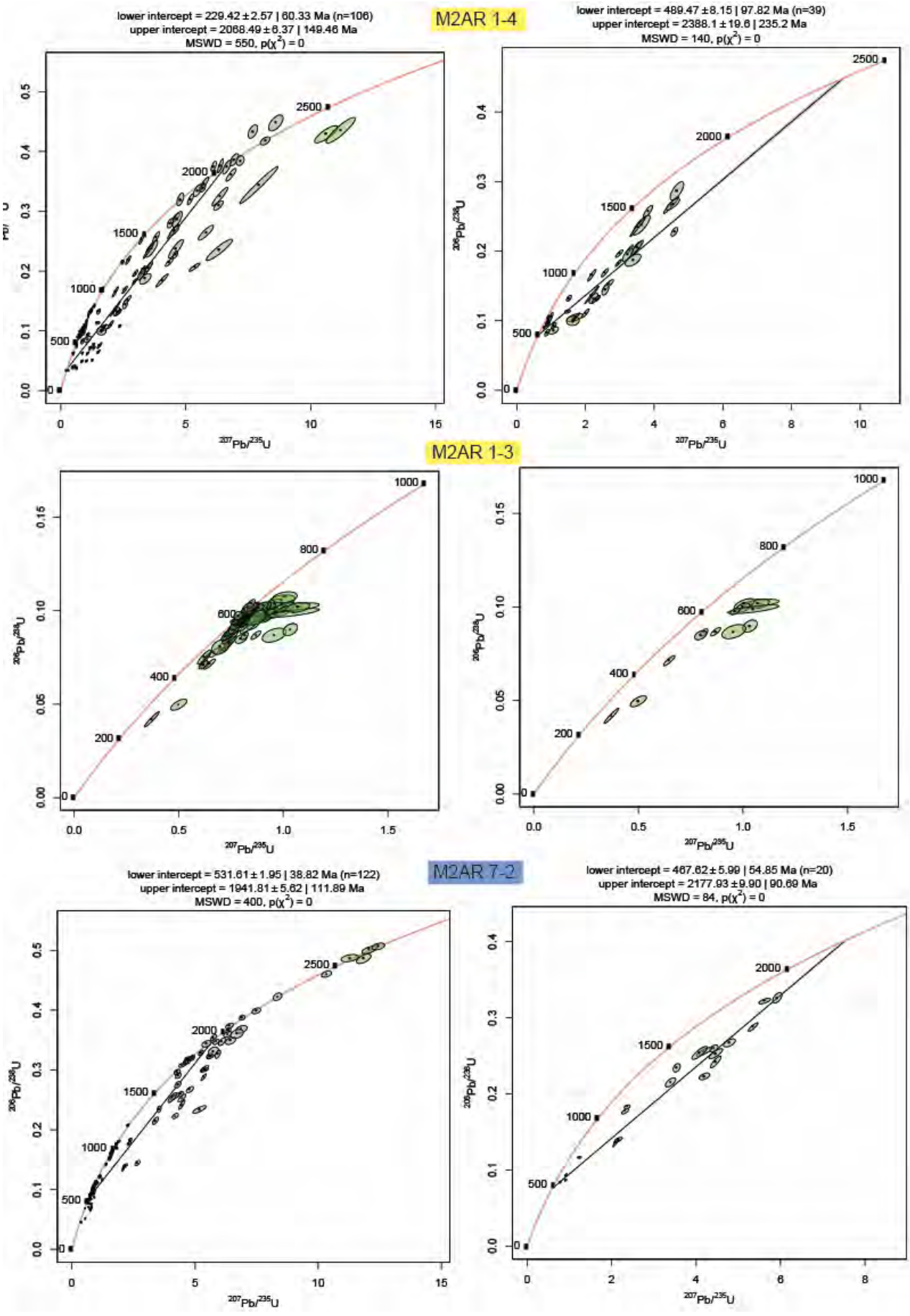
M2AR 1-4
lower intercept = 229.42 ± 2.57 | 60.33 Ma (n=106)
upper intercept = 2068.49 ± 6.37 | 149.46 Ma
MSWD = 550, p(χ²) = 0
lower intercept = 489.47 ± 8.15 | 97.82 Ma (n=39)
upper intercept = 2388.1 ± 19.6 | 235.2 Ma
MSWD = 140, p(χ²) = 0
M2AR 1-3
M2AR 7-2
lower intercept = 531.61 ± 1.95 | 38.82 Ma (n=122)
upper intercept = 1941.81 ± 5.62 | 111.89 Ma
MSWD = 400, p(χ²) = 0
lower intercept = 467.62 ± 5.99 | 54.85 Ma (n=20)
upper intercept = 2177.93 ± 9.90 | 90.69 Ma
MSWD = 84, p(χ²) = 0
207Pb/235U
206Pb/238U

M2AR 7-5

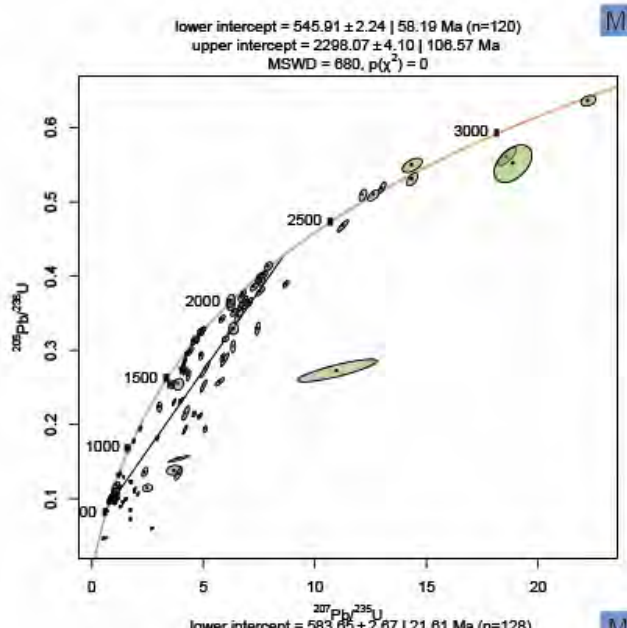

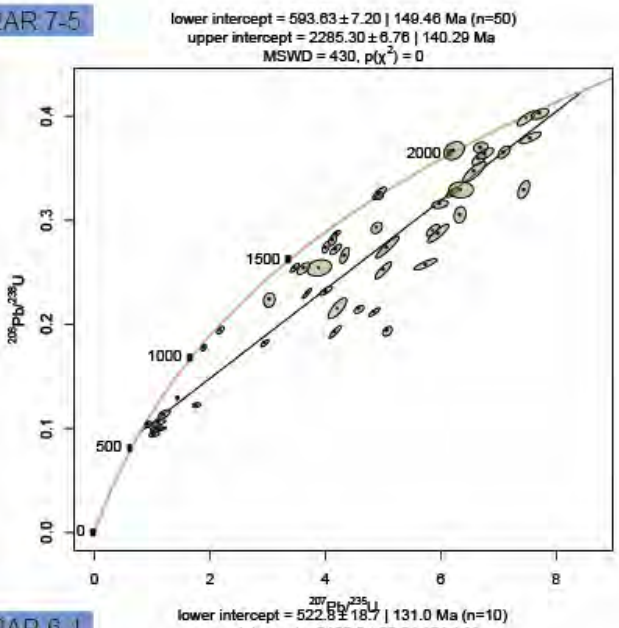

M2AR 6-1

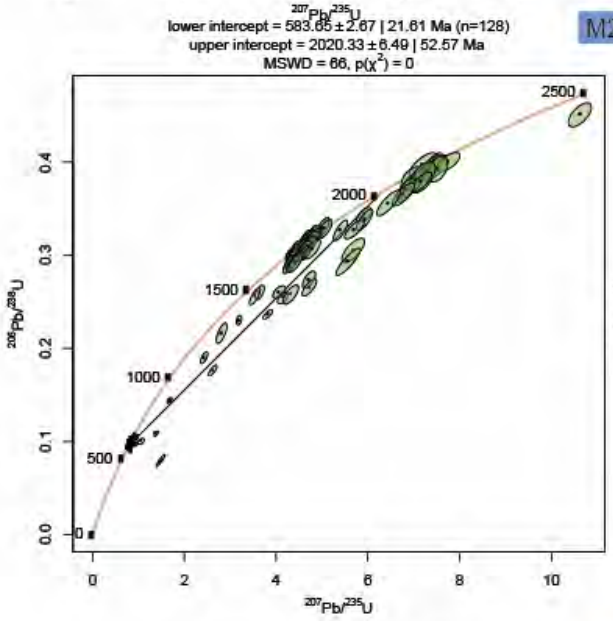

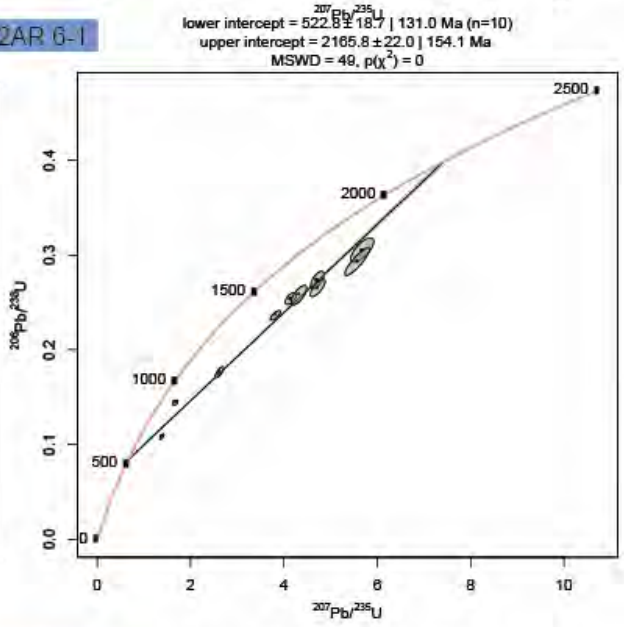

M2AR 6-9D

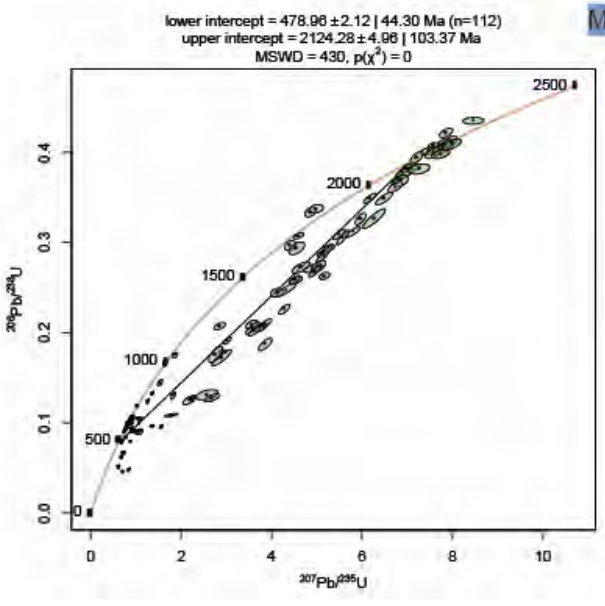

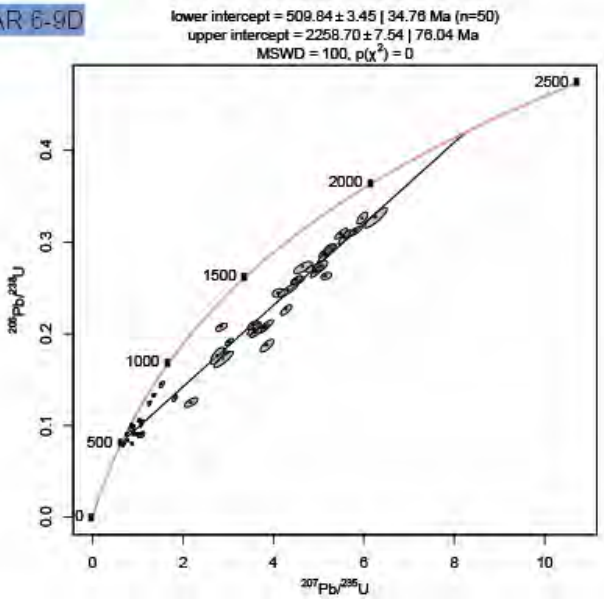

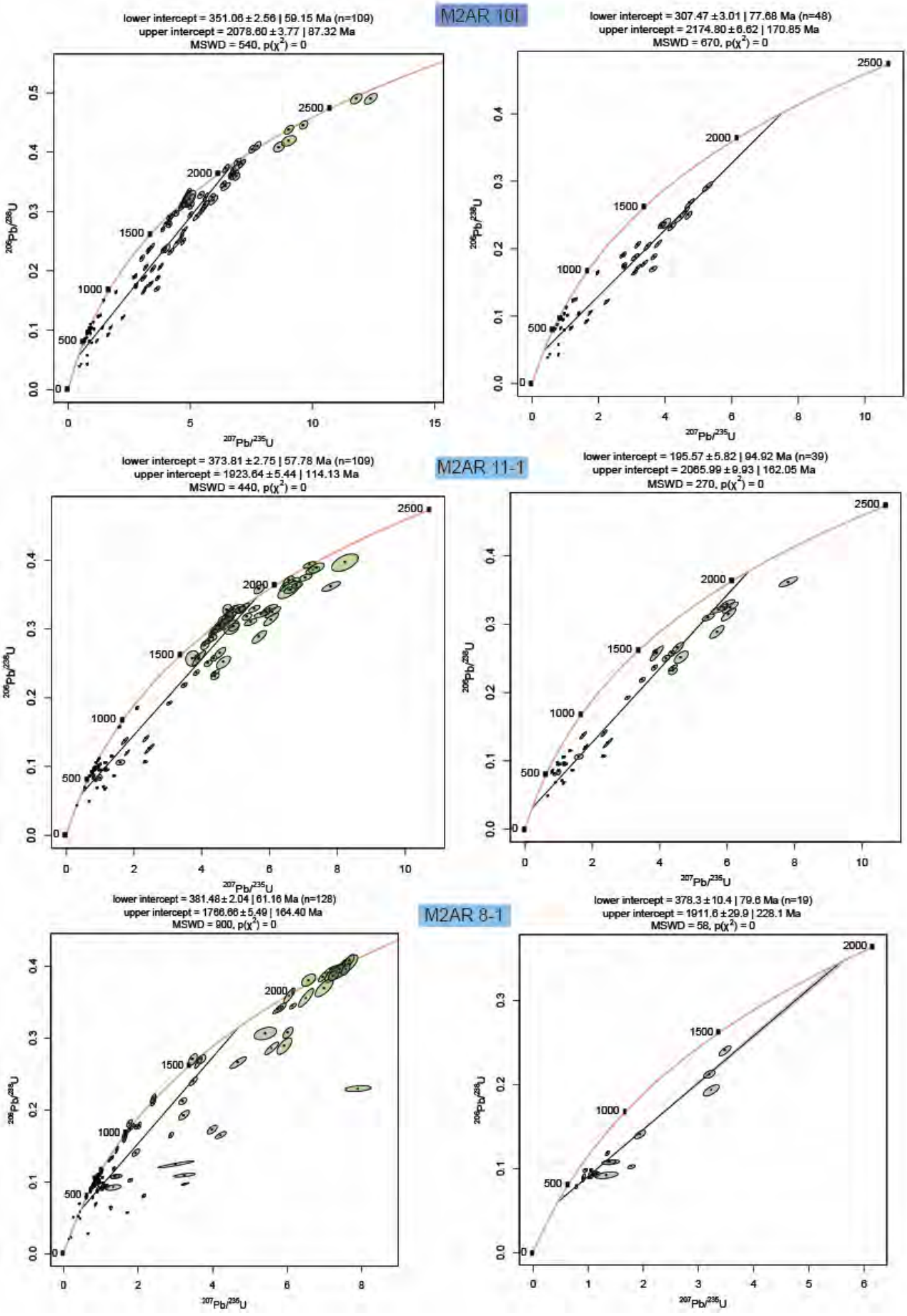
M2AR 10I
lower intercept = 351.08 ± 2.56 | 59.15 Ma (n=109)
upper intercept = 2078.60 ± 3.77 | 87.32 Ma
MSWD = 540, p(χ²) = 0
lower intercept = 307.47 ± 3.01 | 77.68 Ma (n=48)
upper intercept = 2174.80 ± 6.62 | 170.85 Ma
MSWD = 670, p(χ²) = 0
M2AR 11-1
lower intercept = 373.81 ± 2.75 | 57.78 Ma (n=109)
upper intercept = 1923.64 ± 5.44 | 114.13 Ma
MSWD = 440, p(χ²) = 0
lower intercept = 195.57 ± 5.82 | 94.92 Ma (n=39)
upper intercept = 2065.99 ± 9.93 | 162.05 Ma
MSWD = 270, p(χ²) = 0
M2AR 8-1
lower intercept = 381.48 ± 2.04 | 61.16 Ma (n=128)
upper intercept = 1766.66 ± 5.49 | 164.40 Ma
MSWD = 900, p(χ²) = 0
lower intercept = 378.3 ± 10.4 | 79.6 Ma (n=19)
upper intercept = 1911.6 ± 29.9 | 228.1 Ma
MSWD = 58, p(χ²) = 0
207Pb/235U
206Pb/238U

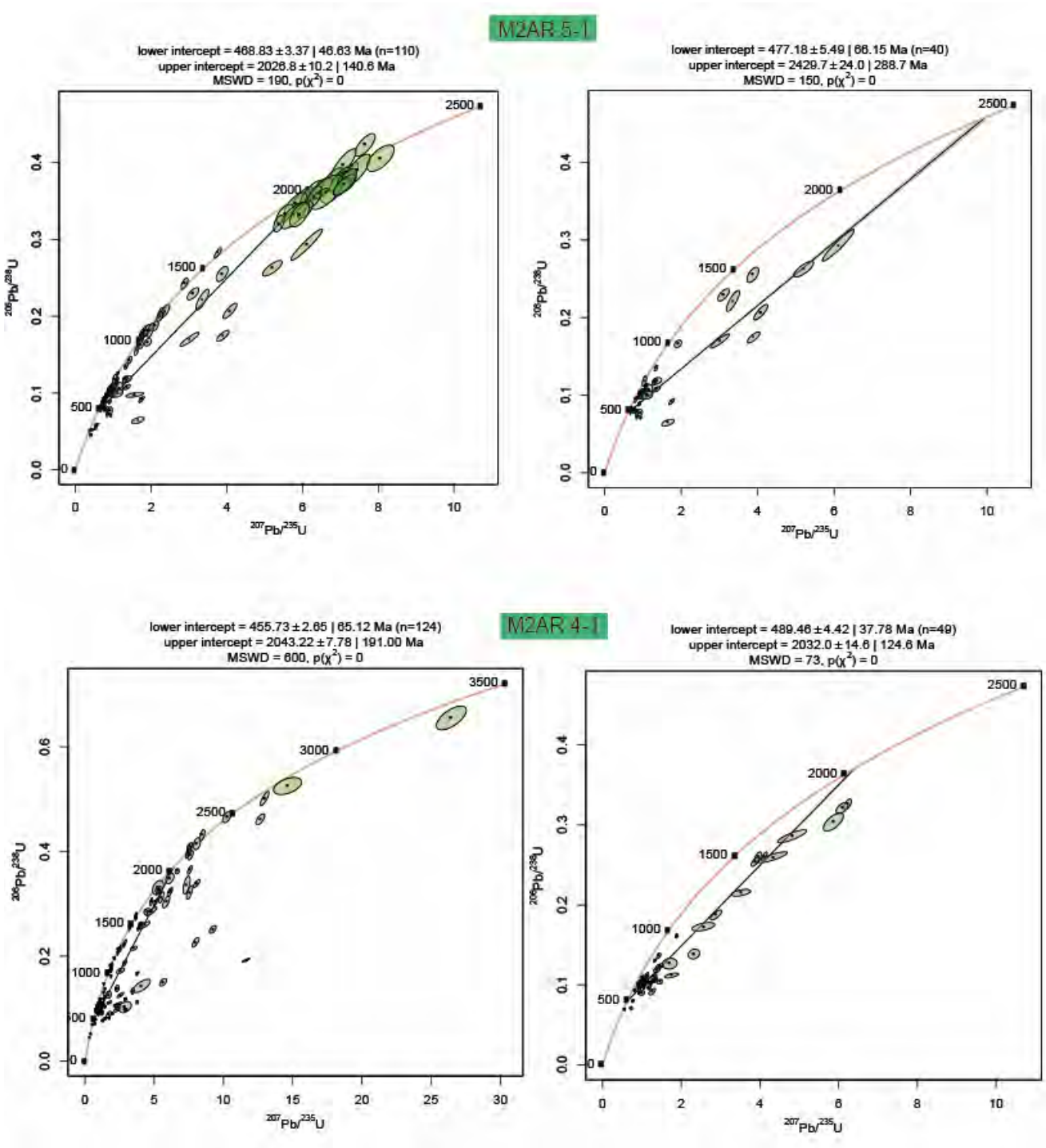

Figure S5: U-Pb Concordia diagrams with analyzed spots of detrital grains from Araripe Basin. Dark green – Rift beginning; Green – Rift; Light blue and blue – Post Rift I, and Yellow – Post-Rift II.

CAPÍTULO 4

EVOLUTION CRETACEE DE LA PARTIE OCCIDENTALE DU SYSTEME ANDES AMAZONIE MARGE EQUATORIALE : RECONSTITUTION DU PALEO RESEAU DE DRAINAGE A PARTIR DE LA PROVENANCE SEDIMENTAIRE DES SEDIMENTS DES BASSINS ANDO AMAZONIENS

NEW INSIGHTS INTO THE CRETACEOUS EVOLUTION OF THE WESTERN AMAZONIAN PALEODRAINAGE SYSTEM

Rodrigues, A. R., Roddaz, M., Santos, R. V., Louterbach, M., D'Apolito, C., Brusset, S., Dantas, E. L., Negri, F. R. 2023. New Insights into The Cretaceous Evolution of The Western Amazonian Paleodrainage System. Sedimentary Geology, 453, 106434. Doi: https://doi.org/10.1016/j.sedgeo.2023.106434.

4 EVOLUTION CRETACEE DE LA PARTIE OCCIDENTALE DU SYSTEME ANDES AMAZONIE MARGE EQUATORIALE : RECONSTITUTION DU PALEO RESEAU DE DRAINAGE A PARTIR DE LA PROVENANCE SEDIMENTAIRE DES SEDIMENTS DES BASSINS ANDO AMAZONIENS

New insights into the Cretaceous evolution of the Western Amazonian paleo drainage system

Les résultats de ce chapitre sont exprimés sous la forme d'un article intitulé « New insights into the Cretaceous evolution of the Western Amazonian paleodrainage system » qui a été publié à Sedimentary Geology (Doi : https://doi.org/10.1016/j.sedgeo.2023.106434*). A partir d'une étude de provenance sédimentaire, l'objectif de ce chapitre est de déterminer les sources des apports sédimentaires des bassins de l'Acre et de Madre du Dios et leur relation avec le système de drainage développé dans la région amazonienne occidentale pendant le Crétacé Supérieur.*

Résumé

L'histoire géologique du fleuve Amazone est complexe et essentiellement contrôlée par les processus géodynamiques opérant dans la plaque supérieure sud-américaine. Malgré quelques études récentes, la configuration pré-Néogène du paléodrainage de l'Amazone est encore mal définie. Une étude récente a suggéré que le système de paléodrainage de l'Amazonie occidentale était inversé par rapport à la configuration actuelle et d'origine cratonique pendant le Crétacé. Cependant, l'étendue et la durée de ce système ne sont pas bien définies. Pour ajouter de nouvelles contraintes, nous avons étudié les sources des roches sédimentaires crétacées dans les bassins brésiliens de l'Acre et péruviens du Madre de Dios, en nous basant sur les concentrations en éléments majeurs et traces, les compositions isotopiques Sm-Nd et la datation U-Pb des zircons détritiques. Les échantillons de la fin du Crétacé du bassin

d'Acre ont des valeurs d'ƐNd (0) entre -21.2 et -8.4 et des zircons avec des âges Ventuari-Tapajos (2,0-1,82 Ga) et Rio Negro-Juruena (1,82-1,54 Ga) provenant de terrains situés dans la partie la plus orientale du craton amazonien. En revanche, les échantillons du bassin Madre de Dios présentent des valeurs d'εNd (0) allant de -15,2 à -7,1 avec des âges variables. Ceux de la partie nord du bassin (MD234 et MD238) sont principalement constitués de contributions de zircons d'âge compris entre 0,9 et 1,3 Ga (Grenville/ Sunsás, 30 % - 43 %) ainsi que de 0,5-0,7 Ga (Brésilien/Pampéen, 26 % - 16 %) de provenance de sources felsiques. L'échantillon le plus vieux (MD234) montre une contribution dominante de zircons paléozoïques (20 %). Les échantillons provenant de la partie sud du bassin Madre de Dios (échantillons MD-2019-4A ; MD-2019-10 ; MD-2019-13 ; MD-2019-11D et MD-2019-12A) ont des distributions d'âge U-Pb dominées par des âges de zircon compris entre 0,9-1,3 Ga (Grenville/Sunsás, 30 % - 45 %) et 1,54-1,3 Ga (Rondonia-San Ignácio, 16 % - 43 %), indiquant une origine cratonique pour ces roches sédimentaires. Pour expliquer la différence de provenance entre les échantillons des parties nord et sud du bassin de Madre de Dios, nous suggérons qu'une barrière structurale (l'arche de Madidi (?)) était active à la fin du Crétacé. Si on suit cette hypothèse, la partie nord du bassin de Madre de Dios avait des sources sédimentaires similaires à celles des bassins voisins comme ceux du Huallaga, de Bagua, d'Ucayali et de Marañón, alors que dans la partie sud du bassin, la sédimentation était influencée par des sources locales. En prenant en compte les résultats des études publiées récemment, ces données indiquent que le paleo réseau de drainage amazonien d'origine cratonique qui s'est développé sur toute la partie occidentale de l'Amazonie entre le Cénomanien et le Maastrichtien est le résultat du probable soulèvement de l'arche de Purus en réponse à un processus géodynamique lié à l'ouverture post-rift de l'océan Atlantique équatorial.

NEW INSIGHTS INTO THE CRETACEOUS EVOLUTION OF THE WESTERN AMAZONIAN PALEODRAINAGE SYSTEM

Mariana de Assunção Rodrigues [a,b,*], Martin Roddaz [b], Roberto Ventura Santos[a], Melanie Louterbach[c], Carlos D'Apolito [e], Stéphane Brusset [b], Elton Luiz Dantas [a], Francisco Ricardo Negri [d]

[a] Universidade de Brasília, Darcy Ribeiro Campus, Asa Norte 70910-900 Brasília, DF, Brazil

[b] Géosciences-Environnement Toulouse, Université de Toulouse; UPS (SVT-OMP); 14 Avenue Édouard Belin, F-31400 Toulouse, France

[c] Harvard Graduate School of Design, Department of Landscape Architecture, 48 Quincy Street, MA 02138 Cambridge, USA

[d] Universidade Federal do Acre, Campus Floresta, Laboratório de Paleontologia. Estrada do Canela Fina, km 12, 69980-000 Cruzeiro do Sul, AC, Brazil

[e] Universidade Federal do Acre, Centro de Ciências Biológicas e da Natureza. Rodovia BR-364; 69920-900 Rio Branco, AC, Brazil

*Corresponding author,

E-mail address: marianarodrigues.geologia@gmail.com (M. A. Rodrigues).

Abstract

The geological history of the Amazon River is a complex story driven by geodynamic processes operating in the South American plate. In spite of recent research, the pre-Neogene structure of Amazon paleodrainage is still underconstrained. A recent study has suggested that the western Amazonian paleodrainage system was reversed,

cratonic in origin during the Cretaceous. However, the extent and duration of this system are not well-constrained. To add new constraints, we investigated the sources of Cretaceous sedimentary rocks in the Brazilian Acre and Peruvian Madre de Dios basins, based on major and trace element concentrations, Sm-Nd isotopic compositions, and U-Pb detrital zircon dating. The late Cretaceous samples of the Acre Basin have ε_{Nd} (0) values between -21.2 and -8.4 and zircon grains derived from terranes situated in the easternmost part of the Amazonian Craton: Ventuari-Tapajos (2.0-1.82 Ga) and Rio Negro -Juruena (1.82-1.54 Ga). In contrast, the Madre de Dios Basin samples have εNd (0) values ranging from -15.2 to -7.1 and a wide range of U-Pb zircon age distributions. The samples from the northern part of the basin (MD234 and MD238) are dominated by zircon ages between 0.9-1.3 Ga (Grenville/ Sunsás, 30% - 43%) and 0.5-0.7 Ga (Brazilian/Pampean, 26% - 16%) with felsic provenance. The oldest MD234 sample also shows a dominant contribution from Paleozoic zircon (20%). On the other hand, the samples from the southern part of the Madre de Dios Basin (samples MD-2019-4A; MD-2019-10; MD-2019-13; MD-2019-11D and MD-2019-12A) have U-Pb age distributions dominated by zircon ages between 0.9-1.3 Ga (Grenville/Sunsás, 30% - 45%) and 1.54-1.3 Ga (Rondonia-San Ignácio, 16% - 43%), pointing to a cratonic origin for these sedimentary rocks. To elucidate the distinction in provenance between the samples from the northern and southern parts of the Madre de Dios Basin, we suggest that a structural barrier (the Madidi Arch (?)) was active during the late Cretaceous. In this scenario, the northern part of the Madre de Dios Basin had similar sedimentary sources as the nearby basins like Huallaga, Bagua, Ucayali, and Marañón, whereas, in the southern part of the basin, sedimentation was influenced by local sources. Together with previously published studies, these data indicate that the continent-wide cratonic drainage developed between the Cenomanian

and Maastrichtian in response to the Purus Arch uplift was probably driven by a geodynamic process related to the post-rift opening of the Atlantic Equatorial Ocean.

Keywords: Cretaceous; provenance, Nd isotopes, zircon U-Pb dating; Western Amazonia; Continent-wide cratonic paleodrainage;

4.1 Introduction

In terms of global mass transfer from continents to oceans, the Amazon River is the most important river contributor, supplying about 20% of the water (Callède et al., 2004), ~10% of the dissolved load (Gaillardet et al., 2003), and ~3% of the suspended load (Milliman & Syvitski, 1992) to the world's oceans. According to Filizola & Guyot, (2004), Andean tributaries supply more than 95% of the median annual suspended sediment flux that the Amazon delivers, with 2/3 and 1/3 from the Solimões and Madeira rivers, respectively. Its basin drainage includes several Meso-Cenozoic basins located between the Andes and the Atlantic Ocean (Fig. 1). The geological history of the Amazon River and its paleodrainage is complex and its Neogene configuration is a much-discussed subject (Albert et al., 2018; Hoorn et al., 2010; Carina Hoorn et al., 2017; Louterbach et al., 2018; Roddaz et al., 2005, 2010; van Soelen et al., 2017a). The majority of previous research has concentrated on two aspects concerning the Amazon River: the precise moment of its transcontinentalization (Figueiredo et al., 2009; Gorini et al., 2014; Hoorn et al., 2017; van Soelen et al., 2017b) and the geodynamic systems, such as Andean uplift, flat-slab subduction or dynamic topography, that potentially drove this (Eakin et al., 2014; Rodríguez Tribaldos et al., 2017; Sacek, 2014; Shephard et al., 2010). In spite of new researches (e.g. Hurtado et al., 2018; Rodríguez Tribaldos et al., 2017; Stewart et al., 2016), the Amazon basin's pre-Neogene arrangement has garnered considerably less focus.

Recent studies on sedimentary rocks from the Peruvian and Ecuadorian retro arc foreland basins have shown major changes in the drainage system of the western Amazon between the Albian and the early Paleocene (Erlich et al., 2018; George et al., 2019; Gutiérrez et al., 2019; Hurtado et al., 2018; et al., 2018). Based on the εNd values (between – 16.8 to -18.6) and the detrital zircon grain, which were originated from the easternmost Brazilian Shield terranes Hurtado et al. (2018) suggested the existence of a long-lived cratonic drainage system originated from the Purus Arch (Fig. 1) in the Central-Eastern part of the Brazilian Shield during the Albian-Maastrichtian (from ca 110 Ma to 66 Ma). This cratonic drainage system may be considered the western part of the Cretaceous continent-wide cratonic drainage of the northern part of South America termed “Sanozama” paleodrainage (Almeida, 1974; Potter, 1997). However, the study of Hurtado et al. (2018) is based on two Cretaceous samples from the Huallaga Basin and one from the northern part of the Madre de Dios Basin. Hence, the extent and duration of this continent-wide cratonic drainage system during the Cretaceous and how it detected other western Amazonian basins is far from being constrained.

In this study, we refine the extent and duration of the long-lived cratonic drainage system in Western Amazonia based on the provenance study of Cretaceous sedimentary rocks deposited in the Acre and Madre de Dios basins. We present whole-rock geochemistry, Sm-Nd isotopic composition, and U-Pb zircon ages to understand the regional configuration and evolution of western Amazonian basins. Through compilations with recent studies, our data indicate that the long-lived paleodrainage system developed between the Cenomanian and Maastrichtian and reached its maximum paleogeographic extension in the Maastrichtian in response to the Purus Arch uplift.

4.2 Geological settings and sampling

4.2.1 Cretaceous stratigraphy of western Amazonian basins

The Cretaceous paleogeography of northern South America was strongly controlled by the geodynamic process related to Gondwana's breakup and the convergence between the Nazca and South America plates (Zamora & Gil, 2018). Since Cretaceous times western Amazonia (Fig. 33) sedimentary basins, such as the Oriente/Marañón, Santiago, Bagua, Ucayali, Huallaga, Madre de Dios, and Acre basins experienced a complex structural evolution (Baby et al., 2005; Erlich et al., 2018; George et al., 2019; Gutiérrez et al., 2019; Hermoza et al., 2006; Louterbach et al., 2018; Martinez et al., 1999; Roddaz et al., 2005; Wine et al., 2001; Zamora & Gil, 2018) (Figs. 1 and 2). These basins are presently divided into two parts, the northern and the southern Amazonian retroarc foreland basin (N. Espurt et al., 2007; Roddaz et al., 2005b), because of the uplift of the Fitzcarrald Arch in the Pliocene (Espurt et al., 2007); (Espurt et al., 2010; Roddaz et al., 2010).

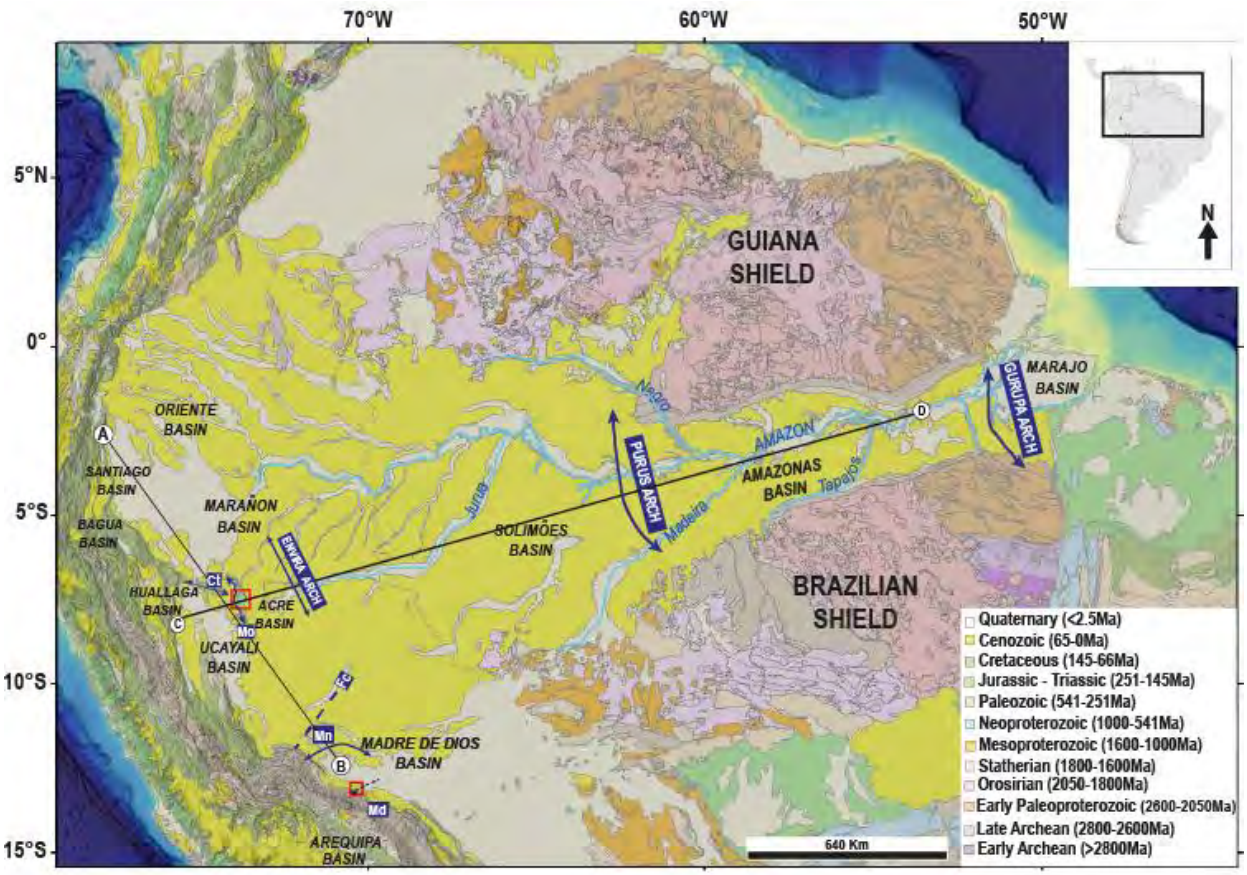

Fig. 33: Geological map of the Andes and Amazon basins modified from the CPRM tectonic map of South America

(http://cprm.maps.arcgis.com/apps/webappviewer/index.html?id=6bd9c72461a142209a34341adbc8d695). The red squares indicate the location of the studied areas. The locations of the Envira, Purus, and Gurupá Arches are based on (Caputo, 2014; Caputo & Soares, 2016). The location of the Manu (Mn) and Madidi (Md) Arches are based on (House et al., 1999). The Location of the Contaya Arch (Ct), Moa Divisor Structure (Mo), and Fitzcarrald Arch (Fc) is based on (Hermoza et al., 2006; Lopez-Gamundi & Lopez-Gamundi, 2018). The black lines (A-B, C-D) indicate the approximate location of the chronostratigraphic diagrams in Fig. 34.

The Oriente Basin is made up of Paleozoic to Quaternary sedimentary rocks and sediments (Christophoul et al., 2002). Prolonged to the north by the Putumayo Basin of Colombia and to the south by the Marañón Basin (Fig. 33), the Oriente Basin displays three stratigraphic units ranging in age from the Carboniferous to the Recent (Baby et al., 1999). The first Cretaceous sequence is formed by the Hollin and Napo Formations, which is composed of sandstones, limestones, and organic-rich shales (Fig. 2). The Albian sandstones from the Hollin Formation were deposited above the pre-Albian unconformity (Baby et al., 2013) and derived from the Amazon craton

(Gutiérrez et al., 2019; Ruiz et al., 2007). The Upper Cretaceous Napo Formation sedimentary rocks are derived from eastern cratonic sources, mainly from the Rondonian-San Ignacio terrane (1.8 – 1.3 Ga) (Gutiérrez et al., 2019). The Tena Formation (Maastrichtian-Paleocene) exhibits fine-grained reddish sediments that were deposited in a fluvial setting within a distal foredeep deposition zone (Baby et al., 2013). The sedimentary sources were related to the exhumation of the Cordillera Real to the west (Ruiz et al., 2004) and the recycling of ancient formations (Hollin and Napo formations) (Gutiérrez et al., 2019).

The Cretaceous sequences of the Oriente Basin are correlated to those of the Marañón Basin (Zamora & Gil, 2018), which is located southward between the Ucayali and Acre basins (Fig. 33). The Cretaceous sedimentary succession within the Marañón Basin begins with the deposition of the sandstones of the Cushabatay Formation in a fluvial to shoreface environments as a product from the Jurua orogeny reactivation (Caputo, 2014; Zamora & Gil, 2018). The Cretaceous sedimentary rocks were deposited after an erosional hiatus (110-120 Ma) and are the calcareous green shales, interbedded with sandstones and platform limestones of the Raya Formation (equivalent to the Napo Basal in the Oriente Basin; Fig. 34) (Zamora and Gil, 2018). The Albian to early Cenomanian Agua Caliente Formation is characterized by sandstones and shales deposited into fluvial-deltaic and marine settings (Zamora & Gil, 2018) The transition between this formation and the Chonta Formation is progressive (Wine et al., 2001; Zamora & Gil, 2018). The Chonta Formation is composed of sandstones, limestones, and shales and consists of the source rock of the Oriente - Marañón prolific oil province (Calderon et al., 2017). This unit defines three transgressive-regressive sequences (Zamora and Gil, 2018). During the Turonian, limestones and black shales were deposited. From the Coniacian to

Santonian marine shales interbedded with sandstones and limestones were deposited. The contact between the Chonta Formation and the middle Campanian -late Maastrichtian, fluvial to shallow marine Vivian Formation is erosive (Calderon et al., 2017; Zamora & Gil, 2018). The late Maastrichtian Vivian-Cachiyacu formations represent the last Cretaceous deposition cycle and were formed by sandstones, shales, and limestones (Calderon et al., 2017) (Fig. 34).

The Ucayali Basin is limited from the Marañón Basin by the NW-SE Contaya Arch and from the Acre Basin, by the NNW-SSE Moa Divisor structure (Fig. 33). The sedimentary thickness of the basin decreases progressively to the south and towards the Fitzcarrald Arch (Hermoza et al., 2006; Lopez-Gamundi & Lopez-Gamundi, 2018). The Cretaceous sedimentation started with the Cushabatay and Raya formations during the Neocomian – Aptian (Martinez et al., 1999). They consist of fluvial to marginal clastics and marine limestones, which progressively disappear to the NNE/SSW (Fig. 34) (Martinez et al., 1999). The Chonta Formation is made up of shales and limestones (Calderon et al., 2017). The end of the Cretaceous is represented by the Maastrichtian quartz-rich sandstones of the Vivian Formation (Martinez et al., 1999).

The Huallaga Basin is bounded by the Eastern Cordillera to the west and the Chazuta thrust-related anticline to the east (Hurtado et al., 2018). An erosional unconformity separates the Cretaceous sedimentary succession which is made up from the bottom to the top, by the Cushabatay, Raya, Agua Caliente, Chonta, Cashiyacu, and Vivian formations. The Cushabatay Formation consists of quartz-rich sandstones interbedded with shales and siltstones and deposited by fluvial-deltaic systems during Aptian-Albian times (Hurtado et al., 2018; Wine et al., 2001). The

middle-late Albian Raya Formation was deposited in a shallow marine environment and consists of shales, siltstones, and sparse calcareous beds (Hurtado et al., 2018;

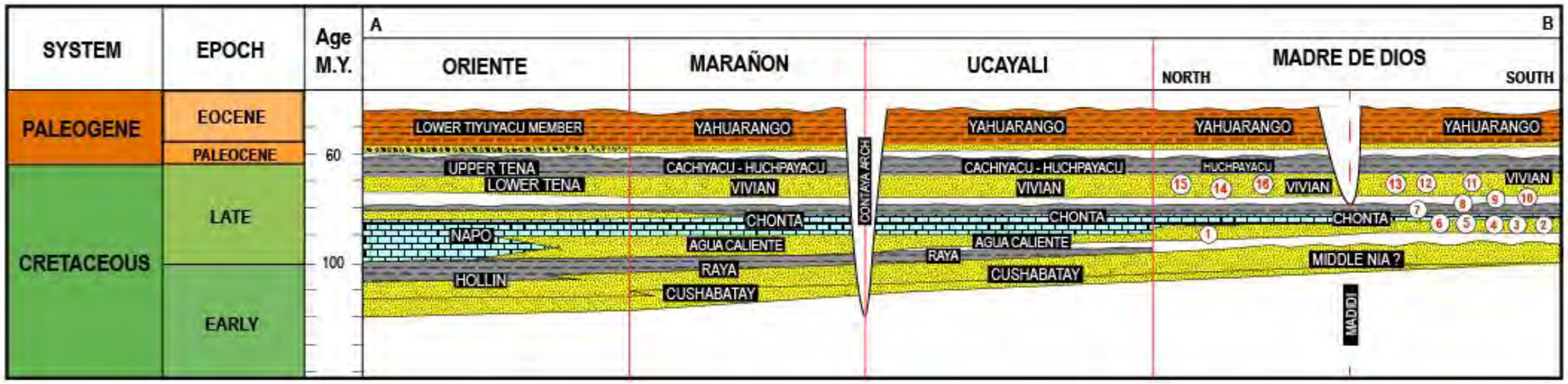

Madre de Dios Basin

	SAMPLE
1	MD 234
2	MD 2019- 1B
3	MD 2019- 3B
4	MD 2019- 4A
5	MD 2019- 4B
6	MD 2019-12C
7	MD 2019-12B
8	MD 2019-12A
9	MD 2019-11D
10	MD 2019-11B
11	MD 2019-11E
12	MD 2019-10
13	MD 2019-13
14	MD 238
15	MD 239
16	MD 176

Acre Basin

	SAMPLE
1	ACRE 38
2	ACRE 49
3	ACRE 42
4	ACRE 39
5	ACRE 37
6	ACRE 33
7	ACRE 30
8	ACRE 29
9	ACRE 27
10	ACRE 22
11	ACRE 20
12	ACRE 16
13	ACRE 15

SHALES & CLAYSTONE

CLAYSTONE & SILSTONE

LIMESTONE

SANDSTONE

Fig. 34: Comparative chronostratigraphic diagrams showing stratigraphic nomenclature, age, and lithology for (A) the Subandean Amazonian Basins and (B) Peruvian and Brazilian Amazonian Basins. The chronostratigraphic diagram (A) was constructed based on (Calderon, 2017; Hermoza et al., 2006; Louterbach et al., 2014; Louterbach et al., 2018; Martinez et al., 1999; Roddaz et al., 2010). The chronostratigraphic diagram (B) is based on (Calderon, 2017; Caputo, 2014; Caputo & Soares, 2016; Cunha, 2007; Hurtado et al., 2018; Wanderley Filho et al., 2007).

Sanchez et al., 1997). The Cenomanian Agua Caliente deposits are composed of fluvial-deltaic sandstones interbedded with shales and siltstones (Sanchez et al., 1997). The Coniacian-Turonian Chonta Formation is composed of marine shales, marls, mudstones, and limestones (Hurtado et al., 2018). This stratigraphic pile ends in the Maastrichtian with the fluvial coastal quartz-rich sandstones of the Vivian Formation whose marine equivalent is the Cachiyacu Formation (Hurtado et al., 2018; Sanchez et al., 1997).

The southern Peruvian Madre de Dios Basin is limited to the southwest by the Azulmayo thrust, to the north and northeast by the Brazilian Shield, and to the north-northwest by the Fitzcarrald Arch (Louterbach et al., 2018). The basement of the basin includes Precambrian to Cambrian metamorphic rocks, Paleozoic metasediments, and tardi-Hercynian igneous rocks (Louterbach et al., 2018). To the east at the boundary with the Eastern Cordillera, the Madre de Dios Basin encompasses a heterogeneous sedimentary succession of sedimentary rocks deposited between the Upper Paleozoic and the Cenozoic (Louterbach et al., 2018). The deposits from the early Cretaceous did not undergo preservation, while the sedimentary succession of the late Cretaceous began above a basal regional unconformity (Louterbach, 2014). It is then followed by estuarine sandstones from the Basal Chonta Formation followed by littoral to intertidal gray carbonaceous shales, mudstones siltstones, and sandstones from the Cenomanian-Turonian Chonta Formation (Louterbach, 2014). The Vivian Formation started with red shales and paleosol horizons formed during the late Campanian in a fluvial-tidal coastal plain (Louterbach et al., 2018). The late Maastrichtian Vivian Formation is characterized by sandstones, deposited in a coastal environment with continental inputs (Louterbach, 2014; Louterbach et al., 2018).

The Acre Basin is limited to the east and north by the Iquitos Arch, to the northwest by the Marañón Basin, to the west by the Ucayali Basin, and to the south by the Madre de Dios Basin (Cunha, 2007; Haag, 2019). According to (Oliveira, 1994), this basin was affected by complex compressional and extensional events from the Paleozoic to the Present. The Albian-Cenomanian sandstones from the lower Moa Formation were followed by transgressive Cenomanian/Turonian black shales of the upper part of this unit. During the Turonian-Campanian, black shales and fine-grained sandstones of the Rio Azul Formation were deposited. The late Campanian Divisor Formation was made up of fluvial sandstones (Cunha, 2007).

The sedimentary units from the late Cretaceous of the Marañón, Ucayali, Huallaga, Madre de Dios, and Acre basins may be correlated with the Alter do Chão Formation from the Solimões and Amazonia basins (Caputo, 2014; Hurtado et al., 2018). The Jurassic Envira Arch separates the Acre from the Solimões Basin and the Purus Arch limited the Solimões and Amazonas basins (Caputo, 2014) (Fig. 33). The Purus Arch formed as a result of Neoproterozoic compressive stress that caused the inversion of the Cachimbo Graben (Caputo & Soares, 2016; Wanderley Filho et al., 2007). The Purus Arch experienced episodes of uplift and subsidence after the Pennsylvanian (Caputo & Soares, 2016; Wanderley Filho et al., 2007). Because of the presence of the Cenozoic deposits and the absence of the Cretaceous sedimentary rocks around the Purus Arch (Caputo & Soares, 2016), the Purus Arch could be topographically high during the Cretaceous as Hurtado et al. (2018) suggested.

4.2.2 Potential sources

Detrital zircon U-Pb ages have been used in provenance studies in the Andes-Amazonian basins to interpret the possible contributions of Cratonic and Andean source rocks during the sedimentary evolution (Chavez et al., 2022; Erlich et al., 2018;

George et al., 2019; Horton et al., 2015; Horton, 2018; Hurtado et al., 2018; Louterbach et al., 2018; Moreno et al., 2020; Nie et al., 2012). The relative sources have different types of terranes and different ages. Precambrian zircon U-Pb ages (>900 Ma) are found in the Amazon craton which is a continental block resulting from lateral crustal accretionary processes that lasted from Archean to Mesoproterozoic (Cordani & Teixeira, 2007; Santos et al., 2000; Tassinari & Macambira, 1999). Neoproterozoic and Phanerozoic zircon U-Pb ages (<900 Ma) could be related to rocks from the fold and thrust belts formed during the amalgamation of the Supercontinent Gondwana. These rocks were affected by the Brazilian Event (Brito Neves, 2002), and by magmatic events on western Gondwana related to a polycyclic orogenic history (Chew et al., 2008; Chew et al., 2007; Chew et al., 2016) (Fig. 35).

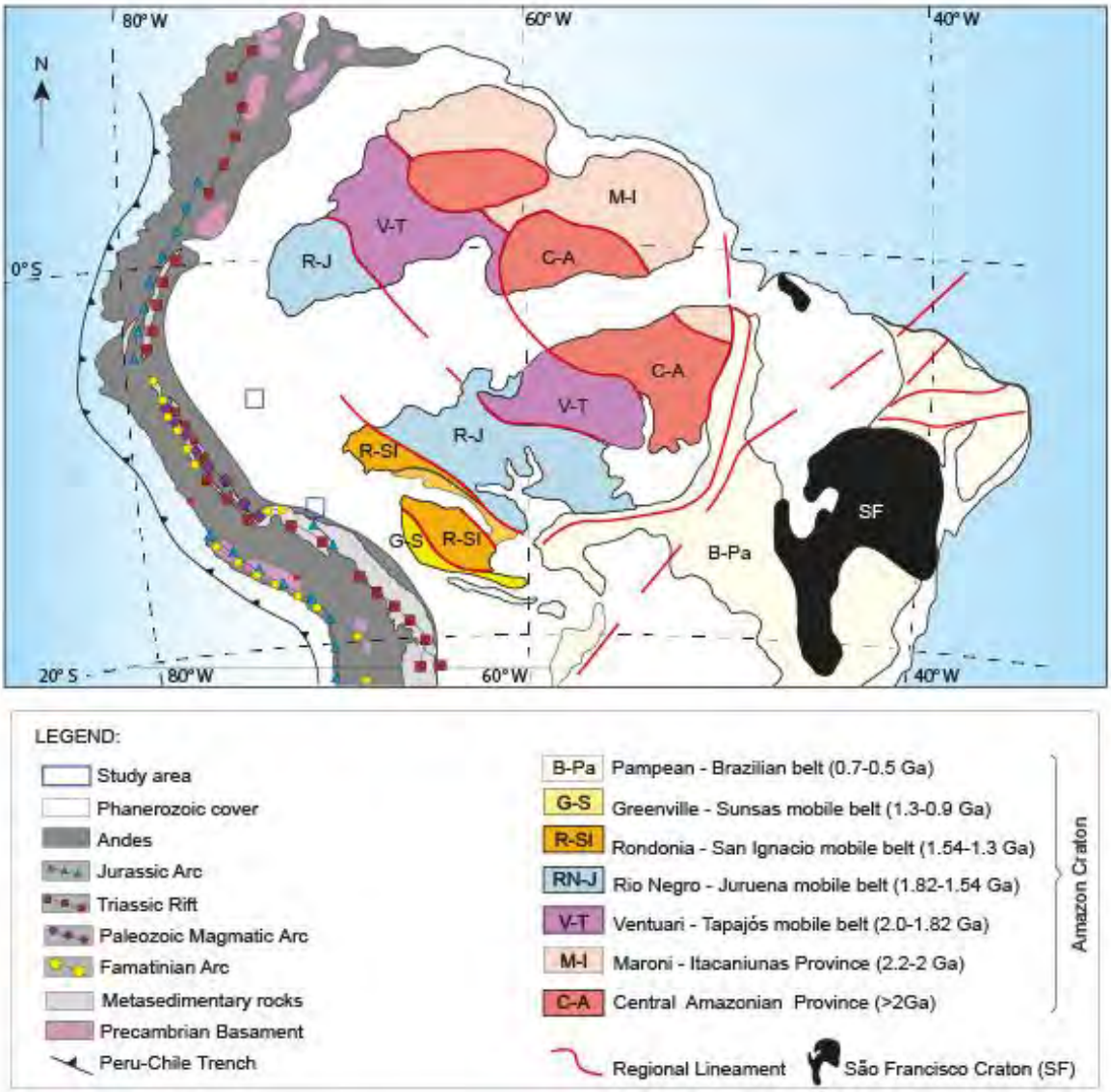

Fig. 35: Map of the northern part of South America illustrating the major tectonic provinces and the ages of their more recent metamorphic events. Modified and adapted from (Chew et al., 2008; Chew et al., 2007; Cordani et al., 2000; Miškovic et al., 2009; Naipauer et al., 2015; Oliveros et al., 2012; Ramos, 2018; Sempere et al., 2002; Spikings et al., 2016). Modified from Hurtado et al. (2018). Nd isotopes may be used as a provenance tool because they are not easily fractionated by sedimentary or post-depositional processes (Konieczna et al., 2015; Mahoney, 2005; McLennan et al., 1990). Cratonic-derived river sediments have εNd(0) values between -14.5 and -20, while Andean-derived sediments have εNd(0) values >-13.8 (Figueiredo et al., 2009; Horbe et al., 2013; Roddaz et al., 2005). This difference in the Nd isotopes recorded in fine-grained sediments has been used to decipher the provenance and reconstruct the paleodrainage systems in Western Amazonia (e. g. Roddaz et al., 2005; Louterbach et al., 2018; Hurtado et al., 2018).

4.3 Sampling and stratigraphic constraints

In total, we collected thirty-five samples from the Cretaceous sedimentary rock successions cropping out in the Madre de Dios and Acre basins (Fig. 34 and details in the supplementary dataset). Among these samples, seven from the Madre de Dios

Basin and seven from the Acre Basin were analyzed for zircon U-Pb dating. For comparisons, we used data from two samples from Louterbach et al. (2018) (MD 239 and MD 176,Tab. 9). Eighteen samples were measured for their major and trace elements concentrations (seven from the Madre de Dios Basin and eleven from the Acre Basin). Twenty-two samples were measured for their whole-rock Sm-Nd isotopic composition (eleven from Madre de Dios Basin and eleven from the Acre Basin). The locations of the analyzed samples can be found in Tab. 9 and the supplementary dataset.

Tab. 9: Label, formation, age, and localization for the analyzed samples of Madre de Dios and Acre basins. Madre de Dios basin: Ages are from Louterbach (2014) and Louterbach et al. (2018) Acre basin: Ages are from Cunha (2007) (*) and Haag (2019) (**) Brito et al. (1994) (***).

Madre de Dios	Sample	Formation	Age	Longitude (W)	Latitude (S)
1	**MD234**	Basal Chonta	Cenomanian or older	71°21'49.54"	12°53'36.13"
2	**MD234 B**	Basal Chonta	Cenomanian or older	71°21'49.54"	12°53'36.13"
3	**MD234 C**	Basal Chonta	Cenomanian or older	71°21'49.54"	12°53'36.13"
4	**MD-2019-1B**	Chonta	Early Cenomanian	70°19'3.82"	13°16'46.80"
5	**MD-2019-3B**	Chonta	Cenomanian	70°22'12.30"	13°12'16.93"
6	**MD-2019-4A**	Chonta	Cenomanian	70°22'14.22"	13°12'11.62"
7	**MD-2019-4B**	Chonta	Cenomanian	70°22'12.39"	13°12'9.20"
8	**MD-2019-12C**	Chonta	Late Cenomanian -Early Turonian	70°23'2.14"	13°11'51.06"
9	**MD-2019-12B**	Chonta	Late Cenomanian -Early Turonian	70°23'1.91"	13°11'50.71"
10	**MD-2019-12A**	Chonta	Late Cenomanian -Early Turonian	70°23'1.29"	13°11'49.33"
11	**MD-2019-11D**	Chonta	Coniacian-Santonian	70°23'21.35"	13°11'23.45"
12	**MD-2019-11B**	Chonta	Coniacian-Santonian	70°23'23.75"	13°11'25.35"
13	**MD-2019-11E**	Vivian	Maastrichtian	70°23'24.80"	13°11'27.37"
14	**MD-2019-10**	Vivian	Maastrichtian	70°23'57.90"	13°11'29.79"
15	**MD-2019-13**	Vivian	Maastrichtian	70°23'53.36"	13° 9'9.98"
16	**MD238**	Vivian	Early Maastrichtian	71°21'44.21"	12°53'34.76"

17	**MD239**	Vivian	Early Maastrichtian	71°21'41.36"	71°21'43.56"
18	**MD176**	Vivian	Late Maastrichtian	71°21'43.56"	12°53'31.20"

Acre	Sample	Formation	Age	Longitude (W)	Latitude (S)
1	**ACRE 38**	Moa	Late Albian-Cenomanian/Late Turonian* Late Cretaceous ***	73°39'59.00"	7°26'52.98"
2	**ACRE 49**	Moa	Late Albian-Cenomanian/Late Turonian* Late Cretaceous ***	73°41'37.67"	7°27'29.60"
3	**ACRE 42**	Rio Azul	Turonian-Campanian*	73°42'8.10"	7°28'14.18"
4	**ACRE 42B**	Rio Azul	Turonian-Campanian*	73°42'8.10"	7°28'14.18"
5	**ACRE 39**	Rio Azul	Turonian-Campanian*	73°42'11.73"	7°28'16.54"
6	**ACRE 37**	Rio Azul	Turonian-Campanian*	73°41'56.09"	7°28'41.81"
7	**ACRE 33**	Rio Azul	Cenomanian** Turonian-Campanian*	73°42'6.12"	7°29'5.41"
8	**ACRE 30**	Divisor	Campanian-Maastrichtian*	73°41'59.12"	7°29'33.14"
9	**ACRE 30A**	Divisor	Campanian-Maastrichtian*	73°41'59.12"	7°29'33.14"
10	**ACRE 29**	Divisor	Campanian-Maastrichtian*	73°41'59.58"	7°29'36.30"
11	**ACRE 27A**	Divisor	Campanian-Maastrichtian*	73°41'57.82"	7°29'50.64"
12	**ACRE 27B**	Divisor	Campanian-Maastrichtian*	73°41'57.82"	7°29'50.64"
13	**ACRE 22**	Divisor	Campanian-Maastrichtian*	73°42'4.49"	7°30'0.91"
14	**ACRE 22A**	Divisor	Campanian-Maastrichtian*	73°42'4.49"	7°30'0.91"
15	**ACRE 20**	Divisor	Campanian-Maastrichtian*	73°42'8.18"	7°30'7.50"
16	**ACRE 20A2**	Divisor	Campanian-Maastrichtian*	73°42'8.18"	7°30'7.50"
17	**ACRE 16**	Divisor	Campanian-Maastrichtian*	73°42'6.08"	7°30'18.15"
18	**ACRE 15**	Divisor	Campanian-Maastrichtian*	73°42'7.38"	7°30'20.17"
19	**ACRE 15A**	Divisor	Campanian-Maastrichtian*	73°42'7.38"	7°30'20.17"

Following Louterbach (2014), the Madre de Dios Basin can be divided into two parts: a northern part that is represented by the Pongo de Coñeq sedimentary succession (Figs. S1 and S5 in the supplementary dataset); and a southern part that is best represented by the Inambari sedimentary succession (see Figs. S1, S3, and S4

in the supplementary dataset). In the northern part of the Madre de Dios Basin, two samples were collected (MD 234 and MD 238) in the Pongo de Coñeq sedimentary succession immediately above the so-called Cretaceous Basal Unconformity (Caputo, 2014; George et al., 2019; Hermoza et al., 2006; Pfiffner & Gonzalez, 2013). Unfortunately, there is no stratigraphic constraint for this outcrop but given its stratigraphic position, it may belong to the basal sandstones of the late Cretaceous Chonta Formation (Cenomanian or older; (Chacaltana et al., 2005; Erlich et al., 2018; Zamora & Gil, 2018). The MD 238 outcrop is stratigraphically above the MD 234 outcrop and is Maastrichtian in age (see supplementary dataset of Louterbach et al., 2018, Table S2). Given that it is stratigraphically below the early Maastrichtian MD 239 outcrop (Louterbach et al., 2018), we ascribed an early Maastrichtian age for the MD 238 outcrop. The MD 176 outcrop is stratigraphically above MD 239 and is late Maastrichtian in age (Louterbach et al., 2018). In the southern part of the basin, nine samples were collected in the Chonta Formation (MD-2019-1B, MD-2019-3B, MD-2019-4A, MD-2019-4B, MD-2019-11B, and MD-2019-11D MD-2019-12A, MD-2019-12B, MD-2019-12C) and the remaining three were collected in the Campanian-Maastrichtian Vivian Formation (MD-2019-10, MD-2019-11E, and MD-2019-13). Stratigraphic constraints for the samples of the Chonta Formation can be found in Table 2. The samples from the MD-2019-12 outcrop (MD-2019-12A e B) are constrained by fossil content found in the MD 275bio outcrop of Louterbach (2014). The presence of *Helvetoglobotruncana* suggests a late Cenomanian-early Turonian age (Loeblich & Tappan, 1988) for this outcrop. The samples belonging to the MD-2019-3 and 4 outcrops are constrained by the fossil contents of outcrops MD 282 of Louterbach (2014). The presence of *Cythereis*, *Timirasevia, Dordoniella,* and *Protocythere* suggest a Cenomanian age for this outcrop. In addition, these outcrops

are located below the MD302 outcrop (see Fig. S3 in the supplementary data set) which is estimated to be Turonian-Conician in age based on the presence of *Ovocytheridea sp.* ostracod (Louterbach, 2014). The sample MD-2019-1B is constrained by fossil content found in the MD 309 Bio A outcrop of Louterbach (2014). The presence of *Cythereis sp.* ostracod suggests an early Cenomanian age (Babinot et al., 2009). The stratigraphic age of the remaining samples of the Chonta and Vivian Formations are based on the stratigraphic ages assigned to these formations (Tab. 10 and Fig. 34).

Tab. 10: Paleontological content of the sedimentary rocks analyzed in this work.

Sample	Palynology	Fossil	Microfossil	Age	Taxonomic composition	References
MD-2019-1B			**x**	*Cythereis*: Early Cenomanian (Babinot et al., 2009)	*Ostracodes: Cytheráceos; Cythereis sp.; Bisulcocpris sp.*	MD 309 Bio A Louterbach et al., 2018 Louterbach, 2014

MD-2019-4A	**x**		**x**	Cenomanian	*Planctonic Foram.: Guembelitria cretacea (Cushman, 1933) Rugoglobigerina rugosa (Plummer, 1926) Hedbergella holmdelensis Olsson, 1964 Archaeoglobigerina blowi Pessagno, 1967 Heterohelix globulosa (Ehrenberg), 1840 Benthic Foram.: Haplophragmoides walteri (Grzybowski), 1898 Haplophragmoides sp. Rzehakina epigona (Rzehak, 1895) Silicosigmoilina sp. Trochammina sp. Retrabajados: Diatomea ? Others: Neocythere sp. (ostracode) Spicul*	MD 281 (Bio) Louterbach et al., 2018 Louterbach, 2014
MD-2019-3B	**x**		**x**	Cenomanian	*Dordoniella sp., Cytherella sp., Isocythereis sp., Cythereis sp., Protocythere sp. y Timiriasevia sp. Dinoflagellates ?*	MD 282 (Bio) Louterbach et al., 2018 Louterbach, 2014
MD-2019-12B			**x**	Late Cenomanian-Early Turonian	*Planctonic Foram.: Globotruncanidaeand Helvetoglobotruncana*	MD 275 BioLouterbach et al., 2018 Louterbach, 2014
MD-2019-12A			**x**	Late Cenomanian -Early Turonian	*Planctonic Foram.: Globotruncanidae and Helvetoglobotruncana*	MD 275 Bio Louterbach et al., 2018 Louterbach, 2014

MD238	**X**			Early Maastrichtian	*Rzehakinalata Cushman & Jarvis, 1928 (5) Rzehakina minima Cushman &Renz (1946) (8) RzehakinaepigonaRzehak (1895) (2) RzehakinafissistomataGrzybowski, 1901 (2) SpirosigmoilinellacompressaMatsunaga (1955) (13) SilicosigmoilinaangustaTurenko, 1983 (2) Ammobaculites sp. Cushman, 1910 (1) cf. Trochammina Parker & Jones, 1859 (2) Miliammina sp. Heron-Allen &Earland, 1930 (2) SigmoilinadistortaPhleger& Parker, 1951 (2)*	Louterbach et al., 2018 Louterbach, 2014
MD239	**X**			Late Maastrichtian	*cf. RotaliidaeEhrenberg, 1839 (1) SpirosigmoilinellacompressaMatsunaga, 1955 (1) SilicosigmoilinaangustaTurenko 1983 (1) Dientes (5)Karrerulina horrida (Mjatlivk, 1970) (2) Karrerulinaconiformis (Grzybowski, 1898) (2) cf. fragmentos de arenáceos indeterminados (2) Foraminíferos ennegrecidos retrabajados (4) Dientes (8)*	Louterbach et al., 2018 Louterbach, 2014
ACRE 33	**x**			Maastrichtian	*PPNSD 09G: Ariadnaesporites spinosusDroseridites senonicus, Gnetaceaepollenites jansonii.,Monocolpopollenites spheroidites, Spirosyncolpites spiralis e Ulmoideipites krempii*	PPNSD 09 (Haag, 2009)
				Santonian-Mastrichtian	*Florentinia berran Heterosphaeridium difficile Steevesipollenites binodosus Ariadnaesporites spinosus Gabonisporis vigourouxii Zlivisporis blanensis*	This study

				Cenomanian?-Santonian/Campanian	*PPNSD 09F: Gnetaceaepollenites barghoornii Cretacaeiporites mulleri, Droseridites senonicus, Monocolpopollenites spheroidites,*	PPNSD 09 (Haag, 2009)
Moa Formation		**x**		Late Cretaceous	*Fish remains: Chondrichthyes - sclerorhynchidae*	Brito et al. (1994)

In the Acre Basin, we built up a log of the Cretaceous to Cenozoic sedimentary succession cropping out along the Moa River (see Figs. S1 and S2 in the supplementary dataset). The ACRE 49 is the oldest outcrop of the sedimentary succession and was collected in the Aptian-Turonian Moa Formation (Brito et al., 1994; Cunha, 2007). Five samples were collected in the Turonian – Campanian Rio Azul Formation (Cunha, 2007) (ACRE 42, ACRE 42B, ACRE 39, ACRE 37, and ACRE 33). Stratigraphic constraints for the samples of the Moa and the Rio Azul Formation can be found in Tab. 10 and Figure S2 in the supplementary dataset. Unfortunately, there is no stratigraphic constraint for the ACRE 38 and ACRE 37 outcrops, but given their stratigraphic position, they may belong to the Moa and Rio Azul Formations, respectively. The samples from the ACRE 33 outcrop are constrained by fossil content found in the PPNSD 09 section (Haag, 2019), and new palynological data (see supplementary dataset). An association of pollen, spores, and dinoflagellate cysts suggests a late Cretaceous age, likely in the Santonian to Maastrichtian range. The stratigraphic age of the outcrops belonging to the Campanian-Maastrichtian Divisor Formation (ACRE 30, ACRE 29, ACRE 27, ACRE 22, ACRE 20, ACRE 16, and ACRE 15) is based on the stratigraphic age reported by Cunha (2007).

4.4 Materials and methods

4.4.1 Major and trace element concentrations

The major and trace element concentrations were measured at the Service d'Analyse des Roches et Mineraux (SARM, INSU facility, Vandoeuvre-Les-Nancy, France) by ICP-OES and ICP-MS. Analytical details are available on http://helium.crpg.cnrs-nancy.fr/SARM/ and in (Carignan et al., 2001). Precision is better than 5% for elements measured by ICP-OES, and 10% for elements measured by ICP-MS (see supplementary dataset for details).

4.4.2 Sm-Nd isotope composition

The Sm-Nd isotope composition of the analyzed was made at the Geochronos Laboratory of the Geosciences Institute, Universidade de Brasília, following the methods described by Goia & Pimentel (2000). The isotopic ratios of Sm and Nd were measured using a Thermo Scientific TRITON Plus thermal ionization mass spectrometer. The precision of the measurements was estimated by analyzing the BHVO-2 standard and repeated analysis gave a $^{143}Nd/^{144}Nd$ ratio of 0.512996 ± 0.000006 (2SD, n=10) (Weis et al., 2005).

The measured $^{143}Nd/^{144}Nd_{sample}$ and $^{143}Sm/^{144}Nd_{sample}$ ratios were expressed in ε notation and reflect the fractional deviation in parts per 104 unit from the $^{143}Sm/^{144}Nd$ from the Chondritic Uniform Reservoir (CHUR) as described by Jacobsen & Wasserburg (1980). The TDM and TDM* ages were calculated following (Augustsson & Bahlburg, 2008; DePaolo et al., 1991; DePaolo, 1981; Albarède & Brouxel, 1987 and Goldstein et al., 1984) as demonstrated in the supplementary dataset.

1.1. Detrital zircon geochronological analysis

The samples were treated at the Geochronos Laboratory of the Geosciences Institute, Universidade de Brasília. Approximately 150 zircon grains were handpicked from each sample, mounted in epoxy resin, and polished to obtain a flat surface, ideal

for U-Pb analyses. Acquisition parameters, data reduction and reference material information are summarized in Table S5 and S6 in the supplementary dataset.

The $^{206}Pb/^{238}U$ ages were utilized for zircons grains with ages ≤1.5 Ga and $^{207}Pb/^{206}Pb$ ages for grains with ages >1.5 Ga (Spencer et al., 2016). Discordance age degrees >10% were not considered, as well as samples with few zircons, because of their low statistical representation (Vermeesch, 2004). The kernel density estimation (KDE) diagrams (Vermeesch, 2013) were used to illustrate and compared detrital zircon age data. To investigate the difference between detrital zircon U-Pb age distributions, we employed the non-matrix metric multi-dimensional scaling (MDS) statistical technique outlined by Vermeesch (2013). In accordance with the latest recommendations by Vermeesch (2018), we utilized the Kolmogorov–Smirnov test to generate an MDS map that compares the analyzed samples.

4.5 Results

4.5.1 Major elements, Large-Ion Lithophile Elements (LILE), High Field Strength Elements (HFSE), and Trace Transition Elements (TTE)

The elemental concentrations of major elements, LILE, HFSE, and TTE of analyzed samples were normalized to the Post Archean Australian Shales (PAAS) concentration (Pourmand et al., 2012; Taylor & McLennan, 1985) (Fig. 36, Tab. 11: Major and trace element concentrations of sedimentary rocks analyzed in this study. D.L.: Detection Limit.). The Chemical Index of Alteration (CIA) can be used to evaluate the level of the paleo-weathering situation of ancient sediments and the weathering of the original area (Fedo et al., 1995; Nesbitt & Young, 1982). The weathering intensity of feldspars in comparation to unaltered rocks is quantified by the CIA= $[Al_2O_3/(Al_2O_3+CaO^*+Na_2)+K_2O)]$ x 100 (in molar proportions), in which CaO* denotes the concentration of CaO within silicate component. Because of the lack of CO_2 data,

to calculate CaO*, we have assumed the value of CaO if Cao ≤ Na_2O or CaO = Na_2O if CaO>Na_2O (Bock et al., 1998). CIA values around 50 are commonly observed for unaltered plagioclase and K-feldspars found in upper crustal rocks, while elevated CIA values indicate increased levels of weathering. The CIA value of the PAAS standard is 67 and represent the upper continental crust configuration (Taylor & McLennan, 1985). The grain-size sorting effect can be valuated using the Al/Si ratio as it can be considered a proxy for sediment grain size (Bouchez et al., 2011). The sedimentary sorting effect favors heavy mineral concentrations such as zircon and quartz dilution in the coarser fraction, which could modify the trace element ratios used as provenance proxies (McLennan et al., 1993; Roddaz et al., 2014).

Tab. 11: Major and trace element concentrations of sedimentary rocks analyzed in this study. D.L.: Detection Limit.

note: Uncertainties for all elements are given in the supplementary material

LREE = LaPAAS + PrPAAS + NdPAAS (in ppm); MREE = GdPAAS + TbPAAS + DyPAAS (in ppm); HREE = TmPAAS + YbPAAS + LuPAAS (in ppm); MREE* = (HREE+LREE) / 2;

CIA=[Al2O3/(Al2O3+CaO*+Na2O+K2O)] ×100 (in molar proportions); Eu/Eu* = EuN/(SmN × GdN)1/2 where XN refers to the chondrite-normalized concentration value (Condie, 1993);

ΩCe = 2 x (Cesample/CePAAS) / [(Lasample/LaPAAS) + (Prsample/PrPAAS)]

Madre de Dios

Sample	MD-2019-01B	MD-2019-03B	MD-2019-04C	MD-2019-11B	MD-2019-11E	MD-2019-12B	MD-2019-12C
wt%							
SiO2	49.28	54.03	53.8	51.14	68.2	53.61	58.03
Al2O3	14.21	18.775	20.67	17.768	13.688	18.275	18.533
Fe2O3	5.74	7.938	6.182	7.419	5.335	6.834	4.505
MnO	0.1895	0.0225	0.0273	0.124	< D.L.	0.0347	0.015
MgO	3.571	1.897	1.32	2.566	0.647	2.347	2.034
CaO	7.633	2.009	0.424	3.645	0.073	3.322	1.648
Na2O	0.912	3.77	0.521	0.19	0.397	2.042	0.915
K2O	2.991	2.039	4.435	6.064	3.723	2.415	4.095
TiO2	0.692	0.746	0.998	0.705	0.962	0.786	0.841
P2O5	0.23	0.17	0.25	0.18	< D.L.	0.24	0.42
LOI	14.61	8.32	11.19	10.28	5.97	9.86	8.58
Total	100.1	99.7	99.8	100.1	99.0	99.8	99.6
Al/Si	0.3	0.4	0.4	0.4	0.2	0.4	0.4
CIA	74.7	70.6	79.3	73.4	76.6	73.8	75.8
ppm							
Sc	13.8	18.2	24.4	18.1	14.3	21.8	21.1
Rb	106.5	83.0	190.1	233.2	154.3	100.6	170.7
Cs	5.8	3.3	6.1	6.4	5.2	3.8	6.7

Ba	387.4	129.9	133.3	521.8	327.3	148.9	191.7
Sr	292.1	176.0	93.6	138.9	108.4	151.9	119.8
Th	12.0	10.8	12.8	11.5	9.2	11.0	11.5
U	2.9	2.8	3.5	3.7	1.9	6.3	2.6
Y	31.7	28.9	40.1	28.3	35.5	34.9	32.3
Zr	166.9	129.6	170.1	113.7	426.2	130.1	131.9
Nb	13.4	10.8	12.8	10.7	11.8	11.1	11.3
Hf	4.6	3.7	4.9	3.3	10.7	3.7	3.8
Cr	61.9	70.5	89.7	64.7	61.5	79.5	81.2
V	85.6	113.3	132.3	72.5	76.0	128.5	120.5
Co	23.8	17.5	18.9	22.2	13.5	19.9	14.6
Cu	7.0	24.6	40.2	7.4	4.3	29.2	21.7
Ni	29.4	33.7	28.8	28.8	14.2	48.5	26.7
Zn	61.0	36.8	86.0	132.8	44.3	45.9	33.7
La	37.0	47.0	43.1	35.2	37.8	40.1	40.6
Ce	76.3	95.5	91.4	69.8	83.8	84.7	82.0
Pr	9.0	11.0	11.0	8.4	9.5	10.7	9.8
Nd	35.1	40.9	43.3	31.4	36.1	43.1	38.0
Sm	7.2	7.2	9.1	6.2	7.1	9.0	7.6
Eu	1.4	1.3	1.7	1.2	1.4	1.6	1.6
Gd	6.1	5.6	7.9	5.3	6.1	7.4	6.7
Tb	0.9	0.9	1.2	0.8	1.0	1.1	1.0
Dy	5.7	5.3	7.5	5.0	6.2	6.5	6.0
Ho	1.2	1.1	1.5	1.0	1.3	1.3	1.2
Er	3.2	3.0	4.1	2.8	3.6	3.6	3.2
Tm	0.5	0.5	0.6	0.4	0.6	0.6	0.5
Yb	3.0	2.9	3.9	2.7	3.8	3.6	3.1
Lu	0.5	0.5	0.6	0.4	0.6	0.5	0.5
Ta	1.2	0.9	1.1	0.9	1.0	1.0	1.0
Sm/Nd	0.2	0.2	0.2	0.2	0.2	0.2	0.2
Eu/Eu*	0.7	0.6	0.6	0.7	0.7	0.6	0.7
ΩCe	1.0	1.0	1.0	1.0	1.1	1.0	1.0
Cr/Th	5.1	6.5	7.0	5.6	6.7	7.2	7.1
Th/Sc	0.9	0.6	0.5	0.6	0.6	0.5	0.5
Zr/Sc	12.1	7.1	7.0	6.3	29.7	6.0	6.3

LREE	2.7	3.2	3.2	2.5	2.8	3.1	2.9
HREE	3.1	3.0	4.1	2.7	3.9	3.7	3.2
MREE	3.1	2.9	4.1	2.7	3.3	3.7	3.4
MREE*	2.9	3.1	3.6	2.6	3.3	3.4	3.0

Acre

Sample	ACRE 15A	ACRE 16	ACRE 20 A2	ACRE 22 A	ACRE 27 A	ACRE 30 A	ACRE 33	ACRE 37	ACRE 38	ACRE 42 B	ACRE 49
wt%											
SiO2	89.35	80.59	64.20	94.12	61.43	83.69	62.62	55.99	96.76	77.19	83.69
Al2O3	5.26	10.28	7.60	0.64	23.95	10.58	23.20	2.03	0.85	10.31	2.53
Fe2O3	0.76	0.93	2.68	3.25	0.93	0.20	0.84	22.30	0.80	0.80	9.63
MnO	< D.L.	< D.L.	0.22	< D.L.	< D.L.	< D.L.	< D.L.	0.07	0.12	< D.L.	0.06
MgO	0.10	0.14	0.64	< D.L.	0.10	< D.L.	0.09	< D.L.	< D.L.	0.05	< D.L.
CaO	0.08	0.07	10.25	< D.L.	0.06	< D.L.	0.05	0.06	< D.L.	< D.L.	< D.L.
Na2O	0.04	0.04	0.06	< D.L.	< D.L.	< D.L.	< D.L.	0.05	< D.L.	0.15	0.05
K2O	0.11	0.19	0.96	0.05	0.61	0.11	0.60	1.54	0.46	5.29	1.60
TiO2	0.38	0.61	0.54	0.15	1.11	0.41	1.09	0.17	0.05	0.33	0.09
P2O5	< D.L.	< D.L.	0.15	0.24	< D.L.	< D.L.	< D.L.	< D.L.	< D.L.	< D.L.	0.34
LOI	2.97	6.20	12.05	0.90	10.78	4.54	10.55	18.28	0.26	5.06	2.03
Total	99.05	99.04	99.34	99.35	98.95	99.53	99.04	100.49	99.30	99.18	100.02
Al/Si	0.07	0.14	0.13	0.01	0.44	0.14	0.42	0.04	0.01	0.15	0.03
CIA	96.64	97.52	87.68	98.38				55.32			
ppm											
Sc	4.21	7.81	10.06	1.80	16.57	4.19	16.21	1.50	< D.L.	3.97	< D.L.
Rb	6.09	10.59	54.01	2.54	44.93	6.32	44.14	44.23	18.08	151.06	48.75
Cs	0.38	0.74	2.64	0.17	3.33	0.31	3.35	0.56	0.36	2.09	0.55
Ba	142.32	205.22	300.24	143.86	151.51	42.93	148.68	314.29	287.23	854.88	357.14
Sr	41.40	78.60	60.19	20.61	37.74	6.81	35.24	61.70	19.77	151.72	41.08
Th	5.88	10.09	9.16	4.95	37.20	14.29	37.39	6.81	3.51	13.18	3.56
U	2.64	2.35	1.98	5.95	9.66	3.62	9.88	1.89	1.23	3.41	1.67
Y	10.49	14.82	33.30	29.20	39.78	29.19	42.87	16.67	7.51	30.70	13.38
Zr	419.57	374.16	479.94	259.22	791.79	903.60	798.45	548.56	85.62	571.71	136.82

Nb	10.73	23.64	29.76	133.37	62.88	33.39	63.94	14.10	11.24	32.77	12.68
Hf	10.42	9.29	11.45	6.44	19.98	23.21	20.00	12.48	2.37	13.54	3.47
Cr	21.13	64.64	37.24	364.67	78.51	14.46	45.29	8.13	750.07	17.42	264.23
V	20.01	38.41	68.99	6.94	57.05	14.27	56.40	3.76	5.71	19.65	3.80
Co	32.88	1.15	21.77	2.44	14.80	26.54	23.75	107.84	4.11	97.80	6.60
Cu	12.39	14.19	11.26	11.94	17.16	5.51	16.74	11.50	7.26	7.53	4.73
Ni	2.57	5.04	16.58	10.60	16.12	< D.L.	13.91	43.60	16.92	10.68	8.74
Zn	< D.L.	< D.L.	55.15	22.16	22.58	< D.L.	21.21	29.21	< D.L.	7.03	27.16
La	24.76	50.82	30.24	50.31	88.02	33.66	89.80	15.66	12.58	36.97	11.82
Ce	44.35	92.62	63.52	166.26	172.22	78.05	175.16	34.95	36.73	82.27	29.42
Pr	3.84	8.44	7.79	27.27	19.13	9.04	19.41	3.81	3.20	8.84	3.19
Nd	10.73	23.64	29.76	133.37	62.88	33.39	63.94	14.10	11.24	32.77	12.68
Sm	1.42	2.94	6.06	30.88	10.70	6.16	10.80	2.77	2.10	6.25	2.77
Eu	0.24	0.48	1.22	5.35	1.70	0.92	1.71	0.42	0.33	1.14	0.53
Gd	1.18	2.14	5.35	20.62	7.57	4.48	7.78	2.30	1.55	5.09	2.51
Tb	0.22	0.34	0.88	2.87	1.16	0.74	1.20	0.39	0.24	0.80	0.41
Dy	1.56	2.36	5.63	14.07	7.18	4.87	7.44	2.56	1.45	5.13	2.55
Ho	0.37	0.53	1.21	2.00	1.49	1.09	1.56	0.58	0.29	1.13	0.55
Er	1.19	1.62	3.46	3.96	4.29	3.32	4.58	1.77	0.82	3.33	1.54
Tm	0.21	0.27	0.55	0.47	0.70	0.56	0.75	0.30	0.13	0.53	0.24
Yb	1.55	1.93	3.66	2.55	4.81	4.09	5.09	2.15	0.86	3.73	1.63
Lu	0.25	0.31	0.56	0.32	0.76	0.66	0.81	0.35	0.13	0.58	0.26
Ta	0.91	1.05	0.96	0.55	3.22	1.18	3.09	1.17	0.21	1.28	0.30
Sm/Nd	0.13	0.12	0.20	0.23	0.17	0.18	0.17	0.20	0.19	0.19	0.22
Eu/Eu*	0.56	0.59	0.65	0.65	0.58	0.54	0.57	0.50	0.56	0.62	0.61
ΩCe	1.08	1.06	1.00	0.99	1.01	1.07	1.01	1.09	1.39	1.10	1.15
Cr/Th	3.59	6.41	4.07	73.60	2.11	1.01	1.21	1.19	213.52	1.63	30.24
Th/Sc	1.40	1.29	0.91	2.75	2.25	3.41	2.31	4.54		0.68	0.64
Zr/Sc	99.66	47.91	47.71	144.01	47.78	215.66	49.26	365.71		7.42	6.02
LREE	1.22	2.61	2.24	7.39	5.55	2.54	5.64	1.10	0.90	2.58	0.92
HREE	1.55	1.96	3.72	2.62	4.87	4.12	5.20	2.17	0.87	3.74	1.67
MREE	0.73	1.18	2.93	9.28	3.90	2.48	4.03	1.30	0.80	2.71	1.36
MREE*	1.38	2.28	2.98	5.00	5.21	3.33	5.42	1.64	0.89	3.16	1.29

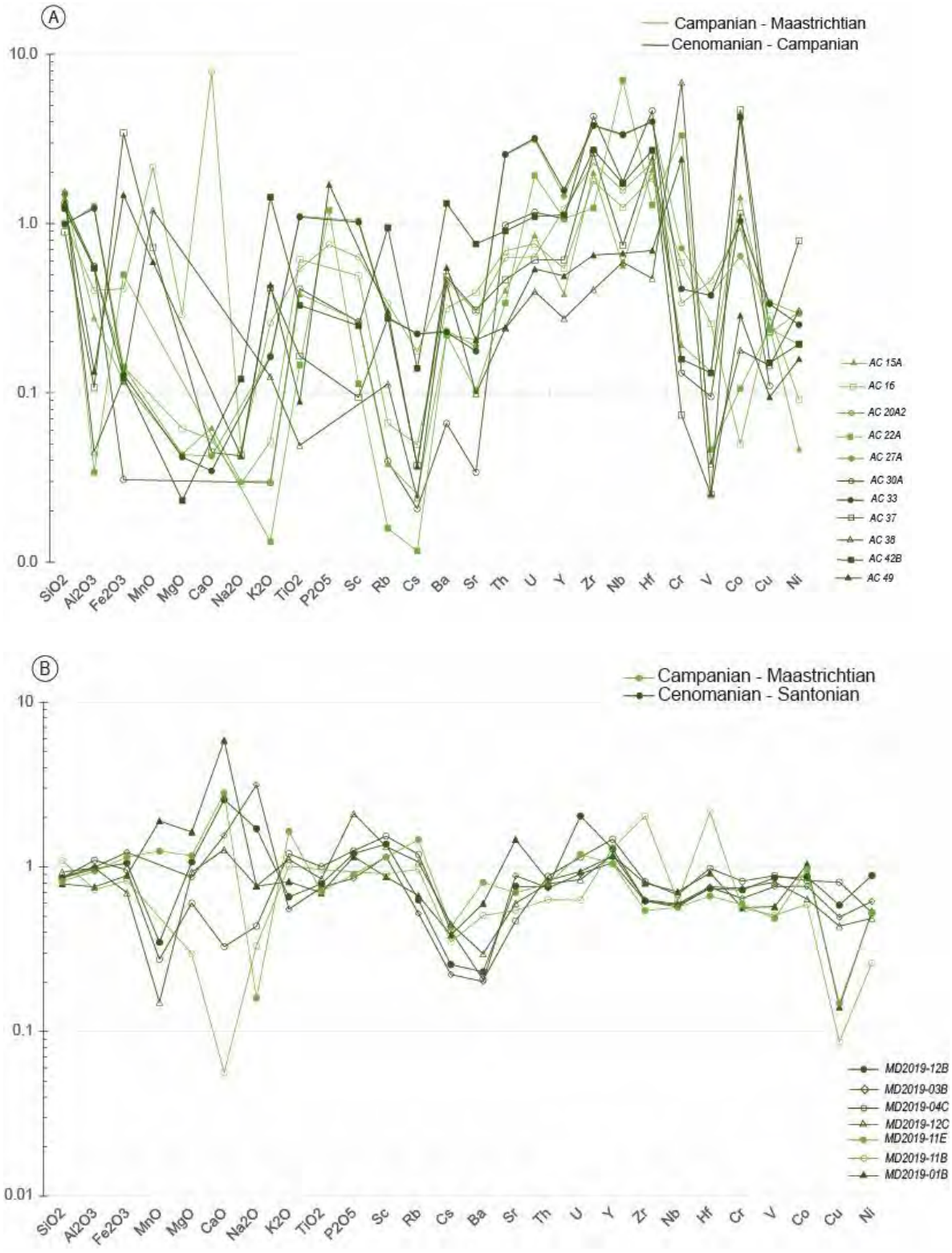

Fig. 36 Major and selected trace element contents of analyzed samples normalized to PAAS (Pourmand et al., 2012; Taylor & McLennan, 1985). From left to right on the diagram, these include the major elements (SiO2, TiO2, Al2O3, Fe2O3, MnO, MgO, CaO, Na2O, K2O, and P2O5), LILE (Rb, Cs, Ba, Sr, Th, and U), HFSE (Y, Zr, Nb, Hf), and TTE (Sc, Cr, Co, V, and Ni). (A) Acre Basin, (B) Madre de Dios Basin.

4.5.1.1 Acre

All the samples are depleted in Fe_2O_3 against PAAS the of except the samples AC 37 and 49 which show enrichment relative to PAAS. All the samples are enriched in SiO_2, except for AC 37 sample. Enrichment in CaO is noted for the AC 20 A2 sample, while all other samples are depleted against PAAS. (Tab. 11 and Fig. 36).

The calculated CIA values, which range between 55 and 98, are higher than those observed in the unaltered plagioclase and K-feldspars typical of unaltered upper crustal rocks, as well as of the PAAS. However, we are unable to calculate CIA values for the following samples: samples AC 30A, 22A, 27A, 33, and 38 because they have concentrations below the detection limit. Overall, ACRE 15A, 16, 20A2, and 21A, have higher CIA values than AC 37, 42B, and 49 (Tab. 11). The samples ACRE 15A, 16, 20A2, 22, 30A, 37, 38, 42, and 49 have low Al/Si ratio, between 0.01 to 0.15. Samples 27A, and 33 have higher Al/Si ratios, 0.44 and 0.42 respectively (Tab. 11).

4.5.1.2 Madre de Dios

All the samples are depleted in TiO2, Cs, Ba, Sr, Th, Nb, Cr, V, Cu, and Ni and enriched in P2O5 and Y. Enrichment in CaO can be noted in MD 2019 12B, 01B, and 11B, while MD 2019 11B is depleted. The same sample is enriched in Zr and Hf, relative to PAAS, whereas other samples have similar contents or are depleted (Tab. 11 and Fig. 36). The analyzed samples have CIA values between 71 and 79, and are higher than those of the PAAS. Overall, the MD-2019-01B and 11B have lower CIA values than MD-2019-12B, 03B, 04C, 11E, and 12C (≥70) (Tab. 11). All of the Madre de Dios samples have high Al/Si ratio, between 0.23 and 0.44 (Tab. 11).

4.5.2 Rare Earth Elements (REE)

The Eu anomaly is calculated relative to chondrites ($Eu/Eu^* = Eu_N/(Sm_N \times Gd_N)^{½}$ where N refers to the chondrite-normalized concentration value (Condie, 1993)) and Th/Sc ratio could be used as a provenance tool (McLennan et al., 1990). This enables the possibility of making comparations with sediments originating from basic or felsic places (Cullers, 2000) and the PAAS (Pourmand et al., 2012; Taylor & McLennan, 1985). Low Eu/Eu* ratios (0.3 to 0.94), and high Th/Sc (> 0.64) are characteristic of felsic and silicic source rocks in fine-grained sedimentary protoliths, whereas higher Eu/Eu* ratios (0.71 - 1.02) and lower Th/Sc (<0.4) of fine-grained sedimentary rocks indicate more mafic and less differentiated source rocks (Cullers, 2000; McLennan et al., 1990).

4.5.2.1 Acre

The analyzed samples display important differences in the REE patterns (Fig. 37) after normalized against PAAS. The AC 33 and 27 samples have similar REE patterns with REE enrichment against PAAS but depletion in Middle REE (MREE) when compared with Light REE (LREE) and Heavy REE (HREE) (Fig. 37). The sample AC22A shows prominent enrichment in MREE with a “belly” shape pattern (Fig. 37). The samples AC 20A2 and 42B have similar patterns, with depletion in LREE, positive Eu anomalies, negative Gd anomalies, and enrichment in HREE against PAAS. The AC 30A and AC 33 samples are enriched in HREE against PAAS. The other samples are depleted in REE against PAAS (Fig. 37 and Tab. 11). The samples AC 15 and AC 16A have similar REE patterns with a strong depletion in MREE against other REE (Fig. 37).

The Ce anomalies exhibit a limited range of values (0.99 – 1.15), which closely resemble those the PAAS (i.e., ΩCe = 1), except for the AC 38 sample (1.39). The observed values consistently surpass those measured in authigenic smectites and

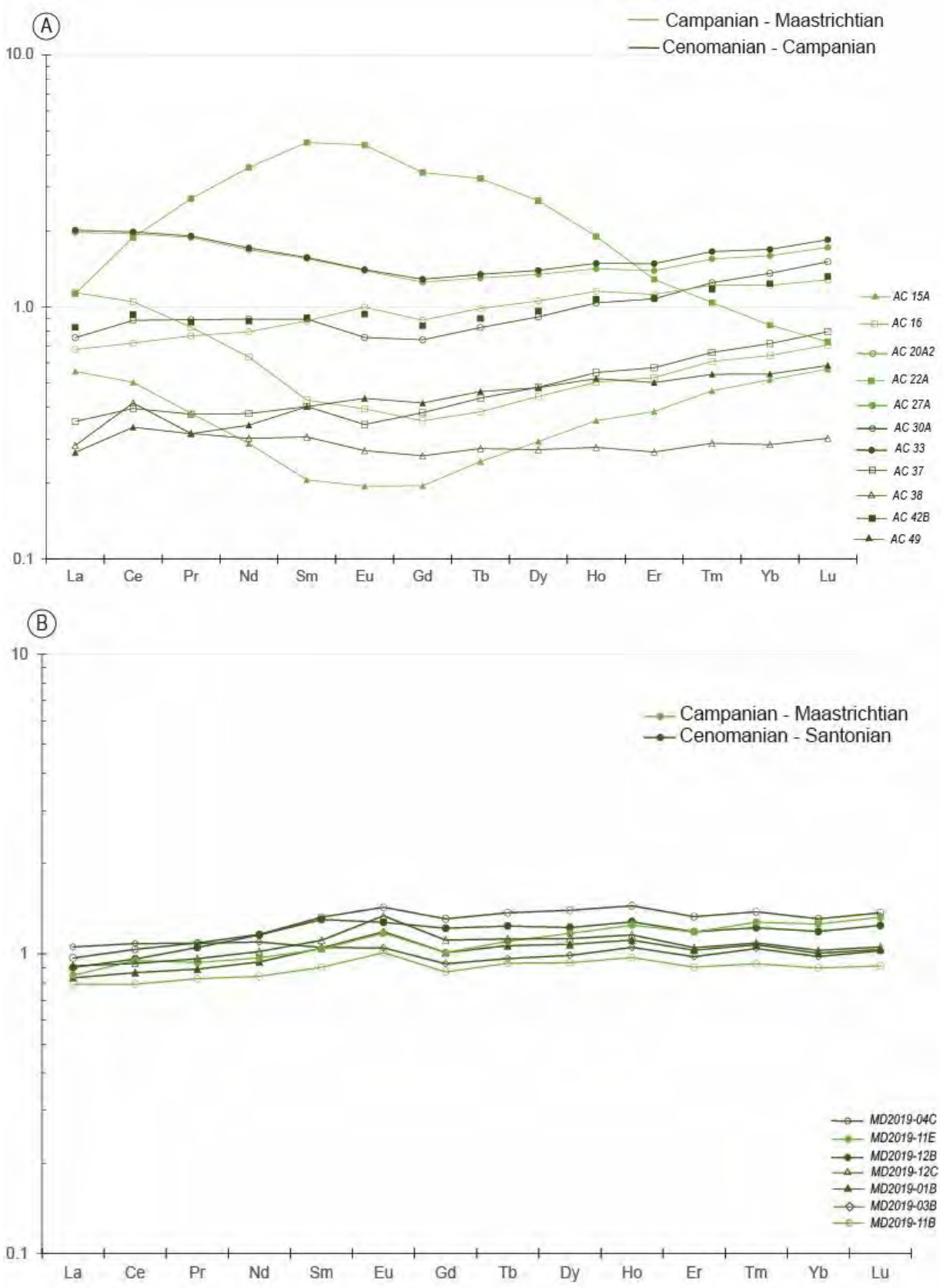

Fig. 37: Rare earth element (REE) contents of studied samples normalized to PAAS. (Pourmand et al., 2012; Taylor and McLennan, 1985). (A) Acre Basin, (B) Madre de Dios Basin.

seawater (ΩCe < 0.50), (De Baar et al., 1985). Similarly, the Eu/Eu* ratios have values from 0.50 to 0.65 (Fig. 37 and Tab. 11). The analyzed sample's Eu/Eu* ratios range between 0.50 to 0.65, and all of them present high Th/Sc (between 0.6 to 3.4) (Fig. 37 and Tab. 11).

4.5.2.2 Madre de Dios

Most of the analyzed samples have relatively flat REE patterns with slight enrichment in HREE, except for MD 2019 11B and variable Eu anomalies after normalized to PAAS (Fig. 37). The Ce anomalies values range between 0.98 to 1.07 similarly to the PAAS (i.e., ΩCe = 1). The values obtained from the analysis surpass than those measured in authigenic smectites and seawater, where the ΩCe values are below 0.50 (De Baar et al., 1985). The Eu/Eu* ratios have values between 0.59 and 0.70 and are higher than that of the PAAS (i.e., Eu/Eu* = 0.58), and the Th/Sc ratios range between 0.5 and 0.9 (Fig. 37 and Tab. 11).

4.5.3 Sm-Nd isotopes

The Sm-Nd isotope composition of analyzed samples from the Madre de Dios and Acre basins are presented in Tab. 12 and Fig. 38. The $^{147}Sm/^{144}Nd$ isotopic composition of the samples from the Acre Basin ranges from 0.1358 to 0.0727, with ε_{Nd} (0) values between -21.2 to -8.4 and ε_{Nd} (T) values ranging from -20.2 to -7.3. $T_{DM\ (0)}$ ages range from 2.66 to 0.91 Ga and $T_{DM\ (*)}$ ages between 2.27 to 1.32 Ga (Table 3). The three youngest samples (AC-15A, AC-16, and AC-20A) have higher ε_{Nd} (0) values (-8.4 to -10.8 vs -18.6 to -21.2) and younger TDM ages (0.91-1.57 Ga vs 1.87-2.45 Ga) than the oldest samples.

The late Cretaceous sedimentary rocks of the northern part of the Madre de Dios Basin (samples MD 234; MD234B, MD234C, MD238) yield present-day

Tab. 12: Sm-Nd systematics of analyzed sedimentary rocks. Madre de Dios basin: Ages are from Louterbach (2014) and Louterbach et al. (2018). The ε_{Nd} (T) values of Made de Dios Basin samples were calculated based on the stratigraphic ages of Louterbach et al. (2018) (75Ma). For all the samples we used 75Ma. Acre basin: Ages are from Cunha (2007) (*) and Haag (2019) (**) Brito et al. (1994) (***). The ε_{Nd} (T) values of Acre Basin samples were calculated based on the stratigraphic interpretation from Cunha (2007), and the palynology ages analyzed in this study and by Haag (2019). For ACRE 49, ACRE 42B, ACRE 38, ACRE 37, ACRE 33, ACRE 30A, ACRE 27A, ACRE 22A, and ACRE 20A2 we used 90Ma, and for ACRE 16 and ACRE 15A 70Ma.

Madre de Dios	Sample	Formation	Age	Longitude (W)	Latitude (S)	Sm (ppm)	Nd (ppm)	$^{147}Sm/^{144}Nd$	$^{143}Nd/^{144}Nd$	$\pm 2\sigma$ (10^{-6})	e_{Nd} (0)	e_{Nd} (T)	TDM (Ga)	TDM* (Ga)
1	**MD234**	Basal Chonta	Cenomanian or older	71°21'49.54"	12°53'36.13"	2.61	12.79	0.1235	0.5119	±9	-14.4	-13.7	2.03	1.78
2	**MD234B**			71°21'49.54"	12°53'36.13"	1.74	10.85	0.0968	0.512271	±7	-7.16	-6.2	1.1	1.24
3	**MD234C**			71°21'49.54"	12°53'36.13"	1.81	9.58	0.1144	0.512276	±4	-7.05	-6.3	1.3	1.24
4	**MD-2019-1B**	Chonta	Early Cenomanian	70°19'3.82"	13°16'46.80"	7.73	39.08	0.1196	0.512075	±3	-10.99	-10.2	1.68	1.53
5	**MD-2019-4C**	Chonta	Cenomanian	70°22'12.39"	13°12'9.20"	9.77	48.65	0.1215	0.512071	±7	-11.06	-10.3	1.72	1.54
6	**MD-2019-3B**	Chonta	Cenomanian	70°22'12.30"	13°12'16.93"	7.91	46.33	0.1032	0.512106	±1	-10.37	-9.5	1.4	1.48
7	**MD-2019-12C**	Vivian	Late Cenomanian -Early Turonian	70°23'2.14"	13°11'51.06"	8.46	42.33	0.1491	0.512266	±7	-7.25	-6.8	1.98	1.28

8	**MD-2019-12B**	Vivian	Late Cenomanian -Early Turonian	70°23'1.91"	13°11'50.71"	9.87	48.94	0.1218	0.51207	±4	-11.08	-10.4	1.72	1.54
9	**MD-2019-11B**	Chonta	Coniacian - Santonian	70°23'23.75"	13°11'25.35"	6.71	34.99	0.116	0.512073	±3	-11.02	-10.3	1.62	1.53
10	**MD-2019-11E**	Vivian	Maastrichtian	70°23'24.80"	13°11'27.37"	8.07	42.68	0.1143	0.512067	±3	-11.13	-10.4	1.6	1.54
11	**MD238**	Vivian	Early Maastrichtian	71°21'44.21"	12°53'34.76"	3.96	21.43	0.1117	0.51186	±1.4	-15.18	-14.4	1.86	1.83

Acre	Sample	Formation	Age	Longitude (W)	Latitude (S)	Sm (ppm)	Nd (ppm)	$^{147}Sm/^{144}Nd$	$^{143}Nd/^{144}Nd$	±2σ (10^{-6})	ε_{Nd} (0)	ε_{Nd} (T)	TDM (Ga)	TDM* (Ga)
1	**ACRE 38**	Moa	Late Albian-Cenomanian/Late Turonian*	73°39'59.00"	7°26'52.98"	2.259	12.448	0.1097	0.511744	±1.3	-17.44	-16.4	1.99	1.99
2	**ACRE 49**	Moa	Late Albian-Cenomanian/Late Turonian*	73°41'37.67"	7°27'29.60"	2.984	13.993	0.1289	0.511676	±1.4	-18.77	-18.0	2.54	2.11

4	**ACRE 42 B**	Rio Azul	Turonian-Campanian*	73°42'8.10"	7°28'14.18"	8.093	45.016	0.1087	0.511664	±1.3	-19	-18.0	2.08	2.11
5	**ACRE 37**	Rio Azul	Turonian-Campanian*	73°41'56.09"	7°28'41.81"	3.224	17.426	0.1118	0.511552	±1.8	-21.19	-20.2	2.31	2.27
3	**ACRE 33 A**	Rio Azul	Cenomanian** Turonian-Campanian*	73°42'6.12"	7°29'5.41"	11.959	72.973	0.0991	0.511641	±1.1	-19.45	-18.3	1.94	2.13
6	**ACRE 30 A**	Rio Azul	Campanian-Maastrichtian*	73°41'59.12"	7°29'33.14"	6.837	38.221	0.1081	0.511653	±7	-19.21	-18.2	2.09	2.12
7	**ACRE 27 A**	Divisor	Campanian-Maastrichtian*	73°41'57.82"	7°29'50.64"	11.734	71.68	0.0990	0.511626	±1.1	-19.73	-18.6	1.96	2.15
8	**ACRE 22 A**	Divisor	Campanian-Maastrichtian*	73°42'4.49"	7°30'0.91"	33.45	148.912	0.1358	0.511682	±6	-18.64	-18.0	2.74	2.1
9	**ACRE 20 A2**	Divisor	Campanian-Maastrichtian*	73°42'8.18"	7°30'7.50"	5.897	29.239	0.1219	0.512087	±7	-10.75	-9.9	1.7	1.52
10	**ACRE 16**	Divisor	Campanian-Maastrichtian*	73°42'6.08"	7°30'18.15"	3.029	25.184	0.0727	0.512205	±1.2	-8.44	-7.3	1	1.32

11	**ACRE 15 A**	Divisor	Campanian-Maastrichtian*	73°42'7.38"	7°30'20.17"	1.574	11.36	0.0837	0.512185	±1.3	-8.83	-7.8	1.10	1.35

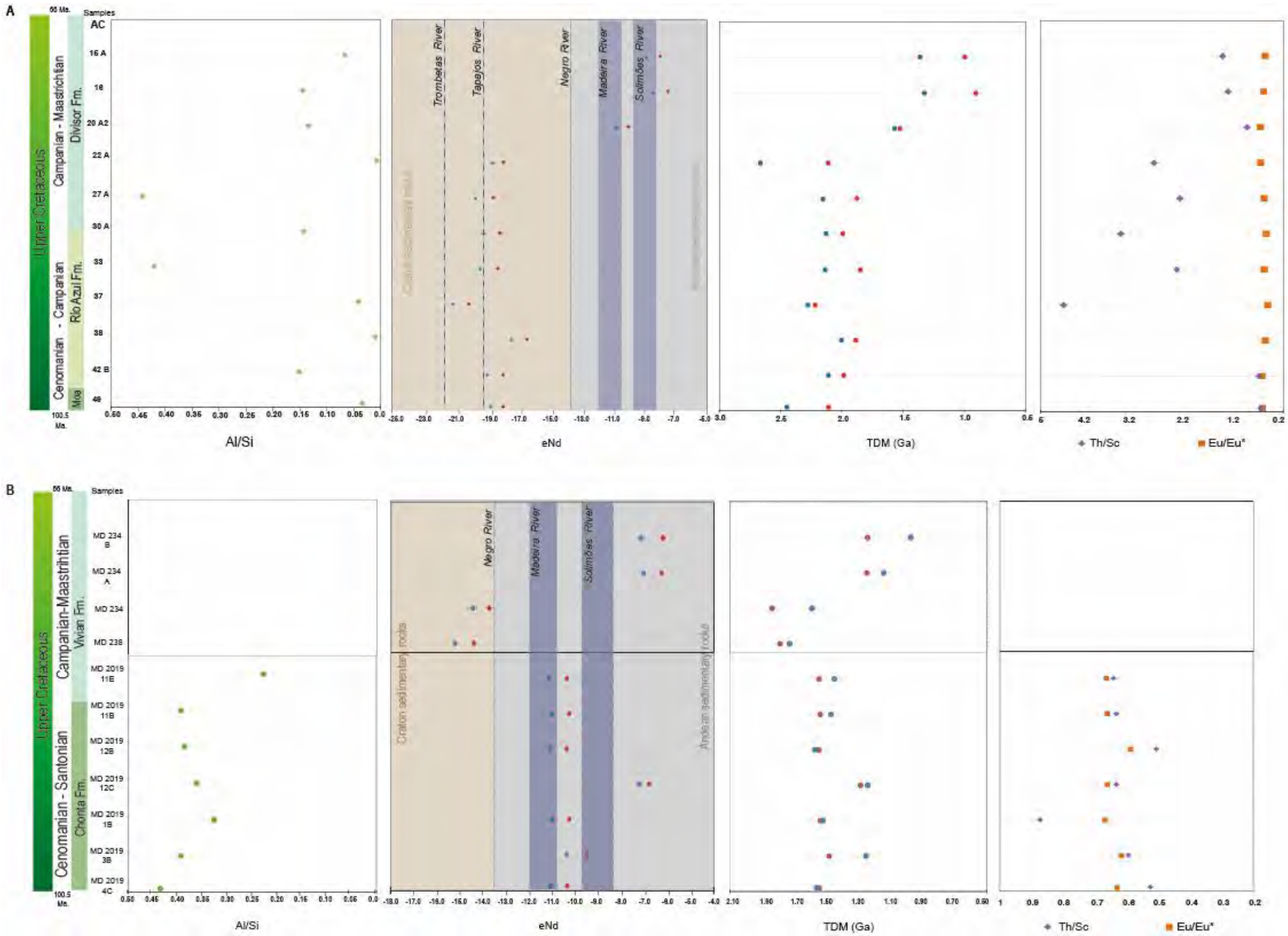

Fig. 38 Stratigraphic variation of Nd isotope composition (expressed as ƐNd(0) / TDM (0) for the blue points, and ƐNd(T) / TDM (T) for the red points) and selected trace element ratios (Th/Sc and Eu/Eu*, see text for details) of analyzed samples A - Acre Basin; B - Madre de Dios Basin. The lengths of the horizontal bar for the Sm-Nd isotopic compositions correspond to 2σ analytical errors (see Table 3). Dashed lines in ƐNd show the Amazonian recent rivers ƐNd values. Purple and orange symbols indicate the values of Th/Sc and Eu/Eu*, respectively. The $Ɛ_{Nd}$ (T) values of Acre Basin samples were calculated based on the stratigraphic interpretation from Cunha (2007), and the palynology ages analyzed in this study and by Haag (2019). For AC49, 42B, 38, 37, 33, 30A, 27A, 22A, and 20A2 we used 90Ma, and for 16 and 15A, 70Ma. The $Ɛ_{Nd}$ (T) values of Made de Dios Basin samples were calculated based on the stratigraphic ages of Louterbach et al. (2018) (75Ma).

$^{147}Sm/^{144}Nd$ isotopic composition ranging from 0.0968 to 0.1235, with ε_{Nd} (0) values between -7.1 to -15.2 and ε_{Nd} (T) values ranging –from 6.2 to -14.4. The $T_{DM(0)}$ ages range from 1.0 to 1.76 Ga and $T_{DM\ (*)}$ ages between 1.24 and 1.83 Ga (Tab. 12). The analyzed sedimentary rocks from the southern part of the Madre de Dios Basin have $^{147}Sm/^{144}Nd$ between 0.1491 and 0.1032 with ε_{Nd} (0) values ranging from -11.1 to -7.3, ε_{Nd} (T) values ranging between -6.8 and -10.4 and T_{DM} ages between 1.6 and 1.27 Ga and $T_{DM(0)}$ ages ranging from 1.28 to 1.54 Ga. (Tab. 12). One sample (MD2019 12C) displays a much higher ε_{Nd} (0) value than the others (-7.3 vs -10.4 to -11.1, Tab. 12). Overall, the Cenomanian (?) sedimentary rocks of the Acre Basin have lower ε_{Nd} (0) values and higher (?) TDM ages than the late Cretaceous sedimentary rocks of the Madre de Dios Basin

4.6 U-Pb detrital zircon

Tab. 13 and Fig. 39 and Fig. 40 present the U-Pb zircon ages obtained across the Cretaceous successions of the Acre and Madre de Dios Basins.

The U-Pb age distribution of analyzed samples from the Acre Basin was dominated by zircon ages between 2.0-1.82 Ga (Ventuari-Tapajós, 15% - 45.9%) and 1.82-1.54 (Rio Negro-Juruena, 16% - 46.4%) and to a lesser extent by zircons ages between 1.54-1.3 Ga (Rondonia-San Ignácio, 5%-32%) and 0.9-1.3 Ga (Grenville/Sunsás, 4% - 46%), (Tab. 13 and Fig. 39).

The U-Pb age distribution of the samples from the northern part of the Madre de Dios Basin (MD234 and MD238) are dominated by zircon ages between 0.9-1.3 Ga (Grenville/Sunsás, 30.2%-36.7%) and 0.5-0.7 Ga (Brazilian/Pampean, 16.3%-26.2%). The MD234 sample also shows a dominant contribution from zircons aged between 0.4 and 0.5 Ga (Famatinian Arch, 19.8% - 6.1%). In contrast, the analyzed samples from the southern part of the Madre de Dios Basin (samples MD-2019-4A; MD-2019-

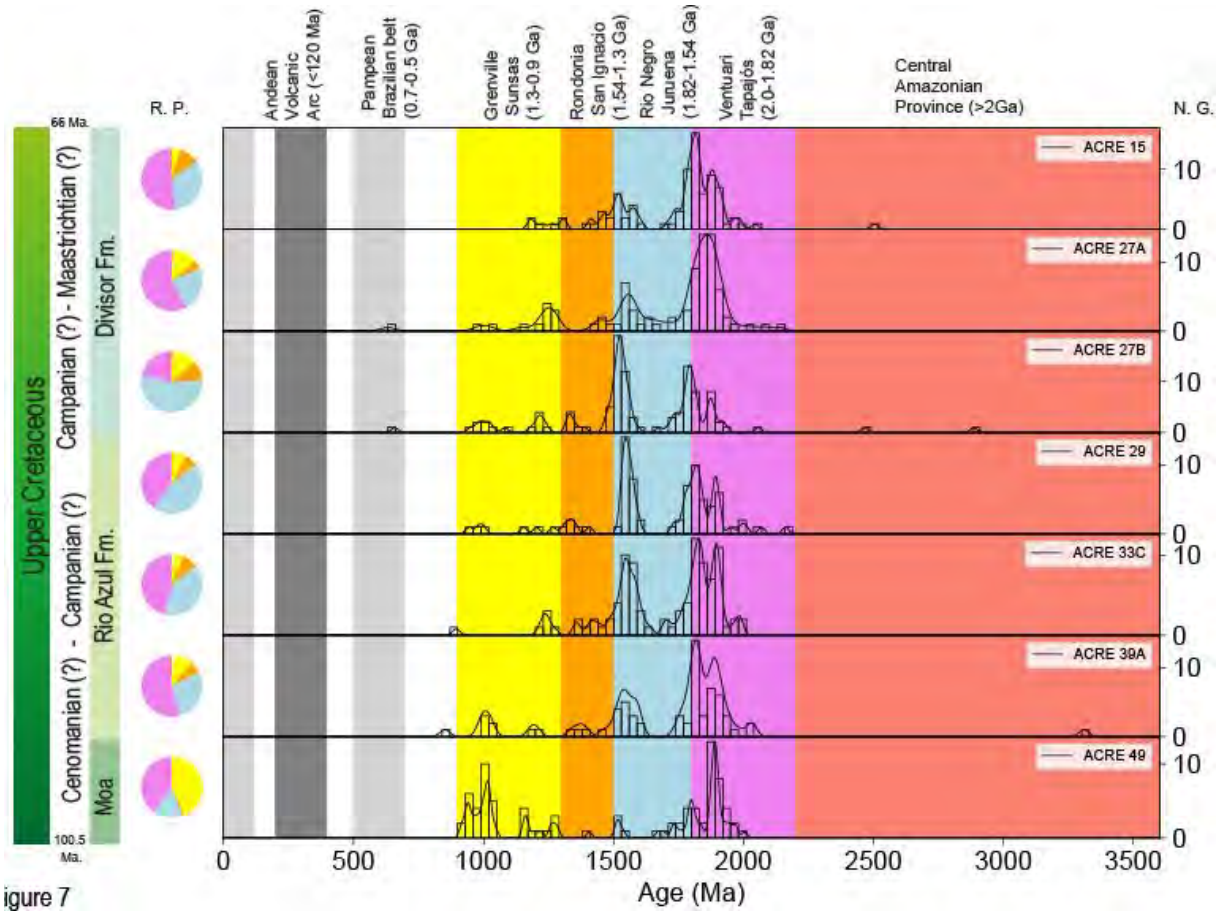

igure 7

Fig. 39: Stratigraphic evolution of Acre U-Pb ages on zircon grains. The detrital age distribution presents the Kernel Density Estimations (KDE) (black line), which were calculated following (Vermeesch, 2012) in the Python-based DetritalPy program (Sharman et al., 2018) and age histogram (bars). N.G.: Number of grains; R.P.: Relative Percentage (Table 5).

Tab. 13: Numbers and percentages (%) of U–Pb ages representing known and distinct geochronological events in probable source regions on the Amazonia craton and the central Andes. Temporal ranges of events according to Bahlburg et al. (2009), Chew et al. (2008), and Calderon et al. (2017). n is the number of samples analyzed for the time interval.

Time (Ga)	Event	MD-2019-4A		MD-2019-10		MD-2019-11D		MD-2019-12A		MD-2019-13		MD-234	
		n = 98		n = 54		n = 72		n = 78		n = 90		n = 126	
Province/terrane		number	%	number	%	number	%	number	%	number	%	number	%
< 0.12	**Andean Arc**	0	0%	0	0%	0	0%	0	0%	0	0%	0	0%
0.25-0.15	**Triassic-Jurassic extension**	0	0%	0	0%	0	0%	0	0%	0	0%	2	2%
0.4-0.26	**Paleozoic Magmatic Arc**	0	0%	0	0%	0	0%	0	0%	0	0%	25	20%
0.5-0.4	**Famatinian**	0	0%	0	0%	0	0%	0	0%	0	0%	2	2%
0.7-0.5	**Brazilian**	3	3%	0	0%	1	1%	3	4%	4	4%	33	26%
0.9-0.7		1	1%	3	6%	1	1%	1	1%	2	2%	6	5%
1.3-0.9	**Greenville Sunsas**	45	46%	30	58%	31	43%	38	49%	39	43%	38	30%
1.54-1.3	**Rondonia - San Ignacio**	43	44%	16	31%	33	46%	25	32%	37	41%	8	6%
1.82-1.54	**Rio Negro-Juruena**	6	6%	4	8%	4	6%	7	9%	7	8%	2	2%
1.82-2	**Ventuari- Tapajos**	0	0%	0	0%	2	3%	3	4%	1	1%	3	2%
2.2-2	**Maroni-Itacaiunas**	0	0%	0	0%	0	0%	1	1%	0	0%	4	3%
>2.2	**Central Amazon**	0	0%	1	2%	0	0%	0	0%	0	0%	3	2%

Time (Ga) / Province/terrane	Event	MD-238 n = 49 number	%	MD-239 n = 74 number	%	MD-176 n = 169 number	%
< 0.12	**Andean Arc**	0	0%	0	0%	0	0%
0.25-0.15	**Triassic-Jurassic extension**	0	0%	0	0%	1	1%
0.4-0.26	**Paleozoic Magmatic Arc**	3	6%	0	0%	1	1%
0.5-0.4	**Famatinian**	2	4%	0	0%	0	0%
0.7-0.5	**Brazilian**	8	16%	10	14%	12	7%
0.9-0.7		7	14%	0	0%	0	0%
1.3-0.9	**Greenville Sunsas**	21	43%	16	22%	47	28%
1.54-1.3	**Rondonia - San Ignacio**	7	14%	22	30%	89	53%
1.82-1.54	**Rio Negro-Juruena**	0	0%	17	23%	9	5%
1.82-2	**Ventuari- Tapajos**	4	8%	6	8%	6	4%
2.2-2	**Maroni-Itacaiunas**	0	0%	3	4%	4	2%
>2.2	**Central Amazon**	1	2%	0	0%	0	0%

Time (Ga) / Province/terrane	Event	ACRE 49 n = 86 number	%	ACRE 39 n = 68 number	%	ACRE 33 n = 95 number	%	ACRE 29 n = 69 number	%	ACRE 27B n = 111 number	%	ACRE 27A n = 85 number	%
< 0.12	**Andean Arc**	0	0%	0	0%	0	0%	0	0%	0	0%	0	0%

0.25-0.15	**Triassic-Jurassic extension**	0	0%	0	0%	0	0%	0	0%	0	0%	0	0%
0.4-0.26	**Paleozoic Magmatic Arc**	0	0%	0	0%	0	0%	0	0%	0	0%	0	0%
0.5-0.4	**Famatinian**	0	0%	0	0%	0	0%	0	0%	0	0%	0	0%
0.7-0.5	**Brazilian**	0	0%	0	0%	0	0%	0	0%	1	1%	1	1%
0.9-0.7		0	0%	1	1%	1	1%	0	0%	0	0%	0	0%
1.3-0.9	**Greenville Sunsas**	37	43%	7	10%	5	5%	6	8%	13	12%	11	13%
1.54-1.3	**Rondonia - San Ignacio**	5	6%	9	13%	14	15%	10	13%	36	32%	8	9%
1.82-1.54	**Rio Negro-Juruena**	14	16%	23	34%	39	41%	35	46%	39	35%	25	29%
1.82-2	**Ventuari-Tapajos**	30	35%	25	37%	36	38%	24	32%	16	14%	40	47%
2.2-2	**Maroni-Itacaiunas**	0	0%	2	3%	0	0%	1	1%	1	1%	0	0%
>2.2	**Central Amazon**	0	0%	1	1%	0	0%	0	0%	5	5%	0	0%

Time (Ga)	Event	ACRE 15 n = 85	
Province/terrane		number	%
< 0.12	**Andean Arc**	0	0%
0.25-0.15	**Triassic-Jurassic extension**	0	0%
0.4-0.26	**Paleozoic Magmatic Arc**	0	0%

0.5-0.4	**Famatinian**	0	0%
0.7-0.5	**Brazilian**	0	0%
0.9-0.7		0	0%
1.3-0.9	**Greenville Sunsas**	6	7%
1.54-1.3	**Rondonia - San Ignacio**	13	15%
1.82-1.54	**Rio Negro-Juruena**	32	38%
1.82-2	**Ventuari- Tapajos**	33	39%
2.2-2	**Maroni-Itacaiunas**	0	0%
>2.2	**Central Amazon**	1	1%

10; MD-2019-13; MD-2019-11D and MD-2019-12A) have U-Pb age distributions dominated by zircon ages between 0.9-1.3 Ga (Grenville/Sunsás, 27.8%-44.9%) and 1.54-1.3 Ga (Rondonia-San Ignácio, 41%-58.3%) (Tab. 13 and Fig. 40).

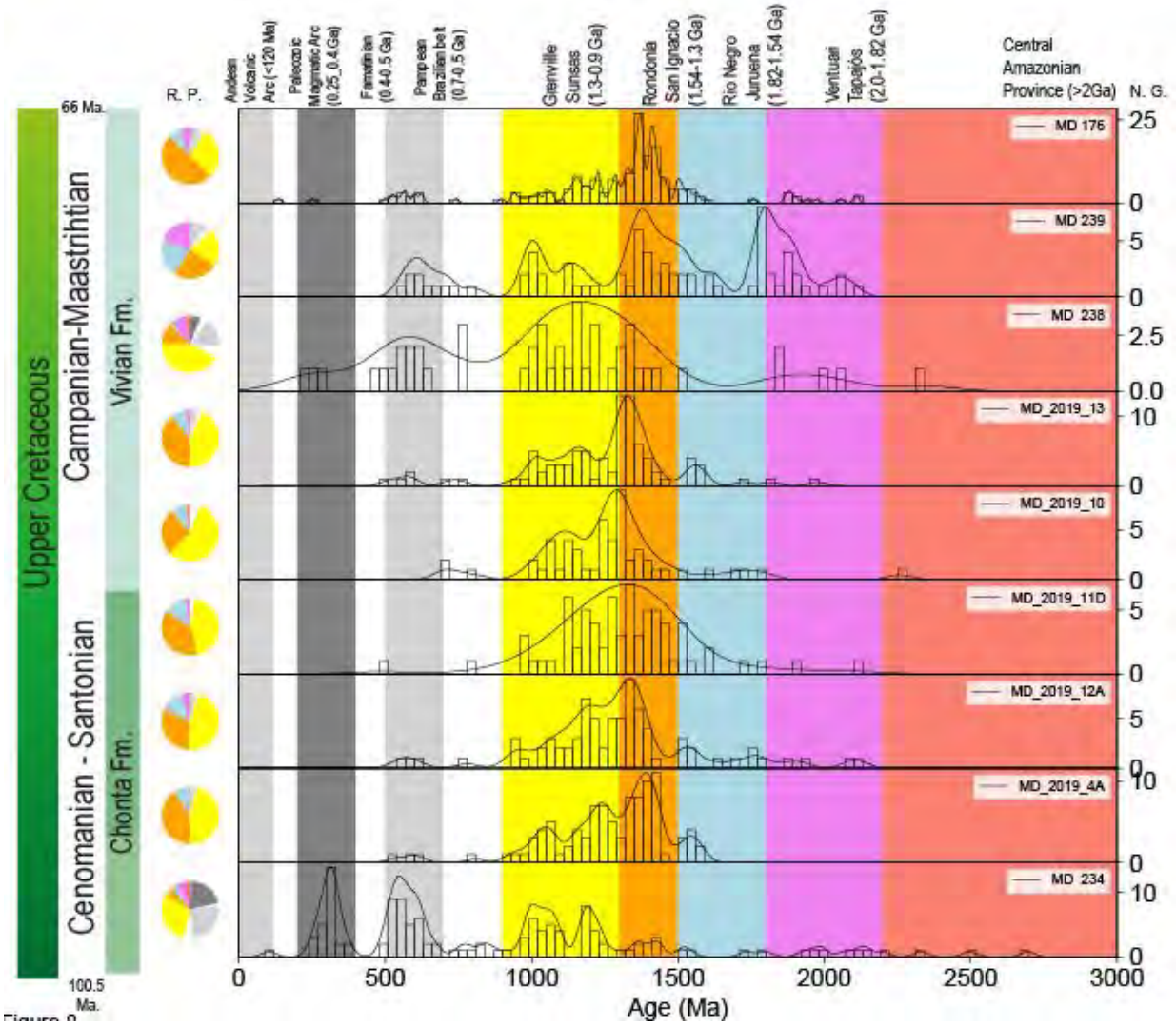

Fig. 40: Stratigraphic evolution of Madre de Dios U-Pb ages on zircon grains. The detrital age distribution presents the Kernel Density Estimations (KDE) (black line), which were calculated following (Vermeesch, 2012) in the Python-based DetritalPy program (Sharman et al., 2018) and age histogram (bars). N.G.: Number of grains; R.P.: Relative Percentage (Table 5).

4.7 Discussion

4.7.1 Influence of geochemical characteristics in the provenance sedimentary interpretation.

The utilization of elemental ratios (Cr/Th, Th/Sc, Zr/Sc), Eu anomalies (Eu/Eu*) and Sm-Nd isotopic compositions of sedimentary rock have proven to be valuable in

determining the source of ancient sediments (McLennan et al., 1993). However, it is essential to consider the potential effects of grain-size sorting and diagenesis on trace element ratios, REE concentration, and radiogenic isotope composition of the analyzed sedimentary rocks.

Except for the samples AC 33 (0.42) and AC 27A (0.44), most of the Acre Basin samples have a low Al/Si ratio (0.01 - 0.27) (Fig. 38), which indicates that they are enriched in quartz. However, the lack of Al/Si with REE content, Eu/Eu*, Cr/Th, and ε_{Nd} (0) correlation (seen in the supplementary dataset) suggests sedimentary sorting has not made any alteration of these provenance indicators. Nevertheless, the REE concentrations of the analyzed samples against PAAS show contrasting patterns. Only one sample of the Acre Basin (Sample AC 38) plots in the shale field (Fig. 41) whereas the remaining ten samples plot outside of the shale field suggesting that the REE concentrations have been perturbed by post-depositional processes (Fig. 41). The AC 22A show strong enrichment in HREE (Fig. 41). This strong HREE enrichment could be associated with a primary phase of the pedologic process. In a study of the lateritic process in a tropical environment, Viers and Wasserburg (2004) indicated that the zircon dissolution could elevate the HREE concentrations at the early stage of the weathering process, and the Zr precipitation could remove the REE during that phase. This could explain the HREE enrichment for samples AC 22, 27A, and 38. The remaining samples (AC 15A, 42B, 30A, 20A2, 37, and 49) show enrichment in LREE over HREE and plot between the “shales” and “seawater” fields in Fig. 41.

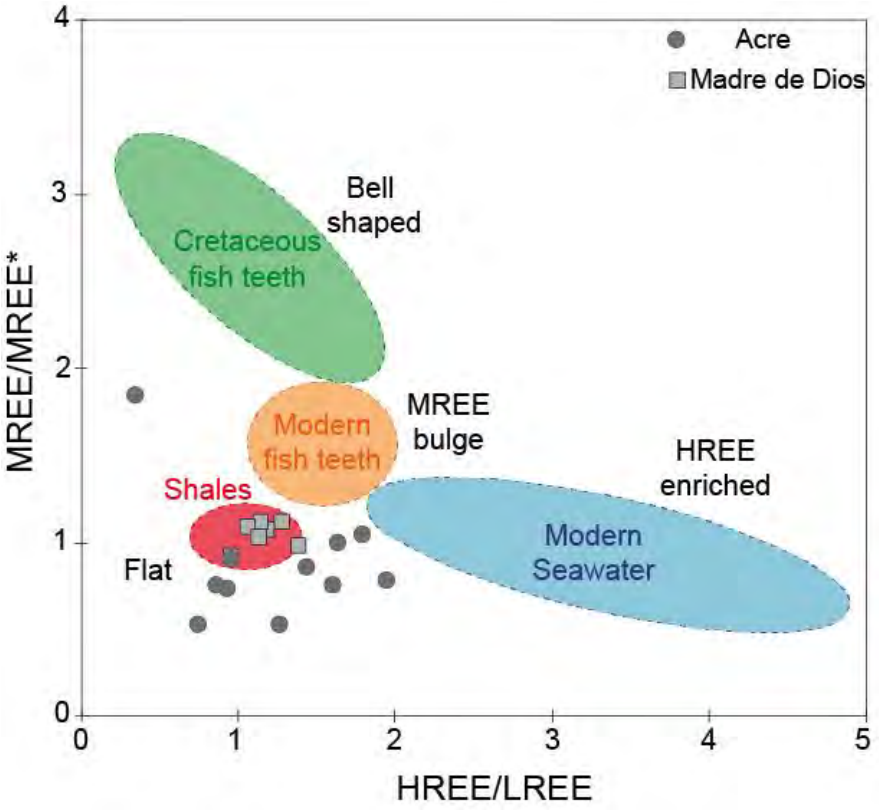

Fig. 41: REE patterns observed in fish teeth, Fe-Mn oxides, organic matter, and pore waters, while "HREE-enriched" profiles correspond to modern seawater (Huck et al., 2016; Moiroud et al., 2016). These end-members reflect the REE contents of marine sediments influenced by seawater or authigenic phases, while "flat" REE patterns are characteristic of continental clays (see Huck et al., 2016; Moiroud et al., 2016 for a review).

The Madre de Dios samples have a high Al/Si ratio which ranges between 0.33 and 0.44 (except for MD-2019-11E, Al/Si = 0.23), which suggests that are fine and clay-rich sediments (Bouchez et al., 2011) (Tab. 11, Fig. 41). The lack of correlation (see in the supplementary dataset) between CIA and Al/Si with REE content, Eu/Eu*, Cr/Th, and ε_{Nd} (0) values implies that the provenance indicators have not been altered by chemical weathering and sedimentary sorting. The samples exhibit low Eu/Eu* ratios (Tab. 11) indicating that diagenetic remobilization of Eu was insignificant in our samples. The Madre de Dios samples have more uniform major and trace elements and REE concentration patterns when compared with those of the Acre Basin (Figs. 5A and 5B). The analyzed samples from Madre de Dios exhibit Ce anomalies (ΩCe) above 0.85 and display flat REE patterns when compared to PAAS, indicating their

classification within “shales” field (Fig. 41). This characteristic, typical of continental clays (see Moiroud et al., (2016), suggest that these samples are unaffected by marine autogenesis.

4.7.2 Interpretation of provenance

The Th/Sc, Cr/Th elemental ratios and the Eu/Eu* ratios of the Acre Basin samples are in favor of a silicic/felsic source *sensu* Cullers (2000) source: the Th/Sc is between 0. and 4.5; the Cr/Th ratios are equal or higher than 1.0 and the Eu/Eu* ratios are between 0.50 - 0.65. This is also the case for the analyzed Madre de Dios sedimentary rocks with Th/Sc ratio range (0.64 - 0.87); Cr/Th ratio (between 5.14 and 7.23), and Eu/Eu* values (0.59 and 0.67 (Tab. 11Tab. 11: Major and trace element concentrations of sedimentary rocks analyzed in this study. D.L.: Detection Limit., Fig. 38) characteristics of silicic/felsic sources (Cullers, 2000). Further insights can be obtained by considering the Nd isotopic composition of the analyzed samples, which can provide additional constrains.

Therefore, the Nd isotopic compositions observed in sedimentary rocks from the Andean and Amazonian regions can be attributed to a combination between juvenile primitive Andean Arc and older cratonic sources (Basu et al., 1990; Roddaz et al., 2005). Cratonic sedimentary rocks are characterized by negative ε_{Nd} (0) values, between -14.5 and -20, and Nd model ages (T_{DM}) from 1.75 to 3.3 Ga, while Andean-derived sediments have more positive ε_{Nd} (0) values and T_{DM} lower than 1.6 Ga (Cordani & Sato, 1999; Figueiredo et al., 2009; Carina Hoorn et al., 2017; Horbe et al., 2013; Roddaz et al., 2005). Within Colombia, a threshold value of -12.7 for εNd(0) has been employed to differentiate sedimentary rocks derived from the Andean or cratonic sources (Nie et al., 2012). Similarly, zircon U-Pb ages have been used in provenance studies of Amazonian sediments to decipher the relative contributions of Andean and cratonic source rocks (Erlich et al., 2018; George et al., 2019; Gutiérrez et al., 2019;

Horton, 2018; Hurtado et al., 2018; Louterbach et al., 2018; Moreno et al., 2020; Perez et al., 2016). The distinct geological ages of the Andean Cordillera and the Amazon craton account for their compositional differences. For instance, the Amazon craton is defined by Precambrian zircon U–Pb ages (>600 Ma, Fig. 35) (Bahlburg et al., 2009; Chew et al., 2008; Chew et al., 2007; Cordani et al., 2000; Cordani & Sato, 1999; Rizzotto & Quadros, 2005; Santos et al., 2000; Tassinari & Macambira, 1999). In contrast, the Andes are mostly characterized by Phanerozoic zircon U-Pb ages (<550 Ma, mainly Mesozoic-Cenozoic ages, Fig. 35) (DeCelles et al., 2011; Horton et al., 2016; Martin-Gombojav & Winkler, 2008; Nie et al., 2012; Perez et al., 2016), except for the Marañón Complex which crops out in the Peruvian Eastern Cordillera. The Marañón complex is composed of metamorphic and plutonic rocks of the Precambrian age (Chew et al., 2007; Ramos & Folguera, 2009).

Except for the three youngest samples of the Campanian-Maastrichtian Divisor Formation (AC 20 A2, AC 16, and AC 15A) that could have been perturbed by pedogenetic processes, the ε_{Nd} (0) values together with the T_{DM} ages of other analyzed samples of the Acre Basin (Tab. 12) suggest that sedimentary rocks were sourced from cratonic rocks. When compared with the Cretaceous sedimentary rocks of the Huallaga Basin (Hurtado et al., 2018), they have similar negative ε_{Nd} (0) values as those of the Cenomanian (Agua Caliente Formation - HUA 245), Coniacian-Turonian (Chonta Formation - HUA 240 and 244) and Maastrichtian (Vivian Formation - HUA 462).

The U-Pb zircon age distribution of Cenomanian to Maastrichtian samples of the Acre Basin also suggests a cratonic source with a dominant population of zircon aged between 1.8 and 2.0 Ga related to the tectonic province of Ventuari-Tapajos (2.0-

1.82 Ga). The sample HUA 462 of the Huallaga Basin (Hurtado et al., 2018), some samples of the Marañón Basin (Chonta 22-06-08-04; Chonta Palo Seco-1X – 2299m; Lower Vivian 20-06-08-19; Lower Vivian #120 Pagoreni 1003-ST1; Upper Vivian #62 Yarina-2X.; Erlich et al., 2018), the early Maastrichtian sample of the Madre de Dios Basin (MD 239, Louterbach et al., 2018) and the sample (SG1616) analyzed in George et al. (2019) also present zircons aged between 1.82 and 2.0 Ga (Venturi-Tapajos), which suggest a common source. The second dominant population consists of zircon aged between 1.54 and 1.82 Ga related to the tectonic province of Rio Negro Juruena (Santos et al., 2000; Tassinari & Macambira, 1999). The sample HUA 266A of the Huallaga Basin (in Hurtado et al., 2018) and some samples (Chonta #141 Tuncheplaya-95X 3201m; Chonta Palo Seco-1X – 2299m; Chonta #64 Yarina-2X 2396-2423m; Lower Vivian #75 San Alejandro-1X; Lower Vivian #120 Pagoreni 1003-ST1; Lower Vivian #149 Yanez-1X; Upper Vivian #135 Plantayacu-83X) of the Marañón Basin (Erlich et al., 2018) have similar 1.54 -1.82 Ga dominant zircon population which suggest a shared source.

In the Madre de Dios Basin, most of the samples have ε_{Nd} (0) values higher than -11, and T_{DM} ages (Tab. 12) younger than 1.6 Ga, which suggests that they are sourced by the Andes. The samples from the southern Madre de Dios Basin (MD 2019-13; 10; 11D; 12A and 4B) are dominated by zircon aged between 1.5 and 1.0 Ga, which could have been sourced by the tectonic provinces of Grenville-Sunsás (0.9-1.3 Ga) and Rondonia-San Ignacio (1.3-1.54 Ga). Similar age peaks can be found for the late Maastrichtian sample of the northern part of the Madre de Dios Basin (MD 176) analyzed by Louterbach et al. (2018). In the northern part of the basin, the oldest Late Cretaceous (MD 234) is characterized by dominant populations of analyzed zircons between 0.5 – 0.7 Ga (Brazilian/Pampean source), and MD 238 sample has a

subordinate population of detrital zircon earlier than 1.0 Ga, which also appears in samples from the Arequipa Basin (ARE 17; ARE 332; ARE 339) located west to the studied area, analyzed in (Chavez et al., 2022); and in the samples of the Eastern Cordillera (145306), Bagua (FTfm145311) and Huallaga (HUA 266A) basins analyzed in George et al., 2019; Moreno et al., 2020 and Hurtado et al. 2018, respectively.

Additional information can be gained from the MDS graph (Fig. 42) which is used to represent statistically the degree of similarity in U-Pb zircon age distribution between analyzed samples (Vermeesch, 2013, 2018). In this map (Fig. 42), “similar” samples cluster closely together and are linked by solid and dashed lines (closest and second-closest neighbors), whereas “dissimilar” samples plot far apart. In the MDS graph, three statistically distinct groups of U-Pb zircon age can be visualized (Fig. 42).

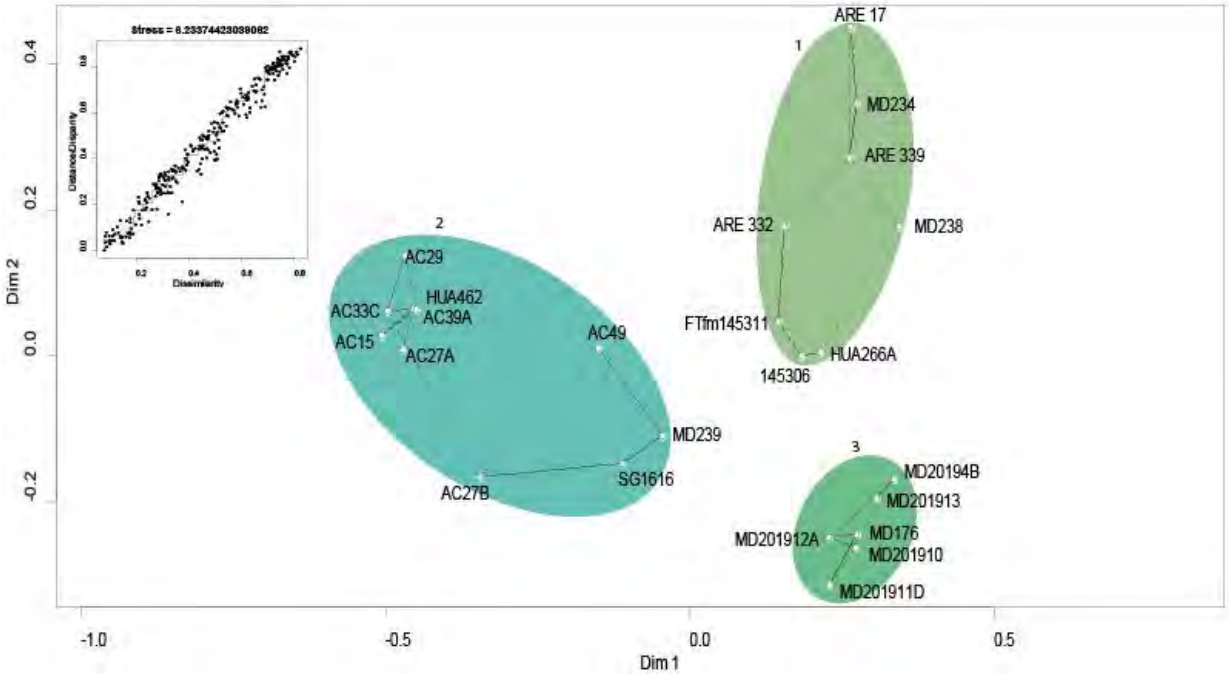

Fig. 42: A) Non-metric multi-dimensional scaling (MDS) plot (Vermeesch, 2013) based on the U-Pb age distributions of detrital zircons in the analyzed samples using the Kolmogorov-Smirnov test. Closest and second closest neighbors are linked by solid and dashed lines, respectively; B) Shepard plot of the U-Pb data showing the transformation from dissimilarity to distances and disparities. Groups 1, 2, and 3 indicate samples with a similar detrital zircon age population (see discussion in the text).

The first group is composed of the late Cretaceous MD 238 and MD 234 samples from the northern part of the Madre de Dios Basin, the Cretaceous samples from the Arequipa Basin (ARE 17; ARE 339; ARE 332 (Chavez et al., 2022), the

Campanian sample from the Bagua Basin (FTfm145311, Moreno, et al., 2020), the early Cretaceous sample from the Eastern Cordillera (145306 sample, George et al., 2019) and the Albian sample of the Huallaga Basin (HUA 266A, Hurtado, et al., 2018). All these samples are linked by solid or dashed lines, suggesting a shared provenance. The late Cretaceous samples of the Bagua Basin are connected by a solid line with the sample of the Eastern Cordillera (145306) and were interpreted to be sourced by sediment recycling from the Cretaceous Goyllarisquizga Group with potential contribution of Amazon Craton (Moreno et al., 2020). The early Cretaceous sample of the Eastern Cordillera and the Albian sample of the Huallaga Basin are also connected by solid lines which indicate a shared provenance. The sample from the Huallaga Basin (HUA 266A) was interpreted to be mainly sourced by the Amazon Craton (Hurtado et al., 2018). The analyzed MD 234 and MD 238 samples are connected by solid lines to the early Cretaceous samples of the Hualhuani and Murco formations of the Arequipa Basin (samples ARE 17 and 339), which were interpreted to be mainly sourced by the Eastern Cordillera (Chavez et al., 2022). Hence, we favor local, mixed Andean (Eastern Cordillera) - Cratonic sources for the samples MD234 and MD238.

The second group is composed of the Cenomanian-Maastrichtian samples of the Acre Basin (AC 49, AC 39A, AC 33C, AC 29, AC 27B, AC 27A, AC 15), the early Maastrichtian sample from the northern part of the Madre de Dios Basin (MD 239, Louterbach et al., 2018), the Maastrichtian sample from the Huallagua Basin (HUA 462, Hurtado et al., 2018) and the Maastrichtian sample from the Santiago Basin (SG 1616, George et al., 2019). The MD 239 and HUA 462 samples are interpreted to have been sourced by the eastern Amazon Craton, most probably the Purus Arch because of the dominance of the Ventuari-Tapajos zircon ages (1.82 - 2-0 Ga) and of the negative ε_{Nd} (0) values (Louterbach et al., 2018; Hurtado et al., 2018). We favor a

similar eastern Amazon Craton provenance interpretation for the Cenomanian-Maastrichtian samples of the Acre Basin because they are dominated by Ventuari - Tapajos (2 – 1.82 Ga) and Rio Negro – Juruena (1.82 – 1.54 Ga) zircon ages, absence of phanerozoic ages (<0.9 Ga), and have very negative ε_{Nd} (0) values.

The third group is represented by the Cenomanian – Maastrichtian samples from the southern part of the Madre de Dios Basin (samples MD 2019 4B; MD 2019 10; MD 2019 11D; MD 2019 12A; MD 2019 13) and the late Maastrichtian sample of the northern part of the Madre de Dios Basin analyzed in Louterbach et al. (2018) (MD 176). The samples from this group exhibit dominant contributions from the Rondonia-San Ignacio (1.82 – 1.54 Ga) and Grenville-Sunsás (0.9 – 1.3 Ga) provinces and a decrease in the contribution from the easternmost Amazon Craton source. Compared with the second group and older samples of the northern part of the Madre de Dios Basin, the data indicate a contribution from more local sources. In addition, the ε_{Nd} (0) values of the fine-grained analyzed samples of the southern part of the Madre de Dios Basin are similar to those of the late Maastrichtian sample of the same basin (MD 176 Louterbach et al., 2018), the Neogene sediments in the South Amazonian Foreland Basin (Roddaz et al., 2005), and of the suspended material of the Madeira River (Viers et al., 2008), thus indicating a similar Andean provenance.

4.7.3 Implications for the paleogeographic evolution of Cretaceous Andes-Amazonian drainage

Our results suggest different sedimentary provenances for the Cenomanian-Maastrichtian samples of the Acre Basin, the late Cretaceous samples of the northern part of the Madre de Dios Basin, and the Cenomanian-Maastrichtian samples of the southern part of the Madre de Dios Basin. We suggest that these distinct source areas reflect different paleodrainage networks. Our provenance results also bring new time

constraints on the Cretaceous continent-wide cratonic paleodrainage of the northern part of South America termed “Sanozama” paleodrainage (Almeida, 1974; Potter, 1997) and on its geographic extension in Western Amazonia. We thus propose the following scenario: 1) during the Albian-Cenomanian, Western Amazonia is fragmented into several sub-basins fed by local sources; 2) during the Cenomanian-Campanian, the provenance of western Amazonian basins located north of the Ucayali Basin (Fig. 33) is dominated by input from Ventuari-Tapajos terranes likely sourced by the incipient uplift of the Purus Arch; the incipient cratonic drainage is estimated to be Cenomanian in age; 3) In the early Maastrichtian, this drainage reached its acme and sourced the northern part of the Madre de Dios Basin but not the southern part that was probably isolated from the northern part by the Madidi Arch (Fig. 43).

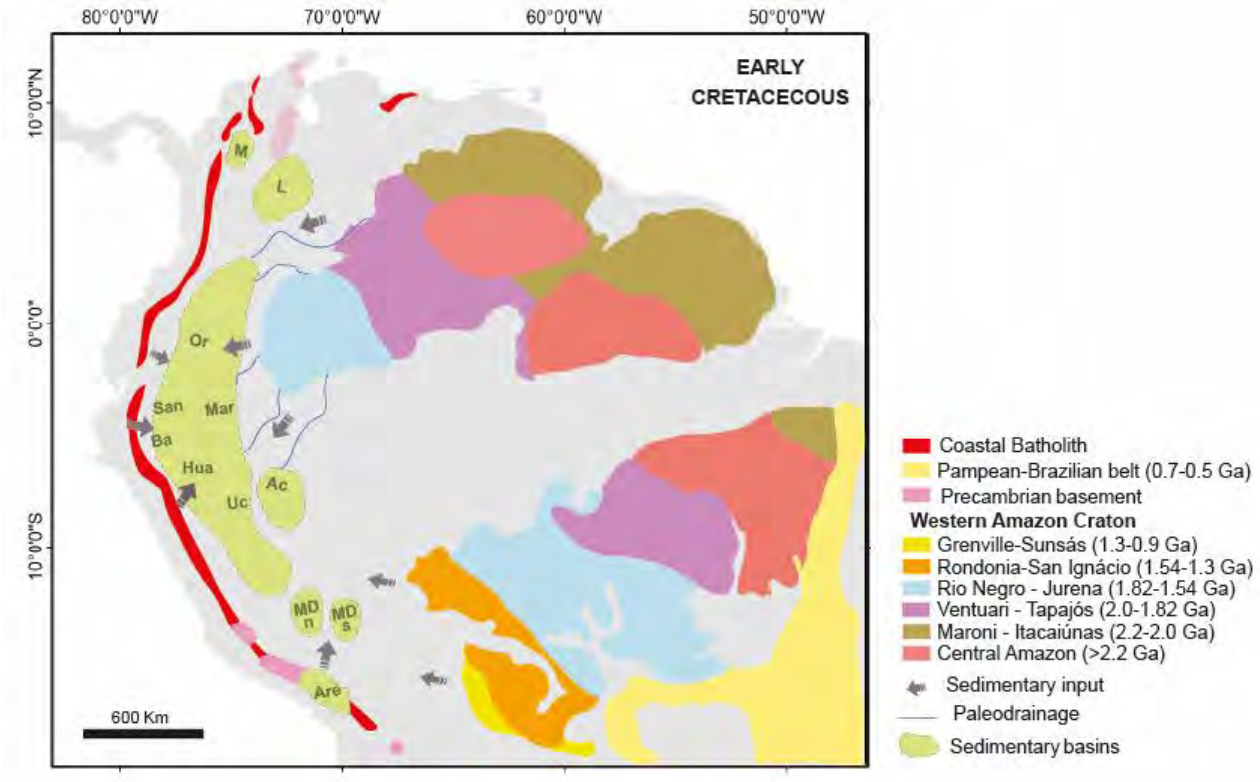

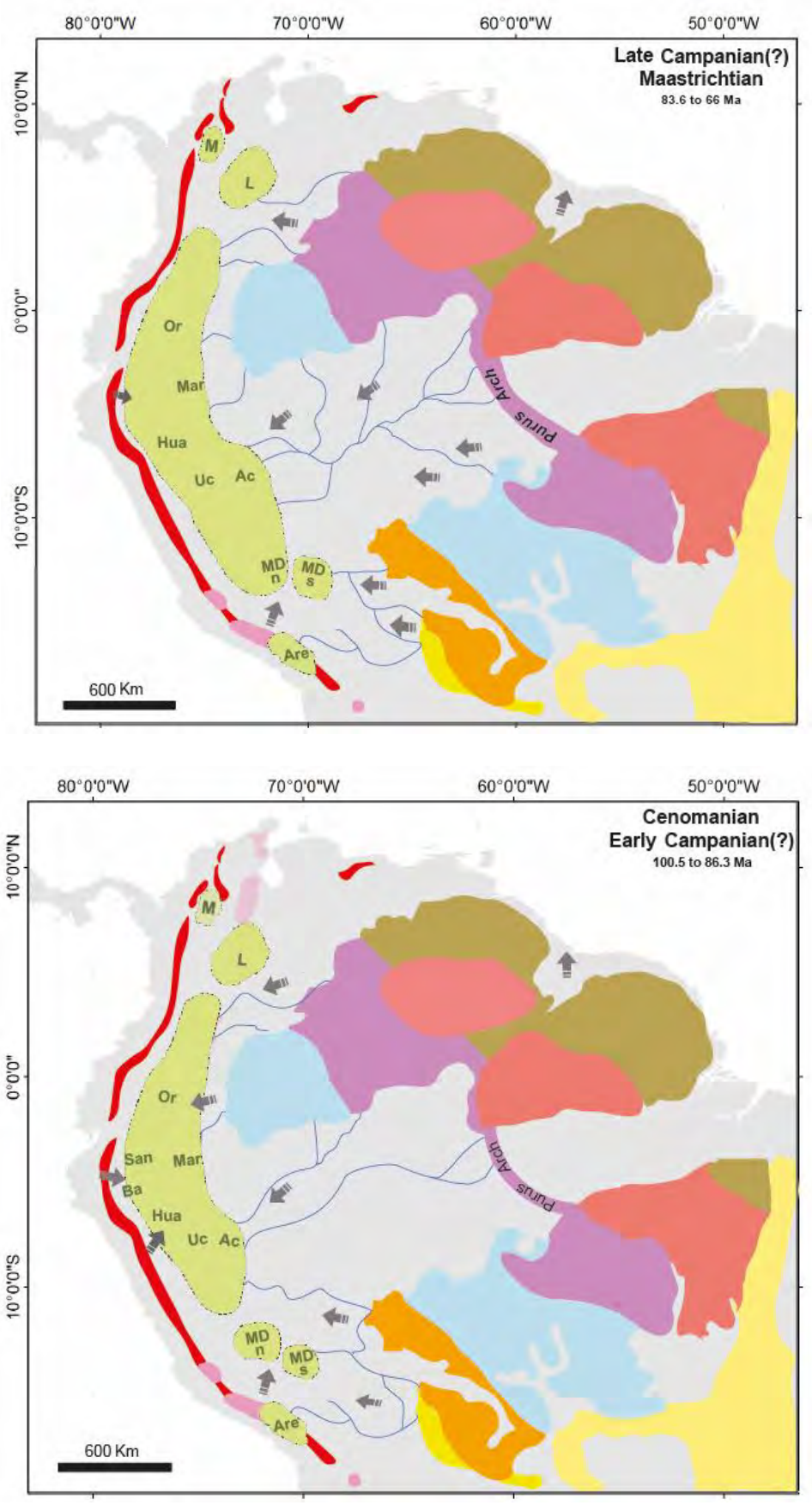

Fig. 43: Schematic paleogeographic maps summarizing the Cenomanian to Maastrichtian paleogeographic evolution of Western Amazonia. See text for details. The paleogeographic maps were

built based on (Hurtado et al., 2018; Roddaz et al., 2010). The position of the Purus Arch is based on Caputo and Soares, (2016) and Hurtado et al. (2018). The position of Coastal Batholith, Precambrian basement, and Geologic terranes is based on (Chew et al., 2008; Chew et al., 2007; Chew et al., 2016; Cordani et al., 2000; Hurtado et al., 2018). The sedimentary input directions are based on Chavez et al. (2022); Erlich et al. (2018); George et al., (2019); Hurtado et al. (2018); Louterbach et al. (2018); Moreno et al. (2020); Roddaz et al. (2021) and U-Pb detrital zircon ages of this study. Are: Arequipa Basin; MDn: North of Madre de Dios Basin; MDs: south of Madre de Dios Basin; Ac: Acre Basin; Uc: Ucayali Basin; Hua: Huallaga Basin; Ba: Bagua Basin; San/ Santiago Basin; Mar: Marañón Basin; Or: Oriente Basin; M: Madaglena Basin and L: Llanos Basin.

Based on our data, it is evident that the source of the late Cretaceous sedimentary rocks in both the northern and southern regions of the Madre de Dios Basin exhibits distinct variations (Fig. 39 and Fig. 40). This difference in provenance may imply the existence of a topographic barrier separating the paleodrainage systems of the northern and southern parts. Middle Permian thrusts were reactivated during the late Cretaceous (Baby et al., 2018; Calderon, 2018). Two cross-basinal arches might act as a topographic barrier during the late Cretaceous: the Manu and Madidi arches (House et al., 1999). The Paleozoic series of both arches have been completely eroded, exposing crystalline basement rocks along their axes during the late Permian to the late Cretaceous period. The Manu Arch is an NW-SE structure that separates the Ucayali Basin from the Madre de Dios Basin (Fig. 33) and hence due to its geographical location, it cannot explain the difference in provenance within the sedimentary rocks of the Madre de Dios Basin. The Madidi Arch is trending westwards from northern Bolivia towards the Sub-Andean Zone (SAZ) in southeastern Peru (House et al., 1999) (Fig. 33). Although its geographical position needs to be better constrained in the SAZ, recent reconstruction suggests that it may separate the analyzed sedimentary rocks of the southern part from those of the northern part (see Fig. 16 in (Baby et al., 2018). Thus, we consider the uplift of Madidi Arch may be the best candidate for a topographic barrier capable of separating the paleodrainage of the northern and southern parts of the Madre de Dios Basin. However, other hypotheses cannot be highlighted, such as SW Amazon Craton uplift (?) or stratigraphic sequence

changes (?). Given that the mechanisms (rift shoulder (?), intracratonic deformation? forebulge uplift?) at the origin of the Cretaceous uplift of the Madidi Arch are unknown, more work is needed to resolve this issue.

Hurtado et al. (2018) based on the dominant Ventuari-Tapajos (1.82 - 2.0 Ga) zircon population of Huallaga Basin samples HUA 266A and HUA 462 and of the early Maastrichtian sample of the northern part of the Madre de Dios Basin (Louterbach et al., 2018) suggest the existence of a long-lived Aptian-Maastrichtian cratonic paleodrainage originated from the Central part of the Amazon craton, likely the Purus Arch with an embouchure in the interior seaway of the Amazonian Basin. For these authors, the beginning of this long-lived paleodrainage is recorded by the presence of the Cretaceous Basal Unconformity which separates the Jurassic and Cretaceous series in the Western Amazonian basins (Hurtado et al., 2018). Our provenance data suggest that the long-lived cratonic paleodrainage started much younger, during the Cenomanian-Turonian times in the Acre Basin. Indeed, in the Acre Basin, our provenance dataset shows that Grenville-Sunsás (0.9 - 1.3 Ga) zircons were a major source of the Cenomanian-Turonian Moa Formation (AC 49) but disappears upward in the section. Based on the palynomorph's age (see Fig. 5.2 in Haag, 2019 and supplementary data: palynological result and Fig. S6) and the zircon grains analyzed in this study (AC 39A, AC 33C, AC 29, AC 27 A and B, AC 15) we argue that the change of the dominant sedimentary input occurred during the deposition of the Rio Azul and Divisor Formations where zircon age distribution is dominated by Rio Negro – Juruena (1.54 – 1.82 Ga) and Ventuari Tapajos (1.82-2.0 Ga) zircons.

The early Cretaceous samples from the Marañón Basin (Forestal 1X; Yanez 1X; Tiruntan 1X; Pagoreni 1003-ST1; Plantayacu 83X; Yarina 2X; Loreto 1X) analyzed by Erlich et al., 2018), the Arequipa Basin (ARE 339 and ARE 17 samples Chavez et al.,

2022), the Eastern Cordillera Basin (145306, George et al. 2019), the Santiago Basin (SG1616, George et al. 2019) and the Huallaga Basin (HUA 462A, Hurtado et al., 2018) show similarly increase in Rio Negro – Juruena (1.54 – 1.82 Ga) and Ventuari Tapajos (1.82-2.0 Ga) zircons after the Campanian. In the northern part of the Madre de Dios Basin, the dominant input of Ventuari-Tapajos zircons (1.82 – 2.0 Ga) is only recorded in the early Maastrichtian MD239 sample analyzed in Louterbach et al. (2018) and not in older sedimentary rocks analyzed in this study (i.e. MD234 and MD238) suggesting that the continent-wide paleodrainage extended to the northern part of the Madre de Dios Basin only during the early Maastrichtian. The difference in provenance between samples from the northern and southern parts of the Madre de Dios Basin and the absence of dominant Ventuari – Tapajos (1.82 – 2.0Ga) zircon population in the samples from the southern part of the Madre de Dios Basin indicate that the extension of the cratonic paleodrainage never reached the southern part of the Madre de Dios Basin. These also suggest that the Sanozama drainage reached its acme (widest paleogeographical extension) in the early Maastrichtian.

The existence of the continent-wide paleodrainage was controlled by the uplift history of the Central part of the Amazon Craton and the Purus Arch. However, the mechanism(s) at the origin of the Cenomanian-Maastrichtian uplift of the Central part of the Amazon Craton and the Purus Arch remains unclear. The Purus Arch is an elevated area, located 240 km west of Manaus and parallel to NW-SE strike-slip faults (Costa et al., 2001) that separate the Amazonas and Solimões Basins. It consists of a regional structure that originated from distension during the Mesoproterozoic Era (Caputo and Soares, 2016 and references therein). The Purus Arch was likely exposed from the Neoproterozoic until the Early of the Pennsylvanian and probably experienced uplift and erosion during the Cretaceous because Cretaceous sedimentary rocks are

absent in the region of the Purus Arch (Caputo and Soares, 2016). This may suggest that the Purus Arch was an important paleogeographic barrier during the late Cretaceous.

Different investigations have recorded an elevation of the eastern sectors of the Central Brazilian and Guyana shields during the late Cretaceous (Caputo & Soares, 2016; Harman et al., 1998; Hurtado et al., 2018; Potter, 1997; Roddaz et al., 2021; Vallejo et al., 2017).The estimation of denudations rates using apatite fission track analysis during the late Cretaceous in the Central Brazilian Shield led to the interpretation that an important phase of tectonic reactivation occurred in the region between the early Campanian and late Maastrichtian (~80 to 60 Ma) (Harman et al., 1998). The elevation and erosion of the Central Brazilian shield were facilitated by the emergence of the Brazilian Carajás region in the northeastern Amazon region around 80 Ma (Monteiro et al., 2018). Furthermore, a similar mechanism was proposed for the central part of the Guiana Shield during the Campanian (Sapin et al., 2016). The uplifted surface likely influenced the paleodrainage evolution of this region after the Coniacian (~86 Ma) (Roddaz et al., 2021). Drainage reorganizations during the late Cretaceous are also identified in the cost line of NW Africa, characterized by an increased influx of Precambrian sediments during the Campanian – Maastrichtian, related to the opening of the South and Equatorial Atlantic Ocean (Mourlot et al., 2018). Similar geodynamic system may be occurred in the northeastern and northwestern South America and West African cratons during the opening of the Aquatorial Ocean, leading to surface uplift. This elevation of the Atlantic margins in the late Cretaceous can be explained by intracontinental deformation resulting from significant changes in plate motions between Africa, Antartica, and South America (see Harman et al., 1998 and references therein), as well as mantle upwelling beneath the margin (Matton and

Jébrak, 2009). These processes may have contributed to the late Cretaceous uplift of the Purus Arch and the Central part of the Amazon Craton, potentially influencing the paleodrainage evolution of Western Amazonia during the Cenomanian-Maastrichtian.

4.8 Conclusions

The analysis based on a multi-proxy dataset, including major and trace elements concentrations, Sm-Nd isotopic composition, and detrital zircon U-Pb ages, used to identify the sources of Cretaceous sedimentary rocks from the Acre and Madre de Dios basins (Brazil and Peru) results in the following conclusions:

- The Cretaceous sedimentary rocks of the northern part of the Madre de Dios Basin have different provenances. The oldest late Cretaceous sedimentary rocks (MD234 and MD238) are sourced by mixed Andean (Eastern Cordillera)-Cratonic sources whereas the early Maastrichtian sedimentary rock (MD239) analyzed in Louterbach et al. (2018) was sourced by the Central Brazilian Shield;
- The Cenomanian – Maastrichtian samples from the southern part of the Madre de Dios Basin have similar Andean provenance as the late Maastrichtian sample (MD176) of the northern part of the Madre de Dios Basin analyzed in Louterbach et al. (2018). They did not share the same provenance as those of the northern part suggesting that a topographic barrier (the Madidi Arch (?)) might have separated the northern part from the southern part during the late Cretaceous;
- The Cenomanian-Maastrichtian sedimentary rocks of the Acre Basin have εNd (0) values consistent with a Cratonic source with silicic contribution and U-Pb zircon age distribution dominated by Amazon Craton zircon grains (Ventuari-Tapajos (2.0-1.8 Ga) and Rio Negro-Juruena (1.8-1.54 Ga)) sourced by the continent-wide drainage system. These data suggest that the cratonic drainage system was initiated younger

than previously thought, probably in response to the uplift of the Purus Arch ascribed to geodynamic process (intracontinental deformation or mantle upwelling) during the opening of the Atlantic Equatorial Ocean.

Our provenance data also suggest that the continent-wide cratonic drainage reached its maximum paleogeographic extension during the early Maastrichtian and was the main source of sediments for the Ecuadorian, Peruvian, and Brazilian western Amazonia Basins. Contrary to the Cenozoic period, the influence of the Andes on Western Amazonia paleogeography was minor during the Cenomanian-early Maastrichtian.

Acknowledgments

We are thankful to the University of Brasilia and University Toulouse III Paul Sabatier for the infrastructure and technical support. We also thank for the financial support of the Brazilian National Council for Scientific and Technological Development (CNP-428843/2916-6; 312941/2018-8), the Coordination for the Improvement of Higher Education Personnel – Brazil (CAPES) and, the French Evaluation Committee of the University and Scientific Cooperation with Brazil (COFECUB) for funding the first author during the PhD degree. This work received financial and institutional support by the IRD (Institut pour la Recherche et le Développement). This study was also supported and funded by CAPES-COFECUB program Te 924/18 “Paléo-Amazone: évolution Néogène de l’Amazonie Brésilienne.” We thank an anonymous reviewer and Brian Horton as well as the editor Massimo Moretti for valuable reviews that improved this contribution.

References

Albarède, F., & Brouxel, M. (1987). The Sm/Nd secular evolution of the continental crust and the depleted mantle. *Earth and Planetary Science Letters*, *82*(1–2), 25–35. https://doi.org/10.1016/0012-821X(87)90104-X

Albert, J. S., Val, P., & Hoorn, C. (2018). The changing course of the Amazon River in the Neogene: center stage for Neotropical diversification. *Neotropical Ichthyology*, *16*(3). https://doi.org/10.1590/1982-0224-20180033

Almeida, L. F. G. de. (1974). A drenagem festonada e seu significado fotogeologico. *Anais do XXVIII Congresso Brasileiro de Geologia*, *7*, 175–199.

Augustsson, C., & Bahlburg, H. (2008). Provenance of late Palaeozoic metasediments of the Patagonian proto-Pacific margin (southernmost Chile and Argentina). *International Journal of Earth Sciences*, *97*(1), 71–88. https://doi.org/10.1007/s00531-006-0158-7

Babinot, J.-F., Colin, J.-P., & Randrianasolo, A. (2009). Les ostracodes de l'Albien-Turonien moyen de la région d'Antsiranana (Nord Madagascar) : systématique, paléoécologie et paléobiogéographie. *Carnets de Géologie*, 25.

Baby, P., Rivadeneira, M., Barragán, R., & Christophoul, F. (2013). Thick-skinned tectonics in the Oriente foreland basin of Ecuador. *Geological Society, London, Special Publications*, *377*(1), 59–76. https://doi.org/10.1144/SP377.1

Baby, P., Rivadeneira, M., Christophoul, F., & Barragan, R. (1999). Style and timing of deformation in the Oriente Basin of Ecuador, 6.

Baby, P., Espurt, N., Brusset, S., Hermoza, W., Antoine, P. O., Roddaz, M., et al. (2005). Influence of the Nazca ridge subduction on the amazonian foreland basin deformation : preliminary analyses, 4.

Baby, P. Calderon, Y., Brusset, S., Roddaz, M., Eude, A., Calves, G., et al. (2018). The Peruvian Sub-Andean Foreland Basin System: Structural Overview, Geochronologic Constraints, and Unexplored Plays. In G. Zamora, K. R. McClay, & V. A. Ramos, *Petroleum Basins and Hydrocarbon Potential of the Andes of Peru and Bolivia* (pp. 91–120). The American Association of Petroleum Geologists. https://doi.org/10.1306/13622118M1173767

Bahlburg, H., Vervoort, J. D., Du Frane, S. A., Bock, B., Augustsson, C., & Reimann, C. (2009). Timing of crust formation and recycling in accretionary orogens: Insights learned from the western margin of South America. *Earth-Science Reviews*, *97*(1–4), 215–241. https://doi.org/10.1016/j.earscirev.2009.10.006

Basu, A. R., Sharma, M., & DeCelles, P. G. (1990). Nd, Sr-isotopic provenance and trace element geochemistry of Amazonian foreland basin fluvial sands, Bolivia and Peru: implications for ensialic Andean orogeny. *Earth and Planetary Science Letters*, *100*(1–3), 1–17. https://doi.org/10.1016/0012-821X(90)90172-T

Brito Neves, B. (2002). Main Stages of the Development of the Sedimentary Basins of South America and their Relationship with the Tectonics of Supercontinents. *Gondwana Research*, *5*(1), 175–196. https://doi.org/10.1016/S1342-937X(05)70901-1

Bock, B., Mclennan, & Hanson. (1998). Geochemistry and provenance of the Middle Ordovician Austin Glen Member (Normanskill Formation) and the Taconian

Orogeny in New England. *Sedimentology*, *45*(4), 635–655. https://doi.org/10.1046/j.1365-3091.1998.00168.x

Bouchez, J., Gaillardet, J., France-Lanord, C., Maurice, L., & Dutra-Maia, P. (2011). Grain size control of river suspended sediment geochemistry: Clues from Amazon River depth profiles: RIVER SEDIMENTS GRAIN SIZE AND CHEMISTRY. *Geochemistry, Geophysics, Geosystems*, *12*(3), n/a-n/a. https://doi.org/10.1029/2010GC003380

Brito, P. M., Negri, F. R., & Bocquentin, J. (1994). Fish Remains From the Upper Cretaceous of the Acre Basin, North Brazil. *Boletim Do 3° Simposio Sobre o Cretaceo Do Brasil*, 113–114.

Bühn, B., Pimentel, M. M., Matteini, M., & Dantas, E. L. (2009). High spatial resolution analysis of Pb and U isotopes for geochronology by laser ablation multi-collector inductively coupled plasma mass spectrometry (LA-MC-ICP-MS). *Anais Da Academia Brasileira de Ciências*, *81*(1), 99–114. https://doi.org/10.1590/S0001-37652009000100011

Calderon, Y. (2018). *Structural arquitecture, sedimentary balance and hydrocarbon potential of a "'wedgetop-foredeep'" transition zone of retro-foreland basin: example of the Marañon and Huallaga basins of northern Peru* (Thèse Doctorat). Université de Toulouse III Paul Sabatier, Toulouse.

Calderon, Y., Baby, P., Hurtado, C., & Brusset, S. (2017). Thrust tectonics in the Andean retro-foreland basin of northern Peru: Permian inheritances and petroleum implications. *Marine and Petroleum Geology*, *82*, 238–250.

Callède, J., Guyot, J. L., Ronchail, J., L'Hôte, Y., Niel, H., & de Oliveira, E. (2004). Evolution du débit de l'Amazone à Óbidos de 1903 à 1999 / Evolution of the River Amazon's discharge at Óbidos from 1903 to 1999. *Hydrological Sciences Journal*, *49*(1), 85–97. https://doi.org/10.1623/hysj.49.1.85.53992

Caputo, M. V. (2014). Juruá Orogeny: Brazil and Andean Countries. *Brazilian Journal of Geology*, *44*(2), 181–190. https://doi.org/10.5327/Z2317-4889201400020001

Caputo, M. V., & Soares, E. A. A. (2016). Eustatic and tectonic change effects in the reversion of the transcontinental Amazon River drainage system. *Brazilian Journal of Geology*, *46*(2), 301–328. https://doi.org/10.1590/2317-4889201620160066

Carignan, J., Hild, P., Mevelle, G., Morel, J., & Yeghicheyan, D. (2001). Routine Analyses of Trace Elements in Geological Samples using Flow Injection and Low Pressure On-Line Liquid Chromatography Coupled to ICP-MS: A Study of Geochemical Reference Materials BR, DR-N, UB-N, AN-G and GH. *Geostandards and Geoanalytical Research*, *25*(2–3), 187–198. https://doi.org/10.1111/j.1751-908X.2001.tb00595.x

Chacaltana, C., Valdivia, W., Robert, E., & Aldana, M. (2005). La Formacion Chonta en el Pongo de Manseriche: nuevos registros, organizacion biozonal y puesta en evidencia del Albiano Inferior. *Boletim Sociedad Geologica del Peru*, *100*, 37–48.

Chavez, C., Roddaz, M., Dantas, E. L., Santos, R. V., & Alván, A. A. (2022). Provenance of the Middle Jurassic-Cretaceous sedimentary rocks of the Arequipa Basin (South Peru) and implications for the geodynamic evolution of the Central Andes. *Gondwana Research*, *101*, 59–76. https://doi.org/10.1016/j.gr.2021.07.018

Chew, D., Magna, T., Kirkland, C., Miskovic, A., Cardona, A., Spikings, R., & Schaltegger, U. (2008). Detrital zircon fingerprint of the Proto-Andes: Evidence for a Neoproterozoic active margin? *Precambrian Research*, *167*(1–2), 186–200. https://doi.org/10.1016/j.precamres.2008.08.002

Chew, D. M., Schaltegger, U., Kosler, J., Whitehouse, M. J., Gutjahr, M., Spikings, R. A., & Miskovic, A. (2007b). U-Pb geochronologic evidence for the evolution of the Gondwanan margin of the north-central Andes. *Geological Society of America Bulletin*, *119*(5–6), 697–711. https://doi.org/10.1130/B26080.1

Chew, David M., Pedemonte, G., & Corbett, E. (2016). Proto-Andean evolution of the Eastern Cordillera of Peru. *Gondwana Research*, *35*, 59–78. https://doi.org/10.1016/j.gr.2016.03.016

Christophoul, F., Baby, P., & Dávila, C. (2002). Stratigraphic responses to a major tectonic event in a foreland basin: the Ecuadorian Oriente Basin from Eocene to Oligocene times. *Tectonophysics*, *345*(1–4), 281–298. https://doi.org/10.1016/S0040-1951(01)00217-7

Condie, K. C. (1993). Chemical composition and evolution of the upper continental crust: Contrasting results from surface samples and shales. *Chemical Geology*, *104*(1–4), 1–37. https://doi.org/10.1016/0009-2541(93)90140-E

Cordani, U. G., & Sato, K. (1999). Crustal evolution of the South American Platform, based on Nd isotopic systematics on granitoid rocks. *Episodes*, *22*(3).

Cordani, U. G., & Teixeira, W. (2007). Proterozoic accretionary belts in the Amazonian Craton. In *Geological Society of America Memoirs* (Vol. 200, pp. 297–320). Geological Society of America. https://doi.org/10.1130/2007.1200(14)

Cordani, U. G., Milani, E. J., Thomas Filho, A., & Campos, D. de A. (2000). *Tectonic evolution of South America* (31th International Geological Congress). Rio de Janeiro.

Costa, J. B. S., Léa Bemerguy, R., Hasui, Y., & da Silva Borges, M. (2001). Tectonics and paleogeography along the Amazon river. *Journal of South American Earth Sciences*, *14*(4), 335–347. https://doi.org/10.1016/S0895-9811(01)00025-6

Cullers, R. L. (2000). The geochemistry of shales, siltstones and sandstones of Pennsylvanian–Permian age, Colorado, USA: implications for provenance and metamorphic studies. *Lithos*, *51*(3), 181–203. https://doi.org/10.1016/S0024-4937(99)00063-8

Cunha, P. R. da C. (2007). Bacia do Acre. *Boletim de Geociências Petrobras*, *15*(2), 207–215.

De Baar, H. J. W., Bacon, M. P., Brewer, P. G., & Bruland, K. W. (1985). Rare earth elements in the Pacific and Atlantic Oceans. *Geochimica et Cosmochimica Acta*, *49*(9), 1943–1959. https://doi.org/10.1016/0016-7037(85)90089-4

DeCelles, P. G., Carrapa, B., Horton, B. K., & Gehrels, G. E. (2011). Cenozoic foreland basin system in the central Andes of northwestern Argentina: Implications for Andean geodynamics and modes of deformation: ANDEAN FORELAND BASIN. *Tectonics*, *30*(6), n/a-n/a. https://doi.org/10.1029/2011TC002948

DePaolo, D. J., Linn, A. M., & Schubert, G. (1991). The continental crustal age distribution: Methods of determining mantle separation ages from Sm-Nd isotopic data and application to the southwestern United States. *Journal of Geophysical Research*, *96*(B2), 2071. https://doi.org/10.1029/90JB02219

DePaolo, Donald J. (1981). Trace element and isotopic effects of combined wallrock assimilation and fractional crystallization. *Earth and Planetary Science Letters*, *53*(2), 189–202. https://doi.org/10.1016/0012-821X(81)90153-9

Eakin, C. M., Lithgow-Bertelloni, C., & Dávila, F. M. (2014). Influence of Peruvian flat-subduction dynamics on the evolution of western Amazonia. *Earth and Planetary Science Letters*, *404*, 250–260. https://doi.org/10.1016/j.epsl.2014.07.027

Erlich, R. N., Fallon, J., & O'Sullivan, P. (2018). Stratigraphy and LA-ICP-MS Zircon U-PB Provenance of middle Permian to Maastrichtian Sandstones from Outcrop and Subsurface Control in the Sub-Andean Basins of Peru. In *Petroleum Basins and Hydrocarbon Potential of the Andes of Peru and Bolivia* (pp. 179–226). The American Association of Petroleum Geologists. https://doi.org/10.1306/13622121M1173769

Espurt, N., Baby, P., Brusset, S., Roddaz, M., Hermoza, W., Regard, V., et al. (2007). How does the Nazca Ridge subduction influence the modern Amazonian foreland basin? *Geology*, *35*(6), 515. https://doi.org/10.1130/G23237A.1

Espurt, Nicolas, Baby, P., Brusset, S., Roddaz, M., Hermoza, W., & Barbarand, J. (2010). The Nazca Ridge and Uplift of the Fitzcarrald Arch: Implications for Regional Geology in Northern South America. In C. Hoorn & F. P. Wesselingh (Eds.), *Amazonia: Landscape and Species Evolution* (pp. 89–100). Oxford, UK: Wiley-Blackwell Publishing Ltd. https://doi.org/10.1002/9781444306408.ch6

Fedo, C. M., Wayne Nesbitt, H., & Young, G. M. (1995). Unraveling the effects of potassium metasomatism in sedimentary rocks and paleosols, with implications for paleoweathering conditions and provenance. *Geology*, *23*(10), 921. https://doi.org/10.1130/0091-7613(1995)023<0921:UTEOPM>2.3.CO;2

Figueiredo, J., Hoorn, C., van der Ven, P., & Soares, E. (2009). Late Miocene onset of the Amazon River and the Amazon deep-sea fan: Evidence from the Foz do Amazonas Basin. *Geology*, *37*(7), 619–622. https://doi.org/10.1130/G25567A.1

Filizola, N., & Guyot, J. L. (2004). The use of Doppler technology for suspended sediment discharge determination in the River Amazon / L'utilisation des techniques Doppler pour la détermination du transport solide de l'Amazone. *Hydrological Sciences Journal*, *49*(1), 143–153. https://doi.org/10.1623/hysj.49.1.143.53990

Gaillardet, J., Viers, J., & Dupré, B. (2003). Trace Elements in River Waters. *Treatise on Geochemistry*, *5*, 225–272. https://doi.org/10.1016/B0-08-043751-6/05165-3

George, S. W. M., Horton, B. K., Jackson, L. J., Moreno, F., Carlotto, V., & Garzione, C. N. (2019). Sediment provenance variations during contrasting Mesozoic-early Cenozoic tectonic regimes of the northern Peruvian Andes and Santiago-Marañón foreland basin. In *Andean Tectonics* (pp. 269–296). Elsevier. https://doi.org/10.1016/B978-0-12-816009-1.00012-5

Goia, S. M. C. L., & Pimentel, M. M. (2000). The Sm-Nd isotopic method in the geochronology laboratory of the University of Brasília. *Anais Da Academia Brasileira de Ciências*, *72*(2), 219–245. https://doi.org/10.1590/S0001-37652000000200009

Goldstein, S. L., O'Nions, R. K., & Hamilton, P. J. (1984). A Sm-Nd isotopic study of atmospheric dusts and particulates from major river systems. *Earth and Planetary Science Letters*, *70*(2), 221–236. https://doi.org/10.1016/0012-821X(84)90007-4

Gorini, C., Haq, B. U., dos Reis, A. T., Silva, C. G., Cruz, A., Soares, E., & Grangeon, D. (2014). Late Neogene sequence stratigraphic evolution of the Foz do Amazonas Basin, Brazil. *Terra Nova*, *26*(179–185). https://doi.org/10.1111/ter.12083

Gutiérrez, E. G., Horton, B. K., Vallejo, C., Jackson, L. J., & George, S. W. M. (2019). Provenance and geochronological insights into Late Cretaceous-Cenozoic foreland basin development in the Subandean Zone and Oriente Basin of Ecuador. In *Andean Tectonics* (pp. 237–268). Elsevier. https://doi.org/10.1016/B978-0-12-816009-1.00011-3

Haag, N. A. (2019). *Palinostratigrafia do Meso-Cenozoico da Bacia do Acre (Amazônia Sul Ocidental, Brasil)* (Tese de doutoramento). Universidade de Coimbra, Coimbra.

Harman, R., Gallagher, K., Brown, R., Raza, A., & Bizzi, L. (1998). Accelerated denudation and tectonic/geomorphic reactivation of the cratons of northeastern Brazil during the Late Cretaceous. *Journal of Geophysical Research: Solid Earth*, *103*(B11), 27091–27105. https://doi.org/10.1029/98JB02524

Hermoza, W., Baby, P., Espurt, N., Martinez, E., & Bolaños, R. (2006). The Ucayali Subandean Basin: A Complex Fold And Thrust Belt And Inverted System. In *9th Simposio Bolivariano - Exploracion Petrolera en las Cuencas Subandinas*. Cartagena, Colombia,: European Association of Geoscientists & Engineers. https://doi.org/10.3997/2214-4609-pdb.111.08

Hoorn, C., Wesselingh, F. P., ter Steege, H., Bermudez, M. A., Mora, A., Sevink, J., et al. (2010). Amazonia Through Time: Andean Uplift, Climate Change, Landscape Evolution, and Biodiversity. *Science*, *330*(6006), 927–931. https://doi.org/10.1126/science.1194585

Hoorn, Carina, Bogotá-A, G. R., Romero-Baez, M., Lammertsma, E. I., Flantua, S. G. A., Dantas, E. L., et al. (2017). The Amazon at sea: Onset and stages of the Amazon River from a marine record, with special reference to Neogene plant turnover in the drainage basin. *Global and Planetary Change*, *153*, 51–65. https://doi.org/10.1016/j.gloplacha.2017.02.005

Horbe, A. M. C., Motta, M. B., de Almeida, C. M., Dantas, E. L., & Vieira, L. C. (2013). Provenance of Pliocene and recent sedimentary deposits in western Amazônia, Brazil: Consequences for the paleodrainage of the Solimões-Amazonas River. *Sedimentary Geology*, *296*, 9–20. https://doi.org/10.1016/j.sedgeo.2013.07.007

Horton, B. K. (2018). Sedimentary record of Andean mountain building. *Earth-Science Reviews*, *178*, 279–309. https://doi.org/10.1016/j.earscirev.2017.11.025

Horton, B. K., Anderson, V. J., Caballero, V., Saylor, J. E., Nie, J., Parra, M., & Mora, A. (2015). Application of detrital zircon U-Pb geochronology to surface and subsurface correlations of provenance, paleodrainage, and tectonics of the Middle Magdalena Valley Basin of Colombia. *Geosphere*, *11*(6), 1790–1811. https://doi.org/10.1130/GES01251.1

Horton, B. K., Fuentes, F., Boll, A., Starck, D., Ramirez, S. G., & Stockli, D. F. (2016). Andean stratigraphic record of the transition from backarc extension to orogenic shortening: A case study from the northern Neuquén Basin, Argentina. *Journal of South American Earth Sciences*, *71*, 17–40. https://doi.org/10.1016/j.jsames.2016.06.003

House, N. J., Carpenter, D. G., Cunningham, P. S., & Berumen, M. (1999). Influence of Paleozoic Arches on Structural Style and Stratigraphy in the Madre de Dios Basin in Southern Peru and Northern Bolivia. In *SEG Technical Program Expanded Abstracts 2000* (pp. 672–676). Society of Exploration Geophysicists. https://doi.org/10.1190/1.1816156

Huck, C. E., van de Flierdt, T., Jiménez-Espejo, F. J., Bohaty, S. M., Röhl, U., & Hammond, S. J. (2016). Robustness of fossil fish teeth for seawater neodymium isotope reconstructions under variable redox conditions in an ancient shallow marine setting: ROBUSTNESS OF FOSSIL FISH TOOTH ND. *Geochemistry, Geophysics, Geosystems*, *17*(3), 679–698. https://doi.org/10.1002/2015GC006218

Hurtado, C., Roddaz, M., Santos, R. V., Baby, P., Antoine, P.-O., & Dantas, E. L. (2018). Cretaceous-early Paleocene drainage shift of Amazonian rivers driven by Equatorial Atlantic Ocean opening and Andean uplift as deduced from the provenance of northern Peruvian sedimentary rocks (Huallaga basin). *Gondwana Research*, *63*, 152–168. https://doi.org/10.1016/j.gr.2018.05.012

Jackson, S. E., Pearson, N. J., Griffin, W. L., & Belousova, E. A. (2004). The application of laser ablation-inductively coupled plasma-mass spectrometry to in situ U–Pb zircon geochronology. *Chemical Geology*, *211*(1–2), 47–69. https://doi.org/10.1016/j.chemgeo.2004.06.017

Jacobsen, S. B., & Wasserburg, G. J. (1980). Sm-Nd isotopic evolution of chondrites. *Earth and Planetary Science Letters*, *50*(1), 139–155. https://doi.org/10.1016/0012-821X(80)90125-9

Konieczna, N., Belka, Z., & Dopieralska, J. (2015). Nd and Sr isotopic evidence for provenance of clastic material of the Upper Triassic rocks of Silesia, Poland. *Annales Societatis Geologorum Poloniae*. https://doi.org/10.14241/asgp.2014.008

Loeblich, A. R., & Tappan, H. N. (1988). *Foraminiferal Genera and Their Classification (Volume I and II)* (Van Nostrand Reinhold Company). New York.

Lopez-Gamundi, O., & Lopez-Gamundi, C. (2018). Exhumation of a Proximal Foredeep and Associated Wedge-Top Basin Evidenced by Porosity versus Depth Trends: The Upper Cretaceous Vivian Sandstones in Northwestern Marañón and Santiago Basins (Peru). In G. Zamora, K. R. McClay, & V. A. Ramos, *Petroleum Basins and Hydrocarbon Potential of the Andes of Peru and Bolivia* (pp. 251–270). The American Association of Petroleum Geologists. https://doi.org/10.1306/13622123M1173531

Louterbach, M. (2014). *Propagation du front orogénique Subandine et réponse sédimentaire a associée dans le bassin d'avant-pays Amazonien (Madre de Dios, Pérou)* (Thèse Doctorat). Université de Toulouse, Toulouse.

Louterbach, M., Roddaz, M., Bailleul, J., Antoine, P.-O., Adnet, S., Kim, J. H., et al. (2014). Evidences for a Paleocene marine incursion in southern Amazonia (Madre de Dios Sub-Andean Zone, Peru). *Palaeogeography, Palaeoclimatology, Palaeoecology*, *414*, 451–471. https://doi.org/10.1016/j.palaeo.2014.09.027

Louterbach, M., Roddaz, M., Antoine, P.-O., Marivaux, L., Adnet, S., Bailleul, J., et al. (2018). Provenance record of late Maastrichtian-late Palaeocene Andean Mountain building in the Amazonian retroarc foreland basin (Madre de Dios basin, Peru). *Terra Nova*, *30*(1), 17–23. https://doi.org/10.1111/ter.12303

MacRae, N. D., Nesbitt, H. W., & Kronberg, B. I. (1992). Development of a positive Eu anomaly during diagenesis. *Earth and Planetary Science Letters*, *109*(3–4), 585–591. https://doi.org/10.1016/0012-821X(92)90116-D

Mahoney, J. B. (2005). Nd and Sr isotopic signatures of fine-grained clastic sediments: A case study of western Pacific marginal basins. *Sedimentary Geology*, *182*(1–4), 183–199. https://doi.org/10.1016/j.sedgeo.2005.07.009

Martinez, E., Fernandez, J., Calderon, Y., & Galdos, C. (1999). *Ucayali/Ene Basin, Peru, Hydrocarbon Evaluation* (p. 10). Lima: Petroperu/PARSEP.

Martin-Gombojav, N., & Winkler, W. (2008). Recycling of Proterozoic crust in the Andean Amazon foreland of Ecuador: implications for orogenic development of the Northern Andes: Multiple recycling of Proterozoic crust in the Northern Andes. *Terra Nova*, *20*(1), 22–31. https://doi.org/10.1111/j.1365-3121.2007.00782.x

McLennan, S. M., Taylor, S. R., McCulloch, M. T., & Maynard, J. B. (1990). Geochemical and Nd ‐ Sr isotopic composition of deep-sea turbidites: Crustal evolution and plate tectonic associations. *Geochimica et Cosmochimica Acta*, *54*(7), 2015–2050. https://doi.org/10.1016/0016-7037(90)90269-Q

McLennan, S. M., Hemming, S., McDaniel, D. K., & Hanson, G. N. (1993). Geochemical approaches to sedimentation, provenance and tectonics. In *Processes Controlling the Composition of Clastic Sediments*. Colorado.

Milliman, J. D., & Syvitski, J. P. M. (1992). Geomorphic/Tectonic Control of Sediment Discharge to the Ocean: The Importance of Small Mountainous Rivers, 20.

Miškovic, A., Spikings, R. A., Chew, D. M., Kosler, J., Ulianov, A., & Schaltegger, U. (2009). Tectonomagmatic evolution of Western Amazonia: Geochemical characterization and zircon U-Pb geochronologic constraints from the Peruvian Eastern Cordilleran granitoidsU-Pb geochronology and geochemistry of the proto-Andean granitoids of Peru. *GSA Bull*, *121*, 1298–1324. https://doi.org/10.1130/B26488.1

Moiroud, M., Pucéat, E., Donnadieu, Y., Bayon, G., Guiraud, M., Voigt, S., et al. (2016). Evolution of neodymium isotopic signature of seawater during the Late Cretaceous: Implications for intermediate and deep circulation. *Gondwana Research*, *36*, 503–522. https://doi.org/10.1016/j.gr.2015.08.005

Monteiro, H. S., Vasconcelos, P. M. P., Farley, K. A., & Lopes, C. A. M. (2018). Age and evolution of diachronous erosion surfaces in the Amazon: Combining (U-Th)/He and cosmogenic 3He records. *Geochimica et Cosmochimica Acta*, *229*, 162–183. https://doi.org/10.1016/j.gca.2018.02.045

Moreno, F., Garzione, C. N., George, S. W. M., Horton, B. K., Williams, L., Jackson, L. J., et al. (2020). Coupled Andean Growth and Foreland Basin Evolution, Campanian–Cenozoic Bagua Basin, Northern Peru. *Tectonics*, *39*(7). https://doi.org/10.1029/2019TC005967

Mourlot, Y., Roddaz, M., Dera, G., Calvès, G., Kim, J., Chaboureau, A., et al. (2018). Geochemical Evidence for Large-Scale Drainage Reorganization in Northwest Africa During the Cretaceous. *Geochemistry, Geophysics, Geosystems*, *19*(5), 1690–1712. https://doi.org/10.1029/2018GC007448

Naipauer, M., Tapia, F., Mescua, J., Farías, M., Pimentel, M. M., & Ramos, V. A. (2015). Detrital and volcanic zircon U–Pb ages from southern Mendoza (Argentina): An insight on the source regions in the northern part of the Neuquén Basin. *Journal of South American Earth Sciences*, *64*, 434–451. https://doi.org/10.1016/j.jsames.2015.09.013

Nesbitt, H. W., & Young, G. M. (1982). Early Proterozoic climates and plate motions inferred from major element chemistry of lutites. *Nature*, *299*.

Nie, J., Horton, B. K., Saylor, J. E., Mora, A., Mange, M., Garzione, C. N., et al. (2012). Integrated provenance analysis of a convergent retroarc foreland system: U–Pb ages, heavy minerals, Nd isotopes, and sandstone compositions of the Middle Magdalena Valley basin, northern Andes, Colombia. *Earth-Science Reviews*, *110*(1–4), 111–126. https://doi.org/10.1016/j.earscirev.2011.11.002

Oliveira, C. M. M. (1994). *Estilos Estruturais e Evolução Tectônica da Bacia do Acre* (Dissertação de mestrado). Universidade Federal de Ouro Preto, Ouro Preto.

Oliveros, V., Labbé, M., Rossel, P., Charrier, R., & Encinas, A. (2012). Late Jurassic paleogeographic evolution of the Andean back-arc basin: New constrains from the Lagunillas Formation, northern Chile (27°30'–28°30'S). *Journal of South American Earth Sciences*, *37*, 25–40. https://doi.org/10.1016/j.jsames.2011.12.005

Paton, C., Hellstrom, J., Paul, B., Woodhead, J., & Hergt, J. (2011). Iolite: Freeware for the visualisation and processing of mass spectrometric data. *Journal of Analytical Atomic Spectrometry*, *26*(12), 2508. https://doi.org/10.1039/c1ja10172b

Perez, N. D., Horton, B. K., McQuarrie, N., Stübner, K., & Ehlers, T. A. (2016). Andean shortening, inversion and exhumation associated with thin- and thick-skinned deformation in southern Peru. *Geological Magazine*, *153*(5–6), 1013–1041. https://doi.org/10.1017/S0016756816000121

Petrus, J. A., & Kamber, B. S. (2012). VizualAge: A Novel Approach to Laser Ablation ICP-MS U-Pb Geochronology Data Reduction. *Geostandards and Geoanalytical Research*, *36*(3), 247–270. https://doi.org/10.1111/j.1751-908X.2012.00158.x

Pfiffner, O., & Gonzalez, L. (2013). Mesozoic–Cenozoic Evolution of the Western Margin of South America: Case Study of the Peruvian Andes. *Geosciences*, *3*(2), 262–310. https://doi.org/10.3390/geosciences3020262

Potter, P. E. (1997). The Mesozoic and Cenozoic paleodrainage of South America: a natural history. *Journal of South American Earth Sciences*, *10*(5–6), 331–344. https://doi.org/10.1016/S0895-9811(97)00031-X

Pourmand, A., Dauphas, N., & Ireland, T. J. (2012). A novel extraction chromatography and MC-ICP-MS technique for rapid analysis of REE, Sc and Y: Revising CI-chondrite and Post-Archean Australian Shale (PAAS) abundances. *Chemical Geology*, *291*, 38–54. https://doi.org/10.1016/j.chemgeo.2011.08.011

Ramos, V. A. (2018). Tectonic Evolution of the Central Andes: From Terrane Accretion to Crustal Delamination. In G. Zamora, K. R. McClay, & V. A. Ramos, *Petroleum Basins and Hydrocarbon Potential of the Andes of Peru and Bolivia* (pp. 1–34). The American Association of Petroleum Geologists. https://doi.org/10.1306/13622115M1172855

Ramos, V. A., & Folguera, A. (2009). Andean flat-slab subduction through time. *Geological Society, London, Special Publications*, *327*(1), 31–54. https://doi.org/10.1144/SP327.3

Rizzotto, G. J., & Quadros, M. L. do E. S. (2005). Geologia do Sudoeste do Craton Amazonico. *Contribuições à Geologia Da Amazônia*, *4*.

Roddaz, M., Viers, J., Brusset, S., Baby, P., & Hérail, G. (2005). Sediment provenances and drainage evolution of the Neogene Amazonian foreland basin. *Earth and Planetary Science Letters*, *239*(1–2), 57–78. https://doi.org/10.1016/j.epsl.2005.08.007

Roddaz, M., Hermoza, W., Mora, A., Baby, P., Parra, M., Christophoul, F., et al. (2010). Cenozoic Sedimentary Evolution of the Amazonian Foreland Basin System. In C. Hoorn & F. P. Wesselingh (Eds.), *Amazonia: Landscape and Species Evolution* (pp. 61–88). Oxford, UK: Wiley-Blackwell Publishing Ltd. https://doi.org/10.1002/9781444306408.ch5

Roddaz, M., Viers, J., Moreira-Turcq, P., Blondel, C., Sondag, F., Guyot, J.-L., & Moreira, L. (2014). Evidence for the control of the geochemistry of Amazonian floodplain sediments by stratification of suspended sediments in the Amazon. *Chemical Geology*, *387*, 101–110. https://doi.org/10.1016/j.chemgeo.2014.07.022

Roddaz, M., Dera, G., Mourlot, Y., Calvès, G., Kim, J.-H., Chaboureau, A.-C., et al. (2021). Provenance constraints on the Cretaceous-Paleocene erosional history of the Guiana Shield as determined from the geochemistry of clay-size fraction of sediments from the Arapaima-1 well (Guyana-Suriname basin). *Marine Geology*, *434*, 106433. https://doi.org/10.1016/j.margeo.2021.106433

Rodríguez Tribaldos, V., White, N. J., Roberts, G. G., & Hoggard, M. J. (2017). Spatial and temporal uplift history of South America from calibrated drainage analysis: SOUTH AMERICAN DRAINAGE. *Geochemistry, Geophysics, Geosystems*, *18*(6), 2321–2353. https://doi.org/10.1002/2017GC006909

Ruiz, G., Seward, D., & Winkler, W. (2004). Detrital thermochronology - a new perspective on hinterland tectonics, an example from the Andean Amazon Basin, Ecuador. *Basin Research*, *16*(3), 413–430. https://doi.org/10.1111/j.1365-2117.2004.00239.x

Ruiz, G. M. H., Seward, D., & Winkler, W. (2007). Evolution of the Amazon Basin in Ecuador with Special Reference to Hinterland Tectonics: Data from Zircon Fission-Track and Heavy Mineral Analysis. In *Developments in Sedimentology* (Vol. 58, pp. 907–934). Elsevier. https://doi.org/10.1016/S0070-4571(07)58036-2

Sacek, V. (2014). Drainage reversal of the Amazon River due to the coupling of surface and lithospheric processes. *Earth and Planetary Science Letters*, *401*, 301–312. https://doi.org/10.1016/j.epsl.2014.06.022

Sanchez F., A., Chira F., J., & Valencia M., M. (1997). *Geología de los Cuadrángulos de Tarapoto, Papa Playa, Utcurarca y Yanayacu* (Carta Geológica Nacional No. 94). Lima: INGEMMET.

Santos, J. O. S., Hartmann, L. A., Gaudette, H. E., Groves, D. I., Mcnaughton, N. J., & Fletcher, I. R. (2000a). A New Understanding of the Provinces of the Amazon Craton Based on Integration of Field Mapping and U-Pb and Sm-Nd Geochronology. *Gondwana Research*, *3*(4), 453–488. https://doi.org/10.1016/S1342-937X(05)70755-3

Santos, J. O. S., Hartmann, L. A., Gaudette, H. E., Groves, D. I., Mcnaughton, N. J., & Fletcher, I. R. (2000b). A New Understanding of the Provinces of the Amazon Craton Based on Integration of Field Mapping and U-Pb and Sm-Nd Geochronology. *Gondwana Research*, *3*(4), 453–488. https://doi.org/10.1016/S1342-937X(05)70755-3

Sapin, F., Mélanie, D., Dall'asta, M., Lahmi, M., Baudot, G., & Ringenbach, J.-C. (2016). Post-rift subsidence of the French Guiana hyper-oblique margin: from roft-inherited subsidence to Amazon deposition effect. *Geological Society of London*, (431), 125–144. https://doi.org/10.1144/SP431.11

Sempere, T., Carlier, G., Soler, P., Fornari, M., Carlotto, V., Jacay, J., et al. (2002). Late Permian–Middle Jurassic lithospheric thinning in Peru and Bolivia, and its bearing on Andean-age tectonics. *Tectonophysics*, *345*(1–4), 153–181. https://doi.org/10.1016/S0040-1951(01)00211-6

Sharman, G. R., Sharman, J. P., & Sylvester, Z. (2018). detritalPy: A Python-based toolset for visualizing and analysing detrital geo-thermochronologic data. *The Depositional Record*, *4*(2), 202–215. https://doi.org/10.1002/dep2.45

Shephard, G. E., Müller, R. D., Liu, L., & Gurnis, M. (2010). Miocene drainage reversal of the Amazon River driven by plate–mantle interaction. *Nature Geoscience*, *3*(12), 870–875. https://doi.org/10.1038/ngeo1017

van Soelen, E. E., Kim, J.-H., Santos, R. V., Dantas, E. L., Vasconcelos de Almeida, F., Pires, J. P., et al. (2017a). A 30 Ma history of the Amazon River inferred from terrigenous sediments and organic matter on the Ceará Rise. *Earth and Planetary Science Letters*, *474*, 40–48. https://doi.org/10.1016/j.epsl.2017.06.025

van Soelen, E. E., Kim, J.-H., Santos, R. V., Dantas, E. L., Vasconcelos de Almeida, F., Pires, J. P., et al. (2017b). A 30 Ma history of the Amazon River inferred from terrigenous sediments and organic matter on the Ceará Rise. *Earth and Planetary Science Letters*, *474*, 40–48. https://doi.org/10.1016/j.epsl.2017.06.025

Spencer, C. J., Kirkland, C. L., & Taylor, R. J. M. (2016). Strategies towards statistically robust interpretations of in situ U–Pb zircon geochronology. *Geoscience Frontiers*, *7*(4), 581–589. https://doi.org/10.1016/j.gsf.2015.11.006

Spikings, R., Reitsma, M. J., Boekhout, F., Mišković, A., Ulianov, A., Chiaradia, M., et al. (2016). Characterisation of Triassic rifting in Peru and implications for the early disassembly of western Pangaea. *Gondwana Research*, *35*, 124–143. https://doi.org/10.1016/j.gr.2016.02.008

Stewart, J. A., Gutjahr, M., James, R. H., Anand, P., & Wilson, P. A. (2016). Influence of the Amazon River on the Nd isotope composition of deep water in the western equatorial Atlantic during the Oligocene–Miocene transition. *Earth and Planetary Science Letters*, *454*, 132–141. https://doi.org/10.1016/j.epsl.2016.08.037

Tassinari, C. C. G., & Macambira, M. J. B. (1999). Geochronological provinces of the Amazonian Craton. *Episodes*, *22*(3).

Taylor, S. R., & McLennan, S. M. (1985). *The Continental Crust: Its Composition and Evolution*. Oxford, UK: Blackwell Scientific.

Vallejo, C., Tapia, D., Gaibor, J., Steel, R., Cardenas, M., Winkler, W., et al. (2017). Geology of the Campanian M1 sandstone oil reservoir of eastern Ecuador: A delta system sourced from the Amazon Craton. *Marine and Petroleum Geology*, *86*, 1207–1223. https://doi.org/10.1016/j.marpetgeo.2017.07.022

Vermeesch, P. (2004). How many grains are needed for a provenance study? *Earth and Planetary Science Letters*, *224*(3–4), 441–451. https://doi.org/10.1016/j.epsl.2004.05.037

Vermeesch, P. (2012). On the visualisation of detrital age distributions. *Chemical Geology*, *312–313*, 190–194. https://doi.org/10.1016/j.chemgeo.2012.04.021

Vermeesch, P. (2013). Multi-sample comparison of detrital age distributions. *Chemical Geology*, *341*, 140–146. https://doi.org/10.1016/j.chemgeo.2013.01.010

Vermeesch, P. (2018). Dissimilarity measures in detrital geochronology. *Earth-Science Reviews*, *178*, 310–321. https://doi.org/10.1016/j.earscirev.2017.11.027

Viers, J., & Wasserburg, G. J. (2004). Behavior of Sm and Nd in a lateritic soil profile. *Geochimica et Cosmochimica Acta*, *68*(9), 2043–2054. https://doi.org/10.1016/j.gca.2003.10.034

Wanderley Filho, J. R., Eiras, J. F., & Vaz, P. T. (2007). Bacia do Solimões. *Boleti, de Geosciências Da Petrobras*, *15*(2), 217–225.

Wiedenbeck, M., Allé, P., Corfu, F., Griffin, W. L., Meier, M., Oberli, F., et al. (1995). Three Natura Zircon Standards for U-Th-Pb, Lu-Hf, Trace Element and REE Analyses. *Geostandards Newsletter*, *19*(1), 1–23.

Wine, G., Vetrici, D., & Arcuri, J. (2001). *The Huallaga Basin and Adjacent Area* (Proyecto de Asistencia para La Reglamentación del Sector Energético del Perú). Lima: PARSEP.

Zamora, G., & Gil, W. (2018). The Marañón Basin: Tectonic Evolution and Paleogeography. In *Petroleum Basins and Hydrocarbon Potential of the Andes of Peru and Bolivia* (pp. 121–144). The American Association of Petroleum Geologists. https://doi.org/10.1306/13622119M1173768

Supporting information for

New insights into the Cretaceous evolution of the Western Amazonian paleodrainage system

Mariana de Assunção Rodrigues [a,b,*], Martin Roddaz [b], Roberto Ventura Santos[a], Melanie Louterbach[c], Carlos D'Apolito [e], Stéphane Brusset [b], Elton Luiz Dantas [a], Francisco Ricardo Negri [d]

[a] Universidade de Brasília, Darcy Ribeiro Campus, Asa Norte 70910-900 Brasília, DF, Brazil

[b] Géosciences-Environnement Toulouse, Université de Toulouse; UPS (SVT-OMP); 14 Avenue Édouard Belin, F-31400 Toulouse, France

[c] Harvard Graduate School of Design, Department of Landscape Architecture, 48 Quincy Street, MA 02138 Cambridge, USA

[d] Universidade Federal do Acre, Campus Floresta, Laboratório de Paleontologia. Estrada do Canela Fina, km 12, 69980-000 Cruzeiro do Sul, AC, Brazil

[e] Universidade Federal do Acre, Centro de Ciências Biológicas e da Natureza. Rodovia BR-364; 69920-900 Rio Branco, AC, Brazil

*Corresponding author,

E-mail address: marianarodrigues.geologia@gmail.com (M. A. Rodrigues).

Contents

Figures S1 to S6

Texts S1 and S2

Tables S2 to S6

Additional Supporting Information (Anexo)

Table S1

Introduction

This supporting information provides a detailed description of instrumentation, including analytical conditions and the methodology used. Furthermore, the full analytical datasets produced during the U-Pb ages analysis are available as separate tables in the annexes section.

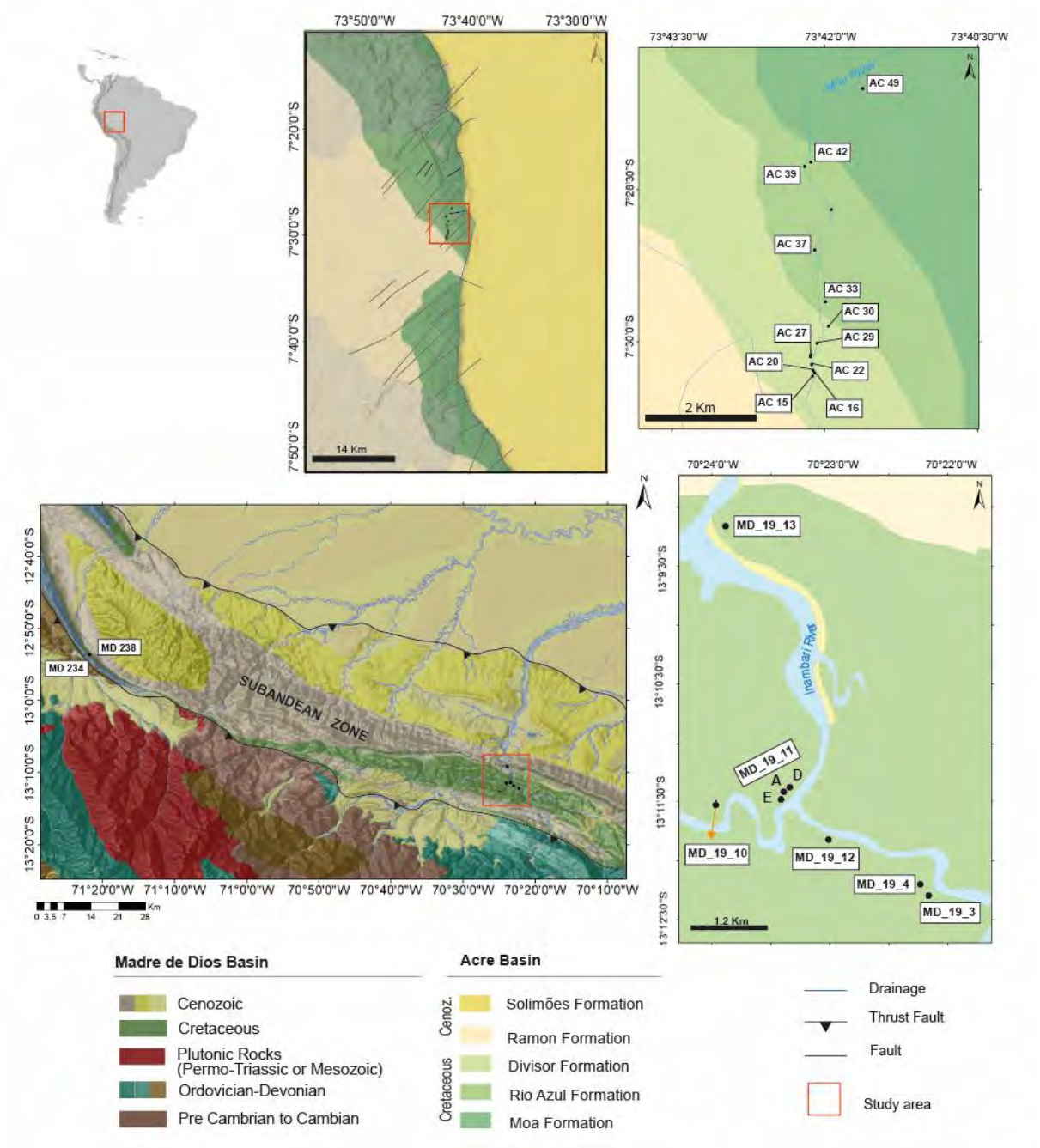

Figure S1: Geological map of the studied areas, modified from the INGEMMET Geological Map of Peru available at http://geocatmin.ingemmet.gob.pe/geocatmin/, Louterbach, et al. (2018) and SGB-CPRM Geological map of Brazil available at http://www.cprm.gov.br/publique/Geologia/Geologia-Basica/Carta-Geologica-do-Brasil-ao-Milionesimo-298.html. (1) Acre Basin: Sedimentary section realized from point A to point B and C to D in the Moa River (yellow bold line) (Fig. S2); (2) Madre de Dios Basin: (a) Pongo de Coñeq section (Fig. S5) and (b) Inambari section (Fig. S3).

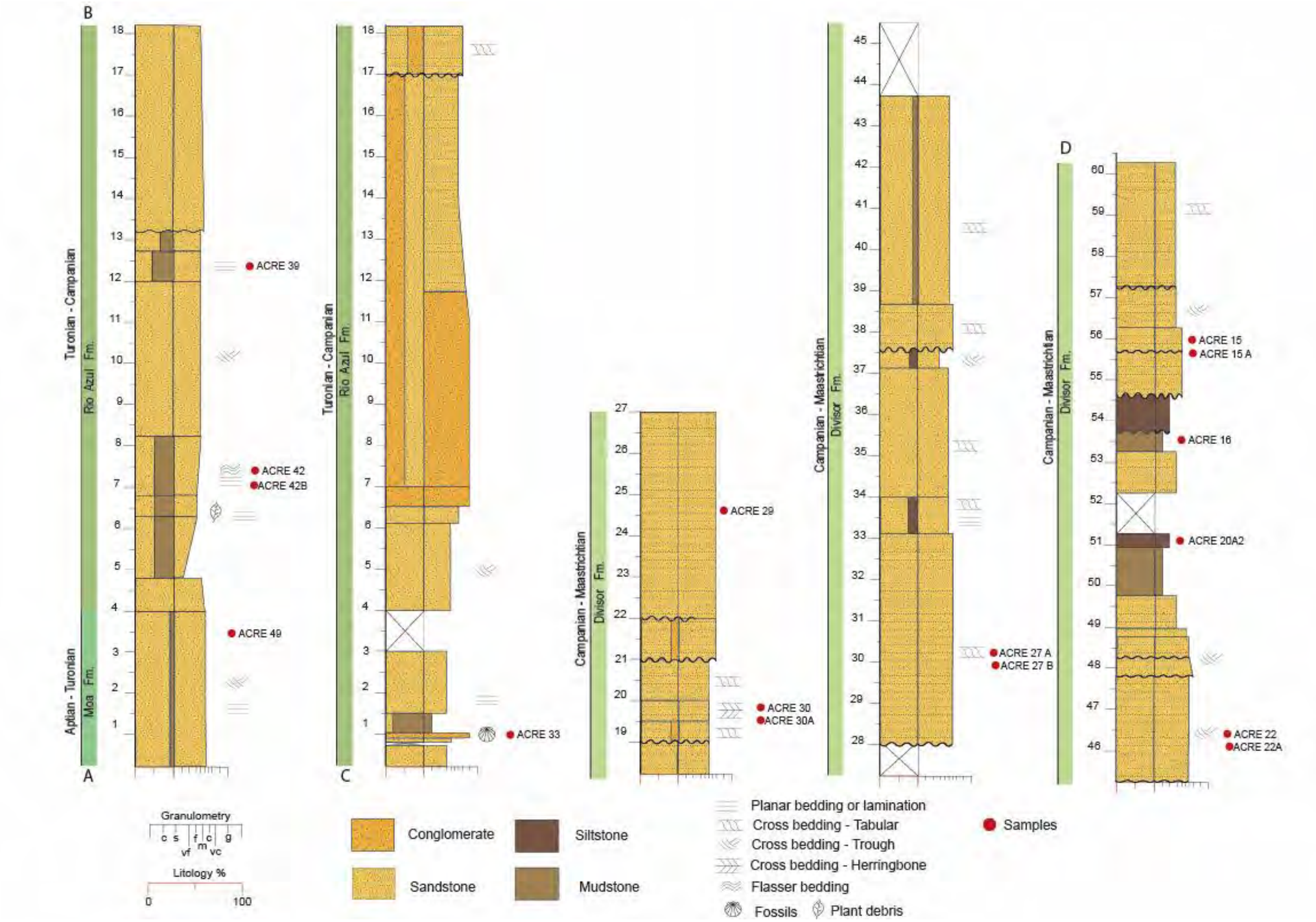

Figure S2: Synthetic sedimentary section presenting the stratigraphic succession of the Acre Basin in the Moa River area. The samples collected and analyzed in this study are indicated.

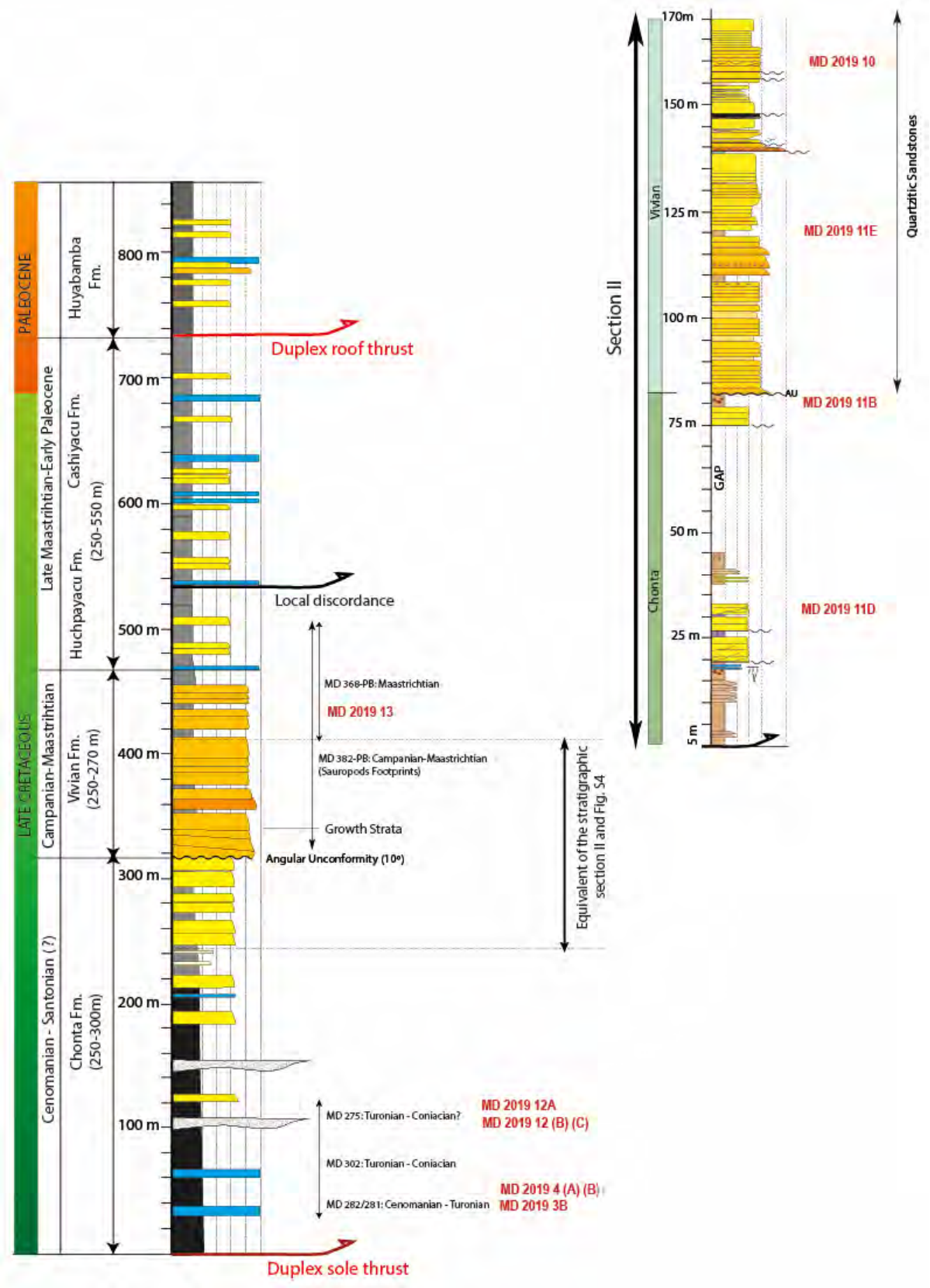

Figure S3: Synthetic sedimentary section presenting the stratigraphic content of the Inambari area indicating the samples collected and analyzed in this study (in red) and in Louterbach (2014) (black). Biostratigraphic results are indicated with their corresponding sample. Modified from Louterbach (2014).

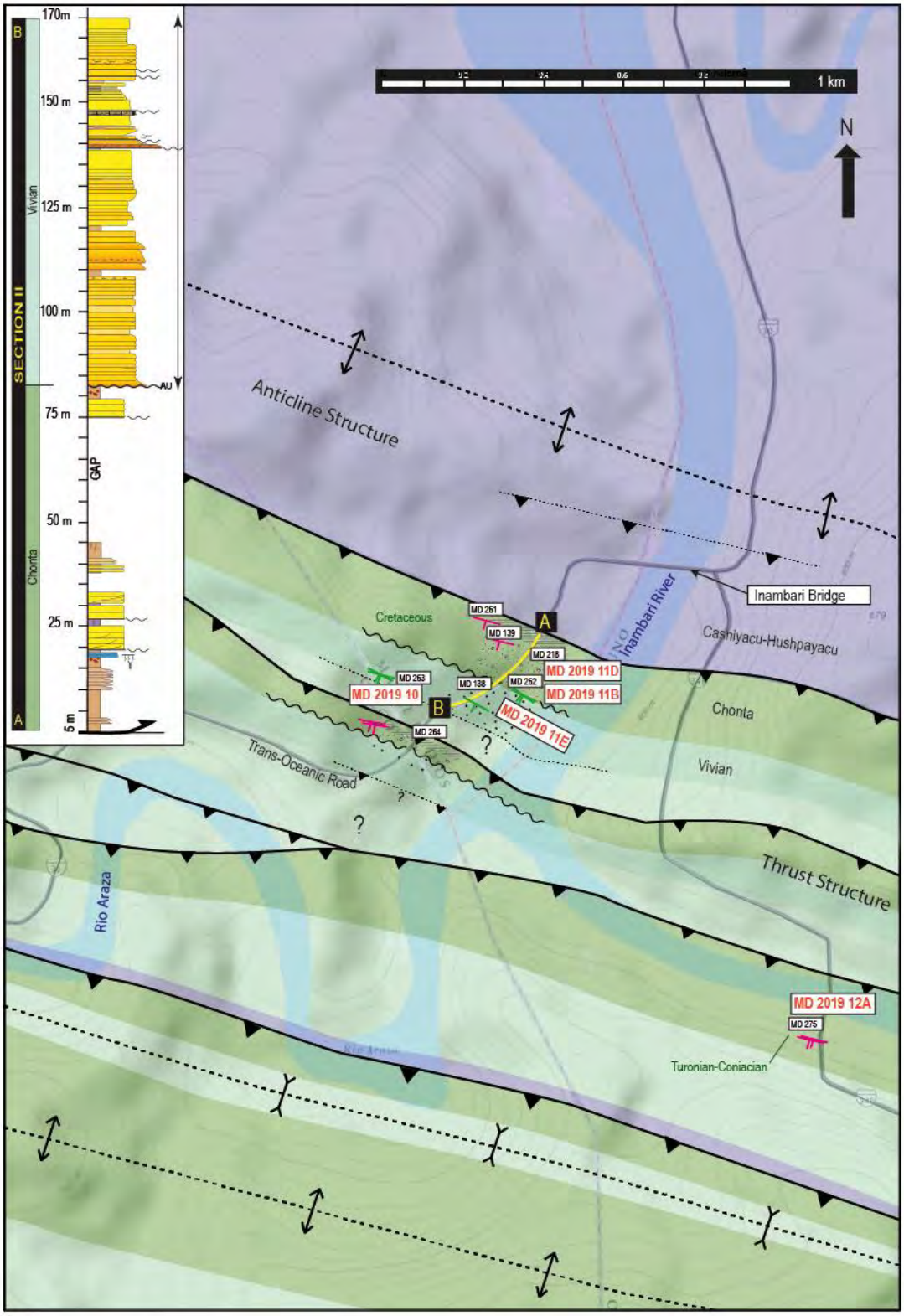

Figure S4: Geological map of the Inambari area indicating the samples collected and analyzed in this study (red) and those analyzed by Louterbach (2014) (black). The sedimentary section (Section II) is realized from point A to point B south of the Inambari Bridge (yellow bold line).

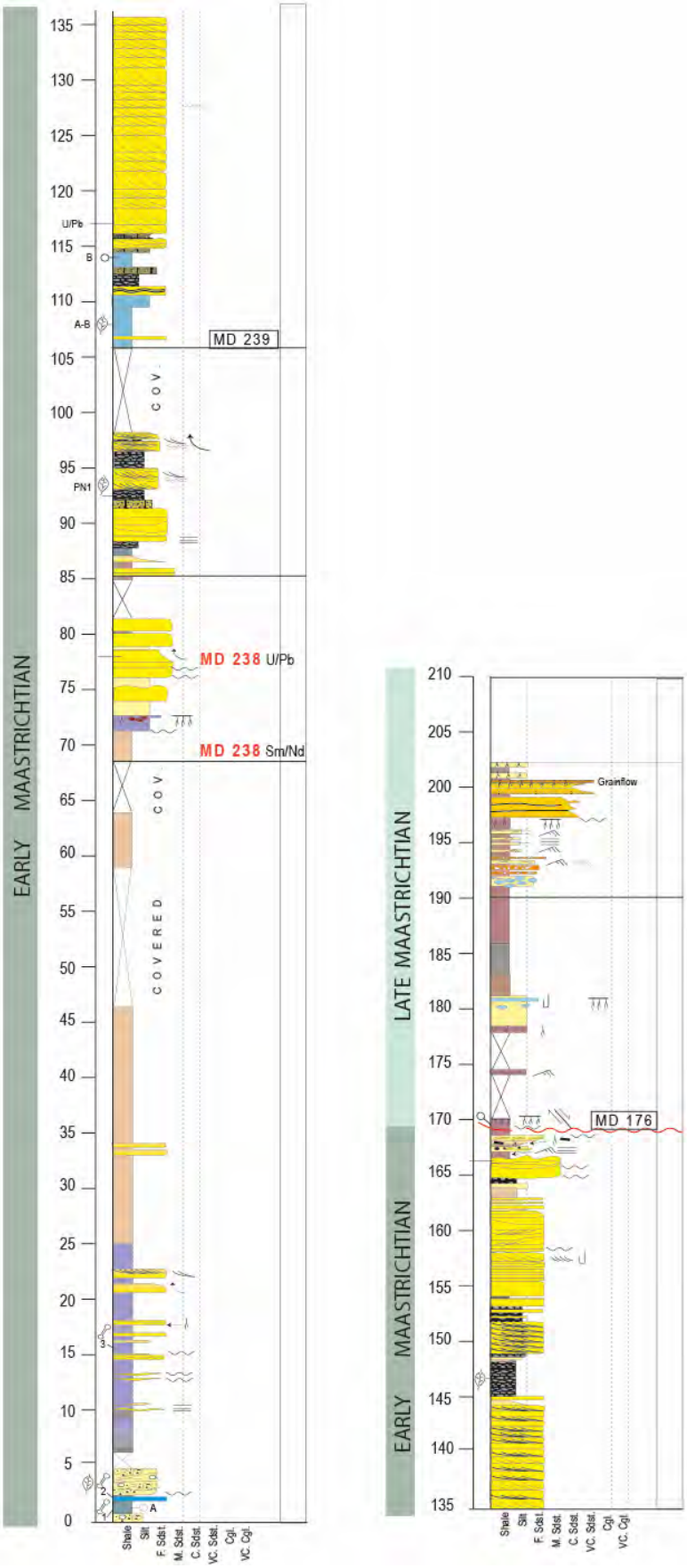
EARLY MAASTRICHTIAN
LATE MAASTRICHTIAN
EARLY MAASTRICHTIAN
U/Pb
B
A-B
PN1
MD 239
MD 238 U/Pb
MD 238 Sm/Nd
MD 176
COV.
COVERED
Grainflow
A
Shale
Silt
F. Sdst.
M. Sdst.
C. Sdst.
VC. Sdst.
Cgl.
VC. Cgl.

Figure S5: Sedimentary section presenting the stratigraphic content of the Pongo de Coñeq area indicating the samples collected and analyzed in this study (in red) and Louterbach et al. (2018). Modified from Louterbach (2014) and Louterbach et al. (2018).

Results of palynology

- **Sample ACRE 33**

We performed a new pollen analysis of a sample at the conglomerate ACRE 33 (Fig. S2) and assessed it critically along with previous pollen data from two other samples (by Haag 2019): one immediately below (PPNSD 09-F) and one immediately above (PPNSD 09-G) the conglomerate.

The record of a polyplicate form attributed to *Gnetaceaepollenites diversus* Stover 1964 (Haag 2019, pg. 412, plate II, Fig. D) was used to suggest a Cenomanian age for sample PPNSD 09-F. However, the specimen illustrated is in fact *Gnetaceaepollenites barghoornii* (Pocock) de Lima 1980, which ranges from Aptian to Maastrichtian. It has been reported up to the Maastrichtian of Patagonia (Vallati et al., 2016) and northern Argentina (Narvaez et al., 2014), as well as the late Santonian of São Paulo (Arai and Dias-Brito, 2018). Other taxa from this sample (e.g. *Cretacaeiporites mulleri* Herngreen 1973 and *Droseridites senonicus* Jardine and Magloire 1965) also have long stratigraphical ranges from Aptian to Maastrichtian.

In sample ACRE 33 we counted a total of 304 specimens and recorded 39 different morphotypes: one freshwater algae (*Pediastrum* spp.), 12 dinoflagellate cysts, 14 pollen, and 11 spore types, as well as foraminiferal organic linings (Fig. S6). Among continental elements, angiosperms are 19% of the counts, gymnosperms are 8%, and ferns are 73%. The proportional species richness of these groups is as follows: angiosperms 40% (n=10); gymnosperms 16% (n=4); and ferns 44% (n=11). Only two Gnetales were recorded (*Equisetosporites* sp. and *Steevesipollenites binodosus*). Marine elements are >61% of the counts, freshwater algae are ca. 5.6%, and the remaining are continental elements and include at least 13% of aquatic ferns. These data suggest a marginal marine environment (e.g., estuaries) with high terrestrial input.

Palynostratigraphy suggests an Upper Cretaceous age (Santonian/Campanian), as discussed below:

Florentinia berran Below 1982 (Albian to Maastrichtian of Brazil; Arai et al. 2000); *Heterosphaeridium difficile* (Manum and Cookson 1964) Ioannides 1986 (late Cenomanian to late Campanian; Bell and Selnes 1997; Prince et al. 1999; Nøhr-Hansen et al. 2016); *Spiniferites bejui* Masure et al. 1998 (Aptian to early Campanian of Brazil and Ghana; Masure et al. 1998; Arai 2007; Carvalho et al. 2001); *Steevesipollenites binodosus* Stover 1964 (Albian to Santonian of Brazil; Herngreen 1973; Lima 1980); *Ariadnaesporites spinosus* (Elsik 1966) Hills 1967 (early Campanian to Maastrichtian of Brazil, Peru and Colombia; Elsik 1966; Regali et al., 1974; Hurtado et al. 2018; Carvalho et al., 2021); *Gabonisporis vigourouxii* Boltenhagen 1967 (Coniacian to Maastrichtian of Brazil and Colombia; Regali et al., 1974; Carvalho et al., 2021); *Zlivisporis blanensis* Pacltova 1961 (usually a longer range from Aptian to Maastrichtian worldwide, but more often in the Campanian to Maastrichtian in northern South America; Regali et al., 1974; Carvalho et al., 2021). Although many of these species have a long range in the Upper Cretaceous, a tentative age from Santonian to late Campanian is advanced for sample ACRE 33. The above sample PPNSD 09-G is more securely dated as Maastrichtian due to the occurrence of *Ulmoideipites krempii* (Anderson 1960) Elsik 1968 (Regali et al., 1974; Vajda and Bercovici 2012; Carvalho et al. 2021).

ACKNOWLEDGMENTS

We thank Mitsuru Arai for helping with palynomorph identifications.

REFERENCES

Arai, M. 2007. Sucessão das associações de dinoflagelados (Protista, Pyrrhophyta) ao longo das colunas estratigráficas do Cretáceo das bacias da margem continental brasileira: uma análise sob ponto de vista paleoceanográfico e

paleobiogeográfico. Tese doutorado, Universidade Federal do Rio Grande do Sul, Instituto de Geociências, Programa de Pós-Graduação em Geociências. 231 pp.

Arai, M., Dias-Brito, D. 2018. The Ibate paleolake in SE Brazil: Record of an exceptional late Santonian palynoflora with multiple significance (chronostratigraphy, paleoecology and paleophytogeography). Cretaceous Research 84: 264-285.

Arai, M., Botelho, J., Lana, C.C, PedrJo, E. 2000. Cretaceous dinoflagellate provincialism in Brazilian marginal basins. Cretaceous Research 21(3): 351- 366.

Bell, D. G., Selnes, H. 1997. The First Appearance Datum (FAD) of *Heterosphaeridium difficile* (Manum & Cookson), dinoflagellata, in clastic deposits offshore Norway. Journal of Micropalaeontology 16: 30 - 30.

Carvalho, M.R., Jaramillo, C., de la Parra, F., Caballero-Rodríguez, D., Herrera, F., Wing, S., Turner, B.L., D'Apolito, C., Romero-Báez, M., Narváez, P., Martínez, C., Gutierrez, M., Labandeira, C., Bayona, G., Rueda, M., Paez-Reyes, M., Cárdenas, D., Duque, Á., Crowley, J.L., Santos, C., Silvestro, D. 2021. Extinction at the end-Cretaceous and the origin of modern Neotropical rainforests. Science 372: 63-68. doi:10.1126/science.abf1969

Elsik, W. C. 1966. New Sporomorph genera from the Upper Cretaceous of Perú: Pollen et Spores 8(3): 553-564.

Herngreen, W. G. F. 1973. Palynology of the Albian-Cenomanian strata of Borehole 1-QS-1-MA, State of Maranhão, Brazil. *Pollen et Spores* **15(3-4)**:515-555

Hurtado, C., Roddaz, M., Santos, R.V., Baby, P., Antoine, P.-O., Dantas, E.L., 2018a. Cretaceous-early Paleocene drainage shift of Amazonian rivers driven by Equatorial Atlantic Ocean opening and Andean uplift as deduced from the provenance of northern Peruvian sedimentary rocks (Huallaga Basin). Gondwana Res. 63, 152–168. https://doi.org/10.1016/j.gr.2018.05.012

Prince I. M., Jarvis I, Tocher, B. A. 1999. High-resolution dinoflagellate cyst biostratigraphy of the Santonian–basal Campanian (Upper Cretaceous): new data from Whitecliff, Isle of Wight, England. Review of Palaeobotany and Palynology 105: 143–169.

Carvalho, M. A. 2001. Paleoenvironmental reconstruction based on palynological and palynofacies analyses of the Aptian-Albian succession in the Sergipe Basin, northeastern Brazil. Ph.D. thesis, University of Heidelberg, 192 pp.

Masure, E., Rauscher, R., Dejax, J., Schuler, M. and Ferré, B., 1998: Cretaceous-Paleocene palynology from the Côte d'Ivoire-Ghana transform margin, sites 959, 960, 961, and 962. Proceedings of the Ocean Drilling Program, Scientific Results, 159: 253-276.

Narvaez, P. L., and Pramparo, M. B., Sabino, I.F. 2014. First palynological record of the Cretaceous La Yesera Formation (Salta Group), Northwestern Argentina: Revista Brasileira de Paleontologia 17: 141-156.

Nøhr-Hansen, H., Williams, G. L., Fensome, R. A. 2016. Biostratigraphic correlation of the western and eastern margins of the Labrador–Baffin Seaway and implications for the regional geology. GEUS Bulletin 37: 1–74.

Regali, M. S. P., Uesugui, N., Santos, A. S. 1974. Palinologia dos sedimentos Meso-Cenozoicos do Brasil (II). Boletim Técnico da Petrobras 17(4): 263-301.

Lima, M.R. 1980. Palinologia da Formacion Santana (Cretaceo do Nordeste do Brasil). III. Descricao sistematica dos polens da turma plicates (subturma costates). Ameghiana Revista de la Asociacion Paleontologica Argentina XVII (1): 15 - 47.

Vajda, V., Bercovici, A. 2012. Pollen and spore stratigraphy of the Cretaceous-Paleogene mass-extinction interval in the southern hemisphere. Journal of Stratigraphy 36(2): 153-164.

Vallati, P., Casal, G., Foix, N., Allard, J., Sosa, A., and Calo, M. 2016. First report of a Maastrichtian palynoflora from the Golfo San Jorge Basin, Central Patagonia, Argentina: Ameghiniana 53: 495-505.

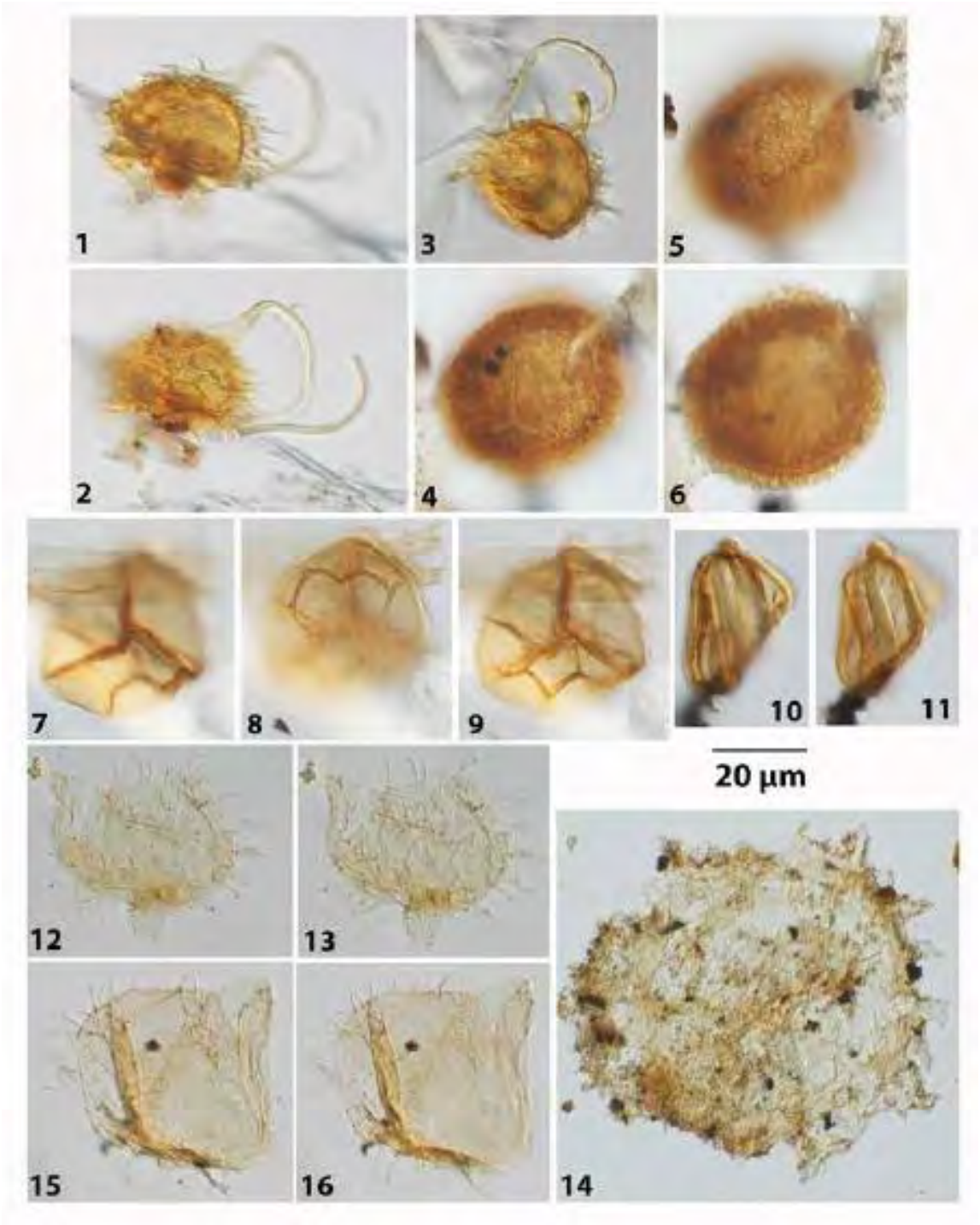

Figure S6: Selected palynomorphs from sample ACRE33 (lab label: PALMA11414_L1), codes in parentheses are coordinates of the England Finder (EF) system. 1-2) Ariadnaesporites spinosus (Elsik 1966) Hills 1967 (EF J18-2); 1-3) A. spinosus (EF K34-3/4); 4-6) Gabonisporis vigourouxii Boltenhagen 1967 (EF N13-1/3); 7-9) Zlivisporis blanensis Pacltova 1961 (EF U34-4); 10-11) Steevesipollenites binodosus Stover 1964 (EF X38-2); 12-13) Florentinia berran Below 1982 (EF S40); 14) Heterosphaeridium diffcile (Manum and Cookson 1964) Ioannides 1986 (EF C8-1); 15-16) Spiniferites beju Masure et al. 1998 (EF C5-2).

Table S1a: U-Pb data of the Acre Basin samples. (Anexo)

Table S1b: U-Pb data of the Madre de Dios Basin samples. (Anexo)

Table S2: Description of the Acre section presented in the supplementary dataset

Section A-B

Wall height	(m)	Roof height	(m)	Base	Lithology 1	Grain size 1
481.7	0	485.7	4	Nette	Sandstone	Medium
485.7	4	486.5	4.8	Nette	Sandstone	Fine
486.5	4.8	488	6.3	Nette	Sandstone	Very Fine
488	6.3	488.5	6.8	Nette	Sandstone	Very Fine
488.5	6.8	490	8.3	Nette	Sandstone	Very Fine
490	8.3	493.7	12	Nette	Sandstone	Fine
493.7	12	494.4	12.7	Nette	Sandstone	Fine
494.4	12.7	495	13.3	Nette	Sandstone	Fine
495	13.3	500	18.3	Erosive	Sandstone	Medium

Section C-D

Wall height	(m)	Roof height	(m)	Base	Lithology 1	Grain size 1
438	0	438.6	0.6	Sharp	Sandstone	Very Fine
438.6	0.6	438.7	0.7	Sharp	Non visible	-
438.7	0.7	438.8	0.8	Sharp	Sandstone	Fine
438.8	0.8	439	1	Sharp	Conglomerate	Gravel
439	1	439.5	1.5	Sharp	Sandstone	Very Fine
439.5	1.5	441	3	Sharp	Sandstone	Very Fine
441	3	442	4	Sharp	Non visible	-
442	4	444.1	6.1	Sharp	Sandstone	Fine
444.1	6.1	444.5	6.5	Sharp	Sandstone	Coarse
444.5	6.5	445	7	Sharp	Conglomerate	Gravel
445	7	455	17	Sharp	Conglomerate	Gravel
455	17	456.2	18.2	Erosive	Sandstone	Coarse
456.2	18.2	457	19	Sharp	Sandstone	Medium
457	19	457.5	19.5	Erosive	Sandstone	Medium
457.5	19.5	458	20	Sharp	Sandstone	Medium
458	20	459	21	Sharp	Sandstone	Medium
459	21	460	22	Erosive	Sandstone	Very Coarse
460	22	465	27	Erosive	Sandstone	Coarse
465	27	466	28	Non visible	Non visible	-
466	28	471.2	33.2	Erosive	Sandstone	Coarse
471.2	33.2	472	34	Sharp	Sandstone	Medium
472	34	475.2	37.2	Sharp	Sandstone	Medium
475.2	37.2	475.7	37.7	Sharp	Sandstone	Very Fine
475.7	37.7	477	39.7	Erosive	Sandstone	Coarse
477	39.7	482	44.7	Sharp	Sandstone	Medium
482	44.7	483.8	46.5	Non visible	Non visible	-
483.8	46.5	486.8	49.5	Erosive	Sandstone	Coarse
486.8	49.5	487.2	49.9	Erosive	Sandstone	Very Coarse
487.2	49.9	487.5	50.2	Erosive	Sandstone	Coarse
487.5	50.2	487.7	50.4	Sharp	Sandstone	Medium
487.7	50.4	488.5	51.2	Sharp	Sandstone	Very Fine
488.5	51.2	489.7	52.4	Sharp	Mudstone	-
489.7	52.4	490	52.7	Sharp	Siltstone	-
490	52.7	491	53.7	Non visible	Mudstone	-
491	53.7	492	54.7	Sharp	Non visible	-
492	54.7	493	55.7	Non visible	Sandstone	Very Fine
493	55.7	493.5	56.2	Sharp	Mudstone	-
493.5	56.2	494.4	57.1	Erosive	Siltstone	-
494.4	57.1	495.5	58.2	Erosive	Sandstone	Fine
495.5	58.2	496.5	59.2	Erosive	Sandstone	Fine
496.5	59.2	497	59.7	Sharp	Sandstone	Very Fine
497	59.7	500	62.7	Erosive	Sandstone	Very Fine

Lithology 1 (%	Lithology 2	Grain size 2	Lithology 2 (%	Base	Top
90	Mudstone	-	10	Medium	Medium
100	Non visible	-	0	Fine	Fine
50	Mudstone	-	50	Mud	Very Fine
50	Mudstone	-	50	Fine	Fine
50	Mudstone	-	50	Mud	Very Fine
100	Non visible	-	0	Fine	Fine
45	Mudstone	-	55	Fine	Fine
65	Mudstone	-	35	Fine	Fine
100	Non visible	-	0	Medium	Medium

Lithology 1 (%	Lithology 2	Grain size 2	Lithology 2 (%	Base	Top
100	Non visible	-	0	Very Fine	Very Fine
100	Non visible	-	0	-	-
100	Non visible	-	0	Fine	Fine
100	Non visible	-	0	Gravel	Gravel
20	Mudstone	-	80	Very Fine	Very Fine
100	Non visible	-	0	Very Fine	Very Fine
100	Non visible	-	0	-	-
100	Non visible	-	0	Medium	Fine
100	Non visible	-	0	Coarse	Coarse
100	Non visible	-	0	Gravel	Gravel
50	Sandstone	Very Coarse	50	pebble	Coarse
60	Conglomerate	Gravel	40	Gravel	Coarse
100	Non visible	-	0	Very Coarse	Medium
75	Conglomerate	Gravel	25	Gravel	Medium
100	Non visible	-	0	Very Coarse	Medium
100	Non visible	-	0	Coarse	Medium
75	Conglomerate	Gravel	25	Gravel	Medium
100	Non visible	-	0	Coarse	Coarse
100	Non visible	-	0	-	-
100	Non visible	-	0	Coarse	Medium
75	Siltstone	-	25	Medium	Silt
100	Non visible	-	0	Medium	Medium
80	Siltstone	-	20	Very Fine	Very Fine
100	Non visible	-	0	Coarse	Coarse
95	Mudstone	-	5	Medium	Medium
100	Non visible	-	0	-	-
100	Non visible	-	0	Coarse	Coarse
100	Non visible	-	0	Very Coarse	Coarse
100	Non visible	-	0	Coarse	Medium
100	Non visible	-	0	Medium	Medium
100	Non visible	-	0	Medium	Very Fine
100	Non visible	-	0	Mud	Mud
100	Non visible	-	0	Silt	Silt
100	Non visible	-	0	Mud	Mud
100	Non visible	-	0	-	-
100	Non visible	-	0	Very Fine	Very Fine
100	Non visible	-	0	Mud	Mud
100	Non visible	-	0	Silt	Silt
95	Mudstone	-	5	Fine	Fine
100	Non visible	-	0	Fine	Fine
100	Non visible	-	0	Very Fine	Very Fine
100	Non visible	-	0	Very Fine	Very Fine

Structure	Fossils	Geometry	vertical stack
Cross bedding (trough) - lamination		-	-
lamination tidal -		-	-
rythmites tidales - flaser - lenticulaire -		-	-
lamination		-	-
flaser - lamination	Plant debris	Tabular	-
Cross bedding trough		Lenticular	stratocroissant
lenticulaire - lamination		Tabular	-
lofting rythmites - rythmites tidales -		-	-
		-	-

Structure	Fossils	Geometry	vertical stack
		-	-
		-	-
		-	-
	bivalves - dents - restes de		
	mollusque - dents vertèbre de poisson - fossiles indéterminés -	-	-
Lenticular -		-	-
cross bedding tabular		tabular	strato-descending
		-	-
cross bedding trough		-	-
cross bedding oblique d'angle faible -		-	-
cross bedding tabular -		-	-
cross bedding tangentielle -		-	-
cross bedding tabular -		tabular	constant
		-	-
cross bedding tabular -		Lenticular	strato-descending
cross bedding herringbone -		-	-
cross bedding tabular -		Lenticular	-
		Lenticular	strato-descending
		Lenticular	stratocroissant
		-	-
cross bedding tabular		-	-
cross bedding tangentielle		tabular	-
trough cross bedding		Lenticular	-
cross bedding trough -		Chenalisé	strato-descending
cross bedding tabular		-	-
cross bedding tabular		-	-
		-	-
cross bedding trough -		amalgamé	strato-descending
cross bedding trough -		-	-
cross bedding trough -		-	-
cross bedding trough -		-	-
		Lenticular	-
paleosols -	racines -	-	-
		-	-
paleosols -	racines -	-	-
		-	-
paleosols -	racines -	-	-
paleosols -		-	-
		-	-
		Lenticular	constant
cross bedding trough -		Chenalisé	-
		Lenticular	constant
cross bedding tabular -		amalgamated	strato-descending

tendance granulométrique	Latitude	Longitude	Altitude	Précision	Samples
-	-7.45821	-73.69354	322.9317	24	Acre 49
-	-7.45752	-73.70102	254.85738	8	
-	-7.46872	-73.70349	247.49956	48	
-	-7.46816	-73.70393	275.81201	128	
-	-7.47096	-73.70259	312.48444	32	Acre 42
granocroissant	-7.4714	-73.70312	309.84018	12	
-	-7.47125	-73.7033	289.86215	16	Acre 39
-	-7.47138	-73.70314	263.47394	8	
-	-7.47147	-73.70281	271.31635	48	

tendance granulométrique	Latitude	Longitude	Altitude	Précision	Samples
-	-7.48243	-73.70019	258.96378	8	
-	-7.48228	-73.69962	303.27667	48	
-	-7.48495	-73.70184	280.79028	8	
-	-7.48494	-73.70184	267.1655	16	Acre 33
-	-7.4849	-73.7017	256.27969	3	Acre 33B
grain-descending	-7.48485	-73.70179	257.45523	4	
-	-7.4863	-73.70147	258.29337	8	
-	-7.48726	-73.70158	265.76889	12	
-	-7.48782	-73.70177	285.99573	24	
-	-7.48862	-73.7019	269.68878	8	
-	-7.48962	-73.70232	183.5629	4	
-	-7.49175	-73.70085	284.92758	4	
-	-7.49189	-73.70024	279.00281	96	
grain-descending	-7.49239	-73.69973	297.63229	8	
-	-7.49237	-73.69971	270.62653	8	Acre 30
-	-7.4928	-73.69966	279.76587	24	
grain-descending	-7.4934	-73.69995	240.98694	16	
granocroissant	-7.49337	-73.69981	281.98477	8	Acre 29
-	-7.49349	-73.69984	270.92136	4	
-	-7.49686	-73.6993	258.65002	64	Acre 27
-	-7.4974	-73.69941	123.49428	8	
-	-7.49796	-73.6998	283.23792	24	
grain-descending	-7.49825	-73.69994	198.97289	8	
-	-7.49915	-73.70033	298.18198	24	
-	-7.49934	-73.70044	159.42477	8	
-	-7.49975	-73.70074	261.90338	8	
grain-descending	-7.50004	-73.70136	219.54144	24	Acre 22
-	-7.50032	-73.70136	315.08243	8	
-	-7.50025	-73.70114	183.00026	4	
-	-7.50091	-73.70193	288.94943	8	
-	-7.50081	-73.70183	266.58197	128	
-	-7.50155	-73.70231	274.40921	8	
-	-7.50203	-73.70236	311.7648	8	
-	-7.5021	-73.70244	243.935	8	Acre 20
-	-7.50363	-73.70219	264.05276	8	
-	-7.50465	-73.70202	232.407	32	
-	-7.50493	-73.7019	272.10403	12	Acre 16
grain-descending	-7.50585	-73.70198	344.35397	96	
-	-7.50564	-73.70173	260.3736	8	
-	-7.50562	-73.70162	300.83679	16	Acre 15
-	-7.50566	-73.70163	238.17412	12	
grain-descending	-7.50568	-73.70166	276.57733	8	

Table S3: Samples correlations based on correlation coefficient (R^2) for geochemical proxies used in this study based on a data matrix without outlier data. (A) Acre Basin and (B) Madre de Dios Basin.

A

Acre	εNd(0)	Eu/Eu*	ΩCe	Cr/Th	Th/Sc	Zr/Sc	LREE	HREE	MREE	MREE*	Al/Si	CIA
εNd(0)	1	0.25	-0.10	-0.11	-0.43	-0.29	-0.27	-0.34	-0.31	-0.33	-0.18	0.99
Eu/Eu*		1	-0.33	-0.01	-0.51	-0.58	0.37	0.11	0.52	0.30	-0.06	0.23
ΩCe			1	0.81	-0.47	-0.23	-0.60	-0.64	-0.53	-0.68	-0.45	-0.61
Cr/Th				1	-0.42	-0.27	-0.13	-0.54	0.00	-0.33	-0.43	-0.30
Th/Sc					1	0.91	0.30	0.31	0.29	0.34	0.13	-0.38
Zr/Sc						1	-0.05	-0.02	0.06	-0.04	-0.23	-0.36
LREE							1	0.60	0.90	0.94	0.52	0.41
HREE								1	0.40	0.84	0.84	-0.11
MREE									1	0.78	0.14	-0.16
MREE*										1	0.71	0.13
Al/Si											1	0.47
CIA												1

B

Madre de Dios	εNd(0)	Eu/Eu*	ΩCe	Cr/Th	Th/Sc	Zr/Sc	LREE	HREE	MREE	MREE*	Al/Si	CIA
εNd(0)	1	0.11	0.09	0.07	0.10	-0.03	0.12	0.16	0.16	-0.02	0.14	0.12
Eu/Eu*		1	1.00	0.97	0.97	0.65	0.98	0.97	0.98	0.71	0.98	1.00
ΩCe			1	0.98	0.96	0.66	0.99	0.98	0.98	0.74	0.99	1.00
Cr/Th				1	0.90	0.63	0.99	0.96	0.96	0.79	0.98	0.98
Th/Sc					1	0.66	0.92	0.92	0.92	0.61	0.92	0.96
Zr/Sc						1	0.63	0.63	0.65	0.67	0.63	0.61
LREE							1	0.98	0.98	0.77	0.99	0.99
HREE								1	0.99	0.73	1.00	0.98
MREE									1	0.71	0.99	0.99
MREE*										1	0.75	0.71
Al/Si											1	0.99
CIA												1

Table S4: Uncertainties–of the major and trace element concentrations.

	ICP-MS iCapQ and ICP-OES iCap6500 (Sc only)							
	Uncertainties in terms of the content							
	>100µg/g	>50 µg/g	>10 µg/g	>1 µg/g	>0.5 µg/g	>0.1 µg/g	>0.01 µg/g	D.L. µg/g
As		<5%	<15%	<20%		**		0.50
Ba		<5%	<15%	**				5.5
Be		<5%	<15%			<20%	**	0.05
Bi			<5%	<10%		<20%	**	0.045
Cd		<10%	<15%			<20%	**	0.02
Co		<5%	<10%	<20%		**		0.08
Cr			<5%	<10%		**		0.50
Cs			<5%	<15%		<20%	**	0.02
Cu		<8%	<20%	**				2.0
Ga			<5%	<10%		<20%	**	0.02
Ge		<5%		<10%		<20%	**	0.04
Hf			<5%	<10%		<15%	**	0.03
In		<5%		<15%		<20%	**	0.03
Mo		<5%	<15%	<20%		**		0.50
Nb		<5%		<10%		<20%	**	0.015
Ni			<5%	**				2.0
Pb		<10%		<20%		**		0.45
Rb		<5%	<15%	<20%		**		0.15
Sb			<5%	<10%		<20%	**	0.06
Sc	<5%	<10%		<15%	**			0.6
Sn		<5%	<15%	<20%		**		0.30
Sr		<5%	<10%	<20%		**		0.70
Ta		<5%		<10%		<20%	**	0.004
Th		<5%		<10%		<20%	**	0.015
U		<5%	<10%	<15%		<20%	**	0.01
V		<5%	<10%	<15%		**		0.85
W		<5%	<10%	<20%		**		0.80
Y		<5%		<15%		<20%	**	0.02
Zn		<10%	<20%	**				7.0
Zr		<5%	<15%	**				1.50
La			<5%	<15%		<20%	**	0.02
Ce		<5%	<10%	<15%		<20%	**	0.03
Pr		<5%	<10%			<20%	**	0.004
Nd		<5%	<15%			<20%	**	0.016
Sm			<5%	<15%		<20%	**	0.005
Eu				<5%		<10%	**	0.002
Gd			<5%	<10%		<20%	**	0.005
Tb		<5%	<10%	<15%		<20%	**	0.001
Dy			<5%	<10%		<15%	**	0.004
Ho		<5%		<10%		<20%	**	0.001
Er				<5%		<10%	**	0.002
Tm		<5%		<10%		<20%	**	0.001
Yb		<5%	<10%	<15%		<20%	**	0.002
Lu			<5%	<10%		<20%	**	0.001

**The measurement uncertainty is calculated for 200mg of prepared sample. It becomes important (>25%) over a concentration range between the limit of determination and the lowest concentration for which a percentage of error is indicated.

	ICP-OES iCap6500							
	Uncertainties in terms of the content							
	>10 %	>5 %	>1 %	>0.5 %	>0.1 %	>0.05 %	>0.01 %	D.L. %
SiO2	<2%			<10%	<20%	**		0.05
Al2O3	<2%	<10%	<15%		<20%	**		0.04
Fe2O3	<2%		<10%	<15%		<20%	**	0.015
MnO			<5%	<15%		<20%	**	0.015
MgO		<2%	<10%	<15%		<20%	**	0.03
CaO	<2%	<5%		<15%		<25%	**	0.03
Na2O		<5%	<10%	<15%		<25%	**	0.02
K2O		<5%	<10%	<20%		<25%	**	0.03
TiO2		<5%	<10%	<20%		<25%	**	0.02
P2O5			<5%	<15%	**			0.10

Text S2 **Methodology description**

Sm-Nd isotope

Before chemical preparation, the samples were dried at 60° C for approximately 12h. Sample digestion and extraction of Sm-Nd isotopes following the procedures described in (Goia & Pimentel, 2000). The isotopic ratios of both elements were measured using a Thermo Scientific TRITON Plus thermal ionization mass spectrometer. During the Nd runs, isotopic normalizations were made using the natural ratios of $^{146}Nd/^{144}Nd = 0.7219$. The accuracy of the measurements was estimated by repeated analysis of the BHVO-2 standard. Repeated analysis of the BHVO-2 standard gave a $^{143}Nd/^{144}Nd$ ratio of 0.512996 ± 0.000006 (2SD, n=10) (Weis et al., 2005).

The measured $^{143}Nd/^{144}Nd_{sample}$ and $^{143}Sm/^{144}Nd_{sample}$ ratios were expressed in epsilon notation and reflect the fractional deviation in parts per 104 unit from the $^{143}Sm/^{144}Nd$ from the Chondritic Uniform Reservoir (CHUR). This notation is defined as:

$$\varepsilon Nd\ (t) = [(^{143}Nd/^{144}Nd)_{sample}\ (t) / (^{143}Nd / {}^{144}Nd)_{CHUR}\ (t) -1] \times 10^4$$

where t indicates the time at which εNd is calculated. Here, no time correction was applied (t = 0), and the $^{143}Nd / {}^{144}Nd_{CHUR}\ (0) = 0.512638$ (Jacobsen & Wasserburg, 1980).

The TDM and TDM* ages were calculated following (Augustsson & Bahlburg, 2008; D. J. DePaolo et al., 1991; Donald J. DePaolo, 1981).

$$T_{DM} = \ln [(^{143}Nd/^{144}Nd_{\ sample,\ today} - {}^{143}Nd/^{144}Nd)_{\ DM,\ today}) / (^{147}Sm/^{144}Nd_{sample,\ today} - {}^{147}Sm/^{144}Nd_{DM,\ today}) + 1] / \lambda;$$

$$T_{DM^*} = \ln [(^{143}Nd/^{144}Nd_{\ sample,Ts} - {}^{143}Nd/^{144}Nd)_{DM,\ Ts}) / (^{147}Sm/^{144}Nd_{crust,\ Ts} - {}^{147}Sm/^{144}Nd_{DM,\ Ts}) + 1] / \lambda + Ts;$$

where Ts is the estimated stratigraphic age. The $^{147}Sm/^{144}Nd_{crust,}$ Ts was calculated assuming that the $^{147}Sm/^{144}Nd_{crust,\ today}$ = 0.11 (Albarède & Brouxel, 1987). The model of (Goldstein et al., 1984) was used, where λ (^{147}Sm) = 6.54 x $10^{-12}a^{-1}$, $^{143}Nd/^{144}Nd_{DM,\ today}$ = 0.51315, $^{147}Sm/^{144}Nd_{DM,\ today}$ = 0.217, ^{143}Nd / $^{144}Nd)_{CHUR}$ = 0.512638, and $^{147}Sm/^{144}Nd_{CHUR,\ today}$ = 0.1967.

Detrital zircon geochronological analysis

The samples were fragmented in a rock crusher, sifted, and concentrated using a pan to separate the heavy mineral fraction. A Frantz magnetic separator was used to remove the magnetic fraction. Approximately 150 zircons were handpicked from each sample under a binocular microscope and mounted in epoxy resin. The resin discs were then polished, cleaned, and carbon-coated, then, backscatter (BSE) images of zircon grains were obtained using a scanning electron microscope SEM FEI Quanta 450, working at 20-25 kV.

The U-Pb zircon dating was undertaken by laser ablation-inductively-coupled-plasm-mass-spectrometer (LA-ICP-MS) using a Neptune (Thermo-Finnigan) coupled to an Nd-YAG (= 213 nm) laser ablation system (New Wave Research, UP213) following the procedures of (Bühn et al., 2009). Some samples were analyzed by Thermo Finnigan Element XR high-resolution single-collector sector field coupled to a 193 nm Iridia Excimer (ArF) laser ablation system (see supplementary dataset for details). Under Neptune, the analysis employed a laser spot diameter of 25 μm, frequency of 10 Hz, and fluence of ~3.0-3.5 J/cm^2. Under Element XR the mass spectrometer was tuned to improve U and Pb sensitivity while minimizing oxide production before each analytical session. Each mass (202, 204, 206-208, 232, 238) was measured using the triple detection mode (SEM + Faraday) by sweeping the electrostatic sector on each mass. Each sweep consisted of 82 ms, resulting in over

800 scans for each ablation. Laser conditions included a spot diameter of 25 μm, 20 Hz, and 2.0 J cm^{-2}. Every analysis incorporated one background acquisition lasting 10 - 20s, followed by 20 - 40s data acquisitions from each sample. GJ-1 standard zircon (Jackson et al., 2004) was used to quantify the amount of ICP-MS fractionation, and zircon 91500 (Wiedenbeck et al., 1995) as secondary/validation. Data processing and correction of laser-induced fractionation (LIEF) were performed using IOLITE v4.0 software (Paton et al., 2011) as a time-resolved signal, and individual signal inspection was done with the assistance of VisualAge (Petrus & Kamber, 2012) with exponential plus linear modeling. Our measurements of 91500 yielded weighted man 206Pb/238U ages of 1063 ± 10 Ma (2σ, *n* = 309) in agreement with the recommended age of 1062.4 ± 0.4 Ma (Wiedenbeck et al., 1995).

The effective U-Pb ages were $^{206}Pb/^{238}U$ ages for zircons grains with ages ≤1.5 Ga and $^{207}Pb/^{206}Pb$ ages for grains with ages >1.5 Ga (Spencer et al., 2016). Ages with discordance degrees >10% and samples with few zircons were not considered because of their low statistical representation (Vermeesch, 2004). Detrital zircon age data are visualized and compared using kernel density estimation (KDE) diagrams (Vermeesch, 2013).

To investigate the difference between detrital zircon U-Pb age distributions, we implemented the non-matrix metric multi-dimensional scaling (MDS) statistical technique (Vermeesch, 2013). The MDS is a “superset of principal component analysis” that, given a table of pairwise ‘dissimilarities’ between samples, produces a ‘map’ of points on which ‘similar’ samples cluster closely together, and ‘dissimilar’ samples plot far apart (Vermeesch, 2018). Following the latest recommendations by (Vermeesch, 2018), we use the Kolmogorov–Smirnov test to produce an MDS map comparing analyzed samples.

References

Albarède, F., & Brouxel, M. (1987). The Sm/Nd secular evolution of the continental crust and the depleted mantle. *Earth and Planetary Science Letters*, *82*(1–2), 25–35. https://doi.org/10.1016/0012-821X(87)90104-X

Augustsson, C., & Bahlburg, H. (2008). Provenance of late Palaeozoic metasediments of the Patagonian proto-Pacific margin (southernmost Chile and Argentina). *International Journal of Earth Sciences*, *97*(1), 71–88. https://doi.org/10.1007/s00531-006-0158-7

Bühn, B., Pimentel, M. M., Matteini, M., & Dantas, E. L. (2009). High spatial resolution analysis of Pb and U isotopes for geochronology by laser ablation multi-collector inductively coupled plasma mass spectrometry (LA-MC-ICP-MS). *Anais Da Academia Brasileira de Ciências*, *81*(1), 99–114. https://doi.org/10.1590/S0001-37652009000100011

Carignan, J., Hild, P., Mevelle, G., Morel, J., & Yeghicheyan, D. (2001). Routine Analyses of Trace Elements in Geological Samples using Flow Injection and Low Pressure On-Line Liquid Chromatography Coupled to ICP-MS: A Study of Geochemical Reference Materials BR, DR-N, UB-N, AN-G and GH. *Geostandards and Geoanalytical Research*, *25*(2–3), 187–198. https://doi.org/10.1111/j.1751-908X.2001.tb00595.x

DePaolo, D. J., Linn, A. M., & Schubert, G. (1991). The continental crustal age distribution: Methods of determining mantle separation ages from Sm-Nd isotopic data and application to the southwestern United States. *Journal of Geophysical Research*, *96*(B2), 2071. https://doi.org/10.1029/90JB02219

DePaolo, Donald J. (1981). Trace element and isotopic effects of combined wallrock assimilation and fractional crystallization. *Earth and Planetary Science Letters*, *53*(2), 189–202. https://doi.org/10.1016/0012-821X(81)90153-9

Goia, S. M. C. L., & Pimentel, M. M. (2000). The Sm-Nd isotopic method in the geochronology laboratory of the University of Brasília. *Anais Da Academia Brasileira de Ciências*, *72*(2), 219–245. https://doi.org/10.1590/S0001-37652000000200009

Goldstein, S. L., O'Nions, R. K., & Hamilton, P. J. (1984). A Sm-Nd isotopic study of atmospheric dusts and particulates from major river systems. *Earth and Planetary Science Letters*, *70*(2), 221–236. https://doi.org/10.1016/0012-821X(84)90007-4

Jackson, S. E., Pearson, N. J., Griffin, W. L., & Belousova, E. A. (2004). The application of laser ablation-inductively coupled plasma-mass spectrometry to in situ U–Pb zircon geochronology. *Chemical Geology*, *211*(1–2), 47–69. https://doi.org/10.1016/j.chemgeo.2004.06.017

Jacobsen, S. B., & Wasserburg, G. J. (1980). Sm-Nd isotopic evolution of chondrites. *Earth and Planetary Science Letters*, *50*(1), 139–155. https://doi.org/10.1016/0012-821X(80)90125-9

Paton, C., Hellstrom, J., Paul, B., Woodhead, J., & Hergt, J. (2011). Iolite: Freeware for the visualisation and processing of mass spectrometric data. *Journal of Analytical Atomic Spectrometry*, *26*(12), 2508. https://doi.org/10.1039/c1ja10172b

Petrus, J. A., & Kamber, B. S. (2012). VizualAge: A Novel Approach to Laser Ablation ICP-MS U-Pb Geochronology Data Reduction. *Geostandards and Geoanalytical Research*, *36*(3), 247–270. https://doi.org/10.1111/j.1751-908X.2012.00158.x

Spencer, C. J., Kirkland, C. L., & Taylor, R. J. M. (2016). Strategies towards statistically robust interpretations of in situ U–Pb zircon geochronology. *Geoscience Frontiers*, *7*(4), 581–589. https://doi.org/10.1016/j.gsf.2015.11.006

Vermeesch, P. (2004). How many grains are needed for a provenance study? *Earth and Planetary Science Letters*, *224*(3–4), 441–451. https://doi.org/10.1016/j.epsl.2004.05.037

Vermeesch, P. (2013). Multi-sample comparison of detrital age distributions. *Chemical Geology*, *341*, 140–146. https://doi.org/10.1016/j.chemgeo.2013.01.010

Vermeesch, P. (2018). Dissimilarity measures in detrital geochronology. *Earth-Science Reviews*, *178*, 310–321. https://doi.org/10.1016/j.earscirev.2017.11.027

Wiedenbeck, M., Allé, P., Corfu, F., Griffin, W. L., Meier, M., Oberli, F., et al. (1995). Three Natura Zircon Standards for U-Th-Pb, Lu-Hf, Trace Element and REE Analyses. *Geostandards Newsletter*, *19*(1), 1–23.

CAPÍTULO 5

DISCUSSÃO

DISCUSSION

5 5. DISCUSSÃO/ DISCUSSION

Ce chapitre présente la discussion sur la paléogéographie de la partie nord de la Plateforme Sud-Américaine pendent le Crétacé. L'intégration des résultats des chapitres 3 et 4 associée à une revue de la littérature a permis de proposer une reconstitution paléogéographique de l'évolution mesozoïque de la partie nord de l'Amérique du Sud par pas de temps. Nous proposons ainsi quatre cartes paléogéographiques :

- La période du Jurassique au Néocomien (~152 à 121 Ma) montre le début et l'apogée du rifting des bassins intérieurs du Nord-Est du Brésil, reflétant l'ouverture de l'océan Atlantique Sud. La situation dans la partie occidentale de l'Amazonie reste peu contrainte ;
- L'intervalle entre l'Aptien et l'Albien (120 -113 Ma) se caractérise par les stades post-rift, la présence d'incursions marines peu profondes et la dernière rupture continentale. Dans ce stade aussi, la configuration de l'Amazonie occidentale reste peu contrainte ;
- La période de l'Albien au Cénomanien (113 - 101 Ma) montre une réorganisation du drainage dans la partie occidentale de la plateforme et la présence de sources locales dans la partie orientale en relation a la géodynamique post rift de l'ouvertures des océans atlantiques sud et équatorial système ;
- La période fini crétacée (Turonien - Maastrichtien, 89 - 66 Ma) est marquée par l'acmée du paléodrainage intracontinental « Sanozama » et les effets de l'ouverture de l'océan Equatorial sur les bassins intracontinentaux.

5.1 Paleogeografia da Plataforma Sul Americana Setentrional durante o Cretáceo

Durante a segunda metade do século XX modelos paleogeográficos globais foram desenvolvidos tendo por base a teoria de tectônica de placas (Barron 1987). Mapas base sobre a paleogeografia do Cretáceo foram produzidos com dados oceânicos e continentais provenientes de estudos geológicos e geofísicos. Modelos mundiais foram propostos (e. g. (Scotese *et al.* 1988a, b; Scotese 1991) com o objetivo de entender a configuração geométrica, tectônica e paleoclimática de várias regiões ao longo do período Cretáceo. Mapas paleogeográficos regionais da América do Sul (Machado Junior *et al.* 1990; Assine 1994), ainda carecem de informações que permitam uma reconstrução mais robusta da paleogeografia na Plataforma Sul Americana durante o Cretáceo. Nesta tese, apresentamos uma contribuição para a reconstrução paleogeográfica da parte norte da América do Sul durante o Cretáceo tendo por base dados de proveniência de sedimentos obtidos em bacias intracratônicas do nordeste do Brasil durante o Cretáceo Inferior (145 – 100 Ma); e da região Andes-Amazônia durante o Cretáceo Superior (100 – 66 Ma).

A evolução geodinâmica da parte setentrional da América do Sul pode ser demonstrada por meio de quatro cenários paleogeográficos:

- Período que compreende o Jurássico - Neocomian (~152 a 121 Ma) – Estágio de início e clímax do rifteamento de bacias interiores do nordeste brasileiro, reflexo da abertura do Oceano Atlântico Sul;
- Intervalo entre o Aptiano – Albiano (120 -113 Ma) – Estagio pós rifte - as incursões marinhas e última ruptura continental;
- Do Albiano - Cenomaniano (113 – 94 Ma) – Reorganização da drenagem na parte oeste da plataforma, sistema Amazônia – Andes;

- Fim do Cretáceo (Turoniano – Maastrichtiano, 94 – 66 Ma) - Clímax da drenagem intercontinental Sanozama e efeitos da Abertura do Oceano Equatorial nas bacias intracontinentais.

5.2 Cretáceo inferior: Fragmentação do Gondwana e as deposições durante o Neocomiano, Aptiano e Albiano.

O ciclo geodinâmico conhecido como Ciclo de Wilson (Wilson, 1968) foi responsável pelo desmembramento e aglutinação dos continentes. Tal processo foi responsável pela formação de crosta juvenil, de montanhas, de bacias sedimentares e depósitos minerais (Wilson 1969). Este complexo ciclo se repete ao longo do tempo geológico e está registrado em diferentes rochas desde aproximadamente 3 bilhões de anos (Bleeker 2003; Van Kranendonk *et al.* 2010; Shirey and Richardson 2011). A fragmentação do Gondwana é um exemplo deste processo e preserva os registros geodinâmicos nos estratos sedimentares.

Dentre as bacias cretáceas, as localizadas no nordeste brasileiro registram diferentes estágios geodinâmicos relacionados à ruptura do supercontinente Pangea e à formação do Oceano Atlântico (Sul e Equatorial). Tentativas de reconstruções paleogeográficas da parte setentrional da Plataforma Sul Americana foram apresentadas por (Petri 1987; Machado Junior *et al.* 1990; Assine 1994). Todos identificaram a presença de magmatismo, rifteamento e incursões marinhas em diferentes episódios geotectônicos que possibilitaram a deposição de sedimentos nas bacias do Nordeste (Figura 44). Como exposto no capítulo 3, a proveniência dos sedimentos da bacia do Araripe fornece informações sobre a configuração tectônica da Plataforma Sul Americana durante o Neocomiano ao Albiano-Cenomaniano.

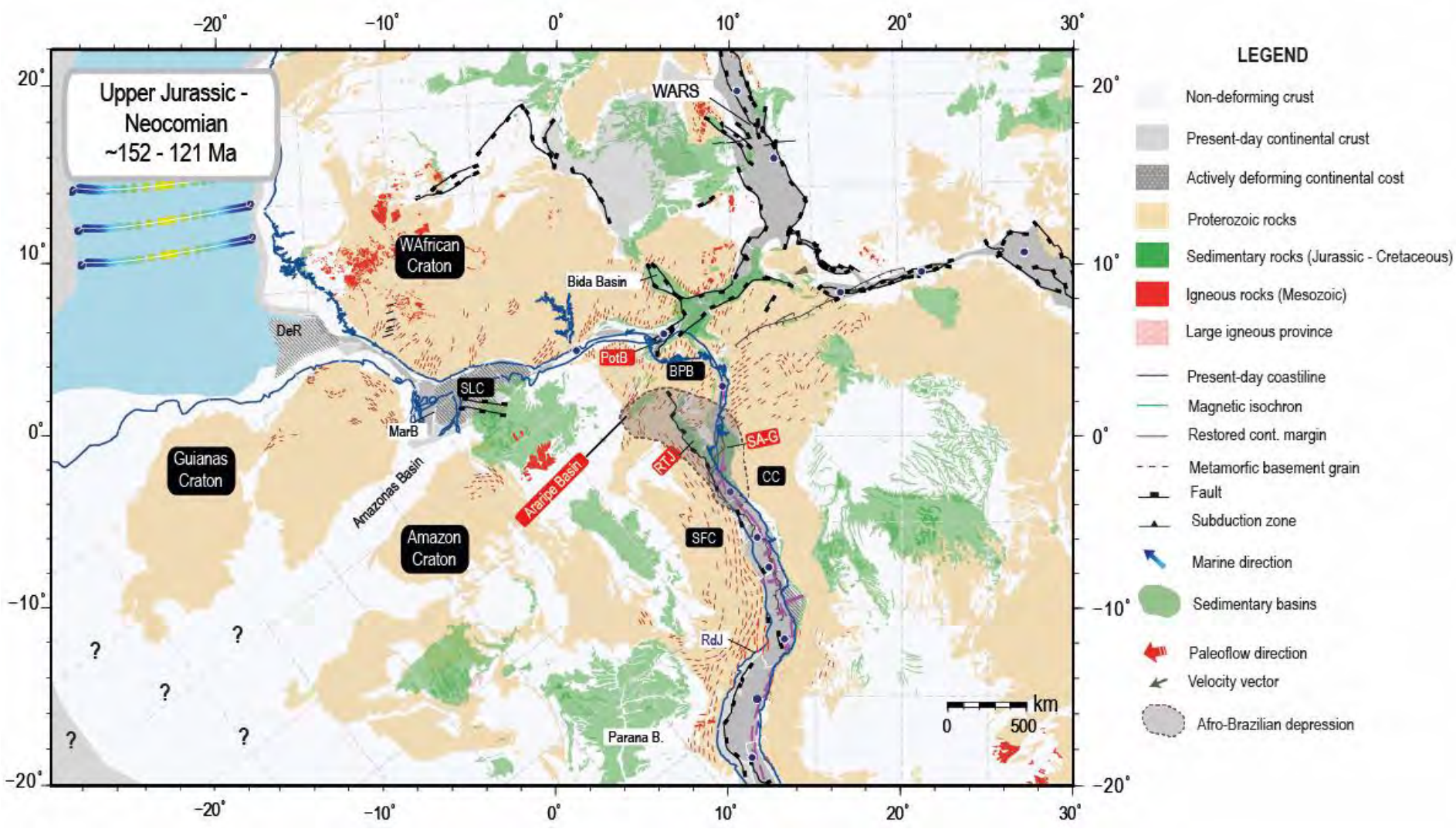

Figura 44 :Reconstrução paleogeográfica proposta para o início do riftiamento entre a América do sul e a África (Jurássico Superior-Neocomiano), baseada no modelo cinemático de Heine et al (2013) e nos dados discutidos ao longo do texto. SLC: Craton São Luís; SFC: Craton São Francisco, CC: Craton do Congo; BPB: Província Borborema; DeR: Plataforma Demerara; MarB: Bacia do Marajó; PotB: Bacia Potiguar; RTJ: Bacia Recôncavo-Tucano-Jatobá; SA-G: Bacia Sergipe-Alagoas-Gabon.

A bacia do Araripe começa seu processo de deposição durante o Ordoviciano (aproximadamente 460 Ma) com a Formação Cariri (Assine 1992; Ponte and Ponte Filho 1996; Fambrini *et al.* 2020). Essa unidade é correlata com o Grupo Serra Grande (Bacia do Parnaíba) e a Formação Tacaratu (Bacia Tucano e Jatobá) (Caputo and Crowell 1985). O processo de ruptura do Gondwana durante o período Juro-Cretáceo reativou estruturas Neoproterozóicas na região nordeste do Brasil e consequentemente, o desenvolvimento de sistema de rifts intracontinentais, controlados pelas estruturas reliquiares das províncias Borborema e Banin-Nigeria (Assine 1994; Matos 1999; Torsvik *et al.* 2009; Heine *et al.* 2013; Matos *et al.* 2021). Entre 152 – 139 Ma (Juro-Neocomiano) houve o estiramento litosférico na região e iniciou-se o estágio *rift* (Assine 2007; Kuchle *et al.* 2011; Scherer *et al.* 2014). Uma grande área depressiva se forma na região Nordeste brasileira e sudoeste africana, acentuando-se os reflexos da fragmentação de Gondwana (Assine 2007; Kuchle *et al.* 2011; Scherer *et al.* 2014).

A depressão Afro-Brasileira (Garcia and Wilbert 1995; Kuchle *et al.* 2011) é formada pelas deposições do Andar Dom João no Brasil (Schaller 1969) e pela Formação N'Dombo na Bacia do Gabon (África) (Mbina Mounguengui *et al.* 2008) (Figura 44). No final do Jurássico e início do Cretáceo, sedimentos lacustres marcam o maior período de inundação (Lago Capianga), sendo observados desde a Bacia do Gabon até a Bacia do Araripe (Figura 44) (Kuchle *et al.* 2011). As paleocorrentes nos depósitos fluviais indicam padrões de drenagem à sudoeste na Bacia do Gabon (Mbina Mounguengui *et al.* 2002, 2008); para sul nas bacias de Sergipe e Alagoas (Kuchle *et al.* 2011); para sudeste na Bacia do Araripe (Assine 2007; Scherer *et al.* 2014; Fambrini *et al.* 2020; Godot Souza *et al.* 2022), e para noroeste nas bacias Almada, Camamu, Recôncavo e Tucano (Kuchle *et al.* 2011). Altos estruturais internos

marcam a reorganização das drenagens no Neocomiano e a reconfiguração das direções de paleofluxo para nordeste nas Bacias Recôncavo e Tucano (Kuchle *et al.* 2011); para oeste na Bacia do Araripe (Scherer *et al.* 2014; Fambrini *et al.* 2020), para nordeste na Bacia Almada e para sudeste nas bacias Sergipe, Alagoas e Gabon (Mbina Mounguengui *et al.* 2002, 2008; Kuchle *et al.* 2011) (Figura 44). Este momento está relacionado ao estágio de *rift* inicial (Matos 1992), no qual começam a se depositar os sedimentos da Formação Abaiara na Bacia do Araripe, discutido no capítulo 3. A deposição dessas rochas marca a separação das bacias da chamada Depressão Afro-Brasileira e iniciam a individualização das bacias brasileiras e africanas.

Estruturas de meio graben se formam no continente, como reflexo dos primeiros processos de rifteamento do Atlântico Sul (*Rift valley* Neocomiano) (Matos 1992; Kuchle *et al.* 2011). Grandes zonas de cisalhamento são reativadas e três rifts-trends são instalados: Gabon-Sergipe Alagoas (GSA); Recôncavo-Tucano-Jatobá (RTJ) e Carriri-Potiguar (CP) (Matos 1992). Na bacia Gabon é possível identificar uma seção *rift* completa com idades que vão desde o Neocomiano até o Barremiano (145 – 120 Ma) (Teisserenc and Villemin 1990; Mbina Mounguengui *et al.* 2008). Por sua vez, na margem brasileira é possível notar uma seção Aptiana (120 - 113 Ma) (com sal) e uma Albiana-Eocenica (113 - 33 Ma) (Matos 1999). A separação entre os *rifts* GSA e RTJ foi controlada pelo rígido embasamento dos cratons São Francisco-Congo e pela zona de cisalhamento Pernambuco – Ngaoundere. As variações cinemáticas regionais fizeram com que a evolução do RTJ tivesse dois estágios, o primeiro de rifiteamento leste-oeste (Barremiano) e o segundo noroeste-sudeste (final do Barremiano, início do Aptiano) (Magnavita *et al.* 1994; Matos 1999). No CP, as zonas falha, o arranjo estrutural das sequências supracrustais (cinturões internos da

Província Borborema), e a heterogeneidade dos terrenos Proterozoicos controlaram a deposição das bacias Rio do Peixe, Iguatu e a fase *rift* da Bacia do Araripe (Matos 1999; Castro *et al.* 2007, 2008; Nogueira *et al.* 2015). Na Bacia do Araripe, as fontes sedimentares indicam áreas soerguidas a leste (capítulo 3), reflexo da ruptura continental e do processo de formação de grabens durante a abertura do Atlântico Sul. Na bacia Potiguar a deposição nesta fase ocorreu sobre estruturas de falhas pré-existentes, relíquias da orogenia Brasiliano-Pan Africana (Matos 1992, 1999). A sedimentação da CP é interrompida no início do processo de ruptura do setor Equatorial (Barremiano superior, ~124Ma) (Matos 1999).

5.2.1 Incursões Marinhas no nordeste brasileiro

A separação entre a América do Sul e a África iniciou-se entre o fim do Barremiano superior e o início do Aptiano (Moulin *et al.* 2010) culminando com a formação do Oceano Atlântico Sul (Heilbron *et al.* 2000; Moulin *et al.* 2010; Chaboureau *et al.* 2013). A abertura desse oceano, que foi controlada inicialmente pelas Zona de Fratura Ascension e Zona de Fratura Agulhas-Falkland (Chaboureau *et al.* 2013; Kukla *et al.* 2018; Cui *et al.* 2023), pode ser separado em 4 segmentos: Equatorial, Central; Austral e Falkland (Moulin *et al.* 2010). O Oceano Atlântico Equatorial teve sua história de formação relacionada ao movimento de margens transformantes ancoradas pelos terrenos Proterozoicos do Craton do Oeste Africano e Craton São Luis, iniciados entre 126-123 Ma (Matos *et al.* 2017, 2021), mas sua constituição propriamente dita, deu-se entre o Albiano-Cenomaniano (113 - 100 Ma) (Matos *et al.* 2021).

Incursões marinhas foram documentadas nas bacias intracontinentais durante o Aptiano (Arai 2014; Assine *et al.* 2014; Custódio *et al.* 2017; Fauth *et al.* 2023).

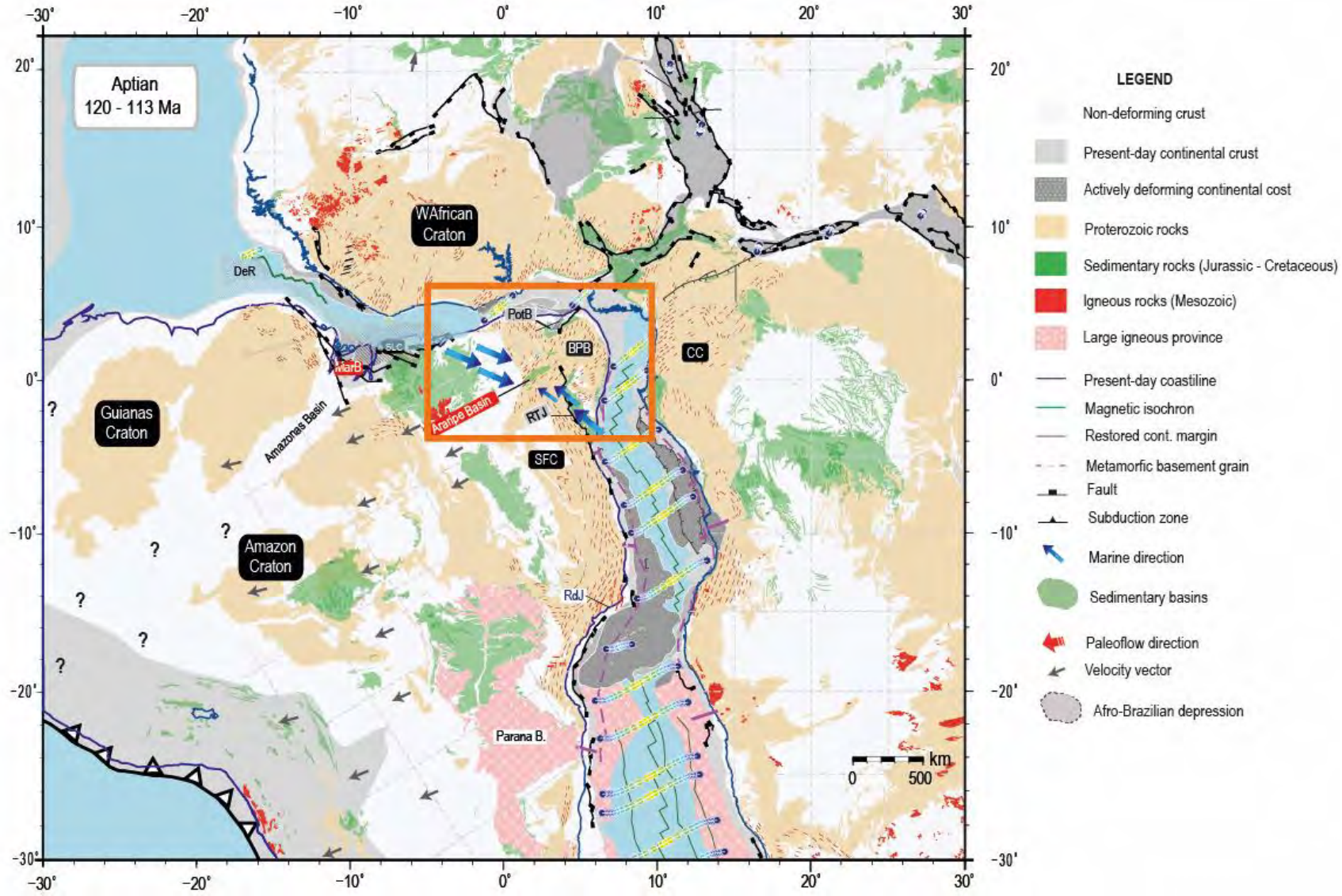

Figura 45 : Reconstrução paleogeográfica proposta para Aptiano, baseada no modelo cinemático de Heine et al (2013) e nos dados discutidos ao longo do texto. SLC: Craton São Luís; SFC: Craton São Francisco, CC: Craton do Congo; BPB: Província Borborema; DeR: Plataforma Demerara; MarB: Bacia do Marajó; PotB: Bacia Potiguar; RTJ: Bacia Recôncavo-Tucano-Jatobá. O retângulo laranja representa as reconstruções paleogeográficas discutidas no capítulo 3 e as setas em azul correspondem as hipóteses da direção de incursão marina discutidas no texto.

Como discutido em vários trabalhos, durante a fase pós-rift I, ingressões marinhas se estenderam por toda região nordeste da Plataforma Sul Americana, inclusive para a Bacia do Araripe (Assine 2007; Arai 2016; Assine *et al.* 2016; Custódio *et al.* 2017; Arai and Assine 2020). No entanto, o caminho dessas ingressões e a conexão com o oceano cretáceo são objetos de discussões. Alguns estudos paleontológicos (Arai 2014, 2016), apontam uma relação com as águas do Mar Tethys. Por outro lado, outros autores utilizam estudos sobre a arquitetura sedimentar e estratigráfica para indicar uma transgressão marinha com conexões a sul (Assine *et al.* 2014; Custódio *et al.* 2017). Em outro estudo, Fauth *et al.* (2023) sugerem que as unidades basais da fase tectônica "Pos rift I" (Assine 2007; Fambrini *et al.* 2020) (Formação Barbalha) possuem material fóssil relacionado ao ambiente marinho. Destacam ainda que os fósseis que possuem características continentais mostram ter sofrido estresse ambiental no local onde foram depositados, marcando uma influência de salinidade fora do comum para esses ambientes e ratificando possíveis incursões de água do mar.

Outros estudos apontam hipóteses diferentes para explicar a trajetória das incursões marinhas da Bacia do Araripe: a partir da Bacia do Parnaíba, a noroeste (Lima 1978; Arai 2009, 2014); via Bacia Potiguar a nordeste (Maisey 2000; Godot Souza *et al.* 2022) ou ainda por sudoeste, via Bacia Recôncavo-Tucano-Jatobá (Assine 2007; Assine *et al.* 2016; Custódio *et al.* 2017; Rodrigues *et al.* 2020; Fauth *et al.* 2023). Baseado na distribuição e porcentagens de idades U-Pb dos zircões detríticos analisados neste trabalho (Capítulo 3), não se pode determinar a paleogeografia da rota marítima existente na Bacia do Araripe, durante o Aptiano - Albiano. Porém, nossos dados contribuem para um melhor entendimento sobre as hipóteses existentes (Figura 45).

Observa-se que o aumento percentual de grãos Neoproterozoicos (Tab. 8, Fig. 30 no capítulo 3) na Formação Romualdo indica relevante contribuição de molasses brasilianos (e plutons) que estão localizados no Domínio Central Ceará e no Terreno Orós Jaguaribe (Figura 45). Esta evidência concorda com os dados de paleocorrentes apresentadas por Assine (1994); Assine *et al.* (2014) e Custódio *et al.* (2017). As rochas siliciclásticas da Bacia Potiguar, na sua fase pós rift, possuem fontes similares (Baesso *et al.* 2021) às das rochas sedimentares da fase pós-rift I da Bacia do Araripe, analisadas neste trabalho. No entanto, a falta de depósitos marinhos nas bacias localizadas entre a Araripe e Potiguar (Arai 2014) e a ausência de depósitos aptianos na Bacia do Rio do Peixe (Nogueira *et al.* 2015), dificultam a confirmação desta rota marítima sugerida por Godot Souza *et al.* (2022). Além disso, como sugerido por Assine (1994) e Assine *et al.* (2014), o Lineamento Patos teria funcionado como uma divisão de sistemas de drenagem entre as duas bacias.

Alimentando a discussão sobre este assunto, Kroth *et al.* (2021) indicam uma deficiência de material terrígeno na parte oeste da Bacia do Araripe durante a sedimentação da Formação Romualdo, relacionada a pouca descarga fluvial. Godot Souza *et al.* (2022) apresentam dados de paleocorrente com direção a sudoeste em estratos aluviais basais da Formação Romualdo e dados paleontológicos indicam afinidade fossilífera com organismos do Mar de Tethys (Maisey 2000; Arai 2009, 2014, 2016). Esses dados sugerem que a rota marítima teve como origem o Oceano Atlântico Equatorial ou da Bacia do Parnaíba. Sendo assim, alternativamente, a Bacia do Araripe poderia representar a junção entre duas incursões marinhas, a primeira vinda de sudeste, via bacia Tucano-Jatobá; e a segunda via noroeste (Bacia do Parnaíba).

Assine *et al.* (2014) sugerem uma divisão de drenagens entre as bacias Parnaíba e Araripe, mas ainda não existem estudos que apontam evidências sobre esta feição. Não obstante, (Heine *et al.* 2013) indicam que não há qualquer característica da influência do lineamento Transbrasiliano como barreira topográfica durante a abertura do Oceano Atlântico. A transgressão marinha que atingiu a Bacia do Araripe poderia ter vindo primeiramente da regiões mais ao sul, conforme proposto por Assine *et al.* (2016); Custódio *et al.* (2017) e Fauth *et al.* (2023). Porém durante a deposição da Formação Romualdo (Aptiano Superior), uma segunda grande incursão marinha pode ter ocorrido proveniente de noroeste, a partir da região do Crato São Luis, passando pela Bacia do Parnaíba, por terrenos da Província Borborema até chegar a Bacia do Araripe. Essa incursão marinha estaria registrada em estratos superiores da Formação Romualdo (Maisey 2000; Valença *et al.* 2003; Arai 2014) (Figura 45).

5.3 Albiano – Cenomaniano (110 – 94 Ma): Formação do Oceano Atlântico Equatorial e os reflexos geodinâmicos no Escudo do Brasil e Guianas e NW África.

No final do Albiano/início do Cenomaniano (~98 Ma), a América do Sul estava totalmente separada da África (Matos *et al.* 2021). No entanto, ajustes litosféricos e processos geodinâmicos continuaram influenciando a deposição sedimentar durante o Cenomaniano. A abertura do Oceano Equatorial promoveu a deposição de bacias sedimentares na parte Sul Americana, dividindo-se em seis sítios de deposição de oeste para leste: Guiana-Suriname; Foz do Amazonas, Pará-Maranhão, Barreirinhas, Ceará e Potiguar. Essas bacias são limitadas pelas zonas de fraturas do oceano Atlântico Equatorial e apresentam múltiplas fases de subsidência e estilos estruturais (Mohriak 2003; Condé *et al.* 2007; Figueiredo *et al.* 2007; Trosdtorf Junior *et al.* 2007; Mohriak *et al.* 2013; Jovane *et al.* 2016; Roddaz *et al.* 2021; Rouby *et al.* 2023). Em

direção oposta, a margem Equatorial Africana consiste numa série de bacias localizadas no Golfo da Guine denominadas de oeste para leste como Sierra Leone-Liberia; Côte-D'Ivoire – Ghana; Togo-Benin-oeste Nigéria; e Benue - Niger Delta, onde zonas de fraturas influenciam a cinemática da região (Matos 2000; Basile *et al.* 2005).

O sistema de rifteamento do Atlântico Equatorial se desenvolveu no Cretáceo Inferior (ca 130-103 Ma) a partir da acreção da primeira crosta oceânica (Basile *et al.* 2005; Figueiredo *et al.* 2007; Zalán and Matsuda 2007). O início da acreção de crosta oceânica é correlata à uma inconformidade observada na Bacia de Côte D'Ivoire (Basile *et al.* 2005) e na Bacia Ceará (Condé *et al.* 2007). A primeira influência marinha que ocorreu nesta área se deu no fim do Aptiano (113 Ma) (Maisey 2000), porém a conexão entre o Atlântico Sul e Central somente ocorreu entre o fim do Albiano e o início do Cenomaniano (100 Ma) (Pletsch *et al.* 2001). O estresse litosférico durante a abertura Equatorial não se deu de forma homogênea, uma vez que segmentos dominados por *rift* e segmentos dominados por movimentos transformantes são identificados ao longo de toda costa equatorial sul americana (Greenroyd *et al.* 2008) e similarmente nas costas do oeste africano (Antobreh *et al.* 2009). A interação entre processos tectônicos e oceânicos fez com que as deposições sedimentares sofressem drásticas mudanças de fácies e de taxas de subsidência. A Margem Transformante da Côte d'Ivoire – Ghana é um exemplo de história deposicional que reflete os estágios de evolução tectônica do Atlântico Equatorial. (Pletsch *et al.* 2001) apontam que este sistema expõe três fases de sedimentação que começa com a fragmentação e deriva continental e a deposição de estratos marinhos no Albiano, passando para o estágio de diferenciação e forte divergência entre as margens (Americana e Africana) e subsidência assíncrona entre as regiões norte e sul do sistema. A evidência de xistos betuminosos com biofácies bentônicas mostram

condições de baixa oxigenação após a conexão entre a parte marinha central e sul (Cenomaniano-Turoniano, ca. 100-89 Ma). O último estágio deste sistema inicia-se no Coniaciano (89 Ma), quando o sistema passa a ser de margem passiva (Pletsch *et al.* 2001). Como exemplo sul americano, a Bacia da Foz do Amazonas, localizada no extremo norte da margem equatorial brasileira, teve a abertura do Oceano Atlântico Equatorial como principal propulsora de sedimentos (Zalán 2004; Soares-Júnior *et al.* 2008). A Formação Calçoene relaciona-se aos primeiros pulsos siliciclásticos deposicionados na fase pré-*rift* da bacia. A Formação Cassiporé teve sua deposição ligada a abertura do Oceano Atlântico Equatorial Sul, por meio de movimentos transformantes *syn rift* (Matos 2000; Zalán 2004; Figueiredo *et al.* 2007; Soares-Júnior *et al.* 2008) e a Formação Limoeiro representa a fase pós movimentos transformantes, iniciada no Cenomaniano (100 Ma) (Brandão and Feijó 1994; Milani and Thomaz-Filho 2000; Figueiredo *et al.* 2007; Soares-Júnior *et al.* 2008).

Processos de denudação, erosão e reativação de estruturas pré cambrianas e paleozóicas são relatadas em diferentes estudos e se relacionam com o desenvolvimento das bacias sedimentares, tanto da margem equatorial, quanto no interior dos continentes durante o Cretáceo Superior (Potter 1997; Harman *et al.* 1998; Caputo and Soares 2016; Sapin *et al.* 2016; Hurtado *et al.* 2018; Loparev *et al.* 2021; Roddaz *et al.* 2021; Rodrigues *et al.* 2023; Rouby *et al.* 2023). No capítulo 4, discutimos e apontamos que estimativas de taxas de denudação feitas por meio de traço de fissão em apatitas mostram que entre o Albiano e Cenomaniano houve uma importante fase de reativação tectônica (Harman *et al.* 1998), que elevou e erodiu regiões do Escudo Brasil Central e Guianas (Sapin *et al.* 2016; Monteiro *et al.* 2018). A reativação tectônica de terrenos reliquiares também foi responsável pelo

soerguimento de arcos estruturais, como o Arco de Purus e Gurupá (Caputo and Soares 2016) e pelo rearranjo dos sistemas de drenagem no interior dos continentes.

O Arco Gurupá está ligado ao rift Marajó, e foi formado na primeira fase de abertura do Oceano Atlântico Central (Caputo and Soares 2016) (Figura 46). Ele funcionou como um divisor de águas entre a Bacia do Marajó e Amazonas, até a separação dessas bacias (Cretáceo Inferior) (Zalán and Matsuda 2007). O soerguimento desse arco trouxe uma área erosiva que funcionou como fonte para sedimentação de bacias a oeste do seu posicionamento (Caputo and Soares 2016). O Arco de Purus é uma área soerguida com direção N-S que separa a Bacia do Amazonas e Solimões (Costa *et al.* 2001; Caputo and Soares 2016) (Figura 46). Durante a orogenia Juruá (157 - 152 Ma) (Caputo 2014), o arco serviu como refrator de esforços cisalhantes (Munis 2009) e como discutido no capitulo 4, ele foi soerguido durante o Cretáceo, funcionando como uma possível barreira paleogeográfica e área fonte de sedimentos para as bacias da Amazônia Ocidental (Rodrigues *et al.* 2023).

As similaridades entre a deposição das bacias ao longo da margem equatorial e no oeste amazônico refletem as mudanças geodinâmicas ocorridas no Escudo Brasil Central e Guianas e nos terrenos neoproterozoicos ligados ao ciclo Basiliano-Pan-Africano durante o Albiano-Turoniano. (Figueiredo *et al.* 2007; Zalán and Matsuda 2007) indicam que durante o Cretáceo, a deposição da Bacia Marajó, continuou lateralmente com a Bacia Parnaíba, mostrando equivalentes estratos sedimentares (Formação Codó, Itapecuru, Ipixuna, Pirabas, Barreiras e Pós-Barreiras). Amostras da Formação Ipixuna, localizada na parte leste da Bacia Marajó, apresentam fontes marcantes com idades Paleoproterozóicas (1.8 - 2.2 Ga), que estariam ligadas aos terrenos do Craton Amazônico (Ventuari – Tapajós e Maroni-Itacaiúnas) (Moizinho *et al.* 2022). (Erlich *et al.* 2018) discutem as fontes dos sedimentos de bacias sub andinas

durante o Cretáceo e apontam que na transição entre o Albiano e o Cenomaniano (107-94 Ma) as fontes das bacias de Marañon e Ucayali (Figura 46) possuíam relevante influência de fontes de cratônicas (1.8 – 1.5 Ga) (Rio Negro-Juruena). (Gutiérrez *et al.* 2019) encontraram padrão detrítico semelhante (1.7 – 1.5 Ga) na Formação Hollin (Cretáceo Inferior) localizada na Bacia Oriente. Tais semelhanças corroboram com o início do soerguimento flexural crustal durante a abertura do Atlântico Equatorial, bem como dos arcos estruturais discutidos acima. Outro ponto importante sobre este momento de deposição (Albiano – Turoniano), seria entender a influência dos terrenos Neoproterozoicos como áreas fonte de sedimentos para as bacias da margem equatorial e da Amazônia Ocidental. Grãos detríticos da Bacia do Araripe levam a assinatura do Evento Brasiliano – Pan-Africano desde a fonte até a deposição (Capítulo 3). O mesmo pode ser observado nos grãos analisados na Formação Ipixuna (Moizinho *et al.* 2022), naqueles dos depósitos Albianos da Bacia São Luís-Grajaú (Nascimento *et al.* 2007) e na Bacia Potiguar (Baesso *et al.* 2021). Populações com idades entre 0.7 – 0.5 Ga também são representativas na plataforma Demerara, Bacia Guiana-Suriname (Girault *et al.* 2023). Nas bacias amazônicas, tais fontes são marcantes durante este período e são indicadas na Bacia Oriente (Gutiérrez *et al.* 2019); Ucayali (Erlich *et al.* 2018), Cordilheira leste (George *et al.* 2019), Baguá (Moreno *et al.* 2020), Huallaga (Hurtado *et al.* 2018) e Madre de Dios (Louterbach 2014; Rodrigues *et al.* 2023). Fontes com estas idades estão presentes na Província Borborema e no Cinturão orogênico Paraguai-Araguaia, na borda no Craton Amazônico. Para as bacias localizadas no nordeste brasileiro e na margem equatorial, fontes Brasilianas são mais proximais. No entanto, as fontes que conduziram sedimentos para as bacias da Amazônia Ocidental ainda são incertas.

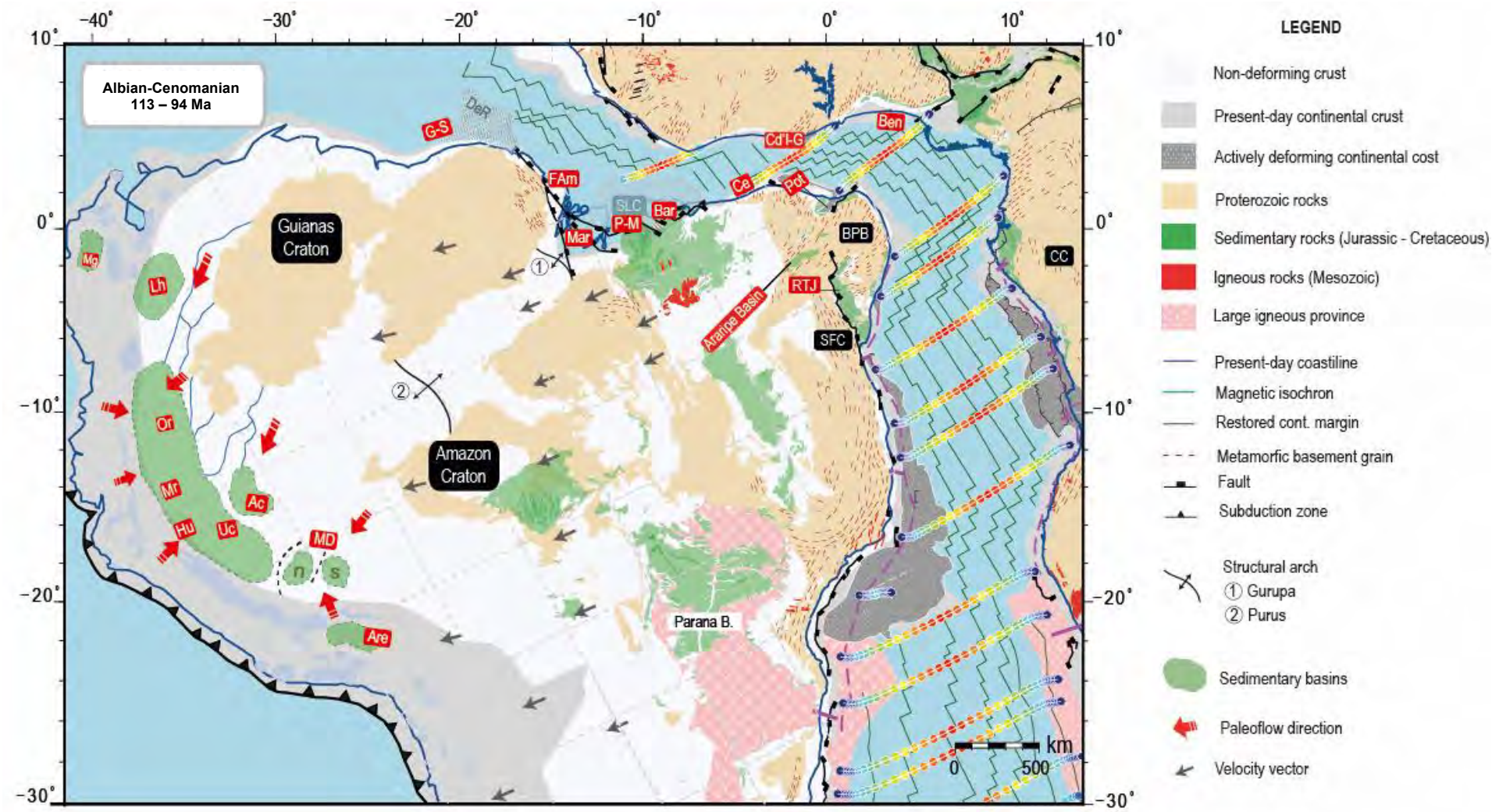

Figura 46 : Reconstrução paleogeográfica proposta para o Albiano-Cenomaniano, baseada no modelo cinemático de Heine et al (2013) e nos dados discutidos ao longo do texto. SLC: Craton São Luís; SFC: Craton São Francisco, CC: Craton do Congo; BPB: Província Borborema; DeR: Plataforma Demerara; Mar: Bacia do Marajó; Pot: Bacia Potiguar; RTJ: Bacia Recôncavo-Tucano-Jatobá; Ben: Bacia do Benin; Cd'I-G: Bacia de Côte d'Ivoire – Gana; G-S: Bacia Guianas-Suriname; FAm: Bacia Foz do Amazonas; P-M: Bacia Parnaíba-Maranhão; Bar: Bacia Barreiras; Ce: Bacia do Ceará; Mg: Bacia Madaglena; Lh: Bacia Lhanos; Or: Bacia Oriente; Mr: Bacia Marañon; Hu: Bacia Huallaga; Uc: Bacia Ucayali; Ac: Bacia do Acre; MD: Bacia de Madre de Dios (n-norte, s-sul); Are: Bacia de Arequipa.

5.4 Turoniano – Maastrichtiano (94 – 66 Ma): Clímax da drenagem intercontinental e as deposições na Amazônia Ocidental.

Movimentos flexurais e soerguimentos terrestres ocorridos durante a abertura do Oceano Atlântico Equatorial fizeram com que houvesse uma reorganização no sistema de drenagens de toda a parte norte da América do Sul. As bacias localizadas na Amazônia ocidental, por exemplo, indicam diferenças de fontes e fluxos hídricos desde o Albiano até o início do Paleoceno (Erlich *et al.* 2018; Hurtado *et al.* 2018; George *et al.* 2019; Gutiérrez *et al.* 2019). Os rios são sensíveis às mudanças tectônicas e a processos de deformação (Holbrook and Schumm 1999) e os dados analisados na bacia do Acre e Madre de Dios mostram diferenças nas fontes dos sedimentos que refletem padrões distintos de sistemas fluviais durante o Cretáceo Superior (Capítulo 4). Além disso, na margem equatorial os sistemas de drenagem apontam para uma fonte predominantemente cratônica oriunda do soerguimento crustal e da denudação dessa área (Harman *et al.* 1998; Roddaz *et al.* 2021; Fellin *et al.* 2023).

Sobre os aportes sedimentares das bacias da Amazônia Ocidental, nota-se que as fontes que alimentam a parte sul da bacia de Madre de Dios possuem uma proveniência diferente quando comparadas com a parte norte, que somente cessa no final do Cretáceo (Maastrichtiano). Discutimos no capitulo 4 que a parte mais ao norte da bacia possui uma história deposicional mais ligada às Bacias Huallaga, Santiago e Bagua, enquanto a parte mais ao sul possuía fontes mais regionais. Tal diferença poderia ter sido causa por uma barreira topográfica, que possivelmente separou a bacia durante o Cretáceo Superior. Altos topográficos relacionados a reativação de estruturas do embasamento também foram sugeridos por De Oliveira and Vidotti (2023) para a subdivisão da Bacia do Acre. A área denominada como Sub-bacia Divisor (De Oliveira and Vidotti 2023), parte ao norte da Bacia do Acre, é a mesma

analisada neste trabalho, e mostra, similaridades de características geofísicas do embasamento com o sistema sedimentar das bacias andinas (Marañon, Ucayali, Huallaga, bem como com a parte norte da bacia de Madre de Dios (Figura 47). No mesmo sentido, o estudo de proveniência dos grãos detríticos apontou áreas fontes comuns entre essas bacias durante a deposição no Cretáceo Superior. É importante destacar que mais estudos sobre proveniência sedimentar precisam ser feitos na sub-bacia do Acre, denominada Xapuri (De Oliveira and Vidotti 2023), para entender quais as fontes influenciaram a deposição naquela região, bem como qual o tamanho e a influência das estruturas do embasamento na deposição sedimentar deste período. Ressalta-se também uma menor influência de fontes andinas durante a deposição sedimentar da bacia de Madre de Dios e do Acre, fato que corrobora com a hipótese de que os escudo das Guianas e do Brasil Central estariam mais elevados.

Estudos realizados nas regiões leste do Escudo das Guianas e Brasil Central e na região nordeste brasileira mostraram que elas estiveram elevadas durante o final do Cretáceo (Potter 1997; Harman *et al.* 1998; Morais Neto *et al.* 2009; Japsen *et al.* 2012; Caputo and Soares 2016; Vallejo *et al.* 2017; Monteiro *et al.* 2018; Sacek *et al.* 2019; Roddaz *et al.* 2021; Rouby *et al.* 2023). Harman *et al.* (1998) indicaram taxas de denudação de 3 a 7 km nas margens norte do Craton São Francisco e no Escudo Brasil Central. Esta taxa, relacionada a dados de traços de fissão em apatitas, demonstram que este evento coincide com a mudança relativa no movimento de placas tectônicas ocorrido no final do Cretáceo (~80 – 60Ma) (Harman *et al.* 1998). Rouby *et al.* (2023) apontam que o volume de sedimentos siliciclásticos depositados na Bacia da Guiana-Suriname e na Foz do Amazonas durante o Cretáceo Superior estão ligados à reorganização de drenagens na região cratônica. Os volumes de sedimentos clásticos acumulados na Bacia da Guiana-Suriname decrescem durante

o Cretáceo Superior (de ~2,7 para ~1,6 × 105 km^3) (Rouby *et al.* 2023). Pode ser que a elevação cratônica tenha alimentado com mais sedimentos a paleorede de drenagens “Sanozama” que o sistema de drenagens Guiana-Suriname (Figura 47), levando mais volume de sedimentos para as bacias da Amazônia Ocidental (Acre e Madre de Dios), discutidas no capítulo 4. Embora não haja um consenso entre quais e como os altos estruturais delimitaram a deposição das bacias entre o Cenomaniano e o Coniaciano, pode-se dizer que houve um grande aporte sedimentar proveniente de um sistema hídrico comum para as bacias da Amazonia Ocidental (exceto Madre de Dios sul) e para a sub-bacia Divisor, na Bacia do Acre.

A região nordeste brasileira passou por períodos de soterramento intenso após a ruptura do Gondwana e abertura do Atlântico Equatorial. Porém, durante o Cretáceo Superior a região passou por fases de soerguimento e denudação até o processo de peneplanação, ocorrido no Eoceno-Oligoceno (Japsen *et al.* 2012). Tais eventos estariam ligados à uma diminuição da taxa de propagação da Dorsal Meso - Atlântica e o crescimento do orógeno Andino (Japsen *et al.* 2012). Morais Neto *et al.* (2009) atribuíram o processo de exumação da Província Borborema, durante o Cretáceo Superior, à um evento termo - isostático ocorrido entre o Cenomaniano e o Turoniano (100 – 90 Ma), reflexo da ascensão anterior de plumas mantélicas (magmatismo Santa Helena (?). Para Sacek *et al.* (2019) o soerguimento regional após o estágio rift teve como mecanismo o efeito combinado entre denudação diferencial do continente e recuperação flexural da litosfera (70%), além da elevação térmica induzida pela erosão parcial da base da litosfera continental embaixo da Província Borborema (30%). A presença de sedimentos marinhos do Grupo Santana da Bacia do Araripe em altitudes de 700-800m atualmente confirma a evidência de soerguimento da região

algum tempo depois de sua deposição (durante a deposição da Formação Exu entre o Albiano-Cenomaniano?).

Tendo em vista que o arco estrutural de Purus estaria ativo na região da Amazônia Ocidental durante o Cretáceo Superior (Caputo and Soares 2016), os mecanismos geodinâmicos (relação isostática com o pulso orogênico andino, a denudação e a posterior recuperação flexural da litosfera) poderiam atuar nas porções ocidentais da Plataforma Sul-Americana. Sendo assim, as fontes dos sedimentos continuaram sendo predominantemente cratônicas (Terrenos Ventuari Tapajós e Rondônia San Ignacio) e o sistema de drenagem Sanozama poderia alimentar as bacias até pelo menos o Maastrichtiano, quando as fontes das bacias ocidentais (Madre de Dios sul e norte) unem-se e começam a receber aporte sedimentar oriundo do sudoeste do Craton Amazônico (ver discussão Capitulo 4 e Figura 47).

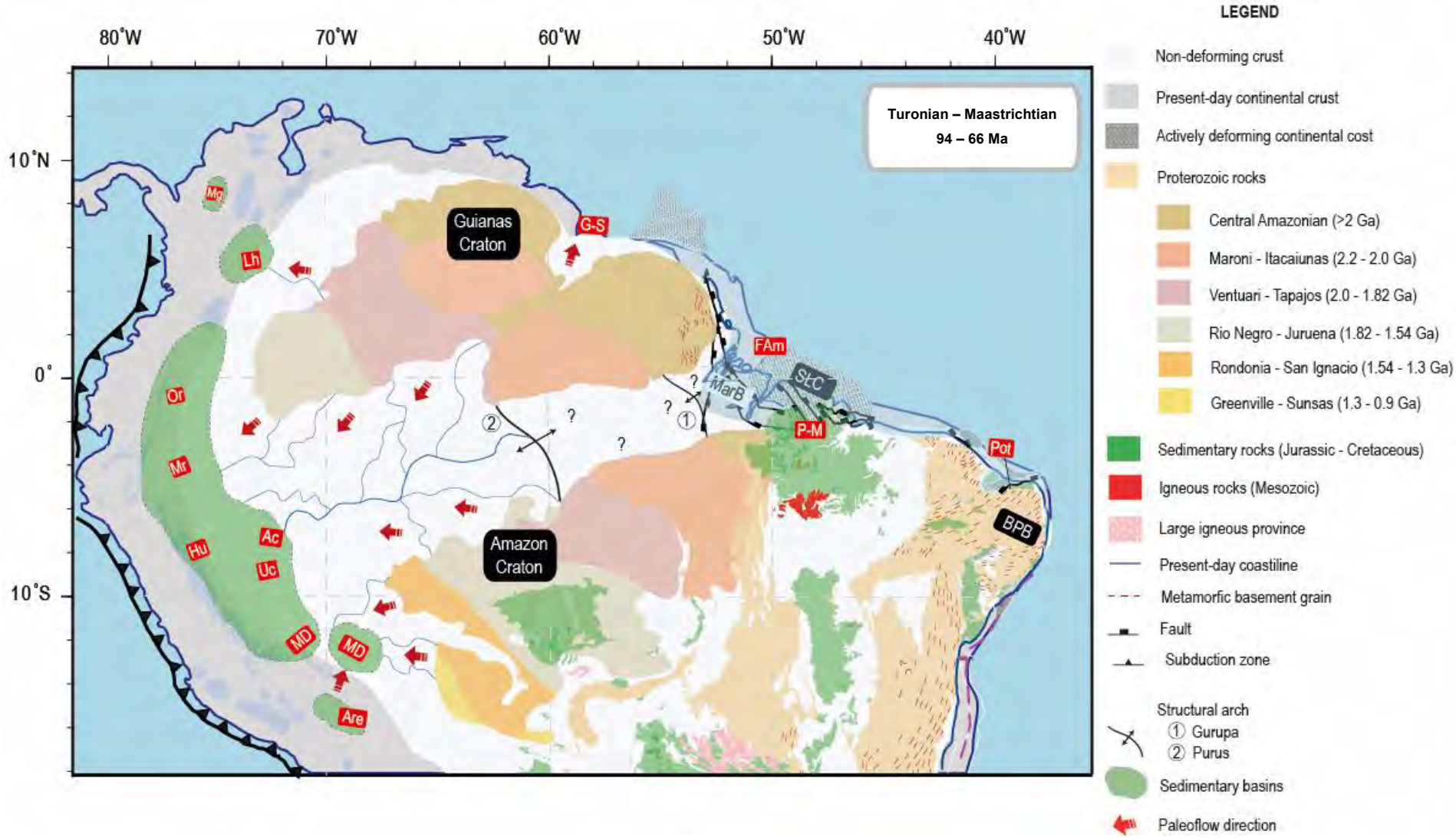

Figura 47 : : Reconstrução paleogeográfica proposta para o período final do Cretaceo, baseada no modelo cinemático de Heine et al (2013) e nos dados discutidos ao longo do texto. As províncias tectônicas do Craton das Guianas e Amazônico, os terrenos andinos, as bacias localizadas na Amazônia Ocidental e o sistema de drenagens continental foram modificados de adaptados de (Cordani et al. 2000; Chew et al. 2007, 2008; Spikings et al. 2016; Hurtado et al. 2018; Rodrigues et al. 2023). SLC: Craton São Luís; SFC: Craton São Francisco, CC: Craton do Congo; BPB: Província Borborema; Mar: Bacia do Marajó; Pot: Bacia Potiguar; RTJ: Bacia Recôncavo-Tucano-Jatobá; Ben: Bacia do Benin; Cd'I-G: Bacia de Côte d'Ivoire – Gana; G-S: Bacia Guianas-Suriname; FAm: Bacia Foz do Amazonas; P-M: Bacia Parnaíba-Maranhão; Bar: Bacia Barreiras; Ce: Bacia do Ceará; Mg: Bacia Madaglena; Lh: Bacia Lhanos; Or: Bacia Oriente; Mr: Bacia Marañon; Hu: Bacia Huallaga; Uc: Bacia Ucayali; Ac: Bacia do Acre; MD: Bacia de Madre de Dios (n-norte, s-sul); Are: Bacia de Arequipa.

Referências

Antobreh, A.A., Faleide, J.I., Tsikalas, F. and Planke, S. 2009. Rift–shear architecture and tectonic development of the Ghana margin deduced from multichannel seismic reflection and potential field data. *Marine and Petroleum Geology*, **26**, 345–368, https://doi.org/10.1016/j.marpetgeo.2008.04.005.

Arai, M. 2009. Paleogeografia do Atlântico Sul no Aptiano: um novo modelo a partir de dados micropaleontológicos recentes. *Boleti, de Geosciências da Petrobras*, **17**, 331–351.

Arai, M. 2014. Aptian/Albian (Early Cretaceous) paleogeography of the South Atlantic: a paleontological perspective. *Brazilian Journal of Geology*, **44**, 339–350, https://doi.org/10.5327/Z2317-4889201400020012.

Arai, M. 2016. Reply to the comments of Assine et al. (Comments on paper by M. Arai 'Aptian/Albian (Early Cretaceous) paleogeography of the South Atlantic: a paleontological perspective'). *Brazilian Journal of Geology*, **46**, 9–13, https://doi.org/10.1590/2317-4889201620150046B.

Arai, M. and Assine, M.L. 2020. Chronostratigraphic constraints and paleoenvironmental interpretation of the Romualdo Formation (Santana Group, Araripe Basin, Northeastern Brazil) based on palynology. *Cretaceous Research*, **116**, 104610, https://doi.org/10.1016/j.cretres.2020.104610.

Assine, M.L. 1992. Analise estratigrafica da Bacia do Araripe, Nordeste do Brasil. *Revista Brasileira de Geociências*, **22**, 289–300, https://doi.org/10.25249/0375-7536.1992289300.

Assine, M.L. 1994. Paleocorrentes e Paleogeografia na Bacia do Araripe, Nordeste do Brasil. *Revista Brasileira de Geociências*, **24**, 223–232, https://doi.org/10.25249/0375-7536.1994223232.

Assine, M.L. 2007. Bacia do Araripe. *Boletim de Geociências da Petrobras*, **15**, 371–389.

Assine, M.L., Neumann, H., Varejão, F.G. and Mescolotti, P.C. 2014. Sequências deposicionais do Andar Alagoas da Bacia do Araripe, Nordeste do Brasil. *Boletim de Geociências da Petrobras*, **22**, 3–28.

Assine, M.L., Quaglio, F., Warren, L.V. and Simões, M.G. 2016. Comments on paper by M. Arai 'Aptian/Albian (Early Cretaceous) paleogeography of the South Atlantic: a paleontological perspective'. *Brazilian Journal of Geology*, **46**, 3–7, https://doi.org/10.1590/2317-4889201620150046A.

Baesso, A., Remus, M.V.D., Pereira, B.R.B., Alkmim, A.R., Lana, C.C., Vignol-Lelarge, M.L. and Porcher, C.C. 2021. Insights into sedimentary provenance and the evolution of the Potiguar Basin, NE Brazil, using U–Pb ages and Lu–Hf isotopes in detrital zircons. *Marine and Petroleum Geology*, **131**, 105170, https://doi.org/10.1016/j.marpetgeo.2021.105170.

Barron, E.J. 1987. Cretaceous plate tectonic reconstructions. *Palaeogeography, Palaeoclimatology, Palaeoecology*, **59**, 3–29, https://doi.org/10.1016/0031-0182(87)90071-X.

Basile, C., Mascle, J. and Guiraud, R. 2005. Phanerozoic geological evolution of the Equatorial Atlantic domain. *Journal of African Earth Sciences*, **43**, 275–282, https://doi.org/10.1016/j.jafrearsci.2005.07.011.

Bleeker, W. 2003. The late Archean record: a puzzle in ca. 35 pieces. *Lithos*, **71**, 99–134, https://doi.org/10.1016/j.lithos.2003.07.003.

Brandão, J.A.S.L. and Feijó, F.J. 1994. Bacia da Foz do Amazonas. *Boletim de Geociências Petrobras*, **8**, 91–99.

Caputo, M.V. 2014. Juruá Orogeny: Brazil and Andean Countries. *Brazilian Journal of Geology*, **44**, 181–190, https://doi.org/10.5327/Z2317-4889201400020001.

Caputo, M.V. and Crowell, J.C. 1985. Migration of glacial centers across Gondwana during Paleozoic Era. *Geological Society of America Bulletin*, **96**, 1020, https://doi.org/10.1130/0016-7606(1985)96<1020:MOGCAG>2.0.CO;2.

Caputo, M.V. and Soares, E.A.A. 2016. Eustatic and tectonic change effects in the reversion of the transcontinental Amazon River drainage system. *Brazilian Journal of Geology*, **46**, 301–328, https://doi.org/10.1590/2317-4889201620160066.

Castro, D.L., de Oliveira, D.C. and Gomes Castelo Branco, R.M. 2007. On the tectonics of the Neocomian Rio do Peixe Rift Basin, NE Brazil: Lessons from gravity, magnetics, and radiometric data. *Journal of South American Earth Sciences*, **24**, 184–202, https://doi.org/10.1016/j.jsames.2007.04.001.

Castro, D.L., Bezerra, F.H.R. and Castelo Branco, R.M.G. 2008. Geophysical evidence of crustal-heterogeneity control of fault growth in the Neocomian Iguatu basin, NE Brazil. *Journal of South American Earth Sciences*, **26**, 271–285, https://doi.org/10.1016/j.jsames.2008.07.002.

Chaboureau, A.-C., Guillocheau, F., Robin, C., Rohais, S., Moulin, M. and Aslanian, D. 2013. Paleogeographic evolution of the central segment of the South Atlantic

during Early Cretaceous times: Paleotopographic and geodynamic implications. *Tectonophysics*, **604**, 191–223, https://doi.org/10.1016/j.tecto.2012.08.025.

Chew, D., Magna, T., Kirkland, C., Miskovic, A., Cardona, A., Spikings, R. and Schaltegger, U. 2008. Detrital zircon fingerprint of the Proto-Andes: Evidence for a Neoproterozoic active margin? *Precambrian Research*, **167**, 186–200, https://doi.org/10.1016/j.precamres.2008.08.002.

Chew, D.M., Schaltegger, U., Kosler, J., Whitehouse, M.J., Gutjahr, M., Spikings, R.A. and Miskovic, A. 2007. U-Pb geochronologic evidence for the evolution of the Gondwanan margin of the north-central Andes. *Geological Society of America Bulletin*, **119**, 697–711, https://doi.org/10.1130/B26080.1.

Condé, V.C., Lana, C.C., Pessoa Neto, O.C., Roesner, E.H., Morais Neto, J.M. and Dutra, D.C. 2007. Bacia do Ceará. *Boletim de Geociências Petrobras*, **15**, 347–355.

Cordani, U.G., Milani, E.J., Thomas Filho, A. and Campos, D. de A. 2000. *Tectonic Evolution of South America*, 31th International Geological Congress.

Costa, J.B.S., Léa Bemerguy, R., Hasui, Y. and da Silva Borges, M. 2001. Tectonics and paleogeography along the Amazon river. *Journal of South American Earth Sciences*, **14**, 335–347, https://doi.org/10.1016/S0895-9811(01)00025-6.

Cui, X., Wignall, B., Freeman, K.H. and Summons, R.E. 2023. Early Cretaceous marine incursions into South Atlantic rift basins originated from the south. *Communications Earth & Environment*, **4**, 6, https://doi.org/10.1038/s43247-022-00668-3.

Custódio, M.A., Quaglio, F., Warren, L.V., Simões, M.G., Fürsich, F.T., Perinotto, J.A.J. and Assine, M.L. 2017. The transgressive-regressive cycle of the Romualdo Formation (Araripe Basin): Sedimentary archive of the Early Cretaceous marine ingression in the interior of Northeast Brazil. *Sedimentary Geology*, **359**, 1–15, https://doi.org/10.1016/j.sedgeo.2017.07.010.

De Oliveira, R.S. and Vidotti, R.M. 2023. The Acre Basin basement (NW Brazil) and the transition from the intracratonic to retroarc foreland basin system. *Basin Research*, **35**, 86–119, https://doi.org/10.1111/bre.12705.

Erlich, R.N., Fallon, J. and O'Sullivan, G. 2018. The Marañón Basin: Tectonic Evolution and Paleogeography. *In*: *Petroleum Basins and Hydrocarbon Potential of the Andes of Peru and Bolivia*. 121–144., https://doi.org/10.1306/13622119M1173768.

Fambrini, G.L., Silvestre, D. da C., Barreto Junior, A.M. and Silva-Filho, W.F. da. 2020. Estratigrafia da Bacia do Araripe: estado da arte, revisão crítica e resultados novos. *Geologia USP. Série Científica*, **20**, 169–212, https://doi.org/10.11606/issn.2316-9095.v20-163467.

Fauth, G., Kern, H.P., et al. 2023. Early Aptian marine incursions in the interior of northeastern Brazil following the Gondwana breakup. *Scientific Reports*, **13**, 6728, https://doi.org/10.1038/s41598-023-32967-w.

Fellin, M.G., Zattin, M., et al. 2023. New detrital petrographic and thermochronologic constraints on the Late Cretaceous–Neogene erosional history of the equatorial margin of Brazil: Implications for the surface evolution of a complex rift margin. *Basin Research*, bre.12808, https://doi.org/10.1111/bre.12808.

Figueiredo, J., Zalán, P.V. and Soares, E.F. 2007. Bacia da Foz do Amazonas. *Boletim de Geociências Petrobras*, **15**, 299–309.

Garcia, A.J.V. and Wilbert, A. 1995. Paleogeographic Evolution of Mesozoic pre-rift Sequences in costal and interior basins of Northeastern Brazil. *In*: *Pangea: Global Environments and Resources.* 123–130.

George, S.W.M., Horton, B.K., Jackson, L.J., Moreno, F., Carlotto, V. and Garzione, C.N. 2019. Sediment provenance variations during contrasting Mesozoic-early Cenozoic tectonic regimes of the northern Peruvian Andes and Santiago-Marañón foreland basin. *In*: *Andean Tectonics*. 269–296., https://doi.org/10.1016/B978-0-12-816009-1.00012-5.

Girault, I., Basile, C., et al. 2023. Thermochronology and U–Pb dating of detrital zircons from the Demerara Plateau (French Guiana-Suriname): Implications for the provenance of the Early Cretaceous syn-rift sedimentation. *Basin Research*, **35**, 1386–1406, https://doi.org/10.1111/bre.12758.

Godot Souza, J.F., Isozaki, Y., et al. 2022. Provenance analysis of the Araripe intracontinental basin, northeast Brazil – Routes for proto-Atlantic marine incursions in northwest Gondwana. *Sedimentary Geology*, **440**, 106243, https://doi.org/10.1016/j.sedgeo.2022.106243.

Greenroyd, C.J., Peirce, C., Rodger, M., Watts, A.B. and Hobbs, R.W. 2008. Do fracture zones define continental margin segmentation? — Evidence from the French Guiana margin. *Earth and Planetary Science Letters*, **272**, 553–566, https://doi.org/10.1016/j.epsl.2008.05.022.

Gutiérrez, E.G., Horton, B.K., Vallejo, C., Jackson, L.J. and George, S.W.M. 2019. Provenance and geochronological insights into Late Cretaceous-Cenozoic foreland basin development in the Subandean Zone and Oriente Basin of Ecuador. *In*: *Andean Tectonics*. 237–268., https://doi.org/10.1016/B978-0-12-816009-1.00011-3.

Harman, R., Gallagher, K., Brown, R., Raza, A. and Bizzi, L. 1998. Accelerated denudation and tectonic/geomorphic reactivation of the cratons of northeastern Brazil during the Late Cretaceous. *Journal of Geophysical Research: Solid Earth*, **103**, 27091–27105, https://doi.org/10.1029/98JB02524.

Heilbron, M., Mohriak, W.U., Valeriano, C.M., Milani, E.J., Almeida, J. and Tupinambá, M. 2000. From collision to extension: the roots of the Southeastern Continental Margin of Brazil. *In*: Mohriak, W. U. and Talwani, M. (eds) *Atlantic Rifts and Continental Margins*. 1–32.

Heine, C., Zoethout, J. and Müller, R.D. 2013. Kinematics of the South Atlantic rift. *Solid Earth*, **4**, 215–253, https://doi.org/10.5194/se-4-215-2013.

Holbrook, J. and Schumm, S.A. 1999. Geomorphic and sedimentary response of rivers to tectonic deformation: a brief review and critique of a tool for recognizing subtle epeirogenic deformation in modern and ancient settings. *Tectonophysics*, **305**, 287–306, https://doi.org/10.1016/S0040-1951(99)00011-6.

Hurtado, C., Roddaz, M., Santos, R.V., Baby, P., Antoine, P.-O. and Dantas, E.L. 2018. Cretaceous-early Paleocene drainage shift of Amazonian rivers driven by Equatorial Atlantic Ocean opening and Andean uplift as deduced from the provenance of northern Peruvian sedimentary rocks (Huallaga basin). *Gondwana Research*, **63**, 152–168, https://doi.org/10.1016/j.gr.2018.05.012.

Japsen, P., Bonow, J.M., et al. 2012. Episodic burial and exhumation in NE Brazil after opening of the South Atlantic. *Geological Society of America Bulletin*, **124**, 800–816, https://doi.org/10.1130/B30515.1.

Jovane, L., Figueiredo, J.J.P., et al. 2016. Seismostratigraphy of the Ceará Plateau: Clues to Decipher the Cenozoic Evolution of Brazilian Equatorial Margin. *Frontiers in Earth Science*, **4**, https://doi.org/10.3389/feart.2016.00090.

Kroth, M., Borghi, L., et al. 2021. Aptian shell beds from the Romualdo Formation (Araripe Basin): Implications for paleoenvironment and paleogeographical reconstruction of the Northeast of Brazil. *Sedimentary Geology*, **426**, 106025, https://doi.org/10.1016/j.sedgeo.2021.106025.

Kuchle, J., Scherer, C.M. dos S., Born, C.C., Alvarenga, R. dos S. and Adegas, F. 2011. A contribution to regional stratigraphic correlations of the Afro-Brazilian depression – The Dom João Stage (Brotas Group and equivalent units – Late Jurassic) in Northeastern Brazilian sedimentary basins. *Journal of South American Earth Sciences*, **31**, 358–371, https://doi.org/10.1016/j.jsames.2011.02.007.

Kukla, P.A., Strozyk, F. and Mohriak, W.U. 2018. South Atlantic salt basins – Witnesses of complex passive margin evolution. *Gondwana Research*, **53**, 41–57, https://doi.org/10.1016/j.gr.2017.03.012.

Lima, M.R. de. 1978. *Palinologia Da Formação Santana (Cretaceo Do Nordeste Do Brasil)*. PhD Thesis, Univesidade de São Paulo.

Loparev, A., Rouby, D., et al. 2021. Superimposed Rifting at the Junction of the Central and Equatorial Atlantic: Formation of the Passive Margin of the Guiana Shield. *Tectonics*, **40**, https://doi.org/10.1029/2020TC006159.

Louterbach, M. 2014. *Propagation du front orogénique Subandine et réponse sédimentaire a associée dans le bassin d'avant-pays Amazonien (Madre de Dios, Pérou)*. Thèse Doctorat, Université de Toulouse.

Machado Junior, D. de L., Dehira, L.K., Carneiro, C.D.R. and Almeida, F.F.M. de. 1990. Reconstruções Paleoambientais do Juto-Cretáceo no Nordeste Oriental Brasileiro. *Revista Brasileira de Geociencias*, **19**, 470–485.

Magnavita, L.P., Davison, I. and Kusznir, N.J. 1994. Rifting, erosion, and uplift history of the Recôncavo-Tucano-Jatobá Rift, northeast Brazil. *Tectonics*, **13**, 367–388, https://doi.org/10.1029/93TC02941.

Maisey, J.G. 2000. Continental break up and the distribution of fishes of Western Gondwana during the Early Cretaceous. *Cretaceous Research*, **21**, 281–314, https://doi.org/10.1006/cres.1999.0195.

Matos, R.M.D. de. 1999. History of the northeast Brazilian rift system: kinematic implications for the break-up between Brazil and West Africa. *Geological Society, London, Special Publications*, **153**, 55–73, https://doi.org/10.1144/GSL.SP.1999.153.01.04.

Matos, R.M.D. de, Krueger, A., Norton, I. and Casey, K. 2021. The fundamental role of the Borborema and Benin–Nigeria provinces of NE Brazil and NW Africa during the development of the South Atlantic Cretaceous Rift system. *Marine*

and Petroleum Geology, **127**, 104872, https://doi.org/10.1016/j.marpetgeo.2020.104872.

Matos, R.M.D. 1992. The Northeast Brazilian Rift System. *Tectonics*, **11**, 766–791, https://doi.org/10.1029/91TC03092.

Matos, R.M.D. 2000. Tectonic evolution of the equatorial South Atlantic. *In*: Mohriak, W. and Taiwani, M. (eds) *Geophysical Monograph Series*. 331–354., https://doi.org/10.1029/GM115p0331.

Matos, R.M.D., Krueger, A., Casey, K. and Norton, I. 2017. The Equatorial Atlantic and the South Atlantic Margins: Cretaceous twins, but so different at birth. *In*: *15th International Congress of the Brazilian Geophysical Society & EXPOGEF, Rio de Janeiro, Brazil, 31 July-3 August 2017* – 15th International Congress of the Brazilian Geophysical Society & EXPOGEF, Rio de Janeiro, Brazil, 31 July-3 August 2017. 499–501., https://doi.org/10.1190/sbgf2017-098.

Mbina Mounguengui, M., Lang, J., Guiraud, M. and Jocktane, O. 2002. Sedimentary dynamics and structural geology of pre-rift deposits of the interior basin of Gabon. *Journal of African Earth Sciences*, **35**, 315–329, https://doi.org/10.1016/S0899-5362(02)00035-0.

Mbina Mounguengui, M., Lang, J. and Guiraud, M. 2008. Sedimentary dynamics and extensional structuring related to early Cretaceous rifting of Neocomian and Barremian deposits of the interior basin of Gabon. *Journal of African Earth Sciences*, **51**, 239–256, https://doi.org/10.1016/j.jafrearsci.2008.01.008.

Milani, E.J. and Thomaz-Filho, A. 2000. Sedimentary Basins of South America. *In*: *Tectonic Evolution of South America*. 389–449.

Mohriak, W.U. 2003. Sedimentary Basins of the Brazilian Continental Margin. *Geologia, Tectônica e Recursos Minerais do Brasil*.

Mohriak, W.U., Danforth, A., Post, P.J., Brown, D.E., Tari, G.C., Nemčok, M. and Sinha, S.T. 2013. Conjugate divergent margins: an introduction. *Geological Society, London, Special Publications*, **369**, 1–10, https://doi.org/10.1144/SP369.26.

Moizinho, G.R., Vieira, L.C., Santos, R.V., Nogueira, A.C.R., Dantas, E.L. and Roddaz, M. 2022. Provenance of Miocene-Pleistocene siliciclastic deposits in the Eastern Amazonia coast (Brazil) and paleogeographic implications. *Palaeogeography, Palaeoclimatology, Palaeoecology*, **587**, 110799, https://doi.org/10.1016/j.palaeo.2021.110799.

Monteiro, H.S., Vasconcelos, P.M.P., Farley, K.A. and Lopes, C.A.M. 2018. Age and evolution of diachronous erosion surfaces in the Amazon: Combining (U-Th)/He and cosmogenic 3He records. *Geochimica et Cosmochimica Acta*, **229**, 162–183, https://doi.org/10.1016/j.gca.2018.02.045.

Morais Neto, J.M., Hegarty, K.A., Karner, G.D. and Alkmim, F.F. 2009. Timing and mechanisms for the generation and modification of the anomalous topography of the Borborema Province, northeastern Brazil. *Marine and Petroleum Geology*, **26**, 1070–1086, https://doi.org/10.1016/j.marpetgeo.2008.07.002.

Moreno, F., Garzione, C.N., et al. 2020. Coupled Andean Growth and Foreland Basin Evolution, Campanian–Cenozoic Bagua Basin, Northern Peru. *Tectonics*, **39**, https://doi.org/10.1029/2019TC005967.

Moulin, M., Aslanian, D. and Unternehr, P. 2010. A new starting point for the South and Equatorial Atlantic Ocean. *Earth-Science Reviews*, **98**, 1–37, https://doi.org/10.1016/j.earscirev.2009.08.001.

Munis, M. de B. 2009. *Caracterização Geomagnética Do Graben Purus e Suas Implicações Na Evolução Das Bacias Do Soimões e Do Amazonas*. Tese de doutorado, Univesidade Federal do Rio de Janeiro.

Nascimento, M.D.S., Góes, A.M., Macambira, M.J.B. and Brod, J.A. 2007. Provenance of Albian sandstones in the São Luís–Grajaú Basin (northern Brazil) from evidence of Pb–Pb zircon ages, mineral chemistry of tourmaline and palaeocurrent data. *Sedimentary Geology*, **201**, 21–42, https://doi.org/10.1016/j.sedgeo.2007.04.005.

Nogueira, F.C.C., Marques, F.O., Bezerra, F.H.R., de Castro, D.L. and Fuck, R.A. 2015. Cretaceous intracontinental rifting and post-rift inversion in NE Brazil: Insights from the Rio do Peixe Basin. *Tectonophysics*, **644–645**, 92–107, https://doi.org/10.1016/j.tecto.2014.12.016.

Petri, S. 1987. Cretaceous paleogeographic maps of Brazil. *Palaeogeography, Palaeoclimatology, Palaeoecology*, **59**, 117–168, https://doi.org/10.1016/0031-0182(87)90077-0.

Pletsch, T., Erbacher, J., et al. 2001. Cretaceous separation of Africa and South America: the view from the West African margin (ODP Leg 159). *Journal of South American Earth Sciences*, **14**, 147–174, https://doi.org/10.1016/S0895-9811(01)00020-7.

Ponte, F.C. and Ponte Filho, F.C. 1996. *Estrutura Geológica e Evolução Tectônica Da Bacia Do Araripe*.

Potter, P.E. 1997. The Mesozoic and Cenozoic paleodrainage of South America: a natural history. *Journal of South American Earth Sciences*, **10**, 331–344, https://doi.org/10.1016/S0895-9811(97)00031-X.

Roddaz, M., Dera, G., et al. 2021. Provenance constraints on the Cretaceous-Paleocene erosional history of the Guiana Shield as determined from the geochemistry of clay-size fraction of sediments from the Arapaima-1 well (Guyana-Suriname basin). *Marine Geology*, **434**, 106433, https://doi.org/10.1016/j.margeo.2021.106433.

Rodrigues, M. de A., Roddaz, M., et al. 2023. New insights into the Cretaceous evolution of the Western Amazonian paleodrainage system. *Sedimentary Geology*, **453**, 106434, https://doi.org/10.1016/j.sedgeo.2023.106434.

Rodrigues, M.G., Matos, S.A., Varejão, F.G., Fürsich, F.T., Warren, L.V., Assine, M.L. and Simões, M.G. 2020. Short-lived “Bakevelliid-Sea” in the Aptian Romualdo Formation, Araripe Basin, northeastern Brazil. *Cretaceous Research*, **115**, 104555, https://doi.org/10.1016/j.cretres.2020.104555.

Rouby, D., Loparev, A., et al. 2023. Sediment routing systems to the Atlantic rifted margin of the Guiana Shield. *Geosphere*, **19**, 957–974, https://doi.org/10.1130/GES02561.1.

Sacek, V., De Morais Neto, J.M., Vasconcelos, P.M. and De Oliveira Carmo, I. 2019. Numerical Modeling of Weathering, Erosion, Sedimentation, and Uplift in a Triple Junction Divergent Margin. *Geochemistry, Geophysics, Geosystems*, **20**, 2334–2354, https://doi.org/10.1029/2018GC008124.

Sapin, F., Mélanie, D., Dall’asta, M., Lahmi, M., Baudot, G. and Ringenbach, J.-C. 2016. Post-rift subsidence of the French Guiana hyper-oblique margin: from roft-inherited subsidence to Amazon deposition effect. *Geological Society of London*, 125–144, https://doi.org/10.1144/SP431.11.

Schaller, H. 1969. *Revisão Estratigrafica Da Bacia de Sergipe/Alagoas*. Boletim técnico da PETROBRAS **12**.

Scherer, C.M. dos S., Jardim de Sá, E.F., Córdoba, V.C., Sousa, D. do C., Aquino, M.M. and Canelas Cardoso, F.M. 2014. Tectono-stratigraphic evolution of the Upper Jurassic–Neocomian rift succession, Araripe Basin, Northeast Brazil.

Journal of South American Earth Sciences, **49**, 106–122, https://doi.org/10.1016/j.jsames.2013.10.007.

Scotese, C.R. 1991. Jurassic and cretaceous plate tectonic reconstructions. *Palaeogeography, Palaeoclimatology, Palaeoecology*, **87**, 493–501, https://doi.org/10.1016/0031-0182(91)90145-H.

Scotese, C.R., Gahagan, L.M. and Larson, R.L. 1988a. Plate tectonic reconstructions of the Cretaceous and Cenozoic ocean basins. *Tectonophysics*, **155**, 27–48, https://doi.org/10.1016/0040-1951(88)90259-4.

Scotese, C.R., Gahagan, L.M. and Larson, R.L. 1988b. Plate tectonic reconstructions of the Cretaceous and Cenozoic ocean basins. *Tectonophysics*, **155**, 27–48, https://doi.org/10.1016/0040-1951(88)90259-4.

Shirey, S.B. and Richardson, S.H. 2011. Start of the Wilson Cycle at 3 Ga Shown by Diamonds from Subcontinental Mantle. *Science*, **333**, 434–436, https://doi.org/10.1126/science.1206275.

Soares-Júnior, A.V., Costa, J.B.S. and Hasui, Y. 2008. Evolução da Margem Atlântica Equatorial do Brasil: Três fases distensivas. *São Paulo*, **27**, 13.

Spikings, R., Reitsma, M.J., et al. 2016. Characterisation of Triassic rifting in Peru and implications for the early disassembly of western Pangaea. *Gondwana Research*, **35**, 124–143, https://doi.org/10.1016/j.gr.2016.02.008.

Teisserenc, P. and Villemin, J. 1990. Sedimentary basin of Gabon - geology and oils systems. *In*: Edwards, J. D. and Santogrossi, P. A. (eds) *Divergent/Passive Margins Basins*. 117–199.

Torsvik, T.H., Rousse, S., Labails, C. and Smethurst, M.A. 2009. A new scheme for the opening of the South Atlantic Ocean and the dissection of an Aptian salt basin. *Geophysical Journal International*, **177**, 1315–1333, https://doi.org/10.1111/j.1365-246X.2009.04137.x.

Trosdtorf Junior, I., Zalán, P.V., Figueiredo, J.J.P. and Soares, E.F. 2007. Bacia de Barreirinhas. *Boletim de Geociências Petrobras*, **15**, 331–339.

Valença, L.M.M., Neumann, V.H. and Mabesoone, J.M. 2003. An overview on Callovian-Cenomanian intracratonic basins of Northeast Brazil: Onshore stratrigraphic record of the opening of the southern Atlantic. *Geologica Acta*.

Vallejo, C., Tapia, D., et al. 2017. Geology of the Campanian M1 sandstone oil reservoir of eastern Ecuador: A delta system sourced from the Amazon Craton.

Marine and Petroleum Geology, **86**, 1207–1223, https://doi.org/10.1016/j.marpetgeo.2017.07.022.

Van Kranendonk, M.J., Hugh Smithies, R., Hickman, A.H., Wingate, M.T.D. and Bodorkos, S. 2010. Evidence for Mesoarchean (~3.2Ga) rifting of the Pilbara Craton: The missing link in an early Precambrian Wilson cycle. *Precambrian Research*, **177**, 145–161, https://doi.org/10.1016/j.precamres.2009.11.007.

Wilson, J.T. 1969. Static or mobile earth: The current scientific revolution. *Tectonophysics*, **7**, 600–601, https://doi.org/10.1016/0040-1951(69)90033-X.

Zalán, P.V. 2004. Evolução Fanerozóica das Bacias Sedimentares Brasileiras. 19.

Zalán, P.V. and Matsuda, N.S. 2007. Bacia do Marajó. *Boletim de Geociências da Petrobras*, **15**, 311–319.

CONCLUSÃO E PERSPECTIVAS

CONCLUSION ET PERSPECTIVES

6 CONCLUSÃO E PERSPECTIVAS / CONCLUSION ET PERSPECTIVES

Les résultats obtenus au cours de cette thèse par l'analyse de la provenance des sédiments des bassins crétacés du système Andes-Amazonie-marge équatoriale ont apporté permis d'apporter de préciser l'évolution paléogéographique du système sédimentaire Andes-Amazonie-marge équatoriale et de discuter les mécanismes contrôlant son évolution. Il a pu être montré que :

1) *Les sources des sédiments des bassins crétacés analysés proviennent des craton des Guyanes, du Bouclier brésilien Central, de la Province Borborema et des plutons du cycle Brasiliano-Pan Africano. Il a détecté des sources andines dans les bassins analysés (Acre) pendant le Crétacé. Ces zones constituent les principales zones sources qui alimentaient ces bassins au cours du Cretacé ;*
2) *Le bassin de l'Araripe possède une histoire sédimentaire liée aux phases de rupture de l'Atlantique Sud et équatorial. Pendant la phase pré-rift (~152-135 Ma), le bassin faisait partie de la dépression Afro-Brésilienne et recevait des sédiments en provenance du N-NO. Lors la phase rift (~135-125 Ma), il y a eu un changement de source due à la rupture continentale et à la formation de l'Atlantique Sud, avec un apport de sédiments en provenance de la partie orientale de la province de Borborema. Au début de la phase, post-rift (121 - 113 Ma), le bassin a cessé d'être alimenté par la partie orientale et les incursions marines ont dominé l'environnement de sédimentation. Enfin, au cours de la phase post-rift II (113 - 100 Ma), un dernier changement de source a été observée dans le bassin avec des sources au NE qui reflètent le moment final de la fragmentation du Gondwana.*

3) *Au cours de l'Albien-Cénomanien, l'ouverture de l'Atlantique équatorial a favorisé la formation de bassins sédimentaires le long des côtes sud-américaines et africaines, ainsi que la réactivation et le soulèvement de zones continentales qui ont reconfiguré le système de drainage et l'apport sédimentaire. Dans la région de l'Amazonie occidentale, le soulèvement du Bouclier du Brésil Central et des Guyanes, ainsi que la réactivation de l'Arche de Purus, ont conduit au développement d'un réseau de drainage intracontinental (« Sanozama »), transportant les sédiments des régions cratoniques à l'est vers les bassins à l'ouest.*
4) *Le développement des bassins sédimentaires de l'Amazonie occidentale n'a pas été homogène. Les bassins de l'Acre, de l'Oriente, du Marañon, de l'Ucayali, de l'Huallaga, du Santiago, du Bagua et la partie nord du bassin de Madre de Dios ont été alimentés par des sédiments cratoniques provenant du système hydrographique de Sanozama, principalement en provenance des terrains Ventuari-Tapajós et Rio Negro-Juruena, pendant le Cénomanien et le Campanien. Le secteur le plus méridional du bassin de Madre de Dios était séparé de la partie septentrionale et a connu un système d'apports sédimentaires provenant de sources liées aux terrains de Rondonia-San Ignacio et de Sunsás-Aguapeí au moins jusqu'au Campanien. Au Maastrichtien, les bassins se sont individualisés et les sources sédimentaires ont présenté des caractéristiques similaires.*

Finalement, afin de poursuivre le développement de ce travail de recherche, je propose de travailler sur les thématiques suivantes :

- La modélisation des structures du socle dans la région de l'Amazonie occidentale.

Cette étude permettrait une meilleure compréhension des structures qui ont délimité et façonné le dépôt des bassins du Madre de Dios et de l'Acre au cours du Crétacé. Les observations structurales pourraient révéler si la structure qui a agi comme une barrière pendant le dépôt du bassin sud du Madre de Dios, proposée dans cette thèse, est la même que celle qu'Oliveira et al (2022, 2023) ont délimitée comme marqueur de séparation entre les sous-bassins de l'Acre.

- Étude de la provenance sédimentaire du sous-bassin de Xapuri, bassin de l'Acre.

Cette étude pourrait contribuer à affiner la paléogéographie de la région en incorporant les données obtenues dans la partie méridionale du bassin de l'Acre aux résultats présentés dans cette thèse.

- Analyse de l'enregistrement du cycle Brasiliano-Pan Africain en Amazonie occidentale.

Avec cette étude, il sera possible de mieux comprendre le rôle des sources provenant du cycle Brasiliano-Pan Africain dans la sédimentation des bassins amazoniens (localisation ? dimension ?). En ce qui concerne cet événement, il serait intéressant d'étudier les sources qui ont laissé une « signature héritée », observable dans les grains détritiques avec des âges U-Pb discordants (quelle est la source ? Est-elle toujours présente lors du dépôt des bassins crétacés ?).

Os resultados obtidos durante esta tese por meio da análise da proveniência dos sedimentos das bacias cretáceas do sistema Andes-Amazônia-Oceano Atlântico e as relações com a paleogeografia e tectônica forneceram novas interpretações sobre o sistema sedimentar e sobre a reconstrução *source-to-sink* das bacias localizadas na Amazônia Ocidental e no Nordeste Brasileiro, permitindo demonstrar que:

- As fontes dos sedimentos das bacias cretáceas analisadas possuem fontes localizadas nos cratons das Guianas e Escudo Brasil Central, da Província Borborema e de plutons oriundos do ciclo transbrasiliano. Além disso, não há influência de fontes andinas nas bacias distais (Acre e Araripe) durante o Cretáceo.
- A bacia do Araripe possui uma história sedimentar relacionada às etapas de ruptura do Oceano Atlântico Sul e Equatorial, na qual, durante o estágio pré-rifte (~152-135 Ma) a bacia compunha a depressão Afro-Brasileira e recebia sedimentos vindos de N-NW; no estágio rifte (~135-125 Ma) houve uma reorganização de drenagens por conta da ruptura continental e da formação do Atlântico Sul, cujo o aporte de sedimentos passou a vir a região leste da Província Borborema; no primeiro momento da fase pós-rifte (121 – 113 Ma) a bacia parou de ser alimentada pela região leste e incursões marinhas dominaram o ambiente de sedimentação; e na fase pós-rifte II (113 - 100 Ma) a bacia refletiu o momento final da fragmentação do Gondwana, em que um sistema de drenagens com fontes a NE depositaram sedimentos na bacia.
- No Albiano-Cenomaniano abertura do Atlântico Equatorial propiciou a formação de bacia sedimentares ao longo da costa sul americana e africana, bem como reativou e soergueu áreas continentais que reconfiguraram o sistema de

drenagens e aporte sedimentar. Na região amazônica ocidental o soerguimento do Escudo Brasileiro Central e das Guianas, bem como a reativação do Arco de Purus fez com que uma drenagem intercontinental (Sanozama) se desenvolvesse, levando sedimentos das regiões cratônicas a leste para bacias a oeste.

- O desenvolvimento das bacias sedimentares do oeste amazônico não foi homogêneo. As bacias Acre, Oriente, Marañon, Ucayali, Huallaga, Santiago, Bagua e a parte norte da bacia de Madre de Dios foram alimentadas pelos sedimentos cratônicos sistema hídrico Sanozama, sobretudo dos terrenos Ventuari-Tapajós e Rio Negro-Juruena, durante o Cenomaniano e o Campaniano. O setor mais ao sul da bacia Madre de Dios esteve separado da parte ao norte e experimentou um sistema de aporte sedimentar de fontes relacionadas aos terrenos Rondonia-San Ignacio e Sunsás-Aguapeí pelo menos até o Campaniano. Durante o Maastrichtiano as bacias se individualizam e as fontes sedimentares dispunham de características similares.

Finalmente, afim de continuar a desenvolver este trabalho de pesquisa, proporemos as seguintes temáticas científicas:

- *Modelização de estruturas do embasamento na região da Amazônia Ocidental*.

Tal estudo permitirá uma melhor compreensão sobre as estruturas que delimitaram e moldaram a deposição das bacias de Madre de Dios e do Acre durante o Cretáceo. As observações estruturais podem desvendar se a estrutura que funcionava como barreira orogênica durante a deposição da bacia de Madre de Dios sul, proposta nesta tese, é a mesma que (De Oliveira and Vidotti 2023; Oliveira 2023) delimitaram como marco de separação entre as sub bacias do Acre.

- *Estudo de proveniência sedimentar da Sub bacia Xapuri, Bacia do Acre.*

Este estudo pode colaborar para o refinamento da paleogeografia da região ao incorporar dados obtidos na parte sul da Bacia do Acre aos resultados apresentados nesta tese.

- *Análise do registro do ciclo Brasiliano-Pan Africano na Amazônia Ocidental.*

Por meio deste estudo será possível entender mais a função das fontes oriundas do ciclo Brasiliano-Pan Africano na deposição das bacias amazônicas (localização? dimensão?). Ainda sobre este evento, seria interessante investigar sobre as fontes que deixaram uma “marca hereditária”, que se observa nos grãos detríticos com idades U-Pb discordantes (qual é a fonte? Ela ainda continua influente durante a deposição das bacias no Cretáceo?).

Referências

De Oliveira, R.S. and Vidotti, R.M. 2023. The Acre Basin basement (NW Brazil) and the transition from the intracratonic to retroarc foreland basin system. *Basin Research*, **35**, 86–119, https://doi.org/10.1111/bre.12705.

Oliveira, R.S.D. 2023. *Compartimentação crustal e evolução tectono-sedimentar da Bacia do Acre*. Tese de doutorado, Universidade de Brasília.

ANEXOS/ ANNEXÉS

Dados de datação U-Pb da Bacia de Madre de Dios

Madre de Dios	Amostra	Lab Name	Methodology	Formation	Age	Longitude (W)	Latitude (S)
1	MD234	LAB 2083 LAB 3684	LA-ICP-MS	Basal Chonta	Cenomanian or older	71°21'49.54"	12°53'36.13"
6	MD-2019-4A	LABXR0019	Element	Chonta	Cenomanian	70°22'14.22"	13°12'11.62"
10	MD-2019-12A	LABXT002	LA-ICP-MS	Chonta	Late Cenomanian -Early Turonian	70°23'1.29"	13°11'49.33"
11	MD-2019-11D	LABXT003	LA-ICP-MS	Chonta	Coniacian-Santonian	70°23'21.35"	13°11'23.45"
14	MD-2019-10	LABXT 001 LABXTXR 001-1	LA-ICP-MS Element	Vivian	Maastrichtian	70°23'57.90"	13°11'29.79"
15	MD-2019-13	LABXT_0005	LA-ICP-MS	Vivian	Maastrichtian	70°23'53.36"	13° 9'9.98"
16	MD238	LAB 1662	LA-ICP-MS	Vivian	Early Maastrichtian	71°21'44.21"	12°53'34.76"
17	MD239	Louterbach et al. 2018	LA-ICP-MS	Vivian	Early Maastrichtian	71°21'41.36"	71°21'43.56"
18	MD176	Louterbach et al. 2019	LA-ICP-MS	Vivian	Late Maastrichtian	71°21'43.56"	12°53'31.20"

Madre de Dios basin: Ages are from Louterbach (2014) and Louterbach et al. (2018)

Amostra MD234 Basal Chonta

			Data for Wetherill plot[4]									Ages[4]								
Comments		Th/U	$^{206}Pb/^{204}Pb$	1σ%	$^{207}Pb/^{206}Pb$	1σ %	$^{207}Pb/^{235}U$	1σ %	$^{206}Pb/^{238}U$	1σ %	Rho	$^{207}Pb/^{206}Pb$	2σ abs	$^{206}Pb/^{238}U$	2σ abs	$^{207}Pb/^{235}U$	2σ abs	% U-Pb disc[5]	% U-Pb disc[6]	Best Age [7]	2σ abs
LAB2083	048-ZR38	0.439	2714	30.76	0.04901	1.50	0.109	1.68	0.0161	0.67	0.40	148	70	103	1	105	3	30.51	1.8	103	1.38
LAB2083	067-ZR53	0.293	16824	25.25	0.05104	0.60	0.273	0.92	0.0388	0.59	0.64	243	27	245	3	245	4	-1.06	-0.1	245	2.85
LAB3684	038-ZR28	0.301	69038	19.62	0.05130	0.90	0.291	1.81	0.0411	1.53	0.84	254	41	260	8	259	8	-2.14	-0.2	260	7.76
LAB2083	010-ZR8	1.062	5895	27.13	0.05204	0.78	0.302	1.10	0.0421	0.69	0.63	287	35	266	4	268	5	7.53	0.8	266	3.61
LAB3684	003-ZR1N	0.587	36965	15.75	0.05202	0.72	0.320	0.97	0.0446	0.52	0.54	286	33	281	3	282	5	1.81	0.2	281	2.87
LAB3684	122-ZR93	0.888	57671	17.55	0.05241	0.42	0.322	0.84	0.0446	0.63	0.74	304	19	281	3	284	4	7.29	0.8	281	3.45
LAB3684	004-ZR1B	0.309	64692	13.71	0.05228	0.53	0.323	0.82	0.0448	0.51	0.62	298	24	282	3	284	4	5.18	0.6	282	2.81
LAB2083	028-ZR22	0.817	17434	27.98	0.05237	0.61	0.324	0.94	0.0448	0.62	0.65	301	28	283	3	285	5	6.22	0.7	283	3.41

LAB2083	017-ZR13	6.288	665	37.82	0.05381	2.26	0.347	2.87	0.0468	1.74	0.60	363	100	295	10	302	15	18.82	2.6	295	10.01
LAB2083	064-ZR50	0.249	6283	29.16	0.05302	1.07	0.352	1.28	0.0481	0.61	0.47	330	48	303	4	306	7	8.11	1.0	303	3.60
LAB3684	120-ZR91	0.673	54628	12.19	0.05478	0.52	0.370	0.81	0.0489	0.50	0.61	403	23	308	3	319	4	23.59	3.6	308	2.98
LAB2083	049-ZR39	0.097	11306	51.92	0.05347	1.21	0.362	1.45	0.0491	0.70	0.48	349	54	309	4	314	8	11.37	1.5	309	4.24
LAB3684	008-ZR5	1.741	6862	12.57	0.05379	1.51	0.364	1.69	0.0491	0.66	0.39	362	68	309	4	315	9	14.67	2.0	309	3.99
LAB3684	097-ZR74	0.114	8439	26.75	0.05308	0.58	0.364	0.83	0.0497	0.46	0.55	332	26	313	3	315	4	5.88	0.7	313	2.81
LAB3684	016-ZR11	0.611	29992	16.35	0.05338	0.79	0.369	1.00	0.0501	0.50	0.50	345	35	315	3	319	5	8.63	1.1	315	3.08
LAB2083	035-ZR27	0.449	6256	31.83	0.05327	0.92	0.369	1.18	0.0502	0.64	0.54	340	41	316	4	319	6	7.11	0.9	316	3.95
LAB3684	084-ZR63	1.775	9377	14.61	0.05281	1.17	0.369	1.34	0.0507	0.53	0.40	320	53	319	3	319	7	0.44	0.1	319	3.33
LAB2083	026-ZR20	0.703	19258	47.85	0.05271	0.47	0.372	0.97	0.0512	0.76	0.79	316	21	322	5	321	5	-1.77	-0.2	322	4.76
LAB3684	123-ZR94	0.987	127664	15.28	0.05307	0.35	0.376	0.67	0.0513	0.44	0.65	332	16	323	3	324	4	2.83	0.4	323	2.76
LAB2083	057-ZR45	4.292	7268	24.40	0.05258	0.87	0.373	1.23	0.0514	0.78	0.64	311	39	323	5	322	7	-3.95	-0.5	323	4.92
LAB3684	109-ZR82	47.494	6234	18.69	0.05421	1.86	0.385	2.00	0.0516	0.64	0.32	380	82	324	4	331	11	14.68	2.1	324	4.01
LAB3684	091-ZR68	3.201	36267	7.01	0.05271	0.88	0.377	1.09	0.0519	0.53	0.49	316	40	326	3	325	6	-3.17	-0.4	326	3.39
LAB3684	099-ZR76	0.419	11448	13.21	0.05338	1.12	0.383	1.34	0.0521	0.64	0.47	345	50	327	4	330	8	5.19	0.7	327	4.06
LAB2083	033-ZR25	0.370	12296	32.57	0.05346	1.01	0.394	1.29	0.0534	0.71	0.55	348	45	335	5	337	7	3.68	0.5	335	4.64
LAB3684	033-ZR23	0.268	73037	14.53	0.05348	0.34	0.409	0.85	0.0554	0.69	0.81	349	15	348	5	348	5	0.53	0.1	348	4.65
LAB2083	068-ZR54	0.352	6524	28.20	0.05377	0.86	0.438	1.12	0.0590	0.62	0.56	361	38	370	4	369	7	-2.27	-0.3	370	4.48
LAB3684	111-ZR84	0.384	19359	45.76	0.05413	1.07	0.444	1.27	0.0595	0.57	0.45	376	48	372	4	373	8	1.10	0.2	372	4.15
LAB2083	014-ZR10	0.299	8050	30.35	0.05706	0.69	0.622	1.08	0.0790	0.75	0.69	494	30	490	7	491	8	0.71	0.1	490	7.06
LAB3684	050-ZR37	0.558	13024	17.22	0.05644	1.06	0.621	1.28	0.0798	0.63	0.49	470	47	495	6	490	10	-5.35	-0.9	495	5.96
LAB3684	073-ZR56	0.434	56716	25.08	0.05830	0.46	0.671	0.78	0.0835	0.51	0.65	541	20	517	5	521	6	4.50	0.9	517	5.04
LAB3684	047-ZR34	0.123	45224	14.25	0.05849	0.52	0.674	0.82	0.0836	0.52	0.63	548	23	517	5	523	7	5.64	1.1	517	5.13
LAB2083	039-ZR31	0.202	34146	30.97	0.05806	0.45	0.673	0.86	0.0840	0.63	0.73	532	20	520	6	522	7	2.26	0.4	520	6.30
LAB2083	008-ZR6	0.308	19339	27.45	0.05933	0.63	0.692	0.95	0.0846	0.60	0.63	579	27	523	6	534	8	9.69	2.0	523	6.02
LAB3684	012-ZR9	0.400	105718	36.57	0.05825	0.60	0.682	0.87	0.0849	0.51	0.59	539	26	526	5	528	7	2.52	0.5	526	5.13
LAB3684	032-ZR22	0.479	42678	16.24	0.05764	0.47	0.675	0.78	0.0850	0.50	0.65	516	21	526	5	524	6	-1.89	-0.3	526	5.09
LAB3684	046-ZR33B	0.191	100777	27.05	0.05784	0.55	0.682	0.91	0.0855	0.62	0.68	524	24	529	6	528	7	-1.05	-0.2	529	6.34
LAB2083	053-ZR41	0.324	27091	30.75	0.05797	0.46	0.688	0.93	0.0861	0.72	0.77	529	20	532	7	532	8	-0.68	-0.1	532	7.37

LAB2083	065-ZR51	0.173	27431	25.90	0.05856	0.45	0.700	0.89	0.0867	0.67	0.75	551	20	536	7	539	7	2.67	0.5	536	6.90
LAB2083	069-ZR55	0.543	43097	24.20	0.05833	0.51	0.720	1.03	0.0895	0.81	0.79	542	22	552	9	550	9	-1.88	-0.4	552	8.60
LAB2083	005-ZR3	0.220	33657	27.30	0.05944	0.46	0.734	0.83	0.0896	0.58	0.70	583	20	553	6	559	7	5.15	1.1	553	6.16
LAB3684	049-ZR36	0.278	35453	14.52	0.05765	0.69	0.713	0.95	0.0897	0.54	0.57	516	30	554	6	547	8	-7.29	-1.3	554	5.73
LAB2083	044-ZR34	0.474	15706	32.84	0.05886	0.54	0.730	0.97	0.0900	0.72	0.74	562	24	555	8	557	8	1.12	0.2	555	7.66
LAB2083	029-ZR23	0.002	39731	30.68	0.05892	0.50	0.733	1.04	0.0902	0.83	0.80	564	22	557	9	558	9	1.26	0.3	557	8.90
LAB2083	038-ZR30	0.358	2880	41.31	0.05926	0.72	0.738	1.08	0.0904	0.72	0.66	577	31	558	8	562	9	3.25	0.7	558	7.64
LAB2083	050-ZR40	0.904	3533	43.18	0.05891	0.83	0.734	1.23	0.0904	0.82	0.67	564	36	558	9	559	11	1.04	0.2	558	8.80
LAB3684	069-ZR52	0.629	24911	21.08	0.05983	0.61	0.755	0.88	0.0916	0.51	0.58	597	27	565	5	571	8	5.43	1.1	565	5.46
LAB2083	023-ZR17	0.526	19988	29.06	0.05936	0.56	0.753	1.08	0.0920	0.85	0.79	580	24	567	9	570	9	2.21	0.5	567	9.24
LAB2083	043-ZR33	0.253	18624	43.04	0.05900	0.68	0.761	1.07	0.0936	0.73	0.69	567	29	577	8	575	9	-1.68	-0.3	577	8.09
LAB3684	074-ZR57	1.927	7507	17.46	0.06036	0.92	0.785	1.23	0.0943	0.72	0.59	616	40	581	8	588	11	5.75	1.2	581	8.00
LAB2083	030-ZR24	0.374	2198	34.16	0.06063	1.47	0.810	1.74	0.0969	0.86	0.49	626	63	596	10	602	16	4.78	1.0	596	9.76
LAB2083	040-ZR32	0.262	31321	34.47	0.06013	0.53	0.804	0.98	0.0970	0.74	0.75	608	23	597	8	599	9	1.89	0.4	597	8.44
LAB2083	056-ZR44	0.431	61570	28.52	0.06027	0.33	0.808	0.80	0.0972	0.63	0.79	613	14	598	7	601	7	2.45	0.5	598	7.18
LAB3684	059-ZR44	0.393	24996	17.67	0.06096	0.70	0.824	0.97	0.0980	0.55	0.57	638	30	603	6	610	9	5.55	1.2	603	6.37
LAB2083	037-ZR29	0.256	32554	29.65	0.06020	0.38	0.818	0.91	0.0985	0.74	0.81	611	16	606	9	607	8	0.78	0.2	606	8.51
LAB2083	063-ZR49	0.176	46720	24.81	0.06005	0.44	0.825	0.84	0.0996	0.61	0.72	605	19	612	7	611	8	-1.10	-0.2	612	7.10
LAB2083	006-ZR4	0.328	15621	32.74	0.06040	0.59	0.830	0.92	0.0997	0.60	0.65	618	26	612	7	614	8	0.87	0.2	612	7.04
LAB3684	043-ZR31	0.243	565056	85.74	0.06048	0.43	0.838	0.76	0.1004	0.51	0.67	621	18	617	6	618	7	0.66	0.1	617	5.99
LAB2083	009-ZR7	0.245	20428	25.46	0.06063	0.46	0.842	1.03	0.1007	0.85	0.82	626	20	618	10	620	10	1.23	0.3	618	10.00
LAB2083	034-ZR26	0.286	41801	32.94	0.06069	0.41	0.866	1.18	0.1034	1.04	0.88	628	17	634	13	633	11	-0.97	-0.2	634	12.56
LAB3684	093-ZR70	0.361	105584	11.54	0.06019	0.38	0.859	0.71	0.1035	0.47	0.66	610	16	635	6	630	7	-4.03	-0.8	635	5.72
LAB3684	107-ZR80	0.437	105993	13.95	0.06096	0.59	0.917	0.88	0.1091	0.54	0.61	638	25	668	7	661	9	-4.64	-1.0	668	6.86
LAB3684	082-ZR61	0.083	115304	23.32	0.06173	0.47	0.930	0.83	0.1093	0.58	0.70	665	20	669	7	668	8	-0.58	-0.1	669	7.35
LAB3684	030-ZR20	0.339	56572	11.37	0.06434	0.57	1.090	0.84	0.1228	0.50	0.59	753	24	747	7	748	9	0.78	0.2	747	7.02
LAB3684	009-ZR6	0.154	60387	16.60	0.06492	0.41	1.139	0.75	0.1272	0.50	0.67	772	17	772	7	772	8	0.00	0.0	772	7.31
LAB2083	007-ZR5	0.195	20313	29.19	0.06600	1.27	1.184	1.50	0.1301	0.70	0.47	806	53	788	10	793	16	2.23	0.6	788	10.45
LAB3684	005-ZR2	0.390	37030	12.70	0.06849	0.51	1.309	0.90	0.1386	0.64	0.71	884	21	837	10	850	10	5.27	1.5	837	10.02

LAB3684	070-ZR53	0.417	52534	15.78	0.06811	0.38	1.304	0.72	0.1388	0.48	0.67	872	16	838	8	847	8	3.89	1.1	838	7.57
LAB3684	007-ZR4	0.462	33570	10.81	0.07032	0.51	1.403	0.85	0.1447	0.57	0.68	938	21	871	9	890	10	7.13	2.1	871	9.36
LAB3684	020-ZR15	0.341	10239	15.49	0.06942	0.79	1.467	1.17	0.1533	0.79	0.67	911	32	919	13	917	14	-0.87	-0.2	919	13.48
LAB2083	016-ZR12	0.116	6433	33.83	0.07313	0.56	1.651	0.93	0.1638	0.64	0.69	1018	23	978	12	990	12	3.92	1.3	978	11.69
LAB3684	053-ZR38	0.243	59498	12.64	0.07199	0.54	1.633	0.86	0.1645	0.55	0.65	986	22	982	10	983	11	0.41	0.1	982	10.05
LAB3684	029-ZR19	0.189	13063	20.21	0.07299	0.88	1.665	1.27	0.1655	0.83	0.66	1014	36	987	15	995	16	2.61	0.8	987	15.21
LAB2083	046-ZR36	0.374	54577	33.56	0.07379	0.36	1.692	0.76	0.1663	0.56	0.74	1036	14	992	10	1006	10	4.27	1.4	992	10.29
LAB3684	017-ZR12	0.265	40683	19.40	0.07254	0.46	1.665	0.83	0.1664	0.57	0.69	1001	19	992	11	995	10	0.87	0.3	992	10.54
LAB3684	121-ZR92	0.088	290674	11.78	0.07475	0.27	1.717	0.70	0.1666	0.53	0.76	1062	11	993	10	1015	9	6.46	2.1	993	9.72
LAB2083	059-ZR47	0.268	16508	29.70	0.07249	0.53	1.762	0.94	0.1762	0.68	0.73	1000	22	1046	13	1031	12	-4.65	-1.4	1000	21.60
LAB3684	119-ZR90	0.180	3627	14.70	0.07277	1.59	1.731	2.57	0.1725	1.99	0.77	1008	64	1026	38	1020	33	-1.78	-0.6	1008	63.85
LAB3684	087-ZR66	0.578	95640	20.22	0.07311	0.44	1.747	0.74	0.1733	0.46	0.63	1017	18	1030	9	1026	10	-1.30	-0.4	1017	17.68
LAB3684	042-ZR30	0.363	29835	11.00	0.07329	0.51	1.723	0.96	0.1705	0.73	0.76	1022	21	1015	14	1017	12	0.70	0.2	1022	20.68
LAB3684	036-ZR26	0.180	70883	20.07	0.07335	0.36	1.751	0.77	0.1732	0.57	0.74	1024	15	1029	11	1028	10	-0.56	-0.2	1024	14.59
LAB3684	055-ZR40	0.338	85104	12.85	0.07378	0.45	1.795	0.81	0.1765	0.57	0.70	1035	18	1048	11	1044	11	-1.19	-0.4	1035	18.11
LAB2083	027-ZR21	0.944	27823	29.47	0.07421	0.42	1.754	0.89	0.1714	0.70	0.78	1047	17	1020	13	1029	12	2.60	0.9	1047	16.78
LAB3684	048-ZR35	0.193	25804	13.51	0.07433	0.58	1.753	0.96	0.1711	0.66	0.70	1050	23	1018	13	1028	12	3.08	1.0	1050	23.19
LAB3684	127-ZR98	0.278	71568	12.28	0.07434	0.36	1.791	0.82	0.1747	0.63	0.77	1051	14	1038	12	1042	11	1.19	0.4	1051	14.44
LAB3684	057-ZR42	0.246	42985	24.09	0.07460	0.51	1.759	0.87	0.1710	0.60	0.68	1058	21	1018	11	1031	11	3.78	1.2	1058	20.66
LAB3684	080-ZR59	0.606	63161	11.22	0.07490	0.47	1.832	0.84	0.1774	0.59	0.71	1066	19	1053	11	1057	11	1.23	0.4	1066	18.66
LAB3684	110-ZR83	0.285	48765	17.98	0.07524	0.41	1.869	0.81	0.1801	0.58	0.72	1075	17	1068	11	1070	11	0.67	0.2	1075	16.62
LAB3684	060-ZR45	0.183	130808	21.88	0.07547	0.33	1.864	0.74	0.1791	0.54	0.74	1081	13	1062	11	1068	10	1.76	0.6	1081	13.26
LAB3684	041-ZR29	0.305	19534	19.75	0.07557	0.49	1.859	0.94	0.1784	0.71	0.75	1084	20	1058	14	1067	12	2.34	0.8	1084	19.73
LAB3684	114-ZR87	0.362	42523	14.32	0.07572	0.43	1.962	0.80	0.1879	0.57	0.71	1088	17	1110	12	1102	11	-2.04	-0.7	1088	17.05
LAB2083	024-ZR18	0.520	69663	29.37	0.07614	0.49	1.860	1.17	0.1772	1.00	0.85	1099	19	1052	19	1067	15	4.30	1.5	1099	19.41
LAB3684	092-ZR69	0.121	96931	45.71	0.07892	0.50	2.155	0.81	0.1980	0.51	0.64	1170	20	1165	11	1167	11	0.45	0.2	1170	19.77
LAB2083	047-ZR37	0.352	81208	24.51	0.07900	0.36	2.020	0.90	0.1855	0.73	0.82	1172	14	1097	15	1122	12	6.44	2.3	1172	14.35
LAB2083	036-ZR28	0.243	23112	32.77	0.07904	0.49	2.127	0.85	0.1952	0.60	0.70	1173	19	1149	13	1158	12	2.03	0.7	1173	19.28
LAB2083	055-ZR43	0.310	27395	29.56	0.07931	0.40	2.222	0.87	0.2032	0.68	0.78	1180	16	1193	15	1188	12	-1.08	-0.4	1180	15.58

LAB3684	098-ZR75	0.799	100177	15.69	0.07931	0.44	2.129	0.77	0.1947	0.51	0.66	1180	17	1147	11	1158	11	2.82	1.0	1180	17.29
LAB2083	070-ZR56	0.204	61539	35.56	0.07966	0.53	2.172	0.85	0.1978	0.55	0.65	1189	21	1163	12	1172	12	2.13	0.8	1189	20.78
LAB3684	065-ZR48	0.131	53915	56.84	0.07977	0.36	2.077	0.72	0.1888	0.50	0.69	1191	14	1115	10	1141	10	6.40	2.3	1191	14.19
LAB3684	106-ZR79	0.138	50192	30.53	0.07983	0.63	2.116	1.21	0.1922	0.97	0.80	1193	25	1133	20	1154	17	4.99	1.8	1193	24.63
LAB3684	021-ZR16	0.487	37526	15.79	0.08041	0.67	2.124	1.32	0.1916	1.08	0.81	1207	26	1130	22	1157	18	6.39	2.3	1207	26.36
LAB3684	018-ZR13	0.531	73177	14.84	0.08061	0.28	2.233	0.69	0.2009	0.51	0.74	1212	11	1180	11	1192	10	2.63	1.0	1212	10.82
LAB2083	018-ZR14	0.190	41135	38.42	0.08093	0.37	2.202	0.85	0.1973	0.67	0.79	1220	14	1161	14	1182	12	4.83	1.8	1220	14.33
LAB3684	010-ZR7	0.258	61395	16.45	0.08129	0.55	2.234	0.83	0.1993	0.49	0.59	1228	22	1172	10	1192	12	4.62	1.7	1228	21.71
LAB3684	067-ZR50	0.314	38528	18.65	0.08153	0.34	2.218	0.78	0.1973	0.60	0.77	1234	13	1161	13	1187	11	5.96	2.2	1234	13.33
LAB3684	037-ZR27	0.191	146044	20.53	0.08181	0.48	2.233	1.08	0.1979	0.89	0.83	1241	19	1164	19	1191	15	6.20	2.3	1241	18.92
LAB3684	044-ZR32	0.280	15428	14.69	0.08399	0.65	2.366	1.12	0.2043	0.83	0.74	1292	25	1198	18	1232	16	7.29	2.8	1292	25.33
LAB2083	025-ZR19	0.251	36514	41.45	0.08647	0.30	2.668	0.80	0.2237	0.64	0.80	1349	12	1302	15	1320	12	3.50	1.4	1349	11.68
LAB3684	072-ZR55	0.255	45232	16.18	0.08719	0.41	2.748	0.79	0.2286	0.57	0.72	1365	16	1327	14	1342	12	2.74	1.1	1365	15.76
LAB3684	071-ZR54	0.298	38088	32.51	0.08751	0.46	2.745	0.81	0.2275	0.55	0.68	1372	18	1321	13	1341	12	3.68	1.5	1372	17.75
LAB2083	004-ZR2	0.127	11174	34.63	0.08947	0.44	2.790	0.91	0.2262	0.71	0.78	1414	17	1314	17	1353	14	7.07	2.9	1414	16.74
LAB3684	054-ZR39	0.149	49734	18.21	0.09025	0.38	3.114	0.87	0.2502	0.69	0.80	1431	14	1440	18	1436	13	-0.61	-0.2	1431	14.36
LAB2083	015-ZR11	0.367	9040	36.03	0.09028	0.48	3.129	1.05	0.2513	0.85	0.81	1431	18	1445	22	1440	16	-0.97	-0.4	1431	18.35
LAB2083	013-ZR9	0.302	18942	38.57	0.09420	0.44	3.242	0.88	0.2496	0.67	0.76	1512	17	1436	17	1467	14	5.03	2.1	1512	16.60
LAB3684	086-ZR65	0.202	91157	12.44	0.09522	0.48	3.510	0.98	0.2673	0.78	0.79	1532	18	1527	21	1529	16	0.35	0.1	1532	17.89
LAB3684	034-ZR24	0.270	100744	18.29	0.10608	0.27	4.508	0.68	0.3082	0.50	0.73	1733	10	1732	15	1732	11	0.08	0.0	1733	9.94
LAB3684	113-ZR86	0.242	2665996	94.13	0.10997	0.44	4.732	0.88	0.3121	0.67	0.76	1799	16	1751	20	1773	15	2.67	1.2	1799	16.05
LAB3684	022-ZR17N	0.640	153685	10.56	0.11840	0.47	5.830	0.85	0.3571	0.61	0.71	1932	17	1968	21	1951	15	-1.87	-0.9	1932	16.62
LAB2083	054-ZR42	0.432	40647	33.99	0.12150	0.31	5.848	0.90	0.3490	0.75	0.84	1978	11	1930	25	1954	15	2.45	1.2	1978	11.14
LAB3684	019-ZR14	0.337	128561	12.79	0.12235	0.33	5.653	0.74	0.3351	0.56	0.75	1991	12	1863	18	1924	13	6.41	3.2	1991	11.62
LAB3684	094-ZR71	0.315	145880	13.35	0.12796	0.29	6.681	0.69	0.3786	0.51	0.73	2070	10	2070	18	2070	12	0.02	0.0	2070	10.27
LAB3684	068-ZR51	0.222	128223	19.53	0.13223	0.23	6.663	0.78	0.3655	0.65	0.83	2128	8	2008	22	2068	14	5.63	2.9	2128	8.00
LAB3684	108-ZR81	0.305	178139	24.01	0.13277	0.34	7.367	0.80	0.4024	0.62	0.78	2135	12	2180	23	2157	14	-2.11	-1.1	2135	11.85
LAB3684	081-ZR60	0.455	64469	12.97	0.13751	0.32	7.560	0.79	0.3987	0.63	0.79	2196	11	2163	23	2180	14	1.51	0.8	2196	10.98

LAB3684	125-ZR96	0.688	229243	16.80	0.14854	0.24	8.861	0.74	0.4326	0.59	0.80	2329	8	2317	23	2324	13	0.51	0.3	2329	8.17
LAB3684	031-ZR21	0.337	143302	16.93	0.16375	0.26	10.587	0.71	0.4689	0.55	0.77	2495	9	2479	23	2488	13	0.64	0.4	2495	8.58
LAB3684	058-ZR43	0.501	45098	21.16	0.18467	0.33	12.357	0.99	0.4853	0.86	0.87	2695	11	2550	36	2632	18	5.38	3.1	2695	10.83
Data not used due to high discordance																					
LAB2083	003-ZR1	0.341	20567	56.77	0.19748	0.42	12.238	1.13	0.4494	0.98	0.87	2805	14	2393	39	2623	21	14.72	8.8		
LAB3684	015-ZR10	0.304	114790	34.19	0.09619	0.43	3.242	0.77	0.2444	0.52	0.67	1551	16	1410	13	1467	12	9.15	3.9		
LAB2083	019-ZR15	0.153	2413	15.46	0.10374	0.53	1.305	2.41	0.0912	2.32	0.96	1692	20	563	25	848	28	66.74	33.6		
LAB2083	020-ZR16	0.908	7261	32.72	0.05421	0.74	0.389	1.14	0.0520	0.80	0.69	380	33	327	5	334	6	13.90	2.0		
LAB3684	024-ZR18	0.284	22033	24.91	0.07931	1.32	1.803	1.55	0.1649	0.71	0.46	1180	52	984	13	1046	20	16.63	6.0		
LAB3684	035-ZR25	0.259	11514	68.53	0.08797	4.07	2.226	4.18	0.1835	0.89	0.21	1382	152	1086	18	1189	58	21.39	8.7		
LAB3684	045-ZR33N	0.269	44957	26.45	0.08448	3.03	0.832	3.86	0.0714	2.36	0.61	1304	116	445	20	615	35	65.88	27.7		
LAB2083	045-ZR35	0.252	1037	6.41	0.09441	1.78	1.584	2.15	0.1217	1.15	0.53	1516	67	740	16	964	27	51.19	23.2		
LAB3684	056-ZR41	0.027	197702	16.47	0.06736	0.40	1.114	1.30	0.1200	1.18	0.91	849	16	730	16	760	14	13.95	3.9		
LAB2083	058-ZR46	0.228	11497	26.65	0.07266	0.63	1.944	1.37	0.1940	1.16	0.85	1004	25	1143	24	1096	18	-13.82	-4.3		
LAB2083	060-ZR48	0.001	17598	27.18	0.05831	0.65	0.825	1.03	0.1026	0.71	0.69	542	28	630	8	611	9	-16.25	-3.1		
LAB3684	062-ZR47	0.101	57000	48.83	0.10765	1.82	2.432	3.43	0.1639	2.88	0.84	1760	66	978	52	1252	49	44.42	21.9		
LAB3684	066-ZR49	0.413	58359	26.58	0.10256	1.31	1.923	1.69	0.1360	1.00	0.59	1671	48	822	15	1089	22	50.80	24.5		
LAB3684	079-ZR58	6.195	5572	16.57	0.07100	2.19	0.484	2.38	0.0494	0.87	0.36	957	88	311	5	401	16	67.53	22.4		
LAB3684	088-ZR67	0.301	632	2.05	0.09713	0.48	1.483	0.85	0.1107	0.60	0.70	1570	18	677	8	923	10	56.88	26.7		
LAB3684	095-ZR72	0.253	17987	12.96	0.07654	1.15	1.758	1.59	0.1665	1.03	0.65	1109	46	993	19	1030	20	10.48	3.6		
LAB3684	105-ZR78	0.378	303810	18.81	0.11809	0.87	4.689	1.37	0.2879	0.99	0.73	1927	31	1631	29	1765	23	15.37	7.6		
LAB3684	124-ZR95	0.277	95221	22.34	0.06664	0.53	0.988	0.85	0.1075	0.55	0.65	827	22	658	7	698	9	20.36	5.6		
LAB3684	126-ZR97	0.383	35933	52.39	0.06433	2.50	1.225	2.70	0.1381	0.97	0.36	752	104	834	15	812	30	-10.83	-2.7		
LAB3684	128-ZR99	0.075	450204	22.66	0.21126	0.62	13.709	0.87	0.4706	0.49	0.56	2915	20	2486	20	2730	16	14.72	8.9		
LAB3684	129-ZR100	0.665	8417	15.91	0.05794	3.36	0.771	3.48	0.0965	0.82	0.23	528	144	594	9	580	31	-12.60	-2.3		
Data not used due high analytical error																					
LAB3684	006-ZR3	0.307	5313	47.20	0.05759	5.09	0.650	5.14	0.0818	0.57	0.11	514	216	507	6	508	41	1.39	0.3		
LAB3684	011-ZR8	0.259	1911	20.05	0.03455	27.86	0.452	27.87	0.0950	0.77	0.03	-745	1288	585	9	379	169	178.52	-54.3		

LAB3684	096-ZR73	209.718	1241	34.77	0.05688	6.34	0.433	7.33	0.0552	3.66	0.50	487	268	346	25	365	44	28.91	5.2
LAB3684	100-ZR77	3.089	1045	8.76	0.05715	3.99	0.368	6.16	0.0467	4.67	0.76	497	171	294	27	318	33	40.77	7.5
LAB3684	112-ZR85	9475.227	32	14.76	0.51473	9.16	1720.425	47.96	24.2395	47.07	0.98	4284	257	20812	4809	7566	795	-385.81	-175.1
LAB3684	118-ZR89	191.288	1013	13.16	0.05842	4.20	0.420	5.10	0.0521	2.86	0.56	546	178	328	18	356	30	39.97	8.0
Data not used due to elevated 204Pb																			
LAB3684	023-ZR17B	0.821	234	1.41	0.14802	1.15	2.381	1.97	0.1167	1.56	0.79	2323	39	711	21	1237	28	69.38	42.5
LAB3684	061-ZR46	0.409	475	12.08	0.10153	0.67	3.207	0.97	0.2290	0.61	0.62	1652	25	1329	15	1459	15	19.54	8.9
LAB2083	066-ZR52	0.093	412	28.65	0.06501	4.30	0.874	7.86	0.0975	6.57	0.84	775	176	600	75	638	73	22.56	6.0
LAB3684	083-ZR62	109.604	300	15.37	0.05540	13.18	0.425	14.86	0.0556	6.87	0.46	429	539	349	47	360	88	18.56	3.0
LAB3684	085-ZR64	1050.829	441	15.45	0.08805	3.41	0.879	6.98	0.0724	6.08	0.87	1384	128	451	53	641	65	67.42	29.6
LAB3684	117-ZR88	14.451	38	7.77	0.79372	3.11	17.637	6.42	0.1611	5.60	0.87	4911	87	963	100	2970	120	80.39	67.6

Data report template (with modifications) from http://www.plasmage.org/recommendations

[1] Convertion factor from mV to CPS is 62500000

[2] concentration uncertainty c.20%

[3] data not corrected for common-Pb

[4] not corrected for common-Pb

[5] Discordance calculated as (1-(^{206}Pb/^{238}U age/^{207}Pb/^{206}Pb age))*100

[6] Discordance calculated as (1-(^{206}Pb/^{238}U age/^{207}Pb/^{205}Pb age))*100

[7]Best age: 207Pb/206Pb (Ages > 1.5 Ga) and 206Pb/238U (Ages < 1.5 Ga)

Decay constants of Jaffey et al 1971 used

Amostra MD-2019-4A

			Ratios										Rho	Ages (Ma)						% conc [1]	Best age	2s
Sample	Spot number	Th/U	206Pb/204Pb	1s	238U/206Pb	1s	207Pb/206Pb	1s	207Pb/235U	1s	206Pb/238U	1s		207Pb/206Pb	2s	206Pb/238U	2s	207Pb/235U	2s			
MD-2019-4A				(%)		(%)		(%)		(%)		(%)			(abs)		(abs)		(abs)			(abs)
LABX0019	LABSMPABC010.FIN2	0.3	1073.8	97.1	3.84	7.0	0.09825	4.17	3.5499	12.8	0.26126	7.2	0.5	1585	156	1496	193	1537	203	94.4	1585	156
LABX0019	LABSMPABC015.FIN2	0.6	4145.6	68.2	3.67	7.0	0.09715	4.04	3.6691	12.8	0.27406	7.2	0.7	1565	153	1561	199	1563	199	99.7	1565	153
LABX0019	LABSMPABC031.FIN2	1.1	1597.4	70.9	4.18	7.1	0.09671	4.01	3.2100	12.7	0.24014	7.2	0.8	1559	150	1387	179	1459	197	89.0	1559	150

LABX0019	LABSMPABC108.FIN2	1.0	4088.6	78.1	3.92	7.3	0.09649	4.00	3.4221	12.7	0.25630	7.2	0.7	1555	150	1470	189	1509	201	94.6	1555	150
LABX0019	LABSMPABC143.FIN2	0.7	3038.1	68.5	4.05	7.1	0.09639	4.23	3.3033	12.8	0.24743	7.2	0.5	1543	156	1425	183	1478	197	92.4	1543	156
LABX0019	LABSMPABC051.FIN2	0.8	5945.2	98.8	3.71	7.3	0.09310	3.98	3.4963	12.8	0.27013	7.2	0.6	1488	151	1541	197	1526	203	103.6	1541	197
LABX0019	LABSMPABC030.FIN2	0.1	178.6	177.7	3.75	7.2	0.09307	4.09	3.4871	12.7	0.26730	7.1	0.4	1483	153	1527	194	1523	199	103.0	1527	194
LABX0019	LABSMPABC052.FIN2	0.5	695.0	122.0	3.87	6.8	0.09418	4.04	3.3677	12.7	0.25900	7.2	0.5	1515	168	1484	189	1496	198	98.0	1515	168
LABX0019	LABSMPABC124.FIN2	0.0	1386.1	114.4	3.72	7.3	0.09421	4.15	3.5225	12.8	0.27024	7.2	0.5	1504	156	1541	198	1530	201	102.5	1504	156
LABX0019	LABSMPABC090.FIN2	0.7	6354.5	37.7	3.91	7.1	0.08993	4.03	3.1795	12.7	0.25586	7.2	0.5	1421	154	1468	188	1452	199	103.3	1468	188
LABX0019	LABSMPABC070.FIN2	1.5	75.9	302.6	4.02	7.1	0.08811	4.24	3.0392	12.8	0.24910	7.2	0.2	1372	152	1434	184	1415	185	104.5	1434	184
LABX0019	LABSMPABC013.FIN2	0.9	376.8	73.4	4.02	7.1	0.08806	4.04	3.0451	12.7	0.24893	7.1	0.2	1379	156	1433	183	1418	194	103.9	1433	183
LABX0019	LABSMPABC032.FIN2	0.5	12933.8	46.6	4.03	7.2	0.09236	4.00	3.1753	12.7	0.24840	7.2	0.4	1472	153	1430	183	1451	196	97.2	1430	183
LABX0019	LABSMPABC102.FIN2	1.1	3944.1	44.2	4.03	7.3	0.08727	4.01	2.9929	12.7	0.24821	7.1	0.2	1363	153	1429	183	1405	194	104.8	1429	183
LABX0019	LABSMPABC054.FIN2	0.6	3434.2	66.8	4.04	7.0	0.08763	3.99	3.0150	12.8	0.24779	7.2	0.8	1372	152	1427	183	1411	193	104.0	1427	183
LABX0019	LABSMPABC099.FIN2	0.9	490.1	83.5	4.05	7.3	0.08916	4.02	3.0515	12.7	0.24725	7.2	0.4	1411	170	1424	183	1420	193	100.9	1424	183
LABX0019	LABSMPABC070.FIN2	0.8	3604.6	52.2	4.07	7.1	0.08710	3.99	2.9595	12.7	0.24631	7.2	0.4	1360	152	1419	182	1397	194	104.3	1419	182
LABX0019	LABSMPABC046.FIN2	0.6	65.6	594.5	4.08	6.7	0.09191	4.11	3.1089	12.8	0.24634	7.2	0.7	1458	156	1419	182	1433	192	97.3	1419	182
LABX0019	LABSMPABC018.FIN2	1.6	228.7	393.1	4.07	7.3	0.08743	3.99	3.0005	12.7	0.24618	7.1	0.6	1367	153	1419	182	1407	194	103.7	1419	182
LABX0019	LABSMPABC069.FIN2	0.8	2810.9	57.6	4.07	7.1	0.08819	4.00	3.0140	12.7	0.24578	7.2	0.2	1384	152	1416	182	1411	192	102.4	1416	182
LABX0019	LABSMPABC032.FIN2	0.1	22490.6	99.5	4.08	7.2	0.08522	4.00	2.9329	12.7	0.24532	7.1	0.5	1318	156	1414	182	1390	192	107.3	1414	182
LABX0019	LABSMPABC081.FIN2	2.0	782.0	106.0	4.13	7.4	0.08620	4.00	2.8960	12.7	0.24296	7.2	0.5	1340	156	1402	181	1380	192	104.6	1402	181
LABX0019	LABSMPABC028.FIN2	0.3	395.2	187.7	4.12	7.1	0.08789	3.98	2.9873	12.7	0.24281	7.1	0.6	1378	154	1401	180	1404	193	101.7	1401	180
LABX0019	LABSMPABC045.FIN2	0.8	1250.7	123.3	4.12	7.4	0.08643	3.98	2.9275	12.8	0.24269	7.2	0.5	1350	138	1401	181	1389	193	103.8	1401	181
LABX0019	LABSMPABC009.FIN2	1.0	3271.2	54.0	4.13	7.2	0.08761	3.99	2.9372	12.7	0.24253	7.2	0.7	1372	154	1400	181	1391	193	102.0	1400	181
LABX0019	LABSMPABC101.FIN2	0.9	1269.6	113.2	4.14	8.4	0.08744	4.01	2.9317	12.7	0.24095	7.2	0.7	1368	155	1397	215	1390	192	102.2	1397	215
LABX0019	LABSMPABC033.FIN2	0.1	346.0	144.7	4.15	7.2	0.08719	4.09	2.9596	12.8	0.24153	7.2	0.7	1358	151	1394	180	1400	208	102.7	1394	180
LABX0019	LABSMPABC064.FIN2	6.6	17.4	1106.0	4.18	7.3	0.08632	4.15	2.8643	12.8	0.23996	7.2	0.5	1336	156	1386	179	1370	188	103.7	1386	179
LABX0019	LABSMPABC013.FIN2	1.2	2672.9	115.8	4.19	6.9	0.08964	4.11	2.9468	12.7	0.23930	7.2	0.4	1412	155	1383	178	1393	192	97.9	1383	178
LABX0019	LABSMPABC036.FIN2	0.8	703.7	74.6	4.18	6.5	0.08826	4.15	2.9139	12.8	0.23877	7.2	0.2	1379	157	1380	178	1384	192	100.1	1380	178
LABX0019	LABSMPABC072.FIN2	0.9	1065.1	54.0	4.19	7.2	0.08718	4.04	2.8779	12.7	0.23874	7.1	0.2	1367	140	1380	178	1375	191	100.9	1380	178
LABX0019	LABSMPABC010.FIN2	0.7	276.5	451.2	4.20	7.2	0.08569	3.99	2.8372	12.7	0.23859	7.1	0.3	1329	155	1379	178	1365	190	103.8	1379	178

LABX0019	LABSMPABC027.FIN2	0.5	724.8	116.2	4.20	7.2	0.08479	4.00	2.8295	12.7	0.23855	7.1	0.5	1308	156	1379	177	1363	191	105.4	1379	177
LABX0019	LABSMPABC089.FIN2	1.5	16887.9	97.1	4.21	7.1	0.08926	4.02	2.9200	12.7	0.23763	7.1	0.4	1407	153	1374	177	1387	193	97.6	1374	177
LABX0019	LABSMPABC068.FIN2	0.9	845.5	120.7	4.23	6.9	0.08857	3.99	2.9014	12.7	0.23681	7.2	0.8	1393	153	1370	176	1381	191	98.4	1370	176
LABX0019	LABSMPABC065.FIN2	0.9	671.5	148.9	4.23	7.2	0.08800	4.10	2.8754	12.7	0.23672	7.2	0.3	1375	155	1369	177	1374	191	99.6	1369	177
LABX0019	LABSMPABC121.FIN2	0.4	807.9	72.4	4.27	8.1	0.08652	4.10	2.8404	12.9	0.23623	7.3	0.9	1342	167	1366	180	1361	201	101.8	1366	180
LABX0019	LABSMPABC046.FIN2	1.5	244.2	136.5	4.26	7.0	0.08636	4.06	2.8336	12.7	0.23517	7.2	0.2	1341	159	1361	175	1367	209	101.5	1361	175
LABX0019	LABSMPABC136.FIN2	0.7	1016.1	120.9	4.27	7.1	0.08607	4.01	2.7984	12.7	0.23465	7.2	0.3	1336	156	1359	175	1355	191	101.7	1359	175
LABX0019	LABSMPABC137.FIN2	0.7	3675.2	39.3	4.30	7.4	0.08676	4.05	2.7984	12.7	0.23283	7.2	0.4	1350	158	1349	175	1354	192	99.9	1349	175
LABX0019	LABSMPABC045.FIN2	5.8	647.4	84.3	4.31	7.1	0.08659	4.02	2.7858	12.7	0.23252	7.2	0.4	1348	152	1348	174	1351	189	100.0	1348	174
LABX0019	LABSMPABC012.FIN2	2.2	2134.2	155.4	4.31	7.1	0.08773	3.98	2.8187	12.7	0.23194	7.1	0.5	1374	155	1345	173	1360	191	97.8	1345	173
LABX0019	LABSMPABC029.FIN2	0.8	552.5	193.5	4.36	7.4	0.08904	4.03	2.8232	12.7	0.23060	7.2	0.7	1401	153	1337	174	1360	193	95.4	1337	174
LABX0019	LABSMPABC144.FIN2	1.1	750.7	60.9	4.35	7.3	0.08402	4.11	2.6779	12.8	0.23031	7.2	0.2	1285	166	1336	173	1321	192	104.0	1336	173
LABX0019	LABSMPABC126.FIN2	1.5	485.2	131.7	4.37	7.2	0.08810	4.09	2.7967	12.8	0.22925	7.2	0.6	1380	155	1330	173	1353	193	96.4	1330	173
LABX0019	LABSMPABC048.FIN2	0.5	284.7	175.6	4.38	6.9	0.08427	4.10	2.6760	12.7	0.22838	7.2	0.9	1302	143	1326	171	1321	189	101.8	1326	171
LABX0019	LABSMPABC018.FIN2	0.7	2415.4	42.6	4.39	6.8	0.08786	4.02	2.7774	12.8	0.22816	7.2	0.7	1376	156	1325	171	1348	184	96.3	1325	171
LABX0019	LABSMPABC067.FIN2	1.6	505.5	60.0	4.42	7.3	0.08699	4.20	2.6900	12.8	0.22659	7.2	0.6	1355	157	1316	172	1333	250	97.2	1316	172
LABX0019	LABSMPABC053.FIN2	1.9	41.4	590.7	4.43	7.2	0.08647	4.16	2.6969	12.8	0.22462	7.2	0.3	1339	160	1306	170	1326	186	97.5	1306	170
LABX0019	LABSMPABC068.FIN2	0.9	1005.6	90.6	4.51	6.9	0.08879	4.04	2.7340	12.7	0.22253	7.2	0.5	1395	153	1295	168	1337	190	92.8	1295	168
LABX0019	LABSMPABC014.FIN2	1.0	2158.0	52.1	4.56	7.2	0.08527	4.09	2.6099	12.8	0.21985	7.2	0.5	1324	174	1281	166	1302	184	96.7	1281	166
LABX0019	LABSMPABC011.FIN2	1.9	236.1	126.6	4.59	7.2	0.08129	4.05	2.4544	12.7	0.21811	7.2	0.3	1223	158	1272	165	1258	182	103.9	1272	165
LABX0019	LABSMPABC083.FIN2	1.2	733.4	93.5	4.59	7.2	0.07994	4.03	2.4100	12.7	0.21793	7.1	0.4	1191	158	1271	165	1245	182	106.7	1271	165
LABX0019	LABSMPABC072.FIN2	0.8	526.7	93.2	4.61	7.2	0.08938	4.30	2.6953	12.9	0.21748	7.2	0.5	1399	162	1268	165	1323	186	90.7	1268	165
LABX0019	LABSMPABC063.FIN2	0.1	681.1	48.1	4.65	6.9	0.08287	4.11	2.4634	12.8	0.21608	7.2	0.7	1259	159	1261	164	1259	185	100.2	1261	164
LABX0019	LABSMPABC016.FIN2	0.7	578.6	114.1	4.65	7.2	0.08105	4.01	2.4233	12.7	0.21546	7.1	0.4	1219	157	1258	163	1249	182	103.2	1258	163
LABX0019	LABSMPABC016.FIN2	1.0	319.6	109.9	4.66	7.1	0.08810	4.02	2.6212	12.7	0.21506	7.2	0.5	1381	156	1255	164	1306	187	90.9	1255	164
LABX0019	LABSMPABC069.FIN2	0.3	386.6	130.3	4.70	7.2	0.08054	4.03	2.3756	12.7	0.21320	7.2	0.6	1206	158	1246	162	1234	179	103.3	1246	162
LABX0019	LABSMPABC029.FIN2	0.4	3810.8	122.4	4.71	7.1	0.07934	4.01	2.3632	12.7	0.21262	7.1	0.5	1177	158	1243	161	1231	180	105.6	1243	161
LABX0019	LABSMPABC036.FIN2	0.0	776.5	95.9	4.72	7.2	0.07874	4.01	2.3401	12.7	0.21199	7.2	0.3	1162	158	1239	161	1224	180	106.6	1239	161
LABX0019	LABSMPABC050.FIN2	0.6	237.6	147.8	4.74	7.6	0.08789	4.30	2.5342	12.8	0.21148	7.2	0.1	1379	166	1236	162	1284	205	89.6	1236	162

LABX0019	LABSMPABC012.FIN2	0.4	1813.2	77.1	4.76	7.3	0.08198	4.14	2.3839	12.8	0.21070	7.2	0.2	1236	155	1232	161	1236	183	99.7	1232	161
LABX0019	LABSMPABC035.FIN2	0.0	610.0	131.5	4.77	6.8	0.07860	4.12	2.3148	12.8	0.21026	7.2	0.6	1157	161	1230	161	1216	179	106.3	1230	161
LABX0019	LABSMPABC100.FIN2	0.8	829.8	73.5	4.77	7.3	0.08007	4.00	2.3284	12.7	0.21000	7.2	0.5	1196	159	1229	160	1221	180	102.8	1229	160
LABX0019	LABSMPABC103.FIN2	0.6	21713.1	111.4	4.79	7.2	0.07850	4.00	2.2721	12.7	0.20910	7.2	0.5	1157	159	1224	160	1203	178	105.8	1224	160
LABX0019	LABSMPABC014.FIN2	1.1	506.9	37.5	4.80	7.1	0.08320	4.53	2.3990	12.9	0.20843	7.2	0.1	1256	177	1220	159	1239	183	97.2	1220	159
LABX0019	LABSMPABC064.FIN2	0.9	558.3	71.4	4.86	7.2	0.08207	4.07	2.3440	12.8	0.20610	7.2	0.6	1241	161	1208	158	1224	184	97.3	1208	158
LABX0019	LABSMPABC063.FIN2	0.4	11773.4	71.6	4.87	7.1	0.08040	4.11	2.2881	12.7	0.20581	7.2	0.3	1199	160	1206	158	1208	179	100.6	1206	158
LABX0019	LABSMPABC084.FIN2	1.0	3179.8	52.0	4.88	7.1	0.07834	4.03	2.2379	12.7	0.20543	7.2	0.4	1151	161	1204	157	1192	177	104.6	1204	157
LABX0019	LABSMPABC071.FIN2	1.2	44.4	316.8	4.95	7.1	0.07900	4.20	2.2132	12.8	0.20222	7.2	0.7	1163	165	1187	155	1184	177	102.1	1187	155
LABX0019	LABSMPABC017.FIN2	0.9	45.0	298.0	5.00	7.4	0.08145	4.20	2.2852	12.8	0.20147	7.2	0.5	1233	178	1183	156	1205	178	95.9	1183	156
LABX0019	LABSMPABC105.FIN2	0.8	93.5	161.1	5.03	7.3	0.08419	4.30	2.3236	12.8	0.19935	7.2	0.4	1282	163	1172	154	1216	179	91.4	1172	154
LABX0019	LABSMPABC054.FIN2	1.3	745.8	141.7	5.06	6.9	0.07892	4.04	2.1662	12.8	0.19837	7.2	0.7	1165	162	1166	153	1169	176	100.1	1166	153
LABX0019	LABSMPABC052.FIN2	0.8	2472.7	82.0	5.11	7.0	0.07628	4.07	2.0932	12.8	0.19630	7.2	0.5	1111	191	1155	152	1145	176	104.0	1155	152
LABX0019	LABSMPABC140.FIN2	0.2	870.6	166.0	5.12	7.7	0.07671	4.00	2.0831	12.7	0.19583	7.2	0.7	1111	158	1153	152	1143	174	103.8	1153	152
LABX0019	LABSMPABC035.FIN2	0.8	148.9	234.3	5.13	7.4	0.07868	4.33	2.1031	12.8	0.19545	7.2	0.2	1151	180	1151	152	1148	178	100.0	1151	152
LABX0019	LABSMPABC125.FIN2	0.7	87.2	971.1	5.19	7.1	0.07675	4.01	2.0481	12.7	0.19321	7.2	0.6	1111	161	1139	149	1134	192	102.5	1139	149
LABX0019	LABSMPABC049.FIN2	1.4	241.0	382.1	5.22	7.1	0.07837	4.05	2.0780	12.8	0.19204	7.2	0.6	1153	157	1132	149	1141	174	98.2	1132	149
LABX0019	LABSMPABC119.FIN2	0.9	172.5	99.1	5.46	6.6	0.07552	4.18	1.9142	12.8	0.18334	7.2	0.3	1071	168	1085	145	1084	169	101.3	1085	145
LABX0019	LABSMPABC120.FIN2	0.7	234.4	116.4	5.52	6.5	0.07350	4.14	1.8413	12.8	0.18087	7.2	0.3	1018	166	1072	142	1059	169	105.3	1072	142
LABX0019	LABSMPABC047.FIN2	0.8	1050.4	48.9	5.55	7.4	0.07468	4.84	1.8880	13.1	0.18073	7.2	0.0	1033	172	1071	142	1071	162	103.6	1071	142
LABX0019	LABSMPABC122.FIN2	2.2	1860.6	48.0	5.57	6.5	0.07620	4.09	1.8899	12.7	0.17916	7.2	0.1	1093	164	1062	140	1077	169	97.2	1062	140
LABX0019	LABSMPABC047.FIN2	0.8	871.1	51.8	5.59	7.0	0.07400	4.08	1.8338	12.7	0.17914	7.1	0.2	1034	167	1062	140	1057	168	102.7	1062	140
LABX0019	LABSMPABC048.FIN2	8.1	30.6	2309.1	5.62	7.5	0.07759	4.03	1.9204	12.8	0.17869	7.2	0.8	1132	160	1060	141	1086	172	93.6	1060	141
LABX0019	LABSMPABC107.FIN2	1.0	1007.2	52.9	5.69	6.7	0.07450	4.03	1.8104	12.7	0.17547	7.2	0.5	1050	163	1042	138	1049	169	99.2	1042	138
LABX0019	LABSMPABC066.FIN2	1.6	383.0	105.5	5.72	7.2	0.07284	4.04	1.7621	12.7	0.17492	7.2	0.3	1005	161	1039	137	1031	163	103.4	1039	137
LABX0019	LABSMPABC034.FIN2	0.5	6828.2	66.2	5.74	7.1	0.07286	4.00	1.7643	12.7	0.17455	7.1	0.4	1007	164	1037	137	1032	165	103.0	1037	137
LABX0019	LABSMPABC071.FIN2	1.0	1129.1	45.8	5.82	7.2	0.07242	4.13	1.7270	12.8	0.17246	7.2	0.2	988	169	1025	136	1018	164	103.8	1025	136
LABX0019	LABSMPABC139.FIN2	1.5	444.0	128.0	5.94	7.6	0.07501	4.72	1.7550	13.0	0.16910	7.3	0.4	1046	195	1007	136	1025	168	96.2	1007	136
LABX0019	LABSMPABC106.FIN2	0.8	119.2	309.2	5.93	7.0	0.07461	4.14	1.7702	12.8	0.16890	7.2	0.4	1053	166	1006	133	1034	165	95.5	1006	133

LABX0019	LABSMPABC087.FIN2	0.9	1021.8	35.0	5.95	7.0	0.07172	4.22	1.6699	12.8	0.16846	7.2	0.2	964	176	1003	133	995	164	104.1	1003	133
LABX0019	LABSMPABC118.FIN2	0.4	27.3	350.4	6.22	7.6	0.07401	4.44	1.6645	13.0	0.16184	7.4	0.7	1032	180	967	133	992	164	93.7	967	133
LABX0019	LABSMPABC027.FIN2	0.6	834.5	75.1	6.40	6.9	0.07217	4.09	1.5571	12.8	0.15698	7.2	0.7	983	163	940	125	960	196	95.6	940	125
LABX0019	LABSMPABC086.FIN2	1.3	193.9	254.6	6.50	7.1	0.07030	4.02	1.4988	12.7	0.15406	7.2	0.5	933	165	924	123	929	154	99.0	924	123
LABX0019	LABSMPABC085.FIN2	1.3	502.9	125.4	7.49	7.2	0.06614	4.00	1.2235	12.7	0.13365	7.1	0.4	807	167	809	109	811	142	100.1	809	109
LABX0019	LABSMPABC051.FIN2	1.7	389.6	80.3	10.02	7.1	0.06110	4.11	0.8461	12.8	0.10001	7.2	0.5	634	176	614	84	622	118	96.9	614	84
LABX0019	LABSMPABC065.FIN2	1.6	289.0	386.2	10.49	7.4	0.05932	3.99	0.7806	12.7	0.09540	7.1	0.7	576	173	587	80	586	113	101.9	587	80
LABX0019	LABSMPABC138.FIN2	0.9	2701.5	199.5	11.67	7.1	0.05817	4.51	0.6852	12.9	0.08599	7.2	0.1	504	193	532	73	532	116	105.4	532	73
Data not used due to high discordance																						
LABX0019	LABSMPABC030.FIN2	2.4	4030.7	64.9	4.74	7.2	0.08889	4.08	2.6100	12.7	0.21161	7.2	0.2	1407	178	1237	162	1303	187	87.9		
LABX0019	LABSMPABC028.FIN2	2.1	121.3	130.7	10.77	7.2	0.06299	4.44	0.8076	12.8	0.09306	7.2	0.3	687	193	574	79	600	116	83.5		
LABX0019	LABSMPABC142.FIN2	1.6	435.7	159.3	4.61	7.1	0.09504	4.09	2.8704	12.8	0.21792	7.3	0.7	1531	167	1270	169	1372	193	82.9		
LABX0019	LABSMPABC017.FIN2	2.3	821.8	101.5	5.13	7.8	0.08972	4.01	2.4568	12.8	0.19747	7.3	0.9	1416	152	1161	156	1257	189	82.0		
LABX0019	LABSMPABC104.FIN2	2.2	194.4	159.2	5.01	7.2	0.09332	4.13	2.5984	12.9	0.20134	7.4	0.8	1490	154	1182	159	1298	188	79.3		
LABX0019	LABSMPABC049.FIN2	1.6	7589.4	102.2	4.88	8.5	0.11624	5.79	3.3361	13.5	0.20725	7.4	0.4	1858	198	1213	166	1477	206	65.3		
LABX0019	LABSMPABC009.FIN2	1.2	16265.3	100.5	5.65	7.4	0.10162	5.25	2.4971	13.2	0.17793	7.2	0.1	1626	189	1055	141	1270	190	64.9		
LABX0019	LABSMPABC053.FIN2	1.6	1851.7	52.2	5.20	7.3	0.11261	4.91	3.0186	13.1	0.19370	7.3	0.4	1817	181	1141	153	1406	197	62.8		
LABX0019	LABSMPABC141.FIN2	1.4	332.1	66.5	5.62	7.8	0.10564	4.31	2.6117	12.8	0.18091	7.5	0.7	1710	156	1070	149	1300	184	62.6		
LABX0019	LABSMPABC050.FIN2	1.6	631.4	22.0	5.95	9.3	0.12370	4.61	2.9869	12.9	0.17964	8.0	0.8	1982	166	1061	158	1399	204	53.5		
LABX0019	LABSMPABC067.FIN2	1.8	549.8	14.2	5.87	8.3	0.12178	4.45	2.9718	13.4	0.17497	7.7	0.9	1970	148	1038	148	1386	195	52.7		
LABX0019	LABSMPABC066.FIN2	2.2	427.3	28.8	5.68	7.1	0.12384	4.18	3.0391	12.8	0.17711	7.2	0.6	2002	152	1051	140	1414	198	52.5		
LABX0019	LABSMPABC135.FIN2	1.9	661.4	46.1	7.01	8.5	0.12282	5.10	2.4461	12.9	0.14686	7.9	0.5	1971	177	882	130	1254	187	44.7		
LABX0019	LABSMPABC117.FIN2	5.1	96.2	120.7	8.99	7.4	0.10927	5.58	1.7395	13.2	0.12006	8.4	0.6	1724	172	728	114	1014	158	42.2		
LABX0019	LABSMPABC034.FIN2	0.1	638.6	47.9	12.59	10.4	0.14106	4.88	1.8338	13.6	0.10010	9.9	1.0	2203	164	609	115	1036	178	27.7		
LABX0019	LABSMPABC015.FIN2	1.1	161.4	5.9	10.00	9.8	0.15778	4.96	2.3123	13.9	0.10441	7.9	0.9	2403	178	639	97	1194	197	26.6		
LABX0019	LABSMPABC088.FIN2	1.4	295.0	11.1	15.42	6.8	0.14980	4.42	1.4246	13.1	0.06975	8.8	1.0	2324	158	433	73	891	144	18.6		
LABX0019	LABSMPABC031.FIN2	0.1	321.8	256.3	9.52	7.2	0.05921	4.05	0.8696	12.7	0.10520	7.1	0.5	569	176	645	88	637	132	113.3		

Amostra MD-2019-12A

			Ratios										Rho	Ages (Ma)						% conc [1]	Best age	2s
Sample	Spot number	Th/U	206Pb/204Pb	1s	238U/206Pb	1s	207Pb/206Pb	1s	207Pb/235U	1s	206Pb/238U	1s		207Pb/206Pb	2s	206Pb/238U	2s	207Pb/235U	2s			
MD-2019-12A				(%)		(%)		(%)		(%)		(%)			(abs)		(abs)		(abs)			(abs)
LABXT_002	LABXT_002-59	1.7	0.000543619	26.84	2.74	0.6	0.13148	0.18	6.5976	0.5	0.36496	0.6	0.00	2116	6	2006	22	2056	10	94.8	2116	6
LABXT_002	LABXT_002-52	1.3	0.000095063	88.55	2.71	0.6	0.12963	0.18	6.6017	0.6	0.36900	0.6	0.70	2091	6	2025	22	2055	11	96.8	2091	6
LABXT_002	LABXT_002-70	1.5	0.000003222	823.90	3.08	0.6	0.11784	0.16	5.3017	0.6	0.32425	0.6	0.41	1922	6	1810	20	1865	11	94.2	1922	6
LABXT_002	LABXT_002-76	7.7	0.000012895	52.50	3.05	0.6	0.11473	0.27	5.1802	0.6	0.32756	0.6	0.27	1874	10	1826	21	1846	10	97.4	1874	10
LABXT_002	LABXT_002-50	2.4	0.000166932	22.92	3.47	0.7	0.10955	0.21	4.3763	0.8	0.28826	0.7	0.92	1791	8	1633	19	1701	14	91.2	1791	8
LABXT_002	LABXT_002-41	1.6	0.000066976	64.22	3.31	0.6	0.10784	0.17	4.5079	0.7	0.30208	0.7	0.92	1762	6	1702	19	1727	12	96.6	1762	6
LABXT_002	LABXT_002-95	1.4	0.000020370	224.12	3.24	1.0	0.10728	0.20	4.5163	0.7	0.31163	0.9	0.72	1752	7	1749	26	1729	12	99.8	1752	7
LABXT_002	LABXT_002-75	2.1	0.000037087	63.63	3.40	0.7	0.10377	0.30	4.2076	0.7	0.29398	0.7	0.44	1689	11	1661	19	1670	12	98.4	1689	11
LABXT_002	LABXT_002-53	0.7	0.000000770	1857.75	3.84	0.6	0.10054	0.52	3.6127	1.2	0.26065	0.7	0.70	1625	18	1493	18	1541	17	91.9	1625	18
LABXT_002	LABXT_002-117	0.9	0.000131718	33.53	3.72	0.8	0.09630	0.24	3.5397	1.0	0.26865	0.8	0.87	1552	9	1533	23	1526	17	98.8	1552	9
LABXT_002	LABXT_002-60	0.6	0.000025337	32.28	3.98	0.7	0.09591	0.41	3.3221	0.7	0.25166	0.7	0.76	1541	16	1447	17	1481	12	93.9	1541	16
LABXT_002	LABXT_002-44	1.3	0.000156522	90.09	4.00	0.8	0.09494	0.17	3.2661	0.6	0.25092	0.7	0.52	1525	6	1443	19	1470	9	94.6	1525	6
LABXT_002	LABXT_002-20	0.3	0.000020621	32.18	3.95	0.6	0.09492	0.24	3.2888	0.6	0.25327	0.6	0.19	1524	9	1455	17	1475	9	95.5	1524	9
LABXT_002	LABXT_002-56	0.6	0.000045901	71.88	3.96	0.7	0.09483	0.23	3.3161	0.8	0.25284	0.7	0.93	1522	9	1453	17	1479	12	95.5	1522	9
LABXT_002	LABXT_002-54	1.5	0.133544277	45.91	4.01	0.7	0.09094	0.42	3.1487	1.0	0.24934	0.7	0.86	1440	16	1435	17	1439	15	99.7	1435	17
LABXT_002	LABXT_002-78	1.0	0.000037872	25.97	4.14	0.7	0.09109	0.28	3.0377	0.6	0.24164	0.7	0.34	1448	11	1395	16	1414	9	96.4	1395	16
LABXT_002	LABXT_002-106	0.9	0.000018631	38.04	4.16	0.6	0.09159	0.24	3.0277	0.6	0.24048	0.6	0.25	1456	9	1389	16	1411	9	95.4	1389	16
LABXT_002	LABXT_002-63	0.6	0.000018407	41.37	4.17	0.6	0.08982	0.27	2.9792	0.7	0.23980	0.7	0.74	1418	10	1386	16	1398	11	97.7	1386	16
LABXT_002	LABXT_002-71	0.7	0.000008753	47.66	4.20	0.7	0.09055	0.45	2.9912	0.8	0.23896	0.7	0.67	1432	18	1381	18	1400	12	96.4	1381	18
LABXT_002	LABXT_002-72	0.9	0.000039015	102.28	4.20	0.7	0.08891	0.16	2.9337	0.7	0.23812	0.6	0.89	1400	6	1377	16	1387	10	98.3	1377	16
LABXT_002	LABXT_002-114	0.3	0.000225900	32.95	4.22	0.6	0.08862	0.30	2.8853	0.7	0.23710	0.6	0.26	1392	11	1372	16	1374	10	98.5	1372	16
LABXT_002	LABXT_002-58	0.8	0.000003825	426.68	4.27	0.7	0.08703	0.26	2.8123	0.7	0.23418	0.6	0.75	1359	10	1356	16	1355	11	99.8	1356	16
LABXT_002	LABXT_002-73	0.9	0.000084244	51.02	4.28	0.6	0.08678	0.21	2.7955	0.7	0.23389	0.6	0.44	1353	8	1355	15	1351	10	100.1	1355	15
LABXT_002	LABXT_002-82	0.8	0.000000290	12563.97	4.28	0.6	0.08724	0.16	2.8017	0.7	0.23380	0.6	0.88	1364	6	1354	16	1352	10	99.3	1354	16
LABXT_002	LABXT_002-119	3.8	0.000173601	37.64	4.29	0.7	0.08683	0.34	2.7799	0.7	0.23346	0.7	0.40	1353	13	1352	16	1346	11	100.0	1352	16

LABXT_002	LABXT_002-66	0.6	0.000104356	37.68	4.31	0.7	0.09046	0.19	2.9129	0.8	0.23229	0.7	0.86	1433	7	1346	16	1380	12	93.9	1346	16
LABXT_002	LABXT_002-85	2.0	0.000003806	162.36	4.33	0.7	0.08451	0.36	2.7080	0.9	0.23151	0.7	0.69	1299	14	1342	17	1324	14	103.3	1342	17
LABXT_002	LABXT_002-57	1.0	0.000004579	209.87	4.33	0.7	0.08803	0.24	2.8100	0.8	0.23120	0.7	0.90	1380	9	1341	16	1353	12	97.1	1341	16
LABXT_002	LABXT_002-97	1.0	0.000951488	36.52	4.33	0.7	0.08907	0.22	2.6728	0.5	0.23096	0.7	0.06	1404	8	1339	16	1319	8	95.4	1339	16
LABXT_002	LABXT_002-102	0.9	0.000029399	53.75	4.33	0.6	0.08765	0.21	2.7910	0.6	0.23095	0.7	0.64	1372	8	1339	16	1350	10	97.6	1339	16
LABXT_002	LABXT_002-24	2.5	0.002955984	40.16	4.35	0.6	0.08868	0.23	2.8031	0.6	0.22992	0.6	0.07	1395	9	1334	15	1353	10	95.6	1334	15
LABXT_002	LABXT_002-18	1.5	0.000019762	164.34	4.36	0.6	0.08789	0.15	2.7613	0.6	0.22917	0.6	0.23	1378	6	1330	15	1342	9	96.5	1330	15
LABXT_002	LABXT_002-92	3.0	0.000064890	61.22	4.37	0.6	0.08742	0.25	2.7503	0.6	0.22878	0.6	0.18	1367	10	1328	15	1339	9	97.2	1328	15
LABXT_002	LABXT_002-74	0.5	0.000270404	24.03	4.40	0.7	0.08686	0.19	2.6421	0.7	0.22747	0.6	0.91	1355	7	1321	16	1310	10	97.5	1321	16
LABXT_002	LABXT_002-47	1.3	0.001759695	32.81	4.41	0.6	0.08646	0.14	2.7139	0.7	0.22689	0.6	0.91	1347	5	1318	15	1329	10	97.9	1318	15
LABXT_002	LABXT_002-32	1.5	0.000000722	3250.47	4.42	0.6	0.08823	0.20	2.7590	0.6	0.22623	0.6	0.02	1385	8	1315	15	1342	9	94.9	1315	15
LABXT_002	LABXT_002-51	1.5	0.000169384	29.94	4.46	0.6	0.08734	0.22	2.6969	0.5	0.22426	0.6	0.50	1366	9	1304	15	1325	8	95.5	1304	15
LABXT_002	LABXT_002-109	1.3	0.000029179	46.78	4.47	0.6	0.08705	0.27	2.6738	0.6	0.22351	0.6	0.38	1358	10	1300	15	1318	9	95.7	1300	15
LABXT_002	LABXT_002-34	1.1	0.000060367	47.90	4.52	0.7	0.08986	0.21	2.7221	0.4	0.22165	0.7	0.42	1420	8	1290	16	1334	6	90.9	1290	16
LABXT_002	LABXT_002-13	1.5	0.000055899	33.13	4.57	0.6	0.08675	0.24	2.6036	0.6	0.21895	0.6	0.27	1352	9	1276	15	1299	8	94.4	1276	15
LABXT_002	LABXT_002-87	1.0	0.000032306	42.04	4.57	0.7	0.08364	0.21	2.5316	0.7	0.21893	0.6	0.87	1282	8	1276	15	1277	10	99.6	1276	15
LABXT_002	LABXT_002-101	2.7	0.000024047	32.39	4.61	0.6	0.08513	0.26	2.5401	0.6	0.21718	0.6	0.06	1316	10	1267	15	1281	8	96.3	1267	15
LABXT_002	LABXT_002-9	0.8	0.000011142	118.22	4.61	0.6	0.08741	0.24	2.6273	0.5	0.21708	0.6	0.49	1366	9	1266	15	1306	8	92.7	1266	15
LABXT_002	LABXT_002-115	2.1	0.000062740	41.76	4.62	0.6	0.08373	0.23	2.4921	0.6	0.21650	0.6	0.59	1283	9	1263	15	1267	9	98.4	1263	15
LABXT_002	LABXT_002-21	1.8	0.000006904	52.52	4.66	0.7	0.08855	2.02	2.5778	2.9	0.21533	0.7	0.86	1308	60	1257	17	1266	36	96.1	1257	17
LABXT_002	LABXT_002-45	0.7	0.000021013	262.19	4.66	0.6	0.08289	0.15	2.4476	0.6	0.21483	0.6	0.12	1265	6	1254	15	1254	9	99.2	1254	15
LABXT_002	LABXT_002-3	1.0	0.000036730	87.73	4.80	0.7	0.08704	0.24	2.4923	0.5	0.20843	0.7	0.63	1359	9	1220	15	1268	7	89.8	1220	15
LABXT_002	LABXT_002-5	0.7	0.000005850	82.70	4.82	0.7	0.08705	0.29	2.4974	0.5	0.20764	0.7	0.53	1358	11	1216	15	1270	7	89.6	1216	15
LABXT_002	LABXT_002-89	0.7	0.000255393	50.89	4.83	0.7	0.08143	0.33	2.3171	0.6	0.20727	0.7	0.24	1227	13	1214	15	1215	9	99.0	1214	15
LABXT_002	LABXT_002-88	1.0	0.000032612	21.10	4.85	0.7	0.08038	0.23	2.2921	0.7	0.20628	0.6	0.58	1204	9	1209	14	1206	10	100.4	1209	14
LABXT_002	LABXT_002-62	0.6	0.000085935	32.03	4.87	0.7	0.08204	0.23	2.3303	0.7	0.20553	0.7	0.83	1244	9	1205	15	1217	11	96.9	1205	15
LABXT_002	LABXT_002-27	1.1	0.000011049	29.84	4.91	0.7	0.08363	0.38	2.3322	0.5	0.20394	0.7	0.40	1279	15	1196	15	1220	7	93.5	1196	15
LABXT_002	LABXT_002-19	0.7	0.000269216	48.11	4.93	0.7	0.07773	0.22	2.1964	0.8	0.20348	0.7	0.76	1138	9	1194	16	1175	11	104.9	1194	16
LABXT_002	LABXT_002-94	1.3	0.000000661	752.30	4.93	0.7	0.08048	0.41	2.2547	0.7	0.20315	0.7	0.35	1202	16	1192	14	1195	10	99.2	1192	14

LABXT_002	LABXT_002-111	0.3	0.000052210	67.29	4.96	0.7	0.08220	0.38	2.2988	0.8	0.20151	0.6	0.23	1244	15	1183	14	1210	12	95.1	1183	14
LABXT_002	LABXT_002-105	0.6	0.000000793	465.56	5.00	0.7	0.08285	0.43	2.2751	0.7	0.20032	0.7	0.20	1258	16	1177	15	1201	10	93.5	1177	15
LABXT_002	LABXT_002-93	0.8	0.000035314	61.34	5.01	0.7	0.07972	0.33	2.2224	0.8	0.20014	0.7	0.84	1188	13	1176	15	1184	11	99.0	1176	15
LABXT_002	LABXT_002-104	1.5	0.000012914	36.75	5.01	0.6	0.08090	0.29	2.2241	0.7	0.19968	0.6	0.30	1215	11	1174	14	1185	9	96.6	1174	14
LABXT_002	LABXT_002-15	0.6	0.000860992	32.93	5.08	0.6	0.08138	0.20	2.1965	0.5	0.19686	0.6	0.51	1229	8	1158	14	1178	8	94.3	1158	14
LABXT_002	LABXT_002-11	0.5	0.000026553	87.15	5.16	0.7	0.08325	0.35	2.2271	0.6	0.19384	0.7	0.01	1271	14	1142	14	1188	9	89.8	1142	14
LABXT_002	LABXT_002-107	0.7	0.000171131	28.39	5.16	0.6	0.08063	0.25	2.1437	0.5	0.19376	0.6	0.53	1209	10	1142	13	1161	8	94.4	1142	13
LABXT_002	LABXT_002-35	0.8	0.000031619	53.73	5.28	0.7	0.08085	0.20	2.1167	0.5	0.18963	0.7	0.21	1215	8	1119	13	1153	7	92.1	1119	13
LABXT_002	LABXT_002-64	0.9	0.000031941	26.19	5.32	0.7	0.07951	0.28	2.0711	0.8	0.18817	0.7	0.75	1182	11	1111	13	1135	10	94.0	1111	13
LABXT_002	LABXT_002-23	0.5	0.000303203	50.66	5.34	0.6	0.07978	0.23	2.0594	0.6	0.18730	0.6	0.03	1189	9	1107	13	1134	8	93.1	1107	13
LABXT_002	LABXT_002-14	0.7	0.000032120	31.27	5.41	0.7	0.07965	0.27	2.0213	0.6	0.18505	0.7	0.12	1186	11	1095	13	1120	8	92.3	1095	13
LABXT_002	LABXT_002-61	1.5	0.000079689	50.75	5.55	0.7	0.07632	0.24	1.8224	0.6	0.18026	0.6	0.45	1101	10	1068	13	1052	8	97.1	1068	13
LABXT_002	LABXT_002-49	0.6	0.000183561	38.71	5.56	0.7	0.07868	0.56	1.9433	0.7	0.18022	0.7	0.05	1149	21	1068	14	1093	9	92.9	1068	14
LABXT_002	LABXT_002-39	0.7	0.000010460	61.71	5.56	0.7	0.07922	0.24	1.9574	0.5	0.18003	0.7	0.58	1175	9	1067	13	1099	7	90.8	1067	13
LABXT_002	LABXT_002-91	0.5	0.000006499	111.34	5.78	0.6	0.07474	0.26	1.7783	0.7	0.17294	0.6	0.53	1059	11	1028	12	1034	9	97.1	1028	12
LABXT_002	LABXT_002-67	0.8	0.000072783	28.56	5.83	0.6	0.07488	0.22	1.7821	0.7	0.17168	0.6	0.86	1063	9	1021	12	1036	9	96.1	1021	12
LABXT_002	LABXT_002-26	0.6	0.000020923	42.98	6.20	0.6	0.07370	0.25	1.6385	0.5	0.16139	0.6	0.23	1030	10	965	11	983	7	93.6	965	11
LABXT_002	LABXT_002-8	0.9	0.000020141	36.39	6.29	0.7	0.07459	0.33	1.6358	0.6	0.15925	0.7	0.07	1052	14	953	12	984	7	90.5	953	12
LABXT_002	LABXT_002-4	0.8	0.000036121	31.94	6.33	0.7	0.07410	0.26	1.6082	0.5	0.15802	0.7	0.53	1041	11	946	12	973	6	90.9	946	12
LABXT_002	LABXT_002-17	0.7	0.000000272	2139.34	6.44	0.7	0.07368	0.28	1.5690	0.6	0.15546	0.7	0.61	1029	11	931	11	956	8	90.5	931	11
LABXT_002	LABXT_002-84	1.7	0.000023653	33.83	7.80	0.7	0.06577	0.46	1.1600	0.7	0.12834	0.7	0.31	793	19	778	10	780	8	98.1	778	10
LABXT_002	LABXT_002-55	1.0	0.000011967	74.75	10.18	0.6	0.06096	0.27	0.8268	0.7	0.09831	0.6	0.70	634	12	605	7	610	6	95.4	605	7
LABXT_002	LABXT_002-96	0.8	0.000294894	34.85	10.82	0.7	0.05981	0.23	0.7650	0.7	0.09246	0.6	0.61	594	10	570	7	576	6	96.0	570	7
LABXT_002	LABXT_002-6	1.8	0.000040628	30.26	11.31	0.7	0.06017	0.30	0.7372	0.5	0.08844	0.7	0.26	605	13	546	7	560	5	90.3	546	7

Data not used due to high discordance																				
LABXT_002	LABXT_002-65	0.5	0.000068806	32.91308518 7	4.69	0.6	0.08866	0.26	2.6214	0.6	0.21332	0.7	0.58	1394	10	1246	15	1304	8	89.4		
LABXT_002	LABXT_002-10	1.0	0.000004711	149.9291337 20	6.59	0.7	0.07362	0.34	1.5366	0.5	0.15230	0.7	0.03	1028	14	914	12	944	6	88.9		
LABXT_002	LABXT_002-99	0.4	0.000005542	330.8804105 51	4.63	1.0	0.09110	0.25	2.7656	1.1	0.21836	0.9	0.97	1446	9	1272	20	1335	18	88.0		

LABXT_002	LABXT_002-68	1.6	0.000319182	39.704142948	2.09	0.7	0.20828	0.16	13.8456	0.7	0.47965	0.7	0.84	2890	5	2525	28	2732	14	87.4
LABXT_002	LABXT_002-36	1.2	0.000053560	44.730310851	6.79	0.7	0.07330	0.20	1.4891	0.5	0.14733	0.7	0.39	1020	8	886	11	925	6	86.9
LABXT_002	LABXT_002-80	-7.2	0.000000290	1.495727006	1.28	1.8	0.84784	0.92	93.1323	1.3	0.83021	1.7	0.76	4467	52	3856	100	4602	28	86.3
LABXT_002	LABXT_002-37	0.9	0.000040266	37.778332747	12.07	0.7	0.06035	0.39	0.6941	0.9	0.08316	0.7	0.53	609	16	515	7	533	7	84.6
LABXT_002	LABXT_002-69	0.0	0.000409205	35.527770837	2.13	0.7	0.21523	0.18	13.9399	0.4	0.47013	0.7	0.13	2943	6	2483	29	2744	8	84.4
LABXT_002	LABXT_002-16	1.0	0.000001787	369.820924295	7.07	0.7	0.07323	0.32	1.4242	0.6	0.14155	0.7	0.09	1014	12	854	11	897	7	84.2
LABXT_002	LABXT_002-98	1.3	0.000052698	26.334872817	5.00	1.7	0.09168	0.33	2.6124	1.4	0.20665	1.3	0.91	1457	12	1207	30	1288	21	82.8
LABXT_002	LABXT_002-1	0.7	0.000000441	1249.122095475	4.68	0.7	0.09661	0.70	2.8450	1.1	0.21423	0.7	0.13	1549	25	1251	16	1363	16	80.8
LABXT_002	LABXT_002-7	0.6	0.000226269	33.870880678	10.61	0.7	0.06359	0.30	0.8234	0.4	0.09459	0.8	0.17	725	13	582	9	610	3	80.4
LABXT_002	LABXT_002-113	0.9	0.000012363	53.706446014	6.16	0.8	0.08163	0.36	1.8215	0.5	0.16339	0.8	0.04	1232	14	975	14	1052	7	79.2
LABXT_002	LABXT_002-12	0.4	0.000082473	73.298630055	5.20	1.1	0.09271	0.30	2.4782	0.6	0.19677	1.1	0.67	1478	12	1156	23	1263	9	78.2
LABXT_002	LABXT_002-30	31.3	0.000027907	0.600486734	6.27	0.7	0.08232	0.52	1.8002	0.6	0.15996	0.7	0.44	1242	20	956	13	1043	8	77.0
LABXT_002	LABXT_002-110	1.7	0.000009223	57.456457436	4.41	1.0	0.12512	3.04	4.1171	4.2	0.22760	1.1	0.83	1852	85	1324	26	1564	51	71.5
LABXT_002	LABXT_002-38	0.5	0.000044922	27.432878380	6.93	1.0	0.08189	0.30	1.6826	1.2	0.14602	0.9	0.78	1240	12	878	14	995	16	70.8
LABXT_002	LABXT_002-90	-2.6	0.000000286	1.761876147	1.75	1.4	0.85357	1.22	59.4121	1.4	0.57690	1.3	0.50	4484	0	2930	63	4156	27	65.3
LABXT_002	LABXT_002-81	1.9	0.000013241	68.014214581	7.51	2.2	0.09476	0.30	1.9090	1.6	0.14781	1.8	0.88	1519	11	884	30	1067	22	58.2
LABXT_002	LABXT_002-28	0.6	0.000016920	91.057115263	9.22	2.1	0.09654	0.40	1.5825	1.7	0.11813	1.6	0.98	1554	14	717	22	946	22	46.2
LABXT_002	LABXT_002-100	0.8	0.000026607	8.620039974	11.18	1.6	0.09971	0.26	1.3004	2.2	0.09407	1.9	0.96	1616	10	579	21	834	22	35.8
LABXT_002	LABXT_002-48	0.5	0.000003867	2.208760755	11.57	2.1	0.16302	0.72	2.0907	1.4	0.09911	2.3	0.90	2471	25	605	27	1135	18	24.5
LABXT_002	LABXT_002-112	0.4	0.000002336	4.744897238	18.39	4.5	0.22876	2.45	2.5758	3.9	0.09031	4.1	0.82	2898	84	549	43	1183	62	18.9
LABXT_002	LABXT_002-116	0.3	0.000006948	10.981568317	17.42	1.7	0.13626	0.76	1.1803	2.3	0.06027	2.3	0.95	2175	28	376	16	779	24	17.3
LABXT_002	LABXT_002-29	1.5	0.000000307	0.666245171	0.50	2.4	0.84973	0.40	289.1050	2.9	2.38999	2.6	0.99	4523	76	7623	229	5634	62	168.5

Data not used due to high analytical error																			
LABXT_002	LABXT_002-83	3.3	0.000000303	0.904558529	0.52	1.2	0.85756	0.50	216.5358	1.4	1.95565	1.3	0.87			6967	107	5448	27	#DIV/0!
LABXT_002	LABXT_002-103	0.5	0.000000310	0.828100408	1.11	2.6	0.83265	0.76	109.3570	4.2	1.03902	3.8	0.98			4451	221	4669	75	#DIV/0!

Amostra MD-2019-11D

		Ratios											Rho	Ages (Ma)						% conc [1]	Best age	2s
Sample	Spot number	Th/U	206Pb/204Pb	1s	238U/206Pb	1s	207Pb/206Pb	1s	207Pb/235U	1s	206Pb/238U	1s		207Pb/206Pb	2s	206Pb/238U	2s	207Pb/235U	2s			
				(%)		(%)		(%)		(%)		(%)			(abs)		(abs)		(abs)			(abs)
LABXT_003	LABXT_003-108	1.3	0.000003	318.8	2.72	0.5	0.13120	0.30	6.4744	0.6	0.36734	0.5	0.02	2112	10	2017	18	2039	10	95.5	2112	10
LABXT_003	LABXT_003-70	3.0	0.000060	36.5	2.88	0.5	0.11753	0.40	5.6069	0.5	0.34813	0.6	0.32	1914	15	1925	19	1916	9	100.6	1914	15
LABXT_003	LABXT_003-13	1.7	0.000060	64.1	3.25	0.5	0.10887	0.18	4.5352	0.8	0.30759	0.5	0.91	1780	7	1729	16	1732	13	97.1	1780	7
LABXT_003	LABXT_003-71	1.0	0.000023	37.0	3.54	0.5	0.10612	0.66	4.1272	1.0	0.28284	0.5	0.84	1723	23	1605	15	1653	17	93.2	1723	23
LABXT_003	LABXT_003-91	1.2	0.000617	34.6	3.92	1.8	0.09872	0.29	3.2527	1.3	0.26000	1.2	0.92	1598	11	1495	30	1470	20	93.5	1598	11
LABXT_003	LABXT_003-30	1.2	0.000111	33.3	3.69	0.5	0.09834	0.22	3.5633	0.7	0.27099	0.5	0.87	1591	8	1546	14	1538	11	97.2	1591	8
LABXT_003	LABXT_003-75	1.2	0.000031	147.1	3.72	0.5	0.09553	0.17	3.5349	0.7	0.26890	0.5	0.88	1537	6	1535	14	1531	11	99.9	1537	6
LABXT_003	LABXT_003-7	0.5	0.000063	79.2	4.16	2.3	0.09457	0.22	3.2186	1.0	0.25513	1.0	0.90	1518	8	1462	29	1454	17	96.3	1518	8
LABXT_003	LABXT_003-45	0.9	0.002511	41.4	3.94	0.5	0.09451	0.22	3.1770	0.7	0.25365	0.5	0.71	1517	8	1457	14	1448	11	96.1	1517	8
LABXT_003	LABXT_003-4	1.0	0.000132	44.8	4.19	0.6	0.09408	0.29	3.1088	0.6	0.23928	0.6	0.41	1507	11	1383	15	1432	9	91.7	1507	11
LABXT_003	LABXT_003-32	0.7	0.000169	42.9	3.88	0.6	0.09425	0.67	3.3162	1.3	0.25790	0.6	0.65	1504	24	1479	15	1473	20	98.3	1504	24
LABXT_003	LABXT_003-119	1.0	0.000128	76.9	3.85	0.6	0.09123	0.21	3.2693	0.8	0.25996	0.6	0.87	1450	8	1489	15	1469	12	102.7	1489	15
LABXT_003	LABXT_003-27	1.1	0.000028	83.2	3.94	0.5	0.09181	0.22	3.2170	0.8	0.25429	0.5	0.92	1461	8	1460	14	1456	12	100.0	1460	14
LABXT_003	LABXT_003-48	0.7	0.000074	29.5	3.94	0.5	0.09282	0.24	3.1311	0.7	0.25414	0.5	0.85	1483	9	1460	14	1437	11	98.4	1460	14
LABXT_003	LABXT_003-88	0.9	0.000166	34.9	3.96	0.5	0.09194	0.22	3.1988	0.7	0.25272	0.5	0.57	1464	8	1452	13	1452	12	99.2	1452	13
LABXT_003	LABXT_003-51	0.9	0.000002	638.8	3.98	0.5	0.09068	0.29	3.1495	0.8	0.25160	0.5	0.67	1436	11	1447	14	1440	12	100.7	1447	14
LABXT_003	LABXT_003-57	3.0	0.000023	31.7	4.04	0.7	0.08804	0.30	3.0364	1.2	0.24952	0.7	0.91	1380	11	1435	19	1405	18	104.0	1435	19
LABXT_003	LABXT_003-23	2.1	0.000023	71.1	4.02	0.5	0.09173	0.23	3.0819	0.7	0.24907	0.5	0.38	1460	9	1434	13	1424	11	98.2	1434	13
LABXT_003	LABXT_003-103	1.3	0.167400	33.8	4.03	0.6	0.08647	0.35	2.9720	0.8	0.24890	0.6	0.68	1343	14	1432	15	1396	12	106.6	1432	15
LABXT_003	LABXT_003-28	1.1	0.000043	25.3	4.07	0.5	0.09143	0.23	3.0832	0.6	0.24604	0.5	0.40	1453	9	1418	13	1426	10	97.6	1418	13
LABXT_003	LABXT_003-93	1.3	0.000006	181.0	4.09	0.6	0.08713	0.23	2.9431	0.8	0.24500	0.5	0.86	1361	9	1412	14	1388	12	103.7	1412	14
LABXT_003	LABXT_003-77	0.4	0.122651	49.6	4.11	0.5	0.09251	0.29	3.1283	0.5	0.24334	0.5	0.26	1475	10	1404	13	1438	8	95.2	1404	13
LABXT_003	LABXT_003-104	0.9	0.000067	81.5	4.12	0.5	0.08960	0.20	2.9851	0.7	0.24253	0.5	0.70	1415	8	1400	13	1400	10	98.9	1400	13
LABXT_003	LABXT_003-98	0.8	0.000012	160.6	4.14	0.5	0.08793	0.19	2.9146	0.7	0.24164	0.5	0.79	1379	7	1395	13	1381	11	101.2	1395	13
LABXT_003	LABXT_003-87	0.8	0.000036	34.1	4.15	0.5	0.09022	0.18	3.0151	0.7	0.24100	0.5	0.68	1428	7	1392	13	1408	10	97.4	1392	13

LABXT_003	LABXT_003-86	0.9	0.000078	43.7	4.19	0.6	0.08775	0.18	2.8863	0.7	0.23886	0.5	0.43	1376	7	1381	13	1374	11	100.4	1381	13
LABXT_003	LABXT_003-16	0.7	0.000027	116.6	4.20	0.6	0.08768	0.26	2.8591	0.8	0.23825	0.5	0.02	1372	10	1377	13	1367	12	100.4	1377	13
LABXT_003	LABXT_003-105	2.0	0.000072	28.4	4.26	0.5	0.08872	0.26	2.8928	0.7	0.23516	0.5	0.38	1396	10	1361	13	1376	11	97.5	1361	13
LABXT_003	LABXT_003-92	2.8	0.000032	28.1	4.28	0.5	0.08592	0.39	2.7484	0.8	0.23370	0.6	0.31	1331	15	1354	13	1337	11	101.7	1354	13
LABXT_003	LABXT_003-10	1.7	0.000088	27.8	4.30	0.5	0.08805	0.19	2.8152	0.6	0.23273	0.5	0.18	1382	7	1349	12	1357	9	97.6	1349	12
LABXT_003	LABXT_003-38	1.1	0.000048	74.4	4.30	0.5	0.08844	0.24	2.8684	0.8	0.23260	0.5	0.84	1390	9	1348	13	1369	12	97.0	1348	13
LABXT_003	LABXT_003-80	0.5	0.000553	48.3	4.33	0.5	0.08829	0.18	2.8071	0.6	0.23084	0.5	0.04	1388	7	1339	12	1355	9	96.5	1339	12
LABXT_003	LABXT_003-113	1.1	0.000012	90.1	4.34	0.5	0.08998	0.38	2.6803	0.6	0.23072	0.5	0.14	1421	14	1338	13	1321	9	94.2	1338	13
LABXT_003	LABXT_003-114	1.5	0.000001	1662.4	4.36	0.6	0.08612	0.39	2.6128	0.7	0.22979	0.6	0.20	1336	15	1333	14	1301	11	99.8	1333	14
LABXT_003	LABXT_003-66	0.9	0.000128	44.6	4.38	0.6	0.08972	0.26	2.6940	0.5	0.22889	0.6	0.11	1419	10	1329	14	1325	8	93.6	1329	14
LABXT_003	LABXT_003-58	2.3	0.000002	356.9	4.39	0.5	0.08734	0.26	2.7178	0.7	0.22800	0.5	0.13	1369	10	1324	12	1330	10	96.7	1324	12
LABXT_003	LABXT_003-8	1.8	0.000020	37.2	4.42	0.5	0.08546	0.27	2.6369	0.8	0.22633	0.5	0.72	1323	11	1315	12	1307	11	99.4	1315	12
LABXT_003	LABXT_003-69	1.0	0.000098	27.7	4.43	0.6	0.08514	0.22	2.6689	0.8	0.22633	0.6	0.92	1316	8	1315	13	1314	12	99.9	1315	13
LABXT_003	LABXT_003-41	1.6	0.000035	31.6	4.45	0.6	0.08909	0.43	2.6231	0.7	0.22464	0.6	0.10	1401	16	1307	14	1306	10	93.3	1307	14
LABXT_003	LABXT_003-21	1.8	0.000081	32.6	4.52	0.5	0.08785	0.32	2.5660	0.6	0.22140	0.5	0.34	1376	12	1289	12	1289	9	93.7	1289	12
LABXT_003	LABXT_003-24	0.9	0.000398	42.4	4.60	1.2	0.08656	0.21	2.5839	0.8	0.22113	0.7	0.75	1349	8	1287	17	1295	12	95.4	1287	17
LABXT_003	LABXT_003-17	0.1	0.000019	61.4	4.61	1.2	0.08858	0.43	2.4823	0.4	0.22014	0.7	0.78	1392	16	1282	16	1266	6	92.1	1282	16
LABXT_003	LABXT_003-39	0.7	0.000068	26.2	4.59	1.0	0.09032	0.34	2.6478	0.6	0.21998	0.7	0.66	1430	13	1281	16	1311	10	89.6	1281	16
LABXT_003	LABXT_003-22	1.1	0.000004	235.5	4.56	0.5	0.08935	0.53	2.5694	1.0	0.21965	0.5	0.50	1406	20	1280	12	1286	15	91.0	1280	12
LABXT_003	LABXT_003-40	1.3	0.000037	42.1	4.59	1.3	0.08908	0.39	2.5690	0.8	0.21995	1.1	0.66	1401	15	1279	26	1287	12	91.3	1279	26
LABXT_003	LABXT_003-115	2.2	0.000101	50.1	4.65	0.6	0.08690	0.24	2.3585	0.9	0.21551	0.6	0.95	1356	9	1258	14	1227	12	92.7	1258	14
LABXT_003	LABXT_003-64	1.7	0.000015	31.3	4.71	0.5	0.08571	0.34	2.5012	0.6	0.21233	0.5	0.06	1327	13	1241	12	1270	8	93.6	1241	12
LABXT_003	LABXT_003-67	0.8	0.000015	83.8	4.81	0.6	0.08026	0.27	2.3082	0.8	0.20847	0.6	0.66	1201	11	1220	13	1210	12	101.6	1220	13
LABXT_003	LABXT_003-82	0.3	0.000161	32.9	4.82	0.5	0.08136	0.17	2.3213	0.6	0.20739	0.5	0.02	1229	7	1215	11	1217	9	98.9	1215	11
LABXT_003	LABXT_003-6	1.2	0.000000	46770.2	4.84	0.5	0.08361	0.32	2.3865	0.5	0.20678	0.5	0.44	1279	12	1212	11	1237	8	94.7	1212	11
LABXT_003	LABXT_003-59	0.7	0.000143	24.4	4.90	0.8	0.08078	0.27	2.2592	0.8	0.20570	0.7	0.55	1213	11	1205	16	1195	12	99.4	1205	16
LABXT_003	LABXT_003-3	0.8	0.000019	58.2	4.90	0.5	0.08104	0.28	2.2899	0.8	0.20432	0.5	0.72	1220	11	1198	12	1205	11	98.3	1198	12
LABXT_003	LABXT_003-68	0.5	0.000641	35.0	4.93	0.5	0.08204	0.18	2.2682	0.7	0.20291	0.5	0.50	1245	7	1191	11	1199	10	95.7	1191	11
LABXT_003	LABXT_003-37	1.2	0.000083	39.0	4.93	0.6	0.08291	0.56	2.2075	0.7	0.20289	0.5	0.35	1259	22	1191	12	1181	10	94.6	1191	12

LABXT_003	LABXT_003-106	1.0	0.000003	543.9	4.96	0.9	0.08228	0.32	2.1896	0.8	0.20271	0.6	0.55	1248	13	1190	13	1176	10	95.3	1190	13
LABXT_003	LABXT_003-60	0.8	0.000075	30.0	4.96	0.5	0.08605	0.54	2.4141	0.6	0.20156	0.5	0.10	1329	19	1184	11	1245	9	89.0	1184	11
LABXT_003	LABXT_003-63	0.7	0.000003	229.4	5.03	0.5	0.08126	0.27	2.2292	0.5	0.19891	0.5	0.32	1224	11	1169	11	1189	7	95.5	1169	11
LABXT_003	LABXT_003-118	1.1	0.000034	36.1	5.05	0.5	0.08414	0.45	2.2562	0.4	0.19829	0.5	0.39	1289	17	1166	12	1198	5	90.5	1166	12
LABXT_003	LABXT_003-19	1.1	0.000008	62.0	5.17	0.5	0.07964	0.32	2.0529	0.6	0.19341	0.5	0.05	1184	13	1140	11	1131	9	96.3	1140	11
LABXT_003	LABXT_003-112	1.3	0.000047	39.0	5.24	0.5	0.07910	0.26	2.0186	0.6	0.19104	0.5	0.24	1172	10	1127	11	1120	9	96.2	1127	11
LABXT_003	LABXT_003-56	0.7	0.000176	37.8	5.24	0.5	0.07739	0.30	2.0242	0.7	0.19101	0.5	0.38	1128	12	1127	11	1121	9	99.8	1127	11
LABXT_003	LABXT_003-90	0.5	0.000035	32.2	5.25	0.5	0.08011	0.36	2.0958	0.9	0.19068	0.5	0.74	1192	11	1125	11	1142	12	94.4	1125	11
LABXT_003	LABXT_003-47	0.5	0.000029	90.7	5.26	0.5	0.07781	0.26	1.9957	0.7	0.19022	0.5	0.37	1140	11	1123	11	1111	10	98.5	1123	11
LABXT_003	LABXT_003-43	1.1	0.000020	24.1	5.29	0.5	0.07745	0.28	2.0031	0.6	0.18925	0.5	0.23	1130	11	1117	11	1114	8	98.8	1117	11
LABXT_003	LABXT_003-109	0.9	0.000001	329.5	5.62	0.6	0.07824	0.39	1.9140	0.5	0.17831	0.6	0.21	1148	16	1058	11	1084	7	92.1	1058	11
LABXT_003	LABXT_003-65	1.3	0.000004	107.7	5.66	0.6	0.07846	0.52	1.9043	0.7	0.17670	0.6	0.21	1155	20	1049	12	1080	10	90.9	1049	12
LABXT_003	LABXT_003-9	0.7	0.000007	285.1	5.93	0.5	0.07427	0.20	1.7061	0.7	0.16870	0.5	0.47	1047	8	1005	10	1010	9	96.0	1005	10
LABXT_003	LABXT_003-96	0.7	0.000035	32.6	6.03	0.5	0.07223	0.28	1.6505	0.8	0.16600	0.5	0.47	989	11	990	10	987	10	100.1	990	10
LABXT_003	LABXT_003-83	1.3	0.000013	83.0	6.11	0.5	0.07391	0.26	1.6507	0.5	0.16396	0.5	0.28	1036	11	979	10	988	7	94.5	979	10
LABXT_003	LABXT_003-26	0.6	0.000002	273.7	6.21	0.5	0.07249	0.31	1.5981	0.7	0.16103	0.5	0.43	995	12	962	9	967	9	96.7	962	9
LABXT_003	LABXT_003-111	2.5	0.000060	38.8	7.50	0.5	0.06653	0.37	1.2236	0.7	0.13343	0.5	0.09	818	16	807	8	809	8	98.7	807	8
LABXT_003	LABXT_003-102	2.0	0.000001	108.5	12.94	0.6	0.05777	0.57	0.6104	0.6	0.07740	0.6	0.03	519	24	481	5	484	5	92.7	481	5
Data not used due to high discordance																						
LABXT_003	LABXT_003-100	0.7	0.000052	40.8	5.09	1.0	0.08474	0.42	2.2234	0.5	0.19798	0.9	0.14	1308	17	1163	19	1187	7	88.9		
LABXT_003	LABXT_003-72	0.4	0.000003	207.4	6.01	0.5	0.07732	0.48	1.7730	1.0	0.16653	0.6	0.16	1120	19	993	10	1030	12	88.7		
LABXT_003	LABXT_003-97	1.1	0.000059	87.2	5.03	1.1	0.08700	0.27	2.4723	1.4	0.20420	1.1	0.96	1359	11	1195	24	1250	20	88.0		
LABXT_003	LABXT_003-53	0.5	0.000110	27.9	4.06	1.0	0.10035	0.20	3.4618	1.3	0.24846	1.1	0.88	1629	7	1427	27	1503	21	87.6		
LABXT_003	LABXT_003-14	1.3	0.000093	23.4	4.75	0.5	0.08987	0.45	2.3693	0.8	0.21041	0.5	0.02	1419	17	1231	12	1231	12	86.8		
LABXT_003	LABXT_003-31	0.5	0.000091	29.9	5.00	0.7	0.08816	0.50	2.1482	0.8	0.19979	0.7	0.29	1382	19	1174	15	1163	11	84.9		
LABXT_003	LABXT_003-95	0.7	0.000030	50.2	6.56	0.5	0.07646	0.78	1.5998	1.3	0.15245	0.5	0.07	1093	30	915	9	963	16	83.7		
LABXT_003	LABXT_003-120	0.6	0.000100	48.1	4.73	0.5	0.09364	0.99	2.6143	1.5	0.21156	0.5	0.01	1486	36	1237	12	1302	23	83.2		
LABXT_003	LABXT_003-94	0.9	0.000094	38.4	4.97	0.6	0.09256	1.48	2.5288	1.8	0.20163	0.6	0.93	1430	49	1184	13	1264	25	82.8		

LABXT_003	LABXT_003-85	0.5	0.000012	119.5	5.25	0.5	0.09022	1.65	2.1796	2.2	0.19050	0.5	0.36	1387	57	1124	11	1159	28	81.0
LABXT_003	LABXT_003-44	0.6	0.000002	702.3	6.57	1.4	0.07938	0.25	1.7400	1.5	0.15830	1.3	0.92	1181	10	945	23	1012	18	80.1
LABXT_003	LABXT_003-25	1.2	0.000866	33.8	3.55	0.5	0.12654	0.16	4.8936	0.5	0.28166	0.5	0.21	2049	6	1600	15	1798	9	78.1
LABXT_003	LABXT_003-29	0.3	0.000052	34.9	5.71	4.1	0.10253	2.08	2.8236	0.9	0.21888	1.9	0.66	1623	64	1265	46	1356	13	77.9
LABXT_003	LABXT_003-50	0.6	0.000089	95.5	5.11	0.9	0.09362	0.57	2.5153	1.4	0.19807	1.0	0.90	1500	24	1165	21	1264	20	77.7
LABXT_003	LABXT_003-74	0.8	0.000124	36.3	5.56	1.1	0.08945	0.24	2.2476	0.8	0.18293	0.8	0.77	1411	9	1082	16	1192	11	76.7
LABXT_003	LABXT_003-49	1.8	0.000040	20.4	5.13	1.2	0.10105	0.84	2.7241	0.8	0.20032	1.1	0.94	1622	30	1175	24	1332	12	72.4
LABXT_003	LABXT_003-34	0.7	0.000029	3.6	5.98	0.7	0.08855	0.23	1.9656	0.7	0.16821	0.7	0.56	1392	9	1002	13	1101	10	72.0
LABXT_003	LABXT_003-42	0.3	0.000009	167.0	5.93	3.1	0.09856	0.52	2.3989	1.9	0.19417	2.5	0.95	1590	19	1133	54	1220	30	71.3
LABXT_003	LABXT_003-62	0.7	0.000020	28.5	5.17	1.3	0.10945	0.79	2.9796	1.1	0.19894	1.1	0.78	1772	29	1167	24	1398	17	65.9
LABXT_003	LABXT_003-11	0.8	0.000017	42.9	5.06	1.6	0.11233	1.02	2.9240	1.6	0.20521	1.6	0.65	1824	35	1200	35	1377	24	65.8
LABXT_003	LABXT_003-20	0.5	0.000041	44.0	7.69	2.8	0.09065	0.41	1.7499	2.1	0.15376	2.8	0.96	1436	16	913	48	1007	28	63.6
LABXT_003	LABXT_003-117	0.7	0.000207	83.3	6.54	1.9	0.10140	0.48	2.2477	1.4	0.16529	1.7	0.87	1642	18	981	32	1182	21	59.8
LABXT_003	LABXT_003-89	1.1	0.000018	74.0	6.82	1.8	0.10047	1.81	2.0740	2.7	0.15237	1.0	0.50	1534	63	913	17	1096	34	59.5
LABXT_003	LABXT_003-33	1.3	0.000054	16.1	6.90	1.7	0.09703	0.71	1.9772	0.7	0.15298	1.5	0.43	1553	24	915	25	1105	10	58.9
LABXT_003	LABXT_003-15	1.4	0.000008	10.5	6.69	0.6	0.09664	0.46	1.8552	0.8	0.14954	0.5	0.20	1559	18	898	9	1063	11	57.6
LABXT_003	LABXT_003-46	0.7	0.000105	33.5	8.09	1.4	0.08977	0.68	1.5986	1.9	0.12850	1.2	0.60	1405	15	778	18	952	23	55.4
LABXT_003	LABXT_003-55	0.9	0.000030	60.2	7.36	2.5	0.11018	0.37	2.1943	2.0	0.15577	2.6	0.96	1798	13	925	44	1158	28	51.4
LABXT_003	LABXT_003-35	0.8	0.000042	38.0	21.85	6.2	0.09545	0.49	1.4995	3.9	0.12739	4.4	0.99	1529	18	751	64	840	53	49.1
LABXT_003	LABXT_003-107	0.7	0.000002	862.1	10.21	3.2	0.08533	0.56	1.3235	2.7	0.10484	3.2	0.98	1323	23	641	38	848	31	48.4
LABXT_003	LABXT_003-54	0.9	0.000032	11.8	11.09	3.2	0.09470	0.30	1.3621	2.1	0.11109	2.7	0.98	1520	11	673	34	854	25	44.3
LABXT_003	LABXT_003-73	0.7	0.000014	22.4	9.10	2.8	0.11309	0.56	1.8250	3.1	0.12540	3.0	0.99	1849	21	756	42	1024	38	40.9
LABXT_003	LABXT_003-61	0.4	0.000017	9.5	10.49	2.0	0.10077	0.68	1.4036	1.8	0.10362	1.6	0.80	1623	25	634	19	882	22	39.1
LABXT_003	LABXT_003-101	1.0	0.000007	164.0	8.38	1.3	0.12769	2.16	2.0617	1.7	0.12447	1.3	0.58	1934	75	755	18	1128	23	39.0
LABXT_003	LABXT_003-52	0.1	0.000009	5.1	10.66	3.1	0.11447	0.80	1.6605	1.6	0.11112	2.3	0.93	1850	29	674	30	975	23	36.5
LABXT_003	LABXT_003-84	1.0	0.000028	23.4	10.31	1.8	0.11696	1.44	1.6211	1.1	0.10699	2.0	0.36	1859	45	652	24	972	14	35.1
LABXT_003	LABXT_003-5	0.8	0.000017	28.3	11.01	2.7	0.13111	2.01	2.1260	3.5	0.11338	3.2	0.84	2033	67	683	40	1077	48	33.6
LABXT_003	LABXT_003-78	1.2	0.000002	3.1	7.41	3.3	0.25919	2.02	5.1798	1.2	0.17316	2.7	0.71	3150	62	1016	52	1842	20	32.3
LABXT_003	LABXT_003-99	0.8	0.000020	12.1	18.64	2.0	0.09751	0.32	0.7830	1.7	0.05992	2.2	0.96	1574	12	374	16	580	15	23.8

LABXT_003	LABXT_003-81	1.4	0.000011	2.8	13.67	1.4	0.13068	0.45	1.3794	1.6	0.07660	1.3	0.79	2103	16	475	12	870	18	22.6
LABXT_003	LABXT_003-18	1.7	0.000001	143.9	44.14	0.9	0.05987	1.88	0.1801	1.9	0.02278	0.9	0.15	712	75	145	3	167	6	20.4
LABXT_003	LABXT_003-79	0.6	0.000006	2.3	17.96	0.7	0.12691	0.50	0.9847	1.0	0.05597	0.7	0.59	2047	18	351	4	692	11	17.2
LABXT_003	LABXT_003-12	0.4	0.000005	6.6	22.77	3.1	0.14169	2.22	0.7478	1.3	0.04712	2.5	0.23	2198	77	296	14	568	12	13.5

Amostra MD-2019-10

			Ratios										Rho	Ages (Ma)						% conc [1]	Best age	2s
Sample	Spot number	Th/U	206Pb/204Pb	1s	238U/206Pb	1s	207Pb/206Pb	1s	207Pb/235U	1s	206Pb/238U	1s		207Pb/206Pb	2s	206Pb/238U	2s	207Pb/235U	2s			
				(%)		(%)		(%)		(%)		(%)			(abs)		(abs)		(abs)			(abs)
LABXT_001	LABXT_001-89	0.8	0.0000239	303.3267717	2.62	0.7	0.14256	0.24	7.5176	0.6	0.38267	0.7	0.2	2256	8	2088	24	2171	10	92.6	2256	8
LABXT_001	LABXT_001-75	2.2	0.0000561	41.8299714	3.17	1.1	0.11010	0.26	4.8210	0.7	0.31859	0.7	0.8	1799	9	1782	23	1783	13	99.0	1799	9
LABXT_001	LABXT_001-63	1.3	0.0000945	42.8804083	3.43	0.6	0.10418	0.18	4.1662	0.7	0.29137	0.6	0.5	1698	6	1648	19	1663	11	97.1	1698	6
LABXT_001	LABXT_001-51	1.1	0.0003381	34.9196477	3.69	0.8	0.10651	0.20	3.8879	0.4	0.27231	0.7	0.4	1739	7	1552	21	1610	7	89.3	1739	7
LABXT_001	LABXT_001-56	0.8	0.0006906	30.2145957	3.83	0.7	0.09948	0.17	3.5858	0.8	0.26134	0.7	0.9	1612	6	1496	18	1540	13	92.8	1612	6
LABXT_001	LABXT_001-85	0.6	0.0000975	28.0148115	3.97	0.6	0.09438	0.24	3.2823	0.6	0.25216	0.6	0.2	1513	9	1450	17	1474	9	95.8	1513	9
LABXT_001	LABXT_001-47	0.5	0.0000777	31.4165681	4.02	0.6	0.09120	0.32	3.1417	0.8	0.24901	0.6	0.7	1446	12	1433	17	1438	12	99.1	1433	17
LABXT_001	LABXT_001-44	0.4	0.0000326	135.0539271	4.12	0.7	0.08863	0.46	2.9346	0.8	0.24347	0.7	0.3	1389	18	1404	17	1387	12	101.1	1404	17
LABXT_001	LABXT_001-49	1.2	0.0000131	170.1880744	4.24	0.8	0.09214	0.37	3.0337	1.1	0.23713	0.8	0.9	1465	14	1371	20	1405	18	93.6	1371	20
LABXT_001	LABXT_001-64	1.1	0.0004473	58.9645330	4.27	0.7	0.09135	0.50	2.9411	1.0	0.23454	0.7	0.3	1449	20	1358	16	1385	14	93.7	1358	16
LABXT_001	LABXT_001-93	0.9	0.0000080	217.6575301	4.28	0.7	0.09013	0.20	2.9080	0.5	0.23385	0.7	0.0	1426	8	1355	16	1382	8	95.0	1355	16
LABXT_001	LABXT_001-48	2.7	0.0000075	125.6105957	4.35	0.6	0.08939	0.50	2.8541	1.0	0.23029	0.7	0.6	1405	19	1336	16	1364	14	95.1	1336	16
LABXT_001	LABXT_001-43	2.0	0.0000330	76.2954755	4.52	0.5	0.08883	0.51	2.6721	0.7	0.22461	1.0	0.1	1395	19	1300	18	1318	11	93.2	1300	18
LABXT_001	LABXT_001-55	1.4	0.0001325	60.7876542	4.66	2.7	0.08717	0.29	2.5724	0.8	0.22419	0.8	0.9	1361	11	1300	22	1288	13	95.5	1300	22
LABXT_001	LABXT_001-65	2.0	0.0000518	32.8138096	4.48	0.6	0.08932	0.33	2.7534	0.8	0.22338	0.7	0.3	1408	13	1300	15	1340	12	92.3	1300	15
LABXT_001	LABXT_001-46	1.1	0.0000174	105.7163378	4.48	0.7	0.08797	0.48	2.7247	1.0	0.22328	0.7	0.5	1375	18	1299	16	1327	15	94.5	1299	16

LABXT_001	LABXT_001-76	0.6	0.0000073	603.0089591	4.49	0.7	0.08884	0.20	2.7379	0.7	0.22312	0.7	0.7	1397	7	1298	16	1335	10	92.9	1298	16
LABXT_001	LABXT_001-79	1.4	0.0001344	33.4829744	4.50	0.8	0.09183	0.37	2.8125	0.5	0.22305	0.7	0.2	1458	14	1298	17	1358	7	89.0	1298	17
LABXT_001	LABXT_001-62	0.6	0.0000519	28.6174426	4.51	0.7	0.08736	0.22	2.6558	0.5	0.22136	0.7	0.0	1366	9	1289	16	1315	8	94.4	1289	16
LABXT_001	LABXT_001-87	4.2	0.0000157	39.1597852	4.69	0.7	0.08761	0.25	2.5701	0.5	0.21359	0.7	0.5	1371	10	1248	15	1290	8	91.0	1248	15
LABXT_001	LABXT_001-80	1.6	0.0000269	98.4184358	4.69	0.6	0.08187	0.28	2.4179	0.8	0.21344	0.6	0.5	1239	11	1247	15	1246	11	100.7	1247	15
LABXT_001	LABXT_001-71	0.8	0.0002639	33.9170869	4.69	0.6	0.08731	0.24	2.4919	0.4	0.21316	0.7	0.3	1365	9	1246	15	1268	6	91.3	1246	15
LABXT_001	LABXT_001-69	2.7	0.0002085	40.5777555	4.71	0.9	0.08881	0.48	2.4733	0.7	0.21306	0.8	0.4	1393	18	1245	18	1261	10	89.3	1245	18
LABXT_001	LABXT_001-70	0.5	0.0000148	248.3205184	4.71	0.7	0.08734	0.20	2.4534	0.6	0.21257	0.7	0.3	1366	8	1242	16	1256	8	90.9	1242	16
LABXT_001	LABXT_001-91	0.7	0.0000676	39.1459119	4.96	1.0	0.08669	0.22	2.4630	1.1	0.20393	0.9	0.9	1351	9	1195	20	1252	16	88.5	1195	20
LABXT_001	LABXT_001-83	0.1	0.0000145	47.7640289	5.21	0.9	0.08220	0.54	2.1710	0.7	0.19384	0.8	0.6	1247	21	1141	17	1168	10	91.6	1141	17
LABXT_001	LABXT_001-92	1.1	0.0000781	52.1110274	5.18	0.7	0.07808	0.29	2.0753	0.6	0.19333	0.7	0.6	1146	12	1139	14	1138	8	99.4	1139	14
LABXT_001	LABXT_001-84	1.2	0.0000256	118.4202407	5.21	0.7	0.08248	0.21	2.1752	0.5	0.19222	0.7	0.1	1254	8	1133	14	1172	8	90.4	1133	14
LABXT_001	LABXT_001-41	1.1	0.0001393	28.3343136	5.31	0.7	0.08158	0.39	2.1332	0.6	0.18873	0.7	0.1	1234	14	1114	14	1157	9	90.3	1114	14
LABXT_001	LABXT_001-72	0.8	0.0001150	41.5482840	5.31	0.6	0.08016	0.24	2.0912	0.6	0.18858	0.6	0.1	1198	9	1114	13	1144	8	93.0	1114	13
LABXT_001	LABXT_001-67	0.3	0.0001627	35.2019131	5.49	0.6	0.07726	0.20	1.9328	0.6	0.18210	0.6	0.4	1126	8	1078	13	1090	7	95.8	1078	13
LABXT_001	LABXT_001-78	0.5	0.0000895	26.4742173	5.70	0.6	0.07649	0.19	1.8488	0.7	0.17552	0.6	0.6	1106	8	1042	12	1060	9	94.2	1042	12
LABXT_001	LABXT_001-54	1.9	0.0000046	245.5827997	6.00	0.6	0.07647	0.34	1.7572	0.6	0.16658	0.6	0.5	1105	13	993	12	1028	8	89.9	993	12
Data not used due to high discordance																				
LABXT_001	LABXT_001-98	1.3	0.0001287	32.0050345	3.63	0.7	0.11072	0.26	4.2478	0.8	0.27682	0.7	0.8	1808	9	1575	20	1678	12	87.1		
LABXT_001	LABXT_001-68	3.2	0.0000017	562.0229378	5.48	2.4	0.08676	0.40	2.3368	1.4	0.20091	1.7	0.9	1349	15	1174	37	1207	23	87.0		
LABXT_001	LABXT_001-100	1.1	0.0000260	67.5483768	6.22	1.0	0.07819	0.29	1.7490	0.7	0.16280	0.9	0.6	1148	11	972	16	1023	9	84.7		
LABXT_001	LABXT_001-50	1.7	0.0000199	53.0849510	5.06	1.2	0.08950	0.49	2.3869	0.9	0.20003	1.0	0.6	1406	18	1176	20	1239	12	83.6		
LABXT_001	LABXT_001-45	1.5	0.0007864	40.5516621	5.22	0.7	0.08823	0.35	2.3104	0.7	0.19207	0.7	0.5	1383	13	1132	15	1212	10	81.9		
LABXT_001	LABXT_001-52	1.1	0.0001463	22.9409319	3.98	0.9	0.10955	0.18	3.8863	1.2	0.25444	0.9	1.0	1790	7	1460	24	1598	18	81.5		

LABXT_001	LABXT_001-59	0.6	0.0001023	24.2583605	5.46	1.8	0.08716	0.28	2.2901	1.6	0.18908	1.4	0.9	1364	10	1112	30	1186	26	81.5
LABXT_001	LABXT_001-81	1.7	0.0000804	35.5463817	4.78	0.8	0.09468	0.35	2.7324	0.5	0.21016	0.8	0.1	1517	13	1229	17	1335	8	81.0
LABXT_001	LABXT_001-42	2.7	0.0000199	89.0808280	4.00	1.5	0.11153	0.33	3.7561	0.7	0.25429	0.8	0.7	1822	12	1460	20	1579	12	80.1
LABXT_001	LABXT_001-58	0.9	0.0000076	642.954716 7	5.07	0.9	0.09714	0.26	2.6562	0.9	0.19945	0.9	0.6	1567	10	1171	19	1311	12	74.8
LABXT_001	LABXT_001-74	2.3	0.0000275	129.559591 8	7.37	2.7	0.08402	0.24	1.8118	2.0	0.15552	1.8	0.9	1291	9	927	33	1023	28	71.8
LABXT_001	LABXT_001-90	0.8	0.0000496	39.4847924	7.77	2.3	0.08109	0.24	1.6770	2.2	0.14598	2.0	1.0	1221	9	873	32	969	30	71.5
LABXT_001	LABXT_001-97	1.7	0.0000111	119.603663 8	8.80	1.9	0.07458	0.41	1.2662	1.6	0.12147	1.4	0.9	1050	16	737	20	818	19	70.2
LABXT_001	LABXT_001-86	1.3	0.0004069	37.0913448	6.30	1.1	0.08935	0.30	1.9588	1.1	0.16000	1.0	0.9	1408	11	956	18	1092	16	67.9
LABXT_001	LABXT_001-53	1.0	0.0000109	10.4603039	4.99	0.7	0.11178	0.47	3.0752	0.8	0.20098	0.7	0.6	1821	17	1180	16	1426	12	64.8
LABXT_001	LABXT_001-57	2.3	0.0000875	84.6511993	4.94	1.2	0.12224	0.26	3.5540	1.4	0.20901	1.2	0.9	1989	10	1221	27	1521	22	61.4
LABXT_001	LABXT_001-61	1.1	0.0000645	17.9099938	7.58	1.4	0.09116	0.27	1.7037	1.7	0.13768	1.5	1.0	1447	10	829	23	996	20	57.3
LABXT_001	LABXT_001-73	1.2	0.0000379	204.557690 4	9.49	5.4	0.09083	0.27	1.5126	2.3	0.12919	2.5	1.0	1440	10	778	37	909	33	54.0
LABXT_001	LABXT_001-95	0.9	0.0000194	3.6092568	6.81	1.2	0.10687	0.38	2.1938	0.7	0.15101	1.2	0.6	1742	14	905	20	1176	10	51.9
LABXT_001	LABXT_001-82	2.4	0.0000327	4.6817430	10.04	1.4	0.09397	0.30	1.3003	1.4	0.10365	1.5	0.9	1506	12	635	18	838	17	42.2
LABXT_001	LABXT_001-94	2.5	0.0000391	13.5177346	13.30	3.2	0.09430	0.31	1.2064	3.5	0.09672	3.5	1.0	1511	12	588	39	768	37	39.0
LABXT_001	LABXT_001-88	1.2	0.0000287	10.9813599	13.66	1.3	0.08575	0.17	0.9063	1.5	0.07557	1.3	1.0	1331	7	469	11	647	14	35.2
LABXT_001	LABXT_001-77	2.1	0.0000011	2870.03548 64	25.06	4.7	0.09834	0.56	0.9349	4.6	0.07960	5.3	1.0	1584	21	483	50	616	43	30.5

LABXTXR-001-1	LABXTXR-001-17	0.4	1257.4	163.4	3.94	1.6	0.09069	0.84	3.1937	1.7	0.25465	1.5	0.7	1437	32	1462	40	1455	27	102	1462	40
LABXTXR-001-1	LABXTXR-001-20	0.5	193.8	873.5	4.15	1.8	0.08989	0.90	3.0205	1.8	0.24238	1.8	0.7	1427	38	1398	45	1411	27	98	1398	45
LABXTXR-001-1	LABXTXR-001-4	0.7	2265.2	90.2	4.34	1.6	0.08642	0.96	2.7641	1.8	0.23122	1.6	0.5	1342	38	1340	38	1345	26	100	1340	38
LABXTXR-001-1	LABXTXR-001-10	0.6	931.1	80.5	4.45	2.2	0.08916	1.11	2.7910	2.1	0.22670	2.2	0.8	1403	42	1316	51	1351	32	94	1316	51
LABXTXR-001-1	LABXTXR-001-23	0.6	2450.0	113.4	4.52	2.5	0.08852	0.78	2.7590	2.2	0.22511	2.3	0.9	1390	30	1307	55	1341	34	94	1307	55
LABXTXR-001-1	LABXTXR-001-15	0.8	3879.9	82.3	4.71	5.2	0.08834	1.22	2.7579	3.9	0.22458	4.1	0.9	1384	46	1301	98	1332	64	94	1301	98
LABXTXR-001-1	LABXTXR-001-19	0.7	5344.3	60.6	4.63	3.3	0.08901	1.43	2.6958	2.6	0.22007	3.0	0.9	1398	54	1280	71	1324	39	92	1280	71

LABXTXR-001-1	LABXTXR-001-29	2.4	2282.2	103.8	4.61	2.5	0.08710	1.4	2.6491	3.0	0.21896	2.4	0.8	1357	56	1276	57	1311	44	94	1276	57
LABXTXR-001-1	LABXTXR-001-26	0.9	254.7	567.6	4.62	1.7	0.08063	1.1	2.4305	1.7	0.21770	1.8	0.5	1207	43	1269	41	1251	24	105	1269	41
LABXTXR-001-1	LABXTXR-001-22	0.6	6776.2	68.7	4.70	2.6	0.08513	1.1	2.5346	2.4	0.21460	2.6	0.9	1315	44	1252	59	1280	36	95	1252	59
LABXTXR-001-1	LABXTXR-001-21	1.1	22.6	1569.4	4.92	2.1	0.07989	1.8	2.2748	2.6	0.20599	2.2	0.6	1175	73	1206	49	1200	36	103	1206	49
LABXTXR-001-1	LABXTXR-001-6	0.2	79616.8	68.5	5.14	1.5	0.08083	0.7	2.1849	1.7	0.19501	1.5	0.7	1215	30	1148	32	1176	24	95	1148	32
LABXTXR-001-1	LABXTXR-001-18	0.4	475.6	152.8	5.16	1.5	0.07971	1.4	2.1371	2.1	0.19447	1.6	0.5	1178	55	1145	33	1158	29	97	1145	33
LABXTXR-001-1	LABXTXR-001-13	0.4	81.3	336.7	5.40	1.6	0.07490	1.0	1.9016	1.6	0.18582	1.5	0.5	1059	40	1098	31	1084	25	104	1098	31
LABXTXR-001-1	LABXTXR-001-25	0.6	335.9	187.3	5.56	1.4	0.07413	0.9	1.8620	1.7	0.18021	1.4	0.2	1048	42	1068	28	1067	22	102	1068	28
LABXTXR-001-1	LABXTXR-001-30	1.8	2314.3	40.5	5.56	1.5	0.07798	1.3	1.9461	1.9	0.18020	1.5	0.3	1138	53	1068	29	1096	26	94	1068	29
LABXTXR-001-1	LABXTXR-001-12	0.9	371.8	130.1	5.60	1.5	0.07550	1.3	1.8630	1.7	0.17904	1.5	0.0	1071	54	1061	30	1067	23	99	1061	30
LABXTXR-001-1	LABXTXR-001-28	0.9	957.1	114.7	6.00	1.5	0.07055	1.1	1.6337	1.7	0.16719	1.5	0.3	936	46	996	27	982	22	106	996	27
LABXTXR-001-1	LABXTXR-001-24	1.4	212.4	90.7	7.59	1.6	0.06855	1.4	1.2561	2.0	0.13224	1.6	0.3	872	59	800	24	825	22	92	800	24
LABXTXR-001-1	LABXTXR-001-16	0.8	1895.8	79.5	8.56	1.4	0.06380	0.9	1.0326	1.8	0.11701	1.4	0.5	730	38	713	19	720	18	98	713	19
LABXTXR-001-1	LABXTXR-001-8	1.4	347.4	110.1	8.68	1.5	0.06174	1.0	0.9869	1.8	0.11549	1.6	0.5	660	45	704	21	697	18	107	704	21
Data not used due to high discordance																						
LABXTXR-001-1	LABXTXR-001-7	0.5	29679.9	64.5	5.03	3.8	0.09484	1.3	2.6793	4.2	0.20358	3.8	0.9	1520	51	1192	82	1315	63	78		
LABXTXR-001-1	LABXTXR-001-27	0.3	1005.7	144.1	5.91	4.1	0.09172	1.0	2.2849	4.3	0.18093	4.8	1.0	1456	40	1066	92	1193	58	73		
LABXTXR-001-1	LABXTXR-001-3	0.9	15314.8	48.8	5.03	2.4	0.10468	0.6	2.9042	2.6	0.19983	2.5	1.0	1706	24	1173	54	1386	36	69		
LABXTXR-001-1	LABXTXR-001-9	2.3	6723.7	78.9	17.18	4.3	0.08840	0.8	0.7558	5.3	0.06203	5.4	1.0	1387	33	387	40	563	44	28		
LABXTXR-001-1	LABXTXR-001-11	2.0	2969.8	62.1	15.06	5.5	0.09981	1.1	0.9994	5.7	0.07237	5.5	1.0	1615	43	449	48	692	57	28		

Amostra MD-2019-13

			Ratios										Rho	Ages (Ma)						% conc [1]	Best age	2s
Sample	**Spot number**	**Th/U**	**206Pb/204Pb**	**1s**	**238U/206Pb**	**1s**	**207Pb/206Pb**	**1s**	**207Pb/235U**	**1s**	**206Pb/238U**	**1s**		**207Pb/206Pb**	**2s**	**206Pb/238U**	**2s**	**207Pb/235U**	**2s**			

				(%)		(%)		(%)		(%)			(abs)		(abs)		(abs)			(abs)
LABXT_0005	LABXT_005-41	0.7	5.81726E-05	46.22437	2.89	0.7	0.12136	0.27	5.7166	0.6	0.34561	0.7	0.45	1974	10	1914	24	1931	10	96.9	1974	10
LABXT_0005	LABXT_005-100	2.8	0.000084	55.91848	3.13	1.5	0.11114	0.30	4.8940	2.0	0.31963	1.5	0.10	1816	11	1788	47	1801	34	98.5	1816	11
LABXT_0005	LABXT_005-81	1.7	0.000122	19.33327	3.32	1.5	0.10543	0.27	4.3828	2.0	0.30151	1.5	0.29	1720	10	1699	45	1709	32	98.8	1720	10
LABXT_0005	LABXT_005-5	0.6	-7.46887E-06	-355.698	3.73	0.7	0.09825	0.30	3.6082	0.7	0.26833	0.7	0.48	1588	11	1532	20	1547	11	96.5	1588	11
LABXT_0005	LABXT_005-84	1.0	-0.000332	-29.5198	4.15	1.7	0.09806	0.29	3.2869	2.1	0.24284	1.6	0.92	1584	11	1400	41	1474	33	88.4	1584	11
LABXT_0005	LABXT_005-50	1.1	-0.000910879	-41.6383	3.72	0.7	0.09716	0.27	3.6265	0.6	0.26895	0.7	0.18	1568	10	1535	20	1552	10	97.9	1568	10
LABXT_0005	LABXT_005-90	0.9	0.000374	53.56244	3.73	1.5	0.09663	0.22	3.5747	2.0	0.26821	1.5	0.33	1559	8	1532	41	1543	32	98.2	1559	8
LABXT_0005	LABXT_005-55	0.8	-0.000311666	-54.2388	4.04	0.7	0.09647	0.69	3.3395	1.2	0.24792	0.7	0.84	1546	24	1428	19	1478	18	92.3	1546	24
LABXT_0005	LABXT_005-63	0.6	0.000231963	31.97656	3.89	0.7	0.09569	0.26	3.3876	0.5	0.25730	0.7	0.56	1539	10	1476	20	1499	9	95.9	1539	10
LABXT_0005	LABXT_005-95	0.8	0.000050	47.62279	3.74	1.5	0.09526	0.25	3.5118	2.0	0.26754	1.5	0.25	1530	9	1528	41	1529	31	99.9	1530	9
LABXT_0005	LABXT_005-99	0.5	0.000092	45.16414	3.98	1.5	0.09159	0.21	3.1707	2.0	0.25126	1.5	0.46	1457	8	1445	39	1450	31	99.1	1445	39
LABXT_0005	LABXT_005-31	1.3	-0.000192046	-45.3965	4.00	0.7	0.09149	0.28	3.1521	0.6	0.24987	0.7	0.15	1455	11	1438	19	1443	9	98.8	1438	19
LABXT_0005	LABXT_005-92	0.5	-0.000206	-47.6817	4.09	1.6	0.09031	0.24	3.0382	2.0	0.24453	1.5	0.69	1429	9	1410	39	1416	31	98.6	1410	39
LABXT_0005	LABXT_005-59	1.2	0.000101048	24.97411	4.10	0.7	0.09310	0.28	3.1346	0.5	0.24435	0.7	0.18	1489	11	1409	19	1439	9	94.6	1409	19
LABXT_0005	LABXT_005-34	0.8	-0.000182208	-61.246	4.15	0.8	0.09015	0.27	2.9988	0.6	0.24131	0.8	0.22	1426	10	1393	19	1404	9	97.7	1393	19
LABXT_0005	LABXT_005-107	1.2	0.000027	41.11904	4.16	1.5	0.08969	0.27	2.9619	2.0	0.24068	1.5	0.12	1416	10	1390	37	1397	30	98.2	1390	37
LABXT_0005	LABXT_005-45	0.3	7.03139E-08	4184.678	4.17	0.8	0.09036	0.46	2.9756	0.6	0.23969	0.8	0.10	1429	17	1385	19	1398	9	96.9	1385	19
LABXT_0005	LABXT_005-58	0.6	6.11372E-05	30.89726	4.20	0.7	0.08817	0.31	2.9084	0.6	0.23826	0.7	0.18	1384	12	1378	18	1381	9	99.5	1378	18
LABXT_0005	LABXT_005-98	1.0	-0.000017	-189.665	4.20	1.5	0.08762	0.21	2.8748	2.0	0.23799	1.5	0.44	1372	8	1376	37	1375	30	100.3	1376	37
LABXT_0005	LABXT_0005	0.5	9.53238E-05	68.96493	4.21	0.8	0.09027	0.43	3.2874	0.8	0.23790	0.8	0.74	1430	17	1376	19	1476	12	96.2	1376	19

LABXT_0005	LABXT_005-9	4.2	-4.34225E-05	-48.3915	4.24	0.7	0.08702	0.31	2.8306	0.7	0.23621	0.7	0.66	1358	12	1367	18	1360	10	100.7	1367	18
LABXT_0005	LABXT_005-61	0.8	0.000869428	31.22098	4.26	0.8	0.08768	0.30	2.8281	0.8	0.23511	0.8	0.43	1372	11	1361	19	1360	12	99.2	1361	19
LABXT_0005	LABXT_005-15	3.4	3.25633E-06	164.4989	4.26	0.8	0.08700	0.36	2.8226	0.8	0.23490	0.8	0.49	1357	14	1360	19	1357	12	100.2	1360	19
LABXT_0005	LABXT_005-2	1.3	-5.61543E-07	-487.492	4.31	0.8	0.08743	0.56	2.7628	0.9	0.23299	0.8	0.40	1361	22	1350	20	1339	13	99.2	1350	20
LABXT_0005	LABXT_005-39	0.5	4.30337E-05	65.34195	4.30	0.7	0.09344	0.40	2.8160	0.7	0.23289	0.7	0.82	1493	15	1350	18	1358	10	90.4	1350	18
LABXT_0005	LABXT_005-7	2.8	4.82413E-05	28.98214	4.30	0.7	0.08735	0.30	2.7784	0.6	0.23284	0.7	0.26	1365	12	1349	18	1346	10	98.8	1349	18
LABXT_0005	LABXT_005-108	0.8	-0.000013	-102.525	4.31	1.5	0.08836	0.33	2.8161	2.0	0.23223	1.5	0.60	1386	13	1346	36	1359	30	97.1	1346	36
LABXT_0005	LABXT_005-75	0.4	3.11837E-05	37.89645	4.32	0.8	0.09250	0.45	2.8794	1.2	0.23219	0.8	0.92	1472	17	1346	20	1367	18	91.4	1346	20
LABXT_0005	LABXT_005-6	1.9	2.2496E-05	34.47701	4.31	0.7	0.08760	0.32	2.7714	0.7	0.23184	0.7	0.19	1371	13	1344	18	1344	10	98.0	1344	18
LABXT_0005	LABXT_005-104	1.8	-0.000078	-66.1976	4.32	1.5	0.09069	0.48	2.8868	2.1	0.23139	1.5	0.72	1432	18	1342	37	1376	30	93.7	1342	37
LABXT_0005	LABXT_005-4	0.6	1.16143E-05	71.27915	4.33	0.7	0.08795	0.32	2.7834	0.7	0.23105	0.7	0.41	1378	12	1340	18	1347	11	97.3	1340	18
LABXT_0005	LABXT_005-37	1.4	-1.82316E-05	-138.05	4.35	0.7	0.08844	0.27	2.8190	0.6	0.23005	0.7	0.14	1390	10	1335	18	1358	9	96.0	1335	18
LABXT_0005	LABXT_005-85	0.4	0.000030	36.94537	4.36	1.5	0.08980	0.39	2.8445	2.0	0.22966	1.5	0.40	1417	15	1333	36	1366	30	94.1	1333	36
LABXT_0005	LABXT_005-53	1.3	3.33782E-05	32.65395	4.39	0.7	0.08519	0.33	2.7009	0.9	0.22828	0.8	0.84	1319	13	1325	18	1323	13	100.5	1325	18
LABXT_0005	LABXT_005-18	0.6	-1.3846E-06	-745.931	4.39	0.7	0.08745	0.37	2.7461	0.6	0.22796	0.7	0.25	1367	14	1324	18	1338	9	96.8	1324	18
LABXT_0005	LABXT_005-116	2.8	0.000004	380.1392	4.40	1.5	0.08728	0.26	2.7066	2.0	0.22727	1.5	0.53	1365	10	1320	36	1330	30	96.7	1320	36
LABXT_0005	LABXT_005-119	0.7	-0.000019	-221.16	4.41	1.5	0.08767	0.20	2.7121	2.0	0.22683	1.5	0.22	1373	8	1318	37	1331	30	96.0	1318	37
LABXT_0005	LABXT_005-93	4.3	0.000014	40.91046	4.43	1.5	0.08491	0.31	2.6466	2.0	0.22602	1.5	0.16	1311	12	1314	36	1313	30	100.2	1314	36
LABXT_0005	LABXT_005-67	1.5	4.53412E-05	35.44938	4.43	0.7	0.08619	0.29	2.6891	0.5	0.22592	0.7	0.74	1341	11	1313	18	1323	8	97.9	1313	18
LABXT_0005	LABXT_005-11	1.0	5.28516E-05	45.41564	4.43	0.7	0.08788	0.30	2.7329	0.6	0.22581	0.8	0.21	1377	12	1312	18	1335	8	95.3	1312	18
LABXT_0005	LABXT_005-60	1.0	4.52499E-06	90.46409	4.45	0.8	0.08892	0.46	2.7549	0.6	0.22534	0.8	0.20	1395	18	1310	19	1345	9	93.9	1310	19
LABXT_0005	LABXT_005-105	0.7	0.000160	47.44179	4.45	1.6	0.09066	0.62	2.8005	2.0	0.22533	1.6	0.06	1433	22	1309	37	1355	30	91.4	1309	37

LABXT_0005	LABXT_005-38	1.0	4.10763E-05	76.20473	4.45	0.8	0.09001	0.36	2.5964	0.6	0.22483	0.8	0.21	1423	14	1307	18	1299	9	91.9	1307	18
LABXT_0005	LABXT_005-71	1.7	-1.25574E-05	-414.905	4.46	0.8	0.08852	0.38	2.4773	0.7	0.22416	0.8	0.47	1391	14	1304	18	1264	10	93.7	1304	18
LABXT_0005	LABXT_005-66	1.8	-1.03569E-05	-172.486	4.46	0.7	0.08726	0.30	2.7008	0.5	0.22409	0.7	0.57	1364	12	1303	17	1326	8	95.6	1303	17
LABXT_0005	LABXT_005-103	0.8	0.000273	36.80875	4.48	1.5	0.08546	0.26	2.6223	2.0	0.22317	1.5	0.69	1323	10	1299	35	1306	29	98.2	1299	35
LABXT_0005	LABXT_005-68	2.3	3.21756E-05	41.48801	4.51	0.7	0.08631	0.32	2.6226	0.6	0.22191	0.7	0.15	1344	12	1292	17	1304	9	96.1	1292	17
LABXT_0005	LABXT_005-74	0.7	8.25092E-05	34.52796	4.51	0.7	0.08625	0.45	2.5593	0.6	0.22189	0.7	0.11	1341	18	1292	17	1287	9	96.3	1292	17
LABXT_0005	LABXT_005-22	3.9	4.54531E-06	98.79999	4.51	0.7	0.08675	0.34	2.6445	0.6	0.22179	0.7	0.52	1352	13	1291	18	1310	9	95.5	1291	18
LABXT_0005	LABXT_005-54	1.1	0.003809181	37.42065	4.52	0.7	0.08715	0.29	2.6864	0.6	0.22131	0.7	0.71	1362	11	1289	17	1321	10	94.6	1289	17
LABXT_0005	LABXT_005-36	2.0	6.23924E-05	54.73991	4.52	0.8	0.08627	0.34	2.5640	0.8	0.22109	0.7	0.47	1341	13	1288	17	1287	11	96.0	1288	17
LABXT_0005	LABXT_005-77	0.7	8.67761E-05	35.43013	4.66	0.8	0.08320	0.38	2.4108	0.5	0.21529	0.8	0.01	1271	15	1257	19	1245	7	98.9	1257	19
LABXT_0005	LABXT_005-62	1.5	-4.60911E-05	-53.5854	4.69	0.8	0.08536	0.39	2.4987	0.5	0.21329	0.8	0.41	1320	15	1246	17	1270	7	94.4	1246	17
LABXT_0005	LABXT_005-1	0.8	-4.85205E-05	-57.7523	4.72	0.8	0.08318	0.27	2.4113	0.7	0.21185	0.8	0.76	1272	10	1239	17	1242	11	97.4	1239	17
LABXT_0005	LABXT_005-51	1.7	6.37147E-05	27.34143	4.76	0.8	0.08433	0.31	2.4529	0.5	0.21068	0.8	0.64	1298	12	1232	17	1257	7	94.9	1232	17
LABXT_0005	LABXT_005-94	0.8	0.000051	40.23032	4.87	1.5	0.08096	0.24	2.2909	2.0	0.20546	1.5	0.49	1219	9	1205	33	1209	28	98.8	1205	33
LABXT_0005	LABXT_005-48	1.6	-0.000151051	-39.2778	4.93	0.7	0.08039	0.32	2.2416	0.6	0.20282	0.7	0.20	1203	13	1190	16	1192	8	99.0	1190	16
LABXT_0005	LABXT_005-17	0.7	5.12404E-05	63.04253	4.94	0.7	0.08109	0.33	2.2605	0.6	0.20262	0.7	0.10	1220	13	1190	16	1197	9	97.5	1190	16
LABXT_0005	LABXT_005-97	1.6	0.000050	33.50527	4.96	1.5	0.07944	0.36	2.2084	2.0	0.20190	1.5	0.37	1181	14	1185	33	1184	29	100.4	1185	33
LABXT_0005	LABXT_005-69	0.8	0.000262064	27.81136	4.98	0.7	0.08158	0.26	2.2481	0.5	0.20101	0.7	0.81	1233	10	1181	16	1194	8	95.8	1181	16
LABXT_0005	LABXT_005-101	0.8	-0.000029	-57.1492	5.01	1.5	0.07941	0.26	2.1873	2.0	0.19972	1.5	0.61	1179	10	1174	32	1177	28	99.5	1174	32
LABXT_0005	LABXT_005-42	1.3	-1.04149E-05	-142.199	5.09	0.7	0.07899	0.31	2.1568	0.7	0.19650	0.7	0.19	1169	13	1156	16	1164	9	98.9	1156	16
LABXT_0005	LABXT_005-49	0.7	0.000933795	28.03009	5.10	0.7	0.07957	0.27	2.1579	0.6	0.19611	0.7	0.40	1184	11	1154	15	1165	8	97.5	1154	15

LABXT_00005	LABXT_005-110	0.6	0.000079	45.32188	5.10	1.5	0.08070	0.23	2.1688	2.0	0.19603	1.5	0.53	1212	9	1154	32	1171	27	95.2	1154	32
LABXT_00005	LABXT_005-64	0.9	7.08976E-06	87.09783	5.11	0.7	0.08085	0.34	2.1861	0.5	0.19572	0.7	0.57	1215	13	1153	16	1175	7	94.9	1153	16
LABXT_00005	LABXT_005-24	2.0	4.7114E-06	67.93604	5.13	0.7	0.08238	0.47	2.2142	0.6	0.19532	0.8	0.28	1247	18	1150	16	1184	8	92.3	1150	16
LABXT_00005	LABXT_005-40	0.8	6.72793E-06	84.00269	5.22	0.8	0.08021	0.39	2.1005	0.7	0.19158	0.7	0.18	1197	15	1130	15	1146	10	94.4	1130	15
LABXT_00005	LABXT_005-112	1.0	0.000006	435.5256	5.26	1.9	0.08131	0.46	2.0933	2.1	0.19111	1.6	0.74	1225	19	1128	33	1145	31	92.1	1128	33
LABXT_00005	LABXT_005-79	0.6	-1.38628E-05	-49.7833	5.28	0.8	0.08029	0.46	2.1074	0.6	0.18968	0.8	0.18	1196	18	1119	16	1149	8	93.6	1119	16
LABXT_00005	LABXT_005-109	0.8	-0.000006	-151.753	5.40	1.5	0.07739	0.54	1.9712	2.1	0.18540	1.5	0.50	1125	21	1096	31	1104	28	97.4	1096	31
LABXT_00005	LABXT_005-26	0.9	-1.20827E-06	-205.129	5.41	0.8	0.07772	0.56	1.9848	0.7	0.18541	0.8	0.16	1128	23	1096	16	1107	10	97.2	1096	16
LABXT_00005	LABXT_005-113	1.1	0.000036	24.12617	5.49	1.5	0.07714	0.44	1.9223	2.0	0.18257	1.5	0.20	1118	17	1081	30	1088	27	96.7	1081	30
LABXT_00005	LABXT_005-76	0.9	1.94613E-06	282.0568	5.50	0.7	0.07826	0.37	1.9537	0.5	0.18187	0.8	0.49	1148	15	1077	15	1098	7	93.8	1077	15
LABXT_00005	LABXT_005-35	0.6	5.56898E-06	51.22134	5.54	0.8	0.07815	0.47	1.9463	0.7	0.18050	0.8	0.12	1142	19	1070	15	1094	9	93.6	1070	15
LABXT_00005	LABXT_005-73	0.8	1.88969E-05	43.19134	5.60	0.8	0.07822	0.34	1.8921	0.5	0.17873	0.8	0.69	1150	14	1060	15	1078	6	92.2	1060	15
LABXT_00005	LABXT_005-120	4.9	0.000098	63.51961	5.84	1.7	0.07821	0.33	1.8331	2.0	0.17192	1.5	0.74	1150	13	1022	29	1056	27	88.9	1022	29
LABXT_00005	LABXT_005-12	0.8	-0.000145999	-31.9197	5.84	0.8	0.07463	0.55	1.7378	0.7	0.17176	0.8	0.03	1047	22	1022	15	1020	9	97.5	1022	15
LABXT_00005	LABXT_005-118	1.1	0.000018	58.40451	5.84	1.5	0.07412	0.30	1.7310	2.0	0.17122	1.5	0.26	1041	12	1019	29	1020	26	97.9	1019	29
LABXT_00005	LABXT_005-21	2.4	-7.43065E-05	-33.9868	5.88	0.7	0.07491	0.34	1.7703	0.7	0.17013	0.7	0.10	1062	14	1013	14	1032	9	95.4	1013	14
LABXT_00005	LABXT_005-16	0.7	3.63446E-05	39.15542	5.89	0.7	0.07377	0.32	1.7225	0.6	0.16975	0.7	0.41	1034	13	1011	14	1015	8	97.8	1011	14
LABXT_00005	LABXT_005-78	0.4	0.000342209	25.06586	5.93	0.7	0.07329	0.27	1.7099	0.5	0.16859	0.7	0.60	1020	11	1004	14	1011	7	98.4	1004	14
LABXT_00005	LABXT_005-57	1.8	4.38751E-05	28.94784	5.94	0.8	0.07452	0.38	1.7397	0.6	0.16839	0.7	0.05	1050	15	1003	14	1022	8	95.5	1003	14
LABXT_00005	LABXT_005-102	1.0	0.000023	55.85109	6.13	1.5	0.07254	0.31	1.6271	2.0	0.16322	1.5	0.40	997	13	975	27	980	25	97.8	975	27
LABXT_00005	LABXT_005-44	0.7	2.07021E-05	31.41689	6.45	0.8	0.07345	0.42	1.5815	0.7	0.15522	0.8	0.30	1021	17	930	13	960	9	91.1	930	13
LABXT_00005	LABXT_005-114	1.6	0.000021	29.56267	8.04	1.5	0.06581	0.52	1.1175	2.0	0.12440	1.5	0.04	794	22	756	21	761	22	95.2	756	21

LABXT_0005	LABXT_005-96	0.6	0.000522	48.10921	8.50	1.5	0.06396	0.25	1.0379	2.0	0.11773	1.5	0.28	737	10	717	20	723	21	97.3	717	20
LABXT_0005	LABXT_005-19	0.6	0.000185548	26.81859	10.40	0.7	0.06026	0.28	0.8010	0.6	0.09619	0.7	0.08	611	12	592	8	596	5	96.9	592	8
LABXT_0005	LABXT_005-8	0.9	5.69973E-05	36.90474	10.66	0.8	0.05920	0.30	0.7657	0.7	0.09380	0.7	0.83	572	13	578	8	576	6	101.1	578	8
LABXT_0005	LABXT_005-86	1.8	0.000240	33.20699	11.32	1.5	0.05991	0.35	0.7341	2.1	0.08867	1.5	0.81	596	15	548	16	558	18	91.8	548	16
LABXT_0005	LABXT_005-46	1.0	8.82654E-05	37.39843	12.28	0.8	0.05750	0.41	0.6549	0.8	0.08159	0.8	0.37	504	17	506	8	510	6	100.3	506	8
Data not used due to high discordance																						
LABXT_0005	LABXT_005-47	1.1	5.9338E-05	29.68241	6.44	0.7	0.07497	0.54	1.6213	1.0	0.15527	0.7	0.65	1058	20	930	13	973	12	87.9		
LABXT_0005	LABXT_005-10	1.8	0.000113847	61.1091	4.46	0.9	0.09352	0.62	2.8707	0.7	0.22426	0.9	0.06	1491	23	1305	20	1370	11	87.5		
LABXT_0005	LABXT_005-3	1.0	5.27507E-05	33.90131	4.61	0.9	0.09172	0.38	2.4498	0.4	0.21773	0.9	0.13	1459	15	1270	20	1258	6	87.0		
LABXT_0005	LABXT_005-89	1.4	0.000006	316.2691	5.98	1.6	0.07812	0.25	1.8046	2.0	0.16737	1.5	0.67	1147	10	998	28	1046	26	87.0		
LABXT_0005	LABXT_005-115	4.4	-0.000018	-50.5113	9.74	1.6	0.06426	0.79	0.8995	2.2	0.10269	1.5	0.63	730	29	630	18	651	20	86.3		
LABXT_0005	LABXT_005-91	1.3	0.000087	40.01959	4.79	1.5	0.08999	0.33	2.5838	2.0	0.20875	1.5	0.59	1422	13	1222	34	1295	30	85.9		
LABXT_0005	LABXT_0005	1.0	-0.000227791	-55.3389	6.22	0.7	0.07722	0.38	1.9243	0.5	0.16081	0.7	0.34	1127	16	961	13	1090	6	85.3		
LABXT_0005	LABXT_005-20	0.9	-0.027216238	-99.873	5.01	0.7	0.08832	0.55	2.3576	0.6	0.19965	0.7	0.55	1381	21	1173	16	1227	9	85.0		
LABXT_0005	LABXT_005-117	0.8	-0.000091	-78.4749	5.63	1.6	0.08200	0.24	1.9847	2.0	0.17773	1.5	0.61	1243	9	1054	29	1110	27	84.8		
LABXT_0005	LABXT_005-23	1.3	7.27449E-06	343.8119	5.99	0.7	0.07981	0.45	1.7374	0.6	0.16698	0.7	0.12	1191	18	995	14	1021	8	83.6		
LABXT_0005	LABXT_005-27	0.5	-0.000117084	-144.944	6.56	0.8	0.07636	0.57	1.6283	0.6	0.15248	0.8	0.58	1101	23	915	13	981	8	83.1		
LABXT_0005	LABXT_005-52	2.0	0.000189204	28.98381	5.05	0.8	0.08922	0.30	2.4477	0.6	0.19808	0.7	0.34	1407	11	1165	16	1254	9	82.8		
LABXT_0005	LABXT_0009_1	1.2	0.000072	32.33615	4.07	1.7	0.10551	0.49	3.6400	2.1	0.24829	1.6	0.78	1731	18	1428	42	1558	33	82.5		
LABXT_0005	LABXT_005-88	1.2	-0.000034	-72.3724	4.88	1.5	0.09383	1.11	2.6423	2.2	0.20505	1.5	0.61	1468	40	1202	33	1306	32	81.9		
LABXT_0005	LABXT_005-32	1.9	4.11151E-05	36.05232	5.66	0.8	0.08472	0.31	2.2170	0.8	0.17735	0.8	0.82	1307	12	1052	16	1184	11	80.5		

LABXT_00 05	LABXT_005-106	1.0	0.000111	23.428 06	5.14	2. 1	0.09567	0.3 5	2.6482	2. 2	0.20342	2. 0	0.9 7	1537	13	1190	43	1307	34	77.4
LABXT_00 05	LABXT_005-70	1.2	2.1348E-05	43.451 73	5.28	0. 8	0.09378	0.9 9	2.4433	1. 2	0.19025	0. 8	0.1 6	1471	32	1122	17	1246	16	76.3
LABXT_00 05	LABXT_005-13	1.4	-9.76135E-06	-219.11	6.01	1. 4	0.08845	0.5 4	2.1080	1. 2	0.17217	1. 3	0.9 8	1383	20	1022	25	1142	16	73.9
LABXT_00 05	LABXT_005-83	1.0	0.000006	167.70 95	4.13	1. 5	0.11822	0.3 3	3.9870	2. 0	0.24302	1. 5	0.5 0	1926	12	1402	38	1630	33	72.8
LABXT_00 05	LABXT_005-33	0.9	6.63985E-05	19.688 84	5.66	1. 0	0.09566	0.3 2	2.3645	1. 0	0.17808	0. 9	0.8 4	1538	12	1056	17	1224	16	68.7
LABXT_00 05	LABXT_005-56	1.7	4.95214E-05	31.488 31	6.44	3. 1	0.09274	0.5 5	2.1549	0. 9	0.16936	1. 5	0.8 7	1471	17	1008	28	1161	15	68.5
LABXT_00 05	LABXT_005-25	1.2	4.86005E-05	31.447 89	6.12	1. 6	0.09204	0.4 2	1.8960	0. 8	0.16801	1. 6	0.8 7	1465	16	999	29	1078	11	68.2
LABXT_00 05	LABXT_005-111	1.4	0.000014	139.50 09	6.04	2. 4	0.09502	0.8 4	2.1958	2. 3	0.17146	1. 9	0.7 4	1504	34	1018	37	1172	32	67.6
LABXT_00 05	LABXT_005-43	0.3	1.80777E-05	114.33 6	6.81	2. 8	0.09325	0.4 4	2.1293	1. 5	0.16900	2. 0	0.9 0	1488	17	1000	38	1141	23	67.2
LABXT_00 05	LABXT_005-65	1.8	3.25134E-05	8.5834 72	6.56	0. 9	0.09803	0.3 0	2.0854	0. 9	0.15406	1. 0	0.6 6	1584	11	923	16	1140	11	58.3
LABXT_00 05	LABXT_005-80	0.6	0.00014975 5	64.026 59	8.65	3. 3	0.09518	0.9 8	1.5319	1. 9	0.13400	3. 0	0.9 2	1522	40	805	46	933	24	52.9
LABXT_00 05	LABXT_0005	1.7	1.5338E-05	26.781 39	7.40	1. 4	0.10678	0.9 1	2.1537	0. 8	0.13756	1. 4	0.7 8	1733	32	830	21	1164	11	47.9
LABXT_00 05	LABXT_005-72	0.5	2.71879E-05	2.8515 03	8.29	1. 2	0.09890	0.3 6	1.6992	0. 9	0.12293	1. 1	0.8 8	1600	13	747	15	1003	13	46.7
LABXT_00 05	LABXT_005-14	3.2	3.57958E-05	24.325 54	9.48	2. 3	0.09476	0.4 4	1.3974	1. 5	0.11609	2. 2	0.9 5	1520	17	705	29	879	18	46.4
LABXT_00 05	LABXT_005-82	1.2	0.000024	37.738 71	9.94	2. 0	0.09070	0.5 2	1.3288	2. 4	0.10859	2. 4	0.9 9	1431	20	662	30	851	27	46.3
LABXT_00 05	LABXT_0005	1.6	1.68816E-05	3.0037 21	9.73	1. 3	0.10006	0.3 5	1.5634	1. 0	0.10336	1. 4	0.9 0	1623	13	634	16	953	12	39.0
LABXT_00 05	LABXT_0005	2.0	1.69764E-05	9.0366 33	12.41	3. 1	0.10469	0.7 4	1.4066	2. 7	0.08974	3. 4	0.9 9	1702	28	551	36	879	31	32.4
LABXT_00 05	LABXT_0009 _1	1.8	0.000012	5.5653 36	12.64	2. 8	0.11092	0.6 2	1.3332	3. 2	0.08946	3. 5	0.9 9	1807	23	549	37	846	35	30.4

Amostra MD-238

			Ratios						Rho		Age (Ma)								
Sample	Spot number	Th/U	6/4 ratio	7/6 ratio	1s(%)	7/5 ratio	1s(%)	6/8 ratio	1s(%)		7/6 age	1s(abs)	7/5 age	1s(abs)	6/8 age	1s(abs)	Conc (%)	Best Age	1s(abs)
MD 238																			
LAB1662	056-Z42	0	54613	0	2	9	2	0	1	1	2332	30	2317	20	2299	26	99	2332	30

LAB1662	037-Z28	0	190917	0	1	6	1	0	1	1	2043	12	2004	9	1968	13	96	2043	12
LAB1662	024-Z17	1	80092	0	1	6	1	0	1	1	1984	19	1914	13	1850	17	93	1984	19
LAB1662	046-Z34	1	148132	0	2	4	2	0	2	1	1851	28	1650	19	1497	22	81	1851	28
LAB1662	008-Z05	1	115653	0	1	5	1	0	1	1	1844	13	1834	9	1826	12	99	1844	13
LAB1662	029-Z22	1	56199	0	1	3	1	0	1	1	1509	20	1479	12	1458	14	97	1509	20
LAB1662	065-Z49	0	5383	0	2	3	3	0	2	1	1611	43	1423	25	1301	28	81	1423	25
LAB1662	069-Z53	1	47345	0	1	3	2	0	1	1	1384	20	1388	13	1391	18	100	1388	13
LAB1662	044-Z32	0	122580	0	1	3	1	0	1	1	1346	15	1357	10	1363	13	101	1357	10
LAB1662	038-Z29	0	121093	0	1	3	1	0	1	1	1388	12	1336	7	1304	9	94	1336	7
LAB1662	077-Z59	0	35682	0	1	3	2	0	1	1	1481	26	1334	14	1244	15	84	1334	14
LAB1662	068-Z52	0	53100	0	1	3	1	0	1	1	1357	18	1329	10	1311	12	97	1329	10
LAB1662	074-Z56	0	105116	0	1	3	1	0	1	1	1328	16	1299	9	1281	11	96	1299	9
LAB1662	039-Z30	0	129170	0	1	3	1	0	1	1	1330	14	1291	8	1268	9	95	1291	8
LAB1662	045-Z33	0	105964	0	1	2	1	0	1	1	1312	15	1269	9	1244	11	95	1269	9
LAB1662	033-Z24	1	81079	0	1	2	1	0	1	1	1266	16	1223	9	1198	10	95	1223	9
LAB1662	049-Z37	0	53858	0	1	2	2	0	1	1	1233	19	1222	11	1215	13	99	1222	11
LAB1662	078-Z60	0	31433	0	1	2	2	0	1	1	1242	24	1210	12	1193	12	96	1210	12
LAB1662	004-Z01	0	114669	0	1	2	1	0	1	1	1220	16	1189	8	1172	8	96	1189	8
LAB1662	026-Z19	0	44385	0	2	2	3	0	1	1	1143	47	1161	19	1170	16	102	1161	19
LAB1662	016-Z11	0	9232	0	2	2	3	0	1	1	1236	45	1158	19	1116	15	90	1158	19
LAB1662	057-Z43	0	60562	0	1	2	1	0	1	1	1177	19	1156	9	1145	10	97	1156	9
LAB1662	025-Z18	0	74638	0	2	2	2	0	2	1	1174	30	1140	15	1123	17	96	1140	15
LAB1662	079-Z61	0	56586	0	1	2	1	0	1	1	1147	19	1129	9	1120	9	98	1129	9
LAB1662	053-Z39	0	61100	0	1	2	2	0	1	1	1108	23	1102	10	1099	10	99	1102	10
LAB1662	009-Z06	0	19929	0	1	2	2	0	2	1	1074	29	1085	14	1091	15	102	1085	14
LAB1662	006-Z03	0	77727	0	2	2	2	0	1	1	1094	33	1052	12	1032	8	94	1052	12
LAB1662	036-Z27	0	135164	0	1	2	1	0	1	1	1040	24	1033	9	1029	7	99	1033	9
LAB1662	047-Z35	0	52812	0	1	2	1	0	1	1	988	20	1031	8	1052	8	107	1031	8
LAB1662	007-Z04	1	261679	0	1	2	1	0	1	1	1008	17	1022	8	1028	8	102	1022	8
LAB1662	059-Z45	0	71824	0	1	2	1	0	1	1	1064	19	998	8	968	8	91	998	8
LAB1662	070-Z54	0	63674	0	3	2	3	0	1	1	989	53	996	18	1000	11	101	996	18
LAB1662	020-Z15	0	168212	0	1	2	2	0	1	1	945	25	975	10	989	8	105	975	10
LAB1662	067-Z51	0	41498	0	1	1	2	0	1	1	773	24	778	9	779	10	101	778	9
LAB1662	035-Z26	0	65115	0	1	1	1	0	1	1	812	17	777	7	765	6	94	777	7
LAB1662	023-Z16	0	72848	0	1	1	1	0	1	1	752	20	771	7	778	6	104	771	7
LAB1662	073-Z55	0	29244	0	1	1	2	0	1	1	609	28	639	9	647	8	106	639	9
LAB1662	075-Z57	2	20112	0	2	1	2	0	1	1	655	42	619	11	609	9	93	619	11
LAB1662	018-Z13	1	17381	0	2	1	3	0	3	1	608	39	608	15	608	16	100	608	15
LAB1662	028-Z21	0	51741	0	1	1	2	0	1	1	608	23	593	7	590	6	97	593	7
LAB1662	043-Z31	0	25228	0	1	1	2	0	1	1	584	23	577	7	575	6	98	577	7
LAB1662	058-Z44	1	16844	0	1	1	2	0	2	1	614	22	568	9	557	9	91	568	9
LAB1662	034-Z25	1	7270	0	1	1	2	0	2	1	534	30	550	10	553	10	104	550	10
LAB1662	054-Z40	0	30836	0	1	1	2	0	1	1	598	24	535	7	521	6	87	535	7
LAB1662	066-Z50	0	109927	0	2	1	2	0	1	1	520	37	491	7	485	4	93	491	7
LAB1662	055-Z41	0	36252	0	2	1	2	0	2	1	554	39	468	9	451	7	81	468	9

LAB1662	050-Z38	2	363043	0	2	0	2	0	1	1	299	39	286	5	284	2	95	286	5
LAB1662	010-Z07	1	85708	0	2	0	2	0	1	1	237	45	255	5	257	3	109	255	5
LAB1662	063-Z47	0	89687	0	1	0	1	0	1	1	252	22	215	3	212	2	84	215	3

Data not used due to high discordance

LAB1662	027-Z20	0	17912	0	2	0	2	0	2	1	182	41	99	2	96	2	53			
LAB1662	013-Z08	0	10850	0	3	0	4	0	3	1	266	62	230	8	227	6	85			
LAB1662	060-Z46	1	15678	0	3	0	4	0	2	1	296	67	237	7	231	4	78			
LAB1662	076-Z58	0	27658	0	2	0	3	0	1	1	334	53	266	6	258	3	77			
LAB1662	030-Z23	1	13214	0	9	1	10	0	4	1	556	176	474	36	457	19	82			
LAB1662	005-Z02	0	39854	0	2	1	2	0	1	1	703	37	545	10	508	7	72			
LAB1662	019-Z14	0	7096	0	7	1	11	0	9	1	853	139	664	53	609	50	71			
LAB1662	040-PAD1	1	244201	0	3	1	3	0	1	1	660	69	670	17	674	9	102			
LAB1662	003-PAD1	1	21748	0	1	1	2	0	1	1	826	25	714	9	679	9	82			
LAB1662	080-PAD1	1	25610	0	3	1	3	0	1	1	685	57	690	15	692	9	101			
LAB1662	014-Z09	0	78323	0	1	1	2	0	1	1	690	21	748	8	768	9	111			
LAB1662	064-Z48	1	19025	0	2	1	3	0	2	1	659	33	770	14	809	16	123			
LAB1662	015-Z10	0	92211	0	1	2	2	0	1	1	986	25	1064	11	1103	12	112			
LAB1662	017-Z12	0	16375	0	3	2	4	0	3	1	1213	60	1202	29	1197	30	99			
LAB1662	048-Z36	1	8536	0	1	3	2	0	2	1	1875	17	1494	15	1241	18	66			

Amostra MD-239

Sample	f(206)%	Th/U	6/4 ratio	7/6 ratio	1s(%)	7/5 ratio	1s(%)	6/8 ratio	1s(%)	Rho	7/6 age	1s(Ma)	7/5 age	1s(Ma)	6/8 age	1s(Ma)	Conc (%) 6/8 - 7/6	Conc (%) 6/8 - 7/5	Best age	
008-Z5	0.009	0.301	155201.5	0.126	0.259	6.497	0.711	0.373	0.662	0.916	2046	5	2045	6	2044	12	100	100	2046	5
015-Z10	0.003	0.512	519111.9	0.130	0.210	7.246	0.882	0.404	0.856	0.968	2101	4	2142	8	2185	16	104	102	2101	4
038-Z29	0.034	0.465	65656.7	0.127	0.318	6.560	1.349	0.375	1.311	0.971	2054	6	2054	12	2054	23	100	100	2054	6
023-Z16	0.114	0.477	15322.7	0.066	1.275	1.213	2.012	0.134	1.557	0.767	796	27	807	11	811	12	102	100	807	11
034-Z25	0.023	0.335	88934.2	0.059	0.374	0.760	1.298	0.093	1.243	0.956	569	8	574	6	576	7	101	100	574	6
049-Z37	0.008	0.260	230732.8	0.060	0.267	0.842	0.627	0.102	0.568	0.873	608	6	620	3	623	3	103	101	620	3
053-Z39	0.025	0.207	69878.5	0.059	0.435	0.799	0.739	0.098	0.597	0.761	561	9	596	3	605	3	108	102	596	3
065-Z49	0.014	0.318	123025.1	0.061	0.319	0.861	0.831	0.103	0.767	0.911	631	7	631	4	631	5	100	100	631	4
079-Z61	0.009	0.251	191376.3	0.061	0.218	0.826	0.665	0.099	0.629	0.931	626	5	611	3	607	4	97	99	611	3
COMP_037-Z27	0.188	0.546	9471.8	0.059	1.156	0.725	1.392	0.089	0.774	0.522	579	25	554	6	547	4	95	99	554	6
018-Z13	0.043	0.283	36660.3	0.072	0.542	1.712	0.844	0.172	0.647	0.723	987	11	1013	5	1025	6	104	101	1013	5
039-Z30	0.069	0.298	24573.1	0.080	0.811	2.039	1.126	0.184	0.780	0.661	1202	16	1129	8	1091	8	91	97	1129	8
050-Z38	0.018	0.180	92192.7	0.079	0.593	2.306	0.864	0.211	0.628	0.849	1183	12	1214	6	1232	7	104	101	1214	6
055-Z41	0.022	0.248	76212.7	0.072	0.413	1.663	0.766	0.166	0.645	0.808	1000	8	994	5	992	6	99	100	994	5

COMP_009-Z06	0.104	0.128	16522.4	0.074	0.737	1.655	1.230	0.162	0.985	0.785	1044	15	991	8	968	9	93	98	991	8
COMP_013-Z08	0.274	0.167	6239.6	0.073	1.462	1.647	2.363	0.163	1.857	0.781	1022	30	989	15	974	17	95	98	989	15
COMP_019-Z14	0.086	0.383	19321.0	0.085	0.600	2.569	1.100	0.219	0.923	0.823	1315	12	1292	8	1278	11	97	99	1292	8
COMP_020-Z15	0.145	0.164	11413.5	0.088	0.710	2.668	1.547	0.220	1.374	0.884	1382	14	1320	11	1282	16	93	97	1320	11
COMP_025-Z18	0.068	0.029	24799.7	0.081	0.450	2.192	1.120	0.197	1.026	0.909	1213	9	1178	8	1160	11	96	98	1178	8
COMP_033-Z23	0.060	0.074	28005.5	0.080	0.598	2.124	1.166	0.192	1.001	0.847	1201	12	1157	8	1133	10	94	98	1157	8
COMP_034-Z24	0.039	0.363	33895.9	0.075	0.899	1.635	1.622	0.158	1.349	0.825	1075	18	984	10	943	12	88	96	984	10
COMP_044-Z32	0.056	0.174	29177.7	0.080	0.419	2.027	0.927	0.185	0.827	0.878	1187	8	1124	6	1092	8	92	97	1124	6
COMP_047-Z35	0.031	0.245	54839.1	0.080	0.326	1.992	0.871	0.182	0.808	0.917	1185	6	1113	6	1076	8	91	97	1113	6
004-Z1	0.030	0.304	64044.0	0.095	0.356	3.554	0.807	0.271	0.724	0.879	1532	7	1539	6	1544	10	101	100	1532	7
005-Z2	0.020	0.290	80834.6	0.101	0.314	3.645	0.929	0.262	0.874	0.934	1640	6	1560	7	1501	12	92	96	1640	6
007-Z4	0.025	0.163	64515.5	0.090	0.409	3.251	0.877	0.261	0.776	0.867	1430	8	1469	7	1497	10	105	102	1469	7
028-Z21	0.013	0.181	119308.2	0.086	0.319	2.855	0.647	0.241	0.563	0.828	1334	6	1370	5	1393	7	104	102	1370	5
033-Z24	0.045	0.558	36188.8	0.087	0.436	2.781	1.323	0.232	1.249	0.941	1357	8	1351	10	1346	15	99	100	1351	10
035-Z26	0.068	0.464	24260.9	0.086	0.511	2.793	1.243	0.236	1.133	0.906	1337	10	1354	9	1364	14	102	101	1354	9
037-Z28	0.022	0.323	74347.1	0.088	0.356	2.990	0.903	0.245	0.830	0.908	1393	7	1405	7	1413	11	101	101	1405	7
044-Z32	0.019	0.287	87722.6	0.093	0.364	3.310	0.725	0.259	0.627	0.832	1484	7	1483	6	1483	8	100	100	1483	6
047-Z35	0.019	0.543	85241.7	0.088	0.261	2.874	1.110	0.238	1.079	0.970	1372	5	1375	8	1377	13	100	100	1375	8
048-Z36	0.005	0.161	288000.9	0.091	0.231	3.244	1.028	0.260	1.002	0.973	1439	4	1468	8	1488	13	103	101	1468	8
056-Z42	0.007	0.191	246160.7	0.095	0.360	3.440	0.812	0.263	0.728	0.945	1524	7	1514	6	1507	10	99	100	1524	7
059-Z45	0.006	0.181	293456.5	0.086	0.223	2.860	0.661	0.240	0.622	0.926	1347	4	1371	5	1387	8	103	101	1371	5
060-Z46	0.010	0.442	159526.7	0.095	0.402	3.446	0.739	0.264	0.621	0.906	1519	8	1515	6	1512	8	99	100	1519	8
070-Z54	0.008	0.324	205489.0	0.088	0.516	3.050	1.423	0.251	1.326	0.976	1386	10	1420	11	1443	17	104	102	1420	11
076-Z58	0.022	0.494	74862.7	0.088	0.564	2.833	0.838	0.233	0.619	0.870	1383	11	1364	6	1352	8	98	99	1364	6
078-Z60	0.012	0.499	256935.0	0.092	0.283	3.127	0.672	0.246	0.610	0.882	1472	5	1439	5	1417	8	96	98	1439	5
COMP_005-Z02	0.009	0.120	174166.2	0.095	0.361	3.330	0.819	0.255	0.735	0.880	1525	7	1488	6	1462	10	96	98	1488	6
COMP_008-Z05	0.108	0.176	14900.4	0.091	0.583	2.981	1.078	0.237	0.907	0.826	1454	11	1403	8	1369	11	94	98	1403	8
COMP_010-Z07	0.052	0.035	31773.6	0.091	0.400	2.902	0.996	0.232	0.912	0.907	1442	8	1382	8	1344	11	93	97	1382	8
COMP_029-Z22	0.018	0.063	89360.7	0.087	0.349	2.751	0.748	0.228	0.661	0.859	1368	7	1342	6	1326	8	97	99	1342	6
COMP_035-Z25	0.016	0.181	101684.5	0.094	0.297	3.143	0.750	0.242	0.689	0.902	1511	6	1443	6	1398	9	93	97	1443	6
COMP_049-Z37	0.025	0.020	65788.7	0.090	0.412	2.948	0.800	0.236	0.686	0.830	1435	8	1394	6	1368	8	95	98	1394	6
026-Z19	0.026	0.213	61709.5	0.096	0.559	3.820	1.387	0.289	1.269	0.970	1548	11	1597	11	1635	18	106	102	1548	11
066-Z50	0.008	0.167	200013.1	0.099	0.467	3.798	1.196	0.278	1.101	0.970	1604	9	1592	10	1583	15	99	99	1604	9
067-Z51	0.009	0.475	183003.9	0.112	0.270	4.947	1.477	0.322	1.452	0.983	1826	5	1810	12	1797	23	98	99	1826	5

068-Z52	0.127	0.174	12583.7	0.100	0.659	3.857	1.589	0.281	1.446	0.907	1617	12	1605	13	1595	20	99	99	1617	12
069-Z53	0.010	0.694	158761.5	0.109	0.241	5.002	0.767	0.332	0.728	0.940	1787	4	1820	6	1848	12	103	102	1787	4
COMP_004-Z01	0.028	0.264	60364.3	0.122	0.342	5.408	0.843	0.322	0.770	0.900	1983	6	1886	7	1799	12	91	95	1983	6
COMP_006-Z03	0.034	0.423	45975.0	0.114	0.374	4.867	0.853	0.309	0.767	0.883	1869	7	1797	7	1735	12	93	97	1869	7
COMP_007-Z04	0.024	0.377	65740.6	0.108	0.352	4.484	0.719	0.301	0.627	0.841	1770	6	1728	6	1694	9	96	98	1770	6
COMP_016-Z11	0.030	0.267	52929.3	0.109	0.331	4.408	0.734	0.292	0.655	0.868	1788	6	1714	6	1654	10	93	97	1788	6
COMP_018-Z13	0.033	0.411	83003.2	0.116	0.381	5.195	0.883	0.325	0.797	0.888	1896	7	1852	8	1813	13	96	98	1896	7
COMP_023-Z16	0.028	0.535	57148.0	0.109	0.308	4.475	0.855	0.297	0.798	0.923	1789	6	1726	7	1676	12	94	97	1789	6
COMP_024-Z17	0.035	0.573	55119.1	0.110	0.381	4.507	0.860	0.298	0.772	0.881	1796	7	1732	7	1680	11	94	97	1796	7
COMP_027-Z20	0.041	0.549	37912.0	0.118	0.599	5.157	1.084	0.318	0.904	0.817	1921	11	1846	9	1780	14	93	96	1921	11
COMP_028-Z21	0.012	0.494	169548.7	0.116	0.286	5.043	0.725	0.316	0.666	0.901	1889	5	1827	6	1772	10	94	97	1889	5
COMP_038-Z28	0.015	0.354	129250.1	0.110	0.345	4.636	0.852	0.306	0.779	0.902	1796	6	1756	7	1722	12	96	98	1796	6
COMP_040-Z30	0.026	0.498	59035.1	0.116	0.339	5.133	0.855	0.321	0.785	0.906	1894	6	1842	7	1795	12	95	97	1894	6
COMP_043-Z31	0.017	0.378	93444.6	0.108	0.353	4.415	0.875	0.295	0.800	0.903	1773	6	1715	7	1668	12	94	97	1773	6
014-Z9	0.015	0.501	109399.9	0.111	0.291	5.105	0.789	0.333	0.734	0.917	1821	5	1837	7	1851	12	102	101	1821	5
029-Z22	0.011	0.319	138781.1	0.114	0.380	5.266	0.703	0.335	0.591	0.798	1866	7	1863	6	1861	10	100	100	1866	7
030-Z23	0.000	0.357	3336629.1	0.110	0.316	5.008	0.755	0.331	0.686	0.934	1797	6	1821	6	1841	11	102	101	1797	6
054-Z40	0.011	0.394	87265.1	0.115	0.261	5.382	0.600	0.341	0.541	0.863	1872	5	1882	5	1891	9	101	100	1872	5
074-Z56	0.007	0.568	214240.9	0.112	0.246	5.064	1.009	0.328	0.979	0.968	1834	4	1830	9	1827	16	100	100	1834	4
COMP_036-Z26	0.037	0.416	41123.8	0.109	0.818	5.124	1.563	0.341	1.332	0.846	1782	15	1840	13	1892	22	106	103	1782	15

Amostra MD-176

Identifier	Th/U	$^{206}Pb/^{204}Pb$	1σ%	$^{207}Pb/^{206}Pb$	1σ %	$^{207}Pb/^{235}U$	1σ %	$^{206}Pb/^{238}U$	1σ %	Rho	$^{207}Pb/^{206}Pb$	2σ abs	$^{206}Pb/^{238}U$	2σ abs	$^{207}Pb/^{235}U$	2σ abs	% U-Pb disc[4]
071-Zr53_Analysis1_MIC	0.523	2396	36.07	0.13100	0.58	7.431	1.72	0.4114	1.58	0.92	2111	20	2221	59	2165	31	-5.20
067-ZR46_Analysis4	0.341	31299	17.65	0.13058	1.39	6.784	2.24	0.3767	1.71	0.77	2106	48	2061	60	2084	39	2.13
023-Zr75_Analysis2	0.417	4298	17.97	0.12129	0.51	6.239	0.92	0.3730	0.67	0.73	1975	18	2044	24	2010	16	-3.47
037-Zr22_Analysis3_MIC	0.245	74461	15.71	0.12689	0.32	6.332	0.98	0.3619	0.85	0.87	2055	11	1991	29	2023	17	3.13
022-Zr13_Analysis3_MIC	0.460	120495	17.06	0.11501	0.28	5.728	0.97	0.3612	0.86	0.88	1880	10	1988	29	1936	17	-5.74
033-Zr24_Analysis1_MIC	0.449	2265	11.01	0.11914	0.27	5.680	0.73	0.3457	0.57	0.78	1943	10	1914	19	1928	13	1.51
009-ZR5_Analysis5	0.408	188235	23.28	0.11574	0.34	5.509	1.07	0.3452	0.94	0.88	1891	12	1911	31	1902	18	-1.06
074-ZR51_Analysis4	0.718	96466	22.90	0.11479	0.50	5.244	0.91	0.3313	0.67	0.73	1877	18	1845	21	1860	15	1.70
035-ZR23_Analysis4	2.892	26450	34.49	0.11413	0.86	5.205	1.27	0.3307	0.87	0.68	1866	31	1842	28	1853	22	1.30
047-Zr33_Analysis1_MIC	0.654	1411	65.05	0.11664	0.50	5.223	1.00	0.3247	0.79	0.79	1905	18	1813	25	1856	17	4.86
056-Zr40_Analysis1_MIC	0.400	10119	79.03	0.10753	0.31	4.500	1.00	0.3035	0.88	0.87	1758	11	1708	26	1731	17	2.82
024-Zr15_Analysis3_MIC	0.316	93708	38.77	0.09540	0.43	3.844	1.32	0.2922	1.19	0.90	1536	16	1653	35	1602	21	-7.60

006-ZR2B_Analysis5	0.140	137231	23.21	0.09836	0.38	3.926	0.86	0.2895	0.67	0.78	1593	14	1639	19	1619	14	-2.87
011-Zr06_Analysis3_MIC	0.148	42093	18.19	0.09418	0.48	3.621	1.55	0.2788	1.43	0.92	1512	18	1585	40	1554	25	-4.87
029-Zr79_Analysis2	0.247	64233	56.02	0.09514	0.40	3.642	1.97	0.2776	1.89	0.96	1531	15	1579	53	1559	31	-3.16
009-Zr04_Analysis3_MIC	0.215	63206	15.29	0.09700	0.44	3.713	1.22	0.2776	1.08	0.88	1567	16	1579	30	1574	19	-0.77
004-Zr1_Analysis1_MIC	0.367	331121	14.95	0.10551	0.42	3.995	3.44	0.2746	3.40	0.99	1723	15	1564	94	1633	55	9.25
028-Zr78_Analysis2	0.233	4750	7.20	0.09456	0.49	3.549	0.81	0.2722	0.52	0.65	1519	19	1552	14	1538	13	-2.16
016-Zr70_Analysis2	0.121	29911	18.73	0.09696	1.26	3.600	1.89	0.2693	1.36	0.72	1566	47	1537	37	1550	30	1.88
047-ZR32_Analysis4	0.386	325760	20.95	0.09225	0.51	3.369	0.84	0.2649	0.55	0.66	1473	19	1515	15	1497	13	-2.86
095-Zr59_Analysis3_MIC	0.494	18095	14.34	0.09016	0.81	3.281	2.13	0.2639	1.94	0.91	1429	31	1510	52	1476	33	-5.65
009-ZR6_Analysis4	0.208	31684	16.91	0.09169	1.36	3.330	2.15	0.2634	1.61	0.75	1461	51	1507	43	1488	33	-3.17
054-Zr32_Analysis3_MIC	0.227	17009	16.34	0.09136	0.59	3.296	1.68	0.2617	1.53	0.91	1454	22	1498	41	1480	26	-3.03
016-ZR10_Analysis5	0.485	48926	25.31	0.08743	0.71	3.150	1.43	0.2613	1.19	0.83	1370	27	1497	32	1445	22	-9.24
028-ZR19_Analysis4	0.312	162602	12.85	0.09128	0.61	3.288	1.06	0.2613	0.78	0.74	1452	23	1496	21	1478	16	-3.02
077-Zr57_Analysis1_MIC	0.353	1291	12.70	0.09172	0.28	3.295	0.93	0.2605	0.80	0.86	1462	11	1493	21	1480	14	-2.12
027-Zr77_Analysis2	0.154	9354	34.50	0.08940	1.34	3.145	1.90	0.2551	1.30	0.68	1413	51	1465	34	1444	29	-3.69
041-Zr24_Analysis3_MIC	0.253	14603	11.36	0.09633	0.89	3.373	2.05	0.2540	1.81	0.88	1554	33	1459	47	1498	32	6.13
059-Zr43_Analysis1_MIC	0.345	645	5.71	0.08644	0.46	3.020	1.40	0.2534	1.27	0.91	1348	18	1456	33	1413	21	-8.00
015-ZR9_Analysis5	0.080	27739	16.55	0.09616	0.49	3.358	1.27	0.2532	1.11	0.88	1551	18	1455	29	1495	20	6.18
075-Zr55_Analysis1_MIC	0.476	73184	96.67	0.08749	0.61	3.038	1.43	0.2518	1.24	0.87	1371	23	1448	32	1417	22	-5.58
073-ZR50_Analysis4	0.368	49240	29.21	0.08710	1.10	3.021	1.47	0.2515	0.90	0.61	1363	42	1446	23	1413	22	-6.14
024-Zr76_Analysis2	0.156	5354	39.57	0.08697	0.71	3.015	1.13	0.2515	0.81	0.71	1360	27	1446	21	1412	17	-6.34
009-Zr6_Analysis1_MIC	0.236	513630	6.04	0.09076	0.35	3.125	0.90	0.2497	0.74	0.82	1442	13	1437	19	1439	14	0.33
065-ZR44_Analysis4	0.464	130194	19.84	0.09101	0.52	3.133	0.88	0.2496	0.60	0.68	1447	20	1437	15	1441	13	0.72
059-Zr35_Analysis3_MIC	0.620	4172	15.45	0.08812	1.28	3.014	3.19	0.2481	2.90	0.91	1385	49	1429	74	1411	48	-3.13
011-Zr67_Analysis2	0.748	34076	16.48	0.08611	1.04	2.940	1.57	0.2476	1.12	0.71	1341	40	1426	29	1392	24	-6.39
078-ZR55_Analysis4	0.147	122508	19.17	0.08919	0.42	3.039	0.97	0.2471	0.80	0.82	1408	16	1424	20	1417	15	-1.09
023-Zr14_Analysis3_MIC	0.408	99835	13.87	0.08727	0.32	2.972	1.20	0.2470	1.09	0.91	1366	12	1423	28	1401	18	-4.14
061-Zr37_Analysis3_MIC	0.357	18034	10.70	0.09021	0.71	3.070	1.69	0.2468	1.49	0.88	1430	27	1422	38	1425	26	0.57
066-ZR45_Analysis4	0.349	74623	17.69	0.08990	0.75	3.052	1.25	0.2462	0.93	0.74	1423	29	1419	24	1421	19	0.32
038-Zr29_Analysis1_MIC	0.480	557	4.09	0.09152	0.41	3.107	0.99	0.2462	0.82	0.83	1457	16	1419	21	1434	15	2.65
026-ZR17_Analysis4	0.389	231880	30.10	0.09018	0.75	3.059	1.13	0.2460	0.77	0.68	1429	28	1418	20	1423	17	0.80
086-Zr54_Analysis3_MIC	0.290	5187	14.35	0.08932	1.28	3.030	3.12	0.2460	2.82	0.90	1411	48	1418	72	1415	47	-0.48
018-ZR12_Analysis4	0.249	79310	24.85	0.08898	0.47	3.011	1.00	0.2454	0.80	0.80	1404	18	1415	20	1410	15	-0.80
017-Zr71_Analysis2	0.224	26414	17.50	0.09198	1.34	3.111	2.08	0.2453	1.55	0.75	1467	50	1414	39	1435	32	3.60
012-Zr07_Analysis3_MIC	0.337	48706	11.04	0.08649	0.46	2.924	1.64	0.2452	1.53	0.93	1349	18	1414	39	1388	25	-4.78
016-Zr09_Analysis3_MIC	0.593	44236	19.49	0.08609	0.38	2.910	1.19	0.2452	1.06	0.89	1340	15	1414	27	1385	18	-5.47
043-Zr26_Analysis3_MIC	0.445	15007	17.67	0.08770	0.74	2.960	1.75	0.2448	1.55	0.88	1376	28	1412	39	1398	26	-2.61
013-Zr8_Analysis1_MIC	0.806	743780	5.08	0.08918	0.28	3.008	1.08	0.2446	0.98	0.90	1408	11	1411	25	1410	16	-0.20
017-Zr10_Analysis3_MIC	0.178	29772	15.29	0.08756	0.48	2.952	1.18	0.2445	1.02	0.86	1373	18	1410	26	1395	18	-2.70
064-ZR43_Analysis4	0.328	177931	37.07	0.08944	0.49	3.011	0.92	0.2442	0.69	0.75	1414	19	1408	18	1410	14	0.37
008-ZR4_Analysis5	0.158	115983	16.30	0.09126	0.33	3.072	0.93	0.2442	0.79	0.84	1452	13	1408	20	1426	14	3.01
016-ZR10B_Analysis4	0.423	3640	15.12	0.08665	0.56	2.913	1.09	0.2438	0.86	0.79	1353	21	1406	22	1385	16	-3.96
044-ZR29_Analysis4	0.415	30845	21.61	0.09054	1.06	3.039	1.65	0.2435	1.20	0.73	1437	40	1405	30	1418	25	2.25
036-Zr27_Analysis1_MIC	0.317	1409	6.40	0.09045	0.31	3.034	0.74	0.2433	0.57	0.76	1435	12	1404	14	1416	11	2.18
045-ZR30_Analysis4	0.137	70360	39.26	0.09054	1.14	3.035	1.76	0.2431	1.30	0.74	1437	43	1403	33	1416	27	2.37
070-ZR49_Analysis4	0.509	169101	24.36	0.08921	0.51	2.990	0.87	0.2430	0.61	0.69	1409	19	1402	15	1405	13	0.46

035-Zr20_Analysis3_MIC	0.326	13401	21.19	0.08907	0.65	2.984	1.68	0.2430	1.51	0.90	1406	25	1402	38	1403	25	0.25
028-ZR20_Analysis5	0.322	14765	31.28	0.09061	1.83	3.029	2.20	0.2424	1.17	0.53	1438	69	1399	29	1415	33	2.73
049-ZR34_Analysis4	0.160	111828	17.48	0.08904	0.72	2.957	1.06	0.2409	0.69	0.65	1405	27	1391	17	1397	16	0.97
071-Zr43_Analysis3_MIC	0.224	21399	18.42	0.09013	0.94	2.977	1.88	0.2396	1.58	0.84	1428	36	1384	39	1402	28	3.07
089-Zr55_Analysis3_MIC	0.158	10341	19.20	0.08607	0.84	2.835	1.56	0.2389	1.26	0.81	1340	32	1381	31	1365	23	-3.07
053-ZR36_Analysis4	0.162	103788	25.28	0.08695	0.62	2.862	1.31	0.2387	1.09	0.84	1359	24	1380	27	1372	20	-1.52
081-Zr61_Analysis1_MIC	0.631	2994	37.69	0.09224	0.67	3.030	1.35	0.2382	1.11	0.82	1472	25	1377	27	1415	20	6.45
042-Zr25_Analysis3_MIC	0.450	37333	14.52	0.08833	0.58	2.901	1.13	0.2382	0.90	0.79	1390	22	1377	22	1382	17	0.88
046-ZR31_Analysis4	0.358	51279	48.31	0.08606	0.42	2.825	0.76	0.2381	0.51	0.67	1340	16	1377	13	1362	11	-2.77
036-ZR24_Analysis4	0.299	202312	18.60	0.08766	0.44	2.877	0.92	0.2380	0.72	0.78	1375	17	1376	18	1376	14	-0.09
060-Zr36_Analysis3_MIC	0.501	137049	91.31	0.08820	0.74	2.893	2.01	0.2379	1.83	0.91	1387	28	1376	45	1380	30	0.81
013-ZR8_Analysis4	1.067	19786	63.64	0.08678	0.62	2.843	1.04	0.2376	0.74	0.72	1356	24	1374	18	1367	15	-1.37
078-Zr58_Analysis1_MIC	0.675	1140	10.41	0.08663	0.49	2.838	1.03	0.2375	0.83	0.81	1352	19	1374	21	1366	15	-1.59
028-Zr21_Analysis1_MIC	0.280	2373	31.47	0.09213	0.70	3.014	1.99	0.2372	1.82	0.92	1470	27	1372	45	1411	30	6.64
015-ZR10N_Analysis4	0.501	179233	15.39	0.08668	0.40	2.835	0.92	0.2372	0.74	0.81	1353	15	1372	18	1365	14	-1.39
048-Zr29_Analysis3_MIC	0.280	7732	14.82	0.08794	1.13	2.875	2.08	0.2371	1.70	0.82	1381	43	1372	42	1375	31	0.69
010-Zr66_Analysis2	0.516	68681	39.20	0.08746	1.05	2.858	1.55	0.2370	1.07	0.69	1371	40	1371	26	1371	23	-0.02
019-ZR13_Analysis4	0.183	392908	27.84	0.08665	0.45	2.830	0.80	0.2368	0.55	0.69	1353	17	1370	14	1363	12	-1.29
079-ZR56_Analysis4	0.427	67274	17.76	0.08798	0.66	2.872	1.27	0.2367	1.02	0.80	1382	25	1369	25	1374	19	0.91
069-ZR48_Analysis4	0.564	79179	22.71	0.08549	1.20	2.788	1.59	0.2365	0.98	0.61	1327	46	1369	24	1352	24	-3.16
032-Zr19_Analysis3_MIC	0.289	20664	16.33	0.08853	0.78	2.887	1.37	0.2365	1.06	0.78	1394	30	1368	26	1379	21	1.83
015-Zr69_Analysis2	0.556	26164	20.01	0.08832	1.20	2.876	1.95	0.2362	1.49	0.77	1389	46	1367	37	1376	29	1.63
051-Zr37_Analysis1_MIC	0.254	519	4.69	0.08908	0.46	2.898	1.14	0.2359	0.98	0.86	1406	18	1365	24	1381	17	2.89
020-ZR14_Analysis4	0.329	99056	15.19	0.08777	0.66	2.848	1.00	0.2353	0.66	0.66	1377	25	1362	16	1368	15	1.09
070-Zr52_Analysis1_MIC	0.139	664	8.00	0.08722	0.42	2.830	1.16	0.2353	1.01	0.87	1365	16	1362	25	1364	17	0.23
018-Zr13_Analysis1_MIC	0.141	25994	54.46	0.08709	0.31	2.823	0.83	0.2351	0.68	0.81	1362	12	1361	17	1362	12	0.10
006-Zr03_Analysis3_MIC	0.220	10602	16.15	0.08818	0.78	2.856	2.08	0.2349	1.89	0.91	1386	30	1360	46	1370	31	1.89
006-ZR3_Analysis4	0.491	137851	18.36	0.08713	0.43	2.820	0.88	0.2347	0.66	0.76	1363	17	1359	16	1361	13	0.31
079-Zr49_Analysis3_MIC	0.771	4810	17.24	0.08821	1.09	2.850	2.59	0.2343	2.32	0.90	1387	42	1357	57	1369	39	2.15
031-Zr18_Analysis3_MIC	0.282	56851	15.36	0.08730	0.43	2.819	1.11	0.2342	0.96	0.86	1367	17	1356	23	1361	17	0.78
017-ZR11_Analysis5	0.180	64298	14.91	0.08676	0.58	2.795	1.07	0.2337	0.82	0.76	1355	22	1354	20	1354	16	0.12
010-ZR6_Analysis5	0.193	29136	27.85	0.08946	0.54	2.880	1.14	0.2335	0.93	0.82	1414	21	1353	23	1377	17	4.34
022-Zr74_Analysis2	0.918	11958	21.65	0.09022	2.30	2.903	3.44	0.2334	2.52	0.73	1430	87	1352	61	1383	51	5.46
049-Zr30_Analysis3_MIC	0.243	382123	84.66	0.09010	0.38	2.878	1.04	0.2316	0.90	0.86	1428	14	1343	22	1376	16	5.93
039-ZR27_Analysis4	0.436	102682	12.17	0.08661	0.86	2.760	1.46	0.2311	1.12	0.77	1352	33	1340	27	1345	22	0.88
018-Zr11_Analysis3_MIC	0.395	48081	15.66	0.08420	0.43	2.671	1.67	0.2300	1.57	0.94	1297	17	1335	38	1320	24	-2.88
030-Zr17_Analysis3_MIC	0.702	42919	14.92	0.08537	0.52	2.704	1.29	0.2297	1.12	0.87	1324	20	1333	27	1330	19	-0.69
055-Zr39_Analysis1_MIC	0.266	548	5.14	0.09108	0.49	2.883	1.13	0.2296	0.95	0.84	1448	19	1332	23	1378	17	8.01
076-Zr56_Analysis1_MIC	0.210	1347	35.80	0.08240	0.66	2.605	1.17	0.2292	0.89	0.76	1255	26	1331	21	1302	17	-6.01
054-ZR37_Analysis4	1.026	177490	14.04	0.08602	0.69	2.710	1.15	0.2285	0.84	0.73	1339	27	1326	20	1331	17	0.92
020-ZR14_Analysis5	0.417	110930	16.20	0.08651	0.96	2.718	1.37	0.2278	0.91	0.66	1350	37	1323	22	1333	20	1.96
014-Zr9_Analysis1_MIC	0.763	1026	5.24	0.08700	0.33	2.732	0.74	0.2277	0.55	0.74	1360	13	1322	13	1337	11	2.79
047-Zr28_Analysis3_MIC	0.541	9098	22.05	0.08988	1.02	2.816	2.76	0.2272	2.54	0.92	1423	39	1320	60	1360	41	7.24
050-Zr36_Analysis1_MIC	0.235	1108	26.69	0.08331	0.70	2.608	1.31	0.2270	1.04	0.79	1276	27	1319	25	1303	19	-3.31
039-Zr30_Analysis1_MIC	0.154	129743	21.62	0.08686	0.27	2.704	0.82	0.2257	0.68	0.83	1357	10	1312	16	1329	12	3.33
017-Zr12_Analysis1_MIC	0.332	4078	36.70	0.08665	0.29	2.674	0.79	0.2238	0.64	0.80	1353	11	1302	15	1321	12	3.77

056-Zr34_Analysis3_MIC	0.217	3601	20.16	0.08398	1.42	2.588	3.23	0.2235	2.87	0.89	1292	55	1300	67	1297	47	-0.64
023-ZR15_Analysis5	0.199	32546	34.53	0.08729	0.98	2.667	1.45	0.2216	1.01	0.70	1367	37	1290	24	1319	21	5.61
068-Zr50_Analysis1_MIC	0.260	5713	18.71	0.08991	0.26	2.737	0.99	0.2207	0.88	0.89	1424	10	1286	20	1338	15	9.69
074-Zr46_Analysis3_MIC	0.170	4568	15.16	0.08914	1.30	2.711	3.39	0.2206	3.11	0.92	1407	49	1285	72	1332	50	8.67
080-ZR57N_Analysis4	0.154	122877	16.55	0.08464	0.48	2.574	0.94	0.2206	0.72	0.76	1307	19	1285	17	1293	14	1.73
007-ZR3_Analysis5	0.292	32661	14.16	0.08264	0.57	2.510	1.17	0.2203	0.95	0.81	1261	22	1283	22	1275	17	-1.79
005-Zr02_Analysis3_MIC	0.676	25928	13.98	0.08504	0.49	2.583	1.14	0.2203	0.96	0.84	1316	19	1283	22	1296	17	2.51
044-Zr27_Analysis3_MIC	0.325	14305	15.33	0.08537	0.65	2.562	1.43	0.2176	1.21	0.85	1324	25	1269	28	1290	21	4.12
065-Zr47_Analysis1_MIC	0.134	650	4.60	0.08394	0.49	2.508	0.97	0.2167	0.74	0.77	1291	19	1264	17	1274	14	2.06
092-Zr58_Analysis3_MIC	0.380	16305	21.70	0.08047	0.91	2.360	1.85	0.2127	1.57	0.85	1209	35	1243	35	1231	26	-2.85
027-Zr20_Analysis1_MIC	0.386	1231	6.11	0.08658	0.33	2.524	1.52	0.2114	1.43	0.95	1351	13	1236	32	1279	22	8.50
090-Zr56_Analysis3_MIC	0.199	9129	17.88	0.07922	1.05	2.299	2.06	0.2105	1.73	0.84	1178	41	1231	39	1212	29	-4.56
072-Zr54_Analysis1_MIC	0.317	4712	20.84	0.08124	1.07	2.353	1.87	0.2100	1.49	0.80	1227	42	1229	33	1228	26	-0.13
027-ZR18_Analysis4	0.155	60382	25.57	0.08066	1.11	2.331	1.70	0.2096	1.23	0.72	1213	44	1226	27	1222	24	-1.09
059-ZR42N_Analysis4	0.300	148753	22.94	0.08088	0.54	2.332	0.88	0.2091	0.59	0.67	1219	21	1224	13	1222	12	-0.45
015-Zr08_Analysis3_MIC	0.325	14924	15.32	0.08020	0.69	2.311	1.92	0.2090	1.75	0.91	1202	27	1223	39	1216	27	-1.79
062-Zr46_Analysis1_MIC	0.728	566	12.32	0.08626	0.63	2.480	1.31	0.2085	1.09	0.83	1344	24	1221	24	1266	19	9.19
036-Zr21_Analysis3_MIC	0.369	13847	12.64	0.08493	0.58	2.438	1.59	0.2082	1.43	0.90	1314	23	1219	32	1254	23	7.20
021-Zr12_Analysis3_MIC	0.297	25005	26.06	0.07910	0.99	2.238	2.15	0.2052	1.87	0.87	1175	39	1203	41	1193	30	-2.41
017-ZR11_Analysis4	0.194	18503	18.08	0.08387	1.62	2.362	2.64	0.2043	2.06	0.78	1289	62	1198	45	1231	37	7.07
038-ZR26_Analysis4	0.336	35379	22.99	0.08141	0.78	2.285	1.28	0.2036	0.95	0.74	1231	31	1195	21	1208	18	2.98
005-Zr63_Analysis2	0.207	76343	59.27	0.08052	1.25	2.241	1.81	0.2018	1.25	0.69	1210	49	1185	27	1194	25	2.03
068-ZR47_Analysis4	0.037	368974	14.32	0.07822	0.40	2.176	0.83	0.2018	0.62	0.75	1152	16	1185	13	1173	11	-2.80
066-Zr48_Analysis1_MIC	0.098	242744	15.86	0.08203	0.27	2.268	1.29	0.2006	1.20	0.93	1246	11	1178	26	1203	18	5.45
048-ZR33_Analysis4	0.354	29935	19.24	0.07842	1.27	2.148	1.96	0.1987	1.45	0.74	1157	50	1168	31	1164	27	-0.93
045-Zr31_Analysis1_MIC	0.325	712	3.38	0.07780	0.40	2.125	0.88	0.1981	0.68	0.78	1142	16	1165	15	1157	12	-2.03
050-ZR35_Analysis4	0.265	61080	15.02	0.07819	0.95	2.127	1.52	0.1973	1.13	0.74	1152	37	1161	24	1158	21	-0.78
062-Zr38_Analysis3_MIC	0.219	9520	13.98	0.08120	0.99	2.206	2.03	0.1970	1.74	0.86	1226	38	1159	37	1183	28	5.47
067-Zr49_Analysis1_MIC	0.271	646	3.41	0.08123	0.36	2.196	0.84	0.1961	0.67	0.79	1227	14	1154	14	1180	12	5.94
055-Zr33_Analysis3_MIC	0.118	32954	18.96	0.07971	0.54	2.144	1.20	0.1950	1.00	0.84	1190	21	1149	21	1163	17	3.46
012-Zr68_Analysis2	0.108	23872	28.26	0.08315	1.72	2.235	2.77	0.1949	2.14	0.77	1273	66	1148	45	1192	38	9.81
073-Zr45_Analysis3_MIC	0.303	41782	13.51	0.07942	0.58	2.132	1.28	0.1947	1.08	0.84	1183	23	1147	23	1159	18	3.02
021-Zr73_Analysis2	0.278	20160	17.11	0.07634	2.37	2.026	3.26	0.1925	2.20	0.68	1104	93	1135	46	1124	44	-2.82
004-Zr62_Analysis2	0.208	27408	24.51	0.07578	2.70	2.010	3.52	0.1924	2.23	0.63	1089	106	1134	46	1119	47	-4.14
033-ZR21_Analysis4	0.141	102862	19.64	0.07838	0.63	2.071	1.23	0.1916	0.99	0.80	1157	25	1130	21	1139	17	2.30
075-ZR52_Analysis4	0.249	19489	14.80	0.07773	2.15	2.023	3.07	0.1888	2.16	0.70	1140	84	1115	44	1123	41	2.23
080-Zr50_Analysis3_MIC	0.369	2563	16.87	0.07823	1.72	2.026	3.73	0.1879	3.28	0.88	1153	68	1110	67	1124	50	3.72
004-ZR1_Analysis5	0.264	61419	13.38	0.07498	0.62	1.864	1.07	0.1803	0.79	0.74	1068	25	1069	15	1068	14	-0.05
014-ZR9_Analysis4	0.253	14234	33.10	0.07538	0.67	1.872	1.23	0.1801	0.96	0.78	1079	27	1068	19	1071	16	1.02
029-Zr16_Analysis3_MIC	0.089	51116	13.40	0.07368	0.48	1.807	1.38	0.1779	1.24	0.90	1033	19	1056	24	1048	18	-2.22
037-Zr28_Analysis1_MIC	0.327	852	4.03	0.07753	0.44	1.888	0.96	0.1766	0.78	0.81	1135	17	1048	15	1077	13	7.64
013-ZR7_Analysis5	0.323	45341	21.01	0.07499	0.54	1.823	1.37	0.1763	1.20	0.88	1068	22	1047	23	1054	18	1.99
005-ZR2_Analysis4	0.249	310423	79.82	0.07313	0.58	1.736	1.04	0.1721	0.78	0.75	1018	23	1024	15	1022	13	-0.61
056-ZR39_Analysis4	0.373	44026	12.48	0.07262	1.26	1.714	1.84	0.1712	1.28	0.70	1003	51	1019	24	1014	23	-1.55
010-Zr7_Analysis1_MIC	0.253	699	3.30	0.07477	0.44	1.741	0.83	0.1689	0.60	0.72	1062	18	1006	11	1024	11	5.29
058-Zr42_Analysis1_MIC	0.691	5308	16.90	0.07535	1.09	1.722	2.12	0.1658	1.79	0.84	1078	43	989	33	1017	27	8.28

037-ZR25_Analysis4	0.227	71924	12.52	0.07097	0.79	1.591	1.25	0.1626	0.90	0.72	957	32	971	16	967	16	-1.55
004-ZR1_Analysis4	0.248	612278	26.41	0.06980	0.32	1.530	0.90	0.1590	0.76	0.84	922	13	951	13	943	11	-3.13
076-ZR53_Analysis4	0.284	35228	17.83	0.07266	1.27	1.570	1.88	0.1567	1.33	0.71	1005	51	939	23	959	23	6.56
004-Zr01_Analysis3_MIC	0.326	14661	21.90	0.07286	0.75	1.569	1.27	0.1561	0.95	0.75	1010	30	935	17	958	16	7.40
078-Zr48_Analysis3_MIC	0.204	3699	18.05	0.07300	1.46	1.503	2.69	0.1493	2.22	0.83	1014	59	897	37	932	33	11.52
068-Zr42_Analysis3_MIC	0.361	5556	9.80	0.06623	1.88	1.115	2.83	0.1221	2.08	0.74	814	78	742	29	760	30	8.73
052-Zr38_Analysis1_MIC	0.458	670	6.53	0.06153	0.59	0.864	1.08	0.1018	0.83	0.77	658	25	625	10	632	10	5.00
026-ZR18_Analysis5	0.727	14308	40.85	0.06172	1.73	0.861	2.36	0.1012	1.56	0.66	664	73	621	18	631	22	6.48
048-Zr34_Analysis1_MIC	0.719	1343	58.32	0.06150	0.70	0.827	1.08	0.0976	0.73	0.68	657	30	600	8	612	10	8.61
091-Zr57_Analysis3_MIC	0.184	5468	13.72	0.06076	1.38	0.816	1.94	0.0974	1.32	0.68	631	59	599	15	606	18	5.02
077-ZR54_Analysis4	0.097	191110	21.55	0.05900	0.59	0.754	0.99	0.0927	0.70	0.71	567	26	572	8	571	9	-0.77
083-Zr51_Analysis3_MIC	0.534	2841	11.65	0.06102	2.34	0.774	4.32	0.0920	3.61	0.84	640	99	568	39	582	38	11.29
069-Zr51_Analysis1_MIC	0.702	3988	24.52	0.06317	1.21	0.794	1.61	0.0911	0.99	0.62	714	51	562	11	593	14	21.27
084-Zr52_Analysis3_MIC	0.964	5088	48.97	0.06112	1.97	0.748	3.09	0.0887	2.35	0.76	644	83	548	25	567	27	14.84
018-ZR12_Analysis5	0.487	63128	19.30	0.05789	0.98	0.680	2.56	0.0852	2.34	0.91	526	43	527	24	527	21	-0.24
096-Zr60_Analysis3_MIC	0.712	7506	11.72	0.05982	1.23	0.698	1.79	0.0847	1.24	0.70	597	53	524	13	538	15	12.24
008-ZR5_Analysis4	0.215	218954	17.43	0.05720	0.39	0.634	0.82	0.0804	0.62	0.76	499	17	499	6	499	6	0.17
097-Zr61_Analysis3_MIC	0.305	7513	12.87	0.05150	1.23	0.280	1.63	0.0394	0.99	0.61	263	56	249	5	251	7	5.32
025-ZR16_Analysis4	0.478	16573	22.85	0.05048	3.50	0.147	5.00	0.0211	3.55	0.71	217	158	135	9	139	13	37.89

Dados de datação U-Pb da Bacia do Acre

Acre	Sample	Lab Name	Methodology	Formation	Age	Longitude (W)	Latitude (S)
2	ACRE 49	LAB3841Final	LA-ICP-MS	Moa	Aptian-Turonian* Late Cretaceous ***	73°41'37.67"	7°27'29.60"
5	ACRE 39	LAB4018	LA-ICP-MS	Rio Azul	Turonian-Campanian*	73°42'11.73"	7°28'16.54"
7	ACRE 33	LAB4013 LABXR4014	LA-ICP-MS Element	Rio Azul	Cenomanian** Turonian-Campanian*	73°42'6.12"	7°29'5.41"
10	ACRE 29	LAB4015	LA-ICP-MS	Divisor	Campanian-Maastrichtian*	73°41'59.58"	7°29'36.30"
11	ACRE 27A	LAB4014 LABXR4013	LA-ICP-MS Element	Divisor	Campanian-Maastrichtian*	73°41'57.82"	7°29'50.64"
12	ACRE 27B	LABXR021_I_II	Element	Divisor	Campanian-Maastrichtian*	73°41'57.82"	7°29'50.64"

19	**ACRE 15**	**LABXR-4012 LAB-4012**	**Element LA-ICP-MS**	Divisor	Campanian-Maastrichtian*	73°42'7.38"	7°30'20.17"

Acre basin: Ages are from Cunha (2007) (*) and Haag (2019) (**) Brito et al. (1994) (***)

Amostra Acre 15

			Ratios									**Rho**	**Ages (Ma)**						**% conc[1]**	**Best age**	**2s**
Sample	Spot number	Th/U	206Pb/204Pb	1s	238U/206Pb	1s	207Pb/206Pb	1s	207Pb/235U	1s	206Pb/238U	1s		207Pb/206Pb	2s	206Pb/238U	2s	207Pb/235U	2s			
				(%)		(%)		(%)		(%)		(%)			(abs)		(abs)		(abs)			(abs)
LAB4012																						
ACRE 015	LAB4012	0.5	0.000091	174.1	3.02	0.7	0.11733	0.38	5.3566	0.8	0.33122	0.7	0.9	1915	14	1844	23	1878	13	96.3	1915	14
ACRE 015	LAB4012	1.4	0.000402	98.7	2.86	0.7	0.11680	0.67	5.5988	0.9	0.34983	0.7	0.4	1907	24	1934	23	1916	15	101.4	1907	24
ACRE 015	LAB4012	1.5	0.000425	84.1	2.88	0.8	0.11667	0.44	5.6016	0.8	0.34757	0.8	0.9	1905	16	1923	26	1916	14	101.0	1905	16
ACRE 015	LAB4012	2.1	0.034912	93.0	2.98	0.7	0.11637	0.39	5.3864	0.7	0.33604	0.7	0.8	1900	14	1868	24	1883	12	98.3	1900	14
ACRE 015	LAB4012	1.2	0.000158	285.0	2.97	0.8	0.11573	0.45	5.3727	0.9	0.33662	0.8	0.9	1890	16	1870	27	1880	15	98.9	1890	16
ACRE 015	LAB4012	1.5	0.010623	93.0	2.99	0.7	0.11465	0.50	5.3092	0.8	0.33451	0.7	0.6	1873	18	1860	22	1870	13	99.3	1873	18
ACRE 015	LAB4012	1.4	0.000388	70.7	3.00	0.7	0.11465	0.47	5.2717	0.7	0.33333	0.7	0.6	1873	17	1854	23	1864	12	99.0	1873	17
ACRE 015	LAB4012	1.5	0.000675	52.2	3.03	0.8	0.11380	0.69	5.1752	1.0	0.32970	0.8	0.7	1859	25	1837	24	1848	17	98.8	1859	25
ACRE 015	LAB4012	1.2	0.000102	25.9	3.02	0.7	0.11290	1.04	5.1799	1.3	0.33119	0.7	0.7	1845	38	1844	23	1849	22	100.0	1845	38
ACRE 015	LAB4012	0.9	0.000196	238.5	3.11	0.8	0.11215	0.78	4.9612	0.8	0.32179	0.8	0.2	1833	28	1798	26	1813	14	98.1	1833	28
ACRE 015	LAB4012	1.1	0.000239	122.0	3.05	1.1	0.11198	0.62	5.0384	1.2	0.32828	1.1	0.9	1831	22	1830	36	1826	20	100.0	1831	22
ACRE 015	LAB4012	1.4	0.001113	50.6	3.25	0.8	0.11158	0.37	4.7275	0.8	0.30806	0.8	1.0	1824	13	1731	24	1772	13	94.9	1824	13
ACRE 015	LAB4012	1.8	0.001088	123.5	3.07	0.8	0.11140	0.48	4.9901	0.7	0.32597	0.8	1.0	1821	17	1819	24	1818	13	99.9	1821	17
ACRE 015	LAB4012	1.2	0.000133	51.3	3.03	0.7	0.11139	0.52	5.0511	0.8	0.32974	0.7	0.6	1821	19	1837	24	1828	13	100.9	1821	19
ACRE 015	LAB4012	1.6	0.001964	104.5	3.09	0.8	0.11140	0.62	4.9338	0.7	0.32321	0.8	0.6	1821	22	1805	24	1808	12	99.1	1821	22
ACRE 015	LAB4012	1.2	0.000169	117.2	3.19	0.7	0.11110	0.58	4.8099	0.8	0.31370	0.7	0.6	1817	21	1759	20	1787	14	96.8	1817	21
ACRE 015	LAB4012	1.9	0.000649	41.0	3.15	0.7	0.11026	0.41	4.8285	0.7	0.31724	0.7	0.7	1803	15	1776	21	1790	11	98.5	1803	15
ACRE 015	LAB4012	1.2	0.000049	695.2	3.10	0.7	0.11018	0.53	4.9012	0.7	0.32283	0.7	0.1	1801	19	1804	22	1802	11	100.1	1801	19
ACRE 015	LAB4012	1.4	0.000270	93.3	3.07	0.7	0.11000	0.40	4.9448	0.7	0.32537	0.7	0.7	1798	15	1816	21	1810	12	101.0	1798	15

ACRE 015	LAB4012	1.7	0.000277	134.8	3.15	0.7	0.10943	0.51	4.7778	0.6	0.31713	0.7	0.4	1789	19	1776	22	1781	11	99.3	1789	19
ACRE 015	LAB4012	1.5	0.000099	233.7	3.20	0.7	0.10897	0.53	4.7079	0.7	0.31203	0.7	0.1	1781	20	1751	20	1769	12	98.3	1781	20
ACRE 015	LAB4012	1.2	0.001805	109.5	2.96	1.0	0.10671	0.69	4.9942	0.8	0.33757	1.0	0.6	1743	25	1875	32	1818	13	107.6	1743	25
ACRE 015	LAB4012	0.7	0.000454	52.6	3.54	0.7	0.09911	0.54	3.8576	0.9	0.28272	0.7	0.8	1606	20	1605	20	1605	15	99.9	1606	20
ACRE 015	LAB4012	1.1	0.000518	143.9	3.61	1.1	0.09766	0.53	3.7058	1.0	0.27719	1.0	0.9	1579	20	1577	29	1572	16	99.9	1579	20
ACRE 015	LAB4012	0.9	0.000204	93.4	3.58	1.1	0.09720	0.40	3.7539	1.2	0.27958	1.0	0.9	1570	15	1589	30	1582	19	101.2	1570	15
ACRE 015	LAB4012	1.4	0.000130	29.3	3.83	0.6	0.09590	0.47	3.4438	0.8	0.26073	0.8	0.8	1545	18	1494	20	1514	12	96.7	1494	20
ACRE 015	LAB4012	2.3	0.000046	304.6	3.74	0.8	0.09522	1.20	3.5025	1.0	0.26753	0.8	0.5	1531	45	1528	23	1528	16	99.8	1528	23
ACRE 015	LAB4012	2.2	0.000101	15.7	3.78	0.8	0.09435	0.70	3.4598	0.9	0.26494	0.9	1.0	1514	27	1515	23	1518	14	100.1	1515	23
ACRE 015	LAB4012	1.7	0.000016	821.9	3.83	0.8	0.09358	1.45	3.3599	1.3	0.26118	0.8	0.4	1497	54	1496	22	1495	20	99.9	1496	22
ACRE 015	LAB4012	1.2	0.000546	105.1	3.91	0.7	0.09294	0.39	3.2617	0.7	0.25575	0.7	0.7	1486	15	1468	18	1472	10	98.8	1468	18
ACRE 015	LAB4012	2.1	0.000975	103.5	3.92	0.8	0.09274	0.74	3.2513	0.7	0.25500	0.8	0.3	1481	28	1464	21	1469	11	98.8	1464	21
ACRE 015	LAB4012	0.7	0.000163	79.6	4.63	0.8	0.08196	0.48	2.4409	0.8	0.21626	0.8	0.8	1243	19	1262	18	1255	12	101.5	1262	18
ACRE 015	LAB4012	1.0	0.001207	43.5	4.95	0.7	0.08194	0.47	2.2920	0.7	0.20212	0.7	0.4	1243	18	1187	14	1210	10	95.5	1187	14
ACRE 015	LAB4012	0.9	0.005052	82.4	4.78	0.6	0.08039	0.50	2.3061	0.7	0.20901	0.6	0.4	1205	20	1224	14	1214	10	101.5	1224	14
ACRE 015	LAB4012	0.8	0.000559	128.3	4.99	0.6	0.07909	0.41	2.1865	0.7	0.20044	0.6	0.4	1173	16	1178	14	1177	9	100.4	1178	14

Data not used due to high discordance

ACRE 015	LAB4012	1.6	0.005900	98.1	3.33	2.2	0.11839	0.89	4.8911	1.7	0.30138	2.1	1.0	1931	31	1698	64	1800	28	87.9		
ACRE 015	LAB4012	1.8	0.000298	36.3	3.62	2.0	0.11222	1.20	4.2534	3.1	0.27680	2.0	1.0	1835	44	1575	56	1684	51	85.9		
ACRE 015	LAB4012	1.4	0.000198	43.5	3.85	1.8	0.11092	0.61	3.9673	1.9	0.26040	1.9	1.0	1813	22	1491	50	1626	31	82.2		
ACRE 015	LAB4012	1.6	0.000122	12.2	4.72	0.9	0.09440	0.53	2.7618	1.1	0.21190	0.9	0.9	1515	20	1239	21	1345	16	81.8		
ACRE 015	LAB4012	1.3	0.000178	9.6	4.01	1.6	0.10978	0.65	3.7732	1.6	0.24975	1.6	0.9	1795	24	1437	42	1586	26	80.1		
ACRE 015	LAB4012	1.3	0.000016	15.2	3.84	0.8	0.12819	2.93	4.6258	3.1	0.26070	0.8	0.3	2069	102	1493	21	1753	50	72.2		
ACRE 015	LAB4012	1.1	0.000023	8.3	4.48	2.9	0.11564	2.10	3.5920	1.5	0.22442	2.7	0.6	1886	78	1305	64	1547	25	69.2		
ACRE 015	LAB4012	1.2	0.000024	7.7	4.59	1.4	0.11791	0.98	3.5550	1.6	0.21797	1.4	0.8	1923	35	1271	33	1539	26	66.1		
ACRE 015	LAB4012	1.0	0.000055	7.3	4.91	1.9	0.11185	0.83	3.1522	1.6	0.20418	1.9	0.9	1829	30	1198	43	1445	25	65.5		
ACRE 015	LAB4012	1.2	0.000042	6.8	5.33	1.0	0.11266	0.76	2.8996	1.1	0.18764	1.0	0.7	1842	27	1109	21	1382	16	60.2		
ACRE 015	LAB4012	0.8	0.000061	8.7	6.11	1.2	0.11004	0.61	2.4942	1.1	0.16377	1.2	0.9	1799	22	978	22	1270	16	54.3		

~~ACRE 015~~	~~LAB4012~~	~~0.8~~	~~0.000054~~	~~9.7~~	~~6.42~~	~~5.1~~	~~0.11215~~	~~0.85~~	~~2.5062~~	~~3.4~~	~~0.16147~~	~~4.2~~	~~1.0~~	~~1833~~	~~30~~	~~963~~	~~77~~	~~1269~~	~~50~~	~~52.6~~
~~ACRE 015~~	~~LAB4012~~	~~2.0~~	~~0.000019~~	~~7.8~~	~~6.34~~	~~0.8~~	~~0.11779~~	~~0.71~~	~~2.5847~~	~~1.2~~	~~0.15791~~	~~0.8~~	~~0.8~~	~~1921~~	~~25~~	~~945~~	~~14~~	~~1296~~	~~18~~	~~49.2~~
~~ACRE 015~~	~~LAB4012~~	~~0.8~~	~~0.000052~~	~~11.4~~	~~11.81~~	~~4.2~~	~~0.10667~~	~~0.57~~	~~1.2566~~	~~4.1~~	~~0.08594~~	~~4.0~~	~~1.0~~	~~1742~~	~~21~~	~~531~~	~~41~~	~~824~~	~~46~~	~~30.5~~
~~ACRE 015~~	~~LAB4012~~	~~0.5~~	~~0.000018~~	~~14.0~~	~~12.57~~	~~4.0~~	~~0.11166~~	~~2.60~~	~~1.2353~~	~~3.6~~	~~0.08039~~	~~4.0~~	~~0.8~~	~~1821~~	~~92~~	~~498~~	~~38~~	~~815~~	~~39~~	~~27.4~~
LABXR-4012																				
ACRE 015	LABXR-4012-54	1.8	3861.980228	45.5	2.03	1.4	0.16478	0.70	11.2524	1.5	0.49307	1.4	0.31	2503	24	2584	58	2544	29	103.2	2503	24
ACRE 015	LABXR-4012-28	0.8	2084.162079	131.0	2.62	1.5	0.12622	0.74	6.6966	1.6	0.38235	1.5	0.53	2044	26	2087	53	2072	28	102.1	2044	26
ACRE 015	LABXR-4012-56	2.0	286.817706	111.6	2.69	1.6	0.12289	3.14	6.3498	4.1	0.37231	1.6	0.64	1985	102	2040	56	2019	65	102.8	1985	102
ACRE 015	LABXR-4012-32	1.1	393.603235	75.3	2.87	1.6	0.12195	1.39	5.9219	2.0	0.34931	1.6	0.42	1976	48	1930	53	1961	35	97.7	1976	48
ACRE 015	LABXR-4012-29	1.1	1647.050106	127.4	2.76	1.6	0.12026	0.92	6.0574	1.7	0.36282	1.6	0.57	1957	32	1995	54	1983	30	101.9	1957	32
ACRE 015	LABXR-4012-2	1.7	97902.785094	82.5	2.82	1.6	0.11823	0.81	5.8400	1.9	0.35640	1.7	0.79	1926	29	1964	57	1950	31	102.0	1926	29
ACRE 015	LABXR-4012-6	1.4	1670.411613	107.7	2.83	1.8	0.11728	0.88	5.7569	2.0	0.35415	1.7	0.81	1912	31	1954	57	1938	35	102.2	1912	31
ACRE 015	LABXR-4012-17	1.9	902.220929	89.4	3.24	1.6	0.11709	1.79	5.0221	2.3	0.30943	1.6	0.37	1906	63	1738	50	1821	39	91.2	1906	63
ACRE 015	LABXR-4012-37	1.5	34.713265	2511.7	2.89	1.4	0.11559	0.69	5.5873	1.6	0.34672	1.5	0.65	1887	25	1919	48	1914	28	101.7	1887	25
ACRE 015	LABXR-4012-10	1.2	15868.253111	70.9	2.90	1.4	0.11534	0.56	5.5112	1.5	0.34555	1.4	0.49	1883	20	1913	45	1902	25	101.6	1883	20
ACRE 015	LABXR-4012-39	1.5	1143.211553	204.3	2.97	1.8	0.11515	0.78	5.4184	2.0	0.33779	1.8	0.86	1880	28	1875	58	1886	35	99.8	1880	28
ACRE 015	LABXR-4012-7	1.0	926.852304	99.4	2.92	1.4	0.11517	0.72	5.4440	1.6	0.34340	1.4	0.65	1880	26	1903	46	1891	28	101.2	1880	26
ACRE 015	LABXR-4012-38	0.6	131.166803	1426.9	2.95	1.5	0.11486	0.80	5.4433	1.6	0.34016	1.5	0.54	1875	29	1887	50	1891	28	100.6	1875	29
ACRE 015	LABXR-4012-52	1.9	2689.371129	61.8	2.88	1.4	0.11485	0.66	5.5388	1.5	0.34811	1.4	0.52	1875	24	1925	47	1906	26	102.7	1875	24
ACRE 015	LABXR-4012-11	0.8	7196.341949	84.1	2.92	1.8	0.11424	0.73	5.4422	1.8	0.34349	1.8	0.84	1866	27	1903	59	1891	31	102.0	1866	27
ACRE 015	LABXR-4012-41	0.7	2204.548638	248.5	2.87	1.8	0.11397	0.99	5.5451	2.2	0.35024	1.7	0.90	1859	37	1935	58	1904	39	104.1	1859	37
ACRE 015	LABXR-4012-26	1.0	871.170988	56.5	3.11	3.0	0.11238	0.87	5.0881	2.2	0.32727	2.3	0.93	1834	31	1822	74	1829	41	99.3	1834	31
ACRE 015	LABXR-4012-59	0.7	2612.102086	78.4	3.12	1.6	0.11177	0.67	4.9854	1.8	0.32171	1.6	0.84	1826	24	1797	52	1815	31	98.4	1826	24
ACRE 015	LABXR-4012-4	1.7	925.505515	110.2	3.07	1.5	0.11172	0.88	5.0433	1.6	0.32498	1.4	0.36	1823	31	1814	43	1826	28	99.5	1823	31
ACRE 015	LABXR-4012-45	1.0	2581.197039	69.8	3.03	1.4	0.11140	0.74	5.0658	1.6	0.33106	1.5	0.63	1819	27	1843	47	1830	27	101.3	1819	27
ACRE 015	LABXR-4012-58	1.0	4980.135979	116.9	3.12	2.6	0.11154	1.66	4.9731	1.9	0.32258	2.5	0.62	1819	61	1801	78	1814	33	99.0	1819	61
ACRE 015	LABXR-4012-5	0.9	835.837871	109.4	3.04	1.6	0.11128	0.91	5.0579	1.7	0.32971	1.6	0.65	1817	32	1836	50	1828	29	101.1	1817	32
ACRE 015	LABXR-4012-18	0.6	1922.422418	109.5	3.18	2.8	0.11101	1.24	4.8892	2.9	0.31748	2.7	0.87	1813	46	1776	84	1797	51	98.0	1813	46

ACRE 015	LABXR-4012-60	0.6	1964.203596	89.4	2.91	1.6	0.11076	0.98	5.2831	1.7	0.34397	1.6	0.55	1809	35	1905	54	1865	29	105.3	1809	35
ACRE 015	LABXR-4012-51	0.9	1556.103785	65.1	3.22	1.6	0.11072	0.94	4.7708	1.5	0.31108	1.7	0.59	1809	35	1746	52	1780	26	96.5	1809	35
ACRE 015	LABXR-4012-25	1.2	2434.316123	66.8	3.20	1.7	0.11074	1.24	4.8272	2.2	0.31329	1.7	0.70	1808	45	1756	54	1788	37	97.1	1808	45
ACRE 015	LABXR-4012-57	0.6	8770.424243	49.5	2.92	1.4	0.10947	0.66	5.2040	1.6	0.34294	1.4	0.59	1794	21	1900	47	1853	27	105.9	1794	21
ACRE 015	LABXR-4012-15	1.4	3645.903357	62.0	3.05	1.4	0.10971	0.62	5.0048	1.6	0.32873	1.4	0.73	1792	23	1832	43	1819	27	102.2	1792	23
ACRE 015	LABXR-4012-35	0.8	5175.124951	50.3	3.23	1.9	0.10953	0.70	4.7469	2.0	0.31075	1.8	0.88	1790	26	1744	55	1774	33	97.4	1790	26
ACRE 015	LABXR-4012-14	1.2	6713.483233	61.7	3.01	1.7	0.10910	1.02	5.0286	1.8	0.33234	1.7	0.61	1782	37	1849	53	1823	31	103.8	1782	37
ACRE 015	LABXR-4012-21	1.3	15323.922488	49.0	3.03	1.4	0.10907	0.61	5.0012	1.7	0.32973	1.6	0.81	1782	22	1836	50	1818	29	103.1	1782	22
ACRE 015	LABXR-4012-53	1.3	1756.740277	110.1	3.03	1.6	0.10905	0.72	5.0173	1.6	0.32960	1.4	0.44	1781	26	1836	45	1824	24	103.1	1781	26
ACRE 015	LABXR-4012-44	1.1	2633.174670	98.6	3.17	1.5	0.10846	0.62	4.7392	1.7	0.31611	1.5	0.84	1772	22	1770	45	1773	28	99.9	1772	22
ACRE 015	LABXR-4012-47	0.7	8301.349747	71.8	3.14	1.4	0.10700	0.79	4.7115	1.7	0.31856	1.4	0.61	1746	29	1782	44	1768	28	102.1	1746	29
ACRE 015	LABXR-4012-40	0.4	2075.545799	167.5	3.14	2.3	0.10682	1.07	4.8284	3.0	0.32303	2.2	0.97	1741	40	1802	71	1781	52	103.5	1741	40
ACRE 015	LABXR-4012-48	0.9	20462.288631	49.7	3.16	1.7	0.10583	0.62	4.6015	1.6	0.31551	1.5	0.73	1727	23	1767	47	1752	30	102.4	1727	23
ACRE 015	LABXR-4012-36	0.5	14.151013	8113.6	3.18	1.8	0.10471	0.73	4.5918	1.6	0.31345	1.4	0.58	1707	27	1757	44	1747	27	103.0	1707	27
ACRE 015	LABXR-4012-31	0.7	327.303874	282.0	3.64	1.4	0.09824	0.68	3.7635	1.7	0.27521	1.4	0.83	1589	25	1567	39	1590	33	98.6	1589	25
ACRE 015	LABXR-4012-46	1.4	4755.253380	72.4	3.57	1.6	0.09748	0.87	3.7794	1.7	0.27951	1.4	0.52	1573	32	1589	40	1588	27	101.0	1573	32
ACRE 015	LABXR-4012-43	0.8	1405.945602	63.6	3.61	1.5	0.09619	0.75	3.6827	1.6	0.27750	1.5	0.49	1554	31	1578	41	1570	28	101.5	1554	31
ACRE 015	LABXR-4012-34	2.2	1151.302443	103.6	3.77	1.4	0.09566	0.80	3.5657	1.6	0.26565	1.4	0.04	1538	30	1519	38	1541	26	98.7	1538	30
ACRE 015	LABXR-4012-1	0.8	1431.835404	88.8	3.60	1.6	0.09513	0.87	3.6768	1.6	0.27893	1.5	0.45	1527	33	1586	43	1566	25	103.8	1527	33
ACRE 015	LABXR-4012-24	0.5	888.598508	111.4	3.52	2.0	0.09467	1.45	3.7472	1.8	0.28487	2.0	0.47	1518	54	1615	58	1581	28	106.4	1518	54
ACRE 015	LABXR-4012-8	1.8	1131.344066	73.0	3.76	1.4	0.09459	0.90	3.5093	1.9	0.26667	1.5	0.56	1515	33	1523	40	1527	29	100.5	1515	33
ACRE 015	LABXR-4012-3	1.3	1786.744112	61.9	3.70	1.4	0.09444	0.73	3.5385	1.6	0.27043	1.4	0.46	1514	28	1543	38	1535	25	101.9	1514	28
ACRE 015	LABXR-4012-33	0.7	577.560151	277.8	3.79	1.5	0.09138	0.75	3.3603	1.6	0.26412	1.5	0.60	1452	28	1511	40	1495	25	104.1	1452	28
ACRE 015	LABXR-4012-9	1.1	2998.053168	59.6	4.15	1.5	0.08978	0.74	2.9995	1.6	0.24092	1.4	0.49	1417	28	1395	38	1407	25	98.4	1417	28
ACRE 015	LABXR-4012-42	1.0	733.610445	127.5	4.13	1.4	0.08936	0.72	2.9897	1.6	0.24281	1.4	0.30	1409	27	1401	36	1404	24	99.5	1409	27
ACRE 015	LABXR-4012-30	0.7	134.270699	266.3	4.68	1.8	0.08686	4.23	2.5691	3.9	0.21296	1.5	0.29	1309	124	1244	34	1283	48	95.0	1309	124
ACRE 015	LABXR-4012-27	0.6	185.722151	405.4	4.20	2.0	0.08469	1.44	2.8052	1.7	0.23883	2.0	0.42	1303	56	1380	48	1356	26	105.9	1303	56

Data not used due to high discordance

ACRE 015	LABXR-4012-19	2.3	415.566069	142.7	3.27	1.9	0.12013	1.03	5.1150	2.1	0.30742	1.8	0.75	1955	37	1727	55	1837	36	88.4	1955	37
ACRE 015	LABXR-4012-50	3.5	28483.163164	103.2	3.64	2.6	0.11532	1.16	4.4651	2.3	0.27962	2.6	0.84	1890	46	1587	72	1720	39	83.9	1890	46
ACRE 015	LABXR-4012-13	1.1	16816.914245	91.0	3.82	3.1	0.11895	0.68	4.4096	2.9	0.26792	3.1	0.98	1938	25	1527	83	1708	49	78.8	1938	25
ACRE 015	LABXR-4012-12	1.3	1314.246542	67.4	4.01	2.8	0.11483	1.10	4.0827	2.0	0.25386	2.5	0.79	1872	39	1456	64	1648	33	77.8	1872	39
ACRE 015	LABXR-4012-23	0.6	10649.845556	85.4	4.32	7.0	0.11658	1.65	4.0578	6.6	0.24884	5.9	0.97	1898	59	1425	153	1620	113	75.0	1898	59
ACRE 015	LABXR-4012-16	0.8	3188.206791	130.3	3.63	2.0	0.13413	1.05	5.1403	2.0	0.27651	2.0	0.78	2150	36	1573	55	1842	34	73.2	2150	36
ACRE 015	LABXR-4012-49	1.5	1929.011767	41.5	4.65	5.1	0.11434	1.11	3.5155	3.8	0.22354	4.4	0.99	1866	39	1297	105	1523	64	69.5	1866	39
ACRE 015	LABXR-4012-20	1.3	1359.765214	56.5	5.90	4.9	0.11651	1.02	2.9410	5.1	0.18305	5.4	0.98	1899	37	1077	105	1373	74	56.7	1899	37
ACRE 015	LABXR-4012-55	1.2	447.610772	82.3	5.84	6.6	0.13658	2.16	3.3906	5.4	0.19090	7.4	0.97	2173	74	1116	150	1511	94	51.4	2173	74
ACRE 015	LABXR-4012-22	0.5	232.115475	13.7	4.34	3.4	0.20997	7.89	6.8479	8.1	0.23507	3.1	0.24	2790	229	1359	78	2039	137	48.7	2790	229

Amostra Acre 27A

	Ratios											Rho	Ages (Ma)						% conc [1]	Best age	2s
Spot number	Th/U	206Pb/204Pb	1s	238U/206Pb	1s	207Pb/206Pb	1s	207Pb/235U	1s	206Pb/238U	1s		207Pb/206Pb	2s	206Pb/238U	2s	207Pb/235U	2s			
			(%)		(%)		(%)		(%)		(%)			(abs)		(abs)		(abs)			(abs)
LAB4014_33	3.3	0.0001	47.3258	2.89	1.2	0.12868	2.28	6.1420	2.7	0.34586	1.2	0.31	2074	80	1915	40	1994	46	92.3	2074	80
LAB4014_31	2.6	0.0000	1384.9951	2.83	1.6	0.12464	2.00	6.1255	3.0	0.35463	1.5	0.83	2017	69	1956	51	1989	53	97.0	2017	69
LAB4014_54	0.3	0.0001	155.5822	2.80	1.1	0.12093	0.83	5.9532	1.3	0.35778	1.1	0.38	1969	29	1972	37	1969	23	100.2	1969	29
LAB4014_51	2.3	0.0006	51.5058	3.15	1.9	0.11788	0.65	5.2283	1.6	0.31893	1.8	0.81	1923	23	1784	58	1857	27	92.7	1923	23
LAB4014_55	2.9	0.0000	3053.6064	3.02	1.3	0.11755	0.91	5.3607	1.3	0.33134	1.3	0.46	1917	32	1845	41	1878	23	96.2	1917	32
LAB4014_18	3.1	0.0002	19.8996	3.19	1.2	0.11706	0.57	5.0738	1.4	0.31413	1.2	0.85	1911	21	1761	36	1832	23	92.2	1911	21
LAB4014_46	2.0	0.0001	548.1956	3.00	1.1	0.11557	0.59	5.3258	1.3	0.33388	1.1	0.92	1888	21	1857	35	1873	23	98.4	1888	21
LAB4014_8	2.6	0.0000	889.0713	2.94	1.1	0.11507	0.71	5.3891	1.3	0.33994	1.1	0.15	1880	26	1886	37	1883	22	100.3	1880	26
LAB4014_2	2.3	0.0007	64.4045	3.03	1.1	0.11466	0.57	5.2082	1.3	0.32981	1.1	0.92	1874	20	1837	35	1854	22	98.1	1874	20
LAB4014_27	1.2	0.0005	77.8374	2.97	1.9	0.11337	1.02	5.2764	2.2	0.33795	1.8	0.92	1851	37	1876	59	1862	38	101.3	1851	37
LAB4014_36	1.7	0.0006	89.0762	3.06	1.1	0.11326	0.89	5.1066	1.6	0.32646	1.1	0.65	1851	32	1821	35	1837	26	98.4	1851	32
LAB4014_35	2.3	0.0002	115.5386	3.06	1.1	0.11322	1.06	5.1120	1.4	0.32693	1.1	0.59	1849	37	1823	34	1838	24	98.6	1849	37
LAB4014_6	4.0	0.0001	778.2348	3.15	1.5	0.11286	0.58	4.9422	1.6	0.31742	1.4	0.98	1845	21	1777	44	1809	27	96.3	1845	21

LAB4014_23	2.1	0.0001	253.0794	3.04	1.1	0.11272	0.96	5.1157	1.4	0.32929	1.1	0.26	1842	34	1835	35	1838	24	99.6	1842	34
LAB4014_50	3.3	0.0036	103.0269	3.09	1.1	0.11225	0.68	4.9809	1.3	0.32328	1.1	0.77	1835	24	1806	34	1816	22	98.4	1835	24
LAB4014_58	1.8	0.0001	62.3075	3.08	1.0	0.11223	0.85	5.0109	1.4	0.32520	1.1	0.96	1834	30	1815	34	1821	23	99.0	1834	30
LAB4014_7	3.0	0.0008	83.3884	3.08	1.0	0.11159	0.65	4.9642	1.3	0.32465	1.0	0.53	1824	23	1812	33	1813	21	99.3	1824	23
LAB4014_56	2.5	0.0000	798.3474	3.19	2.0	0.11099	0.63	4.8208	2.0	0.31476	1.8	0.98	1815	23	1763	56	1787	35	97.2	1815	23
LAB4014_4	2.9	0.0013	112.5291	3.11	1.4	0.11051	0.63	4.9114	1.5	0.32148	1.3	0.82	1813	34	1797	41	1804	26	99.1	1813	34
LAB4014_19	3.0	0.0007	89.5868	3.10	1.1	0.11033	0.61	4.8936	1.3	0.32229	1.1	0.79	1804	22	1801	35	1801	22	99.8	1804	22
LAB4014_57	2.8	0.0000	3181.9529	3.66	1.8	0.10200	2.43	3.8491	2.6	0.27179	1.4	0.30	1648	88	1550	37	1600	42	94.0	1648	88
LAB4014_32	0.4	0.0001	145.5143	3.46	1.2	0.10103	0.72	4.0402	1.5	0.28946	1.2	0.87	1642	27	1639	34	1642	24	99.8	1642	27
LAB4014_34	1.1	0.0001	210.0881	3.51	1.1	0.09873	0.78	3.8802	1.3	0.28505	1.1	0.06	1599	29	1617	32	1610	20	101.1	1599	29
LAB4014_42	0.9	0.0005	34.7117	3.62	2.0	0.09801	0.64	3.7652	2.0	0.27781	1.9	0.98	1586	24	1580	53	1584	34	99.6	1586	24
LAB4014_21	3.6	0.0003	27.3049	3.92	1.3	0.09664	0.71	3.3957	1.4	0.25538	1.3	0.99	1559	27	1466	34	1503	23	94.0	1559	27
LAB4014_40	2.9	0.0002	146.8790	3.73	1.1	0.09640	0.71	3.5652	1.3	0.26780	1.1	0.01	1554	27	1530	30	1542	20	98.4	1554	27
LAB4014_1	1.4	0.0007	44.5795	3.77	1.1	0.09598	0.72	3.5056	1.4	0.26523	1.1	0.56	1546	27	1516	31	1528	22	98.1	1546	27
LAB4014_39	1.3	0.0027	155.7817	3.71	1.1	0.09589	0.72	3.5732	1.3	0.26939	1.1	0.36	1544	27	1538	30	1544	20	99.6	1544	27
LAB4014_10	2.4	0.0003	58.9641	3.95	1.0	0.09424	0.80	3.2959	1.5	0.25324	1.0	0.72	1512	30	1455	27	1480	23	96.3	1455	27
LAB4014_9	2.2	0.0017	101.4011	3.96	1.1	0.09141	0.83	3.1714	1.4	0.25236	1.1	0.98	1453	31	1451	29	1450	21	99.8	1451	29
LAB4014_25	1.2	0.0002	43.5021	4.02	1.4	0.08978	0.90	3.0699	1.4	0.24886	1.4	0.66	1419	35	1432	35	1425	22	100.9	1432	35
LAB4014_24	1.4	0.0001	39.1346	4.83	1.3	0.08538	1.50	2.4005	1.6	0.20738	1.3	0.42	1320	56	1215	28	1242	22	92.1	1215	28
LAB4014_0	1.7	0.0001	48.9196	4.76	1.2	0.08273	0.87	2.3776	1.4	0.21035	1.2	0.64	1261	33	1231	27	1236	19	97.6	1231	27
LAB4014_14	4.1	0.0002	71.0897	5.15	1.1	0.07981	1.07	2.1309	1.5	0.19407	1.1	0.31	1190	41	1143	22	1159	20	96.0	1143	22
LAB4014_5	1.8	0.0009	61.2728	9.73	1.1	0.06100	0.74	0.8613	1.3	0.10280	1.1	0.39	638	32	631	14	631	12	98.9	631	14

~~**LAB4014_52**~~	~~2.2~~	~~0.0001~~	~~28.2605~~	~~3.44~~	~~1.7~~	~~0.11393~~	~~0.82~~	~~4.5964~~	~~1.9~~	~~0.29214~~	~~1.6~~	~~0.91~~	~~1861~~	~~30~~	~~1652~~	~~47~~	~~1747~~	~~33~~	~~88.7~~		
~~**LAB4014_45**~~	~~1.9~~	~~0.0016~~	~~121.5227~~	~~4.25~~	~~4.4~~	~~0.09899~~	~~1.14~~	~~3.3009~~	~~3.0~~	~~0.24304~~	~~3.7~~	~~0.99~~	~~1602~~	~~41~~	~~1399~~	~~95~~	~~1476~~	~~49~~	~~87.3~~		
~~**LAB4014_16**~~	~~3.0~~	~~0.0001~~	~~45.9128~~	~~3.50~~	~~1.8~~	~~0.11974~~	~~2.33~~	~~4.6947~~	~~1.5~~	~~0.28639~~	~~1.8~~	~~0.54~~	~~1943~~	~~81~~	~~1623~~	~~52~~	~~1766~~	~~25~~	~~83.5~~		
~~**LAB4014_49**~~	~~1.8~~	~~0.0000~~	~~10.3678~~	~~3.50~~	~~1.4~~	~~0.11946~~	~~0.83~~	~~4.7886~~	~~1.7~~	~~0.28621~~	~~1.4~~	~~0.43~~	~~1947~~	~~29~~	~~1622~~	~~40~~	~~1782~~	~~28~~	~~83.3~~		
~~**LAB4014_29**~~	~~2.2~~	~~0.0001~~	~~36.8896~~	~~3.62~~	~~2.0~~	~~0.12381~~	~~6.22~~	~~4.8605~~	~~8.5~~	~~0.27849~~	~~2.1~~	~~0.95~~	~~1938~~	~~187~~	~~1583~~	~~59~~	~~1752~~	~~122~~	~~81.7~~		
~~**LAB4014_37**~~	~~2.8~~	~~0.0000~~	~~151.0265~~	~~6.51~~	~~3.3~~	~~0.07689~~	~~2.63~~	~~1.6773~~	~~1.9~~	~~0.15586~~	~~2.8~~	~~0.56~~	~~1144~~	~~76~~	~~933~~	~~50~~	~~999~~	~~25~~	~~81.5~~		

LAB4014_13	2.5	0.0004	28.2951	3.75	3.9	0.11758	0.56	4.3749	3.9	0.27065	4.0	1.00	1919	20	1542	109	1703	64	80.4		
LAB4014_48	2.2	0.0000	24.9417	4.50	1.9	0.10242	2.84	3.1288	1.7	0.22290	1.8	0.93	1656	104	1297	43	1439	27	78.3		
LAB4014_59	2.7	0.0002	75.4001	4.36	7.3	0.11094	1.84	3.6956	5.2	0.24544	6.6	1.00	1809	65	1407	168	1559	86	77.8		
LAB4014_43	1.2	0.0000	94.5314	3.38	2.1	0.14170	7.73	5.9521	10.0	0.29734	2.2	0.99	2161	255	1677	66	1919	163	77.6		
LAB4014_26	1.7	0.0005	98.4343	3.50	3.3	0.13608	2.64	5.3802	3.6	0.28878	3.6	0.73	2170	91	1633	102	1877	65	75.3		
LAB4014_22	3.0	0.0011	103.1018	3.87	5.4	0.13692	4.01	4.9793	3.9	0.27074	4.7	0.50	2156	141	1538	132	1807	65	71.3		
LAB4014_17	1.9	0.0001	21.6644	4.85	10.1	0.11424	2.88	3.6530	5.6	0.22797	7.7	0.85	1858	90	1315	187	1549	92	70.8		
LAB4014_47	2.0	0.0001	21.3391	4.75	8.7	0.12317	1.62	3.8522	6.1	0.23791	6.3	0.83	1996	57	1365	160	1576	107	68.4		
LAB4014_12	2.8	0.0000	15.1839	4.53	4.9	0.12127	2.38	3.7384	3.1	0.22707	4.6	0.95	1967	80	1316	109	1576	50	66.9		
LAB4014_53	1.1	0.0007	76.0124	5.55	15.1	0.11503	2.55	3.2449	9.0	0.20931	10.9	0.99	1874	91	1215	248	1443	157	64.8		
LAB4014_41	3.5	0.0000	29.0438	4.95	4.0	0.11658	2.67	3.2947	3.7	0.20596	4.1	0.70	1894	101	1205	90	1476	55	63.6		
LAB4014_20	2.4	0.0001	24.5755	6.17	21.2	0.12192	3.47	3.2703	10.8	0.20079	13.0	1.00	1970	115	1159	291	1415	209	58.8		
LAB4014_30	0.7	0.0000	24.5068	4.79	2.5	0.16426	14.02	4.0761	8.0	0.21087	2.2	0.30	2224	353	1233	50	1655	144	55.4		
LAB4014_15	2.4	0.0001	89.3528	4.98	13.3	0.19566	9.07	6.9233	14.7	0.25088	9.3	0.65	2669	280	1424	246	1965	257	53.3		
LAB4014_11	1.1	0.0000	8.6762	4.86	1.2	0.16986	3.04	4.8191	3.6	0.20603	1.2	0.49	2543	102	1208	27	1783	59	47.5		
LAB4014_38	3.0	0.0000	7.6670	5.73	4.8	0.14911	1.62	3.8109	5.1	0.18679	5.9	0.96	2329	54	1097	117	1576	79	47.1		
LAB4014_44	2.1	0.0000	10.0739	7.29	6.1	0.11849	0.99	2.2981	5.6	0.14092	6.3	1.00	1932	35	848	101	1207	78	43.9		
LAB4014_28	0.7	0.0000	10.6033	12.57	11.5	0.10349	1.05	1.3473	10.4	0.09543	11.2	1.00	1686	39	583	125	841	121	34.6		
LAB4014_3	2.0	0.0000	10.1466	8.21	3.3	0.16301	3.97	2.7881	6.8	0.12308	3.4	0.92	2470	139	748	49	1340	100	30.3		
LABXR-4013-2	1.7	1431.9	41.2	2.60	1.5	0.13361	2.01	7.0646	2.6	0.38555	1.5	0.4	2135	70	2102	54	2115	46	98	2135	70
LABXR-4013-38	0.7	306.6	56.6	2.87	1.6	0.11868	1.36	5.6735	2.1	0.34980	1.6	0.4	1927	47	1933	54	1924	35	100	1927	47
LABXR-4013-8	1.2	1970.4	101.4	3.23	1.9	0.11712	0.67	5.0225	2.0	0.31193	2.0	0.9	1910	24	1749	60	1821	34	92	1910	24
LABXR-4013-55	1.1	1048.9	83.5	2.90	1.3	0.11664	0.60	5.5746	1.6	0.34501	1.3	0.6	1903	21	1911	44	1912	27	100	1903	21
LABXR-4013-43	2.2	1560.8	87.3	2.89	1.5	0.11653	0.78	5.5964	1.7	0.34620	1.5	0.6	1901	28	1916	49	1915	29	101	1901	28
LABXR-4013-17	1.6	240.5	825.9	2.89	1.5	0.11582	0.68	5.5167	1.7	0.34643	1.5	0.8	1891	24	1917	49	1902	29	101	1891	24
LABXR-4013-39	1.2	1125.1	46.1	2.96	1.4	0.11561	0.61	5.3564	1.6	0.33804	1.4	0.7	1887	22	1877	47	1877	27	99	1887	22
LABXR-4013-24	1.0	785.8	220.3	2.85	1.4	0.11538	1.07	5.6670	1.9	0.35171	1.4	0.5	1883	38	1943	48	1926	32	103	1883	38
LABXR-4013-52	1.6	931.2	106.6	2.95	1.3	0.11529	0.59	5.3890	1.5	0.33913	1.3	0.5	1882	21	1882	44	1883	26	100	1882	21

LABXR-4013-42	1.1	908.7	145.6	2.88	1.4	0.11531	0.62	5.5609	1.6	0.34786	1.4	0.6	1882	22	1924	46	1909	27	102	1882	22
LABXR-4013-57	0.5	2282.2	186.7	2.90	1.3	0.11520	0.45	5.4931	1.5	0.34507	1.3	0.7	1882	16	1911	44	1899	26	102	1882	16
LABXR-4013-27	1.4	614.3	140.4	2.84	1.4	0.11520	0.51	5.6518	1.5	0.35237	1.4	0.7	1881	19	1946	46	1923	27	103	1881	19
LABXR-4013-59	1.1	1103.3	107.6	2.94	1.3	0.11514	0.54	5.4208	1.5	0.34046	1.3	0.5	1880	19	1889	44	1888	25	100	1880	19
LABXR-4013-15	1.4	792.8	310.0	2.89	1.7	0.11492	0.71	5.5133	1.8	0.34653	1.7	0.8	1877	26	1917	57	1902	31	102	1877	26
LABXR-4013-36	1.1	174.7	200.7	3.30	1.6	0.11538	2.06	4.8177	2.2	0.30407	1.5	0.4	1869	65	1711	45	1784	35	92	1869	65
LABXR-4013-44	1.1	2404.9	48.7	2.87	1.4	0.11429	0.73	5.5305	1.6	0.34835	1.4	0.5	1866	27	1926	47	1905	27	103	1866	27
LABXR-4013-19	1.1	4811.2	169.4	3.37	1.7	0.11416	0.84	4.7011	1.8	0.29735	1.7	0.8	1865	30	1678	49	1767	31	90	1865	30
LABXR-4013-1	1.6	1026.4	75.0	3.06	1.3	0.11355	0.68	5.0854	1.6	0.32751	1.3	0.4	1855	25	1826	42	1833	26	98	1855	25
LABXR-4013-58	1.1	549.3	156.4	3.12	1.6	0.11342	1.07	5.0226	1.9	0.32058	1.6	0.3	1852	39	1792	50	1822	32	97	1852	39
LABXR-4013-14	1.9	2577.0	48.9	3.06	1.4	0.11335	0.75	5.1296	1.6	0.32710	1.4	0.5	1851	27	1824	45	1840	28	99	1851	27
LABXR-4013-32	1.1	39.8	1154.7	3.05	1.8	0.11259	1.06	5.0678	2.0	0.32941	1.8	0.7	1838	39	1835	57	1829	33	100	1838	39
LABXR-4013-31	1.4	695.6	139.8	3.18	1.5	0.11247	0.73	4.8543	1.6	0.31498	1.5	0.6	1838	26	1765	45	1794	27	96	1838	26
LABXR-4013-25	1.2	2823.9	75.3	3.07	1.5	0.11210	0.76	5.0920	1.6	0.32572	1.5	0.5	1832	27	1817	46	1834	27	99	1832	27
LABXR-4013-7	1.1	1820.5	152.0	3.11	1.7	0.11205	0.89	4.9620	1.7	0.32214	1.6	0.6	1830	32	1800	51	1812	29	98	1830	32
LABXR-4013-34	0.4	5139.0	73.5	3.05	1.3	0.11071	0.47	4.9774	1.5	0.32852	1.3	0.5	1810	17	1831	42	1815	25	101	1810	17
LABXR-4013-22	2.0	978.6	147.2	3.01	1.3	0.11071	0.53	5.1373	1.5	0.33246	1.3	0.3	1809	19	1850	42	1842	25	102	1809	19
LABXR-4013-20	0.8	202.2	465.9	2.99	1.7	0.11059	0.62	5.1676	1.6	0.33472	1.6	0.9	1807	22	1861	52	1847	28	103	1807	22
LABXR-4013-23	2.1	309.0	613.8	3.02	1.3	0.11057	0.88	5.1096	1.7	0.33176	1.3	0.6	1805	30	1847	43	1836	28	102	1805	30
LABXR-4013-46	1.5	4695.5	77.4	3.03	1.4	0.11033	0.69	5.0657	1.7	0.33044	1.4	0.7	1802	25	1840	44	1829	29	102	1802	25
LABXR-4013-47	1.0	2247.7	82.0	2.96	1.6	0.10961	1.26	5.1468	2.0	0.33776	1.6	0.5	1790	46	1876	54	1843	34	105	1790	46
LABXR-4013-26	1.2	1461.0	130.4	2.98	1.4	0.10936	0.67	5.1194	1.6	0.33555	1.4	0.7	1787	24	1865	45	1839	28	104	1787	24
LABXR-4013-33	0.6	1905.3	52.2	3.07	1.6	0.10885	0.88	4.8614	2.0	0.32593	1.6	0.8	1778	32	1818	51	1794	34	102	1778	32
LABXR-4013-12	1.3	482.8	107.3	3.10	1.5	0.10548	0.63	4.7210	1.5	0.32264	1.3	0.3	1720	23	1802	42	1771	25	105	1720	23
LABXR-4013-11	1.0	628.3	85.9	3.05	1.4	0.10521	0.72	4.7825	1.7	0.32813	1.4	0.6	1715	27	1829	43	1781	28	107	1715	27
LABXR-4013-37	1.4	515.9	290.7	3.38	1.4	0.10259	0.79	4.1555	1.6	0.29596	1.4	0.4	1669	29	1671	42	1665	26	100	1669	29
LABXR-4013-51	1.1	1702.4	85.2	3.69	2.5	0.09781	0.59	3.7002	2.0	0.27291	2.1	1.0	1580	22	1553	61	1568	35	98	1580	22
LABXR-4013-54	0.9	708.3	238.7	3.57	1.3	0.09725	0.66	3.7593	1.6	0.28003	1.3	0.2	1569	24	1591	37	1583	25	101	1569	24
LABXR-4013-3	1.3	1372.2	68.4	3.66	1.4	0.09651	0.59	3.6220	1.7	0.27345	1.4	0.8	1555	22	1558	39	1553	26	100	1555	22

LABXR-4013-40	1.0	305.7	61.8	3.69	1.4	0.09659	0.91	3.5930	1.7	0.27125	1.4	0.5	1555	33	1547	39	1547	27	99	1555	33
LABXR-4013-60	0.9	5880.3	61.8	3.68	1.5	0.09609	0.74	3.6269	1.6	0.27237	1.5	0.6	1548	28	1553	41	1555	26	100	1548	28
LABXR-4013-48	0.6	446.4	260.0	3.62	1.2	0.09494	0.60	3.6306	1.5	0.27553	1.3	0.5	1525	23	1569	37	1556	25	103	1525	23
LABXR-4013-45	1.1	272.8	269.0	3.53	1.5	0.09380	1.15	3.6956	1.7	0.28365	1.5	0.2	1500	44	1609	42	1570	28	107	1500	44
LABXR-4013-28	1.5	220.6	539.1	4.68	2.7	0.08296	0.85	2.4754	2.7	0.21469	2.5	0.9	1265	33	1252	59	1260	41	99	1252	59
LABXR-4013-5	0.5	399.7	116.2	4.59	1.4	0.08224	1.12	2.4640	1.8	0.21822	1.4	0.2	1246	45	1272	33	1261	26	102	1272	33
LABXR-4013-53	0.9	18.3	3296.9	4.58	1.4	0.08147	0.89	2.4555	1.6	0.21867	1.4	0.3	1228	35	1275	32	1258	24	104	1275	32
LABXR-4013-13	1.8	12.3	755.4	4.64	1.6	0.08124	1.60	2.4273	1.9	0.21653	1.6	0.1	1213	60	1263	36	1249	27	104	1263	36
LABXR-4013-41	1.1	29.5	1405.9	4.75	1.7	0.08087	1.67	2.3634	1.9	0.21082	1.6	0.0	1211	66	1233	36	1231	27	102	1233	36
LABXR-4013-21	1.3	347.7	195.6	4.65	1.4	0.08029	0.80	2.4097	1.6	0.21535	1.4	0.2	1200	31	1257	31	1245	22	105	1257	31
LABXR-4013-10	0.7	527.7	167.9	5.84	1.4	0.07311	0.78	1.7279	1.6	0.17160	1.4	0.3	1013	32	1021	26	1018	20	101	1021	26
LABXR-4013-30	1.3	605.8	83.0	6.08	1.6	0.07463	2.41	1.7063	3.3	0.16428	1.5	0.6	1007	42	980	28	1005	34	97	980	28
~~**LABXR-4013-16**~~	~~1.1~~	~~2424.7~~	~~71.9~~	~~4.14~~	~~2.3~~	~~0.11366~~	~~0.64~~	~~3.8566~~	~~2.3~~	~~0.24532~~	~~2.2~~	~~0.9~~	~~1856~~	~~23~~	~~1413~~	~~55~~	~~1600~~	~~37~~	~~76~~		
~~**LABXR-4013-35**~~	~~1.1~~	~~363.5~~	~~343.9~~	~~3.99~~	~~2.1~~	~~0.11999~~	~~0.77~~	~~4.1674~~	~~2.3~~	~~0.25397~~	~~2.1~~	~~0.9~~	~~1953~~	~~27~~	~~1457~~	~~55~~	~~1663~~	~~37~~	~~75~~		
~~**LABXR-4013-4**~~	~~2.4~~	~~2507.8~~	~~44.3~~	~~5.30~~	~~5.1~~	~~0.10194~~	~~1.69~~	~~2.7707~~	~~4.5~~	~~0.19831~~	~~4.2~~	~~0.9~~	~~1651~~	~~61~~	~~1163~~	~~90~~	~~1334~~	~~70~~	~~70~~		
~~**LABXR-4013-6**~~	~~0.6~~	~~563.8~~	~~229.0~~	~~5.62~~	~~4.2~~	~~0.10182~~	~~0.84~~	~~2.6011~~	~~3.3~~	~~0.18723~~	~~3.6~~	~~1.0~~	~~1662~~	~~27~~	~~1103~~	~~74~~	~~1292~~	~~50~~	~~66~~		
~~**LABXR-4013-49**~~	~~1.2~~	~~453.4~~	~~113.1~~	~~4.78~~	~~3.9~~	~~0.11926~~	~~2.39~~	~~3.6141~~	~~4.0~~	~~0.21472~~	~~4.0~~	~~0.7~~	~~1935~~	~~73~~	~~1251~~	~~91~~	~~1545~~	~~62~~	~~65~~		
~~**LABXR-4013-29**~~	~~1.0~~	~~2509.6~~	~~37.6~~	~~5.04~~	~~3.4~~	~~0.11601~~	~~1.14~~	~~3.3274~~	~~3.2~~	~~0.20822~~	~~3.5~~	~~1.0~~	~~1889~~	~~39~~	~~1215~~	~~77~~	~~1477~~	~~48~~	~~64~~		
~~**LABXR-4013-50**~~	~~0.8~~	~~1197.7~~	~~138.4~~	~~5.37~~	~~2.6~~	~~0.11929~~	~~0.75~~	~~3.1067~~	~~2.4~~	~~0.18787~~	~~2.5~~	~~0.9~~	~~1944~~	~~27~~	~~1109~~	~~52~~	~~1433~~	~~38~~	~~57~~		
~~**LABXR-4013-56**~~	~~1.0~~	~~432.0~~	~~21.9~~	~~4.64~~	~~5.4~~	~~0.16077~~	~~4.18~~	~~5.0875~~	~~6.8~~	~~0.23493~~	~~4.9~~	~~0.8~~	~~2401~~	~~123~~	~~1349~~	~~120~~	~~1798~~	~~118~~	~~56~~		
~~**LABXR-4013-18**~~	~~0.3~~	~~3976.3~~	~~64.6~~	~~5.93~~	~~4.7~~	~~0.12129~~	~~0.74~~	~~3.1123~~	~~5.0~~	~~0.18690~~	~~5.3~~	~~1.0~~	~~1972~~	~~26~~	~~1096~~	~~106~~	~~1408~~	~~74~~	~~56~~		

Amostra Acre 27B

		Ratios									Rho	Dates						% conc [1]	Best age	2s
Spot number	Th/U	206Pb/204Pb	1s	238U/206Pb	1s	207Pb/206Pb	1s	207Pb/235U	1s	206Pb/238U	1s		207Pb/206Pb	2s	206Pb/238U	2s	207Pb/235U	2s			
			(%)		(%)		(%)		(%)		(%)			(abs)		(abs)		(abs)			(abs)
Z-26	1.0	1149.7	103.4	1.74	1.0	0.20760	0.70	16.7458	1.0	0.57738	1.0	0.7	2885	23	2937	48	2919	19	101.8	2885	23
Z-41	1.3	83500.1	73.4	2.80	0.8	0.11851	0.48	5.8771	0.7	0.35817	0.8	0.8	1932	17	1973	28	1957	12	102.1	1932	17

Z-40	1.4	207.3	222.5	2.76	0.9	0.11712	0.95	5.8542	1.0	0.36072	1.1	0.0	1909	34	1985	36	1953	17	104.0	1909	34
Z-21	0.7	1384.7	123.9	2.96	0.8	0.11490	1.74	5.3363	1.7	0.33831	0.8	0.6	1883	62	1878	26	1871	24	99.7	1883	62
Z-27	2.1	359.6	200.1	2.89	0.9	0.11484	0.76	5.5787	1.1	0.34757	0.9	0.7	1874	27	1922	29	1911	18	102.6	1874	27
Z-46	1.0	248.3	253.1	2.92	0.9	0.11464	0.75	5.4847	0.8	0.34401	0.9	0.3	1871	27	1905	28	1897	13	101.8	1871	27
Z-24	1.0	27839.5	56.7	2.84	1.1	0.11437	0.74	5.6378	1.0	0.35137	1.2	0.6	1867	27	1940	40	1921	18	103.9	1867	27
Z-43	1.9	464.4	393.3	3.37	1.4	0.11410	0.83	4.6466	1.2	0.29502	1.6	0.1	1862	30	1676	44	1756	20	90.0	1862	30
Z-47	1.7	326.1	163.3	3.07	0.9	0.11158	0.77	5.0603	0.8	0.32715	0.8	0.5	1822	28	1824	27	1829	13	100.1	1822	28
Z-11	2.4	3547.6	51.2	3.19	0.8	0.11127	0.96	4.8523	1.0	0.31387	0.7	0.6	1815	34	1759	23	1793	16	96.9	1815	34
Z-44	1.1	2555.9	83.0	3.00	0.9	0.11037	0.58	5.1129	0.8	0.33466	0.9	0.8	1803	21	1860	29	1837	13	103.2	1803	21
Z-38	1.9	1053.7	109.7	3.35	1.0	0.10998	0.61	4.5679	1.0	0.29954	1.0	0.8	1796	22	1688	30	1742	17	94.0	1796	22
Z-12	1.3	79020.9	94.7	3.01	0.9	0.10984	0.72	5.0935	1.0	0.33336	0.9	0.6	1793	26	1854	29	1833	17	103.4	1793	26
Z-54	1.0	15.1	9278.3	3.38	0.9	0.10969	0.41	4.5220	1.0	0.29693	0.9	0.9	1793	15	1675	26	1733	17	93.5	1793	15
Z-55	0.4	690.6	205.0	3.02	0.6	0.10961	0.53	5.0350	0.7	0.33160	0.6	0.7	1791	19	1846	20	1824	12	103.1	1791	19
Z-19	0.6	1193.0	131.0	3.08	1.2	0.10949	0.68	4.9844	1.4	0.32633	1.2	0.5	1788	25	1819	38	1814	23	101.8	1788	25
Z-28	1.0	3537.7	52.1	3.04	0.8	0.10951	0.73	5.0459	0.9	0.33008	0.8	0.5	1788	27	1838	26	1830	17	102.8	1788	27
Z-7	1.7	365.7	105.1	3.01	0.8	0.10936	0.72	5.0701	0.8	0.33332	0.8	0.5	1785	27	1854	25	1830	14	103.8	1785	27
Z-1	1.3	356.1	176.2	3.03	0.6	0.10884	0.58	5.0148	0.8	0.33116	0.6	0.7	1778	21	1844	20	1821	13	103.7	1778	21
Z-49	0.7	622.0	222.4	3.01	0.6	0.10826	0.60	4.9733	0.8	0.33155	0.7	0.7	1768	22	1845	23	1814	14	104.4	1768	22
Z-32	1.2	1532.6	114.5	3.27	0.7	0.10632	0.67	4.5281	0.8	0.30694	0.7	0.6	1734	24	1725	22	1735	13	99.5	1734	24
Z-25	1.3	972.6	133.9	3.23	1.0	0.10502	0.77	4.5591	1.0	0.31072	0.9	0.7	1711	28	1744	29	1740	16	101.9	1711	28
Z-39	2.1	138.4	584.4	3.48	0.7	0.09707	0.95	3.8729	1.1	0.28780	0.7	0.4	1563	34	1630	20	1606	18	104.3	1563	34
Z-52	0.2	14.5	5189.2	3.58	0.7	0.09709	0.97	3.7569	1.1	0.28026	0.7	0.5	1563	36	1592	20	1582	17	101.9	1563	36
Z-34	1.1	46011.9	62.7	3.68	0.8	0.09654	0.75	3.6601	0.9	0.27275	0.8	0.2	1555	28	1554	22	1561	15	100.0	1555	28
Z-22	0.6	1647.0	128.3	3.62	0.8	0.09647	0.67	3.7292	0.7	0.27714	0.8	0.1	1554	25	1576	23	1577	12	101.5	1554	25
Z-57	3.6	274.1	152.6	3.71	0.9	0.09578	0.79	3.5938	0.8	0.27024	0.9	0.5	1539	30	1542	24	1547	13	100.1	1539	30
Z-23	0.8	4230.8	94.9	3.58	0.9	0.09565	0.66	3.7201	0.9	0.28035	0.9	0.8	1538	25	1593	26	1575	14	103.6	1538	25
Z-48	2.5	175.7	247.3	3.66	0.8	0.09563	0.94	3.6273	1.1	0.27378	0.8	0.5	1535	36	1560	21	1554	18	101.6	1535	36
Z-33	1.8	4734.5	71.5	3.76	0.8	0.09531	0.70	3.5296	0.8	0.26702	0.8	0.6	1531	26	1525	21	1533	13	99.6	1531	26
Z-37	1.7	628.6	63.3	3.64	0.9	0.09515	0.85	3.6249	0.8	0.27458	0.9	0.5	1527	31	1563	27	1557	12	102.4	1527	31
Z-29	1.1	2721.8	75.7	3.72	0.9	0.09504	0.80	3.5525	0.8	0.26957	0.9	0.6	1525	30	1538	24	1538	13	100.9	1525	30
Z-20	0.6	3456.2	50.4	3.64	0.8	0.09492	0.76	3.6249	0.8	0.27575	0.8	0.6	1523	29	1570	22	1554	13	103.1	1523	29
Z-60	3.2	1337.6	98.8	3.57	1.1	0.09500	1.27	3.7025	1.1	0.28139	1.1	0.4	1519	47	1598	30	1570	18	105.2	1519	47
Z-16	1.2	120.6	341.6	3.55	0.8	0.09469	0.65	3.7151	0.9	0.28256	0.8	0.5	1519	25	1604	22	1574	14	105.6	1519	25
Z-35	1.6	3370.2	47.6	3.73	1.0	0.09486	1.04	3.5487	1.3	0.26922	1.0	0.6	1519	39	1536	28	1536	21	101.1	1519	39
Z-56	1.3	2036.7	64.0	3.67	0.9	0.09471	0.84	3.5951	0.9	0.27331	0.8	0.5	1518	32	1557	23	1547	14	102.6	1518	32
Z-4	1.7	2946.2	43.7	3.67	0.8	0.09464	1.11	3.5799	1.0	0.27359	0.8	0.3	1513	43	1559	23	1548	17	103.0	1513	43
Z-53	1.8	75.4	478.6	3.70	0.8	0.09437	0.89	3.5498	1.1	0.27100	0.8	0.3	1511	34	1545	23	1537	17	102.3	1511	34
Z-5	2.5	1412.1	138.2	3.65	1.1	0.09399	1.80	3.5855	1.7	0.27525	1.1	0.2	1507	76	1567	31	1549	30	103.9	1507	76
Z-2	1.7	6081.8	101.0	3.65	0.8	0.09386	0.85	3.5868	0.9	0.27484	0.7	0.4	1501	32	1565	20	1546	14	104.3	1565	20
Z-50	1.6	1121.6	48.9	3.72	0.9	0.09317	0.99	3.4506	0.8	0.26874	1.0	0.6	1486	37	1534	29	1515	13	103.2	1534	29
Z-9	1.9	507.0	204.2	3.78	1.0	0.09276	0.99	3.4272	1.2	0.26561	0.9	0.6	1477	37	1518	26	1509	19	102.8	1518	26
Z-13	1.0	3930.4	59.8	3.67	1.0	0.09257	0.68	3.5330	1.0	0.27397	1.0	0.4	1476	26	1560	27	1533	15	105.7	1560	27
Z-10	1.9	40788.4	97.4	3.88	0.8	0.09238	0.75	3.3158	1.0	0.25837	0.8	0.7	1471	28	1481	22	1483	16	100.7	1481	22
Z-45	1.1	1392.7	127.3	4.13	0.8	0.08807	0.74	2.9580	0.8	0.24256	0.8	0.6	1387	26	1400	19	1396	13	100.9	1400	19
Z-30	0.5	9005.6	216.0	4.23	0.7	0.08697	0.63	2.8717	0.8	0.23692	0.7	0.6	1357	24	1370	18	1374	12	101.0	1370	18
Z-17	1.3	4771.4	52.4	4.19	0.7	0.08572	0.67	2.8369	0.8	0.23832	0.7	0.6	1329	25	1378	17	1365	12	103.7	1378	17
Z-42	0.8	1957.5	110.0	4.59	0.8	0.08199	0.85	2.4798	1.0	0.21847	0.8	0.5	1240	34	1273	18	1265	14	102.7	1273	18
Z-36	1.4	908.2	84.9	4.70	1.0	0.08156	0.89	2.4195	1.2	0.21352	1.0	0.7	1230	35	1247	23	1247	17	101.4	1247	23
Z-14	0.6	944.0	135.4	4.53	0.9	0.08080	0.85	2.4864	1.0	0.22143	0.9	0.5	1212	33	1289	21	1267	14	106.4	1289	21
Z-58	0.7	2896.6	34.2	5.82	1.0	0.07577	1.08	1.8221	1.1	0.17270	0.9	0.3	1081	43	1027	18	1052	14	94.9	1027	18
Z-59	0.5	4388.5	86.8	5.48	0.8	0.07365	0.76	1.8700	0.9	0.18315	0.8	0.6	1027	31	1084	16	1070	12	105.5	1084	16

Z-3	0.6	54.4	477.7	5.80	0.6	0.07303	0.89	1.7589	0.8	0.17270	0.5	0.1	1018	39	1027	10	1030	11	100.9	1027	10
Z-15	0.4	220.4	357.8	6.14	1.0	0.07226	1.08	1.6443	1.2	0.16373	1.0	0.6	985	44	977	19	986	16	99.2	977	19
Z-6	1.3	185.4	54.9	9.35	1.1	0.06152	2.27	0.9182	2.1	0.10751	1.1	0.1	646	97	658	14	659	21	101.9	658	14
Data not used due to high discordance																					
~~**Z-51**~~	~~2.1~~	~~548.8~~	~~98.3~~	~~4.18~~	~~0.8~~	~~0.10956~~	~~0.71~~	~~3.6408~~	~~0.8~~	~~0.24004~~	~~0.8~~	~~0.4~~	~~1789~~	~~26~~	~~1387~~	~~20~~	~~1557~~	~~13~~	~~77.5~~		
~~**Z-8**~~	~~0.9~~	~~323.5~~	~~29.1~~	~~5.45~~	~~1.3~~	~~0.12476~~	~~5.94~~	~~3.2680~~	~~7.3~~	~~0.18441~~	~~1.3~~	~~0.8~~	~~1925~~	~~192~~	~~1091~~	~~27~~	~~1432~~	~~103~~	~~56.7~~		
~~**Z-18**~~	~~2.8~~	~~59.7~~	~~9.6~~	~~6.49~~	~~8.4~~	~~0.37472~~	~~4.14~~	~~10.7348~~	~~12.0~~	~~0.20361~~	~~11.5~~	~~1.0~~	~~3765~~	~~139~~	~~1163~~	~~237~~	~~2343~~	~~213~~	~~30.9~~		
Z-84	0.5	125.0	5.1	10.89	2.6	0.21858	1.91	2.9373	4.8	0.09514	3.0	0.96	2955	61	585	34	1365	67	19.8	2955	61
Z-101	0.3	37.5	706.9	2.81	1.8	0.20049	4.31	10.3062	6.2	0.36091	1.9	0.95	2749	143	1983	64	2394	111	72.1	2749	143
Z-67	0.9	1619.5	89.3	2.72	2.3	0.17989	6.53	10.1426	10.7	0.37997	3.0	0.96	2499	182	2066	103	2298	146	82.7	2499	182
Z-89	1.2	1125.5	66.2	2.01	0.9	0.16125	0.71	11.1504	1.3	0.49780	0.8	0.71	2466	24	2603	36	2535	25	105.6	2466	24
Z-114	1.5	268.6	294.0	3.83	1.1	0.13578	3.28	4.9320	4.0	0.26205	1.0	0.78	2118	121	1500	28	1782	70	70.8	2118	121
Z-69	1.4	447.3	62.2	3.47	2.8	0.15679	12.40	8.2316	24.7	0.31116	6.0	1.00	2081	284	1721	159	1855	202	82.7	2081	284
Z-98	1.2	133.5	956.0	2.59	0.7	0.12703	0.65	6.8418	1.2	0.38679	0.7	0.57	2055	23	2108	25	2091	21	102.5	2055	23
Z-76	1.7	1161.2	101.4	3.09	1.2	0.11883	2.43	5.2918	3.0	0.32557	1.3	0.78	1915	72	1816	40	1856	45	94.8	1915	72
Z-115	0.9	316.2	280.2	10.87	6.7	0.11568	0.90	1.8894	8.2	0.12133	8.8	1.00	1886	32	725	119	1020	98	38.5	1886	32
Z-118	1.2	3418.6	46.8	2.97	0.9	0.11520	0.60	5.3528	1.3	0.33795	0.9	0.77	1881	22	1876	30	1876	22	99.7	1881	22
Z-107	2.0	2485.9	120.5	2.82	0.7	0.11477	0.59	5.6276	1.1	0.35490	0.7	0.57	1875	22	1958	22	1920	20	104.4	1875	22
Z-85	1.2	421.6	669.0	3.04	0.9	0.11513	1.23	5.2542	1.7	0.33018	0.8	0.57	1874	44	1839	26	1858	30	98.1	1874	44
Z-99	0.4	2726.6	43.5	5.88	13.1	0.11407	1.01	3.7213	6.3	0.23986	6.5	1.00	1860	35	1361	168	1496	130	73.2	1860	35
Z-71	1.1	4567.9	41.5	4.54	4.6	0.11197	0.76	3.7321	3.7	0.23945	3.9	0.99	1829	27	1375	98	1558	65	75.2	1829	27
Z-92	1.0	21806.6	44.4	3.00	0.8	0.11108	0.70	5.1603	1.3	0.33373	0.8	0.65	1815	25	1856	26	1845	21	102.3	1815	25
Z-64	1.5	412.7	125.8	2.80	0.7	0.11096	0.83	5.4395	1.3	0.35797	0.7	0.47	1812	30	1972	24	1890	23	108.9	1812	30
Z-73	2.4	4215.7	78.5	3.13	0.7	0.11086	0.63	4.9557	1.2	0.31916	0.6	0.53	1812	23	1785	19	1811	20	98.6	1812	23
Z-96	1.0	21845.3	55.2	3.10	0.6	0.11033	0.65	4.9818	1.1	0.32331	0.6	0.46	1803	23	1806	20	1816	19	100.2	1803	23
Z-66	1.6	9374.6	112.2	3.06	0.7	0.11004	0.65	4.9324	1.2	0.32733	0.7	0.66	1798	23	1825	23	1807	21	101.5	1798	23
Z-119	1.2	1336.2	96.2	3.02	0.7	0.10990	0.70	5.0409	1.2	0.33195	0.7	0.60	1795	25	1848	23	1825	21	102.9	1795	25
Z-95	1.2	20782.5	48.0	2.98	0.7	0.10930	0.76	5.1109	1.2	0.33571	0.7	0.41	1785	27	1866	23	1837	20	104.5	1785	27
Z-81	1.1	18753.9	160.3	2.98	0.7	0.10920	0.68	5.0697	1.2	0.33576	0.7	0.57	1784	25	1866	22	1830	21	104.6	1784	25
Z-78	0.7	596.0	335.8	2.99	0.6	0.10853	0.56	5.0363	1.2	0.33392	0.7	0.64	1773	20	1857	22	1825	20	104.7	1773	20
Z-116	1.4	206.9	225.8	2.97	1.0	0.10819	0.64	5.0159	1.2	0.33732	0.9	0.79	1767	24	1873	30	1821	21	106.0	1767	24
Z-104	1.3	2727.5	72.2	3.07	0.7	0.10678	0.64	4.7972	1.3	0.32640	0.7	0.72	1743	24	1821	23	1784	21	104.4	1743	24
Z-86	1.0	350.2	771.6	3.36	1.9	0.10667	0.60	4.4070	2.3	0.29691	2.0	0.97	1741	22	1686	55	1714	38	96.8	1741	22
Z-109	1.0	1230.3	39.5	3.13	1.2	0.10598	0.73	4.6953	1.6	0.32193	1.2	0.82	1729	27	1798	38	1764	27	104.0	1729	27
Z-70	1.2	924.3	165.2	7.23	10.1	0.10521	1.35	2.6450	5.6	0.18586	5.9	0.98	1709	48	1086	122	1268	96	63.5	1709	48
Z-82	1.7	2154.9	61.7	3.72	2.1	0.11020	7.13	4.9850	18.0	0.27541	2.8	0.98	1675	148	1563	72	1608	84	93.3	1675	148
Z-77	-0.5	4.4	183.0	1.25	13.0	0.10337	6.23	44.0617	18.4	3.43281	18.7	0.92	1620	207	7332	1666	3212	377	452.6	1620	207
Z-106	1.4	1309.2	71.2	3.57	0.7	0.09854	0.99	3.8161	1.3	0.28060	0.7	0.10	1591	37	1594	20	1595	21	100.2	1591	37
Z-93	1.6	12469.8	57.4	3.60	0.9	0.09670	0.92	3.7498	1.5	0.27841	0.9	0.63	1564	31	1583	26	1580	24	101.2	1564	31
Z-68	1.5	449.7	123.4	3.69	0.8	0.09805	1.55	3.6596	2.3	0.27154	0.8	0.78	1560	38	1548	23	1548	21	99.3	1560	38
Z-63	1.8	6574.7	88.4	3.65	1.0	0.09604	0.83	3.6064	1.3	0.27355	0.8	0.69	1545	31	1558	23	1554	25	100.9	1545	31
Z-97	0.9	4491.7	50.6	3.71	0.7	0.09597	0.98	3.6026	1.3	0.26961	0.7	0.12	1542	37	1539	19	1549	21	99.8	1542	37
Z-72	0.4	131.4	1556.3	3.68	1.4	0.09554	0.69	3.6561	1.6	0.27368	1.3	0.93	1536	26	1558	36	1560	26	101.4	1536	26
Z-103	0.7	1436.3	100.6	3.52	0.8	0.09549	0.59	3.7604	1.2	0.28483	0.8	0.74	1536	22	1615	23	1584	19	105.2	1536	22
Z-100	1.1	707.3	74.8	3.66	0.8	0.09545	0.81	3.6288	1.2	0.27363	0.8	0.36	1533	30	1559	21	1555	19	101.7	1533	30
Z-94	1.4	22572.8	94.1	3.89	3.6	0.09535	1.00	3.4743	1.9	0.26738	1.2	0.96	1530	37	1527	33	1517	36	99.8	1530	37
Z-117	1.3	2220.3	87.0	3.48	1.2	0.09520	0.83	3.7650	1.4	0.28743	1.1	0.78	1528	31	1635	35	1584	22	107.0	1528	31
Z-87	2.0	3484.9	61.9	3.61	0.9	0.09471	0.78	3.6493	1.5	0.27749	0.9	0.75	1519	29	1578	25	1559	23	103.9	1519	29
Z-91	2.4	17.8	891.9	3.63	1.4	0.09434	1.09	3.6601	1.8	0.27754	1.3	0.63	1518	45	1578	36	1560	28	104.0	1518	45

Z-65	1.5	1035.8	116.6	3.62	0.8	0.09440	0.75	3.5467	1.3	0.27559	0.9	0.71	1513	28	1569	25	1537	21	103.7	1513	28
Z-90	1.1	292.9	148.9	3.51	1.1	0.09396	0.97	3.7399	1.7	0.28641	1.2	0.75	1502	36	1623	33	1577	27	108.0	1502	36
Z-108	1.6	591.4	78.4	3.53	0.7	0.09381	0.83	3.6754	1.3	0.28364	0.7	0.34	1500	31	1609	19	1565	20	107.3	1500	31
Z-110	2.3	2046.8	53.6	3.57	0.7	0.09362	0.90	3.6143	1.4	0.27970	0.8	0.46	1496	34	1590	22	1552	22	106.2	1496	34
Z-80	0.4	1168.3	87.9	4.08	0.7	0.08611	0.79	2.9219	1.3	0.24549	0.7	0.50	1337	31	1415	18	1389	18	105.8	1415	18
Z-83	1.0	24.3	4099.3	4.14	0.7	0.08572	0.84	2.8613	1.2	0.24187	0.7	0.27	1328	33	1396	17	1373	17	105.1	1396	17
Z-105	0.9	303.7	183.9	4.10	0.7	0.08561	0.78	2.8858	1.3	0.24410	0.7	0.47	1326	30	1408	17	1377	19	106.2	1408	17
Z-111	1.1	28151.0	42.3	4.52	0.6	0.08071	0.64	2.4530	1.1	0.22134	0.6	0.35	1212	26	1289	14	1258	16	106.3	1289	14
Z-88	1.2	35656.0	101.7	4.57	0.6	0.08073	0.73	2.4539	1.2	0.21886	0.6	0.24	1212	29	1276	14	1258	17	105.3	1276	14
Z-74	0.9	2195.5	90.5	4.89	1.0	0.07959	0.86	2.2804	1.4	0.20544	1.1	0.94	1183	34	1204	24	1205	20	101.8	1204	24
Z-113	0.7	57.6	55.6	5.49	1.3	0.07350	2.04	1.8417	2.1	0.18251	1.2	0.16	1001	87	1085	26	1057	28	108.5	1085	26
Z-120	0.6	1322.7	62.4	6.06	0.6	0.07081	1.13	1.6274	1.4	0.16526	0.6	0.22	944	47	986	12	980	18	104.5	986	12
Z-79	1.5	225.8	73.8	6.33	1.2	0.07136	2.61	1.5612	2.5	0.15891	1.2	0.02	924	110	950	21	950	32	102.9	950	21

Data not used due to high discordance

~~**Z-112**~~	~~0.6~~	~~350.5~~	~~79.1~~	~~7.56~~	~~5.1~~	~~0.07488~~	~~3.00~~	~~1.3904~~	~~3.1~~	~~0.13731~~	~~4.0~~	~~0.80~~	~~1019~~	~~108~~	~~826~~	~~63~~	~~877~~	~~40~~	~~81.1~~	~~826~~	~~63~~
~~**Z-75**~~	~~6.5~~	~~11.5~~	~~71.5~~	~~1.81~~	~~13.1~~	~~0.05666~~	~~27.43~~	~~13.6096~~	~~22.0~~	~~1.24120~~	~~16.1~~	~~0.77~~	~~999~~	~~666~~	~~4529~~	~~1009~~	~~2305~~	~~430~~	~~453.5~~	~~4529~~	~~1009~~
~~**Z-102**~~	~~0.9~~	~~176.3~~	~~394.4~~	~~5.64~~	~~0.7~~	~~0.08216~~	~~1.31~~	~~1.9975~~	~~1.6~~	~~0.17739~~	~~0.7~~	~~0.31~~	~~1240~~	~~51~~	~~1053~~	~~14~~	~~1113~~	~~21~~	~~84.9~~	~~1053~~	~~14~~

Amostra Acre 29

			Ratios								Rho	Ages (Ma)						% conc [1]	Best age	2s
Spot number	Th/U	206Pb/204Pb	1s	238U/206Pb	1s	207Pb/206Pb	1s	207Pb/235U	1s	206Pb/238U	1s		207Pb/206Pb	2s	206Pb/238U	2s	207Pb/235U	2s			
			(%)		(%)		(%)		(%)		(%)		(abs)		(abs)		(abs)				(abs)
LAB4015_2	1.5	0.0	84.7	2.52	1.1	0.13487	0.63	7.3391	1.3	0.39704	1.1	0.8	2161	22	2155	39	2153	23	99.7	2161	22
LAB4015_55	2.6	0.0	17.8	3.04	1.2	0.12931	3.61	5.8382	3.5	0.32880	1.2	0.3	2069	107	1832	37	1946	55	88.6	2069	107
LAB4015_13	2.1	0.0	40.7	3.02	1.3	0.12363	0.72	5.6408	1.5	0.33195	1.4	0.9	2008	25	1848	43	1922	26	92.0	2008	25
LAB4015_44	2.9	0.0	106.1	3.11	2.3	0.12289	1.92	5.4872	2.7	0.32463	2.1	0.6	1990	65	1811	66	1894	47	91.0	1990	65
LAB4015_20	1.1	0.0	90.6	2.80	1.1	0.11972	0.74	5.8776	1.4	0.35697	1.1	0.9	1951	26	1968	37	1958	25	100.9	1951	26
LAB4015_0	2.0	0.0	68.7	3.11	1.5	0.11766	3.19	5.3340	4.7	0.32202	1.6	0.7	1905	102	1799	48	1864	73	94.4	1905	102
LAB4015_37	2.5	0.0	121.4	2.75	1.1	0.11636	0.59	5.8110	1.3	0.36336	1.1	0.9	1900	21	1998	38	1948	23	105.1	1900	21
LAB4015_21	2.7	0.0	171.5	2.93	1.1	0.11623	0.58	5.4663	1.3	0.34126	1.1	0.9	1898	21	1893	37	1895	23	99.7	1898	21
LAB4015_26	3.2	0.0	49.5	2.94	1.1	0.11609	0.67	5.4423	1.3	0.34047	1.1	0.5	1896	24	1889	35	1891	22	99.6	1896	24
LAB4015_76	2.2	0.0	75.4	2.91	1.1	0.11593	0.69	5.4766	1.3	0.34401	1.1	0.9	1893	25	1906	35	1897	23	100.7	1893	25
LAB4015_50	3.2	0.0	74.3	2.89	1.0	0.11580	0.57	5.5170	1.3	0.34608	1.0	0.8	1891	21	1916	35	1903	22	101.3	1891	21
LAB4015_32	2.2	0.0	84.6	2.92	1.2	0.11568	0.69	5.4542	1.3	0.34221	1.2	0.7	1889	25	1897	39	1893	22	100.4	1889	25
LAB4015_52	2.3	0.0	362.5	2.90	1.1	0.11544	0.59	5.4843	1.3	0.34466	1.0	0.7	1886	21	1909	35	1898	22	101.2	1886	21
LAB4015_68	3.5	0.0	41.7	3.20	1.5	0.11556	1.26	4.9613	1.3	0.31344	1.4	0.1	1885	44	1757	45	1813	22	93.2	1885	44
LAB4015_25	1.8	0.0	45.3	3.39	3.0	0.11519	1.30	4.7161	2.1	0.29882	2.8	1.0	1880	45	1684	83	1768	36	89.6	1880	45
LAB4015_78	2.2	0.0	158.7	2.92	1.1	0.11338	0.76	5.3300	1.4	0.34247	1.1	1.0	1853	27	1899	35	1873	23	102.5	1853	27
LAB4015_60	2.9	0.0	143.4	3.17	1.2	0.11288	0.71	4.9108	1.3	0.31566	1.2	0.7	1845	25	1768	36	1804	22	95.8	1845	25
LAB4015_14	2.3	0.0	12.9	3.48	1.9	0.11284	1.27	4.4778	2.9	0.28855	1.9	1.0	1843	45	1634	56	1724	47	88.6	1843	45
LAB4015_19	2.3	0.0	98.5	3.10	1.2	0.11206	0.78	4.9679	1.3	0.32278	1.1	0.9	1832	28	1803	36	1814	23	98.5	1832	28
LAB4015_71	2.8	0.0	291.2	2.98	1.1	0.11224	1.95	5.1875	2.6	0.33554	1.1	1.0	1831	64	1865	35	1848	40	101.9	1831	64

LAB4015_27	2.3	0.0	244.0	3.01	1.1	0.11180	0.91	5.1103	1.8	0.33252	1.2	0.9	1827	32	1850	38	1837	29	101.3	1827	32
LAB4015_31	3.0	0.0	501.1	3.07	1.1	0.11174	0.81	4.9726	1.3	0.32531	1.1	0.5	1826	29	1816	34	1815	22	99.4	1826	29
LAB4015_49	2.5	0.0	284.4	3.09	1.2	0.11169	0.71	4.9816	1.3	0.32387	1.1	0.4	1826	26	1808	36	1816	22	99.0	1826	26
LAB4015_58	1.8	0.0	129.5	3.11	1.2	0.11139	0.67	4.9539	1.4	0.32186	1.2	0.9	1821	24	1799	38	1811	25	98.8	1821	24
LAB4015_42	2.3	0.0	224.7	2.99	1.2	0.11114	0.74	5.1290	1.5	0.33513	1.2	0.9	1817	27	1863	38	1840	26	102.6	1817	27
LAB4015_23	2.3	0.0	223.2	3.11	1.2	0.11104	0.66	4.9462	1.5	0.32198	1.2	0.8	1815	24	1799	37	1810	25	99.1	1815	24
LAB4015_53	1.7	0.0	3681.4	3.09	1.1	0.11086	0.66	4.9507	1.3	0.32418	1.1	0.7	1813	24	1810	34	1811	22	99.9	1813	24
LAB4015_65	2.0	0.0	114.0	3.00	1.1	0.11078	0.63	5.0837	1.3	0.33337	1.0	0.3	1811	23	1855	34	1833	21	102.4	1811	23
LAB4015_56	2.1	0.0	25.5	3.05	1.1	0.11055	0.68	4.9996	1.3	0.32798	1.1	0.6	1807	24	1829	36	1819	22	101.2	1807	24
LAB4015_28	2.6	0.0	48.3	3.10	1.1	0.11013	0.61	4.8896	1.3	0.32219	1.1	0.9	1801	22	1800	34	1800	22	100.0	1801	22
LAB4015_11	1.6	0.0	379.7	3.12	1.1	0.11005	0.64	4.8844	1.3	0.32105	1.1	0.0	1799	23	1795	34	1799	22	99.8	1799	23
LAB4015_30	1.9	0.0	78.2	3.04	1.2	0.10987	0.93	4.9693	1.3	0.32861	1.2	0.1	1796	34	1832	37	1814	22	102.0	1796	34
LAB4015_38	1.4	0.0	67.5	3.10	1.1	0.10924	0.70	4.8377	1.3	0.32250	1.1	0.6	1786	25	1802	35	1791	22	100.9	1786	25
LAB4015_64	2.7	0.0	112.2	3.04	1.0	0.10912	0.58	4.9453	1.3	0.32861	1.0	0.5	1784	21	1832	33	1810	21	102.7	1784	21
LAB4015_9	1.8	0.0	71.0	3.21	1.1	0.10892	0.58	4.6691	1.3	0.31166	1.1	0.9	1780	21	1749	34	1762	22	98.2	1780	21
LAB4015_1	1.5	0.0	32.3	3.15	1.1	0.10873	0.56	4.7347	1.3	0.31711	1.1	0.9	1777	21	1776	35	1773	22	99.9	1777	21
LAB4015_3	3.6	0.0	71.3	3.22	1.1	0.10832	0.59	4.6178	1.3	0.31081	1.1	0.8	1770	22	1745	32	1752	21	98.5	1770	22
LAB4015_47	1.3	0.0	301.2	3.04	1.1	0.10826	0.63	4.8930	1.3	0.32853	1.1	1.0	1769	23	1831	34	1801	22	103.5	1769	23
LAB4015_69	2.8	0.0	74.2	3.29	1.0	0.10667	0.63	4.4819	1.3	0.30391	1.0	0.4	1742	23	1711	31	1728	21	98.2	1742	23
LAB4015_57	2.5	0.0	112.5	3.18	1.1	0.10586	0.68	4.5948	1.3	0.31436	1.1	0.4	1728	25	1762	34	1748	21	102.0	1728	25
LAB4015_75	2.6	0.0	30.5	3.76	1.1	0.09863	0.81	3.6142	1.3	0.26615	1.1	0.0	1597	30	1521	30	1553	21	95.3	1597	30
LAB4015_73	2.3	0.0	110.6	3.60	1.4	0.09844	1.17	3.7655	1.3	0.27810	1.4	0.2	1591	44	1582	39	1585	21	99.4	1591	44
LAB4015_24	0.9	0.0	29.8	3.63	1.2	0.09786	0.98	3.7212	1.5	0.27582	1.2	0.2	1582	35	1570	32	1585	40	99.3	1582	35
LAB4015_12	6.2	0.0	1159.3	3.84	3.1	0.09588	2.15	3.4938	1.7	0.26456	3.1	0.7	1571	105	1511	83	1525	27	96.2	1571	105
LAB4015_40	1.0	0.0	35.9	3.61	1.1	0.09716	0.64	3.6956	1.3	0.27679	1.1	0.3	1569	24	1575	31	1570	21	100.4	1569	24
LAB4015_34	3.8	0.0	36.4	3.55	1.1	0.09721	0.91	3.7691	1.4	0.28173	1.1	0.9	1569	35	1600	32	1586	22	102.0	1569	35
LAB4015_61	3.0	0.0	94.0	3.58	1.1	0.09707	0.68	3.7380	1.3	0.27904	1.1	0.5	1567	25	1587	31	1579	21	101.2	1567	25
LAB4015_77	2.1	0.0	52.1	3.61	1.1	0.09703	0.90	3.6955	1.5	0.27680	1.1	0.7	1566	32	1575	31	1570	24	100.6	1566	32
LAB4015_70	2.9	0.0	54.6	3.64	1.1	0.09699	0.67	3.6927	1.3	0.27515	1.1	0.3	1566	25	1567	30	1570	21	100.1	1566	25
LAB4015_22	3.7	0.0	68.3	3.65	1.4	0.09690	1.47	3.6441	2.5	0.27384	1.4	0.9	1563	54	1560	40	1558	38	99.8	1563	54
LAB4015_51	3.3	0.0	111.9	3.78	1.4	0.09651	0.94	3.5212	1.4	0.26490	1.4	0.5	1555	36	1515	37	1532	22	97.4	1555	36
LAB4015_18	1.2	0.0	38.8	3.65	1.1	0.09632	0.63	3.6298	1.4	0.27404	1.1	0.9	1553	24	1561	31	1556	22	100.5	1553	24
LAB4015_5	0.8	0.0	44.5	3.64	1.1	0.09623	0.55	3.6369	1.3	0.27465	1.1	0.5	1551	21	1564	29	1558	20	100.8	1551	21
LAB4015_4	3.6	0.0	60.7	3.67	1.1	0.09620	0.63	3.5988	1.3	0.27231	1.1	0.5	1551	24	1553	29	1549	20	100.1	1551	24
LAB4015_45	3.8	0.0	196.4	3.55	1.2	0.09589	0.70	3.7171	1.3	0.28178	1.2	0.8	1544	26	1600	34	1575	21	103.6	1544	26
LAB4015_17	3.4	0.0	784.1	3.64	1.0	0.09582	0.65	3.6250	1.3	0.27494	1.1	0.3	1543	24	1566	29	1555	21	101.5	1543	24
LAB4015_72	2.7	0.0	76.2	3.63	1.5	0.09581	0.84	3.6779	1.4	0.27548	1.4	0.6	1543	31	1568	39	1566	22	101.7	1543	31
LAB4015_29	2.3	0.0	80.7	3.73	1.1	0.09580	0.82	3.5389	1.3	0.26791	1.1	0.8	1542	30	1530	30	1536	21	99.2	1542	30
LAB4015_41	1.3	0.0	134.1	3.67	1.1	0.09565	0.65	3.5864	1.3	0.27250	1.1	0.5	1540	24	1553	30	1547	20	100.9	1540	24
LAB4015_33	1.3	0.0	79.9	3.62	1.1	0.09565	0.63	3.6339	1.3	0.27606	1.1	0.5	1540	24	1571	30	1557	20	102.1	1540	24
LAB4015_35	2.3	0.0	86.7	3.54	1.0	0.09560	0.68	3.7115	1.3	0.28239	1.0	0.2	1539	26	1603	30	1574	21	104.2	1539	26
LAB4015_16	3.3	0.0	2036.4	3.72	1.1	0.09557	0.82	3.5344	1.4	0.26872	1.1	0.1	1538	30	1534	30	1535	22	99.8	1538	30
LAB4015_59	4.9	0.0	185.1	3.83	1.7	0.09588	1.82	3.4527	1.7	0.26191	1.6	0.1	1538	65	1499	43	1516	27	97.5	1538	65
LAB4015_46	3.3	0.0	84.2	3.66	1.1	0.09541	0.96	3.5797	1.4	0.27336	1.1	0.1	1535	36	1558	30	1545	22	101.5	1535	36
LAB4015_54	3.7	0.0	95.8	3.68	1.3	0.09488	0.61	3.5623	1.4	0.27229	1.3	0.9	1525	23	1552	36	1541	23	101.8	1525	23
LAB4015_62	1.7	0.0	64.5	4.38	1.5	0.09188	1.32	2.8960	1.4	0.22853	1.5	0.1	1461	51	1327	35	1381	21	90.8	1327	35

LAB4015_79	1.0	0.0	109.0	4.11	1.5	0.08739	0.93	2.9289	1.7	0.24388	1.6	0.8	1367	36	1407	41	1389	25	102.9	1407	41
LAB4015_43	1.8	0.0	111.9	4.30	2.4	0.08640	1.30	2.7527	1.5	0.23071	1.7	0.8	1343	50	1338	40	1342	22	99.6	1338	40
LAB4015_15	1.6	0.0	68.4	4.45	1.1	0.08532	0.62	2.6376	1.3	0.22476	1.1	0.9	1322	24	1307	25	1311	19	98.9	1307	25
LAB4015_39	1.1	0.0	105.3	4.28	1.1	0.08531	0.98	2.7395	1.3	0.23368	1.2	0.2	1321	38	1354	28	1339	20	102.5	1354	28
LAB4015_6	3.5	0.0	127.3	4.61	1.1	0.08356	0.86	2.4917	1.5	0.21704	1.1	1.0	1280	34	1266	26	1269	21	98.9	1266	26
LAB4015_8	2.1	0.0	56.3	4.88	1.4	0.08247	1.25	2.3236	1.3	0.20523	1.4	0.0	1253	47	1203	30	1219	19	96.0	1203	30
LAB4015_67	1.6	0.0	88.7	5.11	1.0	0.07863	0.58	2.1199	1.3	0.19583	1.0	0.5	1162	23	1153	22	1155	17	99.2	1153	22
LAB4015_36	2.5	0.0	57.8	6.61	5.1	0.07524	4.82	1.3361	7.0	0.15825	5.5	0.7	1023	193	944	96	845	96	92.3	944	96
LAB4015_74	2.1	0.0	70.5	6.12	1.7	0.07327	1.30	1.6516	1.4	0.16399	1.7	0.5	1017	53	979	31	990	17	96.2	979	31
LAB4015_63	1.8	0.0	47.1	5.99	1.7	0.07223	2.21	1.6921	1.7	0.16768	1.7	0.4	979	92	999	32	1005	22	102.1	999	32

Data not used due to high discordance

~~**LAB4015_7**~~	~~2.5~~	~~0.0~~	~~20.9~~	~~3.73~~	~~3.7~~	~~0.11222~~	~~0.87~~	~~4.2377~~	~~2.7~~	~~0.27207~~	~~3.5~~	~~0.9~~	~~1834~~	~~31~~	~~1549~~	~~98~~	~~1679~~	~~45~~	~~84.5~~	
~~**LAB4015_66**~~	~~3.0~~	~~0.0~~	~~19.8~~	~~3.58~~	~~4.0~~	~~0.11852~~	~~0.66~~	~~4.6380~~	~~3.7~~	~~0.28464~~	~~3.7~~	~~1.0~~	~~1933~~	~~24~~	~~1612~~	~~107~~	~~1750~~	~~64~~	~~83.4~~	
~~**LAB4015_10**~~	~~1.5~~	~~0.0~~	~~7.7~~	~~6.01~~	~~3.9~~	~~0.11478~~	~~1.18~~	~~2.6576~~	~~3.5~~	~~0.16918~~	~~3.8~~	~~1.0~~	~~1874~~	~~43~~	~~1006~~	~~72~~	~~1313~~	~~51~~	~~53.7~~	
~~**LAB4015_48**~~	~~5.1~~	~~0.0~~	~~19.2~~	~~10.72~~	~~10.0~~	~~0.13341~~	~~2.52~~	~~1.8017~~	~~9.3~~	~~0.10012~~	~~11.8~~	~~1.0~~	~~2139~~	~~88~~	~~613~~	~~137~~	~~1036~~	~~116~~	~~28.7~~	

Amostra Acre 33C

		Ratios										Rho	Ages (Ma)						% conc [1]	Best age	2s
Spot number	Th/U	206Pb/204Pb	1s	238U/206Pb	1s	207Pb/206Pb	1s	207Pb/235U	1s	206Pb/238U	1s		207Pb/206Pb	2s	206Pb/238U	2s	207Pb/235U	2s			
			(%)		(%)		(%)		(%)		(%)			(abs)		(abs)		(abs)			(abs)
LAB4013	1.4	0.000088	19.199754	3.18	0.9	0.12193	1.04	5.2658	1.7	0.31412	0.9	0.96	1983	37	1761	29	1863	29	88.8	1983	37
LAB4013	0.9	0.000682	39.763183	2.78	0.7	0.12146	0.63	6.0025	0.9	0.36032	0.7	0.52	1977	23	1984	25	1976	15	100.3	1977	23
LAB4013	0.9	0.000187	23.204080	2.97	1.0	0.11771	0.79	5.4626	0.9	0.33677	1.0	0.55	1920	28	1871	33	1895	15	97.4	1920	28
LAB4013	1.8	0.000161	140.915997	2.83	0.7	0.11697	0.56	5.6779	0.7	0.35311	0.7	0.01	1909	20	1949	22	1928	12	102.1	1909	20
LAB4013	1.0	0.006964	90.498074	2.93	0.7	0.11692	0.45	5.4898	0.8	0.34104	0.7	0.81	1909	16	1892	24	1899	13	99.1	1909	16
LAB4013	1.1	0.000243	43.709962	3.16	1.0	0.11655	0.57	5.0661	1.1	0.31635	1.0	0.86	1903	21	1772	31	1830	18	93.1	1903	21
LAB4013	1.8	0.000091	72.514318	2.98	0.9	0.11594	1.24	5.3540	1.7	0.33588	0.8	0.67	1892	44	1867	27	1877	28	98.7	1892	44
LAB4013	1.4	0.000075	352.746534	2.85	0.7	0.11579	0.37	5.6052	0.7	0.35075	0.7	0.52	1891	13	1938	22	1917	12	102.5	1891	13
LAB4013	1.2	0.002358	95.625053	2.83	0.7	0.11522	0.36	5.6120	0.7	0.35334	0.7	0.87	1883	13	1951	22	1918	12	103.6	1883	13
LAB4013	1.1	0.000052	312.508867	3.12	0.7	0.11267	0.65	4.9569	0.9	0.32020	0.7	0.65	1842	23	1791	22	1812	15	97.2	1842	23
LAB4013	1.8	0.001878	84.359315	3.08	0.7	0.11234	0.61	5.0251	0.8	0.32501	0.7	0.53	1836	22	1814	21	1823	14	98.8	1836	22
LAB4013	0.9	0.000124	13.535211	3.40	0.8	0.11217	1.07	4.5164	1.0	0.29392	0.8	0.04	1833	39	1661	25	1734	17	90.6	1833	39
LAB4013	1.6	0.000463	83.345707	3.08	0.7	0.11196	0.85	4.9852	1.0	0.32432	0.8	0.33	1830	30	1811	24	1817	16	99.0	1830	30
LAB4013	1.2	0.000149	60.899783	3.14	0.9	0.11139	0.52	4.8714	0.9	0.31906	0.9	0.90	1821	19	1785	27	1804	25	98.0	1821	19
LAB4013	1.1	0.000059	190.478630	2.99	0.7	0.11114	0.47	5.1069	0.6	0.33444	0.7	0.01	1817	17	1860	22	1837	11	102.4	1817	17
LAB4013	0.7	0.000343	81.406422	3.06	0.7	0.11107	0.38	5.0124	0.7	0.32700	0.7	0.80	1816	14	1824	22	1821	12	100.4	1816	14
LAB4013	3.0	0.000145	120.377875	3.07	1.1	0.11106	0.85	4.9875	0.7	0.32669	1.1	0.53	1815	31	1822	35	1817	13	100.4	1815	31
LAB4013	1.6	0.000244	242.871780	3.05	0.7	0.11036	0.54	4.9992	0.8	0.32766	0.7	0.34	1811	26	1827	22	1819	14	100.9	1811	26
LAB4013	1.1	0.000468	17.458192	3.13	0.8	0.11053	0.39	4.8622	0.7	0.32002	0.7	0.85	1807	14	1790	23	1796	13	99.0	1807	14
LAB4013	0.6	0.000503	126.291609	2.95	0.8	0.11023	0.50	5.1513	0.8	0.33923	0.8	0.76	1802	18	1883	25	1844	13	104.5	1802	18
LAB4013	1.1	0.000072	541.066157	3.15	0.7	0.10865	0.47	4.7476	0.7	0.31754	0.7	0.50	1776	17	1778	21	1776	12	100.1	1776	17
LAB4013	1.5	0.000715	34.840882	3.17	0.7	0.10810	0.59	4.6829	0.7	0.31560	0.7	0.09	1767	21	1768	22	1764	12	100.1	1767	21

LAB4013	1.0	0.000206	19.940008	3.29	0.9	0.10784	0.69	4.5045	0.8	0.30381	0.9	0.49	1762	25	1710	26	1732	13	97.0	1762	25
LAB4013	0.6	0.000966	109.236181	3.61	1.2	0.10094	1.30	3.8349	1.5	0.27726	1.2	0.55	1640	48	1578	33	1600	25	96.2	1640	48
LAB4013	1.3	0.000042	13.195551	3.81	1.1	0.09981	1.14	3.6093	1.0	0.26247	1.1	0.30	1618	42	1502	30	1551	16	92.9	1618	42
LAB4013	1.0	0.000251	11.064854	3.78	0.7	0.09894	0.40	3.5940	0.7	0.26425	0.7	0.88	1603	15	1512	20	1548	11	94.3	1603	15
LAB4013	0.7	0.000277	186.969337	3.51	1.2	0.09823	0.56	3.8470	1.0	0.28502	1.1	0.93	1590	21	1616	33	1602	15	101.7	1590	21
LAB4013	1.5	0.000249	46.313490	3.57	0.9	0.09795	0.64	3.7611	0.7	0.28011	0.8	0.49	1584	24	1592	24	1588	17	100.5	1584	24
LAB4013	1.1	0.000046	66.374769	3.65	1.6	0.09752	0.91	3.6657	1.7	0.27444	1.6	0.87	1576	34	1563	44	1563	27	99.2	1576	34
LAB4013	0.5	0.000249	188.300545	3.77	0.7	0.09628	0.40	3.5243	0.7	0.26553	0.7	0.51	1552	15	1518	18	1533	11	97.8	1552	15
LAB4013	1.2	0.000827	128.784944	3.73	0.6	0.09593	0.40	3.5413	0.7	0.26797	0.6	0.72	1545	15	1530	17	1536	11	99.0	1545	15
LAB4013	2.6	0.000108	266.015599	3.74	0.8	0.09596	0.64	3.5367	0.8	0.26721	0.8	0.34	1545	24	1527	21	1535	13	98.8	1545	24
LAB4013	0.9	0.000606	105.112038	3.74	0.7	0.09590	0.55	3.5305	0.8	0.26773	0.7	0.27	1545	20	1529	18	1534	12	99.0	1545	20
LAB4013	1.0	0.000344	54.587290	3.77	0.9	0.09591	0.71	3.5053	0.7	0.26569	0.9	0.34	1544	26	1519	23	1528	12	98.3	1544	26
LAB4013	0.7	0.002644	72.752365	3.68	0.6	0.09553	0.38	3.5798	0.7	0.27175	0.6	0.47	1538	14	1550	17	1545	11	100.8	1538	14
LAB4013	0.6	0.002581	79.050728	3.76	0.7	0.09488	0.37	3.4901	0.8	0.26606	0.7	0.91	1525	14	1521	19	1525	12	99.7	1525	14
LAB4013	1.7	0.000490	100.628893	3.63	0.8	0.09467	0.44	3.5838	0.8	0.27578	0.7	0.24	1520	17	1570	21	1546	13	103.3	1520	17
LAB4013	1.8	0.001576	123.702793	3.81	1.0	0.09351	0.49	3.3619	1.0	0.26235	1.0	0.89	1497	18	1502	26	1495	16	100.3	1502	26
LAB4013	1.1	0.000220	45.907311	3.84	0.7	0.09312	0.44	3.3412	0.7	0.26035	0.7	0.72	1489	17	1492	18	1491	11	100.2	1492	18
LAB4013	1.5	0.000145	45.608346	4.03	1.2	0.09214	0.70	3.1743	0.8	0.24885	1.2	0.48	1480	36	1432	30	1451	12	96.8	1432	30
LAB4013	0.5	0.000153	191.240322	4.07	1.1	0.09235	0.88	3.1426	1.1	0.24603	1.1	0.60	1473	34	1418	28	1443	17	96.3	1418	28
LAB4013	0.8	0.000105	132.241066	3.88	0.8	0.09224	0.55	3.2947	1.0	0.25803	0.8	0.51	1471	21	1480	22	1480	15	100.6	1480	22
LAB4013	1.3	0.000852	498.524469	4.12	0.8	0.09105	0.49	3.0447	0.7	0.24299	0.8	0.73	1446	19	1402	20	1419	11	96.9	1402	20
LAB4013	1.0	0.002167	102.319332	4.26	0.8	0.08836	1.64	2.8117	1.1	0.23492	0.8	0.12	1386	60	1360	20	1358	16	98.2	1360	20
LAB4013	0.7	0.000641	55.521717	4.28	0.7	0.08661	0.66	2.8013	0.7	0.23369	0.7	0.19	1350	26	1354	17	1356	11	100.3	1354	17
LAB4013	1.1	0.000000	638373.796367	4.73	1.3	0.08471	1.47	2.4554	2.0	0.21150	1.3	0.71	1307	57	1237	29	1259	29	94.6	1237	29
LAB4013	1.3	0.000287	230.022696	4.82	0.9	0.08327	0.65	2.3813	0.9	0.20763	0.9	0.67	1274	25	1216	20	1237	13	95.4	1216	20
LAB4013	0.7	0.000111	140.592040	4.71	0.8	0.08145	0.51	2.3859	0.7	0.21260	0.8	0.61	1231	20	1243	18	1238	10	100.9	1243	18

Data not used due to high discordance

~~**LAB4013**~~	~~1.2~~	~~0.000610~~	~~22.782274~~	~~3.66~~	~~2.1~~	~~0.11028~~	~~0.37~~	~~4.1717~~	~~2.2~~	~~0.27424~~	~~2.1~~	~~1.00~~	~~1803~~	~~13~~	~~1562~~	~~58~~	~~1667~~	~~36~~	~~86.6~~		
~~**LAB4013**~~	~~1.1~~	~~0.000060~~	~~27.270022~~	~~3.73~~	~~1.3~~	~~0.11932~~	~~1.64~~	~~4.3964~~	~~1.3~~	~~0.26845~~	~~1.2~~	~~0.08~~	~~1942~~	~~58~~	~~1533~~	~~33~~	~~1711~~	~~22~~	~~78.9~~		
~~**LAB4013**~~	~~0.8~~	~~0.000104~~	~~5.338024~~	~~4.04~~	~~1.4~~	~~0.11376~~	~~0.88~~	~~3.8705~~	~~1.3~~	~~0.24772~~	~~1.5~~	~~0.80~~	~~1859~~	~~32~~	~~1427~~	~~37~~	~~1607~~	~~21~~	~~76.7~~		
~~**LAB4013**~~	~~0.7~~	~~0.000029~~	~~13.344713~~	~~4.39~~	~~1.0~~	~~0.10789~~	~~3.10~~	~~3.4000~~	~~2.6~~	~~0.22804~~	~~0.9~~	~~0.53~~	~~1750~~	~~107~~	~~1324~~	~~22~~	~~1502~~	~~40~~	~~75.6~~		
~~**LAB4013**~~	~~0.7~~	~~0.000025~~	~~5.488210~~	~~4.81~~	~~1.8~~	~~0.10561~~	~~2.94~~	~~3.0378~~	~~3.4~~	~~0.20808~~	~~1.8~~	~~0.48~~	~~1721~~	~~111~~	~~1219~~	~~39~~	~~1416~~	~~52~~	~~70.8~~		
~~**LAB4013**~~	~~0.6~~	~~0.000138~~	~~11.167971~~	~~5.03~~	~~1.5~~	~~0.10783~~	~~0.46~~	~~2.9525~~	~~1.6~~	~~0.19920~~	~~1.5~~	~~0.98~~	~~1762~~	~~17~~	~~1171~~	~~32~~	~~1395~~	~~23~~	~~66.4~~		
~~**LAB4013**~~	~~0.7~~	~~0.000017~~	~~9.461633~~	~~5.26~~	~~1.5~~	~~0.11256~~	~~1.98~~	~~2.9518~~	~~1.6~~	~~0.19034~~	~~1.4~~	~~0.16~~	~~1837~~	~~70~~	~~1123~~	~~30~~	~~1395~~	~~25~~	~~61.1~~		
~~**LAB4013**~~	~~2.7~~	~~0.000002~~	~~4.089845~~	~~5.29~~	~~2.7~~	~~0.22655~~	~~2.39~~	~~6.0395~~	~~4.6~~	~~0.19160~~	~~2.9~~	~~0.88~~	~~3018~~	~~74~~	~~1129~~	~~60~~	~~1967~~	~~78~~	~~37.4~~		
~~**LAB4013**~~	~~2.8~~	~~0.000006~~	~~13.542132~~	~~7.67~~	~~1.4~~	~~0.15245~~	~~6.36~~	~~2.7581~~	~~7.5~~	~~0.13067~~	~~1.4~~	~~0.79~~	~~2332~~	~~202~~	~~792~~	~~21~~	~~1329~~	~~103~~	~~33.9~~		
~~**LAB4013**~~	~~0.5~~	~~0.000008~~	~~5.384134~~	~~11.97~~	~~5.2~~	~~0.12016~~	~~2.73~~	~~1.4132~~	~~5.1~~	~~0.08532~~	~~5.2~~	~~0.90~~	~~1952~~	~~91~~	~~527~~	~~52~~	~~891~~	~~59~~	~~27.0~~		
~~**LAB4013**~~	~~0.4~~	~~0.000003~~	~~10.610950~~	~~15.23~~	~~4.5~~	~~0.12580~~	~~2.98~~	~~1.1545~~	~~3.2~~	~~0.06738~~	~~5.7~~	~~0.88~~	~~2030~~	~~107~~	~~420~~	~~46~~	~~778~~	~~34~~	~~20.7~~		

LABXR-4014-48	2.0	1278.517252	89.63	2.86317	1.3	0.12241	0.6	5.9131	1.5	0.34958	1.3	0.42	1989.5	21	1932.4	45	1962.7	26	97.1	1989.5	21
LABXR-4014-26	0.8	4415.204257	51.82	2.80292	1.4	0.11987	0.6	5.9408	1.6	0.35755	1.4	0.73	1952.1	21	1970.0	49	1966.3	28	100.9	1952.1	21
LABXR-4014-35	1.1	4094.122471	97.84	3.10640	1.6	0.11710	1.4	5.2046	1.9	0.32136	1.4	0.12	1904.5	46	1796.1	43	1856.8	35	94.3	1904.5	46
LABXR-4014-41	1.0	1362.89378	202.08	3.04560	1.4	0.11653	0.4	5.2873	1.6	0.32905	1.4	0.87	1902.2	15	1833.3	46	1866.1	27	96.4	1902.2	15
LABXR-4014-18	1.4	3939.53602	69.14	2.98991	1.4	0.11655	0.7	5.3917	1.5	0.33486	1.4	0.40	1901.3	24	1861.7	44	1883.1	26	97.9	1901.3	24
LABXR-4014-47	2.0	40.78327279	2840.01	3.07046	1.4	0.11628	0.6	5.2436	1.6	0.32622	1.4	0.78	1898.0	20	1819.7	45	1858.9	27	95.9	1898.0	20

LABXR-4014-43	1.3	1401.222108	101.30	3.06199	1.6	0.11607	0.5	5.2472	1.6	0.32778	1.5	0.88	1894.9	17	1827.0	49	1859.2	29	96.4	1894.9	17
LABXR-4014-55	1.3	1997.614832	73.84	2.95282	1.4	0.11596	0.5	5.4672	1.5	0.33915	1.4	0.49	1893.0	19	1882.3	45	1894.9	26	99.4	1893.0	19
LABXR-4014-33	0.6	52522.94978	51.22	3.04253	1.4	0.11576	0.5	5.2540	1.6	0.32914	1.4	0.73	1890.0	19	1833.9	44	1860.7	27	97.0	1890.0	19
LABXR-4014-16	1.9	419.6405428	173.92	3.24602	1.8	0.11587	2.0	4.9544	2.0	0.30872	1.8	0.00	1887.9	68	1734.0	55	1810.8	33	91.8	1887.9	68
LABXR-4014-56	1.3	248.8113222	300.49	2.94039	1.3	0.11517	0.5	5.4490	1.5	0.34042	1.3	0.35	1880.7	19	1888.5	44	1892.2	26	100.4	1880.7	19
LABXR-4014-6	1.9	2608.243647	65.31	3.03653	1.5	0.11491	0.5	5.2400	1.6	0.33009	1.4	0.74	1876.5	20	1838.4	46	1858.4	27	98.0	1876.5	20
LABXR-4014-17	1.2	17406.61558	61.01	2.94424	1.6	0.11483	0.5	5.3490	2.0	0.33835	1.8	0.96	1875.4	18	1877.3	59	1872.7	39	100.1	1875.4	18
LABXR-4014-22	2.3	2719.520684	44.41	3.01028	1.3	0.11400	0.6	5.2360	1.5	0.33256	1.3	0.64	1862.0	20	1850.6	43	1860.4	29	99.4	1862.0	20
LABXR-4014-37	1.9	4036.100116	71.47	3.13404	1.3	0.11296	0.6	4.9855	1.5	0.31938	1.3	0.51	1845.2	22	1786.5	42	1816.4	26	96.8	1845.2	22
LABXR-4014-42	1.5	59.91004557	483.82	3.19495	1.4	0.11290	0.7	4.8780	1.6	0.31343	1.4	0.35	1843.3	27	1757.3	42	1797.8	26	95.3	1843.3	27
LABXR-4014-23	1.2	365.645523	320.46	3.19534	1.6	0.11312	1.2	4.9663	2.2	0.31378	1.5	0.04	1843.2	41	1758.8	45	1809.9	33	95.4	1843.2	41
LABXR-4014-58	1.1	38.40040664	1526.63	3.15639	1.3	0.11274	0.8	4.9770	1.6	0.31709	1.3	0.37	1840.7	27	1775.3	41	1814.5	27	96.4	1840.7	27
LABXR-4014-51	1.5	392.0570508	116.86	3.28495	1.5	0.11284	1.5	4.7754	1.8	0.30487	1.5	0.14	1839.3	51	1715.2	44	1779.5	30	93.3	1839.3	51
LABXR-4014-52	1.2	467.1324342	116.08	3.39244	1.7	0.11220	0.9	4.6138	1.9	0.29603	1.7	0.65	1831.4	33	1670.9	49	1749.8	31	91.2	1831.4	33
LABXR-4014-28	1.8	1282.844245	45.99	3.20138	1.4	0.11201	0.9	4.8488	1.8	0.31295	1.4	0.66	1828.2	30	1754.8	43	1791.6	28	96.0	1828.2	30
LABXR-4014-44	1.0	106.3862527	273.89	3.18949	1.4	0.11190	0.8	4.8599	1.5	0.31388	1.3	0.26	1827.1	27	1759.6	42	1794.8	26	96.3	1827.1	27
LABXR-4014-20	0.8	617.5874732	159.88	3.16147	1.5	0.11080	0.7	4.8676	1.6	0.31689	1.5	0.67	1810.5	26	1774.2	47	1796.1	27	98.0	1810.5	26
LABXR-4014-13	1.0	8790.179566	141.39	3.14992	1.4	0.11056	0.5	4.8678	1.5	0.31764	1.4	0.69	1807.3	19	1778.1	42	1796.4	26	98.4	1807.3	19
LABXR-4014-4	1.3	2772.676106	77.41	3.26164	1.9	0.10982	0.4	4.6953	1.8	0.30797	1.6	0.97	1795.3	14	1730.0	50	1764.9	31	96.4	1795.3	14
LABXR-4014-12	0.8	12592.18101	50.36	3.13324	1.6	0.10912	0.6	4.8253	1.6	0.31886	1.4	0.75	1787.4	25	1789.4	50	1788.2	28	100.1	1787.4	25
LABXR-4014-31	1.0	3415.637937	71.24	3.22455	1.3	0.10913	0.6	4.6615	1.5	0.31048	1.4	0.58	1782.9	20	1742.9	41	1762.1	28	97.8	1782.9	20
LABXR-4014-24	1.3	442.3083757	208.66	3.38415	1.7	0.10703	0.6	4.4025	1.7	0.29678	1.6	0.86	1747.3	20	1674.6	47	1711.2	30	95.8	1747.3	20
LABXR-4014-29	0.7	597.3900755	272.63	3.18616	1.3	0.10556	0.6	4.5966	1.5	0.31414	1.3	0.48	1721.8	22	1760.9	41	1748.1	26	102.3	1721.8	22
LABXR-4014-49	1.2	503.9592002	114.42	3.35602	1.4	0.10454	0.8	4.3334	1.7	0.29836	1.4	0.30	1702.2	30	1682.9	40	1698.5	27	98.9	1702.2	30
LABXR-4014-50	0.1	171.0263846	2603.83	3.21549	2.2	0.10410	0.6	4.5088	2.1	0.31280	2.0	0.95	1697.0	21	1753.5	63	1730.8	36	103.3	1697.0	21
LABXR-4014-14	2.0	14848.43649	51.44	3.89354	1.5	0.09907	1.2	3.5309	1.8	0.25737	1.4	0.24	1600.5	41	1476.1	38	1532.6	28	92.2	1600.5	41
LABXR-4014-32	0.5	24481.23784	41.01	3.68744	1.3	0.09790	0.5	3.6651	1.5	0.27145	1.3	0.56	1582.6	20	1548.0	37	1563.4	24	97.8	1582.6	20
LABXR-4014-39	0.6	2510.205163	55.04	3.74204	1.3	0.09770	0.7	3.6019	1.6	0.26759	1.4	0.57	1577.6	26	1528.4	37	1549.1	26	96.9	1577.6	26
LABXR-4014-19	2.9	63.5087544	882.20	3.77504	1.7	0.09773	1.3	3.6004	2.1	0.26560	1.6	0.56	1576.0	49	1518.1	45	1547.9	34	96.3	1576.0	49
LABXR-4014-38	1.1	1335.800573	69.10	3.78939	1.4	0.09770	0.9	3.5560	1.7	0.26442	1.4	0.33	1575.7	35	1512.1	38	1538.8	26	96.0	1575.7	35
LABXR-4014-60	1.2	1075.92092	105.49	3.60390	1.4	0.09682	0.6	3.7159	1.5	0.27789	1.4	0.51	1561.1	24	1580.5	39	1574.4	24	101.2	1561.1	24
LABXR-4014-21	1.5	930.5465703	48.53	3.76776	1.4	0.09687	0.8	3.5726	1.7	0.26588	1.4	0.18	1560.4	32	1519.6	38	1542.4	27	97.4	1560.4	32

LABXR-4014-54	0.9	1312.229394	89.43	3.61095	1.6	0.09638	0.6	3.7234	1.6	0.27762	1.5	0.77	1553.0	23	1579.0	42	1575.6	27	101.7	1553.0	23
LABXR-4014-59	2.5	478.2012793	177.11	3.64889	1.3	0.09608	0.6	3.6573	1.5	0.27434	1.3	0.52	1547.1	21	1562.6	37	1561.7	24	101.0	1547.1	21
LABXR-4014-36	1.0	24421.10508	48.78	3.82935	1.4	0.09580	0.6	3.4386	1.5	0.26153	1.4	0.71	1541.9	22	1497.4	38	1512.9	24	97.1	1541.9	22
LABXR-4014-7	1.6	45.70127632	1223.76	3.74950	1.4	0.09546	0.8	3.5211	1.6	0.26722	1.4	0.26	1532.9	32	1526.4	38	1531.4	25	99.6	1532.9	32
LABXR-4014-5	0.7	7939.093438	56.01	3.78068	1.5	0.09452	1.2	3.4605	1.7	0.26490	1.5	0.19	1514.5	44	1514.7	41	1517.7	27	100.0	1514.5	44
LABXR-4014-30	0.7	2991.237349	64.07	3.95763	1.4	0.09114	0.6	3.1963	1.5	0.25290	1.4	0.56	1447.8	22	1453.3	36	1456.0	24	100.4	1453.3	36
LABXR-4014-57	0.8	1231.24415	45.12	4.60417	1.7	0.08410	1.2	2.5409	1.8	0.21798	1.7	0.40	1288.7	47	1270.8	38	1283.0	25	98.6	1270.8	38
LABXR-4014-25	0.9	1529.016337	57.01	4.73722	1.4	0.08064	1.0	2.3626	1.7	0.21138	1.4	0.29	1207.9	39	1236.0	32	1230.7	24	102.3	1236.0	32
LABXR-4014-10	1.1	256.1972686	67.00	6.73339	1.4	0.06989	1.5	1.4353	2.0	0.14886	1.4	0.21	910.9	62	894.4	24	902.1	24	98.2	894.4	24

Data not used due to high discordance

~~**LABXR-4014-27**~~	~~1.4~~	~~2104.370895~~	~~54.36~~	~~3.36487~~	~~1.7~~	~~0.11936~~	~~1.5~~	~~4.9127~~	~~2.7~~	~~0.29806~~	~~1.7~~	~~0.84~~	~~1941.1~~	~~50~~	~~1681.2~~	~~51~~	~~1801.0~~	~~42~~	~~86.6~~		
~~**LABXR-4014-53**~~	~~1.7~~	~~481.1629897~~	~~226.61~~	~~3.99790~~	~~2.7~~	~~0.11384~~	~~0.7~~	~~4.0368~~	~~2.4~~	~~0.25504~~	~~2.3~~	~~0.94~~	~~1858.7~~	~~25~~	~~1462.2~~	~~61~~	~~1635.9~~	~~41~~	~~78.7~~		
~~**LABXR-4014-8**~~	~~1.5~~	~~3207.077971~~	~~131.66~~	~~3.85027~~	~~1.7~~	~~0.12291~~	~~0.8~~	~~4.4172~~	~~1.7~~	~~0.26055~~	~~1.7~~	~~0.80~~	~~1996.2~~	~~31~~	~~1492.2~~	~~45~~	~~1714.7~~	~~29~~	~~74.8~~		
~~**LABXR-4014-46**~~	~~1.0~~	~~4668.50359~~	~~99.64~~	~~4.53835~~	~~3.2~~	~~0.10926~~	~~0.8~~	~~3.3596~~	~~2.9~~	~~0.22243~~	~~2.8~~	~~0.96~~	~~1785.4~~	~~29~~	~~1293.8~~	~~67~~	~~1492.4~~	~~47~~	~~72.5~~		
~~**LABXR-4014-34**~~	~~1.1~~	~~208300.9971~~	~~60.83~~	~~6.27020~~	~~2.9~~	~~0.08702~~	~~0.8~~	~~1.9602~~	~~2.6~~	~~0.16367~~	~~2.6~~	~~0.94~~	~~1357.1~~	~~29~~	~~975.6~~	~~47~~	~~1096.8~~	~~36~~	~~71.9~~		
~~**LABXR-4014-9**~~	~~0.5~~	~~919.0752292~~	~~100.32~~	~~4.59181~~	~~2.7~~	~~0.11070~~	~~1.5~~	~~3.3678~~	~~3.1~~	~~0.21967~~	~~2.5~~	~~0.86~~	~~1806.2~~	~~53~~	~~1279.3~~	~~59~~	~~1492.9~~	~~50~~	~~70.8~~		
~~**LABXR-4014-15**~~	~~0.7~~	~~167.0090947~~	~~232.41~~	~~5.35318~~	~~4.1~~	~~0.11445~~	~~4.9~~	~~2.9072~~	~~3.7~~	~~0.19341~~	~~3.6~~	~~0.23~~	~~1802.3~~	~~172~~	~~1137.2~~	~~75~~	~~1392.3~~	~~62~~	~~63.1~~		
~~**LABXR-4014-40**~~	~~3.4~~	~~1207.280439~~	~~46.57~~	~~6.95745~~	~~3.1~~	~~0.13953~~	~~1.1~~	~~2.8756~~	~~3.1~~	~~0.14972~~	~~3.3~~	~~0.93~~	~~2223.5~~	~~41~~	~~897.0~~	~~55~~	~~1365.7~~	~~46~~	~~40.3~~		
~~**LABXR-4014-45**~~	~~1.0~~	~~287.8598748~~	~~14.65~~	~~6.42231~~	~~5.0~~	~~0.17536~~	~~1.8~~	~~4.0016~~	~~4.1~~	~~0.16869~~	~~5.0~~	~~0.93~~	~~2597.5~~	~~62~~	~~999.5~~	~~91~~	~~1618.2~~	~~65~~	~~38.5~~		
~~**LABXR-4014-11**~~	~~1.3~~	~~1063.994641~~	~~165.25~~	~~7.37264~~	~~2.7~~	~~0.13959~~	~~1.6~~	~~2.6265~~	~~2.1~~	~~0.13766~~	~~2.7~~	~~0.76~~	~~2210.2~~	~~55~~	~~830.3~~	~~42~~	~~1305.1~~	~~32~~	~~37.6~~		

Amostra Acre 39

			Ratios									Rho	Ages (Ma)						% conc [1]	Best age	2s
Spot number	Th/U	206Pb/204Pb	1s	238U/206Pb	1s	207Pb/206Pb	1s	207Pb/235U	1s	206Pb/238U	1s		207Pb/206Pb	2s	206Pb/238U	2s	207Pb/235U	2s			
			(%)		(%)		(%)		(%)		(%)			(abs)		(abs)		(abs)			(abs)
LAB4018	2.0	0.00017	134.44	1.49	1.0	0.27059	0.66	24.8213	0.8	0.66912	1.0	0.36	3309	21	3302	50	3301	16	99.8	3309	21
LAB4018	2.9	0.00002	12.27	3.05	0.9	0.12551	1.31	5.6809	1.6	0.32760	0.9	0.90	2034	47	1827	29	1928	27	89.8	2034	47
LAB4018	1.4	0.00173	79.03	2.71	0.9	0.12488	0.59	6.3499	0.8	0.36835	0.9	0.46	2026	21	2022	32	2025	14	99.8	2026	21
LAB4018	1.2	0.00014	22.91	2.77	1.0	0.12170	1.09	6.0637	1.1	0.36165	1.0	0.10	1980	38	1990	34	1985	19	100.5	1980	38
LAB4019	4.0	0.00007	16.55	2.96	1.0	0.11951	0.65	5.5745	0.8	0.33784	1.0	0.56	1948	23	1876	31	1912	15	96.3	1948	23
LAB4018	3.0	0.00002	898.63	3.02	1.0	0.11876	0.60	5.4175	1.0	0.33074	1.0	0.97	1937	21	1842	32	1888	17	95.1	1937	21
LAB4018	0.2	0.00214	67.75	2.93	0.9	0.11779	0.61	5.5333	0.8	0.34096	0.9	0.28	1922	22	1891	30	1906	14	98.4	1922	22
LAB4018	1.4	0.00118	17.99	2.85	0.9	0.11758	0.58	5.6948	0.8	0.35107	0.9	0.73	1919	21	1940	31	1931	14	101.1	1919	21
LAB4018	2.8	0.00466	88.60	2.94	1.1	0.11695	0.62	5.4786	0.9	0.33981	1.1	0.89	1909	22	1886	35	1897	15	98.8	1909	22

LAB4018	3.7	0.00004	515.24	3.00	1.0	0.11634	0.78	5.3351	0.9	0.33356	1.0	0.19	1900	28	1856	31	1874	15	97.7	1900	28
LAB4019	1.8	0.00015	133.66	2.93	1.1	0.11627	1.00	5.4830	0.9	0.34144	1.1	0.08	1898	36	1894	37	1898	16	99.7	1898	36
LAB4018	2.9	0.00001	14349.55	2.95	0.9	0.11610	0.61	5.4355	0.8	0.33894	0.9	0.62	1896	22	1882	30	1890	14	99.2	1896	22
LAB4018	2.5	0.00192	79.62	2.92	1.0	0.11586	0.66	5.4653	0.8	0.34213	1.0	0.21	1892	24	1897	31	1895	13	100.2	1892	24
LAB4018	3.0	0.00033	135.24	3.05	1.0	0.11570	0.59	5.2159	0.9	0.32827	1.0	0.92	1890	21	1830	33	1855	16	96.8	1890	21
LAB4018	3.5	0.00091	72.74	2.99	0.9	0.11566	0.65	5.3376	0.8	0.33416	0.9	0.32	1889	23	1858	29	1875	14	98.4	1889	23
LAB4018	1.6	0.00341	92.76	2.97	1.0	0.11519	0.62	5.3350	0.8	0.33678	1.0	0.69	1882	22	1871	32	1874	14	99.4	1882	22
LAB4018	3.1	0.00042	20.67	2.97	1.0	0.11510	0.58	5.3453	0.9	0.33668	1.0	0.94	1881	21	1871	32	1876	15	99.5	1881	21
LAB4018	1.0	0.00016	9.69	3.19	1.1	0.11494	0.63	4.9824	0.9	0.31398	1.1	0.85	1878	23	1760	33	1816	15	93.7	1878	23
LAB4018	3.7	0.00056	25.66	2.97	1.1	0.11462	0.60	5.3150	0.9	0.33699	1.1	0.91	1873	22	1872	35	1871	16	99.9	1873	22
LAB4018	1.9	0.00031	149.09	3.06	0.9	0.11442	0.72	5.1671	0.9	0.32725	0.9	0.04	1870	26	1825	30	1847	16	97.6	1870	26
LAB4018	1.4	0.00302	77.70	3.07	0.9	0.11364	0.60	5.0836	0.8	0.32586	0.9	0.70	1858	22	1818	30	1833	14	97.9	1858	22
LAB4018	3.4	0.00056	107.98	3.21	1.0	0.11302	0.72	4.8550	0.9	0.31141	1.0	0.47	1847	26	1748	29	1794	15	94.6	1847	26
LAB4018	2.3	0.00010	5.17	3.19	1.0	0.11297	0.67	4.8817	0.8	0.31398	1.0	0.33	1847	24	1760	30	1799	13	95.3	1847	24
LAB4018	3.8	0.00032	94.68	3.12	1.0	0.11189	0.89	4.9396	0.9	0.32012	1.0	0.13	1829	32	1790	31	1809	15	97.9	1829	32
LAB4018	2.4	0.00024	29.04	3.06	1.0	0.11182	0.88	5.0385	1.1	0.32636	1.0	0.56	1828	32	1821	30	1826	19	99.6	1828	32
LAB4018	2.0	0.00015	19.34	3.28	0.9	0.11173	0.60	4.6876	0.8	0.30460	0.9	0.75	1827	22	1714	28	1765	14	93.8	1827	22
LAB4018	2.7	0.00032	95.46	3.05	1.0	0.11157	0.85	5.0430	0.9	0.32775	1.0	0.02	1824	31	1827	32	1826	15	100.2	1824	31
LAB4018	2.0	0.00187	53.70	3.30	1.0	0.11150	0.59	4.6622	0.9	0.30335	1.0	0.89	1823	22	1708	30	1760	15	93.7	1823	22
LAB4018	1.7	0.00010	143.40	3.14	1.1	0.11129	0.68	4.8608	1.0	0.31826	1.1	0.75	1819	25	1781	33	1795	16	97.9	1819	25
LAB4018	2.3	0.00053	31.91	3.14	1.1	0.11106	0.76	4.8733	0.9	0.31853	1.0	0.41	1816	28	1783	32	1798	14	98.2	1816	28
LAB4018	2.6	0.00020	176.36	3.14	1.0	0.11096	0.62	4.8852	0.9	0.31873	1.0	0.92	1814	23	1784	30	1800	16	98.3	1814	23
LAB4018	3.0	0.00013	159.90	3.10	1.0	0.11069	0.59	4.9075	0.9	0.32288	1.0	0.72	1810	21	1804	32	1803	14	99.7	1810	21
LAB4018	3.0	0.00011	11.46	3.19	1.0	0.11059	0.63	4.7527	0.9	0.31329	1.0	0.82	1808	23	1757	31	1776	15	97.2	1808	23
LAB4018	3.1	0.04849	96.53	3.10	1.0	0.11058	0.61	4.9079	0.9	0.32283	1.0	0.82	1808	22	1803	32	1804	14	99.7	1808	22
LAB4018	2.3	0.00114	42.90	3.07	1.0	0.11049	0.64	4.9728	0.9	0.32609	1.0	0.67	1807	23	1819	31	1815	15	100.7	1807	23
LAB4018	2.0	0.00029	164.51	3.06	0.9	0.11033	0.72	4.9691	0.9	0.32635	0.9	0.00	1804	26	1821	29	1814	15	100.9	1804	26
LAB4018	2.7	0.00003	755.26	3.12	1.0	0.11029	0.61	4.8539	0.9	0.32013	1.0	0.88	1803	22	1790	31	1794	15	99.3	1803	22
LAB4018	2.9	0.00004	11.63	3.46	1.0	0.10949	0.64	4.3740	0.8	0.28925	1.0	0.79	1790	23	1638	30	1707	13	91.5	1790	23
LAB4018	2.8	0.00036	72.85	3.26	1.0	0.10860	0.70	4.5998	0.9	0.30725	1.0	0.49	1775	25	1727	29	1749	15	97.3	1775	25
LAB4018	1.3	0.00044	36.95	3.22	1.0	0.10798	0.59	4.6280	0.8	0.31101	1.0	0.78	1765	22	1746	29	1754	14	98.9	1765	22
LAB4018	2.2	0.00034	130.86	3.24	0.9	0.10787	0.65	4.5868	0.9	0.30849	0.9	0.56	1763	24	1733	28	1747	14	98.3	1763	24
LAB4018	1.7	0.00050	19.07	3.33	0.9	0.10658	0.65	4.3950	0.9	0.30054	0.9	0.57	1741	24	1694	28	1711	14	97.3	1741	24
LAB4018	8.7	0.00026	53.47	3.72	1.0	0.09878	1.48	3.6588	1.3	0.26896	1.0	0.34	1598	54	1536	28	1562	21	96.1	1598	54
LAB4018	1.9	0.00933	92.09	3.74	1.0	0.09843	0.83	3.6229	1.0	0.26713	1.0	0.38	1593	31	1526	28	1554	15	95.8	1593	31
LAB4018	6.3	0.00001	926.42	3.86	1.1	0.09800	0.73	3.4996	0.9	0.25889	1.2	0.78	1585	28	1484	31	1527	14	93.6	1585	28
LAB4018	1.4	0.00003	900.91	3.69	0.9	0.09800	0.69	3.6566	0.8	0.27074	0.9	0.27	1585	26	1545	26	1562	14	97.4	1585	26
LAB4018	3.0	0.00163	80.71	4.05	1.1	0.09763	0.86	3.3023	0.8	0.24683	1.1	0.20	1578	32	1422	29	1482	13	90.1	1578	32
LAB4018	3.0	0.00086	81.33	3.70	1.2	0.09629	0.85	3.5763	1.1	0.27077	1.2	0.70	1552	32	1545	34	1544	18	99.5	1552	32
LAB4018	1.8	0.00026	23.81	3.87	1.0	0.09626	0.75	3.4196	0.9	0.25809	0.9	0.37	1552	28	1480	25	1509	14	95.4	1552	28
LAB4018	2.9	0.00055	140.04	3.73	1.0	0.09614	0.75	3.5586	1.0	0.26791	1.0	0.52	1550	28	1530	26	1540	15	98.7	1550	28
LAB4018	3.3	0.20388	96.05	3.92	1.0	0.09573	0.69	3.3514	0.9	0.25517	1.0	0.52	1541	26	1465	25	1493	14	95.1	1541	26
LAB4018	1.9	0.00087	30.44	3.78	1.1	0.09535	0.69	3.4776	1.0	0.26433	1.0	0.82	1534	26	1512	28	1522	16	98.6	1534	26
LAB4019	5.5	0.00004	132.80	3.70	1.2	0.09508	1.42	3.5430	1.6	0.27046	1.3	0.41	1527	52	1543	34	1536	25	101.1	1527	52
LAB4018	2.6	0.00009	148.24	3.76	1.0	0.09497	0.75	3.4792	0.8	0.26593	1.0	0.09	1526	28	1520	27	1522	13	99.6	1526	28
LAB4018	2.5	0.00158	68.38	3.75	1.2	0.09418	0.71	3.4624	0.9	0.26652	1.2	0.80	1511	27	1523	32	1519	15	100.8	1511	27
LAB4018	1.1	0.00035	92.47	3.81	0.9	0.09365	0.68	3.3932	0.8	0.26261	0.9	0.09	1500	26	1503	25	1503	13	100.2	1503	25
LAB4018	1.3	0.00051	52.02	3.93	1.0	0.09243	0.68	3.2487	0.8	0.25449	1.0	0.52	1475	26	1462	26	1469	12	99.1	1462	26
LAB4018	2.3	0.00055	85.72	4.22	1.0	0.08791	0.89	2.8723	1.0	0.23685	1.0	0.38	1379	34	1370	26	1375	15	99.4	1370	26

LAB4018	0.8	0.00027	55.88	4.33	1.0	0.08673	0.71	2.7676	0.8	0.23110	1.0	0.09	1353	27	1340	23	1347	12	99.0	1340	23
LAB4018	1.0	0.00057	44.00	4.15	1.1	0.08564	0.98	2.8364	0.9	0.24088	1.2	0.24	1329	38	1391	29	1365	14	104.7	1391	29
LAB4018	2.6	0.00017	55.26	4.87	1.0	0.08150	0.77	2.3029	0.8	0.20521	1.0	0.12	1232	30	1203	21	1213	12	97.7	1203	21
LAB4018	0.4	0.00020	65.76	4.97	1.0	0.08054	0.63	2.2364	0.8	0.20139	1.0	0.66	1209	25	1183	21	1192	12	97.8	1183	21
LAB4018	0.8	0.00028	47.40	6.01	1.0	0.07663	0.85	1.7577	1.1	0.16648	1.0	0.55	1110	34	993	19	1030	14	89.4	993	19
LAB4018	2.5	0.00065	129.91	5.78	1.0	0.07599	0.76	1.8140	1.0	0.17322	1.0	0.61	1093	31	1030	19	1050	13	94.2	1030	19
LAB4018	3.8	0.00004	256.30	5.83	1.1	0.07523	0.80	1.7656	1.0	0.17164	1.1	0.09	1073	32	1021	20	1033	13	95.2	1021	20
LAB4018	1.0	0.00032	247.27	5.91	1.0	0.07339	0.68	1.7129	0.9	0.16926	1.0	0.74	1024	27	1008	19	1013	12	98.5	1008	19
LAB4018	1.6	0.00019	75.06	6.03	1.1	0.07291	0.81	1.6660	0.9	0.16601	1.0	0.26	1010	34	990	19	996	11	98.0	990	19
LAB4018	1.6	0.00005	80.96	7.10	1.4	0.06747	1.25	1.3120	1.1	0.14122	1.4	0.32	848	52	851	23	851	12	100.4	851	23

Data not used due to high discordance

~~**LAB4018**~~	~~1.9~~	~~0.00005~~	~~5.20~~	~~4.49~~	~~1.1~~	~~0.10127~~	~~0.72~~	~~3.1073~~	~~1.3~~	~~0.22282~~	~~1.1~~	~~0.95~~	~~1647~~	~~27~~	~~1297~~	~~26~~	~~1434~~	~~19~~	~~78.8~~	
~~**LAB4018**~~	~~3.2~~	~~0.00002~~	~~7.39~~	~~3.85~~	~~1.0~~	~~0.12594~~	~~1.22~~	~~4.5087~~	~~1.4~~	~~0.25977~~	~~1.0~~	~~0.41~~	~~2041~~	~~43~~	~~1489~~	~~27~~	~~1732~~	~~23~~	~~72.9~~	
~~**LAB4018**~~	~~1.2~~	~~0.00003~~	~~2.45~~	~~3.67~~	~~1.0~~	~~0.13497~~	~~0.75~~	~~5.0797~~	~~1.0~~	~~0.27256~~	~~1.0~~	~~0.64~~	~~2163~~	~~26~~	~~1554~~	~~27~~	~~1833~~	~~17~~	~~71.8~~	
~~**LAB4018**~~	~~6.7~~	~~0.00005~~	~~15.53~~	~~5.26~~	~~2.1~~	~~0.09883~~	~~1.46~~	~~2.5867~~	~~1.4~~	~~0.19055~~	~~2.1~~	~~0.73~~	~~1600~~	~~53~~	~~1124~~	~~43~~	~~1297~~	~~20~~	~~70.3~~	
~~**LAB4018**~~	~~2.0~~	~~0.00002~~	~~3.43~~	~~5.06~~	~~1.4~~	~~0.10921~~	~~0.67~~	~~2.9769~~	~~1.5~~	~~0.19773~~	~~1.4~~	~~0.97~~	~~1785~~	~~24~~	~~1163~~	~~31~~	~~1401~~	~~23~~	~~65.1~~	
~~**LAB4018**~~	~~0.4~~	~~0.00001~~	~~2.72~~	~~4.99~~	~~1.2~~	~~0.14073~~	~~1.42~~	~~3.8899~~	~~1.9~~	~~0.20066~~	~~1.2~~	~~0.73~~	~~2234~~	~~48~~	~~1179~~	~~26~~	~~1611~~	~~31~~	~~52.8~~	
~~**LAB4018**~~	~~1.9~~	~~0.00001~~	~~9.06~~	~~6.52~~	~~1.3~~	~~0.11547~~	~~1.87~~	~~2.4444~~	~~2.0~~	~~0.15342~~	~~1.3~~	~~0.29~~	~~1884~~	~~68~~	~~920~~	~~23~~	~~1255~~	~~28~~	~~48.8~~	
~~**LAB4018**~~	~~2.4~~	~~0.00001~~	~~6.17~~	~~5.62~~	~~1.7~~	~~0.15034~~	~~1.73~~	~~3.6878~~	~~1.1~~	~~0.17845~~	~~1.7~~	~~0.07~~	~~2345~~	~~60~~	~~1058~~	~~32~~	~~1568~~	~~17~~	~~45.1~~	
~~**LAB4018**~~	~~1.5~~	~~0.00001~~	~~3.88~~	~~6.92~~	~~1.2~~	~~0.12337~~	~~1.54~~	~~2.4588~~	~~2.2~~	~~0.14460~~	~~1.2~~	~~0.83~~	~~2003~~	~~55~~	~~871~~	~~20~~	~~1259~~	~~32~~	~~43.5~~	
~~**LAB4018**~~	~~2.1~~	~~0.00001~~	~~7.45~~	~~8.67~~	~~1.1~~	~~0.11157~~	~~1.81~~	~~1.7748~~	~~2.0~~	~~0.11537~~	~~1.1~~	~~0.33~~	~~1819~~	~~66~~	~~704~~	~~15~~	~~1035~~	~~26~~	~~38.7~~	
~~**LAB4018**~~	~~3.2~~	~~0.00000~~	~~4.48~~	~~8.68~~	~~1.5~~	~~0.15702~~	~~1.77~~	~~2.4970~~	~~2.2~~	~~0.11546~~	~~1.6~~	~~0.62~~	~~2420~~	~~59~~	~~704~~	~~21~~	~~1270~~	~~33~~	~~29.1~~	

Amostra Acre 49

		Ratios									Ages								
Spot number	**Th/U**	**$^{206}Pb/^{204}Pb$**	**1σ%**	**$^{207}Pb/^{206}Pb$**	**1σ %**	**$^{207}Pb/^{235}U$**	**1σ %**	**$^{206}Pb/^{238}U$**	**1σ %**	**Rho**	**$^{207}Pb/^{206}Pb$**	**2σ abs**	**$^{206}Pb/^{238}U$**	**2σ abs**	**$^{207}Pb/^{235}U$**	**2σ abs**	**% conc1**	**Best Age**	**2σ abs**
003-ZR1	0.282	22851	20.95	0.07076	0.48	1.483	0.98	0.1520	0.77	0.79	951	20	912	13	923	12	95.94	912	13
004-ZR2	0.379	9254	22.03	0.07220	0.92	1.530	1.57	0.1536	1.21	0.77	992	37	921	21	942	19	92.91	921	21
006-ZR4	0.276	73869	6.07	0.07075	0.35	1.518	0.82	0.1556	0.64	0.79	950	14	933	11	938	10	98.15	933	11
007-ZR5	0.235	114961	12.56	0.07167	0.33	1.546	0.87	0.1565	0.71	0.82	977	13	937	12	949	11	95.95	937	12
008-ZR6	0.306	150229	41.84	0.07042	0.58	1.521	1.22	0.1566	1.01	0.83	940	24	938	18	939	15	99.75	938	18
009-ZR7	0.716	75528	16.71	0.06920	0.36	1.499	0.88	0.1571	0.71	0.81	905	15	940	12	930	11	103.96	940	12
010-ZR8	0.278	58613	15.36	0.07240	0.44	1.581	0.81	0.1583	0.57	0.70	997	18	947	10	963	10	94.99	947	10
012-ZR10N	0.508	64705	72.13	0.07166	0.98	1.566	1.36	0.1585	0.87	0.64	976	40	948	15	957	17	97.14	948	15
015-ZR10B	0.317	44571	15.89	0.07213	0.51	1.602	0.93	0.1611	0.68	0.73	990	21	963	12	971	12	97.29	963	12
016-ZR11	0.311	31096	18.02	0.07047	0.54	1.579	1.11	0.1625	0.89	0.81	942	22	970	16	962	14	103.02	970	16
017-ZR12	0.246	51344	8.81	0.07060	0.47	1.583	0.90	0.1626	0.68	0.75	946	19	971	12	964	11	102.67	971	12
018-ZR13	0.419	46625	23.77	0.07204	0.42	1.636	0.92	0.1647	0.73	0.79	987	17	983	13	984	12	99.55	983	13
020-ZR15	0.280	81121	12.54	0.07198	0.47	1.652	0.91	0.1664	0.69	0.76	986	19	993	13	990	11	100.71	993	13
022-ZR17	0.296	91671	16.93	0.07248	0.42	1.666	1.00	0.1667	0.83	0.83	999	17	994	15	996	13	99.47	994	15
023-ZR18	0.291	86760	3.78	0.07224	0.42	1.662	0.81	0.1669	0.58	0.71	993	17	995	11	994	10	100.21	995	11
024-ZR19	0.364	76771	83.07	0.07261	0.84	1.645	1.42	0.1643	1.07	0.76	1003	34	980	20	987	18	97.75	1003	34

028-ZR21	0.197	161458	13.55	0.07284	0.33	1.606	1.09	0.1599	0.98	0.89	1009	13	956	17	972	14	94.72	1009	13
030-ZR23	0.280	27929	17.94	0.07295	0.58	1.700	1.18	0.1690	0.95	0.81	1013	23	1007	18	1009	15	99.42	1013	23
031-ZR24	0.381	112508	12.14	0.07297	0.46	1.609	1.00	0.1599	0.80	0.81	1013	18	956	14	974	12	94.40	1013	18
033-ZR26N	0.369	260952	83.76	0.07299	0.47	1.595	0.90	0.1585	0.67	0.75	1014	19	948	12	968	11	93.54	1014	19
035-ZR27	0.217	67998	11.34	0.07311	0.52	1.646	0.92	0.1632	0.67	0.72	1017	21	975	12	988	12	95.86	1017	21
040-ZR30	0.407	37930	25.47	0.07313	0.67	1.653	1.17	0.1639	0.89	0.76	1018	27	979	16	991	15	96.17	1018	27
041-ZR31	0.296	122944	1.51	0.07326	0.75	1.617	1.02	0.1601	0.58	0.57	1021	30	957	10	977	13	93.73	1021	30
042-ZR32	0.227	85592	21.74	0.07329	0.41	1.693	0.73	0.1676	0.48	0.66	1022	16	999	9	1006	9	97.72	1022	16
043-ZR33	0.177	66014	13.34	0.07337	0.50	1.704	0.90	0.1685	0.66	0.72	1024	20	1004	12	1010	12	98.00	1024	20
046-ZR35	0.174	177518	33.41	0.07379	0.36	1.698	0.78	0.1669	0.59	0.75	1036	15	995	11	1008	10	96.08	1036	15
047-ZR36	0.390	156536	16.46	0.07421	0.34	1.755	0.87	0.1715	0.70	0.81	1047	14	1020	13	1029	11	97.45	1047	14
048-ZR37	0.257	65425	19.97	0.07829	0.42	2.131	0.86	0.1974	0.66	0.76	1154	17	1161	14	1159	12	100.60	1154	17
053-ZR38	0.303	71391	21.51	0.07850	0.30	2.215	0.80	0.2047	0.64	0.80	1160	12	1200	14	1186	11	103.51	1160	12
054-ZR39	0.253	67045	16.56	0.07868	0.43	2.021	0.89	0.1863	0.69	0.77	1164	17	1101	14	1123	12	94.59	1164	17
055-ZR40	0.160	167011	3.31	0.07881	0.35	2.070	0.80	0.1905	0.62	0.77	1167	14	1124	13	1139	11	96.31	1167	14
056-ZR41	0.219	158451	3.37	0.07994	0.30	2.220	0.90	0.2014	0.76	0.85	1195	12	1183	16	1187	12	98.95	1195	12
058-ZR43	0.297	292395	2.48	0.08092	0.35	2.317	0.81	0.2077	0.62	0.77	1220	14	1216	14	1218	11	99.74	1220	14
059-ZR44	0.197	120609	15.74	0.08256	0.43	2.331	0.91	0.2048	0.71	0.78	1259	17	1201	16	1222	13	95.41	1259	17
060-ZR45	0.341	579992	4.15	0.08265	0.33	2.205	0.78	0.1934	0.60	0.77	1261	13	1140	12	1183	11	90.40	1261	13
061-ZR46	0.317	90418	19.17	0.08329	0.37	2.445	1.02	0.2129	0.87	0.86	1276	14	1244	20	1256	15	97.49	1276	14
062-ZR47	0.177	139247	4.86	0.08369	0.42	2.565	0.88	0.2223	0.67	0.77	1285	16	1294	16	1291	13	100.67	1285	16
065-ZR48	0.235	19577	19.15	0.08910	0.47	2.777	1.03	0.2261	0.83	0.81	1406	18	1314	20	1349	15	93.43	1406	18
067-ZR50	0.591	76758	15.98	0.09411	0.39	3.143	0.91	0.2422	0.74	0.81	1510	15	1398	19	1443	14	92.59	1510	15
068-ZR51	0.605	113683	16.98	0.09439	0.26	3.426	0.80	0.2633	0.66	0.82	1516	10	1507	18	1510	12	99.38	1516	10
069-ZR52N	0.503	61552	15.46	0.09456	0.37	3.545	0.96	0.2719	0.81	0.84	1519	14	1550	22	1537	15	102.04	1519	14
071-ZR53	0.721	33252	14.03	0.09545	0.57	3.438	1.09	0.2612	0.85	0.78	1537	21	1496	23	1513	17	97.34	1537	21
072-ZR54	0.113	204189	26.16	0.10250	0.38	4.012	1.08	0.2839	0.94	0.87	1670	14	1611	27	1637	17	96.46	1670	14
073-ZR55	0.336	285030	2.87	0.10382	0.33	4.180	0.82	0.2920	0.65	0.79	1693	12	1652	19	1670	13	97.53	1693	12
074-ZR56	0.299	279128	8.71	0.10585	0.32	4.452	0.97	0.3050	0.83	0.86	1729	12	1716	25	1722	16	99.24	1729	12
077-ZR57	0.412	102867	13.13	0.10587	0.37	4.538	0.73	0.3109	0.51	0.70	1730	14	1745	16	1738	12	100.89	1730	14
078-ZR58	0.893	165338	37.07	0.10699	0.45	4.477	0.96	0.3035	0.77	0.80	1749	16	1708	23	1727	16	97.69	1749	16
079-ZR59	0.576	153355	22.48	0.10818	0.33	4.697	0.83	0.3149	0.67	0.81	1769	12	1765	21	1767	14	99.76	1769	12
080-ZR60	0.598	171809	15.23	0.10953	0.25	4.855	0.77	0.3215	0.63	0.81	1792	9	1797	20	1795	13	100.29	1792	9
081-ZR61	0.914	109646	14.34	0.10957	0.35	4.616	0.83	0.3055	0.65	0.79	1792	13	1719	20	1752	14	95.89	1792	13
083-ZR62B	0.390	68569	14.86	0.10962	0.34	4.851	0.93	0.3209	0.79	0.84	1793	12	1794	25	1794	16	100.06	1793	12
084-ZR63	0.349	234132	13.95	0.10974	0.28	4.800	0.80	0.3172	0.66	0.82	1795	10	1776	20	1785	13	98.93	1795	10
089-ZR66	0.473	232723	19.46	0.11006	0.37	4.958	0.90	0.3267	0.73	0.81	1800	13	1822	23	1812	15	101.22	1800	13
090-ZR67	0.596	154130	12.81	0.11048	0.35	4.849	1.00	0.3183	0.86	0.86	1807	13	1781	27	1793	17	98.57	1807	13
092-ZR69	0.079	252196	12.04	0.11077	0.28	4.786	0.81	0.3134	0.66	0.82	1812	10	1757	20	1783	14	96.97	1812	10
093-ZR70	0.537	83291	30.37	0.11084	0.33	4.639	0.88	0.3035	0.73	0.83	1813	12	1709	22	1756	15	94.24	1813	12
094-ZR71	0.434	168120	17.13	0.11213	0.33	5.298	0.79	0.3426	0.62	0.78	1834	12	1899	20	1868	13	103.55	1834	12
095-ZR72	0.680	273832	11.81	0.11227	0.32	4.834	0.83	0.3122	0.67	0.81	1836	12	1752	21	1791	14	95.38	1836	12
096-ZR73	0.576	30419	55.03	0.11416	0.93	5.121	1.34	0.3253	0.89	0.66	1867	33	1816	28	1840	23	97.28	1867	33
097-ZR74	0.397	134174	15.25	0.11458	0.29	5.093	0.80	0.3224	0.64	0.81	1873	10	1801	20	1835	14	96.16	1873	10
098-ZR75	0.401	68538	14.59	0.11469	0.34	5.088	0.82	0.3218	0.65	0.79	1875	12	1798	20	1834	14	95.91	1875	12
103-ZR76	0.465	153475	13.41	0.11497	0.33	5.195	0.87	0.3277	0.71	0.82	1879	12	1827	23	1852	15	97.22	1879	12

104-ZR77	0.834	111202	20.09	0.11510	0.34	5.369	0.83	0.3383	0.67	0.80	1881	12	1878	22	1880	14	99.84	1881	12
105-ZR78	0.575	99433	23.31	0.11523	0.37	5.366	0.88	0.3377	0.70	0.80	1883	13	1876	23	1879	15	99.58	1883	13
106-ZR79	0.435	214216	9.87	0.11533	0.30	4.966	0.77	0.3123	0.61	0.78	1885	11	1752	19	1814	13	92.94	1885	11
107-ZR80	0.870	214451	13.08	0.11542	0.27	5.447	0.76	0.3422	0.61	0.80	1886	10	1897	20	1892	13	100.58	1886	10
108-ZR81	0.402	161843	18.34	0.11544	0.19	5.318	0.79	0.3341	0.67	0.85	1887	7	1858	22	1872	13	98.48	1887	7
109-ZR82	0.408	996503	80.53	0.11554	0.31	5.462	0.74	0.3428	0.56	0.76	1888	11	1900	19	1895	13	100.63	1888	11
110-ZR83	0.372	205355	26.41	0.11560	0.31	4.824	1.61	0.3026	1.53	0.95	1889	11	1704	46	1789	27	90.21	1889	11
111-ZR84	0.538	979731	80.86	0.11562	0.30	5.432	0.73	0.3407	0.55	0.75	1890	11	1890	18	1890	12	100.04	1890	11
112-ZR85	0.656	130416	15.39	0.11565	0.30	5.200	0.71	0.3261	0.52	0.74	1890	11	1819	17	1853	12	96.27	1890	11
115-ZR86	0.584	381581	1.89	0.11578	0.29	5.568	0.95	0.3488	0.83	0.87	1892	10	1929	28	1911	16	101.94	1892	10
116-ZR87N	0.456	185922	14.74	0.11594	0.33	5.648	1.02	0.3533	0.89	0.87	1895	12	1950	30	1923	17	102.94	1895	12
117-ZR87B	0.633	89960	15.89	0.11597	0.37	5.554	0.80	0.3473	0.61	0.76	1895	13	1922	20	1909	14	101.41	1895	13
118-ZR88	0.532	186077	18.80	0.11603	0.32	5.342	0.94	0.3339	0.80	0.85	1896	11	1857	26	1876	16	97.95	1896	11
119-ZR89	0.422	216903	25.56	0.11618	0.28	5.338	0.97	0.3332	0.86	0.88	1898	10	1854	28	1875	17	97.66	1898	10
120-ZR90	0.618	306157	11.00	0.11641	0.29	5.506	0.87	0.3430	0.74	0.84	1902	11	1901	24	1901	15	99.96	1902	11
121-ZR91	0.524	171858	13.80	0.11642	0.38	5.276	0.93	0.3287	0.77	0.82	1902	14	1832	24	1865	16	96.31	1902	14
122-ZR92	0.319	447357	11.13	0.11656	0.26	5.133	0.77	0.3194	0.62	0.81	1904	9	1787	19	1842	13	93.83	1904	9
123-ZR93	0.808	506135	32.30	0.11778	0.40	5.233	0.82	0.3222	0.62	0.75	1923	14	1800	19	1858	14	93.64	1923	14
127-ZR95	0.555	244660	32.89	0.11799	0.35	5.320	0.86	0.3270	0.69	0.80	1926	13	1824	22	1872	15	94.69	1926	13
128-ZR96	0.699	555587	32.49	0.11926	0.34	5.283	0.74	0.3213	0.55	0.73	1945	12	1796	17	1866	13	92.33	1945	12
129-ZR97	0.274	143697	14.84	0.11927	0.29	5.764	0.86	0.3504	0.72	0.84	1945	10	1937	24	1941	15	99.56	1945	10
130-ZR98	0.376	346632	6.16	0.12070	0.23	5.578	0.88	0.3352	0.77	0.87	1967	8	1863	25	1913	15	94.75	1967	8
131-ZR99	0.327	70926	19.26	0.12091	0.29	5.756	0.84	0.3453	0.69	0.83	1970	10	1912	23	1940	14	97.07	1970	10
132-ZR100	0.301	307416	20.04	0.12325	0.32	5.728	0.81	0.3370	0.64	0.79	2004	11	1872	21	1936	14	93.44	2004	11

Data not used due to high discordance

005-ZR3	0.604	5712	32.62	0.07783	2.33	1.823	3.24	0.1699	2.22	0.69	1143	91	1012	42	1054	42	88.53		
019-ZR14	0.268	258305	31.89	0.11631	0.52	4.255	1.48	0.2653	1.34	0.90	1900	19	1517	36	1685	24	79.83		
027-ZR20	0.677	15199	51.17	0.09610	0.42	2.729	1.16	0.2060	1.02	0.88	1550	16	1207	22	1336	17	77.91		
029-ZR22	0.376	5065	9.60	0.11265	0.36	3.818	0.81	0.2458	0.63	0.78	1843	13	1417	16	1597	13	76.90		
032-ZR25	0.566	98513	19.39	0.11014	0.31	3.555	1.06	0.2340	0.95	0.89	1802	11	1356	23	1539	17	75.24		
034-ZR26B	0.110	6469	6.39	0.09366	0.35	2.535	1.01	0.1962	0.87	0.86	1501	13	1155	18	1282	15	76.94		
036-ZR28	0.687	52639	34.06	0.10987	0.47	4.166	1.89	0.2750	1.79	0.95	1797	17	1566	50	1667	31	87.13		
039-ZR29	0.492	82874	45.96	0.10080	0.45	3.539	1.73	0.2546	1.63	0.94	1639	17	1462	43	1536	27	89.22		
044-ZR34N	0.797	12337	71.52	0.08594	3.57	0.744	3.94	0.0628	1.61	0.41	1337	135	392	12	565	34	29.36		
045-ZR34B	0.604	10155	55.15	0.06093	0.56	0.566	0.93	0.0674	0.65	0.69	637	24	421	5	456	7	66.06		
057-ZR42	0.421	19604	27.61	0.07788	0.58	1.634	1.80	0.1521	1.66	0.92	1144	23	913	28	983	22	79.83		
070-ZR52B	0.290	6551	11.94	0.11196	0.51	4.432	1.17	0.2871	0.98	0.84	1831	18	1627	28	1718	19	88.83		
085-ZR64	0.294	12564	10.87	0.07470	1.33	1.639	1.72	0.1591	1.02	0.60	1061	53	952	18	985	22	89.74		
086-ZR65	0.417	164137	14.20	0.11327	0.37	4.122	1.42	0.2639	1.32	0.93	1852	13	1510	36	1659	23	81.50		
091-ZR68	0.741	94400	30.28	0.12255	0.77	5.363	1.09	0.3173	0.67	0.62	1994	27	1777	21	1879	19	89.12		

Data not used due high analytical error

011-ZR9	0.460	26486	28.89	0.06898	6.11	1.859	6.18	0.1955	0.86	0.14	898	242	1151	18	1067	80	128.15		
021-ZR16	0.538	77905	44.94	0.11412	0.44	6.109	2.24	0.3882	2.17	0.97	1866	16	2115	78	1991	39	113.32		
066-ZR49	0.575	5740	22.03	0.12693	0.69	4.810	2.51	0.2748	2.39	0.95	2056	24	1565	66	1787	42	76.14		

082-ZR62N	0.548	179552	25.25	0.11058	0.44	5.088	3.25	0.3337	3.20	0.98	1809	16	1856	103	1834	54	102.62

Data not used due to elevated 204Pb																	
124-ZR94	0.332	176	10.92	0.40269	3.95	22.185	4.90	0.3995	2.87	0.59	3919	116	2167	105	3192	93	55.29

Dados de datação U-Pb da Bacia do Araripe

Sample	Formation	Age	Longitude (W)	Latitude (S)
M2AR 4-1	Brejo Santo	Jurassic	-39.006662°	-7.464279°
M2AR 5-1	Abaiara	Berriasian-Hauterivian	-38.936652°	-7.339516°
M2AR 8-1	Barbalha	Aptian	-39.356768°	-7.327129°
M2AR 11-1	Barbalha	Aptian	-39.453280°	-7.248347°
M2AR 10I	Crato	Aptian	-39.697751°	-7.116543°
M2AR 6-9	Romualdo	Aptian	-39.098551°	-7.358631°
M2AR 6-1	Romualdo	Aptian	-39.099406°	-7.362347°
M2AR 7-5	Romualdo	Aptian	-39.163554°	-7.572288°
M2AR 7-2	Romualdo	Aptian	-39.163729°	-7.574154°
M2AR 1-3	Araripina	Albian	-40.652910°	-7.365121°
M2AR 1-4	Exu	Albian-Cenomanian	-40.652910°	-7.365121°

Amostra M2AR 1-3

		Ratios										Rho	Ages (Ma)						% conc [1]	% conc [2]	Best age	2s
Spot number	Th/U	206Pb/204Pb	1s	238U/206Pb	1s	207Pb/206Pb	1s	207Pb/235U	1s	206Pb/238U	1s		207Pb/206Pb	2s	206Pb/238U	2s	207Pb/235U	2s				
			(%)		(%)		(%)		(%)		(%)			(abs)		(abs)		(abs)				(abs)
MAR1_3_36	1.9	142.8	473.6	10.38	1.2	0.06875	2.20	0.9269	1.9	0.09667	1.2	0.41	873	94	595	13	665	18	68.1	89.4	595	13
MAR1_3_32	2.7	890.9	122.4	12.71	1.2	0.06742	2.88	0.7106	1.7	0.07884	1.3	0.57	835	112	489	12	545	14	58.6	89.8	489	12
MAR1_3_117	2.4	1982.5	64.3	10.18	1.5	0.07058	2.34	0.9505	2.8	0.09878	1.4	0.57	926	96	607	16	676	28	65.5	89.8	607	16
MAR1_3_68	2.6	1272.6	123.4	10.00	1.2	0.06745	2.30	0.9425	2.8	0.10036	1.2	0.44	872	116	616	15	683	33	70.7	90.3	616	15
MAR1_3_27	2.4	6554.8	73.4	10.18	1.9	0.06894	3.26	0.9435	2.9	0.09891	2.0	0.13	871	130	608	23	673	29	69.8	90.3	608	23
MAR1_3_111	1.9	391.1	219.9	10.52	1.9	0.06778	2.01	0.9073	2.8	0.09596	1.9	0.25	848	78	590	21	653	26	69.6	90.4	590	21
MAR1_3_22	2.3	423.5	85.8	14.14	2.5	0.06396	3.29	0.6221	2.6	0.07132	2.4	0.16	718	138	444	21	490	20	61.8	90.5	444	21
MAR1_3_57	3.1	803.9	116.3	12.53	3.5	0.06524	1.67	0.7417	2.3	0.08224	3.4	0.90	772	68	509	33	562	20	65.9	90.5	509	33
MAR1_3_71	1.8	3050.6	94.3	14.22	2.5	0.06254	2.42	0.6181	2.9	0.07096	2.5	0.65	681	100	442	22	488	22	64.9	90.6	442	22
MAR1_3_83	2.3	1553.2	60.9	9.88	1.6	0.06874	2.92	0.9661	2.9	0.10164	1.5	0.31	872	118	624	18	685	29	71.6	91.1	624	18
MAR1_3_76	2.1	29844.3	66.4	12.28	3.6	0.06513	1.73	0.7456	3.2	0.08304	3.2	0.87	770	73	514	32	564	28	66.7	91.1	514	32
MAR1_3_38	1.9	918.8	109.5	10.32	3.0	0.06819	3.78	0.9196	3.7	0.09801	2.7	0.33	846	157	602	31	660	36	71.2	91.3	602	31

MAR1_3_99	2.1	139.7	204.9	10.93	2.9	0.06579	1.87	0.8572	3.1	0.09297	2.7	0.58	821	102	573	30	626	29	69.8	91.4	573	30
MAR1_3_18	1.7	280.4	207.1	10.42	3.0	0.06718	2.48	0.9090	4.4	0.09745	3.1	0.81	827	107	599	36	653	40	72.4	91.7	599	36
MAR1_3_10	1.8	4903.8	80.3	10.45	1.3	0.06705	1.61	0.8850	2.0	0.09593	1.3	0.60	833	66	590	15	643	19	70.9	91.8	590	15
MAR1_3_61	2.4	6947.8	47.3	11.08	3.1	0.06565	2.21	0.8320	3.9	0.09140	3.0	0.80	785	91	564	32	613	34	71.8	92.0	564	32
MAR1_3_35	2.0	570.4	157.5	13.32	2.2	0.06110	1.27	0.6331	2.3	0.07492	2.7	0.88	636	55	465	24	503	15	73.2	92.6	465	24
MAR1_3_97	2.0	4507.6	64.8	13.11	2.6	0.06291	2.02	0.6705	2.8	0.07751	2.5	0.75	689	87	481	23	519	23	69.8	92.6	481	23
MAR1_3_114	2.5	108.4	234.9	12.15	2.2	0.06324	1.82	0.7196	2.9	0.08221	2.5	0.77	703	80	509	25	549	25	72.4	92.8	509	25
MAR1_3_48	2.7	179.1	88.5	9.85	1.0	0.06662	2.14	0.9416	1.9	0.10182	1.1	0.40	809	89	625	13	673	18	77.3	92.9	625	13
MAR1_3_126	2.2	385.3	78.1	9.59	2.2	0.06735	4.31	0.9939	5.0	0.10552	2.2	0.32	854	183	646	26	694	46	75.7	93.2	646	26
MAR1_3_80	2.7	3282.3	149.7	10.27	1.5	0.06550	2.55	0.8934	3.2	0.09786	1.4	0.26	770	101	602	17	646	29	78.1	93.2	602	17
MAR1_3_60	1.2	457.8	56.7	12.74	4.6	0.06246	4.42	0.6978	4.7	0.08048	3.9	0.33	738	127	499	38	535	40	67.6	93.2	499	38
MAR1_3_121	1.8	1112.5	96.0	11.74	2.8	0.06315	1.57	0.7555	3.0	0.08614	2.8	0.86	707	68	532	28	570	26	75.3	93.4	532	28
MAR1_3_125	2.2	450.6	60.0	10.51	1.4	0.06450	2.51	0.8608	2.5	0.09558	1.4	0.17	734	106	588	15	629	23	80.1	93.6	588	15
MAR1_3_109	2.1	1403.7	68.0	9.70	1.7	0.06681	2.81	0.9589	2.9	0.10387	1.7	0.34	804	114	637	20	680	28	79.2	93.6	637	20
MAR1_3_100	1.6	2873.3	69.2	10.33	2.5	0.06622	2.15	0.8887	2.6	0.09821	2.3	0.49	796	88	604	26	644	24	75.8	93.7	604	26
MAR1_3_101	2.6	4082.0	80.8	10.45	1.9	0.06555	3.09	0.8468	2.1	0.09628	1.9	0.24	770	118	592	21	632	27	77.0	93.8	592	21
MAR1_3_43	2.0	5464.1	95.0	10.20	1.3	0.06484	2.78	0.8898	3.0	0.09838	1.2	0.18	748	112	605	14	644	27	80.8	93.9	605	14
MAR1_3_130	1.9	340.8	73.3	11.06	2.2	0.06319	1.58	0.8084	2.4	0.09148	2.2	0.74	705	65	564	24	600	21	80.0	94.0	564	24
MAR1_3_30	2.4	2190.7	77.8	9.78	1.2	0.06565	3.31	0.9339	2.6	0.10247	1.3	0.20	774	128	629	15	669	25	81.3	94.1	629	15
MAR1_3_129	2.7	562.2	120.3	10.18	1.5	0.06434	1.80	0.8866	1.5	0.09874	1.5	0.23	740	80	607	17	644	15	82.0	94.3	607	17
MAR1_3_56	2.0	778.9	98.7	10.64	2.1	0.06248	1.60	0.8171	2.6	0.09377	2.5	0.82	680	68	577	28	612	19	84.9	94.3	577	28
MAR1_3_118	2.2	1571.5	103.8	10.02	2.0	0.06492	2.20	0.9062	2.7	0.10072	1.9	0.47	754	87	618	23	653	26	82.0	94.7	618	23
MAR1_3_75	2.5	364.7	103.3	11.95	2.7	0.06212	1.78	0.7283	2.1	0.08521	3.0	0.66	665	85	527	30	555	18	79.2	95.0	527	30
MAR1_3_87	1.9	477.7	60.6	9.80	1.6	0.06522	1.96	0.9185	2.1	0.10255	1.7	0.45	769	84	629	20	660	21	81.8	95.3	629	20
MAR1_3_65	2.3	558.2	162.5	10.76	1.2	0.06250	1.10	0.8116	1.2	0.09326	1.2	0.59	686	48	575	13	603	11	83.8	95.3	575	13
MAR1_3_5	2.0	848.7	148.3	13.69	4.6	0.05955	1.73	0.6214	4.1	0.07515	4.1	0.90	580	74	467	37	489	33	80.5	95.5	467	37
MAR1_3_19	2.3	885.8	102.0	11.58	2.0	0.06173	1.38	0.7407	2.4	0.08684	2.0	0.61	660	60	537	20	562	20	81.4	95.5	537	20
MAR1_3_116	1.9	534.7	112.3	10.57	1.7	0.06200	2.17	0.8342	2.8	0.09533	1.6	0.60	688	108	587	19	614	26	85.2	95.6	587	19
MAR1_3_1	2.1	696.4	30.2	10.04	1.8	0.06369	2.61	0.8881	3.3	0.10019	1.8	0.40	712	113	615	22	643	30	86.5	95.7	615	22
MAR1_3_86	2.2	719.3	55.8	10.21	1.7	0.06433	2.61	0.8704	3.0	0.09866	1.6	0.48	732	93	606	19	634	26	82.8	95.7	606	19
MAR1_3_102	1.9	2157.2	50.3	10.59	1.8	0.06194	2.70	0.8327	3.5	0.09521	1.8	0.25	648	103	586	20	612	30	90.5	95.7	586	20
MAR1_3_24	2.1	762.2	132.3	10.77	1.7	0.06255	1.81	0.8083	2.0	0.09339	1.7	0.52	683	79	575	19	601	19	84.2	95.8	575	19
MAR1_3_110	2.1	2105.8	55.5	10.19	1.6	0.06390	3.21	0.8542	2.5	0.09877	1.7	0.20	705	123	607	19	634	28	86.1	95.8	607	19
MAR1_3_4	2.4	878.8	53.5	11.56	3.5	0.06099	1.90	0.7470	3.6	0.08767	3.3	0.87	632	80	541	34	565	32	85.7	95.8	541	34
MAR1_3_42	2.1	400.7	117.3	11.65	2.4	0.06091	1.96	0.7317	3.2	0.08648	2.5	0.77	627	86	535	25	556	28	85.2	96.1	535	25
MAR1_3_44	2.3	2856.2	68.7	10.72	2.0	0.06171	1.80	0.7976	3.1	0.09406	1.7	0.80	650	82	579	19	602	23	89.1	96.3	579	19
MAR1_3_16	1.8	2267.3	85.1	11.40	2.2	0.06182	2.26	0.7534	2.2	0.08881	2.3	0.44	647	102	548	24	569	19	84.7	96.3	548	24
MAR1_3_15	2.3	1159.0	66.3	10.84	1.8	0.06180	2.83	0.7962	3.5	0.09271	1.8	0.66	647	126	571	20	593	32	88.4	96.4	571	20
MAR1_3_92	2.4	3489.0	63.6	9.73	2.1	0.06326	2.38	0.9007	2.4	0.10227	1.8	0.47	696	102	627	21	651	22	90.2	96.5	627	21
MAR1_3_128	2.6	207.1	353.0	10.61	1.3	0.06213	1.30	0.8134	1.2	0.09469	1.3	0.58	672	54	583	14	604	11	86.8	96.5	583	14
MAR1_3_13	2.3	39577.4	50.1	11.77	2.3	0.06087	1.65	0.7202	1.7	0.08603	2.1	0.67	623	71	532	21	550	15	85.3	96.7	532	21
MAR1_3_46	3.1	71.0	471.1	10.63	1.9	0.06162	1.58	0.8142	1.8	0.09486	1.7	0.62	650	70	584	20	604	17	89.8	96.7	584	20
MAR1_3_53	1.3	205.3	53.7	9.84	5.0	0.06077	5.98	0.8518	6.0	0.09736	4.1	0.07	649	212	598	47	618	56	92.2	96.7	598	47
MAR1_3_103	2.0	2181.1	78.1	11.21	2.8	0.06172	2.69	0.7612	3.1	0.08996	2.4	0.55	650	114	555	26	574	27	85.4	96.8	555	26
MAR1_3_88	2.4	123.8	310.9	10.49	1.6	0.06221	2.20	0.8224	2.1	0.09573	1.6	0.36	670	95	589	18	609	20	88.0	96.8	589	18
MAR1_3_8	2.0	124.9	658.4	11.40	4.3	0.06350	3.36	0.7635	2.6	0.09020	2.7	0.38	690	126	556	29	574	23	80.6	96.9	556	29

MAR1_3_47	3.0	1787.0	135.6	10.61	1.9	0.06154	2.14	0.8119	2.8	0.09482	1.9	0.63	645	91	584	21	602	25	90.5	97.0	584	21
MAR1_3_37	2.3	223.6	326.7	11.20	2.0	0.06096	1.79	0.7565	1.9	0.08988	2.1	0.60	629	78	555	22	571	16	88.2	97.1	555	22
MAR1_3_81	2.5	236.3	375.6	10.81	2.1	0.06185	1.63	0.7953	1.9	0.09355	2.2	0.71	659	67	576	24	593	17	87.5	97.1	576	24
MAR1_3_69	1.8	1278.5	42.6	9.90	1.5	0.06261	2.07	0.8835	2.1	0.10159	1.5	0.41	680	87	624	18	642	20	91.7	97.2	624	18
MAR1_3_50	2.7	506.2	187.4	10.49	1.3	0.06102	0.95	0.8163	1.4	0.09576	1.4	0.79	635	41	589	15	605	13	92.8	97.4	589	15
MAR1_3_105	1.8	1016.6	132.0	10.26	1.5	0.06213	1.60	0.8414	1.8	0.09809	1.6	0.59	668	69	603	18	619	17	90.3	97.4	603	18
MAR1_3_112	2.4	2652.1	44.6	10.52	1.6	0.06213	1.75	0.8150	1.7	0.09571	1.7	0.78	691	61	589	19	605	15	85.3	97.4	589	19
MAR1_3_90	3.3	17227.8	98.7	10.97	2.3	0.06146	1.72	0.7793	2.3	0.09233	2.3	0.73	644	71	569	25	584	20	88.3	97.5	569	25
MAR1_3_29	2.6	8088.4	61.1	11.45	1.2	0.06001	1.41	0.7290	1.5	0.08763	1.2	0.50	596	61	541	13	556	13	90.8	97.5	541	13
MAR1_3_113	2.1	1555.5	74.7	10.39	1.4	0.06164	1.50	0.8252	1.4	0.09676	1.5	0.39	652	65	595	17	610	13	91.3	97.5	595	17
MAR1_3_95	2.3	4281.9	56.3	10.60	1.7	0.06165	1.76	0.8061	1.9	0.09509	1.7	0.61	649	76	585	19	599	18	90.1	97.7	585	19
MAR1_3_127	2.3	120.2	279.2	10.49	1.7	0.06084	1.66	0.8165	1.9	0.09607	1.7	0.59	622	73	591	19	605	17	95.1	97.7	591	19
MAR1_3_74	2.9	615.3	82.4	10.10	2.0	0.06193	1.94	0.8548	1.6	0.09970	1.8	0.37	659	85	612	22	627	16	92.9	97.7	612	22
MAR1_3_93	2.3	10125.0	44.1	10.46	2.4	0.06139	1.57	0.8176	2.5	0.09649	2.2	0.80	645	66	594	25	605	23	92.0	98.0	594	25
MAR1_3_40	2.1	654.2	49.0	10.67	1.7	0.05960	1.15	0.7913	2.1	0.09424	1.7	0.66	605	64	580	19	591	18	95.9	98.2	580	19
MAR1_3_79	2.0	84499.2	47.4	10.55	1.7	0.06089	1.52	0.8034	1.8	0.09546	1.7	0.60	625	66	588	19	598	16	93.9	98.3	588	19
MAR1_3_123	0.4	2130.2	52.4	10.39	1.6	0.05991	0.96	0.8188	1.7	0.09693	1.6	0.63	596	42	596	18	607	15	100.1	98.3	596	18
MAR1_3_9	2.4	2275.0	60.1	11.02	2.6	0.06031	1.87	0.7645	1.9	0.09218	2.5	0.67	602	77	568	27	576	17	94.4	98.7	568	27
MAR1_3_78	2.5	44738.9	97.5	10.04	1.4	0.06111	1.25	0.8489	1.7	0.10016	1.5	0.03	636	54	615	17	623	16	96.7	98.7	615	17
MAR1_3_51	2.5	187.4	223.0	10.26	1.2	0.06031	1.18	0.8237	1.4	0.09787	1.2	0.54	609	51	602	14	610	12	98.9	98.7	602	14
MAR1_3_7	2.1	478.5	240.3	10.40	1.6	0.06147	1.40	0.8115	1.4	0.09673	1.6	0.69	648	59	595	18	603	13	91.9	98.7	595	18
MAR1_3_94	2.1	4133.7	60.4	10.47	2.1	0.06092	2.01	0.8068	1.7	0.09642	2.1	0.46	623	83	593	23	600	16	95.2	98.9	593	23
MAR1_3_119	1.9	3787.7	65.8	10.42	1.4	0.06026	1.24	0.8063	1.4	0.09640	1.4	0.75	606	54	593	16	600	12	97.8	98.9	593	16
MAR1_3_39	2.0	1601.4	75.9	10.67	1.8	0.06006	1.84	0.7871	1.9	0.09457	1.9	0.51	592	81	582	21	589	17	98.3	98.9	582	21
MAR1_3_66	2.7	753.7	115.5	10.50	1.8	0.05980	1.02	0.7996	1.7	0.09592	1.8	0.83	592	44	590	20	596	15	99.7	99.0	590	20
MAR1_3_107	2.1	1476.8	76.2	10.53	1.7	0.06044	2.15	0.7964	2.1	0.09559	1.7	0.30	601	95	588	19	594	18	97.9	99.1	588	19
MAR1_3_72	3.0	5813.7	100.3	10.61	1.3	0.06009	1.76	0.7838	2.4	0.09444	1.3	0.69	599	77	582	14	587	21	97.1	99.1	582	14
MAR1_3_21	2.0	518.2	122.0	10.69	1.4	0.05990	0.98	0.7778	1.4	0.09404	1.4	0.76	595	42	579	16	584	13	97.3	99.2	579	16
MAR1_3_28	2.3	8689.8	72.3	10.52	2.0	0.06028	1.41	0.7984	1.7	0.09599	2.0	0.73	605	61	591	23	595	15	97.6	99.2	591	23
MAR1_3_17	1.9	876.1	68.4	10.52	1.5	0.06035	1.79	0.7938	1.7	0.09561	1.4	0.28	603	75	589	16	593	15	97.6	99.3	589	16
MAR1_3_64	1.9	957.5	166.4	9.88	2.0	0.06014	2.05	0.8556	2.3	0.10157	2.0	0.56	602	88	623	24	627	22	103.6	99.4	623	24
MAR1_3_84	2.6	600.4	158.9	9.89	1.9	0.06130	1.74	0.8602	2.4	0.10198	2.0	0.72	640	71	626	24	629	22	97.8	99.5	626	24
MAR1_3_115	1.9	2514.8	64.7	9.86	1.7	0.06088	1.62	0.8616	1.8	0.10217	1.7	0.62	624	69	627	21	630	17	100.5	99.5	627	21
MAR1_3_63	2.0	1376.5	76.9	10.01	1.3	0.06026	1.53	0.8320	1.4	0.10031	1.3	0.47	603	67	616	15	619	16	102.1	99.5	616	15
MAR1_3_31	1.9	1857.9	59.4	10.61	1.4	0.06040	2.14	0.7803	1.4	0.09458	1.4	0.19	604	91	582	16	585	12	96.4	99.5	582	16
MAR1_3_98	2.4	3502.9	62.0	10.15	2.4	0.06108	1.64	0.8362	2.4	0.09979	2.3	0.77	632	71	613	27	616	22	97.0	99.5	613	27
MAR1_3_122	2.5	2097.1	45.9	10.28	1.3	0.05941	1.62	0.8111	1.8	0.09756	1.3	0.47	573	71	600	15	602	16	104.7	99.6	600	15
MAR1_3_77	2.1	203.7	168.0	10.11	1.7	0.06042	2.20	0.8323	2.5	0.09965	1.7	0.45	599	97	612	20	613	23	102.2	99.8	612	20
MAR1_3_45	2.6	1640.2	108.2	10.18	1.1	0.05947	1.16	0.8175	1.3	0.09851	1.1	0.52	578	51	606	13	606	12	104.7	99.9	606	13
MAR1_3_106	2.5	807.4	63.2	9.85	1.8	0.06063	1.59	0.8571	2.1	0.10227	1.7	0.68	615	72	627	20	627	20	102.0	100.0	627	20
MAR1_3_20	1.8	3267.0	61.6	10.32	1.3	0.05984	1.36	0.8021	1.2	0.09726	1.2	0.36	590	57	598	14	598	11	101.4	100.1	598	14
MAR1_3_91	2.0	13573.5	45.8	10.55	2.0	0.05976	1.52	0.7846	1.5	0.09568	1.9	0.62	585	67	589	22	588	14	100.6	100.2	589	22
MAR1_3_73	2.3	351.2	135.7	10.57	1.8	0.05940	1.64	0.7754	1.7	0.09493	1.9	0.57	577	73	585	21	583	15	101.3	100.3	585	21
MAR1_3_34	3.2	582.8	106.8	10.39	1.3	0.05914	1.60	0.7931	2.0	0.09661	1.3	0.60	561	71	594	14	592	18	105.9	100.4	594	14
MAR1_3_23	2.4	991.6	190.7	10.65	2.3	0.05939	1.56	0.7697	2.0	0.09450	2.3	0.74	577	67	582	26	579	18	100.9	100.5	582	26
MAR1_3_25	2.7	915.7	54.9	10.66	1.0	0.05868	1.93	0.7631	1.6	0.09402	1.0	0.06	541	89	579	12	575	14	107.0	100.7	579	12

MAR1_3_62	1.6	201.4	311.4	10.11	1.3	0.05995	1.23	0.8171	1.9	0.09934	1.3	0.80	595	54	610	15	605	17	102.6	100.8	610	15
MAR1_3_41	2.3	428.2	61.3	10.04	1.9	0.05913	1.67	0.8218	2.0	0.10015	1.9	0.63	564	74	615	22	608	19	109.1	101.1	615	22
MAR1_3_104	2.5	4327.3	70.5	9.68	1.4	0.05930	2.71	0.8385	3.3	0.10194	2.2	0.55	560	115	626	27	616	31	111.7	101.5	626	27
MAR1_3_89	2.8	43009.9	54.6	10.01	1.2	0.05905	1.30	0.8150	1.4	0.10025	1.2	0.53	562	56	616	14	605	13	109.6	101.8	616	14
MAR1_3_124	2.2	172.2	159.3	10.32	1.8	0.05811	2.56	0.7841	2.1	0.09731	1.8	0.20	520	111	599	21	587	19	115.0	101.9	599	21
MAR1_3_70	2.1	412.9	353.3	9.74	2.0	0.05913	1.68	0.8468	1.8	0.10353	1.9	0.58	562	73	635	23	622	17	113.0	102.0	635	23
MAR1_3_120	2.2	149.0	77.9	9.43	2.3	0.06785	4.36	1.0080	4.7	0.10712	2.2	0.31	809	180	656	27	702	46	81.0	93.4	656	27
Data not used due to high discordance																						
~~**MAR1_3_67**~~	~~2.0~~	~~337.0~~	~~80.7~~	~~9.96~~	~~2.4~~	~~0.07112~~	~~3.03~~	~~1.0065~~	~~3.9~~	~~0.10153~~	~~2.4~~	~~0.62~~	~~937~~	~~123~~	~~623~~	~~28~~	~~704~~	~~38~~	~~66.5~~	~~88.5~~		
~~**MAR1_3_49**~~	~~2.6~~	~~294.5~~	~~63.2~~	~~11.88~~	~~2.4~~	~~0.06737~~	~~2.91~~	~~0.7976~~	~~2.9~~	~~0.08494~~	~~2.3~~	~~0.43~~	~~831~~	~~116~~	~~525~~	~~24~~	~~594~~	~~26~~	~~63.2~~	~~88.4~~		
~~**MAR1_3_96**~~	~~1.5~~	~~5010.7~~	~~72.4~~	~~11.66~~	~~1.8~~	~~0.06867~~	~~1.78~~	~~0.8151~~	~~1.7~~	~~0.08645~~	~~1.8~~	~~0.54~~	~~877~~	~~70~~	~~534~~	~~18~~	~~605~~	~~16~~	~~60.9~~	~~88.4~~		
~~**MAR1_3_54**~~	~~2.1~~	~~580.1~~	~~78.1~~	~~10.29~~	~~1.5~~	~~0.07047~~	~~1.60~~	~~0.9623~~	~~1.9~~	~~0.09778~~	~~1.5~~	~~0.58~~	~~931~~	~~70~~	~~601~~	~~17~~	~~683~~	~~19~~	~~64.5~~	~~88.0~~		
~~**MAR1_3_3**~~	~~2.2~~	~~1269.4~~	~~87.6~~	~~14.17~~	~~3.0~~	~~0.06536~~	~~1.78~~	~~0.6476~~	~~3.4~~	~~0.07139~~	~~3.1~~	~~0.88~~	~~780~~	~~73~~	~~444~~	~~27~~	~~506~~	~~27~~	~~57.0~~	~~87.8~~		
~~**MAR1_3_58**~~	~~2.5~~	~~1265.1~~	~~62.5~~	~~10.13~~	~~2.0~~	~~0.07383~~	~~2.96~~	~~0.9997~~	~~2.6~~	~~0.09971~~	~~2.0~~	~~0.46~~	~~1008~~	~~116~~	~~612~~	~~24~~	~~702~~	~~26~~	~~60.8~~	~~87.3~~		
~~**MAR1_3_85**~~	~~2.5~~	~~3136.4~~	~~55.6~~	~~9.86~~	~~1.6~~	~~0.08825~~	~~14.33~~	~~1.0818~~	~~6.7~~	~~0.10208~~	~~1.6~~	~~0.55~~	~~1129~~	~~289~~	~~626~~	~~19~~	~~731~~	~~63~~	~~55.5~~	~~85.7~~		
~~**MAR1_3_108**~~	~~2.1~~	~~843.7~~	~~84.4~~	~~10.20~~	~~1.7~~	~~0.07559~~	~~6.76~~	~~1.0502~~	~~9.4~~	~~0.09881~~	~~1.9~~	~~0.75~~	~~993~~	~~194~~	~~607~~	~~22~~	~~709~~	~~75~~	~~61.1~~	~~85.6~~		
~~**MAR1_3_82**~~	~~2.0~~	~~177.2~~	~~150.1~~	~~9.91~~	~~2.1~~	~~0.07615~~	~~4.09~~	~~1.0703~~	~~4.2~~	~~0.10175~~	~~2.1~~	~~0.37~~	~~1062~~	~~149~~	~~624~~	~~25~~	~~735~~	~~42~~	~~58.8~~	~~85.0~~		
~~**MAR1_3_12**~~	~~2.2~~	~~18610.0~~	~~55.3~~	~~11.62~~	~~2.2~~	~~0.07234~~	~~1.47~~	~~0.8696~~	~~2.2~~	~~0.08688~~	~~2.1~~	~~0.79~~	~~989~~	~~60~~	~~537~~	~~22~~	~~634~~	~~20~~	~~54.3~~	~~84.6~~		
~~**MAR1_3_26**~~	~~2.9~~	~~19293.3~~	~~50.4~~	~~26.28~~	~~8.7~~	~~0.06459~~	~~2.37~~	~~0.3714~~	~~7.7~~	~~0.04185~~	~~7.9~~	~~0.96~~	~~749~~	~~100~~	~~264~~	~~41~~	~~318~~	~~41~~	~~35.2~~	~~83.0~~		
~~**MAR1_3_2**~~	~~0.6~~	~~289.0~~	~~278.1~~	~~11.66~~	~~2.9~~	~~0.07918~~	~~4.49~~	~~0.9565~~	~~4.8~~	~~0.08687~~	~~3.5~~	~~0.45~~	~~1148~~	~~156~~	~~537~~	~~36~~	~~678~~	~~45~~	~~46.8~~	~~79.1~~		
~~**MAR1_3_52**~~	~~1.8~~	~~742.6~~	~~91.2~~	~~11.16~~	~~2.8~~	~~0.08385~~	~~2.70~~	~~1.0335~~	~~2.7~~	~~0.08986~~	~~2.9~~	~~0.39~~	~~1267~~	~~100~~	~~554~~	~~31~~	~~718~~	~~28~~	~~43.7~~	~~77.2~~		
~~**MAR1_3_14**~~	~~1.5~~	~~6966.4~~	~~93.0~~	~~20.93~~	~~5.4~~	~~0.07334~~	~~4.41~~	~~0.4999~~	~~6.2~~	~~0.04966~~	~~4.8~~	~~0.68~~	~~986~~	~~170~~	~~312~~	~~29~~	~~408~~	~~42~~	~~31.6~~	~~76.4~~		

Amostra M2AR 1-4

			Ratios									**Rho**	**Ages (Ma)**						**% conc** [1]	**% conc** [2]	**Best age**	**2s**
Spot number	Th/U	206Pb/204Pb	1s	238U/206Pb	1s	207Pb/206Pb	1s	207Pb/235U	1s	206Pb/238U	1s		207Pb/206Pb	2s	206Pb/238U	2s	207Pb/235U	2s				
			(%)		(%)		(%)		(%)		(%)			(abs)		(abs)		(abs)				(abs)
Mar1_4_14	5.9	2410.6	71.0	30.32	1.7	0.05086	1.91	0.2347	2.2	0.03324	1.8	0.50	218	89	211	8	214	8	97	99	211	8
Mar1_4_61	0.7	75.2	251.4	11.48	2.8	0.05804	3.52	0.6982	3.3	0.08873	2.6	0.39	480	166	548	28	535	28	114	102	548	28
Mar1_4_37	1.3	1817.6	87.8	11.47	3.0	0.05882	2.67	0.7179	3.9	0.08885	2.8	0.23	532	129	548	29	546	33	103	100	548	29
Mar1_4_99	0.7	86.4	633.1	11.18	2.3	0.05943	2.74	0.7461	3.5	0.09067	2.3	0.62	554	117	559	24	563	29	101	99	559	24
Mar1_4_19	1.2	991.2	146.8	11.01	3.2	0.05826	2.86	0.7401	1.9	0.09185	3.1	0.50	526	122	566	33	562	17	108	101	566	33
Mar1_4_60	1.1	5699.7	58.9	10.97	2.5	0.06099	2.49	0.7631	2.4	0.09202	2.3	0.50	624	102	567	25	575	21	91	99	567	25
Mar1_4_16	0.8	1079.6	92.2	10.75	2.2	0.05976	1.81	0.7729	2.0	0.09411	2.1	0.49	582	76	580	23	580	18	100	100	580	23
Mar1_4_17	1.2	1654.2	66.1	10.51	1.6	0.06179	2.19	0.8099	2.6	0.09468	2.0	0.33	650	87	583	23	601	23	90	97	583	23
Mar1_4_23	0.9	154.3	101.9	10.48	1.8	0.05844	3.50	0.7964	3.6	0.09618	1.8	0.17	499	150	592	20	592	32	119	100	592	20
Mar1_4_88	1.3	625.6	88.8	10.28	2.6	0.05829	3.62	0.7931	3.6	0.09897	2.6	0.13	539	191	608	30	601	39	113	101	608	30
Mar1_4_123	1.4	562.1	87.8	10.05	2.0	0.06283	1.68	0.8855	2.5	0.10050	1.9	0.71	691	72	617	23	642	23	89	96	617	23
Mar1_4_15	1.0	678.9	99.3	10.02	3.6	0.06298	6.04	0.8764	4.6	0.10244	3.9	0.09	673	351	628	46	634	45	93	99	628	46
Mar1_4_48	1.9	364.0	76.5	9.68	2.1	0.06242	2.13	0.8922	2.8	0.10304	1.9	0.07	670	95	632	23	645	27	94	98	632	23
Mar1_4_62	1.8	1196.8	47.6	9.71	2.5	0.06456	2.80	0.9156	2.4	0.10430	2.5	0.39	739	111	639	30	659	23	87	**97**	639	30
Mar1_4_100	1.9	643.5	63.5	9.33	4.4	0.06454	3.29	0.9740	3.9	0.10906	3.5	0.65	743	127	667	45	689	38	90	97	667	45
Mar1_4_30	1.0	1213.8	76.0	8.70	2.2	0.06570	2.64	1.0444	2.3	0.11597	2.1	0.23	776	114	707	28	725	23	91	98	707	28

Mar1_4_111	0.5	993.9	135.0	8.04	4.2	0.06342	3.07	1.1165	2.7	0.12754	4.0	0.62	701	134	773	59	760	29	110	102	773	59
Mar1_4_13	1.3	485.8	151.7	7.59	2.2	0.06526	1.69	1.2096	2.5	0.13338	2.1	0.47	772	70	807	32	803	28	105	100	807	32
Mar1_4_2	1.0	962.8	285.3	7.55	4.0	0.06532	2.31	1.2296	3.4	0.13438	3.3	0.73	775	101	812	51	812	39	105	100	812	51
Mar1_4_32	0.8	2656.2	67.0	7.10	1.8	0.06924	1.69	1.3487	1.9	0.14165	1.8	0.59	897	69	854	28	866	22	95	99	854	28
Mar1_4_63	1.2	156.9	448.9	5.95	2.1	0.07168	2.25	1.6643	3.0	0.16932	2.1	0.62	966	88	1008	39	992	37	104	102	1008	39
Mar1_4_8	1.5	397.5	50.5	4.67	1.4	0.08220	1.66	2.4729	1.8	0.21486	1.4	0.23	1245	65	1254	31	1263	26	101	99	1254	31
Mar1_4_54	0.7	876.1	195.2	4.68	3.0	0.09036	1.52	2.6993	3.1	0.21814	2.7	0.88	1425	58	1270	62	1321	48	89	96	1270	62
Mar1_4_28	1.0	13109.2	68.6	4.01	2.3	0.09287	1.21	3.2223	2.2	0.25193	2.3	0.85	1481	45	1447	59	1460	33	98	99	1447	59
Mar1_4_6	1.0	996.2	183.8	3.16	2.7	0.10728	2.33	4.7833	2.3	0.31975	2.7	0.55	1745	88	1787	84	1780	39	102	100	1745	88
Mar1_4_10	1.8	68.8	2030.8	3.60	2.4	0.11247	2.27	4.3879	2.3	0.27991	2.3	0.53	1831	83	1590	66	1708	37	87	93	1831	83
Mar1_4_121	1.2	13980.6	71.8	3.50	2.0	0.11570	1.83	4.5869	3.1	0.28863	2.2	0.82	1880	67	1633	62	1755	44	87	93	1880	67
Mar1_4_91	0.2	29725.8	84.0	3.12	1.8	0.11785	1.30	5.1942	1.9	0.31996	2.3	0.79	1918	47	1787	70	1848	34	93	97	1918	47
Mar1_4_5	2.2	15802.0	98.2	2.95	3.1	0.11875	1.31	5.7292	2.7	0.34546	2.7	0.88	1933	48	1909	91	1930	48	99	99	1933	48
Mar1_4_34	0.6	699.3	83.5	3.02	2.5	0.11950	1.93	5.4798	2.5	0.33473	2.4	0.65	1942	71	1859	79	1894	44	96	98	1942	71
Mar1_4_71	0.3	2503.8	183.9	2.68	1.9	0.11944	1.40	6.1236	1.4	0.37507	1.8	0.64	1943	51	2052	63	1992	23	106	103	1943	51
Mar1_4_42	1.4	3839.8	98.8	2.97	1.5	0.12289	1.46	5.6792	1.7	0.33811	1.5	0.59	1994	53	1877	49	1926	30	94	97	1994	53
Mar1_4_57	0.9	28052.8	94.8	2.68	2.6	0.12467	1.59	6.3918	1.5	0.37603	2.5	0.83	2020	55	2056	88	2030	26	102	101	2020	55
Mar1_4_66	0.4	2327.0	73.6	2.33	2.0	0.13024	1.96	7.6885	2.0	0.43327	2.1	0.53	2090	70	2317	83	2191	36	111	106	2090	70
Mar1_4_22	1.9	9977.7	81.1	2.61	2.3	0.13030	1.75	6.9458	2.0	0.38627	2.1	0.62	2096	64	2104	76	2102	36	100	100	2096	64
Mar1_4_81	1.6	1764.3	72.7	2.67	2.0	0.13110	1.12	6.6453	2.0	0.37368	2.5	0.74	2109	40	2043	89	2073	28	97	99	2109	40
Mar1_4_43	1.4	2367.3	134.5	2.62	1.7	0.13432	1.37	7.1775	1.8	0.38461	1.7	0.24	2151	46	2096	62	2131	31	97	98	2151	46
Mar1_4_38	0.7	1270.7	97.1	2.80	2.5	0.13722	1.96	6.8168	2.4	0.36094	2.4	0.87	2185	66	1984	82	2084	42	91	95	2185	66
Mar1_4_87	0.9	6857.7	65.5	2.25	2.6	0.13928	2.45	8.6075	2.7	0.44771	2.4	0.60	2212	84	2383	98	2295	48	108	104	2212	84
Mar1_4_114	0.5	28639.7	67.0	2.40	1.3	0.14013	1.64	8.1791	1.9	0.41750	1.3	0.52	2223	56	2248	51	2248	34	101	100	2223	56
Mar1_4_44	0.6	12257.7	49.6	2.31	2.2	0.18068	1.98	10.6219	3.5	0.42875	2.7	0.81	2651	65	2296	106	2480	68	87	93	2651	65
Data not used due to high discordance																						
~~**Mar1_4_21**~~	~~0.3~~	~~36793.3~~	~~87.5~~	~~2.38~~	~~4.4~~	~~0.18612~~	~~1.72~~	~~11.1995~~	~~4.2~~	~~0.43516~~	~~4.0~~	~~0.90~~	~~2702~~	~~56~~	~~2319~~	~~159~~	~~2524~~	~~82~~	~~86~~	**92**		
~~**Mar1_4_7**~~	~~1.4~~	~~10049.8~~	~~66.2~~	~~3.95~~	~~3.1~~	~~0.10672~~	~~1.78~~	~~3.8183~~	~~2.8~~	~~0.25668~~	~~2.8~~	~~0.81~~	~~1738~~	~~66~~	~~1471~~	~~74~~	~~1593~~	~~45~~	~~85~~	**92**		
~~**Mar1_4_80**~~	~~2.5~~	~~156.7~~	~~224.8~~	~~3.61~~	~~4.0~~	~~0.12050~~	~~3.32~~	~~4.6622~~	~~3.4~~	~~0.28645~~	~~3.7~~	~~0.71~~	~~1935~~	~~122~~	~~1619~~	~~106~~	~~1751~~	~~58~~	~~84~~	**92**		
Mar1_4_65	2.3	475.2	4177.8	9.52	1.5	0.06613	1.86	0.9558	2.2	0.10557	1.5	0.08	798	80	647	18	680	22	81	**95**		
~~**Mar1_4_3**~~	~~0.8~~	~~2882.3~~	~~66.7~~	~~3.21~~	~~4.1~~	~~0.14036~~	~~1.45~~	~~6.3705~~	~~4.0~~	~~0.32441~~	~~3.9~~	~~0.93~~	~~2225~~	~~50~~	~~1804~~	~~124~~	~~2012~~	~~73~~	~~81~~	**90**		
Mar1_4_31	2.0	98.9	171.8	10.01	7.3	0.06755	2.62	0.9918	5.1	0.10507	5.0	0.80	830	107	642	62	690	55	77	**93**		
~~**Mar1_4_112**~~	~~0.6~~	~~6349.9~~	~~84.0~~	~~3.74~~	~~3.2~~	~~0.12064~~	~~1.13~~	~~4.4959~~	~~4.0~~	~~0.26600~~	~~3.7~~	~~0.96~~	~~1962~~	~~40~~	~~1517~~	~~102~~	~~1719~~	~~73~~	~~77~~	88		
~~**Mar1_4_11**~~	~~1.1~~	~~130.4~~	~~138.1~~	~~4.36~~	~~5.9~~	~~0.11024~~	~~3.36~~	~~3.6311~~	~~5.5~~	~~0.23721~~	~~4.8~~	~~0.80~~	~~1787~~	~~124~~	~~1369~~	~~119~~	~~1544~~	~~96~~	~~77~~	89		
~~**Mar1_4_40**~~	~~0.8~~	~~31.5~~	~~5758.5~~	~~3.77~~	~~2.5~~	~~0.12343~~	~~2.26~~	~~4.5487~~	~~3.4~~	~~0.26732~~	~~2.5~~	~~0.78~~	~~1999~~	~~84~~	~~1526~~	~~67~~	~~1735~~	~~60~~	~~76~~	88		
~~**Mar1_4_68**~~	~~1.1~~	~~1759.3~~	~~86.6~~	~~4.44~~	~~4.9~~	~~0.10925~~	~~1.13~~	~~3.5217~~	~~5.1~~	~~0.23462~~	~~4.8~~	~~0.98~~	~~1784~~	~~41~~	~~1354~~	~~116~~	~~1518~~	~~79~~	~~76~~	89		
~~**Mar1_4_26**~~	~~0.2~~	~~576.1~~	~~256.7~~	~~3.27~~	~~2.1~~	~~0.14800~~	~~1.57~~	~~6.3142~~	~~2.5~~	~~0.30939~~	~~2.1~~	~~0.76~~	~~2315~~	~~56~~	~~1736~~	~~65~~	~~2014~~	~~44~~	~~75~~	86		
Mar1_4_27	1.5	638.1	65.0	10.24	2.7	0.06627	1.39	0.9168	2.9	0.09935	2.7	0.81	828	70	610	31	658	28	74	**93**		
~~**Mar1_4_46**~~	~~1.1~~	~~5801.3~~	~~147.2~~	~~3.45~~	~~8.7~~	~~0.16805~~	~~1.30~~	~~7.9307~~	~~7.8~~	~~0.34380~~	~~7.3~~	~~0.98~~	~~2547~~	~~36~~	~~1876~~	~~242~~	~~2157~~	~~146~~	~~74~~	87		
Mar1_4_76	0.7	4251.3	50.8	10.50	2.7	0.06721	2.22	0.8639	2.7	0.09534	3.1	0.62	827	91	586	35	630	25	71	**93**		
Mar1_4_78	1.3	1454.7	41.4	11.21	2.1	0.06613	2.09	0.8051	2.9	0.09032	2.3	0.81	794	84	557	24	607	31	70	**92**		
~~**Mar1_4_102**~~	~~0.4~~	~~5741.5~~	~~77.7~~	~~5.17~~	~~2.5~~	~~0.10904~~	~~1.46~~	~~2.9840~~	~~2.9~~	~~0.19628~~	~~2.3~~	~~0.87~~	~~1776~~	~~53~~	~~1154~~	~~49~~	~~1397~~	~~45~~	~~65~~	83		
~~**Mar1_4_18**~~	~~2.0~~	~~102.8~~	~~260.8~~	~~7.71~~	~~2.9~~	~~0.08286~~	~~2.32~~	~~1.5178~~	~~3.8~~	~~0.13210~~	~~2.7~~	~~0.61~~	~~1250~~	~~88~~	~~799~~	~~41~~	~~932~~	~~46~~	~~64~~	86		
~~**Mar1_4_41**~~	~~1.7~~	~~2992.5~~	~~55.8~~	~~6.32~~	~~4.3~~	~~0.09656~~	~~1.57~~	~~2.1848~~	~~4.5~~	~~0.16509~~	~~4.2~~	~~0.94~~	~~1551~~	~~59~~	~~982~~	~~76~~	~~1165~~	~~62~~	~~63~~	84		
Mar1_4_85	0.1	592.8	70.0	16.59	5.4	0.06085	2.94	0.5189	5.2	0.06201	4.4	0.83	618	128	388	33	423	36	63	**92**		

Mar1_4_20	0.2	685.2	50.6	10.68	3.0	0.07060	3.78	0.9228	4.6	0.09598	3.1	0.72	947	163	590	35	658	43	62	**90**
Mar1_4_113	0.7	5085.8	96.1	3.88	4.4	0.15730	2.01	5.8101	4.2	0.26403	3.8	0.87	2421	66	1508	103	1938	76	62	78
Mar1_4_47	0.3	7206.7	1829.8	5.02	2.7	0.11862	1.03	3.2833	2.5	0.20234	2.6	0.91	1932	37	1186	56	1472	40	61	81
Mar1_4_59	1.8	1151.6	62.3	13.90	3.1	0.06461	1.67	0.6483	3.0	0.07347	2.7	0.80	751	71	457	24	506	24	61	**90**
Mar1_4_56	0.6	2174.4	148.9	4.44	5.3	0.14291	2.46	4.6088	5.1	0.23700	5.3	0.88	2251	85	1365	131	1735	87	61	79
Mar1_4_82	0.7	8312.6	79.9	4.91	2.8	0.12401	1.84	3.5020	2.8	0.20598	2.9	0.79	2009	65	1206	64	1525	43	60	79
Mar1_4_95	1.8	843.1	94.6	4.93	3.4	0.12291	1.57	3.5011	4.2	0.20476	4.2	0.92	2010	66	1197	92	1514	65	60	79
Mar1_4_90	0.3	735.4	210.7	5.26	3.9	0.12062	2.68	3.2270	3.7	0.19466	3.9	0.73	1952	97	1145	81	1457	59	59	79
Mar1_4_64	0.7	93.5	1509.1	4.43	2.0	0.14784	1.79	4.5900	1.7	0.22761	2.2	0.62	2314	62	1321	53	1746	29	57	76
Mar1_4_4	0.6	5112.4	73.8	6.04	3.2	0.10847	1.56	2.5642	3.3	0.16877	2.9	0.88	1767	58	1004	54	1284	51	57	78
Mar1_4_24	0.2	11521.0	62.1	5.54	2.2	0.11725	1.06	2.9602	2.5	0.18274	2.2	0.91	1911	40	1081	44	1393	37	57	78
Mar1_4_50	0.5	568.7	274.2	4.72	2.5	0.14797	1.46	4.3400	2.9	0.21442	2.5	0.85	2318	48	1251	56	1696	47	54	74
Mar1_4_77	0.8	1687.0	105.9	5.46	3.9	0.12725	2.65	3.3863	5.4	0.18685	3.8	0.60	2104	141	1103	77	1489	82	52	74
Mar1_4_122	0.7	1113.6	86.9	4.64	8.1	0.18828	1.60	6.3482	6.6	0.23546	6.1	0.92	2748	74	1355	152	1990	131	49	68
Mar1_4_124	0.4	2.2	1145.5	12.38	3.9	0.08033	5.70	0.8848	6.8	0.08275	4.8	0.67	1075	264	511	47	651	75	48	79
Mar1_4_1	1.7	1761.9	63.5	11.21	4.1	0.08110	3.26	1.0780	5.3	0.09254	4.0	0.68	1236	153	570	43	734	54	46	78
Mar1_4_72	1.2	180.3	543.3	8.89	1.8	0.09520	3.88	1.4750	4.6	0.11314	1.7	0.36	1504	126	691	23	914	50	46	76
Mar1_4_25	0.4	2070.7	41.5	6.70	3.6	0.12718	2.23	2.6700	4.3	0.15204	3.6	0.86	2051	75	911	60	1312	66	44	69
Mar1_4_35	0.4	1600.7	142.8	5.58	4.4	0.16030	1.57	4.0547	4.8	0.18426	4.8	0.95	2452	53	1086	97	1624	84	44	67
Mar1_4_110	0.9	1366.9	79.1	8.09	7.7	0.11416	1.23	2.1848	7.7	0.13678	7.5	0.99	1863	45	822	116	1152	109	44	71
Mar1_4_39	0.7	2596.3	87.2	4.93	2.7	0.19008	1.18	5.3547	3.3	0.20646	2.7	0.90	2739	39	1208	59	1868	57	44	65
Mar1_4_92	1.6	237.3	98.9	7.82	4.9	0.12334	3.56	2.2327	4.6	0.13198	4.5	0.68	1985	123	798	68	1184	65	40	67
Mar1_4_45	0.8	804.8	111.3	7.18	3.7	0.13282	2.88	2.5778	3.2	0.14401	4.0	0.53	2155	76	865	64	1288	47	40	67
Mar1_4_106	0.5	181.1	270.1	12.21	5.4	0.08878	6.79	1.0737	10.4	0.08586	4.9	0.51	1333	190	530	50	761	121	40	70
Mar1_4_128	0.3	313.5	401.5	7.56	2.1	0.12525	1.79	2.3484	2.8	0.13210	2.5	0.71	2045	73	799	38	1222	40	39	65
Mar1_4_125	0.5	381.1	508.2	7.72	3.4	0.12514	1.70	2.2946	4.1	0.13034	3.6	0.90	2022	61	788	55	1199	62	39	66
Mar1_4_36	2.8	211.5	45.6	9.96	5.0	0.11559	8.47	1.6874	10.9	0.10432	4.5	0.60	1778	265	639	55	969	125	36	66
Mar1_4_107	0.5	277.2	34.4	9.58	4.7	0.11884	9.33	1.6334	9.2	0.09966	5.4	0.09	1884	539	643	90	954	116	34	67
Mar1_4_51	1.3	2991.0	36.4	9.94	4.0	0.11824	1.70	1.7160	5.4	0.10519	4.5	0.96	1923	60	643	54	1001	66	33	64
Mar1_4_9	0.8	2406.9	103.6	9.42	4.8	0.13026	1.85	2.0002	4.4	0.11051	4.7	0.90	2094	65	674	60	1108	59	32	61
Mar1_4_104	0.3	378.1	656.2	10.18	3.4	0.11880	1.49	1.6599	2.6	0.10083	2.9	0.88	1931	53	619	35	990	34	32	63
Mar1_4_130	0.3	1417.6	54.6	29.80	2.6	0.06587	2.67	0.3049	4.0	0.03406	2.4	0.77	777	109	216	10	269	19	28	80
Mar1_4_74	0.2	5357.9	66.9	9.37	2.2	0.16042	1.49	2.3661	1.8	0.10793	2.0	0.66	2454	52	660	25	1230	25	27	54
Mar1_4_96	0.5	770.2	86.1	16.25	3.0	0.10141	1.50	0.8800	2.8	0.06277	2.7	0.86	1643	56	392	21	639	27	24	61
Mar1_4_33	0.7	396.9	127.9	12.95	1.9	0.12618	1.70	1.3266	2.5	0.07668	2.5	0.77	2039	62	476	23	856	28	23	56
Mar1_4_98	0.8	868.3	34.3	14.61	4.2	0.12049	1.74	1.1849	4.0	0.07125	4.1	0.89	1955	64	443	35	788	44	23	56
Mar1_4_12	2.4	421.1	56.4	14.22	3.6	0.13441	3.26	1.3274	3.2	0.07162	3.3	0.61	2140	107	446	29	855	36	21	52
Mar1_4_115	1.3	97.6	218.3	13.03	3.5	0.14891	2.64	1.5512	5.1	0.07546	5.4	0.89	2322	93	468	49	943	65	20	50
Mar1_4_126	0.7	10308.8	56.1	16.87	4.3	0.12413	1.96	1.0827	4.8	0.06221	4.3	0.89	2005	70	389	32	737	49	19	53
Mar1_4_89	0.5	11.3	231.5	28.05	6.1	0.09443	9.61	0.4921	11.2	0.03928	6.6	0.17	1527	282	248	32	390	75	16	64
Mar1_4_86	0.4	135.5	45.9	15.88	4.1	0.17080	2.25	1.5097	3.2	0.06479	4.1	0.87	2557	72	404	32	931	39	16	43
Mar1_4_116	0.6	279.3	275.7	24.91	2.7	0.10284	2.07	0.5803	2.4	0.04056	2.5	0.67	1668	78	256	13	464	18	15	55
Mar1_4_103	0.5	173.0	61.4	21.54	4.7	0.12600	3.17	0.8506	4.5	0.04885	4.3	0.78	2014	113	307	26	619	43	15	50
Mar1_4_118	0.8	2423.8	57.3	20.41	3.0	0.14803	2.47	1.0296	4.1	0.04980	3.2	0.73	2312	86	313	20	715	40	14	44
Mar1_4_119	0.8	166.0	15.8	20.05	2.7	0.17904	1.63	1.2640	2.4	0.05081	2.7	0.64	2637	53	319	17	827	27	12	39

~~Mar1_4_55~~	~~0.6~~	~~150.4~~	~~418.9~~	~~28.79~~	~~5.5~~	~~0.12296~~	~~2.78~~	~~0.6378~~	~~5.3~~	~~0.03713~~	~~4.8~~	~~0.74~~	~~1975~~	~~106~~	~~235~~	~~22~~	~~495~~	~~42~~	~~12~~	47			

Amostra M2AR 4-1

		Ratios										Rho	Dates						% conc [1]	% conc [2]	Best age	2s
Spot number	Th/U	206Pb/204Pb	1s	238U/206Pb	1s	207Pb/206Pb	1s	207Pb/235U	1s	206Pb/238U	1s		207Pb/206Pb	2s	206Pb/238U	2s	207Pb/235U	2s				
			(%)		(%)		(%)		(%)		(%)			(abs)		(abs)		(abs)				(abs)
MAR4_1_128	0.7	124.4	231.3	22.71	1.6	0.05473	2.25	0.3371	1.9	0.04435	1.5	0.19	377	100	280	8	295	9	74	95	280	8
MAR4_1_63	0.7	582.4	93.7	19.76	1.4	0.05843	2.01	0.4144	2.4	0.05087	1.3	0.56	528	82	320	8	351	14	61	91	320	8
MAR4_1_45	0.9	133.8	204.4	14.47	1.6	0.05842	1.87	0.5649	2.1	0.06898	1.4	0.18	529	82	430	12	454	15	81	95	430	12
MAR4_1_80	2.4	5861.9	51.7	10.87	2.1	0.06357	2.03	0.8180	2.4	0.09317	2.0	0.53	708	90	574	22	605	21	81	95	574	22
MAR4_1_97	1.3	2244.0	62.0	10.70	2.5	0.06211	1.74	0.8182	2.3	0.09510	2.4	0.48	665	73	585	26	606	21	88	97	585	26
MAR4_1_20	2.1	3082.5	81.0	10.52	1.8	0.06788	1.99	0.9192	2.6	0.09590	1.7	0.65	848	83	590	19	660	25	70	89	590	19
MAR4_1_58	0.3	952.8	70.3	10.51	1.8	0.06132	1.91	0.8190	2.3	0.09602	1.8	0.57	634	82	591	20	606	21	93	98	591	20
MAR4_1_65	2.1	103.4	444.0	10.45	1.4	0.06062	1.40	0.8117	1.6	0.09625	1.4	0.82	616	59	592	16	603	14	96	98	592	16
MAR4_1_14	2.4	643.2	102.1	10.32	1.7	0.06254	2.10	0.8352	1.9	0.09767	1.7	0.49	675	87	601	19	615	17	89	98	601	19
MAR4_1_99	0.4	10246.9	111.1	10.42	2.4	0.06188	2.08	0.8415	2.9	0.09777	2.5	0.69	650	88	601	29	617	26	92	97	601	29
MAR4_1_101	2.0	615.3	127.4	10.19	2.0	0.06289	1.82	0.8655	2.1	0.09939	2.1	0.44	689	80	611	24	632	19	89	97	611	24
MAR4_1_109	0.4	560.3	58.5	9.93	1.6	0.06505	3.07	0.8938	2.9	0.10159	1.7	0.55	744	108	623	21	660	37	84	94	623	21
MAR4_1_27	1.3	7312.8	72.5	9.96	2.6	0.06158	1.94	0.8600	1.9	0.10234	2.5	0.65	642	85	628	30	634	21	98	99	628	30
MAR4_1_54	1.7	3264.2	65.6	9.78	2.4	0.06817	2.65	0.9762	2.5	0.10393	2.3	0.28	844	110	637	28	689	25	75	92	637	28
MAR4_1_89	1.0	146.1	305.2	9.58	1.8	0.06806	3.29	0.9907	3.8	0.10443	2.0	0.24	827	133	640	24	694	37	77	92	640	24
MAR4_1_17	1.2	1009.3	105.2	9.55	2.5	0.06131	2.14	0.9039	2.5	0.10493	2.2	0.66	630	91	643	27	652	24	102	99	643	27
MAR4_1_10	0.4	566.3	78.8	9.60	2.1	0.06329	2.04	0.9246	2.3	0.10544	2.0	0.57	700	85	646	25	663	22	92	97	646	25
MAR4_1_32	0.7	248.2	172.1	9.31	1.7	0.06826	2.86	1.0267	3.0	0.10811	1.7	0.37	851	115	662	21	715	31	78	93	662	21
MAR4_1_118	2.4	377.7	59.4	9.12	3.6	0.06389	3.61	0.9839	4.0	0.10888	2.6	0.67	717	171	666	33	690	39	93	96	666	33
MAR4_1_81	0.8	302.2	113.5	9.24	1.8	0.06750	2.22	1.0232	2.4	0.10906	1.8	0.45	835	92	667	22	714	24	80	93	667	22
MAR4_1_98	0.5	1138.7	53.6	9.10	1.6	0.06698	2.16	1.0230	2.5	0.10979	1.8	0.50	817	91	671	23	713	25	82	94	671	23
MAR4_1_113	1.1	41.9	428.1	9.03	2.1	0.08500	21.18	1.0774	3.5	0.11216	2.0	0.13	773	170	685	25	737	37	89	93	685	25
MAR4_1_82	1.3	6.9	580.4	8.55	1.9	0.06766	5.61	1.1087	5.5	0.11788	2.0	0.23	771	219	718	27	748	58	93	96	718	27
MAR4_1_16	0.8	349.7	109.2	7.70	1.3	0.07341	1.84	1.3318	2.3	0.13036	1.3	0.57	1014	77	790	20	858	27	78	92	790	20
MAR4_1_92	1.3	271.1	220.7	7.38	2.0	0.07505	2.96	1.4280	3.0	0.13662	2.0	0.40	1047	111	825	30	897	36	79	92	825	30
MAR4_1_103	1.1	1628.8	97.1	6.86	1.3	0.06703	1.44	1.3689	1.8	0.14646	1.4	0.57	829	62	881	22	874	21	106	101	881	22
MAR4_1_115	1.3	1793.7	49.2	5.86	1.7	0.07399	1.03	1.7754	1.7	0.17205	1.7	0.82	1036	42	1023	31	1035	23	99	99	1023	31
MAR4_1_57	1.3	1096.8	44.9	5.83	1.7	0.07710	1.90	1.8607	2.5	0.17303	1.7	0.18	1109	77	1028	33	1063	32	93	97	1028	33
MAR4_1_112	1.0	3331.1	31.2	5.84	2.1	0.07927	1.98	1.9113	2.5	0.17325	2.0	0.59	1163	82	1029	38	1081	32	89	95	1029	38
MAR4_1_71	0.6	581.0	63.6	5.64	1.1	0.07625	1.09	1.8905	1.3	0.17797	1.1	0.55	1096	44	1056	21	1077	17	96	98	1056	21
MAR4_1_105	0.2	162.2	506.8	5.59	1.8	0.07281	1.06	1.8308	1.4	0.18067	1.7	0.77	1003	44	1070	34	1061	16	107	101	1070	34
MAR4_1_106	1.0	5504.8	96.6	5.54	2.1	0.07651	2.01	1.9596	2.4	0.18281	2.1	0.26	1091	85	1081	41	1098	32	99	98	1081	41
MAR4_1_124	1.3	507.7	137.9	5.44	1.5	0.07607	1.80	1.9548	1.7	0.18491	1.5	0.23	1084	70	1093	29	1098	23	101	100	1093	29
MAR4_1_48	1.3	3120.6	51.9	5.12	1.5	0.07760	1.49	2.1342	1.6	0.19643	1.4	0.00	1128	61	1156	31	1166	27	102	99	1156	31
MAR4_1_129	0.9	596.1	407.9	4.87	1.7	0.08415	3.53	2.3531	2.0	0.20610	1.8	0.19	1276	125	1208	39	1245	46	95	97	1208	39

MAR4_1_67	0.8	615.8	111.9	4.70	1.4	0.08551	1.58	2.5334	2.3	0.21233	1.6	0.70	1318	60	1240	36	1278	34	94	97	1240	36
MAR4_1_95	0.6	19229.4	73.3	4.66	1.5	0.07998	1.54	2.4121	2.1	0.21417	1.3	0.68	1187	60	1251	29	1243	30	105	101	1251	29
MAR4_1_8	2.6	476.6	99.9	4.66	1.9	0.08392	1.16	2.5465	1.9	0.21680	1.9	0.79	1285	45	1264	43	1283	27	98	99	1264	43
MAR4_1_91	0.9	1399.9	54.7	4.52	2.5	0.09154	2.18	2.8626	3.6	0.22420	2.9	0.81	1446	87	1302	67	1366	54	90	95	1302	67
MAR4_1_119	1.0	1388.8	80.9	3.97	2.1	0.09141	1.50	3.2460	2.2	0.25510	2.1	0.75	1446	60	1463	55	1464	33	101	100	1463	55
MAR4_1_21	0.4	931.9	2604.3	3.65	1.8	0.09593	1.50	3.6824	1.7	0.27338	1.5	0.58	1556	48	1557	42	1565	27	100	99	1556	48
MAR4_1_49	0.8	1353.4	150.2	3.58	2.1	0.09361	1.41	3.6734	1.8	0.27818	1.8	0.75	1493	56	1581	52	1563	29	106	101	1581	52
MAR4_1_46	1.2	22947.1	64.4	3.54	1.8	0.11025	4.13	4.5508	5.2	0.28465	1.9	0.09	1829	174	1614	55	1725	81	88	94	1829	174
MAR4_1_78	0.9	6589.2	67.5	3.05	3.3	0.11411	5.59	5.2719	6.1	0.33121	3.3	0.39	1836	178	1842	106	1853	94	100	99	1836	178
MAR4_1_61	2.0	2030.5	63.0	3.33	2.1	0.11251	1.46	4.7933	1.6	0.30416	2.0	0.59	1850	62	1710	60	1781	27	92	96	1850	62
MAR4_1_23	0.5	2416.4	120.6	3.86	1.7	0.11334	1.08	4.1080	1.5	0.26057	1.7	0.76	1850	39	1492	45	1654	24	81	90	1850	39
MAR4_1_100	0.1	295.4	665.0	3.10	2.0	0.11668	1.92	5.2460	2.4	0.32561	1.9	0.04	1895	69	1815	60	1855	41	96	98	1895	69
MAR4_1_12	1.4	18164.3	73.8	3.09	1.9	0.11760	1.49	5.3356	2.1	0.32674	1.9	0.74	1913	52	1821	59	1870	35	95	97	1913	52
MAR4_1_96	0.8	9803.7	56.1	3.29	1.5	0.12085	1.39	5.1130	2.1	0.30328	1.8	0.77	1962	49	1706	53	1846	28	87	92	1962	49
MAR4_1_70	2.3	192.1	46.3	2.92	2.5	0.12646	3.51	6.1258	3.9	0.34862	2.3	0.42	2011	124	1925	76	1978	67	96	97	2011	124
MAR4_1_87	0.9	2683.1	90.2	3.26	2.7	0.12500	1.62	5.5171	2.6	0.31250	2.7	0.62	2020	61	1749	83	1897	46	87	92	2020	61
MAR4_1_28	0.5	1524.4	86.8	2.77	1.1	0.13028	1.39	6.6556	1.8	0.36242	1.1	0.14	2120	67	1993	38	2064	31	94	97	2120	67
MAR4_1_111	1.9	33767.6	104.9	2.46	1.5	0.13292	1.58	7.5565	2.2	0.40913	1.5	0.59	2143	64	2209	57	2184	34	103	101	2143	64
MAR4_1_59	0.7	1179.2	87.3	2.52	2.0	0.13450	1.56	7.4860	2.0	0.40066	1.9	0.70	2149	54	2169	72	2167	35	101	100	2149	54
MAR4_1_41	0.7	7767.9	101.7	2.55	2.1	0.13535	1.26	7.4695	2.2	0.39682	2.0	0.82	2163	44	2152	75	2165	38	99	99	2163	44
MAR4_1_64	0.6	26328.5	71.0	2.45	2.2	0.13940	1.80	8.0814	2.5	0.41487	2.2	0.32	2209	60	2233	83	2233	44	101	100	2209	60
MAR4_1_38	0.7	46963.2	64.4	2.56	1.8	0.13991	1.70	7.6233	2.0	0.39267	1.8	0.61	2219	59	2134	66	2184	37	96	98	2219	59
MAR4_1_35	1.7	7.7	1276.9	2.32	1.6	0.14152	1.72	8.4539	1.9	0.43099	2.0	0.58	2237	61	2307	76	2277	35	103	101	2237	61
MAR4_1_13	1.9	624.8	64.4	2.17	2.0	0.15699	1.81	10.2420	2.4	0.46570	1.8	0.52	2412	61	2461	77	2449	43	102	100	2412	61
MAR4_1_53	1.8	1568.7	149.9	2.02	2.2	0.18618	1.21	12.9647	2.0	0.50113	2.2	0.83	2704	40	2614	94	2672	37	97	98	2704	40
MAR4_1_107	1.5	1308.9	68.5	1.92	2.5	0.19878	5.00	14.6252	5.6	0.52520	2.5	0.46	2787	147	2718	112	2773	100	98	98	2787	147
MAR4_1_85	0.8	988.2	12.2	2.18	1.8	0.19694	1.58	12.6581	2.0	0.46170	1.8	0.64	2794	52	2444	73	2650	38	87	92	2794	52
MAR4_1_9	0.7	25837.4	48.9	1.56	2.8	0.29143	2.62	26.4544	3.3	0.65525	2.8	0.64	3407	83	3238	143	3349	66	95	97	3407	83
Data not used due to high discordance																						
~~**MAR4_1_83**~~	~~0.7~~	~~43.4~~	~~3.6~~	~~5.22~~	~~1.5~~	~~0.43328~~	~~1.47~~	~~11.6233~~	~~2.1~~	~~0.19243~~	~~1.5~~	~~0.90~~	~~4025~~	~~43~~	~~1134~~	~~32~~	~~2572~~	~~37~~	28.2	44.1		
~~**MAR4_1_18**~~	~~1.4~~	~~635.9~~	~~17.9~~	~~5.42~~	~~2.6~~	~~0.11036~~	~~2.72~~	~~2.8833~~	~~4.1~~	~~0.18724~~	~~2.7~~	~~0.75~~	~~1786~~	~~99~~	~~1105~~	~~55~~	~~1368~~	~~59~~	61.9	80.8		
~~**MAR4_1_26**~~	~~1.3~~	~~22407.8~~	~~65.9~~	~~3.97~~	~~1.8~~	~~0.10969~~	~~1.61~~	~~3.8784~~	~~2.2~~	~~0.25396~~	~~1.8~~	~~0.69~~	~~1786~~	~~60~~	~~1458~~	~~47~~	~~1605~~	~~37~~	81.6	90.8		
~~**MAR4_1_22**~~	~~1.0~~	~~2005.6~~	~~136.5~~	~~3.89~~	~~2.0~~	~~0.10961~~	~~1.63~~	~~3.9487~~	~~1.8~~	~~0.26000~~	~~1.9~~	~~0.62~~	~~1783~~	~~59~~	~~1488~~	~~52~~	~~1621~~	~~29~~	83.5	91.8		
~~**MAR4_1_66**~~	~~1.1~~	~~91.8~~	~~181.8~~	~~9.08~~	~~2.1~~	~~0.11693~~	~~7.90~~	~~1.7558~~	~~8.2~~	~~0.11165~~	~~2.2~~	~~0.61~~	~~1714~~	~~285~~	~~682~~	~~29~~	~~1018~~	~~113~~	39.8	67.0		
~~**MAR4_1_127**~~	~~1.6~~	~~576.7~~	~~81.2~~	~~5.89~~	~~2.5~~	~~0.10677~~	~~6.76~~	~~2.5622~~	~~9.0~~	~~0.17257~~	~~2.5~~	~~0.51~~	~~1621~~	~~219~~	~~1025~~	~~47~~	~~1238~~	~~120~~	63.2	82.8		
~~**MAR4_1_62**~~	~~1.1~~	~~19.9~~	~~285.7~~	~~9.76~~	~~2.3~~	~~0.10141~~	~~4.30~~	~~1.4525~~	~~4.2~~	~~0.10388~~	~~2.2~~	~~0.18~~	~~1593~~	~~163~~	~~637~~	~~27~~	~~903~~	~~48~~	40.0	70.5		
~~**MAR4_1_31**~~	~~1.8~~	~~59.1~~	~~27.9~~	~~6.84~~	~~3.9~~	~~0.28284~~	~~4.04~~	~~5.6363~~	~~3.6~~	~~0.15024~~	~~3.9~~	~~0.50~~	~~3352~~	~~129~~	~~901~~	~~66~~	~~1941~~	~~81~~	26.9	46.4		
~~**MAR4_1_76**~~	~~1.2~~	~~2865.1~~	~~71.5~~	~~11.36~~	~~3.7~~	~~0.09670~~	~~3.83~~	~~1.2605~~	~~5.4~~	~~0.09129~~	~~3.6~~	~~0.58~~	~~1559~~	~~157~~	~~562~~	~~39~~	~~817~~	~~58~~	36.1	68.9		
~~**MAR4_1_55**~~	~~3.1~~	~~94.0~~	~~3.8~~	~~4.01~~	~~2.7~~	~~0.26369~~	~~2.22~~	~~9.2270~~	~~2.1~~	~~0.25122~~	~~2.4~~	~~0.51~~	~~3263~~	~~71~~	~~1444~~	~~63~~	~~2359~~	~~39~~	44.3	61.2		
~~**MAR4_1_33**~~	~~0.3~~	~~171.8~~	~~35.9~~	~~4.57~~	~~3.5~~	~~0.25455~~	~~2.76~~	~~7.9848~~	~~2.6~~	~~0.22687~~	~~3.3~~	~~0.73~~	~~3219~~	~~95~~	~~1314~~	~~79~~	~~2221~~	~~46~~	40.8	59.2		
~~**MAR4_1_72**~~	~~1.5~~	~~91.2~~	~~7.5~~	~~9.03~~	~~1.8~~	~~0.24398~~	~~2.08~~	~~3.7763~~	~~2.1~~	~~0.11168~~	~~1.8~~	~~0.19~~	~~3136~~	~~64~~	~~682~~	~~23~~	~~1584~~	~~34~~	21.8	43.1		
~~**MAR4_1_29**~~	~~1.2~~	~~97.7~~	~~6.6~~	~~10.14~~	~~1.8~~	~~0.21618~~	~~4.86~~	~~2.9191~~	~~4.0~~	~~0.09843~~	~~2.1~~	~~0.01~~	~~2889~~	~~153~~	~~605~~	~~24~~	~~1373~~	~~63~~	20.9	44.1		
~~**MAR4_1_2**~~	~~1.9~~	~~5.1~~	~~1076.9~~	~~7.68~~	~~3.6~~	~~0.18967~~	~~3.39~~	~~3.4502~~	~~2.3~~	~~0.13333~~	~~3.8~~	~~0.33~~	~~2718~~	~~119~~	~~806~~	~~57~~	~~1513~~	~~36~~	29.6	53.2		
~~**MAR4_1_1**~~	~~0.9~~	~~191.9~~	~~94.6~~	~~10.61~~	~~7.2~~	~~0.19799~~	~~9.00~~	~~2.8885~~	~~12.6~~	~~0.10304~~	~~8.3~~	~~0.34~~	~~2716~~	~~252~~	~~629~~	~~97~~	~~1390~~	~~215~~	23.2	45.3		

MAR4_1_126	0.8	200.4	51.4	8.46	1.9	0.17790	2.83	2.9142	2.8	0.11812	2.2	0.42	2611	93	719	30	1379	43	27.5	52.1
MAR4_1_43	0.7	260.8	44.2	2.98	1.9	0.17124	1.98	8.0675	2.4	0.33887	1.8	0.80	2558	65	1879	59	2232	43	73.5	84.2
MAR4_1_74	1.3	298.2	17.0	3.05	2.5	0.16850	2.55	7.5547	2.4	0.32186	3.3	0.68	2552	93	1793	106	2173	44	70.3	82.5
MAR4_1_40	1.3	200.9	136.6	7.94	5.8	0.20915	10.08	4.0940	12.3	0.14329	7.1	0.69	2523	397	855	111	1531	220	33.9	55.9
MAR4_1_30	2.1	651.0	53.8	10.38	3.8	0.16861	6.07	2.3280	8.3	0.09855	4.0	0.63	2487	209	605	46	1197	112	24.3	50.6
MAR4_1_93	0.3	207.6	5.8	6.02	1.8	0.16292	1.34	3.7902	2.3	0.16697	1.8	0.81	2482	45	995	33	1588	37	40.1	62.7
MAR4_1_56	0.8	4814.2	71.3	3.07	4.0	0.16426	3.45	7.3328	2.8	0.33588	4.1	0.55	2465	113	1856	133	2157	62	75.3	86.1
MAR4_1_104	0.8	155.0	9.2	11.17	1.6	0.15990	2.18	2.0042	2.1	0.09008	1.6	0.33	2442	74	556	17	1115	28	22.8	49.9
MAR4_1_130	1.3	147.7	5.7	12.49	1.6	0.15540	1.81	1.7640	1.8	0.08054	1.5	0.18	2397	57	499	14	1031	23	20.8	48.4
MAR4_1_3	1.2	182.8	28.9	9.27	2.4	0.15558	7.40	2.3817	9.2	0.10868	2.4	0.76	2337	252	665	31	1211	127	28.4	54.9
MAR4_1_44	0.9	1511.7	19.8	2.76	1.7	0.14927	1.38	7.5726	1.8	0.36478	1.8	0.71	2332	47	2003	62	2178	32	85.9	91.9
MAR4_1_42	2.0	182.7	13.4	9.60	2.1	0.15180	6.32	2.2290	6.3	0.10546	2.1	0.08	2258	206	646	26	1164	84	28.6	55.5
MAR4_1_69	1.3	234.3	19.1	8.14	3.1	0.14495	5.01	2.5609	7.6	0.12592	3.3	0.80	2233	150	764	47	1258	97	34.2	60.7
MAR4_1_90	0.7	1354.5	48.5	3.14	1.7	0.13905	2.05	6.0857	2.0	0.32103	1.7	0.54	2226	60	1793	52	1984	35	80.6	90.4
MAR4_1_102	2.5	123.3	164.8	3.35	3.1	0.13909	2.88	5.8643	3.5	0.30357	3.0	0.66	2200	100	1706	90	1947	63	77.6	87.6
MAR4_1_125	0.3	1232.4	62.1	3.09	1.7	0.13724	1.36	6.2294	1.2	0.32605	1.6	0.57	2187	47	1818	51	2007	21	83.1	90.6
MAR4_1_88	0.5	1618.8	50.5	11.69	4.2	0.16389	10.40	1.7265	9.0	0.08878	5.6	0.50	2171	372	546	58	977	104	25.2	55.9
MAR4_1_121	1.0	301.3	25.5	12.15	2.9	0.12764	4.23	1.4683	5.5	0.08125	2.8	0.43	2017	138	503	27	905	56	24.9	55.6
MAR4_1_36	1.7	347.0	68.9	3.48	2.9	0.12551	6.36	4.8150	6.2	0.28583	2.3	0.84	1957	183	1619	66	1762	88	82.7	91.9
MAR4_1_79	0.1	18.5	138.8	7.48	3.5	0.12281	5.27	2.3213	5.0	0.13846	3.6	0.19	1908	205	834	56	1202	72	43.7	69.4
MAR4_1_11	0.6	4659.3	122.0	3.89	2.1	0.11568	4.13	4.3265	6.8	0.25963	2.1	0.83	1899	171	1487	55	1708	119	78.3	87.0
MAR4_1_108	1.2	801.1	34.9	13.22	2.6	0.12664	7.28	1.2868	6.0	0.07724	2.6	0.00	1893	248	479	24	824	65	25.3	58.2
MAR4_1_37	2.3	134.6	76.8	4.67	1.7	0.11702	4.88	3.5162	5.6	0.21508	1.6	0.53	1863	163	1255	37	1513	84	67.4	83.0
MAR4_1_123	1.4	208.1	62.1	8.31	3.7	0.09946	9.33	1.7086	8.8	0.12629	4.3	0.11	1445	374	764	62	969	106	52.9	78.9
MAR4_1_114	1.7	1641.8	56.8	10.51	2.0	0.08868	2.58	1.1863	2.8	0.09622	1.9	0.39	1401	109	592	22	800	35	42.2	74.0
MAR4_1_86	1.2	3620.4	56.9	9.48	2.1	0.08970	3.00	1.3364	3.6	0.10673	1.9	0.54	1385	117	653	24	855	42	47.2	76.4
MAR4_1_34	0.7	258.3	53.4	9.91	2.5	0.08854	1.97	1.2263	3.0	0.10153	2.8	0.65	1378	82	623	33	809	34	45.2	77.0
MAR4_1_117	1.3	144.4	294.6	9.62	1.9	0.09014	4.82	1.3144	4.7	0.10476	1.8	0.19	1359	195	642	22	843	56	47.3	76.1
MAR4_1_51	1.4	30.1	3615.7	6.24	1.5	0.08483	1.95	1.8757	1.5	0.16107	1.4	0.29	1323	86	962	25	1078	24	72.8	89.3
MAR4_1_4	0.4	1481.2	40.1	9.20	2.7	0.08523	4.05	1.3052	4.3	0.11050	2.4	0.41	1269	158	675	31	841	49	53.2	80.3
MAR4_1_60	3.0	290.8	120.7	8.20	2.0	0.08408	4.53	1.4550	5.5	0.12350	2.0	0.52	1220	167	750	29	897	61	61.5	83.6
MAR4_1_15	1.3	1186.8	63.7	8.53	2.2	0.08071	3.84	1.3768	5.0	0.11870	2.2	0.35	1214	172	723	30	868	57	59.5	83.2
MAR4_1_68	0.7	1428.7	43.6	10.47	1.8	0.07973	2.19	1.0522	2.4	0.09646	1.7	0.56	1172	85	593	20	728	25	50.7	81.5
MAR4_1_120	1.0	603.1	86.8	9.71	2.4	0.08128	4.81	1.1823	6.5	0.10280	2.1	0.84	1163	172	630	25	779	65	54.2	81.0
MAR4_1_52	1.9	8226.8	86.4	9.67	2.1	0.07616	4.59	1.0728	6.6	0.10440	2.0	0.69	1101	204	640	24	751	54	58.1	85.2
MAR4_1_116	0.8	155.6	92.1	11.34	3.0	0.07888	5.05	1.0003	5.5	0.08966	2.8	0.25	1095	220	553	30	697	55	50.5	79.4
MAR4_1_19	0.3	12.0	1036.6	10.24	2.7	0.07595	2.95	1.0454	3.3	0.09938	2.6	0.54	1066	117	610	30	723	35	57.3	84.4
MAR4_1_110	0.1	357.2	106.4	10.12	2.1	0.07437	3.86	1.0346	4.6	0.10009	2.0	0.56	1040	174	615	24	713	45	59.1	86.1
MAR4_1_75	1.3	76.7	164.2	11.10	2.7	0.07637	4.19	0.9397	3.9	0.09051	2.3	0.65	1032	177	558	25	667	39	54.1	83.7
MAR4_1_77	1.0	113.7	94.8	14.36	2.2	0.07480	3.46	0.7285	3.5	0.07043	2.5	0.13	1029	142	439	21	553	29	42.6	79.2
MAR4_1_7	1.2	1084.2	107.4	9.47	2.5	0.07449	4.38	1.1122	4.9	0.10764	2.5	0.43	996	146	658	31	750	47	66.1	87.8
MAR4_1_122	0.2	3230.5	63.8	9.31	3.5	0.07183	2.66	1.1222	3.5	0.11105	3.1	0.59	979	117	678	40	759	38	69.2	89.4
MAR4_1_5	1.3	606.9	29.9	9.68	1.7	0.07233	2.15	1.0463	2.7	0.10421	1.7	0.49	976	87	639	20	724	28	65.4	88.2

MAR4_1_24	1.0	322.6	135.7	10.62	3.7	0.07267	3.43	0.9545	3.9	0.09854	4.0	0.74	953	147	605	46	675	39	63.5	89.6
MAR4_1_50	0.7	799.2	76.6	10.66	1.7	0.07017	3.24	0.9276	3.9	0.09459	1.7	0.57	892	128	582	18	661	37	65.3	88.1
MAR4_1_84	1.1	248.9	108.5	12.67	1.6	0.07001	3.12	0.7707	3.4	0.07956	1.6	0.58	891	121	493	15	577	29	55.4	85.5

Amostra M2AR 5-1

			Ratios								Rho	Ages (Ma)						% conc [1]	% conc [2]	Best age	2s
Spot number	Th/U	206Pb/204Pb	1s	238U/206Pb	1s	207Pb/206Pb	1s	207Pb/235U	1s	206Pb/238U	1s		207Pb/206Pb	2s	206Pb/238U	2s	207Pb/235U	2s				
			(%)		(%)		(%)		(%)		(%)			(abs)		(abs)		(abs)				(abs)
MAR5_1_9	2.0	8625.0	51.0	20.19	3.6	0.05375	2.56	0.3805	3.7	0.05111	3.5	0.68	335	117	321	22	326	20	96.0	98.4	321	22
MAR5_1_44	0.6	3467.2	113.9	13.14	3.7	0.06300	3.29	0.6821	3.5	0.07874	3.8	0.67	673	133	488	36	526	28	72.6	92.8	488	36
MAR5_1_48	1.7	3705.9	50.3	12.79	3.5	0.06215	3.48	0.6758	2.7	0.08034	3.3	0.51	639	141	498	31	523	22	77.8	95.2	498	31
MAR5_1_82	2.9	530.2	87.8	12.19	2.6	0.06277	3.25	0.7101	2.1	0.08197	2.8	0.12	668	127	508	27	544	17	75.9	93.3	508	27
MAR5_1_50	0.5	394.1	90.0	12.29	3.3	0.06092	4.17	0.6758	4.4	0.08246	3.3	0.45	609	164	511	33	522	36	83.9	97.7	511	33
MAR5_1_35	1.4	2018.6	124.6	12.20	3.7	0.05905	3.29	0.6919	4.0	0.08440	3.5	0.61	532	141	522	35	531	33	98.2	98.3	522	35
MAR5_1_15	0.4	291.9	495.5	11.80	3.6	0.05847	2.55	0.7071	3.4	0.08729	3.5	0.72	523	112	539	36	541	29	103.0	99.7	539	36
MAR5_1_70	0.8	1543.3	171.6	11.82	4.4	0.06026	3.17	0.7398	4.1	0.08751	4.2	0.72	584	142	540	44	560	35	92.5	96.5	540	44
MAR5_1_12	1.0	2513.2	43.8	11.64	3.1	0.06102	3.36	0.7488	4.1	0.08784	3.3	0.58	601	152	542	34	564	36	90.3	96.1	542	34
MAR5_1_93	0.7	3193.9	110.9	11.60	3.3	0.05940	2.75	0.7324	3.5	0.08840	3.2	0.62	554	118	546	33	555	30	98.4	98.2	546	33
MAR5_1_39	1.4	135.0	328.4	11.28	2.9	0.06158	2.67	0.7966	3.4	0.09019	2.6	0.21	635	114	556	28	592	30	87.6	93.9	556	28
MAR5_1_42	0.1	1484.1	37.4	11.18	3.5	0.05966	3.32	0.7531	3.6	0.09191	3.5	0.56	555	142	566	38	567	32	102.0	99.8	566	38
MAR5_1_81	0.2	2467.8	81.6	11.19	3.9	0.05882	2.54	0.7596	4.3	0.09235	3.9	0.78	539	110	569	42	570	37	105.6	99.8	569	42
MAR5_1_99	0.3	2076.5	138.9	10.83	2.5	0.06003	1.51	0.7826	3.1	0.09353	2.4	0.82	597	65	576	26	585	27	96.6	98.5	576	26
MAR5_1_30	0.9	345.8	203.0	10.89	3.6	0.06394	3.80	0.8160	3.8	0.09438	3.5	0.73	699	146	581	39	616	42	83.1	94.3	581	39
MAR5_1_77	0.9	305.0	283.8	10.52	2.3	0.06217	1.97	0.8400	2.8	0.09612	2.3	0.67	667	86	591	26	617	26	88.7	95.8	591	26
MAR5_1_58	1.7	1867.5	49.8	10.45	2.4	0.06157	1.68	0.8249	2.1	0.09687	2.2	0.66	648	72	596	25	610	19	91.9	97.7	596	25
MAR5_1_31	0.7	264.0	139.2	10.40	3.0	0.06688	2.69	0.9097	3.1	0.09809	2.8	0.64	809	112	603	32	654	30	74.5	92.1	603	32
MAR5_1_105	1.3	157.1	169.1	10.33	2.7	0.06282	2.51	0.8654	2.5	0.09835	2.6	0.49	682	104	604	30	632	23	88.6	95.7	604	30
MAR5_1_66	1.9	79.9	458.7	10.33	2.9	0.06273	3.09	0.8517	2.7	0.09889	2.9	0.34	663	133	607	34	624	25	91.6	97.4	607	34
MAR5_1_49	4.3	545.4	86.6	10.17	2.0	0.06952	3.83	0.9626	4.0	0.09804	1.8	0.28	874	140	611	25	680	38	69.9	89.8	611	25
MAR5_1_27	1.1	4856.1	98.3	10.03	2.6	0.05981	2.01	0.8293	2.9	0.09971	3.1	0.80	582	87	612	36	611	26	105.2	100.1	612	36
MAR5_1_68	0.3	335.3	435.8	10.05	3.2	0.06589	5.93	0.9194	5.0	0.10176	3.2	0.15	731	182	624	38	656	45	85.4	95.1	624	38
MAR5_1_97	0.7	2172.7	54.8	10.06	3.6	0.06940	2.82	0.9779	3.3	0.10239	3.3	0.53	880	125	628	40	689	33	71.3	91.1	628	40
MAR5_1_62	0.8	1027.7	45.8	10.05	3.7	0.06316	2.23	0.8949	3.1	0.10274	3.5	0.75	694	96	630	42	646	30	90.7	97.4	630	42
MAR5_1_89	0.2	1037.1	69.9	9.64	1.8	0.06331	2.09	0.9059	2.8	0.10300	2.4	0.70	705	88	632	28	653	27	89.6	96.7	632	28
MAR5_1_85	1.5	1240.6	100.3	9.82	3.9	0.07220	3.99	0.9991	3.9	0.10376	3.6	0.31	961	171	636	44	701	38	66.2	90.7	636	44
MAR5_1_29	1.3	12682.2	96.2	9.86	3.4	0.06369	3.12	0.9171	3.5	0.10421	3.3	0.64	698	131	638	41	657	34	91.5	97.1	638	41
MAR5_1_91	1.6	1752.1	136.2	9.74	3.2	0.06604	2.25	0.9662	4.1	0.10418	3.2	0.31	796	92	638	38	684	39	80.2	93.4	638	38
MAR5_1_102	1.2	116.4	909.9	9.72	3.2	0.06093	2.56	0.8891	3.1	0.10542	3.2	0.62	612	113	645	39	643	29	105.4	100.3	645	39
MAR5_1_37	0.2	1944.0	89.8	9.64	3.1	0.06698	2.30	1.0177	4.7	0.10586	2.8	0.64	819	94	648	35	706	46	79.1	91.8	648	35
MAR5_1_18	0.9	211.5	140.2	9.58	4.0	0.06507	2.91	0.9750	4.0	0.10835	3.9	0.68	746	125	662	49	686	40	88.7	96.5	662	49
MAR5_1_73	1.7	1822.1	68.5	9.23	2.2	0.06347	2.59	0.9480	3.5	0.10924	2.1	0.52	706	110	668	27	674	34	94.7	99.1	668	27
MAR5_1_36	1.2	324.9	71.4	9.22	3.2	0.07039	3.27	1.0833	3.9	0.11095	3.2	0.52	906	137	678	41	741	41	74.8	91.5	678	41

MAR5_1_25	1.1	287.6	107.8	9.08	2.6	0.07232	2.96	1.0763	3.3	0.11096	2.5	0.40	979	125	678	32	740	35	69.2	91.6	678	32
MAR5_1_8	0.4	313.1	330.1	8.63	2.5	0.06689	2.87	1.1017	2.9	0.11736	2.6	0.40	812	115	715	35	752	31	88.1	95.1	715	35
MAR5_1_63	1.1	58.6	406.9	8.75	4.8	0.06859	5.22	1.0357	4.4	0.11800	4.5	0.54	836	199	718	61	743	66	85.9	96.6	718	61
MAR5_1_75	0.7	4323.8	64.1	8.01	1.8	0.06541	1.24	1.1302	1.6	0.12571	1.8	0.71	782	52	763	25	767	17	97.6	99.5	763	25
MAR5_1_24	1.3	402.4	87.6	7.52	2.3	0.07326	2.56	1.3400	2.9	0.13487	2.3	0.51	999	98	815	36	860	33	81.6	94.8	815	36
MAR5_1_28	0.7	293.0	147.2	7.11	2.7	0.06998	2.18	1.4328	3.5	0.14282	2.7	0.57	950	114	860	43	898	41	90.5	95.7	860	43
MAR5_1_57	0.8	3027.4	56.8	6.59	3.2	0.07474	2.60	1.6183	2.9	0.15523	3.3	0.67	1042	103	929	57	974	37	89.1	95.4	929	57
MAR5_1_79	0.9	2070.9	76.1	6.12	2.4	0.07625	2.69	1.7184	3.3	0.16345	2.8	0.11	1073	122	975	52	1009	45	90.8	96.6	975	52
MAR5_1_67	0.5	721.1	159.3	6.11	2.4	0.07221	2.38	1.6551	1.7	0.16557	2.2	0.24	975	94	987	41	990	21	101.2	99.7	987	41
MAR5_1_115	1.0	3893.5	71.5	6.11	2.5	0.08309	3.63	1.9140	4.0	0.16613	2.3	0.33	1236	120	990	43	1078	49	80.1	91.8	990	43
MAR5_1_86	0.9	147.2	266.3	5.94	2.6	0.07460	1.89	1.7540	2.3	0.17058	2.5	0.62	1047	75	1014	47	1026	30	96.9	98.8	1014	47
MAR5_1_2	2.5	9943.0	45.7	6.03	4.5	0.07306	2.95	1.7367	3.8	0.17401	4.4	0.74	987	121	1031	83	1015	49	104.5	101.6	1031	83
MAR5_1_90	1.5	3583.0	78.5	5.71	2.6	0.07404	2.99	1.8095	3.5	0.17706	2.6	0.60	1024	122	1050	51	1045	45	102.6	100.5	1050	51
MAR5_1_56	0.2	1593.5	162.8	5.84	3.9	0.07286	2.59	1.7931	3.6	0.17780	4.2	0.77	990	102	1052	81	1037	47	106.3	101.5	1052	81
MAR5_1_72	0.6	495.2	115.0	5.57	3.4	0.07967	3.09	1.9832	3.3	0.18158	4.1	0.60	1160	120	1073	81	1104	45	92.5	97.2	1073	81
MAR5_1_1	2.2	1191.1	88.8	5.65	3.5	0.07547	3.09	1.8993	3.8	0.18176	3.4	0.62	1052	126	1075	67	1074	49	102.1	100.0	1075	67
MAR5_1_43	0.6	415.1	286.6	5.31	3.6	0.07912	3.40	2.1141	3.0	0.18740	2.7	0.47	1145	135	1106	54	1149	41	96.6	96.3	1106	54
MAR5_1_53	0.7	2429.4	113.8	5.09	2.8	0.08011	2.72	2.2303	2.9	0.19970	2.6	0.50	1178	108	1172	56	1186	40	99.5	98.8	1172	56
MAR5_1_7	0.9	684.1	89.5	5.01	2.9	0.08083	3.04	2.2688	3.0	0.20356	3.0	0.45	1190	118	1193	64	1197	43	100.2	99.6	1193	64
MAR5_1_10	0.5	17772.6	116.3	4.94	3.2	0.08166	3.11	2.3677	4.1	0.20682	3.3	0.68	1211	124	1210	72	1224	58	99.9	98.8	1210	72
MAR5_1_55	0.8	230.4	291.0	4.16	2.3	0.08713	2.10	2.8832	2.5	0.24239	2.4	0.63	1353	83	1398	60	1375	38	103.3	101.7	1398	60
MAR5_1_83	0.6	1856.6	35.7	3.57	2.0	0.09608	1.20	3.7622	2.0	0.28232	1.9	0.83	1545	45	1602	55	1582	32	103.7	101.3	1545	45
MAR5_1_3	2.5	1185.4	148.3	3.05	3.0	0.12008	2.79	5.5344	3.3	0.33317	3.0	0.62	1941	100	1850	96	1899	54	95.3	97.4	1941	100
MAR5_1_20	9.1	347.8	112.8	2.97	3.4	0.12128	2.72	5.8206	4.0	0.34635	3.4	0.71	1956	99	1911	114	1937	67	97.7	98.7	1956	99
MAR5_1_61	1.5	6706.9	60.7	2.88	3.1	0.12173	2.22	6.0077	3.5	0.35486	3.0	0.75	1968	79	1953	100	1965	62	99.2	99.4	1968	79
MAR5_1_46	1.7	410.6	132.0	3.17	2.7	0.12363	2.63	5.3777	2.1	0.32058	2.7	0.49	1991	94	1789	84	1878	35	89.9	95.3	1991	94
MAR5_1_4	2.9	717.9	218.2	3.15	4.2	0.12561	3.37	5.7678	4.8	0.33105	4.2	0.73	2008	123	1835	134	1923	79	91.4	95.4	2008	123
MAR5_1_26	1.2	4618.2	91.3	2.88	3.7	0.12554	2.65	6.2367	3.9	0.36021	3.7	0.78	2017	92	1975	127	1995	69	97.9	99.0	2017	92
MAR5_1_40	1.2	325.2	50.8	2.88	6.2	0.12860	4.30	6.6131	5.4	0.36135	5.0	0.65	2054	147	1981	176	2046	97	96.5	96.8	2054	147
MAR5_1_113	1.9	869.0	175.3	2.88	3.1	0.12834	2.61	6.3150	2.5	0.35577	3.1	0.58	2057	89	1957	105	2015	44	95.1	97.1	2057	89
MAR5_1_45	2.0	1097.4	66.5	3.11	3.7	0.12921	3.23	5.9232	3.5	0.33233	3.9	0.60	2061	114	1843	125	1954	61	89.4	94.3	2061	114
MAR5_1_38	0.9	3793.9	61.1	3.00	2.5	0.12866	2.10	6.0665	2.7	0.33834	2.6	0.62	2069	77	1876	83	1980	46	90.7	94.7	2069	77
MAR5_1_96	1.2	201.9	281.8	2.80	4.8	0.13003	4.48	6.8017	4.0	0.36984	5.0	0.57	2069	153	2021	172	2078	68	97.7	97.2	2069	153
MAR5_1_88	0.9	969.1	77.8	2.73	2.4	0.12930	2.71	6.5797	2.9	0.36966	2.2	0.44	2075	95	2026	77	2051	52	97.6	98.8	2075	95
MAR5_1_33	1.0	30.3	1612.2	2.60	4.0	0.13022	2.13	7.0793	3.8	0.39760	4.1	0.83	2090	75	2149	149	2110	67	102.8	101.9	2090	75
MAR5_1_101	1.6	3516.5	91.8	2.72	3.2	0.13259	2.50	6.9838	3.0	0.37439	3.0	0.62	2119	87	2046	107	2102	55	96.5	97.3	2119	87
MAR5_1_17	0.7	573.8	131.2	2.72	3.5	0.13306	2.18	6.9931	3.2	0.37805	3.5	0.79	2126	77	2060	123	2101	59	96.9	98.1	2126	77
MAR5_1_103	0.8	466.9	77.3	2.39	2.6	0.13283	2.01	7.6503	2.8	0.42278	2.8	0.72	2129	68	2270	104	2186	50	106.6	103.8	2129	68
MAR5_1_34	0.7	1404.9	190.5	2.79	1.6	0.13308	1.44	6.4701	2.6	0.35930	1.6	0.82	2136	51	1978	55	2039	46	92.6	97.0	2136	51
MAR5_1_107	0.8	590.3	131.3	2.63	2.8	0.13527	1.63	7.2916	2.0	0.38767	2.6	0.71	2160	56	2108	95	2144	36	97.6	98.3	2160	56
MAR5_1_5	0.6	1207.9	62.6	2.65	3.9	0.13707	2.84	7.4484	3.7	0.39057	4.2	0.76	2173	95	2116	151	2155	67	97.4	98.2	2173	95
MAR5_1_23	1.1	788.1	148.3	2.62	1.7	0.13694	2.36	7.1598	2.6	0.37924	2.2	0.58	2176	82	2070	79	2126	45	95.1	97.4	2176	82
MAR5_1_22	0.4	263.4	105.6	2.70	3.2	0.13703	2.41	7.2158	2.4	0.37764	3.1	0.53	2177	87	2061	108	2134	43	94.7	96.6	2177	87
MAR5_1_110	2.0	3598.9	52.7	2.76	2.7	0.13780	1.99	7.0562	2.6	0.36862	2.7	0.71	2188	70	2019	92	2112	47	92.2	95.6	2188	70
MAR5_1_19	0.9	14858.8	81.2	2.73	2.9	0.13996	1.97	7.1022	3.3	0.37110	2.9	0.76	2219	68	2031	100	2117	57	91.5	95.9	2219	68

MAR5_1_21	0.9	2617.4	171.2	2.54	3.5	0.14361	2.88	8.0584	3.6	0.40559	3.4	0.64	2249	103	2187	126	2225	64	97.2	98.3	2249	103
MAR5_1_41	2.0	5646.6	95.9	1.92	4.0	0.19767	2.91	14.7246	3.3	0.53873	4.1	0.69	2789	95	2764	182	2787	63	99.1	99.2	2789	95
MAR5_1_94	1.0	854.6	130.2	1.80	3.0	0.23848	2.11	18.8093	3.5	0.57012	3.3	0.79	3100	67	2898	150	3020	64	93.5	96.0	3100	67
Data not used due to high discordance																						
~~**MAR5_1_13**~~	~~1.8~~	~~61.2~~	~~156.2~~	~~16.19~~	~~5.6~~	~~0.18598~~	~~6.16~~	~~1.6527~~	~~7.9~~	~~0.06454~~	~~5.3~~	~~0.53~~	~~2654~~	~~199~~	~~403~~	~~41~~	~~972~~	~~100~~	~~15.2~~	41.4		
~~**MAR5_1_52**~~	~~0.7~~	~~1813.0~~	~~41.9~~	~~5.81~~	~~3.3~~	~~0.16467~~	~~2.00~~	~~3.8957~~	~~3.4~~	~~0.17446~~	~~3.3~~	~~0.78~~	~~2499~~	~~69~~	~~1036~~	~~63~~	~~1608~~	~~56~~	~~41.5~~	64.4		
~~**MAR5_1_16**~~	~~1.0~~	~~879.0~~	~~71.9~~	~~3.56~~	~~5.9~~	~~0.15420~~	~~1.62~~	~~6.1098~~	~~5.5~~	~~0.29307~~	~~5.6~~	~~0.95~~	~~2389~~	~~56~~	~~1650~~	~~163~~	~~1977~~	~~98~~	~~69.1~~	83.5		
~~**MAR5_1_104**~~	~~1.1~~	~~296.1~~	~~950.8~~	~~3.86~~	~~3.1~~	~~0.14642~~	~~2.32~~	~~5.2041~~	~~4.0~~	~~0.26237~~	~~3.1~~	~~0.78~~	~~2297~~	~~80~~	~~1500~~	~~84~~	~~1846~~	~~64~~	~~65.3~~	81.2		
~~**MAR5_1_65**~~	~~0.4~~	~~468.2~~	~~29.7~~	~~11.11~~	~~3.7~~	~~0.14166~~	~~2.06~~	~~1.7487~~	~~3.4~~	~~0.09167~~	~~3.5~~	~~0.80~~	~~2240~~	~~73~~	~~565~~	~~38~~	~~1023~~	~~44~~	~~25.2~~	55.2		
~~**MAR5_1_111**~~	~~0.8~~	~~1107.2~~	~~16.7~~	~~5.03~~	~~4.2~~	~~0.14206~~	~~2.14~~	~~4.0842~~	~~3.6~~	~~0.20689~~	~~3.9~~	~~0.82~~	~~2240~~	~~74~~	~~1209~~	~~85~~	~~1640~~	~~62~~	~~54.0~~	73.7		
~~**MAR5_1_95**~~	~~0.3~~	~~322.9~~	~~112.7~~	~~6.09~~	~~4.3~~	~~0.12502~~	~~3.80~~	~~3.0144~~	~~6.7~~	~~0.16973~~	~~4.3~~	~~0.91~~	~~2000~~	~~137~~	~~1008~~	~~80~~	~~1388~~	~~103~~	~~50.4~~	72.7		
~~**MAR5_1_54**~~	~~0.4~~	~~1829.8~~	~~139.3~~	~~4.76~~	~~4.9~~	~~0.11121~~	~~3.13~~	~~3.3539~~	~~4.1~~	~~0.22154~~	~~4.9~~	~~0.81~~	~~1795~~	~~112~~	~~1284~~	~~114~~	~~1483~~	~~61~~	~~71.6~~	86.6		
~~**MAR5_1_76**~~	~~0.9~~	~~725.9~~	~~64.4~~	~~4.01~~	~~3.0~~	~~0.10972~~	~~2.72~~	~~3.8764~~	~~3.2~~	~~0.25501~~	~~3.1~~	~~0.59~~	~~1774~~	~~99~~	~~1461~~	~~82~~	~~1601~~	~~52~~	~~82.4~~	91.3		
~~**MAR5_1_64**~~	~~1.8~~	~~406.1~~	~~88.0~~	~~10.41~~	~~2.8~~	~~0.11321~~	~~10.43~~	~~1.5694~~	~~11.9~~	~~0.09783~~	~~2.7~~	~~0.57~~	~~1629~~	~~313~~	~~601~~	~~31~~	~~908~~	~~122~~	~~36.9~~	66.2		
~~**MAR5_1_60**~~	~~2.4~~	~~9390.9~~	~~56.6~~	~~4.46~~	~~3.2~~	~~0.10107~~	~~3.20~~	~~3.1071~~	~~4.0~~	~~0.22913~~	~~2.8~~	~~0.68~~	~~1615~~	~~115~~	~~1328~~	~~68~~	~~1423~~	~~61~~	~~82.2~~	93.3		
~~**MAR5_1_32**~~	~~1.2~~	~~397.1~~	~~16.2~~	~~14.17~~	~~2.1~~	~~0.09805~~	~~3.04~~	~~0.9373~~	~~2.3~~	~~0.07097~~	~~2.1~~	~~0.08~~	~~1572~~	~~120~~	~~442~~	~~18~~	~~671~~	~~22~~	~~28.1~~	65.9		
~~**MAR5_1_92**~~	~~1.8~~	~~280.4~~	~~28.2~~	~~9.05~~	~~4.4~~	~~0.08829~~	~~3.81~~	~~1.3662~~	~~5.0~~	~~0.10780~~	~~2.5~~	~~0.60~~	~~1364~~	~~151~~	~~660~~	~~32~~	~~869~~	~~59~~	~~48.4~~	75.9		
~~**MAR5_1_51**~~	~~0.5~~	~~97.1~~	~~316.9~~	~~14.17~~	~~2.7~~	~~0.08551~~	~~2.89~~	~~0.8445~~	~~3.0~~	~~0.07169~~	~~2.7~~	~~0.58~~	~~1303~~	~~116~~	~~446~~	~~23~~	~~620~~	~~27~~	~~34.2~~	72.0		
~~**MAR5_1_80**~~	~~1.6~~	~~1036.7~~	~~69.6~~	~~8.57~~	~~3.6~~	~~0.08370~~	~~5.55~~	~~1.3115~~	~~4.1~~	~~0.11698~~	~~3.1~~	~~0.75~~	~~1217~~	~~183~~	~~712~~	~~42~~	~~845~~	~~47~~	~~58.5~~	84.3		
~~**MAR5_1_87**~~	~~0.9~~	~~89.6~~	~~90.0~~	~~8.48~~	~~4.0~~	~~0.07666~~	~~5.61~~	~~1.3646~~	~~7.1~~	~~0.11835~~	~~3.0~~	~~0.34~~	~~1159~~	~~225~~	~~720~~	~~41~~	~~855~~	~~76~~	~~62.1~~	84.2		
~~**MAR5_1_59**~~	~~1.2~~	~~150.7~~	~~64.2~~	~~13.01~~	~~4.0~~	~~0.09436~~	~~14.35~~	~~0.9223~~	~~5.8~~	~~0.07765~~	~~4.2~~	~~0.03~~	~~1150~~	~~196~~	~~481~~	~~39~~	~~654~~	~~54~~	~~41.9~~	73.5		
~~**MAR5_1_69**~~	~~0.5~~	~~123.8~~	~~276.2~~	~~9.35~~	~~4.1~~	~~0.07864~~	~~5.83~~	~~1.1603~~	~~6.7~~	~~0.10623~~	~~5.7~~	~~0.12~~	~~1085~~	~~231~~	~~674~~	~~52~~	~~769~~	~~75~~	~~62.2~~	87.7		
~~**MAR5_1_78**~~	~~0.6~~	~~1337.4~~	~~61.9~~	~~13.40~~	~~4.6~~	~~0.07519~~	~~3.39~~	~~0.8399~~	~~4.3~~	~~0.07798~~	~~4.2~~	~~0.33~~	~~1041~~	~~127~~	~~483~~	~~39~~	~~615~~	~~39~~	~~46.4~~	78.6		
~~**MAR5_1_14**~~	~~2.0~~	~~6.2~~	~~771.7~~	~~10.26~~	~~4.3~~	~~0.07963~~	~~11.03~~	~~1.1132~~	~~10.3~~	~~0.09994~~	~~4.2~~	~~0.30~~	~~1026~~	~~353~~	~~613~~	~~49~~	~~741~~	~~101~~	~~59.8~~	82.8		
~~**MAR5_1_108**~~	~~4.0~~	~~170.6~~	~~479.4~~	~~11.24~~	~~2.1~~	~~0.07304~~	~~3.04~~	~~0.9047~~	~~3.5~~	~~0.08894~~	~~2.7~~	~~0.50~~	~~1025~~	~~100~~	~~549~~	~~28~~	~~651~~	~~34~~	~~53.6~~	84.4		
~~**MAR5_1_109**~~	~~1.3~~	~~385.2~~	~~75.2~~	~~19.03~~	~~3.3~~	~~0.07139~~	~~4.12~~	~~0.5344~~	~~5.1~~	~~0.05388~~	~~3.1~~	~~0.47~~	~~962~~	~~204~~	~~338~~	~~20~~	~~431~~	~~35~~	~~35.1~~	78.5		
~~**MAR5_1_100**~~	~~2.4~~	~~678.3~~	~~41.4~~	~~9.92~~	~~2.1~~	~~0.07340~~	~~5.38~~	~~1.0438~~	~~5.0~~	~~0.10183~~	~~2.0~~	~~0.24~~	~~959~~	~~173~~	~~625~~	~~24~~	~~719~~	~~48~~	~~65.1~~	86.9		
~~**MAR5_1_6**~~	~~0.4~~	~~288.5~~	~~131.3~~	~~12.84~~	~~4.2~~	~~0.07118~~	~~2.35~~	~~0.7734~~	~~3.3~~	~~0.08035~~	~~4.2~~	~~0.74~~	~~948~~	~~95~~	~~498~~	~~40~~	~~580~~	~~30~~	~~52.5~~	85.8		
~~**MAR5_1_47**~~	~~1.6~~	~~103.9~~	~~101.6~~	~~10.28~~	~~3.3~~	~~0.07040~~	~~6.05~~	~~0.9991~~	~~6.3~~	~~0.09824~~	~~3.1~~	~~0.25~~	~~897~~	~~222~~	~~604~~	~~36~~	~~699~~	~~59~~	~~67.3~~	86.4		
~~**MAR5_1_112**~~	~~1.3~~	~~374.1~~	~~114.4~~	~~17.34~~	~~4.6~~	~~0.07033~~	~~9.94~~	~~0.5641~~	~~8.9~~	~~0.05823~~	~~3.7~~	~~0.91~~	~~708~~	~~314~~	~~365~~	~~26~~	~~442~~	~~60~~	~~51.5~~	82.5		
~~**MAR5_1_98**~~	~~1.6~~	~~539.1~~	~~141.2~~	~~19.62~~	~~2.4~~	~~0.06197~~	~~2.94~~	~~0.4478~~	~~3.3~~	~~0.05155~~	~~2.3~~	~~0.35~~	~~693~~	~~152~~	~~324~~	~~15~~	~~375~~	~~21~~	~~46.8~~	86.5		
~~**MAR5_1_11**~~	~~3.5~~	~~71.1~~	~~215.9~~	~~22.92~~	~~3.4~~	~~0.06618~~	~~6.45~~	~~0.4082~~	~~5.9~~	~~0.04492~~	~~3.5~~	~~0.31~~	~~689~~	~~239~~	~~283~~	~~19~~	~~344~~	~~34~~	~~41.1~~	82.3		

Amostra M2AR 6-1

			Ratios								Rho	Ages (Ma)						% conc [1]	% conc [2]	Best age	2s
Spot number	Th/U	206Pb/204Pb	1s	238U/206Pb	1s	207Pb/206Pb	1s	207Pb/235U	1s	206Pb/238U	1s		207Pb/206Pb	2s	206Pb/238U	2s	207Pb/235U	2s				
			(%)		(%)		(%)		(%)		(%)			(abs)		(abs)		(abs)				(abs)
MAR6_1_128	2.1	810.4	77.5	11.21	2.1	0.06717	2.77	0.8338	2.2	0.09028	2.2	0.26	814	114	557	23	614	20	68	91	557	23
MAR6_1_13	1.6	574.2	65.7	11.06	2.8	0.06241	2.10	0.8047	3.1	0.09237	2.8	0.76	670	92	569	30	597	27	85	95	569	30
MAR6_1_130	1.1	844.3	108.4	10.92	1.9	0.06020	1.76	0.7703	2.0	0.09256	2.0	0.62	597	78	570	22	579	18	96	99	570	22
MAR6_1_126	2.3	5106.6	101.5	10.88	1.6	0.06039	1.83	0.7748	2.4	0.09258	1.6	0.85	602	81	571	18	581	20	95	98	571	18
MAR6_1_124	1.6	127.6	128.2	10.77	1.7	0.06257	1.54	0.8092	1.6	0.09361	1.7	0.34	683	67	577	18	601	14	84	96	577	18

MAR6_1_91	4.2	1708.0	42.6	10.89	2.8	0.06061	2.25	0.7851	3.1	0.09367	2.7	0.69	604	103	577	30	586	27	96	98	577	30
MAR6_1_109	1.0	151.2	118.3	10.82	2.4	0.05927	2.06	0.7679	2.3	0.09377	2.3	0.61	560	89	577	25	577	20	103	100	577	25
MAR6_1_14	1.1	67.3	320.3	10.82	3.2	0.05889	2.14	0.7772	3.1	0.09484	3.1	0.76	575	79	583	34	581	27	101	100	583	34
MAR6_1_119	1.4	71.6	249.3	10.69	2.3	0.06121	2.50	0.8042	2.9	0.09498	2.3	0.53	620	105	585	25	597	26	94	98	585	25
MAR6_1_117	3.4	219.5	116.0	10.71	2.5	0.05959	2.22	0.7849	2.9	0.09500	2.4	0.67	565	104	585	27	586	27	104	100	585	27
MAR6_1_30	1.1	48807.7	83.8	10.60	1.8	0.05980	1.97	0.7925	2.3	0.09513	1.8	0.53	581	85	586	20	591	20	101	99	586	20
MAR6_1_100	1.1	236.9	137.4	10.76	3.0	0.06169	1.95	0.8126	3.1	0.09520	2.8	0.79	647	83	586	32	601	27	91	97	586	32
MAR6_1_55	1.2	2024.1	33.3	10.67	2.5	0.05930	1.98	0.7827	2.5	0.09530	2.5	0.68	561	89	586	28	585	22	105	100	586	28
MAR6_1_11	2.0	228.9	1442.5	10.69	2.8	0.06246	2.84	0.8274	2.9	0.09542	2.9	0.48	660	121	587	32	610	26	89	96	587	32
MAR6_1_26	1.0	1153.9	61.2	10.63	2.5	0.05665	2.48	0.7578	3.9	0.09550	2.7	0.74	456	112	588	30	570	33	129	103	588	30
MAR6_1_79	1.0	342.0	182.1	10.66	2.6	0.05876	1.99	0.7794	3.0	0.09553	2.6	0.75	540	89	588	29	583	27	109	101	588	29
MAR6_1_93	1.1	672.8	78.9	10.65	2.5	0.05943	1.92	0.7860	2.5	0.09561	2.5	0.69	567	84	588	28	587	22	104	100	588	28
MAR6_1_125	1.1	0.6	29036.0	10.58	2.1	0.06387	1.87	0.8455	2.4	0.09562	2.1	0.68	723	81	588	23	620	23	81	95	588	23
MAR6_1_110	0.9	198.7	87.4	10.64	2.6	0.05960	2.22	0.7933	3.0	0.09567	2.6	0.82	567	103	589	29	591	27	104	100	589	29
MAR6_1_84	1.1	396.5	119.4	10.67	3.0	0.05985	2.47	0.7896	2.6	0.09575	3.0	0.61	576	109	589	34	589	23	102	100	589	34
MAR6_1_32	1.4	2705.1	36.9	10.55	2.1	0.05977	2.24	0.7952	2.3	0.09580	2.0	0.44	576	97	589	22	593	21	102	99	589	22
MAR6_1_120	1.4	1534.8	37.2	10.50	1.5	0.06531	1.73	0.8693	2.2	0.09580	1.4	0.59	772	74	590	16	634	21	76	93	590	16
MAR6_1_18	1.1	214.1	115.2	10.49	2.5	0.06059	2.18	0.8178	2.9	0.09666	2.4	0.67	608	92	594	27	605	26	98	98	594	27
MAR6_1_31	1.1	195.3	227.8	10.46	2.3	0.05910	2.10	0.7954	2.7	0.09679	2.2	0.61	553	91	595	25	592	24	108	100	595	25
MAR6_1_62	2.1	10.6	469.6	10.47	2.4	0.05995	2.12	0.8065	2.8	0.09688	2.4	0.66	614	77	596	27	599	25	97	100	596	27
MAR6_1_4	0.8	395.4	128.3	10.45	2.5	0.05782	2.11	0.7814	2.1	0.09702	2.5	0.58	506	97	597	28	585	19	118	102	597	28
MAR6_1_115	1.0	1660.3	91.0	10.44	2.2	0.05941	2.01	0.7995	2.7	0.09705	2.2	0.69	565	87	597	26	595	24	106	100	597	26
MAR6_1_59	0.9	138.4	62.1	10.55	3.0	0.05970	2.21	0.8041	3.3	0.09715	2.9	0.74	571	99	597	33	596	29	105	100	597	33
MAR6_1_74	1.0	12171.7	46.3	10.42	2.2	0.06754	3.00	0.9397	4.7	0.09711	2.1	0.56	861	147	597	24	667	44	69	90	597	24
MAR6_1_72	1.0	5671.2	54.7	10.56	3.3	0.05752	2.63	0.7773	3.9	0.09731	3.2	0.76	483	117	598	36	580	34	124	103	598	36
MAR6_1_68	1.1	4947.1	74.1	10.46	2.5	0.06080	3.00	0.8207	3.6	0.09735	2.5	0.57	592	133	598	28	605	32	101	99	598	28
MAR6_1_104	1.6	513.4	60.8	10.41	2.3	0.06007	1.82	0.8119	2.7	0.09738	2.3	0.72	592	80	599	26	602	24	101	100	599	26
MAR6_1_38	1.0	263.1	120.5	10.44	2.7	0.06051	2.87	0.8142	2.7	0.09751	2.6	0.36	588	130	599	30	603	24	102	99	599	30
MAR6_1_87	1.0	3478.0	112.3	10.46	2.6	0.06058	1.93	0.8153	2.2	0.09753	2.6	0.65	607	86	599	30	604	20	99	99	599	30
MAR6_1_106	0.9	30728.5	107.7	10.21	2.1	0.06150	2.10	0.8324	2.9	0.09764	2.4	0.73	639	89	600	28	613	27	94	98	600	28
MAR6_1_42	1.9	117.2	100.5	10.39	2.5	0.05850	3.20	0.7908	3.0	0.09770	2.6	0.31	512	142	601	30	590	26	117	102	601	30
MAR6_1_80	1.4	90.3	288.4	10.41	2.5	0.05980	2.62	0.8095	3.1	0.09784	2.6	0.61	567	113	601	29	600	27	106	100	601	29
MAR6_1_43	0.9	1559.8	72.7	10.37	2.7	0.06341	2.16	0.8625	2.6	0.09796	2.7	0.66	707	90	602	30	630	24	85	96	602	30
MAR6_1_77	0.9	2451.2	101.1	10.49	3.3	0.06160	2.39	0.8332	3.2	0.09802	3.2	0.71	638	99	602	36	613	29	94	98	602	36
MAR6_1_90	0.8	1323.0	127.4	10.27	1.6	0.06607	1.43	0.9001	1.9	0.09809	1.6	0.71	800	60	603	18	651	18	75	93	603	18
MAR6_1_78	0.9	177.9	48.6	10.34	2.6	0.06038	2.67	0.8194	2.7	0.09834	2.6	0.48	590	115	604	29	606	24	102	100	604	29
MAR6_1_16	1.6	98.5	92.5	10.34	2.6	0.05970	2.58	0.8146	2.5	0.09852	2.5	0.55	565	109	605	29	603	22	107	100	605	29
MAR6_1_67	0.9	515.8	54.9	10.37	2.9	0.05907	2.54	0.8024	2.6	0.09865	2.8	0.58	543	110	606	33	596	23	112	102	606	33
MAR6_1_50	1.1	900.7	98.3	10.26	2.3	0.06039	2.08	0.8269	2.4	0.09870	2.3	0.60	602	89	606	27	610	22	101	99	606	27
MAR6_1_122	1.2	1240.1	73.8	10.18	1.6	0.06004	1.72	0.8260	2.6	0.09890	1.6	0.76	593	75	608	19	610	24	103	100	608	19
MAR6_1_19	1.4	235.3	246.2	10.20	2.0	0.06291	2.28	0.8702	2.7	0.09911	2.0	0.54	684	100	609	23	634	25	89	96	609	23
MAR6_1_57	1.2	458.8	113.4	10.24	2.5	0.06089	2.28	0.8379	2.7	0.09918	2.4	0.65	615	97	609	28	616	25	99	99	609	28
MAR6_1_3	0.8	1856.0	84.7	10.25	2.5	0.06056	2.11	0.8421	3.2	0.09926	2.6	0.75	605	93	610	30	617	30	101	99	610	30
MAR6_1_81	1.1	153.9	148.2	10.20	2.7	0.06007	2.30	0.8277	2.5	0.09983	2.7	0.63	586	97	613	31	611	23	105	100	613	31

MAR6_1_118	1.1	104.0	534.9	10.20	2.5	0.05986	2.20	0.8245	2.4	0.09984	2.6	0.65	578	94	613	30	609	22	106	101	613	30
MAR6_1_76	1.3	22.5	161.8	10.18	2.6	0.07635	4.81	1.0557	5.2	0.09998	2.6	0.40	1022	194	614	30	722	52	60	85	614	30
MAR6_1_52	1.6	345.3	123.1	10.01	2.0	0.05907	2.14	0.8211	2.9	0.09999	2.3	0.68	548	98	614	27	606	27	112	101	614	27
MAR6_1_73	0.9	1834.9	76.9	10.09	2.0	0.06032	2.06	0.8370	2.2	0.10009	2.0	0.56	599	88	615	23	616	20	103	100	615	23
MAR6_1_6	1.1	2024.1	92.3	10.00	1.7	0.05611	2.52	0.7892	3.2	0.10048	1.6	0.62	436	119	617	19	589	29	142	105	617	19
MAR6_1_45	1.1	320.0	43.8	10.08	2.3	0.05790	2.27	0.8085	2.6	0.10065	2.3	0.55	504	102	618	28	600	23	123	103	618	28
MAR6_1_35	1.0	1184.3	66.2	10.06	2.8	0.06151	1.93	0.8643	2.5	0.10146	2.7	0.72	641	84	622	32	631	23	97	99	622	32
MAR6_1_60	0.3	1431.2	72.2	9.91	1.7	0.06136	1.74	0.8671	2.0	0.10165	1.7	0.57	640	73	624	20	633	19	97	99	624	20
MAR6_1_85	0.9	14.7	617.8	9.81	2.1	0.05842	2.80	0.8304	2.2	0.10305	2.0	0.20	518	115	632	24	613	20	122	103	632	24
MAR6_1_37	0.7	736.2	37.5	9.68	2.2	0.06630	2.16	0.9652	2.8	0.10461	2.2	0.65	797	94	641	27	683	28	80	94	641	27
MAR6_1_51	1.2	163.8	77.3	9.49	2.4	0.06178	3.05	0.9059	2.6	0.10635	2.4	0.19	703	175	651	30	654	25	93	100	651	30
MAR6_1_25	0.5	111.5	312.0	5.37	2.6	0.09086	1.85	2.4301	2.6	0.18996	2.7	0.68	1453	81	1119	55	1247	37	77	90	1119	55
MAR6_1_10	0.5	295.6	204.8	4.77	4.4	0.09437	3.22	2.8120	3.3	0.21627	4.1	0.69	1495	118	1259	94	1354	49	84	93	1259	94
MAR6_1_48	0.4	2537.9	70.6	4.00	2.9	0.09993	1.87	3.5349	2.7	0.25570	2.8	0.77	1611	70	1465	74	1529	42	91	96	1611	70
MAR6_1_127	0.6	20.3	3289.0	4.37	1.8	0.09976	1.94	3.1903	1.5	0.23030	1.8	0.30	1611	73	1335	43	1454	22	83	92	1611	73
MAR6_1_95	0.7	16743.3	50.6	3.90	2.5	0.10100	2.06	3.6409	2.2	0.26015	2.4	0.57	1630	78	1489	64	1555	35	91	96	1630	78
MAR6_1_9	1.2	358.6	51.1	3.34	2.1	0.10290	2.26	4.3693	3.0	0.30290	2.3	0.68	1661	83	1703	69	1699	47	103	100	1661	83
MAR6_1_21	1.2	4600.0	67.5	3.26	1.8	0.10362	2.01	4.4743	2.1	0.30951	1.7	0.48	1678	73	1737	53	1722	35	104	101	1678	73
MAR6_1_20	0.9	487.8	113.6	3.39	2.4	0.10410	2.30	4.3428	2.5	0.29990	2.3	0.56	1680	87	1688	69	1696	41	100	100	1680	87
MAR6_1_22	1.0	186.6	176.1	3.19	2.1	0.10452	1.74	4.6196	2.3	0.31626	2.1	0.71	1697	64	1770	65	1749	37	104	101	1697	64
MAR6_1_63	0.8	2623.1	47.3	3.37	2.9	0.10489	1.90	4.3811	2.1	0.30269	2.7	0.73	1701	68	1701	82	1705	36	100	100	1701	68
MAR6_1_71	0.8	3275.6	51.0	3.41	2.6	0.10602	2.12	4.3617	2.0	0.29881	2.8	0.63	1717	78	1682	81	1702	32	98	99	1717	78
MAR6_1_129	0.8	21.5	2065.2	3.19	1.6	0.10580	1.59	4.6283	1.6	0.31625	1.7	0.52	1719	59	1770	51	1752	27	103	101	1719	59
MAR6_1_112	0.6	18132.8	72.2	3.45	2.6	0.10593	1.79	4.3161	2.2	0.29524	2.6	0.74	1720	64	1664	76	1692	37	97	98	1720	64
MAR6_1_123	0.6	3276.0	94.4	3.46	2.0	0.10600	1.28	4.2809	1.6	0.29217	2.0	0.75	1726	47	1651	57	1687	27	96	98	1726	47
MAR6_1_33	0.9	1120.9	103.1	3.28	2.5	0.10666	1.97	4.5948	2.7	0.31006	2.6	0.72	1731	74	1738	78	1742	44	100	100	1731	74
MAR6_1_121	1.3	49643.3	103.2	3.15	1.8	0.10652	1.56	4.7107	1.8	0.32019	1.7	0.14	1732	59	1789	53	1766	29	103	101	1732	59
MAR6_1_116	1.1	22591.0	81.6	3.28	2.1	0.10688	1.98	4.5672	2.3	0.30858	2.1	0.61	1734	73	1732	63	1738	39	100	100	1734	73
MAR6_1_113	1.3	6313.7	55.1	3.52	2.7	0.10691	2.03	4.2694	2.2	0.29002	2.7	0.70	1735	72	1638	78	1683	36	94	97	1735	72
MAR6_1_101	2.0	172.6	201.7	3.45	3.0	0.10712	2.11	4.3767	2.5	0.29713	3.0	0.70	1736	79	1673	87	1702	40	96	98	1736	79
MAR6_1_111	1.3	883.8	67.6	3.20	2.5	0.10763	1.99	4.7244	2.4	0.31749	2.4	0.65	1746	73	1774	74	1766	39	102	100	1746	73
MAR6_1_86	0.9	444.7	73.5	3.39	2.1	0.10742	1.50	4.4407	2.2	0.29789	2.0	0.76	1749	56	1679	61	1716	36	96	98	1749	56
MAR6_1_92	1.2	517.3	28.7	3.18	2.7	0.10824	2.01	4.7933	2.2	0.32165	2.7	0.67	1755	77	1794	85	1779	37	102	101	1755	77
MAR6_1_66	0.8	837.6	45.7	3.17	2.7	0.10868	2.64	4.8206	3.0	0.32084	2.7	0.57	1757	98	1790	83	1781	49	102	101	1757	98
MAR6_1_114	1.0	444.6	150.1	3.51	3.1	0.10825	1.56	4.3790	3.0	0.29272	3.1	0.87	1761	59	1650	91	1700	49	94	97	1761	59
MAR6_1_49	1.3	13349.2	97.2	3.29	2.5	0.10875	1.71	4.6462	1.9	0.30898	2.5	0.72	1769	63	1733	75	1754	32	98	99	1769	63
MAR6_1_96	0.7	946.7	80.7	3.18	2.5	0.10889	1.87	4.8191	2.6	0.31954	2.4	0.73	1770	67	1785	75	1782	43	101	100	1770	67
MAR6_1_83	1.1	318.2	238.5	3.27	2.9	0.10947	2.34	4.7493	3.1	0.31409	3.0	0.70	1772	86	1756	91	1767	51	99	99	1772	86
MAR6_1_28	1.1	209.3	362.8	3.36	2.3	0.10920	1.52	4.5931	2.1	0.30185	2.2	0.75	1778	57	1698	67	1744	35	95	97	1778	57
MAR6_1_97	1.2	1506.6	74.7	3.50	2.8	0.10959	2.02	4.4218	2.8	0.29214	2.8	0.75	1778	74	1648	82	1709	45	93	96	1778	74
MAR6_1_82	1.7	20.6	1367.0	3.35	2.9	0.10999	2.60	4.6231	2.7	0.30485	2.8	0.55	1780	97	1712	84	1747	45	96	98	1780	97
MAR6_1_89	0.7	1.1	268260.5	3.29	2.7	0.10958	1.64	4.7112	2.8	0.30986	2.6	0.81	1784	60	1737	81	1762	46	97	99	1784	60
MAR6_1_41	1.0	2295.0	174.5	3.09	2.7	0.10973	1.89	5.0083	2.5	0.32922	2.7	0.74	1785	69	1831	86	1816	42	103	101	1785	69
MAR6_1_99	1.3	8050.0	64.0	3.29	2.8	0.11008	2.00	4.7158	2.6	0.31041	2.7	0.71	1787	75	1739	83	1764	43	97	99	1787	75
MAR6_1_88	1.3	1147.8	69.9	3.09	2.4	0.11128	2.05	5.0599	2.5	0.32801	2.5	0.70	1808	74	1826	78	1824	42	101	100	1808	74

MAR6_1_36	1.0	593.3	184.8	3.88	2.3	0.11220	2.30	4.0664	2.7	0.26044	2.1	0.56	1821	83	1491	57	1642	43	82	91	1821	83
MAR6_1_61	1.2	272.6	106.7	3.33	2.8	0.11289	2.12	4.7911	2.9	0.30659	2.8	0.71	1832	76	1720	83	1775	48	94	97	1832	76
MAR6_1_15	0.3	1776.8	201.9	3.13	2.7	0.11889	1.80	5.4031	2.3	0.32656	2.7	0.77	1929	64	1818	86	1880	40	94	97	1929	64
MAR6_1_23	0.1	1722.1	26.7	2.95	2.0	0.12378	1.79	5.9173	2.2	0.34291	2.0	0.62	2002	64	1899	66	1959	38	95	97	2002	64
MAR6_1_8	0.6	4625.9	40.3	3.09	2.3	0.12457	1.94	5.7071	3.0	0.32766	2.5	0.77	2013	68	1824	78	1926	49	91	95	2013	68
MAR6_1_94	2.0	6505.5	61.1	3.03	2.9	0.12709	1.74	5.9295	2.4	0.33801	2.7	0.78	2048	61	1873	89	1959	42	91	96	2048	61
MAR6_1_1	0.6	4098.0	101.9	2.56	2.5	0.12926	2.25	7.1955	3.3	0.39730	2.6	0.75	2074	80	2152	95	2126	58	104	101	2074	80
MAR6_1_24	0.5	584.6	168.2	2.87	2.7	0.12981	1.85	6.4471	3.2	0.35602	3.1	0.82	2085	65	1958	102	2029	55	94	97	2085	65
MAR6_1_70	0.7	384.3	381.1	2.65	2.5	0.13139	2.53	6.9505	2.6	0.38256	2.6	0.54	2100	87	2084	91	2099	46	99	99	2100	87
MAR6_1_17	0.5	1683.9	88.2	2.72	3.4	0.13213	2.02	6.9418	3.4	0.37618	3.3	0.81	2117	71	2053	116	2095	60	97	98	2117	71
MAR6_1_7	1.6	748.8	185.6	2.79	2.6	0.13261	1.96	6.7732	2.9	0.36525	2.7	0.77	2122	70	2003	93	2074	50	94	97	2122	70
MAR6_1_12	0.6	503.8	435.8	2.71	2.4	0.13294	1.66	6.9591	2.6	0.37265	2.2	0.79	2130	59	2039	78	2101	46	96	97	2130	59
MAR6_1_107	0.9	26749.9	223.0	2.75	2.7	0.13341	2.12	6.8285	2.4	0.36974	2.7	0.67	2133	74	2025	93	2085	43	95	97	2133	74
MAR6_1_105	0.9	1353.5	117.7	2.54	2.2	0.13419	1.57	7.4177	2.3	0.39862	2.3	0.75	2146	55	2159	85	2158	40	101	100	2146	55
MAR6_1_64	1.2	1375.0	57.5	2.57	2.4	0.13477	2.13	7.3922	2.8	0.39514	2.5	0.70	2148	74	2142	91	2152	50	100	100	2148	74
MAR6_1_29	1.0	2128.3	118.7	2.65	2.2	0.13500	1.63	7.0591	1.8	0.38161	2.2	0.73	2156	57	2081	77	2116	32	97	98	2156	57
MAR6_1_65	1.3	1066.4	115.7	2.60	2.4	0.13542	1.89	7.2954	1.7	0.38982	2.2	0.63	2159	64	2119	80	2145	31	98	99	2159	64
MAR6_1_75	0.8	1476.9	384.1	2.58	2.8	0.13639	2.15	7.4643	3.0	0.39367	2.8	0.71	2171	77	2136	103	2162	54	98	99	2171	77
MAR6_1_5	1.2	1415.0	77.7	2.68	3.6	0.13619	1.74	7.1829	3.2	0.38363	3.5	0.58	2172	61	2086	126	2126	57	96	98	2172	61
MAR6_1_103	1.0	3548.7	62.4	2.68	2.5	0.13637	1.65	7.1648	2.6	0.37868	2.3	0.78	2173	57	2067	82	2125	46	95	97	2173	57
MAR6_1_2	0.9	253.1	289.9	2.59	2.9	0.13815	2.63	7.5234	2.3	0.39244	2.8	0.44	2186	96	2130	101	2171	39	97	98	2186	96
MAR6_1_44	1.3	547.4	147.4	2.53	2.0	0.13920	2.00	7.7480	2.7	0.40000	2.1	0.67	2206	71	2166	77	2195	47	98	99	2206	71
MAR6_1_47	0.3	4790.9	107.6	2.25	2.4	0.17037	1.82	10.6213	1.9	0.45075	2.3	0.63	2552	63	2394	94	2487	36	94	96	2552	63
Data not used due to high discordance																						
~~**MAR6_1_56**~~	~~0.8~~	~~2372.9~~	~~64.6~~	~~3.36~~	~~3.8~~	~~0.13441~~	~~2.50~~	~~5.6796~~	~~3.5~~	~~0.30524~~	~~3.4~~	~~0.72~~	~~2142~~	~~89~~	~~1713~~	~~104~~	~~1919~~	~~60~~	~~80~~	~~89~~		
~~**MAR6_1_58**~~	~~0.8~~	~~3921.0~~	~~133.4~~	~~3.71~~	~~2.7~~	~~0.12462~~	~~2.27~~	~~4.7168~~	~~2.4~~	~~0.27370~~	~~2.7~~	~~0.62~~	~~2011~~	~~79~~	~~1557~~	~~76~~	~~1766~~	~~40~~	~~77~~	~~88~~		
~~**MAR6_1_98**~~	~~0.4~~	~~2260.1~~	~~46.8~~	~~3.98~~	~~2.1~~	~~0.11788~~	~~1.97~~	~~4.1483~~	~~2.3~~	~~0.25414~~	~~2.0~~	~~0.58~~	~~1911~~	~~72~~	~~1458~~	~~53~~	~~1659~~	~~37~~	~~76~~	~~88~~		
~~**MAR6_1_40**~~	~~1.3~~	~~3197.4~~	~~71.1~~	~~3.50~~	~~4.0~~	~~0.13642~~	~~2.05~~	~~5.5704~~	~~3.8~~	~~0.29298~~	~~4.0~~	~~0.88~~	~~2174~~	~~71~~	~~1652~~	~~117~~	~~1903~~	~~65~~	~~76~~	~~87~~		
~~**MAR6_1_69**~~	~~0.5~~	~~3106.8~~	~~62.1~~	~~3.98~~	~~3.1~~	~~0.12143~~	~~2.36~~	~~4.3214~~	~~3.1~~	~~0.25772~~	~~3.2~~	~~0.71~~	~~1961~~	~~87~~	~~1475~~	~~83~~	~~1690~~	~~50~~	~~75~~	~~87~~		
~~**MAR6_1_34**~~	~~0.9~~	~~390.7~~	~~221.2~~	~~3.83~~	~~2.8~~	~~0.12836~~	~~1.89~~	~~4.7257~~	~~2.7~~	~~0.26531~~	~~2.8~~	~~0.75~~	~~2067~~	~~67~~	~~1515~~	~~75~~	~~1767~~	~~44~~	~~73~~	~~86~~		
~~**MAR6_1_54**~~	~~0.4~~	~~3504.1~~	~~49.3~~	~~4.26~~	~~1.8~~	~~0.11610~~	~~1.53~~	~~3.8192~~	~~2.2~~	~~0.23639~~	~~1.7~~	~~0.73~~	~~1890~~	~~56~~	~~1367~~	~~43~~	~~1593~~	~~35~~	~~72~~	~~86~~		
~~**MAR6_1_39**~~	~~0.6~~	~~58.7~~	~~476.8~~	~~6.97~~	~~1.7~~	~~0.08306~~	~~2.00~~	~~1.6772~~	~~2.6~~	~~0.14407~~	~~1.6~~	~~0.58~~	~~1262~~	~~78~~	~~867~~	~~27~~	~~998~~	~~32~~	~~69~~	~~87~~		
~~**MAR6_1_53**~~	~~1.1~~	~~1337.1~~	~~87.3~~	~~5.77~~	~~2.6~~	~~0.10704~~	~~1.81~~	~~2.6178~~	~~2.8~~	~~0.17618~~	~~2.7~~	~~0.78~~	~~1740~~	~~67~~	~~1045~~	~~53~~	~~1301~~	~~40~~	~~60~~	~~80~~		
~~**MAR6_1_108**~~	~~0.6~~	~~1069.9~~	~~43.1~~	~~9.34~~	~~2.2~~	~~0.09211~~	~~1.92~~	~~1.3846~~	~~2.6~~	~~0.10826~~	~~2.2~~	~~0.72~~	~~1458~~	~~74~~	~~662~~	~~27~~	~~880~~	~~31~~	~~45~~	~~75~~		
~~**MAR6_1_46**~~	~~0.8~~	~~938.4~~	~~40.0~~	~~13.59~~	~~7.3~~	~~0.13603~~	~~2.72~~	~~1.4804~~	~~5.3~~	~~0.07938~~	~~6.8~~	~~0.94~~	~~2164~~	~~93~~	~~491~~	~~64~~	~~914~~	~~64~~	~~23~~	~~54~~		

Amostra M2AR 6-9

		Ratios										Rho	Ages (Ma)						% conc[1]	% conc[2]	Best age	2s	
Spot number	Th/U	206Pb/204Pb	1s	238U/206Pb	1s	207Pb/206Pb	1s	207Pb/235U	1s	206Pb/238U	1s		207Pb/206Pb	2s	206Pb/238U	2s	207Pb/235U	2s					
			(%)		(%)		(%)		(%)		(%)			(abs)		(abs)		(abs)					(abs)
6_9_67	0.9	756	102	12.95	1.6	0.06313	1.92	0.6803	2.2	0.07792	1.6	0.29	693	81	484	14	526	18	70	**92**	484	14

6_9_105	1.3	13604	65	12.50	1.1	0.06370	2.58	0.7093	2.4	0.08013	1.1	0.11	714	113	497	10	543	21	70	**91**	497	10
6_9_73	1.3	254	79	11.12	2.3	0.06152	2.26	0.7548	3.9	0.09062	2.0	0.82	644	97	559	21	568	36	87	**98**	559	21
6_9_9	1.6	1	16522	10.68	1.6	0.06167	2.30	0.8074	2.6	0.09434	1.6	0.51	637	98	581	17	599	23	91	97	581	17
6_9_66	1.2	376	1640	10.58	1.2	0.05873	1.82	0.7694	2.2	0.09444	1.3	0.56	539	80	582	14	578	19	108	101	582	14
6_9_8	0.8	712	50	10.36	1.5	0.05996	3.40	0.8022	3.4	0.09687	1.5	0.25	574	142	596	17	596	30	104	100	596	17
6_9_117	1.3	941	115	10.36	1.1	0.06006	1.92	0.8094	2.1	0.09689	1.1	0.42	587	80	596	12	601	19	102	99	596	12
6_9_21	1.1	23	633	10.40	2.7	0.06412	6.03	0.8554	4.7	0.09698	2.6	0.20	690	234	596	30	625	43	86	**95**	596	30
6_9_46	0.8	10767	76	10.25	1.7	0.06213	2.79	0.8447	2.5	0.09814	1.7	0.15	653	123	603	19	620	24	92	97	603	19
6_9_22	1.2	51894	95	10.11	1.1	0.06748	2.43	0.9172	2.1	0.09916	1.0	0.65	834	103	609	12	660	20	73	**92**	609	12
6_9_116	1.4	498	110	10.11	1.2	0.06326	2.85	0.8745	3.1	0.09923	1.2	0.41	690	122	610	14	636	29	88	**96**	610	14
6_9_18	2.1	59	573	10.12	1.2	0.06272	1.92	0.8638	2.1	0.09928	1.2	0.31	679	83	610	14	631	19	90	97	610	14
6_9_81	0.8	70	308	10.10	1.2	0.06069	3.00	0.8371	3.0	0.09928	1.2	0.22	603	131	610	14	616	28	101	99	610	14
6_9_65	0.6	60	457	10.00	1.0	0.05915	1.94	0.8181	2.1	0.09975	1.1	0.41	576	75	613	13	605	19	106	101	613	13
6_9_126	1.5	201	58	10.06	1.2	0.06312	3.50	0.8855	3.7	0.09976	1.2	0.33	676	149	613	14	641	35	91	96	613	14
6_9_98	2.1	228	47	10.05	1.2	0.06298	2.71	0.8714	3.0	0.09993	1.1	0.33	700	127	614	13	641	31	88	**96**	614	13
6_9_123	1.8	179	86	10.03	1.2	0.05911	2.65	0.8295	3.0	0.10021	1.2	0.46	532	127	615	14	610	28	116	101	615	14
6_9_51	1.9	512	122	10.04	1.5	0.06132	2.05	0.8532	2.4	0.10031	1.4	0.56	629	90	616	17	624	23	98	99	616	17
6_9_30	1.6	920	76	9.83	1.1	0.05977	2.17	0.8422	2.6	0.10120	0.9	0.59	579	98	621	11	619	24	107	100	621	11
6_9_120	1.0	251	99	9.72	1.3	0.06095	2.24	0.8738	2.8	0.10286	1.5	0.59	639	85	631	18	635	26	99	99	631	18
6_9_31	0.7	183	54	9.72	1.2	0.06339	2.83	0.9096	3.5	0.10314	1.2	0.64	697	119	633	15	654	33	91	97	633	15
6_9_45	0.8	1390	67	9.72	1.2	0.06118	2.80	0.8759	3.1	0.10334	1.2	0.39	605	120	634	14	635	29	105	100	634	14
6_9_39	1.7	86	148	9.68	1.1	0.06164	2.48	0.8839	2.5	0.10370	1.0	0.20	629	111	636	12	641	24	101	99	636	12
6_9_121	1.0	196	83	9.70	1.5	0.06031	3.29	0.8752	3.5	0.10384	1.5	0.41	560	142	637	18	634	33	114	100	637	18
6_9_110	2.2	625	64	9.60	1.1	0.06338	1.86	0.9138	2.1	0.10399	1.2	0.49	701	82	638	15	657	20	91	97	638	15
6_9_96	2.3	997	266	9.53	1.0	0.07180	3.09	1.0381	3.7	0.10519	0.9	0.63	951	124	645	12	719	38	68	**90**	645	12
6_9_112	1.0	370	63	9.44	0.9	0.06376	1.94	0.9432	2.3	0.10614	1.0	0.50	718	82	650	12	673	22	91	97	650	12
6_9_17	1.3	597	36	9.35	1.4	0.06134	2.57	0.9081	3.2	0.10681	1.6	0.60	617	111	654	19	652	30	106	100	654	19
6_9_52	1.1	23	2315	8.46	0.9	0.06289	1.47	1.0338	1.7	0.11850	0.8	0.55	693	64	722	11	719	18	104	100	722	11
6_9_3	1.3	442	76	8.12	2.0	0.07309	1.40	1.2660	2.2	0.12400	2.0	0.78	1011	56	753	28	829	26	75	**91**	753	28
6_9_82	1.2	27	1565	7.56	1.4	0.07474	1.75	1.3610	2.3	0.13282	1.3	0.63	1050	71	804	20	870	27	77	**92**	804	20
6_9_26	2.7	535	170	6.98	2.1	0.07637	2.45	1.5327	3.0	0.14471	2.0	0.58	1086	96	871	33	940	37	80	**93**	871	33
6_9_5	1.3	290	335	6.07	1.7	0.07130	1.80	1.6476	2.2	0.16550	1.7	0.61	959	74	987	31	987	28	103	100	987	31
6_9_32	1.0	3385	211	6.01	1.0	0.07038	1.38	1.6264	1.7	0.16679	1.0	0.54	930	58	994	18	979	21	107	102	994	18
6_9_25	1.5	2362	62	5.75	1.4	0.07688	2.17	1.8618	2.5	0.17492	1.4	0.32	1098	88	1039	27	1064	33	95	98	1039	27
6_9_57	1.1	678	100	3.01	1.3	0.10507	1.97	4.8615	2.1	0.33370	1.3	0.40	1700	75	1855	40	1791	36	109	104	1700	75
6_9_48	1.3	465	72	2.97	1.1	0.10674	2.40	4.9933	2.4	0.33750	1.1	0.22	1729	88	1874	37	1814	40	108	103	1729	88
6_9_91	0.7	5610	61	3.39	1.6	0.10716	2.29	4.4114	2.3	0.29654	1.5	0.31	1740	84	1673	43	1711	38	96	98	1740	84
6_9_49	1.5	1199	153	3.26	0.9	0.10744	1.55	4.5918	2.0	0.30729	0.9	0.63	1750	57	1727	26	1745	33	99	99	1750	57
6_9_119	1.1	2376	53	3.44	1.9	0.11185	2.61	4.5579	3.1	0.29355	1.9	0.55	1810	97	1658	55	1733	53	92	96	1810	97
6_9_59	0.8	8276	67	2.87	1.3	0.12695	1.16	6.1774	1.9	0.34904	1.3	0.82	2053	42	1929	43	1999	35	94	97	2053	42
6_9_63	0.7	740	73	2.71	1.1	0.13186	1.14	6.7964	1.7	0.36958	1.1	0.77	2120	39	2027	39	2083	31	96	97	2120	39
6_9_35	0.7	5753	59	2.62	0.9	0.13217	1.15	6.9859	1.3	0.38217	1.0	0.50	2121	40	2086	34	2107	23	98	99	2121	40
6_9_15	0.6	1300	117	2.67	1.1	0.13282	1.71	6.9141	1.9	0.37617	1.1	0.41	2127	60	2058	39	2097	33	97	98	2127	60
6_9_61	0.8	2761	879	2.55	1.3	0.13326	1.49	7.2103	1.6	0.39415	1.3	0.62	2133	50	2140	49	2142	33	100	100	2133	50
6_9_74	0.9	641	138	2.73	1.3	0.13445	1.87	6.8679	1.8	0.36877	1.3	0.35	2144	63	2022	44	2090	33	94	97	2144	63

6_9_36	1.1	1261	63	2.88	1.6	0.13388	1.41	6.4861	2.3	0.34851	1.6	0.80	2145	50	1926	53	2040	42	90	94	2145	50
6_9_79	0.8	3569	94	2.78	1.3	0.13428	1.44	6.7359	1.9	0.36166	1.3	0.63	2146	53	1989	43	2073	33	93	96	2146	53
6_9_64	2.4	14995	81	2.46	0.8	0.13422	1.22	7.5740	1.3	0.40706	0.7	0.38	2148	43	2201	28	2180	23	102	101	2148	43
6_9_78	1.0	3139	123	2.62	1.0	0.13442	1.37	7.1382	1.7	0.38249	1.0	0.63	2149	48	2087	35	2124	32	97	98	2149	48
6_9_19	1.2	220	733	2.50	0.9	0.13481	1.83	7.4804	2.1	0.40138	0.9	0.47	2153	63	2175	32	2167	37	101	100	2153	63
6_9_40	1.1	58	1519	2.37	0.9	0.13468	1.21	7.8602	1.5	0.42165	1.0	0.57	2154	42	2277	34	2212	26	106	103	2154	42
6_9_128	1.2	27367	131	2.45	1.1	0.13661	1.66	7.8490	1.7	0.41039	1.0	0.33	2174	58	2216	38	2210	31	102	100	2174	58
6_9_54	0.8	3404	41	2.63	1.3	0.13716	2.49	7.2618	2.6	0.38137	1.2	0.37	2177	87	2082	44	2138	47	96	97	2177	87
6_9_55	1.2	935	349	2.52	1.3	0.13690	1.65	7.5804	2.0	0.39942	1.3	0.58	2179	57	2165	47	2178	36	99	99	2179	57
6_9_6	0.9	958	100	2.46	1.1	0.13702	1.37	7.7877	1.9	0.40689	1.1	0.74	2186	48	2200	41	2204	35	101	100	2186	48
6_9_77	0.9	1679	118	2.48	0.9	0.13849	1.71	7.7287	1.8	0.40256	1.0	0.37	2197	59	2180	36	2195	33	99	99	2197	59
6_9_76	1.3	274	131	2.52	1.0	0.13926	1.89	7.7419	2.1	0.39788	1.0	0.51	2205	64	2158	36	2195	37	98	98	2205	64
6_9_111	1.4	278	139	2.44	1.4	0.13894	1.25	7.9562	1.4	0.41124	1.4	0.58	2210	43	2220	52	2225	25	100	100	2210	43
6_9_93	0.8	794	185	2.30	0.8	0.14001	2.39	8.4624	2.2	0.43492	0.7	0.08	2218	83	2328	29	2279	40	105	102	2218	83
6_9_100	0.9	1506	263	2.46	1.2	0.14092	1.50	7.9875	2.1	0.40853	1.2	0.67	2231	53	2207	46	2225	37	99	99	2231	53
Data not used due to high discordance																						
~~**6_9_60**~~	~~1.9~~	~~2751~~	~~108~~	~~3.81~~	~~1.2~~	~~0.14135~~	~~1.70~~	~~5.1704~~	~~1.8~~	~~0.26293~~	~~1.2~~	~~0.36~~	~~2237~~	~~59~~	~~1504~~	~~33~~	~~1846~~	~~30~~	~~67~~	~~82~~		
~~**6_9_106**~~	~~1.9~~	~~2874~~	~~50~~	~~11.96~~	~~1.4~~	~~0.06713~~	~~2.15~~	~~0.7830~~	~~2.2~~	~~0.08397~~	~~1.3~~	~~0.35~~	~~826~~	~~92~~	~~520~~	~~13~~	~~586~~	~~20~~	~~63~~	~~89~~		
~~**6_9_68**~~	~~0.9~~	~~3309~~	~~54~~	~~4.80~~	~~1.8~~	~~0.12209~~	~~2.50~~	~~3.5580~~	~~2.9~~	~~0.20912~~	~~1.9~~	~~0.55~~	~~1978~~	~~86~~	~~1224~~	~~42~~	~~1537~~	~~46~~	~~62~~	~~80~~		
~~**6_9_124**~~	~~0.7~~	~~42~~	~~915~~	~~5.29~~	~~1.7~~	~~0.11296~~	~~1.68~~	~~3.0231~~	~~2.3~~	~~0.19108~~	~~1.7~~	~~0.73~~	~~1836~~	~~60~~	~~1126~~	~~34~~	~~1408~~	~~37~~	~~61~~	~~80~~		
~~**6_9_127**~~	~~2.6~~	~~148~~	~~159~~	~~11.04~~	~~3.7~~	~~0.07113~~	~~2.51~~	~~0.9074~~	~~3.0~~	~~0.09258~~	~~3.3~~	~~0.77~~	~~932~~	~~101~~	~~570~~	~~37~~	~~652~~	~~29~~	~~61~~	~~87~~		
~~**6_9_104**~~	~~1.4~~	~~739~~	~~66~~	~~4.46~~	~~2.0~~	~~0.13636~~	~~1.64~~	~~4.2829~~	~~2.3~~	~~0.22593~~	~~2.0~~	~~0.73~~	~~2176~~	~~56~~	~~1312~~	~~47~~	~~1687~~	~~39~~	~~60~~	~~78~~		
~~**6_9_13**~~	~~0.9~~	~~2157~~	~~81~~	~~4.96~~	~~2.6~~	~~0.12523~~	~~1.69~~	~~3.5785~~	~~3.4~~	~~0.20531~~	~~2.7~~	~~0.85~~	~~2024~~	~~58~~	~~1202~~	~~59~~	~~1536~~	~~51~~	~~59~~	~~78~~		
~~**6_9_38**~~	~~0.2~~	~~1612~~	~~76~~	~~10.88~~	~~1.6~~	~~0.07168~~	~~2.39~~	~~0.9164~~	~~1.9~~	~~0.09228~~	~~1.7~~	~~0.05~~	~~964~~	~~102~~	~~569~~	~~18~~	~~660~~	~~19~~	~~59~~	~~86~~		
~~**6_9_118**~~	~~1.0~~	~~4504~~	~~118~~	~~4.93~~	~~2.8~~	~~0.13149~~	~~2.05~~	~~3.8251~~	~~3.7~~	~~0.20813~~	~~2.8~~	~~0.85~~	~~2102~~	~~73~~	~~1216~~	~~61~~	~~1583~~	~~61~~	~~58~~	~~77~~		
~~**6_9_108**~~	~~1.9~~	~~1391~~	~~143~~	~~5.04~~	~~2.1~~	~~0.12939~~	~~1.84~~	~~3.6164~~	~~2.9~~	~~0.20120~~	~~2.0~~	~~0.78~~	~~2077~~	~~65~~	~~1180~~	~~44~~	~~1544~~	~~45~~	~~57~~	~~76~~		
~~**6_9_34**~~	~~1.7~~	~~55123~~	~~98~~	~~4.87~~	~~1.8~~	~~0.13286~~	~~1.27~~	~~3.8082~~	~~1.8~~	~~0.20623~~	~~1.8~~	~~0.76~~	~~2133~~	~~44~~	~~1208~~	~~39~~	~~1593~~	~~29~~	~~57~~	~~76~~		
~~**6_9_72**~~	~~1.6~~	~~208~~	~~296~~	~~10.07~~	~~3.7~~	~~0.07710~~	~~1.83~~	~~1.0919~~	~~3.1~~	~~0.10235~~	~~3.4~~	~~0.84~~	~~1112~~	~~71~~	~~627~~	~~40~~	~~746~~	~~33~~	~~56~~	~~84~~		
~~**6_9_42**~~	~~2.0~~	~~1989~~	~~37~~	~~5.61~~	~~1.2~~	~~0.11729~~	~~2.22~~	~~2.9156~~	~~2.5~~	~~0.17872~~	~~1.2~~	~~0.44~~	~~1907~~	~~79~~	~~1060~~	~~23~~	~~1383~~	~~37~~	~~56~~	~~77~~		
~~**6_9_20**~~	~~1.1~~	~~101~~	~~74~~	~~5.88~~	~~4.3~~	~~0.11386~~	~~2.96~~	~~2.7633~~	~~4.4~~	~~0.17589~~	~~4.2~~	~~0.69~~	~~1885~~	~~81~~	~~1042~~	~~81~~	~~1335~~	~~67~~	~~55~~	~~78~~		
~~**6_9_33**~~	~~0.4~~	~~59~~	~~82~~	~~5.99~~	~~4.1~~	~~0.12005~~	~~2.94~~	~~2.8979~~	~~6.0~~	~~0.17206~~	~~4.2~~	~~0.88~~	~~1940~~	~~106~~	~~1021~~	~~80~~	~~1364~~	~~90~~	~~53~~	~~75~~		
~~**6_9_29**~~	~~0.7~~	~~2785~~	~~54~~	~~11.10~~	~~1.2~~	~~0.07805~~	~~3.28~~	~~0.9789~~	~~3.5~~	~~0.09041~~	~~1.3~~	~~0.30~~	~~1116~~	~~133~~	~~558~~	~~13~~	~~690~~	~~35~~	~~50~~	~~81~~		
~~**6_9_56**~~	~~0.6~~	~~1437~~	~~111~~	~~7.76~~	~~2.7~~	~~0.10094~~	~~2.04~~	~~1.8230~~	~~2.4~~	~~0.13002~~	~~2.4~~	~~0.63~~	~~1634~~	~~75~~	~~788~~	~~36~~	~~1052~~	~~31~~	~~48~~	~~75~~		
~~**6_9_14**~~	~~1.0~~	~~9189~~	~~70~~	~~5.42~~	~~2.9~~	~~0.14860~~	~~2.20~~	~~3.8585~~	~~3.1~~	~~0.18699~~	~~3.0~~	~~0.74~~	~~2321~~	~~75~~	~~1104~~	~~60~~	~~1600~~	~~50~~	~~48~~	~~69~~		
~~**6_9_53**~~	~~3.0~~	~~576~~	~~64~~	~~11.21~~	~~2.6~~	~~0.08381~~	~~3.94~~	~~1.0529~~	~~4.8~~	~~0.09005~~	~~2.6~~	~~0.59~~	~~1256~~	~~172~~	~~556~~	~~28~~	~~726~~	~~51~~	~~44~~	~~77~~		
~~**6_9_129**~~	~~1.3~~	~~3163~~	~~71~~	~~12.66~~	~~1.3~~	~~0.07967~~	~~1.94~~	~~0.8809~~	~~1.7~~	~~0.07947~~	~~1.3~~	~~0.52~~	~~1172~~	~~75~~	~~493~~	~~12~~	~~640~~	~~16~~	~~42~~	~~77~~		
~~**6_9_11**~~	~~1.4~~	~~403~~	~~170~~	~~11.21~~	~~2.7~~	~~0.08916~~	~~3.44~~	~~1.1042~~	~~3.6~~	~~0.09018~~	~~2.8~~	~~0.43~~	~~1386~~	~~128~~	~~556~~	~~30~~	~~753~~	~~37~~	~~40~~	~~74~~		
~~**6_9_23**~~	~~5.0~~	~~41~~	~~132~~	~~7.91~~	~~2.6~~	~~0.12565~~	~~4.02~~	~~2.1852~~	~~5.4~~	~~0.12525~~	~~3.3~~	~~0.67~~	~~2005~~	~~146~~	~~760~~	~~48~~	~~1164~~	~~74~~	~~38~~	~~65~~		
~~**6_9_24**~~	~~1.9~~	~~608~~	~~99~~	~~9.28~~	~~1.4~~	~~0.11665~~	~~5.51~~	~~1.7783~~	~~6.4~~	~~0.10849~~	~~1.4~~	~~0.73~~	~~1769~~	~~231~~	~~664~~	~~18~~	~~1008~~	~~86~~	~~38~~	~~66~~		
~~**6_9_2**~~	~~0.9~~	~~2173~~	~~22~~	~~7.94~~	~~2.1~~	~~0.12699~~	~~1.67~~	~~2.2439~~	~~1.5~~	~~0.12654~~	~~2.0~~	~~0.64~~	~~2053~~	~~58~~	~~768~~	~~30~~	~~1194~~	~~21~~	~~37~~	~~64~~		
~~**6_9_99**~~	~~2.7~~	~~462~~	~~79~~	~~15.35~~	~~2.8~~	~~0.07841~~	~~3.80~~	~~0.7165~~	~~3.9~~	~~0.06602~~	~~2.8~~	~~0.40~~	~~1126~~	~~148~~	~~412~~	~~22~~	~~546~~	~~33~~	~~37~~	~~75~~		
~~**6_9_16**~~	~~0.4~~	~~1577~~	~~95~~	~~10.38~~	~~1.2~~	~~0.10117~~	~~2.74~~	~~1.3580~~	~~2.9~~	~~0.09665~~	~~1.2~~	~~0.37~~	~~1628~~	~~103~~	~~595~~	~~14~~	~~868~~	~~34~~	~~37~~	~~68~~		
~~**6_9_80**~~	~~1.7~~	~~5319~~	~~65~~	~~14.96~~	~~1.8~~	~~0.07921~~	~~1.60~~	~~0.7426~~	~~2.4~~	~~0.06736~~	~~1.8~~	~~0.74~~	~~1168~~	~~65~~	~~420~~	~~14~~	~~563~~	~~20~~	~~36~~	~~75~~		
~~**6_9_83**~~	~~4.4~~	~~384~~	~~97~~	~~7.58~~	~~2.7~~	~~0.14153~~	~~7.11~~	~~2.5740~~	~~7.4~~	~~0.13111~~	~~3.5~~	~~0.44~~	~~2216~~	~~271~~	~~793~~	~~52~~	~~1250~~	~~142~~	~~36~~	~~63~~		
~~**6_9_12**~~	~~3.8~~	~~118~~	~~44~~	~~8.04~~	~~2.9~~	~~0.15019~~	~~3.96~~	~~2.6820~~	~~5.3~~	~~0.12772~~	~~2.8~~	~~0.67~~	~~2295~~	~~137~~	~~774~~	~~41~~	~~1299~~	~~78~~	~~34~~	~~60~~		

6_9_114	0.7	32	1027	16.35	2.3	0.07990	2.96	0.6848	2.8	0.06177	2.1	0.29	1171	118	386	16	528	23	33	73
6_9_62	0.6	628	248	10.52	1.5	0.11741	1.82	1.5621	2.3	0.09552	1.6	0.62	1910	63	588	17	953	28	31	62
6_9_44	1.0	160	94	19.80	3.8	0.08781	3.83	0.6160	3.5	0.05137	3.7	0.48	1356	147	323	24	486	27	24	66
6_9_88	0.9	629	23	22.30	2.0	0.11237	1.81	0.7058	2.4	0.04524	1.9	0.66	1828	67	285	11	541	20	16	53
6_9_89	0.6	704	47	21.03	3.7	0.12563	2.09	0.8438	3.6	0.04831	3.3	0.81	2030	77	304	20	619	34	15	49
6_9_95	0.6	406	326	3.10	2.6	0.13786	1.67	6.2685	3.2	0.32645	2.7	0.88	2195	57	1819	84	2007	58	82.9	90.6
6_9_92	0.6	167	303	3.08	1.7	0.13370	1.59	5.9673	1.6	0.32610	1.6	0.64	2141	54	1818	51	1980	34	84.9	91.8
6_9_122	0.7	9742	43	3.21	1.3	0.13279	1.38	5.8028	2.3	0.31158	1.5	0.83	2128	49	1747	45	1951	35	82.1	89.6
6_9_47	0.5	7897	59	3.25	1.6	0.12768	1.16	5.4975	2.0	0.30902	1.5	0.82	2063	42	1735	47	1898	35	84.1	91.4
6_9_27	2.1	3186	94	3.30	2.2	0.13159	1.10	5.5772	2.0	0.30533	2.1	0.87	2117	38	1716	65	1910	35	81.1	89.9
6_9_7	0.8	1278	114	3.42	1.1	0.12869	1.72	5.2653	2.0	0.29382	1.1	0.48	2071	59	1660	33	1860	33	80.1	89.3
6_9_86	0.5	8347	84	3.49	1.2	0.12804	1.31	5.1263	1.8	0.28765	1.3	0.68	2067	48	1629	36	1839	31	78.8	88.6
6_9_37	0.6	826	108	3.53	2.1	0.12958	1.24	5.1647	2.9	0.28694	3.0	0.92	2089	44	1624	87	1843	49	77.7	88.1
6_9_102	1.5	37619	67	3.68	2.0	0.13251	2.07	5.0336	2.6	0.27334	2.0	0.60	2123	71	1557	55	1821	44	73.3	85.5
6_9_58	0.9	1861	69	3.72	1.9	0.12274	2.38	4.6539	3.5	0.27223	1.9	0.71	1977	82	1550	52	1747	55	78.4	88.8
6_9_41	0.8	743	120	3.70	1.4	0.12996	2.80	4.9149	3.4	0.27143	1.4	0.61	2081	100	1548	37	1797	58	74.4	86.1
6_9_113	0.6	9013	68	3.73	1.9	0.13307	1.16	4.9582	2.2	0.26794	2.0	0.85	2134	40	1529	54	1807	38	71.6	84.6
6_9_97	0.9	1307	174	3.90	1.5	0.12607	1.41	4.5146	2.0	0.25832	1.6	0.71	2037	49	1480	41	1730	33	72.7	85.6
6_9_4	0.7	271	225	3.88	1.3	0.12562	2.17	4.5330	2.6	0.25792	1.3	0.56	2033	78	1479	34	1735	44	72.8	85.2
6_9_103	0.7	75	396	4.10	2.6	0.12903	1.93	4.3236	4.1	0.24737	2.4	0.86	2074	71	1423	63	1710	53	68.6	83.2
6_9_75	0.9	1744	38	4.12	1.5	0.12155	2.77	4.1194	2.7	0.24432	1.6	0.22	1957	97	1408	39	1652	43	71.9	85.2
6_9_10	0.3	32	1372	4.85	1.8	0.09856	2.91	2.8512	3.6	0.20718	1.6	0.57	1582	110	1213	37	1364	53	77	89

Amostra M2AR 7-2

	Ratios											Rho	Ages (Ma)						% conc [1]	% conc [2]	Best age	2s
Spot number	Th/U	206Pb/204Pb	1s	238U/206Pb	1s	207Pb/206Pb	1s	207Pb/235U	1s	206Pb/238U	1s		207Pb/206Pb	2s	206Pb/238U	2s	207Pb/235U	2s				
			(%)		(%)		(%)		(%)		(%)			(abs)		(abs)		(abs)				(abs)
7_2_98	1.0	63.6	1362.5	14.59	0.8	0.05720	2.07	0.5386	2.1	0.06828	0.9	0.21	481	93	426	8	437	15	88	97	426	8
7_2_13	1.5	427.1	83.4	13.05	1.2	0.06155	2.08	0.6528	2.5	0.07679	1.2	0.54	648	86	477	11	509	20	74	94	477	11
7_2_82	2.3	236.8	81.7	12.52	1.9	0.06180	2.44	0.6842	2.5	0.08038	1.9	0.37	650	102	498	18	528	20	77	94	498	18
7_2_15	1.2	7003.5	50.6	12.47	1.1	0.06111	2.01	0.6714	2.6	0.08037	1.1	0.65	632	86	498	10	521	21	79	96	498	10
7_2_84	0.7	3661.7	52.8	12.30	0.9	0.05811	1.06	0.6550	1.1	0.08152	0.8	0.41	527	46	505	8	511	9	96	99	505	8
7_2_19	1.2	263.5	153.6	12.11	2.5	0.06222	2.47	0.7155	2.7	0.08346	2.4	0.51	664	107	517	24	547	23	78	94	517	24
7_2_49	1.9	603.8	75.6	11.50	1.6	0.06212	3.23	0.7489	3.2	0.08730	1.6	0.30	655	136	539	17	566	28	82	95	539	17
7_2_129	1.2	617.9	52.1	11.18	1.2	0.06095	2.34	0.7573	2.5	0.08991	1.2	0.36	610	100	555	13	570	22	91	97	555	13
7_2_69	3.0	975.8	80.3	11.09	1.9	0.06087	2.78	0.7583	2.2	0.09061	2.1	0.17	620	118	559	22	572	19	90	98	559	22
7_2_2	1.2	1215.4	65.1	10.99	1.0	0.05820	2.06	0.7353	2.2	0.09081	0.9	0.29	514	89	560	9	558	18	109	100	560	9
7_2_68	0.7	1758.6	132.0	11.02	1.4	0.06765	2.12	0.8514	2.2	0.09096	1.4	0.41	849	85	561	15	625	20	66	90	561	15
7_2_5	3.2	81.5	104.8	10.99	1.0	0.05935	1.95	0.7507	2.3	0.09132	1.0	0.49	558	86	563	10	567	20	101	99	563	10
7_2_6	1.4	3455.3	142.9	10.94	1.3	0.06091	1.97	0.7712	1.9	0.09180	1.3	0.26	620	88	566	14	580	17	91	98	566	14

7_2_61	1.7	276.5	48.5	10.90	1.1	0.06582	4.66	0.8382	5.1	0.09197	1.1	0.48	747	192	567	12	613	46	76	**92**	567	12
7_2_52	1.3	86.7	1266.1	10.81	1.0	0.06082	1.95	0.7714	2.1	0.09275	0.9	0.58	614	84	572	10	584	21	93	98	572	10
7_2_125	1.5	4209.4	59.1	10.60	1.7	0.06586	2.16	0.8618	2.6	0.09456	1.8	0.62	795	90	582	20	630	25	73	**92**	582	20
7_2_64	3.2	108.0	191.0	10.67	2.2	0.06186	2.11	0.8051	2.2	0.09465	2.0	0.50	654	90	583	23	599	20	89	97	583	23
7_2_87	1.2	602.3	56.6	10.61	1.4	0.06270	2.78	0.8187	2.8	0.09467	1.4	0.27	669	125	583	15	605	26	87	**96**	583	15
7_2_9	0.9	31020.2	93.0	10.56	1.7	0.06317	2.27	0.8348	2.3	0.09491	1.6	0.32	707	97	584	18	616	20	83	**95**	584	18
7_2_91	1.6	2483.3	89.7	10.44	1.1	0.06487	3.01	0.8443	2.8	0.09592	1.0	0.20	747	130	590	12	620	26	79	**95**	590	12
7_2_94	0.8	1683.8	129.1	10.42	1.1	0.06651	3.01	0.8795	2.6	0.09606	1.1	0.22	808	125	591	12	640	25	73	**92**	591	12
7_2_30	0.8	381.9	274.7	10.37	1.1	0.06339	2.59	0.8481	2.8	0.09660	1.1	0.38	703	117	594	13	622	27	85	**96**	594	13
7_2_57	1.3	23593.1	104.6	10.30	0.8	0.06182	2.86	0.8328	2.9	0.09717	0.8	0.16	655	125	598	9	614	27	91	97	598	9
7_2_112	1.2	1394.3	39.8	10.31	1.1	0.06072	2.10	0.8192	2.1	0.09744	1.1	0.12	630	98	599	13	606	19	95	99	599	13
7_2_34	1.2	1736.5	73.7	10.21	1.5	0.06901	3.50	0.9359	3.8	0.09821	1.4	0.32	873	154	604	16	668	38	69	**90**	604	16
7_2_45	1.2	446.5	68.9	10.15	1.1	0.06576	2.20	0.8961	2.3	0.09868	1.1	0.36	787	94	607	12	649	23	77	**94**	607	12
7_2_38	2.2	1043.6	84.7	10.14	1.0	0.06221	2.57	0.8484	2.4	0.09888	1.0	0.09	658	114	608	12	622	23	92	98	608	12
7_2_53	1.5	499.6	174.8	10.07	1.1	0.06119	1.82	0.8413	1.6	0.09970	1.1	0.11	629	77	613	12	619	14	97	99	613	12
7_2_1	0.9	664.5	65.4	10.07	1.5	0.06095	2.86	0.8411	2.9	0.09975	1.5	0.29	615	125	613	17	618	27	100	99	613	17
7_2_42	2.0	2207.4	101.9	9.94	0.9	0.05993	2.82	0.8315	2.7	0.10073	0.9	0.09	582	127	619	10	613	25	106	101	619	10
7_2_63	1.4	1110.5	58.6	9.93	1.4	0.06111	1.49	0.8579	2.0	0.10142	1.4	0.68	630	65	623	17	627	19	99	99	623	17
7_2_39	2.1	1323.0	47.8	9.79	1.5	0.06154	2.53	0.8696	2.4	0.10264	1.4	0.27	635	110	630	17	634	23	99	99	630	17
7_2_116	2.8	3345.9	46.7	9.59	0.8	0.06165	1.91	0.8854	1.9	0.10342	0.8	0.22	644	82	634	10	643	18	98	99	634	10
7_2_104	0.8	414.7	40.4	9.59	0.9	0.06277	2.76	0.9015	2.8	0.10398	1.1	0.22	662	121	641	12	649	27	97	99	641	12
7_2_18	0.8	66.5	223.4	9.51	1.5	0.06223	4.13	0.9050	4.4	0.10546	1.5	0.30	643	171	646	18	651	41	100	99	646	18
7_2_65	1.0	481.3	78.6	9.44	1.1	0.06281	1.72	0.9164	2.0	0.10559	1.2	0.50	688	73	647	15	659	19	94	98	647	15
7_2_44	1.2	3127.7	66.9	9.36	1.0	0.06277	1.31	0.9257	1.8	0.10658	1.2	0.66	691	58	656	12	664	17	95	99	656	12
7_2_26	0.8	778.0	83.2	9.20	1.2	0.06564	2.83	0.9888	3.5	0.10891	1.2	0.62	775	118	666	16	696	34	86	**96**	666	16
7_2_66	1.0	214.4	238.9	9.19	1.1	0.06316	1.42	0.9518	1.7	0.10916	1.1	0.47	706	61	668	14	678	16	95	98	668	14
7_2_114	0.9	2618.9	79.3	9.06	1.7	0.06818	2.06	1.0457	2.6	0.11087	1.6	0.63	864	84	678	21	725	27	78	**93**	678	21
7_2_108	1.2	122.7	229.6	9.00	0.8	0.06221	1.88	0.9535	2.1	0.11139	0.8	0.49	663	79	681	11	678	21	103	100	681	11
7_2_55	0.8	1805.5	196.1	8.79	1.1	0.06308	1.62	0.9922	2.2	0.11360	1.2	0.66	698	68	693	16	698	22	99	99	693	16
7_2_54	3.6	516.6	70.1	8.29	2.2	0.06733	3.33	1.1200	2.7	0.12139	2.1	0.02	825	150	738	30	762	29	89	97	738	30
7_2_128	2.4	2238.4	45.6	8.17	1.2	0.06865	2.83	1.1617	2.4	0.12268	1.1	0.11	871	113	746	16	781	26	86	**95**	746	16
7_2_11	0.9	49799.7	55.3	7.10	1.5	0.07082	1.49	1.3900	2.4	0.14190	1.6	0.77	943	61	855	25	882	28	91	97	855	25
7_2_50	5.7	117.7	404.8	6.66	1.4	0.07336	2.76	1.5286	2.9	0.15094	1.4	0.33	994	107	906	23	938	34	91	97	906	23
7_2_75	3.6	914.3	54.0	6.54	1.1	0.07330	2.10	1.5515	2.7	0.15322	1.1	0.64	1010	82	919	19	948	32	91	97	919	19
7_2_28	2.5	688.6	61.8	6.42	0.9	0.07302	1.81	1.5752	1.8	0.15630	0.9	0.21	1000	74	936	16	959	22	94	98	936	16
7_2_92	1.2	3096.4	80.2	6.34	1.4	0.07403	1.59	1.6257	2.0	0.15876	1.3	0.58	1030	66	949	24	978	25	92	97	949	24
7_2_59	1.0	9842.6	82.7	6.23	1.5	0.07003	1.60	1.5662	1.9	0.16187	1.5	0.52	915	67	967	26	954	23	106	101	967	26
7_2_110	0.6	1657.9	192.3	6.14	0.9	0.07470	1.02	1.6865	1.2	0.16343	0.9	0.60	1055	41	976	17	1002	16	92	97	976	17
7_2_106	1.6	810.5	84.6	5.92	0.9	0.07799	1.88	1.8201	2.1	0.16911	0.8	0.38	1136	77	1007	16	1051	27	89	**96**	1007	16
7_2_73	0.8	2.6	24180.4	5.91	1.3	0.07416	1.28	1.7450	1.6	0.17013	1.2	0.64	1038	51	1012	23	1023	21	98	99	1012	23
7_2_3	0.2	1554.1	229.6	5.77	1.0	0.07491	1.57	1.8004	1.8	0.17391	1.0	0.44	1055	63	1033	19	1044	23	98	99	1033	19
7_2_123	2.1	1608.6	58.5	5.72	1.0	0.07565	2.18	1.8066	2.0	0.17545	1.1	0.37	1068	85	1042	20	1054	30	98	99	1042	20
7_2_103	1.3	500.6	159.0	5.70	0.9	0.07532	1.24	1.8335	1.4	0.17597	0.9	0.47	1069	50	1045	17	1056	19	98	99	1045	17
7_2_122	0.8	8024.9	38.0	5.55	1.0	0.07656	2.15	1.9089	2.5	0.18063	1.0	0.52	1095	88	1070	20	1081	33	98	99	1070	20
7_2_29	1.3	2260.9	178.0	4.82	0.9	0.07926	1.43	2.2769	1.7	0.20769	0.8	0.60	1171	58	1216	19	1211	21	104	100	1216	19

7_2_33	0.8	12234.8	73.6	3.38	1.2	0.10434	2.41	4.2784	2.4	0.29646	1.2	0.31	1691	84	1673	34	1686	40	99	99	1691	84
7_2_25	0.8	4250.9	73.0	3.25	0.9	0.10524	2.14	4.4693	2.3	0.30784	0.9	0.36	1707	80	1730	26	1722	38	101	100	1707	80
7_2_14	1.0	1394.6	44.9	3.16	1.1	0.10676	1.78	4.6846	1.8	0.31785	1.0	0.33	1733	64	1779	32	1761	30	103	101	1733	64
7_2_10	1.7	1956.0	76.3	3.20	0.7	0.10683	1.76	4.6204	1.8	0.31278	0.7	0.27	1734	64	1754	22	1750	30	101	100	1734	64
7_2_72	1.0	2529.6	114.6	3.21	1.0	0.10695	1.77	4.6065	1.7	0.31213	1.0	0.29	1737	63	1751	31	1747	29	101	100	1737	63
7_2_24	1.6	1853.7	59.8	3.46	1.3	0.10783	2.04	4.3174	2.2	0.29049	1.3	0.38	1752	74	1643	37	1693	35	94	97	1752	74
7_2_100	1.2	236.6	177.1	3.12	1.1	0.10926	2.09	4.8465	2.2	0.31934	1.0	0.30	1771	78	1796	38	1788	36	101	100	1771	78
7_2_43	1.0	18357.3	37.8	3.12	1.0	0.10963	1.44	4.8777	1.8	0.32139	1.0	0.62	1784	53	1796	31	1795	30	101	100	1784	53
7_2_60	0.6	1341.4	77.8	3.19	1.0	0.11027	1.09	4.7526	0.9	0.31446	1.0	0.43	1799	40	1762	30	1776	15	98	99	1799	40
7_2_126	1.4	1619.4	137.2	3.65	1.7	0.11344	1.94	4.3024	2.4	0.27536	1.7	0.53	1846	71	1567	47	1690	38	85	**93**	1846	71
7_2_41	1.4	3293.9	68.9	2.92	1.4	0.11544	2.53	5.4705	2.8	0.34365	1.3	0.44	1873	89	1903	44	1891	48	102	101	1873	89
7_2_119	2.2	4915.6	123.5	3.06	1.2	0.11558	1.29	5.2420	1.5	0.32843	1.1	0.54	1882	46	1830	36	1857	26	97	99	1882	46
7_2_80	0.9	2552.4	169.5	2.83	1.1	0.11781	1.37	5.7473	1.7	0.35396	1.1	0.57	1919	49	1953	38	1937	29	102	101	1919	49
7_2_70	2.4	1546.8	76.4	2.89	1.0	0.12223	1.38	5.8590	1.7	0.34678	1.0	0.57	1986	50	1919	34	1954	30	97	98	1986	50
7_2_12	1.0	17209.7	121.5	2.68	1.0	0.12370	1.71	6.4015	2.0	0.37368	1.0	0.51	2003	61	2046	35	2029	35	102	101	2003	61
7_2_62	0.9	1425.9	72.5	3.10	1.1	0.12532	1.61	5.5897	1.8	0.32330	1.1	0.38	2027	58	1805	33	1912	30	89	94	2027	58
7_2_48	1.7	2678.5	186.1	2.72	0.8	0.12569	1.18	6.3506	1.3	0.36613	1.0	0.47	2034	42	2011	33	2024	23	99	99	2034	42
7_2_99	1.9	387.5	146.4	3.03	1.8	0.12605	2.83	5.7413	2.9	0.33094	1.8	0.36	2037	96	1842	56	1935	50	90	95	2037	96
7_2_89	2.0	1472.9	85.4	2.89	1.5	0.12730	1.65	6.0925	1.8	0.34707	1.5	0.60	2057	56	1920	50	1988	32	93	97	2057	56
7_2_79	0.3	290.0	833.0	3.32	1.4	0.12840	1.64	5.3825	2.5	0.30211	1.4	0.78	2072	58	1701	42	1879	43	82	**91**	2072	58
7_2_102	1.0	2101.4	145.4	2.79	1.1	0.12885	1.92	6.3182	2.0	0.35943	1.1	0.47	2072	67	1979	39	2017	35	95	98	2072	67
7_2_7	0.8	7014.1	42.4	3.34	0.9	0.12977	1.72	5.4035	2.2	0.29987	0.9	0.74	2091	61	1691	26	1883	39	81	**90**	2091	61
7_2_97	1.2	877.6	248.1	2.59	0.9	0.13004	1.44	6.9138	1.3	0.38746	0.9	0.20	2091	50	2110	31	2099	22	101	101	2091	50
7_2_83	1.3	685.3	238.1	2.88	1.6	0.13359	2.36	6.4480	2.6	0.34888	1.5	0.44	2136	83	1929	50	2035	46	90	95	2136	83
7_2_88	0.9	6789.1	82.7	2.73	1.4	0.13561	2.54	6.8806	2.7	0.36781	1.4	0.40	2154	86	2018	48	2089	47	94	97	2154	86
7_2_78	0.6	11322.1	70.5	2.79	1.6	0.13515	2.97	6.7049	3.1	0.36024	1.7	0.34	2154	103	1983	57	2069	55	92	96	2154	103
7_2_101	1.3	1577.6	77.9	2.52	1.1	0.13600	1.79	7.4878	1.9	0.39880	1.0	0.39	2167	61	2163	38	2167	34	100	100	2167	61
7_2_120	1.3	20872.1	86.9	2.35	1.6	0.14184	1.94	8.3510	1.7	0.42238	1.2	0.37	2242	68	2271	46	2268	30	101	100	2242	68
7_2_51	1.0	1909.7	99.1	2.18	0.9	0.16260	1.41	10.3411	1.6	0.46007	0.9	0.43	2475	49	2439	35	2462	29	99	99	2475	49
7_2_121	0.8	35037.8	49.5	2.06	1.0	0.16791	2.29	11.2787	2.5	0.48695	1.0	0.39	2527	77	2557	42	2542	46	101	101	2527	77
7_2_27	0.8	1242.5	113.7	2.00	1.0	0.17417	1.62	12.0739	2.0	0.50065	1.0	0.58	2589	55	2615	43	2604	39	101	100	2589	55
7_2_35	1.1	5000.8	189.3	2.06	1.3	0.17570	1.67	11.8489	2.0	0.48586	1.3	0.58	2608	56	2552	56	2590	36	98	99	2608	56
7_2_93	0.7	7710.8	78.7	1.98	0.9	0.17763	1.58	12.4393	1.7	0.50647	0.9	0.39	2622	53	2641	37	2634	32	101	100	2622	53
7_2_90	1.7	3468.5	94.2	1.62	0.9	0.23355	1.97	19.9644	2.0	0.61816	0.9	0.34	3066	62	3102	44	3084	40	101	101	3066	62
7_2_56	1.2	4054.5	310.7	1.50	1.1	0.27381	1.78	25.3627	2.2	0.66928	1.1	0.55	3318	56	3301	57	3315	42	99	100	3318	56
Data not used due to high discordance																						
7_2_76	0.7	6.0	27690.9	4.17	2.6	0.13354	1.32	4.4636	2.3	0.24189	2.6	0.86	2142	46	1395	64	1722	39	65.2	81.0		
7_2_77	1.2	330.7	168.8	8.58	1.0	0.07674	3.01	1.2376	3.0	0.11671	1.0	0.16	1093	122	712	14	815	34	65.1	87.3		
7_2_124	1.0	1891.8	59.7	11.93	1.2	0.06745	1.98	0.7830	2.5	0.08404	1.3	0.62	842	83	520	13	586	22	61.8	88.7		
7_2_74	3.2	2842.8	112.1	10.79	1.8	0.07128	1.52	0.9170	2.2	0.09313	1.7	0.74	960	62	574	19	660	22	59.8	87.0		
7_2_71	0.5	274.9	544.3	4.50	1.6	0.13612	2.12	4.1978	2.4	0.22294	1.6	0.50	2171	74	1297	39	1671	40	59.7	77.6		
7_2_20	0.9	2608.3	58.8	13.08	1.3	0.06629	1.82	0.7037	2.1	0.07668	1.3	0.53	807	77	476	12	540	18	59.0	88.1		
7_2_95	0.8	1288.5	10.3	4.30	2.2	0.15975	2.77	5.1782	4.2	0.23381	2.2	0.79	2442	93	1354	54	1841	71	55.4	73.5		
7_2_105	1.2	443.6	233.8	11.56	1.0	0.07611	2.12	0.9121	2.5	0.08664	1.0	0.57	1086	86	536	11	657	24	49.3	81.6		
7_2_96	0.1	84.9	1302.8	7.07	1.3	0.11158	2.49	2.1600	3.5	0.13980	1.9	0.68	1813	93	843	30	1164	48	46.5	72.5		

7_2_130	0.8	1924.0	58.3	14.39	1.4	0.07131	1.42	0.6860	1.3	0.06976	1.4	0.45	961	58	435	12	530	11	45.3	82.0
7_2_109	0.4	189.9	2214.1	7.50	2.7	0.11218	0.97	2.0957	2.6	0.13531	2.9	0.92	1832	36	817	44	1145	35	44.6	71.4
7_2_67	1.9	559.3	148.8	13.38	1.7	0.07651	2.65	0.7931	3.3	0.07516	1.7	0.42	1090	99	467	15	591	28	42.9	79.1
7_2_115	1.6	459.6	109.0	22.42	2.2	0.06298	3.47	0.3899	3.2	0.04493	2.0	0.15	677	157	283	11	334	18	41.8	84.9
7_2_8	1.3	1879.5	54.3	7.01	2.7	0.13366	2.62	2.6617	3.2	0.14430	2.6	0.61	2135	88	868	42	1313	47	40.7	66.1
7_2_31	1.3	1661.1	43.0	14.64	3.0	0.08344	2.50	0.7938	2.5	0.06941	3.2	0.58	1264	104	432	26	592	22	34.2	73.0
7_2_58	1.8	1568.3	63.4	15.48	2.1	0.08396	2.34	0.7534	2.8	0.06510	2.0	0.54	1278	93	406	16	569	25	31.8	71.5
7_2_107	0.6	647.7	137.6	19.25	2.4	0.07702	2.13	0.5466	2.7	0.05163	2.9	0.71	1109	84	324	18	442	20	29.3	73.4
7_2_16	0.3	16606.8	52.3	3.08	1.6	0.13194	1.55	5.9220	1.5	0.32626	1.7	0.56	2120	54	1820	53	1963	26	85.8	**92.7**
7_2_21	2.1	958.6	69.6	3.11	0.9	0.12797	1.53	5.6245	2.0	0.32195	0.9	0.67	2066	55	1799	28	1918	36	87.1	**93.8**
7_2_47	1.0	14.7	5321.5	3.49	1.7	0.13460	1.57	5.3484	1.7	0.28780	1.6	0.88	2154	55	1630	47	1875	30	75.7	86.9
7_2_85	0.8	4192.8	148.3	3.77	1.6	0.12996	1.98	4.7887	2.4	0.26696	1.6	0.59	2087	70	1525	44	1778	41	73.0	85.7
7_2_46	0.6	33450.6	69.8	3.86	1.4	0.12324	1.64	4.4194	1.8	0.25965	1.4	0.46	1998	58	1488	36	1714	29	74.5	86.8
7_2_81	0.8	447.5	434.6	3.93	1.7	0.11828	2.21	4.1930	3.5	0.25536	1.8	0.82	1924	79	1466	47	1668	56	76.2	87.8
7_2_4	0.3	4001.9	120.5	3.98	2.7	0.11632	2.05	4.0833	3.6	0.25378	2.7	0.83	1894	74	1457	69	1645	59	76.9	88.5
7_2_37	1.1	565.2	121.9	3.98	2.1	0.12770	1.77	4.4668	2.9	0.25287	2.1	0.80	2061	62	1452	54	1720	49	70.5	84.4
7_2_113	0.8	1250.9	199.8	4.29	1.9	0.10954	2.18	3.5400	1.9	0.23428	1.9	0.36	1784	79	1356	45	1535	30	76.0	88.4
7_2_17	1.7	9086.4	49.1	4.69	2.5	0.11419	2.24	3.3942	2.9	0.21512	2.3	0.65	1857	79	1255	54	1499	46	67.6	83.7
7_2_127	0.4	459.6	219.0	5.48	1.2	0.09360	2.18	2.3698	2.4	0.18292	1.2	0.39	1491	84	1083	24	1232	34	72.6	87.9
7_2_32	0.5	1881.6	133.0	5.67	1.6	0.09452	2.15	2.3188	2.8	0.17693	1.5	0.64	1511	82	1050	29	1216	40	69.5	86.4

Amostra M2AR 7-5

	Ratios											Rho	Ages (Ma)						% conc [1]	% conc [2]	Best age	2s
Spot number	Th/U	206Pb/204Pb	1s	238U/206Pb	1s	207Pb/206Pb	1s	207Pb/235U	1s	206Pb/238U	1s		207Pb/206Pb	2s	206Pb/238U	2s	207Pb/235U	2s				
			(%)		(%)		(%)		(%)		(%)			(abs)		(abs)		(abs)				(abs)
MAR7_5_35	0.1	7457.5	78.1	12.05	1.2	0.06260	0.80	0.7140	1.7	0.08328	1.2	0.59	692	33	516	12	547	14	74.5	94.3	516	12
MAR7_5_65	1.0	1489.6	64.2	11.86	1.5	0.06093	1.44	0.6708	1.7	0.08486	1.6	0.51	628	63	525	16	525	11	83.6	100.0	525	16
MAR7_5_47	1.7	694.4	121.4	10.71	1.2	0.05710	1.83	0.7864	2.4	0.09361	1.2	0.41	485	81	577	13	588	21	118.8	98.1	577	13
MAR7_5_11	1.2	77727.1	75.2	10.65	1.5	0.06636	2.53	0.8527	2.3	0.09449	1.6	0.16	795	105	582	17	625	22	73.2	93.2	582	17
MAR7_5_8	0.8	1020.0	73.2	10.51	1.3	0.05901	1.92	0.7685	2.6	0.09554	1.3	0.65	553	83	588	15	577	23	106.4	101.9	588	15
MAR7_5_89	0.9	754.3	94.5	10.42	1.7	0.08716	1.53	0.8529	2.6	0.09670	1.6	0.42	1356	57	595	18	624	23	43.9	95.3	595	18
MAR7_5_19	1.0	2284.6	87.1	10.35	1.3	0.06470	1.64	0.8834	1.4	0.09698	1.2	0.43	754	70	597	14	642	14	79.1	92.9	597	14
MAR7_5_77	1.4	2282.9	75.2	10.25	1.1	0.07293	1.35	0.7985	1.7	0.09785	1.1	0.46	1025	67	602	13	595	16	58.7	101.1	602	13
MAR7_5_91	1.2	3.2	9721.3	10.15	1.0	0.09043	1.13	0.8206	1.7	0.09818	1.2	0.60	1430	43	604	14	608	15	42.2	99.3	604	14
MAR7_5_6	1.0	2589.1	58.8	10.12	1.9	0.06685	2.80	0.9091	3.3	0.09970	1.9	0.58	809	105	612	22	654	31	75.7	93.7	612	22
MAR7_5_56	1.5	1950.6	82.1	10.07	1.3	0.06070	2.05	0.8655	1.9	0.09969	1.3	0.31	612	85	612	15	632	18	100.0	96.9	612	15
MAR7_5_62	1.0	16103.6	69.4	10.01	1.2	0.06274	1.47	0.8329	2.0	0.10025	1.2	0.51	691	63	616	14	614	18	89.1	100.3	616	14
MAR7_5_5	1.2	2352.1	71.7	9.85	1.0	0.06432	1.83	0.8951	2.6	0.10180	1.1	0.50	740	78	625	13	647	25	84.5	96.5	625	13
MAR7_5_17	0.4	8087.9	45.5	9.83	0.8	0.06208	1.25	0.9004	2.1	0.10186	0.8	0.53	687	44	625	10	651	20	90.9	96.1	625	10
MAR7_5_42	0.1	281.5	63.8	9.76	1.5	0.06223	2.54	0.8950	3.3	0.10303	1.5	0.49	659	106	632	18	646	31	96.0	97.8	632	18
MAR7_5_60	1.3	1908.7	87.1	9.77	1.8	0.06991	5.98	1.0961	9.6	0.10317	1.7	0.82	838	182	633	20	726	82	75.5	87.2	633	20

MAR7_5_81	0.5	64.9	824.6	9.44	1.5	0.08293	1.74	0.9585	2.1	0.10650	1.5	0.10	1258	69	652	19	681	21	51.9	95.7	652	19
MAR7_5_1	1.6	10129.8	56.2	9.35	1.9	0.06636	2.96	0.9612	5.3	0.10797	1.8	0.26	784	123	661	23	699	36	84.3	94.6	661	23
MAR7_5_21	0.3	18518.9	47.5	8.97	1.1	0.06068	1.58	0.9627	2.0	0.11175	1.1	0.42	618	68	683	14	684	20	110.4	99.9	683	14
MAR7_5_74	2.0	32.1	94.5	8.62	3.3	0.07371	10.49	1.1017	11.8	0.11797	2.8	0.45	953	371	718	39	721	123	75.4	99.7	718	39
MAR7_5_66	0.3	2215.4	61.0	7.72	1.3	0.07250	1.53	1.2156	1.6	0.13017	1.3	0.37	991	62	789	19	807	18	79.6	97.8	789	19
MAR7_5_22	1.4	1637.5	102.6	7.44	1.7	0.06693	3.29	1.2870	3.4	0.13385	1.5	0.07	802	126	810	22	836	37	100.9	96.9	810	22
MAR7_5_43	1.1	3149.0	36.3	3.39	1.3	0.10318	1.57	4.2808	2.2	0.29596	1.3	0.78	1674	57	1671	37	1686	36	99.8	99.1	1674	57
MAR7_5_24	0.6	3550.7	101.9	3.37	1.1	0.10396	0.99	4.3893	1.6	0.29725	1.1	0.60	1693	37	1677	32	1709	27	99.1	98.2	1693	37
MAR7_5_57	1.3	31197.9	52.4	3.33	1.1	0.10487	1.34	4.4569	1.8	0.30120	1.1	0.31	1707	49	1697	32	1721	30	99.4	98.6	1707	49
MAR7_5_15	0.8	62.0	409.5	3.21	1.5	0.10597	1.40	4.5421	1.8	0.31290	1.5	0.67	1727	50	1754	47	1737	30	101.6	101.0	1727	50
MAR7_5_2	2.1	16762.1	64.9	3.07	1.2	0.10702	2.22	4.9228	3.1	0.32657	1.2	0.59	1742	76	1821	37	1803	49	104.5	101.0	1742	76
MAR7_5_40	1.2	750.4	88.8	3.21	1.1	0.10729	1.37	4.6190	2.0	0.31229	1.2	0.70	1748	52	1751	35	1750	33	100.2	100.1	1748	52
MAR7_5_30	1.2	14506.1	51.6	3.19	1.2	0.10806	1.08	4.7322	1.6	0.31432	1.2	0.45	1778	29	1761	36	1771	27	99.0	99.4	1778	29
MAR7_5_27	1.1	2558.3	58.1	2.79	1.8	0.11959	1.35	6.2420	2.2	0.36136	1.7	0.25	1945	48	1987	59	2007	37	102.2	99.0	1945	48
MAR7_5_9	0.8	21231.6	32.5	2.91	1.4	0.12404	1.17	5.8351	1.8	0.34225	1.2	0.63	2024	34	1897	39	1949	31	93.7	97.3	2024	34
MAR7_5_33	2.1	1839.8	95.9	2.85	1.2	0.13069	1.26	6.3773	1.8	0.35109	1.2	0.64	2104	44	1939	39	2027	32	92.2	95.7	2104	44
MAR7_5_58	1.5	1441615.9	73.6	2.60	1.1	0.13135	1.30	7.2798	1.9	0.38532	1.1	0.61	2111	46	2100	40	2143	34	99.5	98.0	2111	46
MAR7_5_51	0.7	3959.9	97.6	2.43	1.1	0.13207	0.79	7.9212	1.7	0.41313	1.1	0.35	2123	27	2228	41	2219	31	105.0	100.4	2123	27
MAR7_5_4	0.6	5079.5	83.1	2.74	1.5	0.13810	1.21	6.8650	1.4	0.36652	1.5	0.65	2199	41	2012	52	2092	26	91.5	96.2	2199	41
MAR7_5_36	1.1	13270.9	69.7	2.55	1.3	0.13875	1.46	7.6035	1.5	0.39280	1.3	0.40	2206	51	2135	46	2183	26	96.8	97.8	2206	51
MAR7_5_61	1.2	804.5	89.3	2.78	1.2	0.13937	1.14	6.8889	1.8	0.36111	1.2	0.62	2233	51	1987	41	2095	32	89.0	94.8	2233	51
MAR7_5_64	0.9	10283.5	48.2	2.53	1.3	0.14510	1.10	7.5132	1.3	0.39626	1.3	0.38	2285	37	2151	47	2173	23	94.1	99.0	2285	37
MAR7_5_49	0.7	1999.1	78.2	2.15	1.4	0.16579	0.78	11.2513	1.8	0.46748	1.4	0.88	2514	26	2471	57	2541	34	98.3	97.2	2514	26
MAR7_5_18	0.8	1255.2	405.6	1.93	1.2	0.17509	0.80	13.0131	1.0	0.51913	1.2	0.71	2605	26	2694	51	2680	19	103.4	100.5	2605	26
MAR7_5_52	1.8	192.8	408.9	1.83	1.4	0.17656	1.26	14.3618	2.5	0.54952	1.4	0.56	2616	43	2821	63	2767	45	107.8	102.0	2616	43
MAR7_5_69	2.8	475.9	175.9	1.97	1.2	0.18903	1.06	12.1479	1.1	0.50911	1.2	0.43	2731	35	2652	52	2615	21	97.1	101.4	2731	35
MAR7_5_41	0.5	2185.6	71.5	1.89	1.2	0.19444	1.29	14.3648	1.4	0.53034	1.3	0.56	2776	41	2741	56	2772	27	98.8	98.9	2776	41
MAR7_5_55	0.5	10465.7	85.0	1.80	2.0	0.23135	1.56	18.6136	1.8	0.56111	1.8	0.78	3055	51	2867	86	3029	30	93.9	94.7	3055	51
MAR7_5_75	1.0	28097.2	68.0	1.57	0.9	0.28194	1.23	22.2506	1.2	0.63639	0.9	0.29	3371	38	3174	46	3194	24	94.2	99.4	3371	38
MAR7_5_34	1.2	442.3	166.0	10.27	2.0	0.06995	2.32	0.9424	3.6	0.09700	1.7	0.50	908	90	597	19	671	32	65.7	89.0		
MAR7_5_87	0.8	672.2	155.6	1.97	1.2	0.23757	1.09	12.6361	1.7	0.50886	1.2	0.64	3101	35	2651	53	2650	33	85.5	100.0		
MAR7_5_122	0.7	1358.1	131.0	9.99	1.7	0.16557	1.61	0.8282	2.2	0.10087	1.9	0.70	2506	55	619	22	611	21	24.7	101.3		
MAR7_5_106	0.5	2915.1	60.5	10.04	1.6	0.12321	1.41	0.8903	2.1	0.10030	1.6	0.06	1997	49	616	19	645	20	30.8	95.5		
MAR7_5_101	1.0	779.4	55.1	10.13	1.3	0.09963	1.11	0.8221	1.6	0.09909	1.2	0.60	1613	41	609	14	609	15	37.8	100.1		
MAR7_5_99	0.9	2903.6	67.9	9.71	2.0	0.10367	2.50	0.9258	4.1	0.10270	1.7	0.58	1671	93	630	21	660	38	37.7	95.4		
Data not used due to high discordance																						
MAR7_5_115	0.4	24461.8	102.1	2.65	1.2	0.31350	0.86	7.5529	2.0	0.37908	1.2	0.76	3536	27	2071	43	2175	36	58.6	95.2		
MAR7_5_113	0.6	2760.0	52.9	2.80	1.3	0.28263	0.61	6.6606	1.4	0.35845	1.3	0.53	3376	19	1974	45	2065	25	58.5	95.6		
MAR7_5_68	0.9	310.4	54.5	9.57	1.8	0.08112	6.49	1.1136	8.7	0.10539	1.9	0.65	1120	220	646	23	739	82	57.7	87.4		
MAR7_5_38	0.6	12009.5	88.8	5.52	1.4	0.11590	1.02	2.9506	1.9	0.18174	1.5	0.75	1891	36	1076	29	1393	28	56.9	77.2		
MAR7_5_20	0.8	8037.5	114.4	10.12	1.8	0.07567	2.04	1.1015	2.6	0.09927	1.7	0.71	1079	78	610	20	753	27	56.5	81.0		
MAR7_5_120	1.4	1807.2	82.7	3.09	1.5	0.25695	1.13	4.9367	1.9	0.32560	1.5	0.75	3224	36	1816	47	1805	32	56.3	100.6		
MAR7_5_45	0.8	8849.3	72.9	4.75	3.9	0.14349	4.11	4.2128	3.0	0.21542	3.7	0.76	2244	131	1255	85	1672	51	55.9	75.1		
MAR7_5_23	1.7	169.9	73.3	9.92	1.9	0.07849	7.20	1.1114	9.6	0.09872	2.1	0.78	1110	275	607	25	736	80	54.6	82.4		
MAR7_5_96	0.5	814.0	4.7	3.46	1.7	0.22420	1.00	5.8620	1.5	0.29034	1.6	0.70	3009	33	1643	47	1954	26	54.6	84.0		

MAR7_5_121	1.7	792.0	68.2	3.10	1.0	0.29908	1.40	4.9313	1.2	0.32382	0.9	0.04	3461	43	1808	30	1806	20	52.2	100.1
MAR7_5_16	1.5	363.0	5.7	4.76	1.6	0.16260	1.16	4.8474	1.6	0.21157	1.6	0.84	2479	39	1237	36	1791	27	49.9	69.0
MAR7_5_59	0.6	17.4	3426.3	5.23	2.6	0.14811	1.10	4.1756	2.1	0.19293	2.6	0.90	2322	38	1136	54	1667	35	48.9	68.2
MAR7_5_3	1.2	117.3	19.0	3.80	4.6	0.27549	9.35	11.0023	13.0	0.27256	4.5	0.85	3190	327	1549	125	2397	251	48.6	64.6
MAR7_5_111	0.8	2780.0	107.1	5.17	1.5	0.16738	1.31	2.1845	2.3	0.19437	1.5	0.64	2527	43	1145	32	1173	31	45.3	97.6
MAR7_5_125	1.3	556.9	13.2	3.07	2.0	0.47907	1.28	7.4374	1.1	0.32927	2.1	0.49	4174	39	1833	67	2164	20	43.9	84.7
MAR7_5_7	1.1	222.5	12.3	5.19	1.9	0.18713	1.60	5.0747	1.3	0.19326	1.9	0.39	2714	53	1139	39	1831	21	42.0	62.2
MAR7_5_114	1.2	49.7	265.3	5.66	1.4	0.16621	1.76	1.8942	1.9	0.17753	1.4	0.41	2511	61	1053	27	1077	24	41.9	97.8
MAR7_5_130	1.0	1415.4	213.1	3.95	1.4	0.31958	0.79	3.4705	1.8	0.25438	1.4	0.78	3566	24	1460	35	1518	29	41.0	96.2
MAR7_5_119	0.4	2981.2	48.4	4.37	1.6	0.26324	0.54	3.6841	1.7	0.22976	1.7	0.90	3273	23	1333	40	1566	27	40.7	85.1
MAR7_5_117	0.8	1283.4	19.7	4.05	2.9	0.32348	1.37	5.0048	2.3	0.25179	2.6	0.86	3582	43	1445	68	1815	40	40.4	79.6
MAR7_5_126	0.8	1215.1	127.0	3.74	3.0	0.39913	1.48	5.0757	3.2	0.27402	3.1	0.92	3901	43	1557	85	1823	53	39.9	85.4
MAR7_5_127	0.2	710.0	12.0	3.54	2.5	0.45626	0.98	5.9555	2.5	0.28725	2.5	0.88	4103	30	1625	72	1963	44	39.6	82.8
MAR7_5_94	1.2	252.9	71.5	9.75	2.1	0.10245	4.20	0.9323	4.9	0.10385	2.3	0.16	1618	146	637	27	662	45	39.3	96.2
MAR7_5_123	0.5	672.1	154.8	4.53	2.4	0.28276	1.74	3.0299	2.6	0.22328	2.5	0.10	3373	52	1298	58	1412	40	38.5	91.9
MAR7_5_98	0.2	26252.9	95.8	7.77	1.1	0.12772	1.00	1.4419	1.1	0.12886	1.1	0.51	2064	36	781	16	906	13	37.8	86.2
MAR7_5_101	1.0	779.4	55.1	10.13	1.3	0.09963	1.11	0.8221	1.6	0.09909	1.2	0.60	1613	41	609	14	609	15	37.8	100.1
MAR7_5_99	0.9	2903.6	67.9	9.71	2.0	0.10367	2.50	0.9258	4.1	0.10270	1.7	0.58	1671	93	630	21	660	38	37.7	95.4
MAR7_5_31	1.4	462.6	63.8	6.38	3.5	0.16848	5.77	3.8970	9.8	0.15356	2.3	0.93	2499	195	921	39	1579	140	36.8	58.3
MAR7_5_109	1.3	508.4	15.8	4.69	1.4	0.31086	1.05	4.5845	1.5	0.21431	1.4	0.51	3522	32	1251	32	1745	24	35.5	71.7
MAR7_5_129	0.6	1281.9	37.6	3.90	1.7	0.49912	1.71	5.7349	2.8	0.25751	1.7	0.84	4234	50	1476	45	1932	48	34.9	76.4
MAR7_5_71	0.7	368.8	10.7	9.09	3.1	0.13656	2.09	1.9263	2.2	0.11159	3.1	0.65	2177	69	682	40	1089	30	31.3	62.6
MAR7_5_106	0.5	2915.1	60.5	10.04	1.6	0.12321	1.41	0.8903	2.1	0.10030	1.6	0.06	1997	49	616	19	645	20	30.8	95.5
MAR7_5_107	1.2	51.7	129.5	8.86	3.0	0.14792	5.10	1.2056	7.3	0.11348	3.3	0.68	2329	137	692	44	785	79	29.7	88.2
MAR7_5_105	0.5	349.1	71.6	7.53	3.4	0.21823	4.75	2.3798	4.5	0.13588	3.7	0.48	2936	133	820	56	1228	63	27.9	66.8
MAR7_5_72	0.7	341.0	9.1	9.44	2.3	0.15270	1.43	2.0790	1.8	0.10662	2.3	0.70	2373	48	653	28	1141	24	27.5	57.2
MAR7_5_79	7.5	65.4	43.9	7.39	3.5	0.25048	8.77	3.6923	7.4	0.13820	3.8	0.17	3068	298	833	58	1541	121	27.2	54.1
MAR7_5_83	1.5	67.7	797.6	10.55	1.4	0.14021	2.61	1.4153	2.4	0.09512	1.5	0.69	2218	83	586	16	907	38	26.4	64.6
MAR7_5_108	0.4	487.5	84.2	8.22	1.5	0.20253	2.55	1.7656	3.1	0.12236	1.5	0.19	2832	79	744	21	1028	38	26.3	72.3
MAR7_5_122	0.7	1358.1	131.0	9.99	1.7	0.16557	1.61	0.8282	2.2	0.10087	1.9	0.70	2506	55	619	22	611	21	24.7	101.3
MAR7_5_92	1.0	478.6	22.4	9.98	2.2	0.16589	2.91	1.5426	2.8	0.09935	1.7	0.51	2498	97	610	20	944	34	24.4	64.6
MAR7_5_86	0.9	172.8	11.7	7.74	5.1	0.27323	2.90	3.8915	3.6	0.13362	5.1	0.78	3314	92	807	78	1606	59	24.3	50.2
MAR7_5_118	0.8	1144.2	111.2	10.71	1.7	0.18326	6.31	1.0383	7.0	0.09406	1.8	0.46	2646	234	579	20	708	70	21.9	81.8
MAR7_5_29	0.6	1714.6	128.7	21.38	4.4	0.10582	17.44	0.5778	19.1	0.04607	3.3	0.95	1366	521	290	19	503	191	21.2	57.7
MAR7_5_73	0.9	219.1	22.0	11.98	2.4	0.17170	3.62	1.7334	2.1	0.08456	2.2	0.28	2543	114	523	22	1019	26	20.6	51.3
MAR7_5_116	0.6	96.0	298.9	11.27	1.2	0.23461	2.71	1.3086	3.7	0.08902	1.2	0.54	3069	79	550	12	845	39	17.9	65.1
MAR7_5_124	0.5	18.6	216.0	8.94	3.5	0.44463	5.76	2.4985	7.2	0.11441	3.5	0.13	4020	172	698	46	1250	98	17.4	55.8
MAR7_5_112	2.6	149.5	10.2	14.09	2.8	0.37045	3.69	1.7330	1.7	0.07247	2.9	0.02	3763	115	451	25	1019	21	12.0	44.2
MAR7_5_88	0.3	58.6	4.1	16.81	2.3	0.43548	1.40	2.6976	2.0	0.05992	2.3	0.66	4033	42	375	17	1326	30	9.3	28.3
MAR7_5_67	1.5	1742.3	66.8	3.49	0.8	0.11345	0.97	4.1959	1.3	0.28709	0.8	0.56	1853	35	1627	24	1672	22	87.8	97.3
MAR7_5_28	0.6	13579.2	42.9	3.06	1.2	0.12943	0.82	6.2056	1.4	0.32682	1.2	0.76	2089	29	1823	39	2004	24	87.3	90.9
MAR7_5_12	0.9	5.3	5551.0	3.43	1.4	0.11791	4.00	4.8907	1.6	0.29258	1.5	0.28	1898	146	1654	43	1799	26	87.1	91.9
MAR7_5_50	0.5	1394.4	58.9	3.06	2.0	0.12804	2.14	6.3523	2.7	0.32911	1.9	0.02	2106	115	1833	61	2021	46	87.0	90.7
MAR7_5_87	0.8	672.2	155.6	1.97	1.2	0.23757	1.09	12.6361	1.7	0.50886	1.2	0.64	3101	35	2651	53	2650	33	85.5	100.0
MAR7_5_53	0.5	892.0	71.4	4.00	2.6	0.10667	3.67	3.8939	4.4	0.25413	2.5	0.20	1706	127	1457	67	1598	67	85.4	91.2

MAR7_5_10	2.2	36772.6	54.8	2.56	1.4	0.16272	1.12	8.7025	1.2	0.38916	1.0	0.70	2480	37	2118	38	2306	21	85.4	91.9
MAR7_5_44	0.7	7456.0	55.3	3.18	1.0	0.13147	1.51	5.9891	1.9	0.31530	1.0	0.30	2113	53	1766	30	1972	32	83.6	89.6
MAR7_5_25	1.0	397.3	124.2	3.79	2.4	0.11236	1.76	4.3337	1.5	0.26612	2.3	0.55	1833	62	1520	64	1699	25	82.9	89.5
MAR7_5_82	1.7	20284.0	101.4	2.66	0.8	0.16617	1.00	6.7989	1.4	0.37659	0.9	0.61	2517	34	2060	30	2084	25	81.8	98.8
MAR7_5_84	1.8	3796.9	81.0	3.17	1.4	0.13958	1.15	4.7340	1.5	0.31646	1.4	0.53	2218	41	1772	42	1772	26	79.9	100.0
MAR7_5_76	1.1	807.8	88.3	2.76	1.2	0.16769	0.95	6.7717	1.7	0.36388	1.2	0.61	2532	32	2000	41	2080	29	79.0	96.1
MAR7_5_85	1.0	1807.9	92.5	2.74	1.2	0.18075	0.94	7.0967	1.2	0.36534	1.3	0.53	2658	31	2007	44	2123	21	75.5	94.5
MAR7_5_93	0.6	4539.4	50.4	2.52	1.5	0.20535	1.13	7.4844	1.7	0.39773	1.4	0.79	2866	36	2158	52	2169	30	75.3	99.5
MAR7_5_37	0.4	523.7	48.2	3.30	2.0	0.14572	1.32	6.3325	1.3	0.30515	2.1	0.15	2293	47	1716	64	2022	22	74.8	84.8
MAR7_5_80	0.8	16773.0	112.7	3.57	1.5	0.13292	1.28	4.1260	1.4	0.28075	1.5	0.47	2133	45	1595	42	1658	23	74.7	96.2
MAR7_5_100	1.1	424.0	212.5	2.49	1.0	0.22699	1.34	7.7162	1.6	0.40186	1.0	0.52	3026	43	2177	37	2196	28	71.9	99.1
MAR7_5_78	0.5	22612.1	101.1	3.97	1.9	0.12519	1.19	3.6257	2.5	0.25366	1.8	0.62	2028	42	1456	48	1551	38	71.8	93.9
MAR7_5_97	0.8	344.7	623.9	2.71	1.0	0.20937	1.22	6.6934	1.5	0.36981	1.1	0.19	2897	40	2028	36	2070	26	70.0	98.0
MAR7_5_102	1.5	0.5	200926.4	2.75	2.0	0.20846	1.10	6.2288	2.3	0.36660	1.9	0.28	2890	36	2011	65	2004	39	69.6	100.4
MAR7_5_54	1.9	257.3	50.8	10.06	1.5	0.07363	7.22	1.0862	8.6	0.09999	1.6	0.50	886	256	614	18	724	83	69.3	84.8
MAR7_5_39	0.9	796.2	169.7	4.33	1.5	0.12519	1.03	4.0110	2.2	0.23218	1.5	0.78	2028	36	1345	36	1633	37	66.3	82.4
MAR7_5_34	1.2	442.3	166.0	10.27	2.0	0.06995	2.32	0.9424	3.6	0.09700	1.7	0.50	908	90	597	19	671	32	65.7	89.0
MAR7_5_90	1.1	768.3	75.6	3.70	1.5	0.15324	0.95	4.1824	1.9	0.27192	1.5	0.75	2379	33	1550	41	1668	31	65.1	92.9
MAR7_5_104	1.2	5267.7	125.8	2.90	2.5	0.23863	1.46	6.5822	2.4	0.34640	2.3	0.81	3109	47	1917	77	2055	43	61.7	93.2
MAR7_5_128	9.4	28.5	73.1	1.85	3.7	0.78064	4.09	18.8751	3.6	0.55147	3.7	0.45	4669	132	2871	197	3020	65	61.5	95.1
MAR7_5_103	1.1	1528.4	64.4	3.67	1.6	0.18072	1.24	4.0120	1.2	0.27386	1.6	0.47	2655	41	1560	43	1636	20	58.7	95.4

Amostra M2AR 8-1

	Ratios											**Rho**	**Ages (Ma)**						**% conc [1]**	**% conc [2]**	**Best age**	**2s**
Spot number	Th/U	206Pb/204Pb	1s	238U/206Pb	1s	207Pb/206Pb	1s	207Pb/235U	1s	206Pb/238U	1s		207Pb/206Pb	2s	206Pb/238U	2s	207Pb/235U	2s				
			(%)		(%)		(%)		(%)		(%)			(abs)		(abs)		(abs)				(abs)
MAR8_1_121	3.0	1082.7	52.5	49.28	1.6	0.05064	4.66	0.1439	4.9	0.02041	1.6	0.22	125	234	130	4	136	12	103.8	95.8	130	4
MAR_8_1_6	1.6	652.7	108.6	19.52	1.8	0.05570	2.08	0.4011	2.3	0.05172	1.8	0.50	419	93	325	11	342	13	77	95	325	11
MAR8_1_67	1.5	55.8	235.3	17.18	1.6	0.05506	2.44	0.4406	2.6	0.05856	1.5	0.45	391	106	367	11	370	16	93.9	99.2	367	11
MAR_8_1_58	0.5	567.2	68.9	13.08	2.2	0.05655	2.15	0.6088	2.8	0.07753	2.3	0.62	454	96	481	21	481	21	106	100	481	21
MAR8_1_95	3.5	117.0	268.6	11.66	1.8	0.06319	2.13	0.7333	2.2	0.08658	1.9	0.59	697	89	535	19	557	19	76.8	96.0	535	19
MAR_8_1_15	0.6	3029.6	75.9	11.67	2.4	0.05927	1.15	0.7166	1.9	0.08693	2.3	0.87	571	51	537	24	548	16	94	98	537	24
MAR8_1_92	0.3	1929.2	74.5	11.59	1.8	0.06102	1.49	0.7237	1.7	0.08699	1.8	0.65	631	64	538	18	552	15	85.2	97.4	538	18
MAR_8_1_65	3.2	202.0	84.5	11.55	2.4	0.05916	1.68	0.7207	2.1	0.08788	2.5	0.73	562	71	543	26	550	18	97	99	543	26
MAR_8_1_1	2.2	204.6	131.0	11.43	2.1	0.06038	2.83	0.7386	2.8	0.08836	2.1	0.29	633	140	546	21	560	24	86	97	546	21
MAR_8_1_34	1.2	342.5	242.5	11.40	2.6	0.05820	1.97	0.7180	2.5	0.08922	2.5	0.70	521	88	551	26	548	21	106	100	551	26
MAR_8_1_3	3.2	71.4	322.0	11.20	2.7	0.05723	2.61	0.7234	3.1	0.09101	2.6	0.59	470	115	561	28	550	26	119	102	561	28
MAR_8_1_2	0.7	1225.4	102.0	10.93	2.1	0.05937	1.65	0.7675	2.4	0.09268	2.1	0.74	568	72	571	23	577	21	100	99	571	23
MAR8_1_66	1.2	515.8	59.8	10.74	1.5	0.06063	2.11	0.7750	2.1	0.09268	1.3	0.37	610	88	571	14	582	18	93.7	98.2	571	14

MAR_8_1_22	1.9	47.0	634.5	10.87	2.4	0.06231	2.46	0.8044	2.6	0.09325	2.3	0.51	660	110	574	25	597	24	87	96	574	25
MAR8_1_80	1.8	2923.3	67.7	10.75	1.5	0.06061	1.83	0.7716	2.4	0.09356	1.5	0.62	612	87	576	17	579	21	94.2	99.5	576	17
MAR8_1_72	0.1	716.9	95.7	10.71	1.5	0.06567	1.88	0.8412	2.6	0.09390	1.6	0.55	783	79	578	17	626	28	73.9	92.3	578	17
MAR_8_1_48	2.4	77.9	254.2	10.74	1.9	0.06027	2.37	0.7840	2.2	0.09405	1.9	0.28	624	86	579	21	586	20	93	99	579	21
MAR_8_1_44	1.1	2618.5	39.3	10.59	1.8	0.05842	1.67	0.7702	1.7	0.09520	1.7	0.52	533	76	586	19	579	16	110	101	586	19
MAR_8_1_7	0.6	1124.0	88.0	10.29	1.4	0.06526	1.74	0.8901	2.1	0.09767	1.3	0.53	771	74	601	15	645	20	78	93	601	15
MAR_8_1_64	0.5	92.1	337.7	10.33	2.4	0.06677	3.49	0.8997	3.6	0.09788	2.3	0.28	801	134	602	27	649	34	75	93	602	27
MAR8_1_128	1.6	4851.1	42.4	10.19	1.3	0.06120	1.59	0.8363	1.8	0.09851	1.2	0.45	636	71	606	14	616	16	95.3	98.3	606	14
MAR_8_1_31	1.0	51.6	849.6	10.21	2.1	0.05910	1.43	0.8124	2.1	0.09909	1.9	0.73	561	64	609	22	603	19	109	101	609	22
MAR_8_1_55	0.7	5887.8	127.0	10.22	2.1	0.06877	3.27	0.9471	3.8	0.09916	2.2	0.42	850	131	609	26	672	36	72	91	609	26
MAR_8_1_61	0.7	138.7	133.8	10.18	2.6	0.06136	2.35	0.8527	3.0	0.10012	2.6	0.67	627	103	615	30	623	28	98	99	615	30
MAR8_1_101	1.8	203.5	130.2	10.02	1.6	0.06481	3.07	0.9000	3.7	0.10026	1.7	0.52	747	122	616	20	649	34	82.4	94.8	616	20
MAR8_1_82	0.8	2191.8	85.0	9.98	1.4	0.06329	1.41	0.8671	1.8	0.10071	1.5	0.64	710	61	618	17	633	17	87.1	97.7	618	17
MAR8_1_84	1.0	2737.9	55.3	9.99	1.8	0.06143	2.27	0.8427	2.4	0.10097	1.8	0.50	636	90	620	21	619	22	97.5	100.1	620	21
MAR8_1_111	3.1	3.8	2413.9	9.89	1.0	0.06696	3.17	0.9347	3.3	0.10124	0.9	0.31	812	128	622	11	668	32	76.6	93.1	622	11
MAR_8_1_12	0.5	843.9	129.7	9.93	2.4	0.05851	2.18	0.8297	2.5	0.10212	2.4	0.60	529	100	626	29	612	23	118	102	626	29
MAR8_1_87	0.9	47.3	266.6	9.78	1.4	0.06773	5.18	0.9419	4.1	0.10243	1.4	0.57	823	196	629	16	672	39	76.3	93.6	629	16
MAR8_1_70	0.3	568.6	52.0	9.76	1.7	0.06203	1.67	0.8739	2.3	0.10319	1.7	0.69	663	70	633	20	636	21	95.4	99.5	633	20
MAR_8_1_20	1.3	4.2	5444.8	9.75	2.4	0.06469	2.04	0.9304	2.3	0.10347	2.3	0.35	754	85	635	28	667	23	84	95	635	28
MAR_8_1_43	0.2	887.6	56.3	9.56	1.6	0.06167	1.30	0.9008	1.9	0.10521	1.5	0.54	656	56	645	19	651	19	98	99	645	19
MAR_8_1_45	1.6	397.1	142.1	9.58	2.2	0.05589	1.92	0.8184	2.1	0.10581	2.2	0.59	431	87	648	27	606	19	150	107	648	27
MAR_8_1_56	1.3	65.8	106.3	9.64	3.1	0.06093	2.42	0.8939	2.9	0.10587	2.9	0.65	615	109	648	35	646	28	105	100	648	35
MAR8_1_88	0.2	1113.2	90.4	9.27	1.4	0.06183	1.17	0.9140	1.7	0.10837	1.4	0.74	663	49	663	18	658	17	100.1	100.7	663	18
MAR8_1_118	1.6	37903.1	54.6	9.22	1.3	0.06415	1.86	0.9730	1.7	0.10884	1.3	0.28	735	77	666	16	689	18	90.6	96.6	666	16
MAR8_1_112	0.6	8300.9	36.8	9.20	1.5	0.06139	1.46	0.9363	1.7	0.10931	1.4	0.56	644	63	669	18	670	16	103.9	99.8	669	18
MAR8_1_75	0.9	437.0	74.2	9.10	1.3	0.06257	2.09	0.9397	2.2	0.11036	1.3	0.39	678	91	675	16	671	22	99.5	100.5	675	16
MAR8_1_99	0.5	696.8	167.8	9.06	1.6	0.06131	1.84	0.9393	2.3	0.11085	1.5	0.56	640	78	678	19	671	22	105.9	100.9	678	19
MAR_8_1_54	1.6	1131.2	43.3	9.02	2.5	0.06471	2.62	1.0069	2.8	0.11279	2.4	0.39	774	125	688	31	705	28	89	98	688	31
MAR8_1_123	0.0	14582.1	47.0	8.70	1.5	0.06411	1.59	1.0299	1.7	0.11564	1.6	0.53	736	68	705	21	718	18	95.8	98.2	705	21
MAR_8_1_38	1.7	694.1	47.4	8.72	1.8	0.06154	1.45	0.9880	1.7	0.11572	1.9	0.72	649	62	706	25	697	17	109	101	706	25
MAR_8_1_49	1.8	884.4	67.2	8.70	1.7	0.06441	1.83	1.0244	2.5	0.11593	1.7	0.54	741	79	707	22	721	22	95	98	707	22
MAR8_1_73	2.2	250.2	56.5	8.68	1.6	0.06546	1.84	1.0318	1.9	0.11593	1.5	0.42	800	67	707	20	719	20	88.4	98.4	707	20
MAR8_1_96	0.8	221.2	147.7	8.66	1.4	0.06388	1.89	1.0190	1.6	0.11599	1.4	0.20	724	80	707	18	713	16	97.7	99.3	707	18
MAR_8_1_37	0.4	43.5	813.8	8.57	2.0	0.06113	2.17	0.9993	2.7	0.11791	2.0	0.65	625	94	718	28	701	28	115	102	718	28
MAR8_1_113	0.6	593.0	117.9	7.74	1.2	0.06775	1.70	1.2261	1.7	0.12969	1.2	0.37	850	72	786	17	811	19	92.4	96.9	786	17
MAR8_1_114	0.9	14031.4	33.0	7.55	1.8	0.06957	1.92	1.3000	2.8	0.13358	1.8	0.71	903	76	808	27	843	31	89.5	95.9	808	27
MAR_8_1_13	1.0	8303.8	76.7	7.04	2.7	0.07243	1.73	1.4277	2.4	0.14465	2.9	0.82	987	72	870	47	908	35	88	96	870	47
MAR8_1_119	1.1	122277.5	36.1	6.38	1.7	0.07422	1.81	1.6313	1.9	0.15796	1.6	0.50	1035	72	945	28	980	24	91.3	96.4	945	28
MAR_8_1_47	0.9	511.6	93.5	6.33	2.2	0.07357	1.90	1.6433	2.9	0.16031	2.3	0.77	1016	77	958	40	983	36	94	97	958	40
MAR8_1_91	1.3	100.9	368.2	6.16	1.4	0.07213	1.89	1.6044	1.7	0.16331	1.5	0.30	976	80	975	26	970	22	99.9	100.4	975	26
MAR_8_1_9	0.7	37391.4	99.6	6.09	2.0	0.07280	1.69	1.6773	1.9	0.16572	1.9	0.62	998	67	988	35	998	25	99	99	988	35
MAR8_1_71	0.5	2852.4	55.4	5.89	1.1	0.07196	1.37	1.6549	1.9	0.17029	1.1	0.70	979	57	1014	20	990	24	103.5	102.4	1014	20
MAR8_1_74	0.9	878.5	81.0	5.81	1.8	0.07506	1.35	1.7729	2.2	0.17316	1.8	0.79	1065	54	1029	34	1034	29	96.7	99.6	1029	34
MAR8_1_125	1.2	8682.0	63.0	5.69	1.7	0.07953	2.23	1.9499	2.2	0.17685	1.6	0.30	1168	93	1049	32	1096	30	89.9	95.8	1049	32
MAR_8_1_27	0.6	503.3	196.5	5.70	2.0	0.07491	1.92	1.8400	2.4	0.17701	1.9	0.63	1053	76	1050	37	1057	31	100	99	1050	37

MAR8_1_104	1.6	2173.6	80.8	5.67	2.2	0.08249	1.98	2.0318	1.6	0.17868	2.2	0.48	1243	78	1059	42	1125	23	85.2	94.2	1059	42
MAR_8_1_35	0.9	346.8	78.8	5.55	2.2	0.06983	2.41	1.7647	3.4	0.18187	2.2	0.68	907	100	1076	44	1028	44	119	105	1076	44
MAR8_1_117	0.6	11103.3	68.7	4.80	1.6	0.08208	1.55	2.4034	2.1	0.20982	1.6	0.70	1239	61	1227	37	1241	31	99.0	98.9	1227	37
MAR8_1_68	1.4	88.6	1058.3	4.68	1.9	0.08249	1.44	2.4224	2.2	0.21476	1.8	0.76	1252	57	1254	40	1247	32	100.2	100.5	1254	40
MAR_8_1_26	0.5	26668.3	106.3	4.69	2.2	0.08017	1.80	2.4038	2.4	0.21628	2.3	0.71	1189	72	1261	53	1240	34	106	102	1261	53
MAR_8_1_11	1.8	48.0	465.5	3.75	2.2	0.09234	2.35	3.4703	2.8	0.27035	2.4	0.53	1455	92	1540	65	1514	43	106	102	1540	65
MAR8_1_90	0.6	2341.8	111.0	3.71	1.8	0.09828	1.31	3.6968	2.6	0.27053	1.9	0.52	1621	80	1543	51	1568	41	95.2	98.4	1543	51
MAR_8_1_23	0.8	1360.0	75.2	3.81	2.2	0.09729	1.12	3.6196	2.2	0.26596	2.4	0.85	1582	49	1518	64	1550	35	96	98	1582	49
MAR_8_1_57	2.1	1264.0	71.8	2.82	2.3	0.12163	1.34	6.0562	2.0	0.35937	2.4	0.84	1974	48	1976	82	1980	35	100	100	1974	48
MAR_8_1_8	1.1	1316.6	63.9	2.94	1.5	0.12212	1.30	5.8278	1.9	0.34227	1.5	0.72	1982	46	1897	49	1947	33	96	97	1982	46
MAR8_1_97	1.5	2936.3	60.9	2.96	1.4	0.12244	1.05	5.7531	1.9	0.33971	1.3	0.85	1989	38	1884	44	1936	34	94.8	97.3	1989	38
MAR_8_1_36	0.8	430.7	100.6	2.64	1.9	0.12517	2.21	6.5739	2.3	0.38091	1.8	0.49	2022	77	2079	64	2052	42	103	101	2022	77
MAR8_1_130	0.5	1319.2	118.3	2.91	0.9	0.12871	0.87	6.1510	1.2	0.34455	0.9	0.68	2078	30	1908	30	1997	20	91.8	95.6	2078	30
MAR_8_1_21	0.4	39218.2	66.0	2.87	2.9	0.13189	1.68	6.5064	2.5	0.35621	2.9	0.84	2115	57	1959	97	2040	44	93	96	2115	57
MAR8_1_85	0.7	905.5	194.4	2.61	1.5	0.13270	1.02	6.9628	1.4	0.38560	1.5	0.77	2131	36	2101	54	2105	26	98.6	99.8	2131	36
MAR8_1_77	1.2	1168.6	69.7	2.54	1.1	0.13321	1.31	7.1778	1.9	0.39530	1.1	0.77	2136	48	2147	41	2131	35	100.5	100.8	2136	48
MAR_8_1_62	1.1	2527.5	48.8	2.61	2.7	0.13255	1.49	7.2390	2.5	0.38999	2.6	0.72	2144	64	2119	94	2136	45	99	99	2144	64
MAR_8_1_60	1.1	1285.6	54.6	2.58	2.2	0.13326	1.63	7.3463	2.3	0.39202	2.1	0.60	2155	70	2129	78	2150	40	99	99	2155	70
MAR_8_1_51	1.1	1157.0	51.3	2.73	2.9	0.13485	2.13	6.9928	2.8	0.37014	2.7	0.73	2155	73	2028	94	2106	50	94	96	2155	73
MAR_8_1_17	0.9	177.9	281.0	2.51	1.9	0.13485	1.38	7.5250	1.9	0.40172	1.9	0.72	2156	47	2174	70	2172	34	101	100	2156	47
MAR_8_1_5	1.4	1047.6	155.7	2.57	2.5	0.13635	1.67	7.4862	2.3	0.39533	2.4	0.75	2174	57	2144	89	2166	41	99	99	2174	57
MAR_8_1_59	1.3	314.1	72.2	2.52	2.5	0.13694	1.93	7.6463	2.6	0.40303	2.6	0.71	2178	68	2178	94	2184	45	100	100	2178	68
MAR8_1_93	0.5	146.3	197.8	2.46	1.6	0.13773	1.23	7.6749	1.3	0.40850	1.6	0.63	2194	43	2206	60	2192	23	100.6	100.7	2194	43
MAR8_1_78	1.0	1504.2	113.0	2.60	1.4	0.13785	1.67	7.2361	1.5	0.38676	1.4	0.39	2194	56	2107	50	2139	27	96.0	98.5	2194	56
MAR_8_1_42	0.9	6381.4	53.6	2.55	1.6	0.13817	1.34	7.5715	1.2	0.39549	1.6	0.56	2199	47	2147	58	2180	21	98	98	2199	47
MAR8_1_86	1.0	4605.0	68.5	2.53	1.3	0.13842	1.26	7.4016	1.1	0.39628	1.3	0.57	2203	43	2151	48	2167	23	97.6	99.3	2203	43
MAR8_1_122	1.5	2313.4	28.6	2.23	1.0	0.16186	1.22	10.1304	1.1	0.44950	1.0	0.36	2471	42	2392	41	2446	21	96.8	97.8	2471	42
MAR_8_1_41	0.9	5068.3	33.7	1.99	1.9	0.17255	1.83	12.1376	1.8	0.50818	1.9	0.53	2573	62	2645	84	2611	35	103	101	2573	62
MAR8_1_83	0.5	2183.5	68.9	2.16	2.0	0.18530	1.78	11.6996	1.4	0.46638	2.1	0.53	2694	59	2465	87	2579	26	91.5	95.6	2694	59
Data not used due to high discordance																						
MAR_8_1_63	1.1	945.1	65.5	3.50	3.4	0.14652	2.98	5.9251	2.7	0.28907	3.2	0.67	2297	95	1635	94	1962	49	71	83		
MAR_8_1_29	0.9	868.3	133.2	5.24	2.8	0.11976	2.56	3.2309	3.6	0.19295	2.8	0.69	1942	90	1136	59	1459	55	59	78		
MAR_8_1_16	0.4	4680.9	116.7	8.54	2.1	0.08232	2.02	1.3506	2.2	0.11829	2.0	0.53	1239	81	720	28	866	26	58	83		
MAR_8_1_33	0.2	1195.7	89.5	7.20	2.8	0.09968	3.17	1.9412	4.1	0.14062	2.9	0.63	1600	116	848	46	1090	54	53	78		
MAR_8_1_18	1.1	763.1	243.3	12.94	2.5	0.07249	2.80	0.7849	2.5	0.07854	2.5	0.34	971	118	487	23	587	22	50	83		
MAR_8_1_24	0.7	2074.6	65.2	10.55	1.8	0.08305	5.80	1.0986	6.5	0.09453	2.1	0.38	1172	197	582	24	738	64	50	79		
MAR_8_1_10	1.0	2010.3	117.1	6.09	1.8	0.12608	1.75	2.8824	1.7	0.16511	1.9	0.52	2039	61	985	34	1376	27	48	72		
MAR_8_1_14	2.4	286.5	86.3	9.39	2.2	0.09233	7.96	1.4114	8.9	0.10765	2.2	0.33	1404	336	659	27	898	119	47	73		
MAR_8_1_30	1.1	944.4	46.6	10.80	2.3	0.08869	5.07	1.1517	4.8	0.09340	2.4	0.19	1346	197	575	26	773	51	43	74		
MAR_8_1_28	0.7	273.7	8.1	5.87	2.9	0.16587	2.34	3.9908	2.7	0.17276	2.9	0.65	2507	80	1026	56	1628	44	41	63		
MAR_8_1_19	1.6	161.7	97.3	10.97	3.3	0.10233	11.68	1.3323	12.7	0.09213	3.4	0.41	1562	346	568	37	840	130	36	68		
MAR_8_1_4	0.5	447.7	17.8	15.02	4.1	0.08910	1.75	0.8631	2.9	0.06857	3.8	0.86	1427	86	427	32	630	27	30	68		
MAR_8_1_25	1.2	96.4	4.2	17.57	1.6	0.21586	1.78	1.7131	1.7	0.05727	1.5	0.47	2942	58	359	11	1012	22	12	35		
MAR_8_1_46	1.5	192.1	66.5	19.90	2.1	0.03806	4.55	0.2673	4.4	0.05083	2.1	0.18	-609	276	320	13	239	19	-52	133		
MAR_8_1_53	2.9	396.9	47.7	14.39	1.6	0.04425	3.55	0.4277	3.8	0.06981	1.6	0.40	-136	182	435	14	360	23	-320	121		

MAR_8_1_52	0.6	1800.5	91.1	3.28	2.2	0.14084	1.76	6.0237	1.8	0.30765	2.0	0.60	2231	62	1728	62	1977	31	77	87
MAR_8_1_39	1.0	3604.1	56.7	4.21	2.0	0.10423	1.59	3.4806	2.5	0.24005	2.0	0.76	1693	59	1386	51	1518	39	82	91
MAR_8_1_50	0.8	235.5	530.5	3.79	2.3	0.12548	2.21	4.6850	3.8	0.26595	2.5	0.85	2027	78	1519	66	1757	62	75	86
MAR8_1_115	0.6	3.8	5370.0	4.73	1.8	0.10801	2.32	3.1986	2.6	0.21221	1.8	0.48	1757	88	1240	42	1454	40	70.6	85.3
MAR8_1_124	1.3	3469.0	54.9	9.46	1.2	0.07229	2.83	1.0464	2.6	0.10612	1.3	0.46	971	108	650	16	735	32	67.0	88.4
MAR8_1_94	2.0	1031.5	74.6	10.27	1.6	0.07071	2.76	0.9488	3.3	0.09799	1.7	0.49	923	110	602	19	674	32	65.2	89.3
MAR8_1_107	1.4	170.2	564.5	10.18	1.2	0.07693	1.94	1.0537	2.1	0.09853	1.3	0.37	1108	78	606	14	730	21	54.7	83.0
MAR8_1_129	1.8	934.7	59.8	11.32	4.4	0.07613	3.75	0.9163	3.0	0.08918	4.6	0.60	1061	151	550	49	658	31	51.8	83.5
MAR8_1_103	3.3	224.0	279.3	11.48	1.6	0.07513	1.97	0.9114	1.9	0.08767	1.6	0.37	1059	78	542	16	657	18	51.2	82.5
MAR8_1_106	1.7	376.7	62.9	9.37	2.0	0.09191	6.81	1.3792	7.3	0.10752	2.0	0.39	1357	279	658	25	864	86	48.5	76.2
MAR8_1_109	1.1	307.2	178.9	10.76	4.0	0.08461	3.41	1.0777	3.1	0.09265	4.1	0.76	1277	144	571	44	740	33	44.7	77.1
MAR8_1_110	1.6	720.0	61.1	11.18	1.4	0.08251	1.99	1.0304	1.6	0.08990	1.3	0.12	1244	77	555	14	718	16	44.6	77.2
MAR8_1_69	0.9	11.5	5345.7	11.21	1.8	0.08347	2.06	1.0232	2.4	0.08989	1.8	0.53	1266	81	555	19	714	24	43.8	77.7
MAR8_1_89	1.1	119.2	12.3	4.36	1.4	0.25245	4.32	7.8998	3.6	0.22987	1.4	0.31	3183	136	1334	35	2214	65	41.9	60.2
MAR8_1_98	1.3	701.3	77.2	20.77	1.3	0.06717	2.80	0.4468	2.3	0.04836	1.3	0.11	815	115	304	8	374	14	37.4	81.3
MAR8_1_76	2.7	485.4	56.2	6.11	2.3	0.18480	1.15	4.2203	2.8	0.16505	2.4	0.72	2694	38	984	43	1674	45	36.5	58.8
MAR8_1_127	1.2	512.4	48.2	8.19	3.0	0.16596	10.15	3.0163	12.9	0.12435	3.1	0.93	2296	385	755	45	1323	195	32.9	57.1
MAR8_1_81	1.8	3476.6	51.4	9.84	1.7	0.13232	3.74	1.7858	3.0	0.10224	1.8	0.42	2102	122	627	21	1054	52	29.9	59.5
MAR8_1_120	0.9	120.3	13.2	9.22	2.2	0.21046	5.98	3.2427	7.2	0.10934	2.0	0.63	2850	191	669	26	1441	108	23.5	46.4
MAR8_1_126	0.2	97.0	9.9	10.27	1.8	0.24309	1.91	3.2604	2.5	0.09707	1.5	0.82	3131	61	597	17	1481	47	19.1	40.3
MAR8_1_79	2.2	160.0	64.4	44.47	1.6	0.06848	6.47	0.2080	6.6	0.02239	2.0	0.21	749	247	143	6	190	22	19.1	75.1
MAR8_1_102	1.5	119.0	14.3	12.55	2.8	0.19375	2.33	2.1523	2.0	0.08045	2.9	0.60	2767	76	499	27	1165	27	18.0	42.8
MAR8_1_105	0.4	211.5	8.5	16.17	3.5	0.14733	3.66	1.2714	2.0	0.06378	3.6	0.26	2281	125	398	28	831	23	17.5	47.9
MAR8_1_116	1.2	9149.5	63.2	3.29	2.2	0.12653	4.25	5.4125	4.5	0.30653	2.3	0.40	2022	139	1722	68	1876	74	85.2	91.8
MAR8_1_108	0.7	128.5	6.7	36.05	2.8	0.16883	2.43	0.6590	3.0	0.02814	2.5	0.81	2533	81	179	9	513	24	7.1	34.9
MAR8_1_100	0.8	37.8	1321.2	3.56	2.8	0.14404	1.96	5.5834	2.7	0.28586	2.5	0.85	2266	62	1618	72	1921	41	71.4	84.2

Amostra M2AR 10I

	Ratios											Rho	Ages (Ma)						% conc [1]	% conc [2]	Best age	2s
Spot number	Th/U	206Pb/204Pb	1s	238U/206Pb	1s	207Pb/206Pb	1s	207Pb/235U	1s	206Pb/238U	1s		207Pb/206Pb	2s	206Pb/238U	2s	207Pb/235U	2s				
			(%)		(%)		(%)		(%)		(%)			(abs)		(abs)		(abs)				(abs)
10I_76	1.2	389.8	148.3	11.64	1.5	0.05914	1.43	0.6990	1.9	0.08619	1.5	0.65	564	63	533	16	538	16	99	94	533	16
10I_85	1.0	263.8	65.7	10.72	1.6	0.05904	2.60	0.7668	3.0	0.09372	1.6	0.47	570	103	577	18	575	27	100	101	577	18
10I_13	1.1	1340.9	118.8	10.56	1.3	0.05970	1.29	0.7841	1.8	0.09494	1.3	0.67	585	55	585	15	587	16	100	100	585	15
10I_14	2.2	24299.3	65.1	9.85	1.8	0.06294	1.89	0.8886	2.3	0.10211	1.8	0.53	692	81	627	21	644	22	97	91	627	21
10I_119	1.9	27.0	8719.7	9.64	1.5	0.06244	1.65	0.8886	1.8	0.10350	1.3	0.49	676	70	635	16	645	17	98	94	635	16
10I_101	0.9	3502.5	59.5	9.15	1.7	0.06153	1.77	0.9367	2.0	0.10998	1.7	0.49	642	76	672	21	670	20	100	105	672	21
10I_109	0.4	750.0	95.8	6.67	1.4	0.07005	1.93	1.4546	1.6	0.15017	1.4	0.17	919	77	902	24	911	19	99	98	902	24
10I_74	0.7	1708.6	144.1	4.54	2.0	0.09857	1.89	3.0217	2.5	0.22120	2.0	0.64	1590	72	1288	46	1411	39	91	81	1590	72

10I_107	1.1	1061.2	96.0	4.30	1.8	0.10099	1.50	3.2663	1.8	0.23378	1.8	0.57	1637	56	1354	45	1472	28	92	83	1637	56
10I_54	0.5	706.3	67.1	4.27	1.5	0.10170	1.12	3.3136	1.6	0.23540	1.5	0.73	1651	41	1362	38	1482	26	92	83	1651	41
10I_60	1.2	275.9	103.4	3.45	1.3	0.10204	2.10	4.1553	2.2	0.29005	1.3	0.26	1654	82	1642	38	1663	36	99	99	1654	82
10I_79	0.8	11963.6	65.5	4.19	2.1	0.10293	1.44	3.4190	2.6	0.24026	2.1	0.86	1673	54	1387	52	1506	42	92	83	1673	54
10I_36	1.5	1251.2	122.3	3.59	1.6	0.10362	1.44	4.0120	2.2	0.27944	1.5	0.74	1685	53	1588	43	1634	35	97	94	1685	53
10I_89	0.7	3055.0	108.4	3.71	1.3	0.10408	1.28	3.8752	1.6	0.26986	1.3	0.52	1694	47	1540	35	1607	26	96	91	1694	47
10I_98	0.9	168.1	690.5	3.47	1.5	0.10423	0.96	4.1736	1.5	0.28883	1.5	0.74	1697	36	1635	42	1667	24	98	96	1697	36
10I_68	1.5	23.0	12656.0	3.54	1.5	0.10455	1.06	4.1302	1.5	0.28354	1.4	0.67	1703	39	1609	41	1665	20	97	94	1703	39
10I_78	0.8	5677.9	74.8	3.40	1.7	0.10517	1.41	4.2843	2.1	0.29441	1.7	0.74	1715	52	1663	51	1689	35	98	97	1715	52
10I_59	0.6	23725.4	69.2	3.60	1.6	0.10616	1.84	4.1348	2.0	0.27807	1.5	0.33	1729	67	1581	43	1660	33	95	91	1729	67
10I_48	1.0	1397.8	62.0	3.23	1.6	0.10676	1.12	4.6188	1.6	0.31077	1.6	0.69	1740	41	1744	48	1751	26	100	100	1740	41
10I_86	1.4	722.1	105.2	3.16	1.4	0.10700	1.34	4.7257	1.3	0.31754	1.4	0.38	1743	51	1777	43	1771	22	100	102	1743	51
10I_49	1.0	1236.1	51.7	3.13	1.9	0.10729	1.75	4.8006	2.2	0.31746	1.4	0.57	1747	63	1777	43	1782	35	100	102	1747	63
10I_111	1.6	942.0	92.2	3.08	1.4	0.10739	1.65	4.8300	2.1	0.32488	1.3	0.66	1748	62	1813	42	1787	36	101	104	1748	62
10I_100	1.2	2216.7	101.1	3.37	1.3	0.10752	1.55	4.4308	1.7	0.29713	1.4	0.27	1752	57	1677	40	1717	28	98	96	1752	57
10I_105	1.2	1571.4	93.2	3.03	1.8	0.10807	1.77	4.9383	1.8	0.33125	1.8	0.41	1761	65	1844	58	1807	31	102	105	1761	65
10I_127	0.8	394.2	617.9	3.05	1.6	0.10823	1.34	4.8982	1.6	0.32938	1.5	0.51	1763	50	1835	49	1800	28	102	104	1763	50
10I_5	1.7	827.7	149.9	3.09	1.9	0.10810	1.26	4.8623	1.9	0.32539	1.8	0.74	1764	46	1815	58	1794	32	101	103	1764	46
10I_6	1.0	996.9	82.8	3.09	1.6	0.10880	1.40	4.8957	1.7	0.32507	1.6	0.56	1774	51	1814	50	1800	28	101	102	1774	51
10I_66	1.8	3861.2	54.3	3.26	1.4	0.10934	1.50	4.6614	2.2	0.30731	1.4	0.75	1780	55	1727	43	1755	37	98	97	1780	55
10I_42	1.4	92.0	110.4	3.17	3.6	0.11153	3.37	4.9750	4.0	0.32160	3.5	0.59	1801	129	1794	110	1805	73	99	100	1801	129
10I_122	1.7	28.1	649.4	3.21	1.3	0.11071	1.57	4.7603	1.8	0.31214	1.3	0.41	1802	56	1751	41	1775	30	99	97	1802	56
10I_40	1.5	3073.3	83.9	3.20	1.5	0.11094	1.59	4.7949	1.9	0.31293	1.5	0.50	1809	58	1755	45	1782	32	98	97	1809	58
10I_71	1.4	418.6	77.9	3.20	1.6	0.11228	1.51	4.8997	1.7	0.31372	1.6	0.46	1830	54	1758	49	1800	29	98	96	1830	54
10I_118	1.2	4535.4	146.2	3.38	1.5	0.11217	1.36		1.7	0.29637	1.4	0.52	1830	50	1673	43	1748	28	96	91	1830	50
10I_57	1.5	4311.2	80.7	3.15	2.4	0.11233	1.67	4.9936	2.7	0.31979	2.4	0.78	1833	61	1788	74	1815	46	98	98	1833	61
10I_81	0.2	4394.8	74.4	3.24	1.6	0.11760	1.31	5.0344	1.9	0.30962	1.6	0.70	1915	47	1738	50	1822	32	95	91	1915	47
10I_24	1.8	4800.9	145.9	3.06	1.6	0.12047	1.51	5.4330	1.9	0.32779	1.5	0.52	1957	53	1827	49	1888	31	97	93	1957	53
10I_50	0.9	6804.5	145.2	3.41	1.5	0.12238	1.15	5.0045	1.6	0.29420	1.5	0.68	1988	41	1662	45	1818	28	91	84	1988	41
10I_130	0.9	4755.9	66.9	2.69	1.4	0.12636	1.09	6.4540	1.7	0.37261	1.5	0.76	2045	39	2041	51	2038	30	100	100	2045	39
10I_126	0.9	2521.9	64.2	3.10	2.0	0.12645	1.05	5.6283	1.5	0.32415	1.8	0.80	2047	36	1809	59	1919	27	94	88	2047	36
10I_58	0.7	568.3	418.4	3.29	2.4	0.12994	1.39	5.5985	2.5	0.30902	2.4	0.85	2090	49	1733	72	1909	44	91	83	2090	49
10I_12	0.7	3927.4	63.8	3.24	2.1	0.13016	1.37	5.6051	2.1	0.31100	2.0	0.76	2096	49	1745	61	1914	37	91	83	2096	49
10I_124	1.4	13.0	5480.0	3.33	1.6	0.13168	1.31	5.4628	1.7	0.30117	1.7	0.67	2116	46	1696	50	1893	29	90	80	2116	46
10I_46	0.8	3005.3	140.3	2.90	1.4	0.13210	1.14	6.3446	1.5	0.34550	1.4	0.63	2123	40	1913	47	2023	27	95	90	2123	40
10I_4	0.8	8017.7	102.2	2.75	1.4	0.13213	0.98	6.6785	1.5	0.36387	1.4	0.75	2123	34	2000	47	2068	27	97	94	2123	34
10I_129	0.8	1863.1	180.8	3.10	1.7	0.13240	1.44	5.8830	1.8	0.32350	1.7	0.60	2125	51	1806	55	1957	32	92	85	2125	51
10I_15	0.7	11439.7	56.6	2.61	1.3	0.13143	1.13	6.9378	1.7	0.38353	1.3	0.53	2126	47	2092	46	2101	30	100	98	2126	47
10I_39	1.4	3855.1	69.7	2.71	1.3	0.13263	1.19	6.7573	1.2	0.36938	1.4	0.28	2131	42	2026	47	2080	21	97	95	2131	42
10I_63	0.6	53161.7	95.6	2.66	1.8	0.13285	1.75	6.9731	2.6	0.37725	1.8	0.75	2132	62	2063	64	2106	46	98	97	2132	62
10I_55	0.6	212.8	203.0	3.15	2.0	0.13322	1.58	5.9494	2.4	0.31913	2.0	0.73	2136	54	1785	61	1965	42	91	84	2136	54
10I_51	0.6	455.8	2285.2	2.47	1.3	0.13351	1.24	7.5377	1.5	0.40497	1.3	0.40	2139	44	2191	49	2175	26	101	102	2139	44
10I_33	0.3	25537.3	93.0	2.78	1.6	0.13472	1.21	6.7113	1.6	0.36144	1.5	0.86	2156	42	1988	52	2072	29	96	92	2156	42
10I_53	0.7	6072.0	63.5	2.94	1.7	0.13524	1.54	6.4531	2.3	0.34186	1.6	0.73	2159	54	1895	54	2034	40	93	88	2159	54
10I_32	0.5	49416.0	103.5	2.63	1.5	0.13555	1.01	7.1211	1.6	0.38080	1.5	0.77	2168	35	2079	52	2132	23	98	96	2168	35

10I_23	1.5	781.8	524.2	2.45	1.5	0.13724	1.29	7.7359	1.6	0.41035	1.5	0.58	2187	45	2216	57	2198	29	101	101	2187	45
10I_99	1.5	6012.2	53.3	2.78	1.8	0.13673	1.17	6.8121	2.0	0.36080	1.7	0.76	2199	53	1985	57	2085	35	95	90	2199	53
10I_112	0.2	3000.3	65.8	2.79	1.4	0.13862	1.53	6.8825	1.7	0.35881	1.4	0.40	2204	53	1976	48	2094	31	94	90	2204	53
10I_19	1.4	455.5	366.8	2.28	1.2	0.15003	1.38	9.0378	1.7	0.43773	1.4	0.57	2341	48	2340	57	2348	27	100	100	2341	48
10I_84	1.7	424.9	124.8	2.46	1.7	0.15314	1.93	8.6291	2.1	0.40872	1.7	0.39	2373	65	2208	64	2296	38	96	93	2373	65
10I_47	1.1	2573.8	161.5	2.39	1.7	0.15490	2.49	9.0250	2.7	0.41893	1.7	0.41	2390	80	2255	64	2336	50	97	94	2390	80
10I_87	0.4	11126.8	47.3	2.25	1.2	0.15634	1.21	9.6367	1.4	0.44582	1.3	0.34	2412	41	2376	50	2399	26	99	99	2412	41
10I_21	2.3	31605.0	53.1	2.05	1.4	0.17537	1.32	11.7921	1.6	0.48980	1.4	0.46	2605	45	2569	59	2586	30	99	99	2605	45
10I_20	1.6	446.5	281.3	2.05	1.5	0.18408	1.37	12.3847	1.7	0.48984	1.5	0.59	2685	45	2569	65	2631	33	98	96	2685	45
Data not used due to high discordance																						
10I_22	0.6	417746.8	36.4	3.45	2.0	0.13068	1.31	5.2713	2.4	0.29179	2.0	0.86	2103	45	1650	57	1861	42	89	78		
10I_96	0.7	998.3	179.5	3.79	2.3	0.12757	0.98	4.7308	2.4	0.26726	2.2	0.93	2061	35	1525	59	1766	41	86	74		
10I_10	0.6	676.8	488.3	3.92	1.9	0.12968	0.90	4.6218	1.8	0.25613	1.9	0.89	2092	32	1469	50	1752	30	84	70		
10I_3	1.0	450.2	288.6	4.03	1.8	0.13575	1.12	4.7030	1.7	0.24952	1.9	0.76	2170	39	1435	48	1766	28	81	66		
10I_27	1.2	20624.1	60.2	4.11	3.1	0.13161	1.49	4.4586	3.0	0.24671	2.7	0.89	2115	52	1420	69	1717	53	83	67		
10I_43	0.4	254.8	130.0	4.24	2.6	0.12269	1.74	4.0197	2.9	0.23778	2.5	0.60	1990	64	1374	63	1634	50	84	69		
10I_16	0.3	329.3	322.9	4.25	1.3	0.11960	1.39	3.8913	1.7	0.23574	1.3	0.50	1945	50	1364	32	1610	28	85	70		
10I_97	0.7	574.8	117.5	4.28	1.7	0.12043	1.71	3.9001	2.3	0.23428	1.6	0.66	1956	65	1357	40	1611	38	84	69		
10I_52	0.7	4570.3	57.2	4.35	2.2	0.12942	1.21	4.1991	2.3	0.23233	2.0	0.84	2085	43	1346	48	1668	38	81	65		
10I_18	0.8	1245.3	18.3	4.88	2.2	0.13257	1.01	3.7839	2.3	0.20719	2.3	0.91	2129	36	1213	50	1585	37	77	57		
10I_9	2.8	2097.5	32.8	4.89	2.0	0.11111	1.23	3.1698	2.3	0.20595	2.0	0.84	1813	44	1206	45	1446	35	83	67		
10I_103	0.8	252.8	426.9	4.93	2.2	0.12230	1.42	3.4729	2.4	0.20362	2.3	0.83	1987	50	1194	50	1519	38	79	60		
10I_26	1.3	4645.3	110.2	5.22	1.5	0.10447	1.21	2.7704	1.4	0.19173	1.5	0.47	1703	45	1131	31	1347	21	84	66		
10I_114	0.2	85.4	979.3	5.29	1.5	0.10276	1.16	2.6980	1.8	0.18961	1.5	0.75	1670	42	1119	31	1326	27	84	67		
10I_11	1.3	120.1	3298.9	5.35	1.8	0.14138	1.42	3.6603	1.9	0.18801	1.9	0.69	2240	47	1110	39	1561	30	71	50		
10I_104	1.7	73147.9	69.6	5.39	2.4	0.11855	1.65	3.0931	2.9	0.18762	2.2	0.85	1927	57	1108	46	1425	46	78	57		
10I_38	1.6	1238.3	39.1	5.67	2.2	0.13714	1.15	3.3730	2.4	0.17810	2.3	0.89	2188	40	1056	44	1494	37	71	48		
10I_75	1.0	1517.8	59.2	5.70	1.5	0.11254	1.69	2.7680	2.2	0.17584	1.5	0.57	1836	60	1044	30	1345	31	78	57		
10I_116	0.4	2720.8	62.8	5.79	1.3	0.11556	1.46	2.7718	1.8	0.17302	1.3	0.49	1884	52	1029	25	1347	26	76	55		
10I_92	1.1	159.0	951.0	5.90	2.7	0.13308	1.14	3.1643	2.6	0.17106	2.7	0.92	2137	40	1017	51	1446	40	70	48		
10I_64	0.8	3177.9	58.4	5.92	1.9	0.15411	1.93	3.6334	2.5	0.16971	2.0	0.64	2386	65	1010	37	1554	41	65	42		
10I_30	3.6	1334.8	14.0	6.10	1.8	0.13639	1.31	3.0774	2.2	0.16440	1.8	0.80	2179	44	981	34	1425	33	69	45		
10I_88	1.0	760.1	111.9	6.10	1.6	0.08654	1.02	1.9675	1.5	0.16439	1.6	0.74	1347	40	981	29	1104	21	89	73		
10I_7	0.9	3364.5	92.6	8.03	1.8	0.07579	2.36	1.3142	3.0	0.12504	1.7	0.60	1075	90	759	25	849	34	89	71		
10I_108	0.2	15.6	3604.9	8.15	1.8	0.07237	2.22	1.2234	2.1	0.12317	1.8	0.27	985	92	749	25	810	23	92	76		
10I_41	0.7	2850.2	32.4	8.44	2.8	0.13316	1.25	2.2427	3.0	0.12141	2.8	0.92	2134	44	738	39	1187	42	62	35		
10I_17	0.4	393.6	269.4	8.90	1.7	0.06652	1.15	1.0313	1.3	0.11268	1.6	0.54	819	48	688	21	719	13	96	84		
10I_72	1.6	2355.2	49.7	9.71	3.3	0.11954	1.03	1.7449	3.0	0.10496	3.0	0.95	1947	37	643	37	1021	40	63	33		
10I_69	1.4	1047.9	58.3	9.67	2.3	0.09621	1.77	1.3970	2.7	0.10420	2.2	0.70	1544	68	639	26	885	32	72	41		
10I_91	1.1	99.5	457.8	9.59	1.5	0.06745	1.63	0.9675	2.1	0.10351	1.9	0.65	845	68	635	23	686	21	92	75		
10I_25	1.8	240.1	138.3	9.89	1.5	0.07648	3.02	1.0647	2.5	0.10129	1.5	0.35	1088	119	622	18	735	26	85	57		
10I_37	2.4	88.8	467.0	10.10	1.4	0.05776	1.93	0.7913	2.0	0.09920	1.4	0.29	507	83	610	16	591	18	103	120		
10I_45	1.6	604.6	73.0	10.13	1.5	0.06295	1.66	0.8628	2.0	0.09902	1.6	0.47	698	69	609	18	631	18	96	87		
10I_35	0.6	9845.9	95.2	10.29	2.1	0.06552	1.83	0.8806	2.1	0.09754	2.0	0.54	785	77	600	23	641	19	94	76		
10I_28	1.4	1567.8	98.2	10.42	1.3	0.06047	1.52	0.7999	1.8	0.09614	1.3	0.39	609	68	592	15	596	16	99	97		

10I_115	1.8	88.3	163.0	10.47	1.7	0.06452	1.91	0.8550	2.1	0.09597	1.6	0.35	741	82	591	18	626	19	94	80
10I_31	1.5	6488.2	59.1	10.55	1.4	0.06318	1.70	0.8236	1.8	0.09500	1.4	0.33	700	73	585	15	609	17	96	84
10I_94	0.6	60.6	1154.3	10.64	2.2	0.07138	1.67	0.9311	2.1	0.09449	2.2	0.65	962	69	582	24	668	21	87	60
10I_34	0.8	7890.2	107.3	10.97	3.1	0.12816	1.53	1.6368	3.1	0.09216	3.1	0.88	2069	52	568	34	982	40	58	27
10I_70	1.9	1077.1	83.8	11.49	1.9	0.06285	2.39	0.7602	2.6	0.08737	2.0	0.42	691	102	540	21	573	22	94	78
10I_77	0.9	1933.2	12.9	12.37	4.0	0.10316	1.70	1.1739	4.1	0.08214	3.3	0.90	1677	63	509	32	785	45	65	30
10I_65	1.5	5031.5	149.5	12.29	2.1	0.07561	1.75	0.8618	3.0	0.08191	2.2	0.82	1077	70	507	22	630	28	81	47
10I_83	0.6	223.3	171.2	12.36	1.5	0.06234	1.64	0.7010	2.0	0.08133	1.6	0.49	673	69	504	16	538	16	94	75
10I_117	1.7	1235.8	39.3	12.72	1.4	0.09007	1.23	0.9793	1.5	0.07878	1.4	0.39	1422	48	489	13	693	16	71	34
10I_73	3.0	437.8	12.1	17.60	2.6	0.10077	1.79	0.7966	1.7	0.05783	2.4	0.62	1625	68	362	17	598	17	61	22
10I_44	0.5	629.7	24.3	23.18	1.5	0.08853	1.86	0.5340	2.1	0.04323	1.5	0.48	1386	70	273	8	434	15	63	20
10I_82	1.7	199.2	7.5	24.43	4.6	0.13700	2.69	0.7900	2.7	0.04268	4.7	0.84	2174	97	269	25	590	24	46	12
10I_8	1.5	549.3	27.1	26.03	2.4	0.08775	1.74	0.4721	2.9	0.03877	2.3	0.81	1369	66	245	11	392	19	63	18

Amostra M2AR 11-1

	Ratios											**Rho**	**Ages (Ma)**						**% conc [1]**	**% conc [2]**	**Best age**	**2s**
Spot number	Th/U	206Pb/204Pb	1s	238U/206Pb	1s	207Pb/206Pb	1s	207Pb/235U	1s	206Pb/238U	1s		207Pb/206Pb	2s	206Pb/238U	2s	207Pb/235U	2s				
			(%)		(%)		(%)		(%)		(%)			(abs)		(abs)		(abs)				(abs)
11_1_88	1.4	2582.1	52.8	23.34	1.1	0.05303	2.34	0.3153	2.6	0.04302	1.1	0.44	299	104	271	6	278	13	90.7	97.8	271	6
11_1_113	1.2	13.0	395.4	15.23	4.2	0.06172	6.78	0.5419	4.5	0.06812	3.9	0.03	515	291	424	32	437	31	82.4	**97.1**	424	32
11_1_66	1.3	925.8	72.2	11.74	1.5	0.05889	2.45	0.6984	3.1	0.08579	1.5	0.57	530	111	530	15	535	25	100.0	99.1	530	15
11_1_107	2.2	267.2	113.4	11.66	1.2	0.05967	2.31	0.7165	2.5	0.08616	1.2	0.40	593	85	533	12	547	21	89.9	97.4	533	12
11_1_57	0.7	2683.6	42.5	11.19	1.4	0.06406	2.08	0.7954	2.0	0.08980	1.4	0.37	728	83	554	15	593	18	76.2	**93.4**	554	15
11_1_46	0.5	914.5	138.0	10.98	1.7	0.06293	1.94	0.7933	2.2	0.08998	1.5	0.64	687	81	555	16	591	19	80.8	**93.9**	555	16
11_1_62	0.9	440.9	87.6	10.92	1.2	0.05924	2.23	0.7483	2.7	0.09196	1.1	0.57	549	100	567	12	565	23	103.3	100.4	567	12
11_1_65	2.0	710.4	99.5	10.81	1.5	0.06217	2.10	0.7991	2.5	0.09315	1.5	0.51	657	94	574	16	594	22	87.4	**96.6**	574	16
11_1_9	1.5	5.9	6555.0	10.56	1.2	0.06510	2.55	0.8568	2.7	0.09506	1.2	0.35	751	105	585	14	626	25	78.0	**93.5**	585	14
11_1_127	1.1	1261.8	47.7	10.56	1.3	0.06226	2.70	0.8234	3.2	0.09527	1.4	0.53	647	112	586	15	606	29	90.7	96.7	586	15
11_1_56	0.8	154.3	244.4	10.49	1.0	0.06637	2.70	0.8723	2.8	0.09566	1.0	0.26	784	109	589	12	634	26	75.1	**92.9**	589	12
11_1_50	0.8	236.6	289.9	10.30	1.0	0.06039	1.74	0.8146	1.9	0.09736	1.0	0.37	601	76	599	11	604	17	99.6	99.2	599	11
11_1_64	1.6	2570.8	114.4	10.10	1.1	0.06210	2.01	0.8524	2.4	0.09932	1.1	0.54	662	84	610	13	624	22	92.2	97.7	610	13
11_1_1	1.1	1899.4	107.3	10.06	1.8	0.06776	2.59	0.9416	2.9	0.10026	1.6	0.42	833	108	616	19	671	28	73.9	**91.8**	616	19
11_1_78	1.5	1261.1	79.1	9.72	1.5	0.07011	3.37	0.9932	4.0	0.10287	1.7	0.51	915	168	631	20	694	40	68.9	**91.0**	631	20
11_1_124	1.0	249.9	233.9	9.57	1.2	0.06126	1.94	0.8908	2.0	0.10503	1.2	0.37	653	73	644	15	645	19	98.5	99.8	644	15
11_1_116	1.3	96.3	389.5	9.44	0.8	0.06022	1.53	0.8955	1.7	0.10613	0.8	0.46	599	66	650	10	648	16	108.5	100.3	650	10
11_1_82	2.0	1954.1	90.0	9.24	1.5	0.06262	1.96	0.9383	2.2	0.10868	1.5	0.46	684	86	665	19	671	21	97.2	99.1	665	19
11_1_34	0.5	6.8	1660.2	8.99	1.1	0.06409	2.22	0.9785	2.2	0.11170	1.1	0.24	719	93	682	14	691	22	94.9	98.8	682	14
11_1_109	2.9	1392.1	92.0	6.37	1.1	0.07150	1.91	1.5717	2.2	0.15765	1.1	0.51	954	78	943	19	956	27	98.9	98.7	943	19
11_1_51	0.6	1745.2	97.8	5.41	1.2	0.08160	1.59	2.0918	1.8	0.18519	1.2	0.47	1230	64	1095	24	1145	24	89.0	95.6	1095	24
11_1_5	1.3	4247.7	98.8	4.26	7.5	0.11897	13.09	3.7294	4.4	0.25701	3.5	0.11	1664	83	1468	96	1552	80	88.2	94.6	1664	83

11_1_117	1.2	236.7	276.9	3.05	1.6	0.10441	1.87	4.7445	2.2	0.32824	1.9	0.20	1689	69	1843	52	1769	36	109.1	104.2	1689	69
11_1_28	0.9	9095.0	95.4	3.25	1.2	0.10519	1.87	4.5096	2.3	0.30685	1.0	0.61	1706	69	1725	31	1728	38	101.1	99.8	1706	69
11_1_10	1.3	667.0	111.6	3.33	1.0	0.10584	1.99	4.3829	2.0	0.29944	1.2	0.31	1713	74	1688	35	1704	33	98.5	99.0	1713	74
11_1_87	0.8	753.3	263.5	3.60	1.1	0.10586	1.47	4.0771	1.8	0.27886	1.1	0.59	1720	56	1585	32	1646	30	92.2	96.3	1720	56
11_1_36	1.0	973.0	128.2	3.34	1.4	0.10640	2.32	4.4533	3.0	0.29865	1.2	0.64	1721	83	1684	36	1714	48	97.8	98.2	1721	83
11_1_126	0.9	2138.6	81.4	3.42	1.5	0.10625	1.90	4.3332	2.4	0.29397	1.4	0.63	1726	70	1661	42	1695	41	96.2	98.0	1726	70
11_1_54	1.5	1405.9	96.3	3.23	1.0	0.10684	1.59	4.5879	1.5	0.31047	1.0	0.22	1736	58	1742	31	1745	25	100.4	99.9	1736	58
11_1_125	1.1	6570.1	54.9	3.21	1.7	0.10697	2.71	4.6209	2.4	0.31250	1.6	0.22	1737	95	1752	48	1750	41	100.9	100.1	1737	95
11_1_40	1.1	632.2	94.3	3.64	1.8	0.10705	2.34	4.0943	2.5	0.27631	1.9	0.46	1738	84	1572	52	1649	40	90.5	95.3	1738	84
11_1_111	1.8	278.5	124.1	3.13	1.5	0.10755	1.98	4.8155	2.0	0.32248	1.5	0.36	1742	74	1800	47	1783	34	103.4	101.0	1742	74
11_1_86	1.0	5667.8	131.5	3.43	1.0	0.10687	1.00	4.3190	1.3	0.29287	1.1	0.66	1742	36	1655	31	1695	21	95.0	97.6	1742	36
11_1_25	1.7	18174.0	45.7	3.31	1.0	0.10741	1.88	4.5002	2.0	0.30262	1.0	0.35	1745	68	1704	29	1727	33	97.7	98.6	1745	68
11_1_106	1.3	542.1	85.1	3.30	1.1	0.10777	1.84	4.5618	1.7	0.30453	1.1	0.13	1748	68	1713	32	1739	27	98.0	98.5	1748	68
11_1_110	0.7	789.8	145.1	3.09	1.0	0.10770	1.71	4.8421	1.7	0.32409	1.0	0.42	1751	63	1809	32	1790	28	103.3	101.1	1751	63
11_1_96	0.7	14520.0	62.3	3.31	1.1	0.10697	1.84	4.5048	2.0	0.30343	1.1	0.39	1752	60	1708	33	1727	33	97.4	98.9	1752	60
11_1_55	1.8	478.2	166.5	3.05	1.2	0.10795	1.78	4.9316	2.2	0.32938	1.2	0.59	1755	66	1835	38	1803	38	104.6	101.8	1755	66
11_1_3	1.4	1622.4	69.9	3.50	1.3	0.10848	2.32	4.3163	2.4	0.28733	1.3	0.32	1757	84	1627	38	1691	39	92.6	96.2	1757	84
11_1_93	1.2	5861.3	80.5	3.16	1.2	0.10653	2.34	4.7764	3.0	0.31694	1.2	0.21	1758	104	1774	37	1774	49	100.9	100.0	1758	104
11_1_123	1.9	913.1	77.6	3.21	1.1	0.10835	1.69	4.7056	2.1	0.31286	1.1	0.57	1760	63	1754	33	1763	35	99.7	99.5	1760	63
11_1_102	1.6	598.9	134.0	3.25	1.1	0.10850	1.83	4.6624	2.2	0.30663	0.9	0.54	1761	67	1724	27	1755	36	97.9	98.2	1761	67
11_1_4	1.1	379.4	179.7	3.55	1.3	0.10903	2.27	4.2222	2.4	0.28340	1.3	0.59	1763	82	1607	38	1683	44	91.2	95.5	1763	82
11_1_2	1.1	2343.9	113.6	3.23	1.1	0.10867	1.92	4.6882	2.3	0.30867	1.0	0.57	1763	69	1734	29	1759	38	98.3	98.6	1763	69
11_1_101	1.0	4151.9	78.7	3.17	1.3	0.10896	1.95	4.8037	2.1	0.31733	1.3	0.42	1767	71	1776	41	1780	35	100.5	99.7	1767	71
11_1_72	1.4	27.4	670.6	3.11	1.5	0.10956	2.15	4.8936	2.7	0.32348	1.4	0.62	1776	77	1805	45	1793	46	101.7	100.7	1776	77
11_1_44	0.9	2751.7	89.8	3.09	1.4	0.11001	2.11	4.9006	2.1	0.32271	1.6	0.37	1782	80	1815	43	1797	36	101.8	101.0	1782	80
11_1_13	1.3	879.6	75.6	3.24	1.6	0.10995	1.95	4.7448	2.5	0.31162	1.6	0.61	1784	70	1747	50	1768	41	97.9	98.8	1784	70
11_1_104	1.8	4011.9	98.7	3.29	2.3	0.11003	2.65	4.6759	2.3	0.30719	2.1	0.27	1784	99	1725	65	1759	39	96.7	98.1	1784	99
11_1_129	1.3	263.9	149.5	3.06	1.6	0.11670	6.04	5.1108	2.9	0.32927	1.5	0.10	1784	60	1833	48	1828	47	102.7	100.3	1784	60
11_1_11	1.7	1461.3	75.6	3.05	1.1	0.11266	1.92	5.1179	1.9	0.32790	1.1	0.27	1836	70	1828	34	1837	33	99.6	99.5	1836	70
11_1_8	1.7	506.7	95.3	3.03	1.4	0.11454	2.48	5.2471	2.4	0.33193	1.5	0.82	1848	95	1846	48	1853	41	99.9	99.6	1848	95
11_1_53	1.2	411.9	405.4	2.81	1.6	0.11485	2.00	5.6918	2.2	0.35797	1.5	0.53	1865	70	1971	53	1925	40	105.7	102.4	1865	70
11_1_12	0.4	354.3	73.8	3.35	2.9	0.11757	3.46	4.8768	3.8	0.30234	2.7	0.34	1896	122	1701	82	1790	60	89.7	95.0	1896	122
11_1_59	1.6	7963.5	43.9	3.32	1.6	0.11793	2.23	4.9396	2.5	0.30285	1.6	0.45	1913	81	1705	47	1804	42	89.1	94.5	1913	81
11_1_27	1.6	1321.1	37.1	3.17	1.3	0.12126	1.90	5.3329	2.1	0.31775	1.3	0.46	1960	69	1778	40	1868	37	90.7	95.2	1960	69
11_1_75	1.7	9538.0	72.0	3.05	1.2	0.12316	1.79	5.5518	2.4	0.32936	1.2	0.67	1990	63	1834	38	1901	43	92.2	96.5	1990	63
11_1_37	1.3	977.5	173.1	2.72	1.3	0.12784	1.58	6.5615	1.9	0.37046	1.4	0.60	2058	57	2030	47	2049	35	98.6	99.1	2058	57
11_1_120	0.4	3653.8	121.5	2.78	1.4	0.12818	1.19	6.4450	1.7	0.36182	1.5	0.69	2069	43	1990	50	2036	30	96.2	97.7	2069	43
11_1_42	0.4	1711.5	162.9	2.71	1.1	0.13131	1.87	6.7329	2.2	0.36971	1.1	0.52	2104	66	2027	38	2072	38	96.3	97.8	2104	66
11_1_30	0.5	7711.0	126.4	2.85	3.3	0.13310	3.10	6.5765	4.1	0.35697	2.9	0.69	2122	105	1965	99	2045	75	92.6	96.1	2122	105
11_1_15	0.4	13487.0	70.3	2.81	1.2	0.13386	2.03	6.6161	2.3	0.35691	1.2	0.53	2137	71	1967	42	2056	41	92.0	95.7	2137	71
11_1_69	1.5	3895.7	101.4	2.55	1.0	0.13401	1.65	7.1757	2.1	0.39300	1.0	0.62	2140	59	2136	36	2138	33	99.8	99.9	2140	59
11_1_103	0.5	1561.2	85.5	2.68	1.1	0.13512	1.75	7.0587	2.2	0.37495	1.1	0.58	2153	62	2052	39	2113	38	95.3	97.1	2153	62
11_1_100	0.7	63.3	2223.7	2.61	1.2	0.13566	1.95	7.2723	2.3	0.38521	1.2	0.52	2158	68	2099	42	2138	41	97.3	98.2	2158	68
11_1_130	1.0	16749.4	81.1	2.76	1.0	0.13533	1.61	6.8095	1.9	0.36331	1.0	0.51	2158	57	1997	35	2082	33	92.5	95.9	2158	57
11_1_98	0.9	2898.0	206.0	2.59	1.6	0.13668	2.06	7.3816	2.5	0.38876	1.5	0.55	2189	63	2115	55	2150	45	96.6	98.4	2189	63

11_1_6	0.8	24525.8	112.2	2.54	2.9	0.14991	3.29	8.2208	3.8	0.39652	2.6	0.54	2331	112	2151	98	2248	70	92.3	95.7	2331	112
11_1_70	0.6	778.4	229.7	1.79	1.9	0.21054	1.83	16.3299	2.2	0.56575	2.3	0.84	2899	59	2884	102	2889	42	99.5	99.8	2899	59
11_1_74	1.0	408.8	660.1	1.60	1.2	0.26599	2.46	22.9056	2.7	0.62513	1.3	0.43	3272	77	3129	62	3217	52	95.6	97.3	3272	77
Data not used due to high discordance																						
11_1_97	1.0	3690.2	68.9	4.31	1.5	0.13712	2.33	4.3874	2.3	0.23113	1.7	0.41	2176	80	1340	42	1705	38	61.6	78.5		
11_1_105	0.9	3182.6	102.8	12.27	3.6	0.06799	1.77	0.8064	4.6	0.08482	3.3	0.78	852	75	524	34	605	36	61.5	86.6		
11_1_108	0.9	409.2	278.6	5.23	1.2	0.11413	1.88	3.0423	2.1	0.19215	1.2	0.66	1852	68	1133	26	1414	31	61.1	80.1		
11_1_71	0.8	2338.9	83.3	10.61	1.4	0.07695	5.76	1.0131	6.3	0.09485	1.4	0.40	991	209	584	16	695	60	58.9	84.1		
11_1_17	1.1	143.9	355.0	7.48	3.2	0.09025	2.52	1.7266	4.5	0.13707	3.1	0.88	1411	96	827	48	1008	60	58.6	82.1		
11_1_92	0.9	692.2	86.2	9.53	1.2	0.07883	3.81	1.1536	4.0	0.10547	1.2	0.30	1104	152	646	15	771	43	58.6	83.8		
11_1_41	1.9	1835.4	76.4	8.77	1.1	0.08463	2.54	1.3440	2.8	0.11454	1.1	0.39	1280	99	699	15	861	32	54.6	81.2		
11_1_16	0.6	2492.0	47.3	10.31	1.0	0.08741	3.42	1.1618	3.3	0.09728	1.0	0.12	1368	146	598	12	791	43	43.7	75.7		
11_1_85	1.4	2315.2	61.9	7.27	2.7	0.12221	1.91	2.3479	3.0	0.14038	2.8	0.87	1977	71	846	44	1221	41	42.8	69.3		
11_1_84	3.0	105.6	93.4	12.30	3.1	0.07789	5.10	0.8764	5.0	0.08045	2.2	0.11	1193	132	499	22	634	48	41.8	78.6		
11_1_45	1.1	8622.6	41.7	8.43	2.8	0.10798	1.58	1.7951	3.3	0.11999	2.8	0.92	1755	58	729	39	1048	49	41.6	69.6		
11_1_21	2.0	1537.6	54.3	10.49	1.8	0.09135	5.18	1.1923	5.1	0.09479	1.5	0.54	1446	213	584	16	789	50	40.4	73.9		
11_1_91	2.9	709.8	85.9	12.42	4.8	0.09037	7.25	0.9985	4.5	0.08378	3.9	0.08	1346	239	518	39	707	48	38.5	73.2		
11_1_29	1.7	320.0	81.7	9.62	2.8	0.10962	5.47	1.5987	6.4	0.10581	2.9	0.25	1731	175	648	35	956	68	37.4	67.8		
11_1_31	2.0	2219.3	80.3	8.22	5.4	0.14093	1.22	2.4570	4.5	0.12577	4.5	0.96	2236	41	763	65	1252	68	34.1	60.9		
11_1_22	2.2	312.9	15.1	11.63	1.3	0.11875	2.50	1.4176	2.4	0.08631	1.3	0.26	1922	90	534	14	894	29	27.8	59.7		
11_1_81	0.3	983.2	33.7	14.63	1.5	0.09689	2.09	0.9139	2.1	0.06890	1.6	0.43	1548	76	429	13	657	20	27.7	65.3		
11_1_79	1.9	242.2	3.4	9.45	1.3	0.16030	2.06	2.3342	2.5	0.10644	1.2	0.59	2443	71	652	16	1217	36	26.7	53.6		
11_1_32	1.9	1793.8	46.3	14.24	1.6	0.11146	1.58	1.0944	2.2	0.07084	1.6	0.73	1813	57	441	14	748	24	24.3	58.9		
11_1_80	3.3	4997.5	45.6	15.22	2.9	0.12419	1.53	1.1557	3.1	0.06753	2.8	0.87	2008	54	421	23	775	34	21.0	54.3		
11_1_49	0.6	1927.0	54.0	20.64	2.4	0.10032	1.61	0.6796	2.3	0.04895	2.5	0.77	1624	61	308	15	526	19	19.0	58.6		
11_1_118	1.6	9195.8	60.5	2.79	1.6	0.15469	1.87	7.8153	2.8	0.36184	1.6	0.76	2386	63	1989	54	2200	49	83.4	**90.4**		
11_1_24	1.1	16187.7	62.2	3.06	1.6	0.13134	2.15	6.0069	2.9	0.32934	1.6	0.71	2101	77	1834	51	1968	52	87.3	**93.2**		
11_1_83	1.9	154.3	158.2	3.11	2.0	0.13569	1.89	6.0907	3.1	0.32441	2.0	0.78	2165	65	1810	62	1982	53	83.6	**91.3**		
11_1_14	0.2	6605.2	77.9	3.10	1.2	0.13286	1.71	5.8962	1.6	0.32415	1.1	0.39	2124	61	1809	35	1965	31	85.2	**92.1**		
11_1_23	0.4	2756.7	190.4	3.12	1.1	0.12730	2.28	5.7408	2.8	0.32094	1.1	0.59	2050	79	1794	33	1932	47	87.5	**92.8**		
11_1_48	0.9	38451.9	80.7	3.18	2.9	0.13937	2.54	6.0442	2.9	0.31403	2.4	0.80	2204	81	1758	74	1975	49	79.7	**89.0**		
11_1_61	0.7	2662.0	104.4	3.24	1.3	0.12673	2.10	5.4386	2.7	0.30972	1.3	0.65	2042	73	1739	38	1885	46	85.2	**92.2**		
11_1_18	1.3	12267.1	52.2	3.53	2.4	0.14290	1.98	5.6955	3.0	0.28847	2.6	0.76	2250	70	1631	75	1921	52	72.5	84.9		
11_1_73	0.7	1996.9	87.8	3.82	2.5	0.12425	2.27	4.5333	3.0	0.26504	2.5	0.71	2006	78	1514	66	1730	50	75.5	87.5		
11_1_60	0.9	16171.4	61.6	3.87	1.3	0.10614	0.87	3.8598	1.6	0.25868	1.3	0.39	1732	32	1483	35	1604	25	85.6	**92.4**		
11_1_33	1.1	35210.3	52.1	3.90	1.2	0.12163	1.49	4.3516	1.7	0.25724	1.3	0.23	1974	53	1475	33	1701	28	74.7	86.7		
11_1_90	0.9	146.4	1019.5	3.98	3.5	0.10975	1.74	3.9103	4.0	0.25714	3.5	0.88	1782	66	1470	92	1597	68	82.4	**92.0**		
11_1_119	1.0	402.6	59.2	4.03	2.8	0.13284	2.94	4.6367	3.6	0.25155	2.9	0.60	2119	106	1445	74	1749	59	68.2	82.6		
11_1_26	0.5	6340.1	84.3	4.03	1.6	0.12121	1.96	4.1867	2.2	0.24997	1.5	0.48	1961	67	1437	39	1667	34	73.3	86.2		
11_1_58	0.4	2264.6	58.3	4.24	1.4	0.11730	1.43	3.8436	1.8	0.23635	1.4	0.62	1911	51	1367	34	1600	29	71.5	85.4		
11_1_122	1.1	19031.2	65.2	4.27	1.6	0.13387	1.54	4.3923	2.4	0.23599	1.6	0.78	2140	54	1365	39	1704	40	63.8	80.1		
11_1_89	0.5	7173.1	45.7	4.57	1.2	0.11547	1.75	3.4811	2.0	0.21839	1.3	0.52	1875	63	1273	30	1519	32	67.9	83.8		
11_1_68	1.2	113.0	256.9	10.24	1.1	0.07160	1.95	0.9597	2.3	0.09809	1.2	0.51	957	80	603	13	681	22	63.0	88.5		

M2AR 1-4 - Zircon compositional data (LA-ICP-MS, n = 31, b.d. = below detection limit)																												
Analysis ID	**Best age (Ma)**	**Geological time**	**Al [ppm]**	**P [ppm]**	**Ca [ppm]**	**Ti [ppm]**	**Y [ppm]**	**Zr [ppm]**	**Nb [ppm]**	**La [ppm]**	**Ce [ppm]**	**Pr [ppm]**	**Nd [ppm]**	**Sm [ppm]**	**Eu [ppm]**	**Gd [ppm]**	**Tb [ppm]**	**Dy [ppm]**	**Ho [ppm]**	**Er [ppm]**	**Tm [ppm]**	**Yb [ppm]**	**Lu [ppm]**	**Hf [ppm]**	**Ta [ppm]**	**Pb[ppm]**	**Th [ppm]**	**U [ppm]**
Mar1_4_14	211	Jurassic/ Triassic	140	2031	157	11.4	2.29E+04	5.03E+05	37.5	0.211	309	2.21	48.3	134.6	5.35	842	289	3000	860	3070	495	3740	527	14390	18.2	103.6	2721	850
Mar1_4_59	457	Ordovician	360	638	500	41.5	1870	5.19E+05	2.83	1.36	83.4	3.45	32.4	42.1	18.7	124.8	30.9	259	65.1	244	46.4	438	80	13400	1.243	160.2	560	573
Mar1_4_61	548	Ediacaran	98	90	4.70E+03	5.9	1096	5.23E+05	1.94	0.42	5.88	0.28	3.8	6	0.6	31.9	9.76	103.8	36.1	169	33.7	332	57.2	13480	2.44	114.1	132.7	351
Mar1_4_78	557	Ediacaran	1080	258	940	49	767	5.27E+05	4.2	0.41	38.3	0.73	5.33	5.58	1.9	21	5.91	66.6	23.9	111.2	24.3	248	52.4	13370	1.47	161	326	471
Mar1_4_99	559	Ediacaran	300	205	590	17.8	572	5.08E+05	3.61	0.23	32.5	0.392	4.49	5.06	2.1	17.4	4.94	53.2	18	78.7	16.6	166	33.6	11870	1.64	77.3	85.4	214
Mar1_4_19	566	Ediacaran	164	710	5.20E+03	9.9	1880	4.66E+05	5.42	0.4	41.8	0.64	6.9	7.2	2.92	37.3	13.2	170	63.9	301	62.9	608	115	1.33E+04	1.8	101.3	180	293
Mar1_4_16	580	Ediacaran	410	192	143	35.9	1002	4.92E+05	4.53	b.l.d	13.4	0.134	1.86	3.72	0.453	20.58	7.32	93.8	34.47	162.4	33.1	316.3	62.8	10910	1.875	61.7	76.6	177
Mar1_4_20	590	Ediacaran	260	155	370	21.3	422	5.22E+05	4.99	0.153	5.15	0.159	1.65	3.9	0.49	23.7	6.87	57.6	13.25	44.7	8.72	86.1	17.9	13470	1.84	84.8	26.8	239
Mar1_4_23	592	Ediacaran	65	195	840	22.6	1005	5.18E+05	3.26	0.32	7.29	0.251	2.91	4.48	1.08	24.7	7.62	93.2	34.6	156	32	305	60.6	10930	1.12	27.8	34.9	77.5
Mar1_4_88	608	Ediacaran	61	300	2220	23	708	5.30E+05	1.42	0.26	36.1	0.191	3.23	6.1	2.59	23.4	5.89	63.1	22	98.2	22	227	44.4	13000	0.67	66.4	127.3	175.1
Mar1_4_27	610	Ediacaran	93	281	460	54	969	5.06E+05	3.1	0.74	40.2	1.39	10.4	9.9	3.39	33.8	9.6	100	30.9	131	26	266	50	10970	0.739	106.9	210	282
Mar1_4_123	617	Ediacaran	77	299	b.l.d	28.6	971	5.17E+05	2.55	b.l.d	35.2	0.214	3.59	6.38	1.73	29.9	8.73	96.7	32.7	142.5	28.2	271	49.3	10570	1.106	65.9	120.9	157
Mar1_4_15	628	Ediacaran	310	360	1.90E+03	32	564	5.06E+05	1.55	0.55	17.1	0.66	5.6	3.6	2.56	16.7	4.61	53	18.8	86.6	18.5	188	34.9	11650	0.32	35.9	49.9	89.2
Mar1_4_48	632	Ediacaran	59	340	1000	32	1780	5.21E+05	3.7	0.245	27.8	0.344	4.39	8.5	1.41	41	13.37	167	59.2	270	51.9	475	85.8	12950	1.25	86.9	220	227

Mar1_4_62	639	Cryogenian	220	115	b.l.d	33.3	1139	5.20E+05	1.86	0.22	14.64	0.529	8.2	11.44	0.788	46	12.4	131.6	42.2	176.6	33.3	304	54.9	10400	0.649	48.1	117.9	122.6
Mar1_4_100	667	Cryogenian	300	b.l.d	b.l.d	b.l.d	1100	2.79E+05	1	b.l.d	64	b.l.d	10.3	14	2.8	120	10.8	93	41	173	33	340	62	6.40E+03	0.3	43	74	62
Mar1_4_30	707	Cryogenian	177	349	405	20.3	876	5.10E+05	5.69	0.37	27.2	0.496	4.5	6.36	1.77	24.1	8.15	91.1	27.7	113.9	21.7	200	36.6	14120	2.92	73.1	100	181
Mar1_4_111	773	Tonian	541	1510	1.76E+04	33	2000	4.93E+05	2.97	1.8	22.8	2.04	18.4	20.6	6.3	67.3	19	198	67.5	305	59.9	589	102.8	14680	1.44	233	129	433
Mar1_4_13	807	Tonian	117	493	1380	12.2	1655	5.21E+05	2.89	0.4	12	1.22	11.4	12.3	2.2	46.8	14.37	160.3	56.8	258	51.7	483	88.5	13760	1.18	239.9	319	480
Mar1_4_63	1008	Stenian	270	468	350	40	1833	5.01E+05	6.5	0.46	17.9	0.58	5.7	8.4	1.41	42.4	15.25	186	63.4	283.5	55.4	511	90.3	12550	2.85	199.9	223	325
Mar1_4_91	1918	Orosirian	169	168	290	21.1	132.4	5.00E+05	1.15	b.l.d	2.56	0.157	1.63	4.63	0.298	18.7	3.87	24.7	3.96	10.1	1.39	10.6	1.47	14900	0.386	596	43.3	492
Mar1_4_5	1933	Orosirian	52	303	610	16.8	1109	5.04E+05	2.28	0.141	26	0.349	6.07	10.1	0.897	40.9	10.93	111.8	35.4	150.4	27.2	240	44.2	12580	0.85	445	418	350
Mar1_4_42	1994	Orosirian	233	612	440	44	1690	5.09E+05	2.93	1.15	32.7	2.67	21.8	21.9	10.6	65.7	19.5	202	59.2	248	45.9	397	70.4	13200	1.05	406	249	332
Mar1_4_57	2020	Orosirian	91	160	1510	6.6	482	5.15E+05	2.26	1.6	15.4	0.72	6.5	4.7	1.37	11.9	3.85	41.6	14.8	76.8	17.9	193.5	43.6	13830	0.921	332	101	237
Mar1_4_22	2096	Rhyacian	144	229	b.l.d	24.5	1606	5.27E+05	2.29	1.21	38.3	2.33	23.7	18.6	5.45	57.6	16.3	172	58.8	250	48	435	81.8	10600	0.442	197.9	173	140.8
Mar1_4_43	2151	Rhyacian	76	128	158	22	497	5.21E+05	1.48	0.87	20.5	0.46	3.49	3.34	1.24	12.5	3.66	41.8	15.05	71.4	15.56	163.3	33.9	11820	0.393	99.1	48.2	68.2
Mar1_4_38	2185	Rhyacian	306	433	1800	23.8	1280	5.05E+05	3.3	1.4	38.4	1.87	16.8	14.2	5.2	32.9	9.8	114	38.9	183	43.9	409	87.2	12210	0.401	181	48.8	141
Mar1_4_114	2223	Rhyacian	450	260	900	30	757	4.78E+05	2.88	0.2	15.84	0.51	7.2	5.8	0.78	24.6	7.03	67.2	24.2	107	21	206	41.1	10630	0.685	642	105	375
Discordant																												
Mar1_4_3			144	440	4.30E+03	25.7	697	4.98E+05	4.67	1.11	45	0.81	4.6	4.4	1.76	15.7	5.23	59.7	20.9	106	23.5	247	51	12190	1.92	699	282	610
Mar1_4_121			89	297	2.10E+03	23.1	1027	5.12E+05	4.4	1.12	45	2.08	16.2	12.3	3.15	31.4	8.88	102	33	141.5	29.5	291	53.3	11030	1.12	175.5	95.6	157
Mar1_4_10			126	446	114	33	1164	5.16E+05	3.1	1.18	39.3	1.6	14.2	13.6	4.7	34.6	10.7	114	38.4	180	37.3	366	70	12450	1.24	227	185.6	250
Mar1_4_18			214	150	4.70E+03	29.2	1281	5.17E+05	1.63	1.18	31.6	1.1	10.6	12.6	3.17	42.4	13.1	129.1	41.2	179	36	323	61.8	12200	2.7	63.8	137	132.9

Detection Limit		Al [ppm]	P [ppm]	Ca [ppm]	Ti [ppm]	Y [ppm]	Zr [ppm]	Nb [ppm]	La [ppm]	Ce [ppm]	Pr [ppm]	Nd [ppm]	Sm [ppm]	Eu [ppm]	Gd [ppm]	Tb [ppm]	Dy [ppm]	Ho [ppm]	Er [ppm]	Tm [ppm]	Yb [ppm]	Lu [ppm]	Hf [ppm]	Ta [ppm]	Pb [ppm]	Th [ppm]	U [ppm]
Minimum Detection Limit		1.2189	3.5592	91.08	0.31392	0.023352	1.22E+00	0.01	0.01	0.0012018	0.01	0.01	0.01	0.01	0.027194	0.01	0.01	0.01	0.01	0.01	0.01	0.01	0.01	0.01	0.013074	0.01	0.013554
Maximum Detection Limit		245.95	822.57	12354	617.55	641.83	2.07E+04	1.9026	2.8783	4.0872	0.58409	3.4145	5.8257	3.4528	13.673	0.6479	17.765	1.0069	4.3873	0.6379	9.5481	1.2092	223.56	3.5022	7.2832	776.34	11.248
Mean Detection Limit		18.5676481	69.1046605	1164.11185	13.9238668	10.2189374	6.44E+02	0.20341244	0.1626133	0.24426043	0.05392479	0.27837365	0.293062	0.13651626	1.24826194	0.0626558	0.56404588	0.07789429	0.40939021	0.05891272	0.68918899	0.13119342	11.5053849	0.10999361	0.38454727	9.98042803	0.41016891
Median Detection Limit		5.8522	21.723	398.91	2.0384	0.54093	8.67E+01	0.046615	0.044439	0.070823	0.022813	0.1237	0.06432	0.054715	0.39429	0.018714	0.11857	0.025426	0.13598	0.019165	0.13996	0.032874	1.5076	0.025108	0.084771	0.032001	0.10277
Associated Error		Al [ppm]	P [ppm]	Ca [ppm]	Ti [ppm]	Y [ppm]	Zr [ppm]	Nb [ppm]	La [ppm]	Ce [ppm]	Pr [ppm]	Nd [ppm]	Sm [ppm]	Eu [ppm]	Gd [ppm]	Tb [ppm]	Dy [ppm]	Ho [ppm]	Er [ppm]	Tm [ppm]	Yb [ppm]	Lu [ppm]	Hf [ppm]	Ta [ppm]	Pb [ppm]	Th [ppm]	U [ppm]
Minimum Absolute Error		11	12	50	3.3	8.9	1.40E+04	0.11	0.027	0.38	0.028	0.22	0.32	0.056	0.94	0.26	1.6	0.24	1.2	0.15	1.4	0.18	390	0.041	1.3	1.3	2.8
Maximum Absolute Error		1200	13000	130000	780	1300	8.60E+04	11	11	21	2.6	7	10	1.6	110	13	120	33	120	21	190	27	2200	4.2	66	90	110
Mean Absolute Error (±2σ)		127.84375	480.4375	4856.59375	33.365625	115.840625	2.33E+04	0.793125	0.6025	4.144375	0.2988125	2.1753125	2.01125	0.5291875	8.115625	1.3646875	12.540625	3.5946875	14.671875	2.8534375	28.046875	4.72125	691.25	0.37225	11.528125	16.553125	22.078125
Median Absolute Error (±2σ)		4.10E+01	54	355	6.55	69	2.10E+04	0.345	0.185	2.75	0.205	1.45	1.2	0.385	3.05	0.755	7.7	2.2	9.95	1.9	17.5	3.05	635	0.13	7.15	10.5	18

M2AR 4-1 - Zircon compositional data (LA-ICP-MS, n = 46, b.d. = below detection limit)

Analysis ID	Best age (Ma)	Geological time	Al [ppm]	P [ppm]	Ca [ppm]	Ti [ppm]	Y [ppm]	Zr [ppm]	Nb [ppm]	La [ppm]	Ce [ppm]	Pr [ppm]	Nd [ppm]	Sm [ppm]	Eu [ppm]	Gd [ppm]	Tb [ppm]	Dy [ppm]	Ho [ppm]	Er [ppm]	Tm [ppm]	Yb [ppm]	Lu [ppm]	Hf [ppm]	Ta [ppm]	Pb[ppm]	Th [ppm]	U [ppm]
MAR4_14	601	Ediacaran	71	172	b.l.d	17.4	886	5.54E+05	1.281	0.156	32.3	0.512	6.16	6.94	3.12	24.2	6.85	78.5	28.7	133.1	30.7	314	70.3	10320	0.44	53.1	187	145.8
MAR4_98	601	Ediacaran	61	182	300	17.4	388	5.19E+05	0.671	0.38	11.4	0.279	2.16	2.04	0.91	8.2	2.63	31.2	11.92	56.3	12.68	127.7	25.5	7220	0.189	41.4	24.21	102.5
MAR4_27	628	Ediacaran	6.5	143	b.l.d	4.5	982	5.30E+05	2.62	b.l.d	32.1	0.271	4.28	6.47	2.65	27.7	8.22	89.9	32.7	150.1	33.9	338	71.4	1.25E+04	1.13	89.8	168.4	240
MAR4_17	643	Cryogenian	83	135	220	9.7	603	5.22E+05	1.051	0.212	25.5	0.365	5.05	6.55	3.18	23.7	6.24	63.8	21	84.4	17.86	172.2	35.5	11100	0.394	46.7	85.3	120.1

MAR4_10	646	Cryogenian	76	271	144	10.7	634	5.41E+05	1.95	0.61	15	0.44	3.27	4.87	1.3	24.3	7	69.2	20.7	80.4	16.4	150	28.7	13360	1.01	104.7	62.2	270
MAR4_113	666	Cryogenian	89	512	1360	18.4	1271	5.06E+05	5.1	0.59	30.4	0.49	4.77	5.7	2.26	27.3	9.9	115.8	43	193	38.3	372	71.4	12580	2.41	94.5	125	214
MAR4_112	685	Cryogenian	169	270	b.l.d	10.1	1460	5.00E+05	3.03	0.67	37.3	0.91	7.2	8.6	2.24	39.3	12.5	147	50.2	221	44.2	399	69.7	12430	1.591	229	203	373
MAR4_100	881	Tonian	300	464	276	26	1444	5.05E+05	12.43	0.83	18	0.63	4.1	5.32	2.65	41.5	14.39	155	45.2	170	33	293	50.8	15090	9.78	250	10.63	215
MAR4_54	1028	Stenian	52	220	100	8.3	954	5.15E+05	2.67	0.77	31.5	1.38	9.8	7.52	2.49	24.4	7.12	84.9	31.15	147.7	33.66	341	75.1	12240	1.046	83.3	214	212
MAR4_110	1029	Stenian	97	203	460	8.8	562	5.13E+05	3.66	1.05	14.7	1.7	8.6	4.1	2.53	10.5	3.7	42.3	16.4	90.2	25	274	61.5	14300	2.52	56.7	5.7	159
MAR4_63	1056	Stenian	245	381	280	52	1580	5.26E+05	2.67	0.67	39.8	0.61	5.7	8.1	3.9	38	11.3	132	49.6	229	52.9	545	122	11930	0.922	94.8	191	497
MAR4_103	1070	Stenian	160	409	127	28.5	1730	5.26E+05	1.86	0.31	21.9	0.349	3.66	6.29	2.9	38.5	12.8	152	55	256	53.3	531	110.4	12660	0.45	154.5	164	285
MAR4_105	1081	Stenian	28.8	100	206	5.2	418	5.28E+05	3.04	0.162	24.5	0.206	1.93	1.94	0.79	7.88	2.54	30.4	12.14	64.1	16.32	190.8	47.1	14540	0.94	332	58.5	496
MAR4_118	1093	Stenian	160	215	1030	32.9	552	5.08E+05	1.3	0.61	31.1	0.73	5.69	6.44	1.69	21.6	5.46	53.5	16.7	71.2	13.66	130.1	24.8	10640	0.458	40.3	133.3	100.5
MAR4_92	1251	Ectasian	650	310	2.00E+03	b.l.d	619	4.91E+05	1.91	0.3	34.2	0.69	4.3	4.3	1.75	17.3	4.91	58.3	21.1	94.7	21.3	227	49.6	12310	0.612	74.3	99	138
MAR4_8	1264	Ectasian	74	278	222	13.6	2227	5.48E+05	1.7	0.348	67.5	1.003	11.8	15.6	5.13	69	19.73	221.3	78.9	339.9	67.6	611	116.6	11370	0.615	132.3	228.5	163.6
MAR4_116	1463	Calymian	249	1199	300	30.8	3060	5.22E+05	1.91	0.38	20.5	0.48	3.64	7.2	2.03	43.1	17.4	244	104.9	552	117.7	1216	236	13340	0.805	28.8	33.1	87.3
MAR4_46	1581	Calymian	152	433	400	23	1580	5.55E+05	2.8	1.9	57.2	2.29	14.6	16.1	6.5	55	15.6	172	56.7	238	50	454	90.5	11920	1.05	194	109.9	176.6
MAR4_45	1829	Orosinian	54	247	184	15.1	699	5.26E+05	1.99	0.18	25.1	0.163	1.6	2.65	0.578	14.09	4.87	59.3	22.12	103.8	22.36	215.3	43.9	13340	1.135	64.2	123.6	245
MAR4_99	1895	Orosinian	274	745	156	19.5	1840	4.91E+05	1.093	b.l.d	1.9	0.136	2.29	6.7	0.294	48.3	16.43	192.4	63.6	262	49.4	439	75.7	13040	0.541	91.1	54.2	260
MAR4_12	1913	Orosinian	63	399	140	22.6	1211	5.29E+05	2.47	0.59	34.7	0.72	7.2	10.7	3.5	34.7	10.6	116.7	41.7	184.6	38.9	356	71.4	10240	0.88	140.8	92.6	111.3
MAR4_86	2020	Orosinian	175	327	102	15.8	1830	5.23E+05	4.03	0.87	18.2	1.05	9.8	9.9	3.35	34.7	11.45	152.3	60.9	293.9	65.1	666	131.7	11140	1.21	44.6	73.7	117.1
MAR4_57	2149	Rhyacian	90	350	1120	43	596	5.25E+05	1.117	1.16	17.8	0.63	2.41	3.02	1.15	13.19	4	48.1	18.58	88.1	20.79	216	50	12630	0.427	66.1	69.4	102.4
MAR4_35	2163	Rhyacian	300	279	520	37	591	5.10E+05	1	0.5	28.1	0.75	6.3	5.7	1.56	16.3	4.72	53.2	19.6	87.3	19.05	180	34.3	10110	0.334	67.1	36.6	40.5
MAR4_32	2237	Rhyacian	47	290	780	17.3	826	5.18E+05	3.01	0.51	16.2	0.58	5	5.3	1.39	22.2	6.85	82.1	28.1	120.3	24.4	225	43.1	12030	1.2	67.7	64.4	173.2

MAR4_49	2704	Neoarchean	101	204	123	20.9	877	5.11E+05	1.9	0.25	18.6	0.171	2.22	3.24	0.5	17.2	5.95	75.9	29.4	135.4	28.7	268	53	12920	0.856	365	156.1	331
MAR4_9	3407	Paleoarchean	116	230	98	15.5	825	5.42E+05	2	0.34	39.9	0.51	3.59	5.23	1.29	19.7	6.53	73.5	26.4	117.6	26.28	251	51.5	12200	1.144	417	72.8	181
Discordant																												
MAR4_11			78	352	310	21.4	1961	5.22E+05	1.28	1.42	13.1	0.98	10.1	13.1	2.39	56.9	17.2	188	65.7	282	56.4	490	91.7	10590	0.377	227	72.7	226
MAR4_15			114	361	1090	24.6	1566	5.30E+05	2.15	0.8	29.6	0.56	5.29	7.46	1.63	34.3	11.12	138.2	53.2	237	52	493	100.3	11380	0.88	86.6	141	191
MAR4_23			102	504	154	13.5	1407	5.44E+05	2.71	0.95	77.6	1.02	8.2	7.29	2.12	30.1	10.15	127	48.4	228	50.8	492	103.3	14980	1.7	419	132.1	428
MAR4_24			127	700	1980	32	1870	5.41E+05	2.57	0.34	10.3	0.53	5.41	7.7	0.92	40.8	13.36	176	64.7	298	63	588	112.9	1.24E+04	0.81	69	107.9	195
MAR4_32			47	290	780	17.3	826	5.18E+05	3.01	0.51	16.2	0.58	5	5.3	1.39	22.2	6.85	82.1	28.1	120.3	24.4	225	43.1	12030	1.2	67.7	64.4	173.2
MAR4_45			54	247	184	15.1	699	5.26E+05	1.99	0.18	25.1	0.163	1.6	2.65	0.578	14.09	4.87	59.3	22.12	103.8	22.36	215.3	43.9	13340	1.135	64.2	123.6	245
MAR4_54			52	220	100	8.3	954	5.15E+05	2.67	0.77	31.5	1.38	9.8	7.52	2.49	24.4	7.12	84.9	31.15	147.7	33.66	341	75.1	12240	1.046	83.3	214	212
MAR4_63			245	381	280	52	1580	5.26E+05	2.67	0.67	39.8	0.61	5.7	8.1	3.9	38	11.3	132	49.6	229	52.9	545	122	11930	0.922	94.8	191	497
MAR4_75			181	1000	2270	18.3	2660	5.20E+05	1.98	0.57	24.4	0.49	4.64	9	2.21	48.7	17.5	231	92.1	392	88	864	155.5	13380	0.77	55.3	114.2	163.1
MAR4_76			166	732	690	32.3	1665	5.28E+05	1.812	0.64	39.3	0.92	7	9	3.06	43.5	13.13	155.1	54.9	244.2	50.3	481	89.8	11690	0.644	26.6	53.4	81.6
MAR4_80			96	255	430	12.6	1200	5.38E+05	6.8	1.68	96.2	1.14	9.8	12.5	2.68	47	12.01	125	40.8	158.9	31.1	272	50.4	11850	1.99	66.7	250	197
MAR4_81			125	174	202	12.6	1130	5.17E+05	2.72	0.292	10.51	0.311	4.42	7.44	1.22	33.4	10.1	113	40.8	172	34.5	306	56.2	9880	0.957	77.7	80.9	193
MAR4_86			175	327	102	15.8	1830	5.23E+05	4.03	0.87	18.2	1.05	9.8	9.9	3.35	34.7	11.45	152.3	60.9	293.9	65.1	666	131.7	11140	1.21	44.6	73.7	117.1
MAR4_89			280	244	1070	23.5	475	5.35E+05	2.48	0.58	33.7	0.35	2.72	2.21	0.74	9.06	3.07	37.5	13.79	65.3	15.19	164.2	33.7	13430	1.11	72.2	99.8	187
MAR4_92			650	310	2.00E+03	-1	619	4.91E+05	1.91	0.3	34.2	0.69	4.3	4.3	1.75	17.3	4.91	58.3	21.1	94.7	21.3	227	49.6	12310	0.612	74.3	99	138
MAR4_98			61	182	300	17.4	388	5.19E+05	0.671	0.38	11.4	0.279	2.16	2.04	0.91	8.2	2.63	31.2	11.92	56.3	12.68	127.7	25.5	7220	0.189	41.4	24.21	102.5
MAR4_109			23.2	111.6	165	5.8	457	5.21E+05	1.687	0.197	14.47	0.165	1.74	2.09	0.667	9.13	2.94	36.1	13.61	65.9	14.36	147.8	32.3	11200	0.381	60.1	37.25	158
MAR4_110			97	203	460	8.8	562	5.13E+05	3.66	1.05	14.7	1.7	8.6	4.1	2.53	10.5	3.7	42.3	16.4	90.2	25	274	61.5	14300	2.52	56.7	5.7	159
MAR4_128			63	154	232	9.4	1576	5.22E+05	4.06	0.163	21	0.117	1.35	2.72	1.74	18.22	6.84	102	46.4	270	67	766	183.3	9790	0.633	47.4	115.4	292

Detection Limit		Al [ppm]	P [ppm]	Ca [ppm]	Ti [ppm]	Y [ppm]	Zr [ppm]	Nb [ppm]	La [ppm]	Ce [ppm]	Pr [ppm]	Nd [ppm]	Sm [ppm]	Eu [ppm]	Gd [ppm]	Tb [ppm]	Dy [ppm]	Ho [ppm]	Er [ppm]	Tm [ppm]	Yb [ppm]	Lu [ppm]	Hf [ppm]	Ta [ppm]	Pb [ppm]	Th [ppm]	U [ppm]
Minimum Detection Limit		2.0497	4.8194	76.553	0.48754	0.030003	1.48E+00	0.0071129	0.0054774	0.0086038	0.01	0.01	0.01	0.01	0.083524	0.01	0.01	0.01	0.01	0.01	0.01	0.01	0.01	0.01	0.0081196	0.01	0.018295
Maximum Detection Limit		16.566	86.545	1629.8	5.6297	0.58605	3.10E+01	0.16761	0.18644	0.14667	0.15316	0.17167	0.20592	0.07637	1.2906	0.030227	0.089923	0.067975	0.31638	0.020837	0.23509	0.045217	0.19601	0.019519	0.10604	0.050759	0.22667
Mean Detection Limit		4.37902708	13.4015854	219.370063	1.32658271	0.10429715	4.34E+00	0.02520225	0.02585043	0.02859513	0.01309128	0.04801019	0.02934617	0.02392047	0.1910274	0.00890581	0.02976183	0.00798408	0.04039977	0.00503158	0.02994804	0.00517918	0.05549931	0.0081838	0.02029307	0.00638346	0.04131663
Median Detection Limit		3.68455	10.362	165.73	1.06565	0.087663	3.37E+00	0.020392	0.0181615	0.021861	0.0097786	0.04172	0.0112065	0.021802	0.150885	0.0073301	0.021279	0.00603505	0.030158	0.0042216	0.024977	0	0.041968	0.00692835	0.01752	0.0016698	0.03569
Associated Error		Al [ppm]	P [ppm]	Ca [ppm]	Ti [ppm]	Y [ppm]	Zr [ppm]	Nb [ppm]	La [ppm]	Ce [ppm]	Pr [ppm]	Nd [ppm]	Sm [ppm]	Eu [ppm]	Gd [ppm]	Tb [ppm]	Dy [ppm]	Ho [ppm]	Er [ppm]	Tm [ppm]	Yb [ppm]	Lu [ppm]	Hf [ppm]	Ta [ppm]	Pb [ppm]	Th [ppm]	U [ppm]
Minimum Absolute Error		4.9	8.1	43	0.62	23	1.60E+04	0.049	0.017	0.32	0.017	0.14	0.2	0.04	0.51	0.17	1.8	0.51	2.5	0.39	5	1	260	0.023	1.2	0.79	3.2
Maximum Absolute Error		380	190	1900	35	170	3.20E+04	0.61	1	8.6	1.1	4.5	3.9	2.1	10	2.6	24	5.8	29	6.2	76	16	1100	0.9	44	25	28
Mean Absolute Error (±2σ)		53.15625	42.83125	241.833333	6.10875	67.7916667	2.19E+04	0.17329167	0.210125	3.1691667	0.18204167	0.98625	0.878125	0.33608333	2.44229167	0.66395833	6.45416667	1.97270833	8.41875	1.87666667	19.6020833	4.18541667	657.708333	0.10120833	7.27083333	6.43354167	12.3125
Median Absolute Error (±2σ)		35	23.5	92.5	3.6	56	2.10E+04	0.15	0.145	2.7	0.135	0.7	0.715	0.25	2	0.455	5.3	1.6	6.9	1.55	16.5	3.6	640	0.073	4.5	5.7	11.5

M2AR 5-1 - Zircon compositional data (LA-ICP-MS, n = 76, b.d. = below detection limit)

Analysis ID	Best age (Ma)	Geological time	Al [ppm]	P [ppm]	Ca [ppm]	Ti [ppm]	Y [ppm]	Zr [ppm]	Nb [ppm]	La [ppm]	Ce [ppm]	Pr [ppm]	Nd [ppm]	Sm [ppm]	Eu [ppm]	Gd [ppm]	Tb [ppm]	Dy [ppm]	Ho [ppm]	Er [ppm]	Tm [ppm]	Yb [ppm]	Lu [ppm]	Hf [ppm]	Ta [ppm]	Pb[ppm]	Th [ppm]	U [ppm]
MAR5_33	522	Cambrian	8.4	192	220	9.9	305	5.21E+05	0.794	0.77	22.7	0.38	1.99	2.05	0.604	7.63	2.23	25.2	9.38	43.7	9.9	104.4	22.7	1.17E+04	0.45	100.9	39.9	73.2
MAR5_15	539	Cambrian	17.9	330	101	7.3	910	5.19E+05	3.47	0.279	9.3	0.192	1.96	3.81	0.22	19.9	7.11	88.9	32.2	152.2	33.3	328	59.8	1.59E+04	2.44	219	155.9	682
MAR5_69	540	Cambrian	122	237	250	14.3	740	5.10E+05	1.19	1.2	57	1.59	12.6	8.8	3.3	20.6	6.4	66.6	23.9	107	23.5	233	47.4	12650	0.466	61	44.3	151
MAR5_12	542	Ediacaran	13.8	464	b.l.d	6.3	1870	5.04E+05	1.071	b.l.d	13.9	0.169	2.54	5.32	1.17	35.8	12.4	155	63.2	302	66.4	643	124	1.16E+04	0.4	33.2	58.8	98
MAR5_89	546	Ediacaran	218	902	197	59	1803	5.07E+05	1.92	0.32	20	0.346	2.77	4.52	1.02	30.3	13.21	178	63.6	277.1	54.6	518	91	13310	0.908	80.6	16.9	199
MAR5_41	566	Ediacaran	6	240	b.l.d	12.4	640	5.12E+05	1.441	b.l.d	23.9	0.087	1.52	3.66	1.34	20.1	5.89	65.1	22.6	96.4	19.3	178	32.9	9.97E+03	0.37	233	127.9	118

MAR5_80	569	Ediacaran	180	270	750	43	853	5.19E+05	5.81	0.36	34.6	0.398	5.03	5.75	1.06	24.2	7.34	82.3	29.4	130.9	26.3	250	46.6	9510	3.2	32	59.4	71
MAR5_98	576	Ediacaran	710	285	640	24.2	1610	4.96E+05	6.03	0.8	82.1	0.88	5.8	6.32	2.07	28.7	9.48	126	49.7	246	56.4	600	120.1	11580	2.57	87.3	357	430
MAR5_76	591	Ediacaran	940	359	2060	30.6	534	5.30E+05	1.3	0.68	21.3	0.384	3.5	4.91	1.18	26.2	7.92	73.1	17.4	48.3	6.99	54.7	9.7	1.37E+04	0.81	92.5	46.3	93
MAR5_57	596	Ediacaran	28	152	103	8.2	544	5.28E+05	2.23	b.l.d	11	0.098	0.94	1.71	0.338	9.4	3.4	44.5	17.2	81.9	18.3	184	37	1.34E+04	3	99.8	78.4	161
MAR5_102	604	Ediacaran	26	160	94	11.4	479	5.04E+05	3.02	0.086	31.7	0.078	1.12	1.77	0.35	9.04	3.11	38.1	14.23	68.4	15.6	163	31.2	1.29E+04	1.65	93.4	157.5	238
MAR5_63	607	Ediacaran	240	196	540	19.9	1490	4.85E+05	23.2	0.56	31.4	0.39	3.59	7.3	0.79	35.6	11.37	145.6	53.6	239	47.1	429	78.6	1.34E+04	7.93	99	151.5	212
MAR5_26	612	Ediacaran	108	109	56	17.9	623	5.34E+05	2.26	0.11	18.7	0.18	2.09	2.99	0.448	16.3	5.01	58.7	21	90.4	18.5	178	31.1	1.21E+04	0.916	182	91	131
MAR5_61	630	Ediacaran	48	242	181	13.7	1090	5.36E+05	3.05	0.33	55.6	0.318	3.32	5.31	1.22	24.6	8.08	97	35.8	169.6	36.8	360	68.7	1.26E+04	1.48	344	222.8	265
MAR5_88	632	Ediacaran	158	205	990	14.3	562	4.82E+05	1.28	0.54	54	0.62	4.3	3.5	1.07	12.8	3.89	49	17.1	77.7	16.3	156	29.8	11690	0.577	132	42.8	97
MAR5_28	638	Cryogenian	91	288	670	17.2	1540	5.03E+05	35.8	1.26	23.4	1	9.8	10.6	1.19	44.7	13.5	151	53.9	236	48.4	466	83.3	1.42E+04	33.2	95.8	69.1	172
MAR5_101	645	Cryogenian	58	104.5	b.l.d	36	289	5.06E+05	0.838	0.128	19.2	0.201	2.13	2.32	0.82	7.49	2.17	24.2	8.46	40.3	9	93.3	18.7	10060	0.316	211	130.8	153
MAR5_18	662	Cryogenian	7.7	81.1	b.l.d	4.74	221	5.03E+05	1.63	b.l.d	17	0.035	0.51	0.95	0.286	4.93	1.59	18.4	6.63	32.7	7.83	83.9	16.2	1.21E+04	0.672	45.1	56.2	108
MAR5_72	668	Cryogenian	103	305	1440	36	741	5.20E+05	3.32	0.298	26.7	0.46	3.77	4.37	1.12	16.5	5.71	70.3	24.9	113.1	23.8	242	45.9	1.26E+04	1.81	113.2	57.1	169
MAR5_8	715	Cryogenian	140	132	112	20	562	5.13E+05	6.56	0.17	14.9	0.207	2.78	4.16	0.68	16.5	4.9	56.9	20.2	84.8	17.5	162	30.9	1.10E+04	3.07	77.3	39.1	177
MAR5_27	860	Tonian	350	181	152	23.2	814	5.29E+05	3.14	0.109	17.2	0.102	1.67	3.6	0.31	19.2	6.31	75	27.61	121.9	24.8	234	43.6	1.21E+04	1.52	68.9	107.4	184
MAR5_56	929	Tonian	8.3	80.6	b.l.d	6.61	136	4.96E+05	1.164	b.l.d	2.14	0.0111	0.226	0.82	0.156	4.19	1.188	12.47	4.19	18.7	4.06	42.3	8.78	1.30E+04	0.446	195	34.8	304
MAR5_77	975	Tonian	48	190	440	14.2	839	5.16E+05	3.02	0.383	30.7	0.431	3.5	3.96	0.95	20.9	6.65	78.9	27.52	120.7	24.6	225	41.1	11590	1.46	83	106.6	223
MAR5_66	987	Tonian	6.3	179	109	18.4	1072	5.20E+05	0.748	0.073	21	0.516	7.58	11.6	2.41	43.9	11.55	116.9	37	153.2	29.1	257	48.7	10780	0.248	26	72.3	70.7
MAR5_83	1014	Stenian	54.7	193	283	37.6	496	5.13E+05	1.64	0.353	32.5	0.62	5.82	6.9	2.06	19.2	5.37	52.7	17	68.4	13.9	132.1	25.4	14770	0.688	313	96.5	287
MAR5_2	1031	Stenian	4.5	599	b.l.d	13.8	2060	5.13E+05	6.97	0.0313	43.6	0.296	5.47	15.3	1.47	69.5	19.9	221	72.6	304	59.8	572	98	1.36E+04	2.6	133.8	294	214
MAR5_53	1052	Stenian	5.5	484	b.l.d	7.8	1680	5.23E+05	2.62	b.l.d	8.6	0.12	2.15	5.15	0.303	33.8	11.82	151.4	57.8	270.5	54.8	517	95	1.47E+04	1.41	266	136.3	350

MAR5_70	1073	Stenian	4.4	19.4	b.l.d	5.3	307	4.75E+05	0.469	b.l.d	21.1	0.204	2.97	3.89	2.02	13.2	2.99	29.4	8.92	37.4	7.36	74	14.4	9.60E+03	0.059	80.3	106.6	245
MAR5_1	1075	Stenian	1.4	404	b.l.d	9.7	1190	5.21E+05	10.37	b.l.d	44	0.097	1.87	5.72	0.676	32	10.04	116.6	40.5	179.6	37.5	348	62.6	1.41E+04	3.29	113.2	205.7	163
MAR5_42	1106	Stenian	10.4	89	b.l.d	2.86	439	5.14E+05	21.9	b.l.d	7.4	0.048	0.68	1.11	0.497	7.29	2.78	36.1	14.34	67.8	14.92	149	29.3	1.01E+04	11.1	151.6	33.3	449
MAR5_50	1172	Stenian	105	318	1450	9.4	1107	5.03E+05	123.4	1.35	39.2	1.6	8.9	6.8	2.45	21.7	7.7	93	33	163.4	37.6	418	84	11810	64.4	114.1	129	359
MAR5_7	1193	Stenian	14.7	281	b.l.d	21	1350	5.43E+05	4.3	0.043	7.92	0.159	2.97	6.57	0.39	36.8	11.49	133.1	48.7	208.1	39.6	355	69	1.34E+04	1.64	61.7	41.9	83
MAR5_10	1210	Calymmian	2.4	177	b.l.d	10.3	839	5.39E+05	2.12	0.0219	5.46	0.0276	0.743	1.93	0.104	14.3	5.53	71.1	27.7	129.5	27.8	277	48.9	1.41E+04	1.14	304	99.3	388
MAR5_82	1545	Calymmian	55	278	410	12.8	919	5.02E+05	4.48	0.45	60	0.339	3.35	5.57	1.23	23.6	7.34	83.9	29.8	135.9	29.5	287	55.5	10300	1.68	59.2	288	175
MAR5_3	1941	Orosinian	58.8	544	b.l.d	8	1360	5.25E+05	1.083	0.053	4.22	0.163	3.07	7.01	0.219	40.4	11.69	136.7	48.1	196	36.9	310	55.3	1.32E+04	0.366	92.7	109	72.1
MAR5_20	1956	Orosinian	7.5	586	b.l.d	43.7	1940	5.14E+05	5.21	0.13	22.3	0.423	7.81	17.9	1.35	91.4	23.6	228	66.4	231	38.3	300	49.5	1.23E+04	1.65	37.5	145	29
MAR5_60	1968	Orosinian	51	147	b.l.d	8.4	636	5.08E+05	2.27	0.51	31.3	0.59	4.9	4.3	1.18	15.8	5.11	61.9	21.4	95.8	19.5	186	34.2	1.42E+04	1.03	135.6	204	160
MAR5_45	1991	Orosinian	7.4	403	b.l.d	11.2	1250	4.91E+05	4.98	0.154	24.6	0.131	2.04	4.69	1.07	28.5	9.69	113.5	41.7	182.9	37.2	354	65.6	1.10E+04	2.4	172	153.5	135
MAR5_4	2008	Orosinian	46.5	498	b.l.d	10.2	1400	5.02E+05	1.183	0.099	3.27	0.219	4.06	8.7	0.271	43.3	12.2	142.4	50.3	193.7	35.5	311	50.7	1.18E+04	0.338	105.6	139.7	87
MAR5_24	2017	Orosinian	173	192	b.l.d	16.9	704	5.13E+05	1.63	0.77	75.3	0.86	6.47	5.72	2.41	19.2	6.16	70	23.2	102.4	21.8	214	42	11360	0.688	77.4	110.8	155
MAR5_112	2057	Rhyacian	88	263	1.80E+03	80	3950	5.12E+05	12.27	0.85	72	1.21	14.5	22.5	4.2	121	37.6	434	146.2	554	101.7	757	115.8	7800	7.5	43.7	144	191
MAR5_44	2061	Rhyacian	93	213	95	12.7	880	5.29E+05	5.71	0.55	39.7	1.34	9.3	9.5	3.3	26.9	8.5	93	29.8	125.8	25.1	245	43	1.46E+04	4.25	228	241	766
MAR5_95	2069	Rhyacian	169	106	1830	41.3	414	4.93E+05	2.29	0.48	31.5	0.53	2.91	1.82	1.09	7.2	2.56	31.8	12.4	61.6	15.2	174	38.4	11260	0.575	99.4	28.6	166
MAR5_87	2075	Rhyacian	149	158	550	39	536	4.91E+05	5.78	0.27	18.1	0.291	2.8	3.79	1.13	16.2	4.9	56.6	19.1	82.1	15.78	145.8	25.3	8640	3.43	25.5	25.2	54.6
MAR5_31	2090	Rhyacian	260	71	130	13.9	238	5.05E+05	0.742	0.37	33	0.206	1.6	1.39	0.63	4.69	1.56	20.2	7.18	37	9.26	102	24.2	12130	0.225	28.01	31.1	74
MAR5_100	2119	Rhyacian	240	677	182	49	1780	5.18E+05	6.44	0.45	29.9	0.38	3.43	5.11	0.68	30.5	11.34	153.2	62.6	323	74	777	154	1.38E+04	2.18	40.3	135.1	100.6
MAR5_17	2126	Rhyacian	4.2	147	b.l.d	8.9	395	5.05E+05	1.138	0.036	17.3	0.065	0.8	1.32	0.407	7.78	2.39	29.1	11.75	57.8	13.4	141	29.4	1.20E+04	0.379	90.9	27.1	63.3
MAR5_105	2160	Rhyacian	46	331	250	9.2	1220	5.14E+05	3.72	0.154	37.4	0.233	3.45	7.01	2.25	35.7	10.44	123	41.4	181	36.3	333	65.9	10890	1.92	52.6	98.6	133.4

MAR5_5	2173	Rhyacian	65.1	181	b.l.d	12.7	297	5.19E+05	1.098	0.0179	2.87	0.061	1.17	2.8	0.121	11.9	3.15	32.2	9.72	37.1	7.29	64	11.8	1.37E+04	0.339	197	48.1	133
MAR5_107	2188	Rhyacian	58	270	141	11.6	2820	5.07E+05	2.83	0.231	18.6	0.453	5.83	10.62	1.91	63.5	21.5	260	98.3	440	87	831	152.6	9720	1.04	152.2	44.5	99.4
MAR5_21	2249	Siderian	110	87.5	b.l.d	8.6	318	5.14E+05	1.213	0.097	19.6	0.072	0.88	1.57	0.61	7.35	2.19	25	10.21	45.6	10.8	116	25.4	9.70E+03	0.51	264	92.4	175
MAR5_36	2789	Neoarchean	26.8	168	b.l.d	21	698	5.13E+05	10.35	0.149	15.3	0.353	3.73	5.68	1.31	23.2	6.73	75.9	25.8	107.6	20.9	190	32.5	9.50E+03	4.01	38.3	63.5	90.1
MAR5_93	3100	Mesoarchean	10.7	304	b.l.d	66	1109	4.97E+05	4.64	0.285	21.9	0.214	2.12	4.52	0.299	25.6	8.4	104.1	37.2	163.6	33.5	316	55.2	1.28E+04	2.35	196.9	213.9	573
Discordant																												
MAR5_113			16	229	-9	24	1310	4.70E+05	0.902	0.077	22.2	0.312	5.23	10.4	3.25	50.5	13.5	150.8	49.3	195	34.8	298	50.7	9830	0.323	57.6	42.2	42
MAR5_14			31	189	90	8.9	968	5.49E+05	1.78	0.63	27.5	0.41	2.46	3.34	1.78	17.1	5.95	80.7	31.9	156.2	35.5	363	76.7	9.60E+03	0.391	6.18	19.8	16
MAR5_22			56.8	159	880	11.9	315	5.28E+05	1.31	0.378	20	0.459	3.52	3.02	1.47	10.5	3.13	31.4	10	42.2	8.6	94	19.9	11460	0.464	87.5	13.6	62.8
MAR5_29			5.9	446	94	7.7	1290	5.28E+05	1.76	0.051	15.1	0.083	1.18	3.61	0.9	23.3	8.49	112.6	44.1	212	45.8	480	98.6	1.31E+04	0.91	45.9	87.7	117
MAR5_30			410	316	190	28.7	691	5.03E+05	1.74	0.3	19.1	0.323	3.53	6.44	2.51	25.9	6.83	68.6	21.7	85.7	15.2	135	22.4	10240	0.563	63.7	90.7	172
MAR5_35			92.1	240	-18	25	497	5.17E+05	1.82	0.0192	4.1	0.16	2.39	5.48	0.072	21.9	5.34	50.9	15.41	59.4	11.52	102.4	17.9	1.31E+04	0.652	63	154.9	201
MAR5_43			57	255	400	27	1056	5.19E+05	4.08	0.219	25.2	0.258	3.28	4.94	1.07	25.6	8.15	100.9	36.6	166	33.7	322	61.9	11610	1.6	152	69	197
MAR5_46			26.8	187	74	10.4	620	4.96E+05	2.41	0.105	48.8	0.144	2.19	4	1.1	17.3	5.24	59.4	21.61	98.1	19.8	187	36.4	11540	0.79	117.4	87.9	94.3
MAR5_48			48	231	550	21.4	897	5.27E+05	4.08	0.36	66.4	0.52	4.66	6.61	1.96	26.6	7.86	87.2	28.8	129.6	27.2	268	49.3	11170	1.78	63.7	196.8	208
MAR5_49			88	109	290	17.1	259	5.09E+05	0.92	0.22	16.3	0.192	1.63	1.61	0.96	7.4	2.23	25.2	8.53	37.9	7.9	76.4	15.7	8700	0.348	38.1	244	100.9
MAR5_58			95	145	180	17.2	267	5.28E+05	1.625	0.309	24.6	0.312	3.43	4.04	0.64	12.22	3.27	28.9	8.7	34.1	6.28	56.1	9.73	12070	0.519	71.6	181.1	189.4
MAR5_59			38	192	120	30.9	845	5.21E+05	1.53	0.44	19	0.36	2.92	3.76	1.66	17.5	5.67	71.8	27.5	130.6	29.3	295	60.7	10150	0.6	13.91	29.6	47.4
MAR5_62			36	260	47	17.5	1420	4.83E+05	1.763	0.142	31.1	0.622	10.8	15.8	2.28	58.3	14.63	146.4	46.9	192	36.1	331	58.1	1.04E+04	0.59	101.9	117.9	265
MAR5_67			47	175	71	16.9	593	5.15E+05	3.1	0.167	18.9	0.178	1.56	2.5	0.482	12.59	4.12	51.8	18.55	87.4	18.52	185	35.4	12710	1.51	112.6	47.6	171
MAR5_68			122	261	31	20.1	433	4.92E+05	1.373	0.186	17.2	0.253	2.25	5.52	1.39	27.3	7.34	58.9	13.7	43.2	7.05	53.4	8.1	1.27E+04	0.82	116	42.5	307

MAR5_73			32.3	162	287	58	319	5.38E+05	0.756	0.333	22.7	0.314	2.37	2.19	1.18	6.75	2.17	26.6	9.92	48.8	11.19	122.8	27.9	7280	0.172	47.3	104.4	116
MAR5_81			78.6	631	38	8.8	1560	5.00E+05	0.992	0.0154	0.749	0.0383	0.66	3.26	0.071	24.9	11.25	149.6	51.7	216	43.1	411	69	1.46E+04	0.616	122.6	34.7	358
MAR5_79			52	294	1170	26	753	4.94E+05	4.43	0.37	48.5	0.36	4.28	5.19	1.28	18.9	6.26	70.6	23.9	105.1	23.6	234	42.4	11720	2.02	100.7	76.7	162
MAR5_86			89	256	580	12.5	1121	5.16E+05	4.18	0.36	23.8	0.196	2.58	4.13	0.63	27	8.58	103.7	38.8	181.7	38.1	379	74.3	13540	1.66	122.8	98.9	182.7
MAR5_94			23.6	139	78	12.1	611	5.18E+05	0.886	0.161	13.4	0.17	1.11	1.96	0.55	10.5	3.76	48.7	18.8	88	18.8	191	35.1	1.11E+04	0.377	72.9	18.6	33.1
MAR5_96			76	294	91	19.1	830	4.93E+05	1.24	0.72	38	1.21	11	12.6	3.9	32.3	9.9	104	32.6	135	25.7	242	42.4	1.04E+04	0.296	77.6	62	65
MAR5_99			380	741	300	43	1910	5.00E+05	1.29	0.87	12.2	0.397	3.11	5.43	0.75	36.3	14.9	188	64.8	292	57	528	90	13720	0.862	139.1	63.2	386
MAR5_110			187	269	480	59	1420	4.91E+05	2.44	0.4	40.9	0.66	8.32	11.1	3.23	43.5	12.63	141.4	48.6	203	39.8	367	65.8	9630	0.738	148.8	115.7	106.6

M2AR 6-1 - Zircon compositional data (LA-ICP-MS, n = 109, b.d. = below detection limit)

Analysis ID	Best age (Ma)	Geological time	Al [ppm]	P [ppm]	Ca [ppm]	Ti [ppm]	Y [ppm]	Zr [ppm]	Nb [ppm]	La [ppm]	Ce [ppm]	Pr [ppm]	Nd [ppm]	Sm [ppm]	Eu [ppm]	Gd [ppm]	Tb [ppm]	Dy [ppm]	Ho [ppm]	Er [ppm]	Tm [ppm]	Yb [ppm]	Lu [ppm]	Hf [ppm]	Ta [ppm]	Pb[ppm]	Th [ppm]	U [ppm]
MAR6_13	569	Ediacaran	153	127	b.l.d	19	737	4.76E+05	2.36	0.14	36.8	0.33	4.98	6.7	2.46	23.6	6.74	71.3	24.7	106.7	21.8	216	41.2	10660	0.512	44.8	99.1	114
MAR6_130	570	Ediacaran	b.l.d	186	b.l.d	8.9	842	4.83E+05	3.64	0.038	16.79	0.089	1.39	3.31	0.305	18.6	6.03	73.8	26.46	117.3	23.87	224	42.2	11030	1.39	73.3	118.6	208
MAR6_126	571	Ediacaran	2.6	193	b.l.d	20.4	2007	5.04E+05	2.32	0.281	20.07	1	13.38	16.7	3.13	69.2	19.55	207	70.1	273.4	49.9	417	76.5	9410	1.2	109	373.9	311
MAR6_124	577	Ediacaran	3.7	152	b.l.d	13.6	797	4.92E+05	1.99	0.266	9.4	0.179	2.84	5.15	0.677	24.1	7.29	79.5	27.34	112.9	22.08	196.3	36.6	9120	0.383	27.22	65.6	75.1
MAR6_91	577	Ediacaran	300	293	b.l.d	13	3780	4.81E+05	4.05	0.469	152	2.38	44	58.2	26.6	193	47.4	461	142.6	562	102.2	859	155	9140	0.752	123.3	820	348
MAR6_109	577	Ediacaran	b.l.d	175	b.l.d	9.7	677	4.72E+05	3.12	0.0279	15.53	0.066	1.11	2.94	0.284	16.9	5.16	63.6	23.52	103.6	21.1	199	36.9	10620	1.329	64	93.3	178
MAR6_14	583	Ediacaran	b.l.d	216	b.l.d	8.6	827	5.06E+05	3.34	0.33	18.5	0.24	2.2	3.79	0.382	18.8	6.45	76	27.26	120.1	24.9	227	43.1	11170	1.41	80.9	124.3	217
MAR6_119	585	Ediacaran	b.l.d	202	134	13.2	1494	4.78E+05	2.1	0.069	13.09	0.334	6.49	11.38	1.39	50.8	14.64	160.6	53.7	225.9	42.6	375	67.4	10280	0.92	58	118.4	160
MAR6_117	585	Ediacaran	5.1	161	92	20.2	991	4.71E+05	1.65	0.127	19.4	0.445	6.7	8.18	2.73	36.7	9.7	105	33.9	138.9	26.6	238	44	9720	0.457	25.7	128.5	70.7
MAR6_55	586	Ediacaran	b.l.d	172	b.l.d	9.8	743	4.94E+05	3.59	0.08	15.74	0.092	1.94	3.32	0.342	18	5.76	69.2	25.02	108	21.37	206	38.4	11210	1.45	64.1	111	173
MAR6_26	588	Ediacaran	b.l.d	154	b.l.d	9.2	600	4.65E+05	2.91	0.027	12.41	0.059	1	2.29	0.278	13.9	4.62	54.9	20.13	88.7	18.22	171	31.6	10850	1.166	47.8	67.2	129
MAR6_79	588	Ediacaran	b.l.d	174	b.l.d	6.7	934	4.86E+05	4.32	0.03	22.6	0.074	1.67	3.31	0.288	19.9	6.89	84.2	30.8	139.3	28.1	255	49.5	12240	2.01	123.3	184.5	345
MAR6_93	588	Ediacaran	b.l.d	199	b.l.d	7.7	847	4.79E+05	3.57	0.312	18.76	0.145	1.78	3.4	0.313	21	6.41	79	28.81	124.8	24.19	235	44.2	11420	1.5	87.3	138	241
MAR6_110	589	Ediacaran	b.l.d	169	b.l.d	6.98	520	4.69E+05	3.01	0.0296	12.43	0.0343	0.84	1.83	0.19	10.85	3.64	46.9	17.53	78.8	16.58	155.9	29.1	10870	1.26	54.4	67	149

MAR6_84	589	Ediacaran	b.l.d	201	b.l.d	9.9	821	4.88E+05	3.34	0.073	17.15	0.113	1.81	3.95	0.358	19.7	6.32	75.2	27.84	119.7	24.4	225	43	11430	1.58	82.4	126.8	226
MAR6_32	589	Ediacaran	6.1	167	b.l.d	5.4	1551	4.84E+05	3.78	0.067	17.33	0.362	6.99	11.87	0.681	52.2	14.82	162.6	55.1	228.6	42.8	380	71.1	10750	1.257	82.9	165.3	223
MAR6_18	594	Ediacaran	b.l.d	185	b.l.d	10.3	758	4.86E+05	3.52	0.031	18.75	0.083	1.33	2.66	0.328	16.32	5.5	65.5	24.49	110.4	22.79	211.1	39.1	11270	1.41	72.4	108.5	187
MAR6_31	595	Ediacaran	22	223	b.l.d	9.8	817	5.02E+05	3.66	0.33	22.4	0.46	4.21	4.84	1.06	20.1	6.43	75.8	26.8	119.6	23.8	214	40.2	11920	1.54	60.9	92.4	160
MAR6_62	596	Ediacaran	b.l.d	159	b.l.d	13.7	862	4.70E+05	1.37	0.085	11.87	0.397	6.69	8.5	2.02	31.8	8.26	86.4	28.8	122	23.9	217	41.6	9300	0.495	27.9	80.8	73.8
MAR6_4	597	Ediacaran	b.l.d	180	b.l.d	5.7	613	4.92E+05	3	0.024	13.73	0.067	0.71	1.6	0.207	10.94	3.9	51.7	20.13	94.2	20.14	195	38.8	12730	1.549	80.6	84.4	204.6
MAR6_115	597	Ediacaran	b.l.d	190	b.l.d	7.9	811	4.84E+05	3.69	0.039	18.67	0.07	1.54	3.04	0.35	18.4	6.23	74.8	27.06	120.6	24.9	228	43.5	11720	1.6	87.9	131.2	241
MAR6_59	597	Ediacaran	b.l.d	141	b.l.d	8	494	4.84E+05	2.47	0.093	10.98	0.072	1.05	2.08	0.251	11.05	3.71	44.6	16.99	75.6	15.54	142.1	27.3	11330	1.061	40.3	51.3	104.7
MAR6_72	598	Ediacaran	b.l.d	154	b.l.d	12.4	581	4.76E+05	2.65	0.029	11.19	0.091	1.12	2.7	0.254	13.9	4.54	56.3	20.46	89.9	18.2	165	31.7	10970	1.08	47.1	66.5	124.9
MAR6_68	598	Ediacaran	b.l.d	162	b.l.d	7.4	735	4.81E+05	3.22	0.036	16.25	0.08	1.29	2.92	0.303	16.38	5.34	65	25	112	22.8	218	40.8	11560	1.371	66.4	96.7	179
MAR6_104	599	Ediacaran	b.l.d	248	b.l.d	13	1583	4.62E+05	2.24	0.28	14.8	0.443	7.9	12.2	1.31	55.8	15.79	171	57.5	236.1	44.9	390	71.2	9560	0.901	61.8	135	169
MAR6_38	599	Ediacaran	b.l.d	190	b.l.d	7.2	624	4.92E+05	3.06	0.044	15.22	0.086	1.05	2.13	0.221	13.3	4.44	55.7	20.41	91.5	18.83	175.5	33	12570	1.61	74.3	100.4	198
MAR6_87	599	Ediacaran	b.l.d	157	b.l.d	7	740	4.77E+05	3.72	0.043	20	0.082	1.51	3.09	0.28	17.1	5.81	70.3	26	117.3	23.26	220	40.5	11530	1.52	90	130.6	242
MAR6_106	600	Ediacaran	36.7	155	b.l.d	6.6	677	4.67E+05	3.65	0.146	17.9	0.214	2.36	2.75	0.479	14.2	4.97	61.1	23.1	103.4	21.15	202	37.8	11580	1.67	80.8	93.8	220
MAR6_42	601	Ediacaran	b.l.d	147	b.l.d	10	583	4.81E+05	1.37	0.05	23.4	0.139	1.74	3.42	0.8	15.1	4.29	51.7	18.6	83.6	16.7	156	30	11350	0.37	34	88.3	89.3
MAR6_80	601	Ediacaran	b.l.d	161	b.l.d	12.1	1451	4.71E+05	2.72	0.077	10.69	0.456	7.21	10.66	0.87	50.5	14.25	154.5	51.1	209.7	38.9	347	64.8	9610	1.07	54.2	110.5	151
MAR6_43	602	Ediacaran	56	146	120	6.1	1272	4.83E+05	7.56	0.77	67.5	1	6.9	6.48	2.66	26.2	8.3	100.5	38.1	183.1	40.8	419	87	12020	1.92	192.9	234	502
MAR6_77	602	Ediacaran	b.l.d	142	b.l.d	5	572	4.72E+05	3.13	0.074	16.1	0.059	0.94	1.96	0.234	10.51	3.78	49.2	18.79	89.1	17.8	174	34.3	1.24E+04	1.52	79.4	98.2	217
MAR6_78	604	Ediacaran	b.l.d	138	b.l.d	8.6	551	4.77E+05	2.84	0.031	8.24	0.067	1.42	2.84	0.197	14.3	4.43	54.3	19.64	84.5	17.26	162	31.6	10620	1.16	33.3	42.6	88
MAR6_16	605	Ediacaran	70	130	100	19.8	788	4.89E+05	1.271	0.043	6.63	0.229	4.22	7.2	0.98	28.9	7.6	80.9	26.3	104.2	20.6	177	33	9390	0.333	18.37	39.1	47.1
MAR6_67	606	Ediacaran	b.l.d	152	b.l.d	7.9	575	4.92E+05	3.08	0.021	14.39	0.059	0.66	2.28	0.226	11.9	4.17	52.1	19.44	86	18.27	171	31.8	12050	1.29	61.6	80.8	164
MAR6_50	606	Ediacaran	b.l.d	194	b.l.d	6.72	871	4.84E+05	4.09	0.038	20.6	0.106	1.73	3.71	0.356	20.1	6.52	79.8	28.9	129	26.1	239	45.1	11770	1.707	100.7	156	271
MAR6_122	608	Ediacaran	5.3	201	180	9.2	925	4.79E+05	3.05	0.06	15.33	0.139	2.17	3.74	0.447	22	6.96	85.8	30.4	133.7	27	248	46.5	10900	1.467	65.5	107.3	173
MAR6_19	609	Ediacaran	5.50E+03	167	600	41	1075	4.32E+05	2.26	1.95	18.4	0.42	3.54	5.42	0.503	28.5	8.58	101.8	36.4	161	30.6	276	51.4	9710	0.873	63.8	114.6	162
MAR6_57	609	Ediacaran	8.2	180	b.l.d	7.8	1227	4.86E+05	2.71	0.091	19.3	0.183	2.93	6.01	0.448	31.3	9.76	115.7	42.2	184	37	327	62.1	12030	1.22	99.6	160	259
MAR6_3	610	Ediacaran	4.5	151	100	9.1	402	4.86E+05	2.01	0.042	8.69	0.055	0.73	1.41	0.23	8.39	2.93	37.2	14.23	64.3	13.44	130.6	26.4	11430	0.932	63.6	66.1	165
MAR6_81	613	Ediacaran	b.l.d	202	102	7.1	833	4.75E+05	4.15	0.034	20.1	0.082	1.52	3.1	0.32	19.2	6.08	76.5	27.6	121	24.5	226	43.3	11480	1.77	91.2	134.3	239
MAR6_118	613	Ediacaran	b.l.d	157	b.l.d	11.9	740	4.82E+05	4.02	0.039	10.25	0.11	2.04	4.23	0.321	20.9	6.19	71.5	25.4	107.3	20.8	196	37.1	9900	1.31	45.4	68	121
MAR6_76	614	Ediacaran	1000	108	125	13.1	655	4.70E+05	1.4	0.063	6.28	0.281	4.55	6.19	0.8	23.9	6.67	70.9	23	92	17.8	165	29.7	9280	0.566	16.03	27.6	41.4
MAR6_52	614	Ediacaran	10	137	b.l.d	11.4	302	4.92E+05	2.33	0.045	28.4	0.064	0.8	1.51	0.866	6.72	2.08	24.9	9.5	46.3	10.82	116.3	24.4	12610	0.942	51.5	110.5	134.8
MAR6_73	615	Ediacaran	200	132	210	12.8	681	4.83E+05	3.52	0.088	15.81	0.112	1.51	2.62	0.258	14.7	4.83	58.9	22.7	101.9	20.86	197	37.7	12440	1.57	75.7	98.3	198
MAR6_6	617	Ediacaran	b.l.d	220	140	7.1	919	4.82E+05	3.49	0.062	18.3	0.09	1.88	2.88	0.36	19.6	6.72	81.4	29.5	129.7	26.5	246	45.9	10870	1.519	85.3	122.6	207

MAR6_45	618	Ediacaran	b.l.d	140	140	11.7	567	4.87E+05	2.83	0.03	8.61	0.099	1.54	2.73	0.271	15.5	4.82	55	19.08	82.2	16.43	152.9	29.6	10390	0.992	35.7	51.1	90
MAR6_35	622	Ediacaran	9.3	55	107	1.8	236	4.92E+05	1.52	0.16	18.79	0.221	1.79	1.4	0.615	3.81	1.174	15.03	6.35	35.8	9.01	109.8	28.6	13340	0.239	83	105.4	207
MAR6_60	624	Ediacaran	303	33	136	2.1	207	4.79E+05	1.44	0.289	10.9	0.468	3.63	1.98	0.88	4.46	1.24	15.6	5.73	30.7	8.27	100.3	27.5	13190	0.358	106.1	35.1	263
MAR6_37	641	Ediacaran	210	103	140	6.5	338	4.85E+05	1.301	0.81	43.8	1.13	6.71	4.46	1.78	9.6	2.82	31.2	10	44.1	9.91	105.7	23	13870	0.238	68.6	62.8	169
MAR6_51	651	Ediacaran	45	370	1.20E+03	17	1363	5.03E+05	4.03	0.4	12.3	0.61	8.2	11.6	1.28	41.9	13.6	154	51.6	218	40.8	353	65.3	11770	1.42	72.8	117.7	174
MAR6_25	1119	Stenian	b.l.d	54	b.l.d	6.56	237	4.61E+05	1.81	0.024	4.69	0.044	0.59	1.07	0.118	5.43	1.81	21.5	7.78	36.1	7.41	75.4	16.1	1.16E+04	0.566	62.5	23.9	83.2
MAR6_10	1259	Ectasian	51	121	b.l.d	12.1	511	4.91E+05	4.07	0.59	19.9	0.72	4.4	3.7	1.3	11.7	3.88	48.1	16.5	73	15.5	148	26	13570	1.38	145.8	54	190
MAR6_48	1611	Statherian	5.2	107	b.l.d	10.4	357	4.87E+05	2.44	0.067	6.8	0.078	0.87	1.75	0.203	8.95	2.77	33.4	11.63	54.7	11.3	107.6	21.9	12670	0.841	175.3	37.3	188
MAR6_127	1611	Statherian	29.2	101	b.l.d	5.7	374	5.02E+05	3.97	0.099	9.69	0.129	1.18	1.7	0.166	7.93	2.38	31.3	11.94	61.1	14.81	168.5	38.2	13950	3.11	128.9	51.4	151.1
MAR6_95	1630	Statherian	183	84	b.l.d	7.6	344	4.70E+05	2.24	0.199	13.1	0.305	1.92	1.62	0.56	6.03	2.018	27	10.86	55	13.21	146	32.1	13710	1.064	462	162	443
MAR6_9	1661	Statherian	2.6	143	b.l.d	12	521	5.11E+05	2.77	0.044	10.59	0.097	1.45	2.45	0.229	12.94	4.16	48	17.09	76.3	15.03	145	27.4	11220	0.944	108.5	53	86.4
MAR6_21	1678	Statherian	46	145	300	13.1	1554	4.84E+05	9	0.13	16.8	0.2	3.29	6.59	0.33	39.1	13	155	56	245	47.8	412	75.1	13330	2.86	260	133.9	203
MAR6_20	1680	Statherian	b.l.d	111	113	8.2	415	4.67E+05	2.51	0.56	12.7	0.22	1.9	1.66	0.128	8.6	2.89	35.1	13.12	61	13.85	141	26.6	1.27E+04	1.18	183.2	68.3	158
MAR6_22	1697	Statherian	b.l.d	178	b.l.d	20.7	625	4.90E+05	2.54	0.055	11.54	0.128	2.05	3.33	0.507	17.1	4.98	58.5	20.43	90.7	18.58	168.1	31.7	10430	0.841	118.1	50.3	93.2
MAR6_63	1701	Statherian	b.l.d	104	b.l.d	4.9	438	4.75E+05	2.19	0.037	9.27	0.074	0.64	1.41	0.159	7.74	2.69	35.7	14.62	72.8	17.01	180	36.9	14090	0.868	290	111	250
MAR6_71	1717	Statherian	b.l.d	122	b.l.d	11.2	572	4.88E+05	3.4	0.049	13.18	0.099	1.39	2.65	0.28	14	4.2	53.8	19.45	90.4	18.56	179.6	35.2	11950	1.39	233	81.2	201
MAR6_129	1719	Statherian	b.l.d	90	b.l.d	6.9	349	4.90E+05	2.29	0.0396	8.8	0.04	0.73	1.41	0.108	7.37	2.45	32.2	11.62	54.5	11.43	111	21.54	12600	1.024	120.5	42.8	101.6
MAR6_112	1720	Statherian	b.l.d	61	b.l.d	3.31	214	4.78E+05	2.02	0.02	5.85	0.039	0.343	0.82	0.1	3.6	1.22	17.7	7.1	36.1	8.37	90.5	18	13170	0.903	168	50.7	139.9
MAR6_123	1726	Statherian	b.l.d	108	b.l.d	10.7	338	4.84E+05	2.56	0.085	9.64	0.116	0.82	1.17	0.22	5.27	1.8	24.8	10.24	52.8	12.84	139.8	29.6	14230	1.35	322	85.2	284
MAR6_33	1731	Statherian	b.l.d	162	b.l.d	17.7	576	4.80E+05	2.34	0.086	11.9	0.117	1.87	2.98	0.503	15.2	4.48	54.3	19.15	85.2	17.23	161	30.2	10200	0.841	116.1	45	95.4
MAR6_121	1732	Statherian	b.l.d	161	b.l.d	14.4	638	4.75E+05	2.81	0.032	11.8	0.088	1.83	3.84	0.268	17.47	5.5	61.7	22.01	95.3	19.14	172.3	32.9	11070	1.013	120.7	68.5	98.6
MAR6_116	1734	Statherian	b.l.d	147	b.l.d	15.1	532	4.87E+05	2.82	0.025	11.33	0.078	1.33	2.93	0.211	13.18	4.2	50.1	17.57	80.1	16.24	159	29.1	11180	1.06	123	61.9	105
MAR6_113	1735	Statherian	818	200	255	16.2	3080	4.60E+05	8.03	0.91	70.8	2.29	23.8	28.9	2.49	102.2	31	337	113.6	475	87.1	738	130.1	11220	3.36	437	268.8	402
MAR6_101	1736	Statherian	b.l.d	106	b.l.d	19.5	1327	4.79E+05	2.89	0.091	12.05	0.639	11.6	15.5	0.85	56.6	15.15	154	49.9	196.8	36.5	310	55.3	10270	0.846	88.5	83.8	78.5
MAR6_111	1746	Statherian	b.l.d	152	b.l.d	14.9	626	4.67E+05	5.18	0.025	12.03	0.139	1.87	3.8	0.275	17.7	5.33	61.4	21.13	91.8	18.33	173	32.1	10750	1.61	109.8	60.9	90.4
MAR6_86	1749	Statherian	27	102	210	25	408	4.76E+05	2.4	0.051	9.22	0.096	1.14	2.05	0.157	9.4	2.9	36.1	13.73	63	13.2	129.4	25.2	12240	0.961	155	62.5	132
MAR6_92	1755	Statherian	3.5	114	b.l.d	13.5	355	4.96E+05	2.02	0.029	6.78	0.068	1.22	1.93	0.11	9.9	2.94	34	12.09	52.3	10.57	94.3	18.7	10840	0.652	63	30.7	49.6
MAR6_66	1757	Statherian	3.4	134	b.l.d	13.1	480	4.80E+05	2.12	0.059	8.23	0.105	1.52	2.59	0.274	12.4	3.81	44.9	16.05	72.7	15.06	138.3	27.2	11060	0.884	113	37.3	93.5
MAR6_114	1761	Statherian	9.2	136	216	11.2	527	4.67E+05	7.15	0.228	15	0.242	2.86	3.12	0.44	14	4.21	48.7	17.76	78.5	16.63	155	30.4	11350	2.24	140.4	66.3	127
MAR6_49	1769	Statherian	6.5	162	161	13.8	699	4.92E+05	3.44	0.038	13.44	0.099	1.85	3.89	0.279	18.8	5.42	64.1	22.78	100.9	20.39	191	35.9	12020	1.28	143.7	81.6	122
MAR6_96	1770	Statherian	b.l.d	102	120	9.9	367	4.74E+05	2.96	0.028	9.45	0.063	0.8	1.8	0.11	9.81	2.81	35.2	12.93	56.4	11.34	105.3	19.6	12590	1.263	77.5	21.84	65.4
MAR6_83	1772	Statherian	30	148	b.l.d	15.7	883	4.80E+05	4.62	0.06	17.1	0.165	2.48	4.64	0.272	22	6.83	81.5	29.3	131.6	26.6	242	43.7	11930	1.76	249	116.1	202

MAR6_28	1778	Stathe rian	14	120	b.l.d	8.6	554	4.73E+05	3.6	0.03	13.55	0.077	1.19	2.27	0.167	13.1	4.18	51	18.95	83.8	17.4	155.8	30.6	12060	1.38	170.3	81.9	138
MAR6_97	1778	Stathe rian	b.l.d	157	b.l.d	14.6	597	4.85E+05	3.24	0.03	12.47	0.095	1.5	2.95	0.289	16.3	4.7	56.3	19.97	90.1	18.28	171	32.2	11470	1.22	130.5	74	121
MAR6_89	1784	Stathe rian	4.5	95	b.l.d	5.6	770	4.75E+05	11.05	0.042	16.21	0.07	1.14	2.68	0.26	14.78	5.11	68.1	26.16	122.1	26.8	259	49.5	1.49E+04	4.53	318.6	99.2	272
MAR6_41	1785	Stathe rian	7.1	127	b.l.d	8.3	655	4.82E+05	4.4	0.039	16.95	0.076	1.22	2.88	0.164	15.2	4.73	59.5	21.72	101.1	20.91	199	37.9	13810	1.55	285	118.2	222
MAR6_99	1787	Stathe rian	b.l.d	140	b.l.d	11.4	708	4.74E+05	7.2	0.031	16.7	0.133	2.18	4.21	0.191	20.4	5.91	69.9	24.31	106.8	21.4	193	36.3	1.16E+04	2.06	143.1	83.9	122
MAR6_36	1821	Orosini an	5.10E+03	101	610	5.1	367	3.87E+05	2.64	0.266	11.45	0.178	1.45	1.31	0.15	6.54	2.13	29.3	11.76	59.7	13.83	138.9	29	11070	1.22	257	127.5	253
MAR6_23	2002	Orosini an	43.5	404	b.l.d	7.2	1111	4.76E+05	10.74	0.202	13.9	0.215	1.98	1.46	0.42	8.15	4.11	68.8	33.6	199.6	52.4	566	112.3	12690	7.89	270	11.8	199
MAR6_8	2013	Orosini an	259	273	330	17.2	467	4.73E+05	1.87	0.728	17.13	0.509	3.26	2.98	0.769	10.4	3.26	39.6	14.75	71.4	15.58	154.8	31.9	12510	0.95	272	59	199
MAR6_94	2048	Orosini an	2.7	188	b.l.d	4.04	944	4.83E+05	5.22	0.041	18.29	0.048	0.78	2.19	0.549	16.7	6.1	77.4	30.18	141.4	30.4	299	59.5	12080	2.08	156.7	130.3	118.3
MAR6_1	2074	Rhyaci an	11.1	106	b.l.d	6.6	188	4.99E+05	0.839	0.053	4.75	0.052	0.59	0.7	0.216	3.68	1.21	15.9	6.21	28.8	6.97	73.3	16.3	11160	0.236	134	26.2	83.7
MAR6_24	2085	Rhyaci an	41	186	b.l.d	13.4	717	4.95E+05	2.22	1.45	22.1	1.4	10	5.79	1.13	17.7	5.27	62	22.1	101.3	21.83	214	42.8	11850	1.4	392	66.9	292
MAR6_70	2100	Rhyaci an	3.6	123	b.l.d	5.7	491	4.94E+05	1.69	0.041	15.67	0.052	0.66	1.32	0.235	6.92	2.6	34.4	14.3	73.8	17.72	185	38.1	12610	1.422	402	97.5	276
MAR6_17	2117	Rhyaci an	9.9	169	b.l.d	4.4	584	4.91E+05	2.51	0.032	12.76	0.045	0.82	1.83	0.37	11.3	3.96	48.7	17.84	82.4	17.7	171	34	1.17E+04	1.45	549	103.6	374
MAR6_7	2122	Rhyaci an	129	164	137	5.6	780	4.89E+05	1.51	0.166	50.1	0.711	10.4	10.8	4.42	29.6	7.07	72.3	24.4	105.1	22.45	221	46.6	11010	0.468	387	222.7	260
MAR6_12	2130	Rhyaci an	121	118	b.l.d	7	840	4.92E+05	1.96	0.179	16.8	0.42	4.51	6	1.06	27	7.1	81	28.3	123	24	231	44.5	11960	1.002	462	103	305
MAR6_107	2133	Rhyaci an	108	258	319	10.1	1090	4.73E+05	2.08	1.15	47.6	1.54	12	10	4.34	30	9.33	100.5	32.9	137.4	29.9	264	49.5	12210	1.02	441	146	312
MAR6_105	2146	Rhyaci an	12.7	148	b.l.d	8.1	597	4.86E+05	1.73	0.064	19.06	0.081	1.04	2.6	0.278	12.36	4.16	51.8	19.29	90.1	18.82	175.6	36.1	12010	0.827	383	123.6	252
MAR6_64	2148	Rhyaci an	5.8	150	b.l.d	12.5	475	4.75E+05	1.41	0.038	14.9	0.075	1.21	2.29	0.395	11.3	3.51	41.9	15.43	69.8	14.35	139	27.4	10850	0.556	235	94.1	155
MAR6_29	2156	Rhyaci an	64	82	b.l.d	18.2	335	4.81E+05	2.3	0.051	17.24	0.113	2.03	2.36	0.207	9.74	2.78	32.6	11.19	47.5	9.71	92.3	17.7	11580	0.819	257	83.4	171
MAR6_65	2159	Rhyaci an	16.3	189	b.l.d	7.7	501	4.89E+05	2.27	0.079	22.3	0.086	1.11	1.84	0.334	9.78	3.37	42.3	16.55	77.9	16.59	163.3	32.9	12700	0.93	416	186.9	271
MAR6_75	2171	Rhyaci an	48.1	211	170	7.4	1036	4.80E+05	3.94	1.09	20	0.494	3.62	3.76	0.611	21.4	6.84	87	34.1	156.7	32.9	319	59.5	1.21E+04	1.78	800	216	530
MAR6_5	2172	Rhyaci an	13.3	234	b.l.d	6.8	721	4.79E+05	1.84	0.023	17.3	0.078	1.2	2.72	0.44	15.9	5.01	63	23.7	104.3	21.59	209	39.3	11420	0.679	253	100.7	171
MAR6_103	2173	Rhyaci an	477	294	360	5.6	674	4.65E+05	1.84	0.79	22	0.54	4.1	3.31	0.77	15.55	4.72	57.7	21.14	97.4	20.8	199	40	10550	0.693	337	119.8	239
MAR6_2	2186	Rhyaci an	2250	220	b.l.d	34	759	4.82E+05	2	0.211	5.17	0.092	1.41	3.02	0.443	17.2	5.38	65.2	24.33	107.3	21.4	205	38.8	9250	0.64	169.3	51.6	105.9
MAR6_44	2206	Rhyaci an	157	162	b.l.d	23.6	508	4.64E+05	1.168	0.087	13.78	0.103	1.65	2.93	0.503	13.7	4.02	47.7	16.76	75.4	15.18	140.8	28.4	9830	0.482	176	76.4	110.6
MAR6_47	2552	Neoarc hean	b.l.d	474	b.l.d	7.6	1374	4.93E+05	10.4	0.0241	9.66	0.0256	0.36	1.54	0.368	14.69	6.66	106	45.8	236.6	54.5	575	118.9	13520	8.4	158.4	14.8	90.1
Discordant																												
MAR6_39			133	104	220	6.1	952	5.01E+05	4.96	0.419	38.1	0.84	6.64	5.65	1.43	18	5.77	73.1	29.1	141.3	30.7	311	64.8	12560	1.79	181.2	100.2	288.4
MAR6_54			30.9	88	10	5.6	445	5.08E+05	1.91	0.152	7.42	0.17	1.21	1.46	0.476	7.3	2.53	33.9	13.7	70.8	16.4	175	36.7	14050	0.658	267	58.3	287
MAR6_56			517	255	160	8.5	1153	4.74E+05	3.06	0.88	64	1.39	12	12.1	2.77	38.5	11.25	121.5	38.8	159.4	30.5	277	49.8	11040	1.076	326	126	286
MAR6_58			452	146	200	11.5	656	4.79E+05	3.02	0.368	27.7	0.447	3.28	3.55	0.75	14.4	4.34	53.5	20.54	95.7	20.72	207	41.1	13270	1.44	496	209	472
MAR6_69			40.3	90	160	4.4	244	4.78E+05	1.41	0.67	18.7	0.85	4.69	3.28	1.03	6.38	1.96	22	7.16	32.8	7.49	78	17.5	14210	0.891	254	63.2	252

Detection Limit			Al [ppm]	P [ppm]	Ca [ppm]	Ti [ppm]	Y [ppm]	Zr [ppm]	Nb [ppm]	La [ppm]	Ce [ppm]	Pr [ppm]	Nd [ppm]	Sm [ppm]	Eu [ppm]	Gd [ppm]	Tb [ppm]	Dy [ppm]	Ho [ppm]	Er [ppm]	Tm [ppm]	Yb [ppm]	Lu [ppm]	Hf [ppm]	Ta [ppm]	Pb [ppm]	Th [ppm]	U [ppm]
Minimum Detection Limit			2.3352	4.9127	65.553	1.4198	0.089795	3.857	0.027457	0.017992	0.021544	0.0090819	0.01	0.01	0.01	0.098874	0.01	0.01	0.01	0.01	0.01	0.01	0.01	0.01	0.0069757	0.014492	0.01	0.031181
Maximum Detection Limit			34.913	61.165	842.54	11.611	6.3321	1269.4	0.153 07	0.561	2.2199	0.167 22	1.1859	0.394 75	0.312 09	0.989 75	0.073 08	1.1447	0.147 06	0.753 42	0.065 933	1.1487	0.160 42	25.587	0.075 883	0.749 01	0.272 52	0.733 48
Mean Detection Limit			6.787 616	16.840838	293.55152	3.243 3531	0.563 4635	223.95648	0.067 1458	0.051 9195	0.089 2782	0.031 0046	0.171 1325	0.124 7235	0.052 4328	0.330 6818	0.022 9716	0.102 6066	0.024 5547	0.123 9594	0.022 2735	0.165 3246	0.028 1686	4.792 3232	0.024 258	0.110 0394	0.038 6914	0.136 6701
Median Detection Limit			6.4659	15.89	286.82	3.0768	0.224 59	7.5217	0.062 156	0.041 236	0.042 122	0.027 563	0.150 89	0.107 37	0.047 711	0.307 81	0.020 565	0.079 07	0.021 09	0.101 68	0.020 36	0.117 75	0.020 016	0.120 58	0.025 185	0.042 045	0.025 6	0.077 24
Associated Error			Al [ppm]	P [ppm]	Ca [ppm]	Ti [ppm]	Y [ppm]	Zr [ppm]	Nb [ppm]	La [ppm]	Ce [ppm]	Pr [ppm]	Nd [ppm]	Sm [ppm]	Eu [ppm]	Gd [ppm]	Tb [ppm]	Dy [ppm]	Ho [ppm]	Er [ppm]	Tm [ppm]	Yb [ppm]	Lu [ppm]	Hf [ppm]	Ta [ppm]	Pb [ppm]	Th [ppm]	U [ppm]
Minimum Absolute Error			1.5	10	53	0.75	11	14000	0.082	0.008 8	0.33	0.008 3	0.099	0.14	0.022	0.29	0.085	0.82	0.31	1.4	0.27	3.4	1.1	370	0.027	0.69	0.5	3.4
Maximum Absolute Error			2300	140	1100	15	330	36000	0.75	0.71	11	0.36	3.4	5.4	2.7	17	4	35	7.9	32	6	41	8.4	1200	0.47	43	46	50
Mean Absolute Error (±2σ)			71.741975	20	115.50617	2.321 358	50.185185	23765 .432	0.207 6173	0.062 7877	1.417 037	0.055 0407	0.482 3333	0.553 4568	0.137 1975	1.627 284	0.416 4444	3.821 1111	1.113 8272	4.893 8272	1.194 4444	13.17 1605	2.750 6173	798.3 9506	0.115 0494	8.027 1605	5.058 642	15.45 8025
Median Absolute Error (±2σ)			2.8	17	93	1.6	42	24000	0.19	0.02	0.9	0.024	0.27	0.37	0.061	1.2	0.31	2.7	0.87	3.9	0.93	12	2.4	810	0.094	4.9	4.1	14

M2AR 7-5 - Zircon compositional data (LA-ICP-MS, n = 78, b.d. = below detection limit)

Analysis ID	Best age (Ma)	Geological time	Al [ppm]	P [ppm]	Ca [ppm]	Ti [ppm]	Y [ppm]	Zr [ppm]	Nb [ppm]	La [ppm]	Ce [ppm]	Pr [ppm]	Nd [ppm]	Sm [ppm]	Eu [ppm]	Gd [ppm]	Tb [ppm]	Dy [ppm]	Ho [ppm]	Er [ppm]	Tm [ppm]	Yb [ppm]	Lu [ppm]	Hf [ppm]	Ta [ppm]	Pb [ppm]	Th [ppm]	U [ppm]
MAR7_65	525	Cambrian	b.d	147	b.d	13.92	746	5.10E+05	5.55	0.047	14.89	0.121	2.06	4.19	0.274	21.8	6.74	75.2	24.58	106.1	20.6	186.5	32.89	12790	2.02	68.2	111.9	213.5
MAR7_47	577	Ediacaran	14	174	b.d	18.3	1171	5.06E+05	1.533	0.069	12.44	0.264	4.38	8.43	1.45	38.7	10.88	120.7	40.6	170.1	32.81	295.6	53.7	10530	0.542	31.45	76.8	88.3
MAR7_11	582	Ediacaran	118	178	b.d	28	940	5.15E+05	5.68	1.49	39.3	2.57	17	14.8	5.5	34.8	10.2	102	29.9	130	27.1	251	46.3	13210	2.2	165.7	286.4	469
MAR7_8	588	Ediacaran	b.d	184	b.d	7.5	986	5.05E+05	4.22	0.047	7.37	0.163	2.97	5.26	0.431	27.4	8.37	97.9	33.44	141.6	27.38	248.8	45.5	10910	1.789	43.8	48.4	120.4
MAR7_89	595	Ediacaran	42	117	b.d	7.1	661	4.90E+05	5.52	0.19	13.94	0.266	2.39	3.78	0.43	15.6	5.03	61	21.4	97.4	19.4	182	33.8	12800	2.23	94.6	125	266

MAR7_19	597	Ediacaran	39.4	191	b.d	9.4	1241	4.97E+05	5.19	0.64	27.3	0.81	6.85	7.5	1.7	35.4	10.7	120.6	39.9	173.6	33.18	308	56.5	11290	2	102.8	147.6	281
MAR7_77	602	Ediacaran	b.d	114	b.d	8.15	678	4.95E+05	3.54	0.047	24.66	0.112	2.28	4.02	0.385	18.91	5.65	65.1	22.32	102.2	20.71	194.9	37.6	11930	1.564	87.6	171.2	240.1
MAR7_6	612	Ediacaran	68	194	b.d	12.6	908	5.00E+05	3.18	0.225	17.12	0.417	4.24	5.34	1.04	23.1	7.21	85.7	29	133.6	26.78	244.5	46.8	11660	1.366	74.5	107.2	199.8
MAR7_56	612	Ediacaran	7.6	144	b.d	4.82	371	4.89E+05	1.74	0.034	8.31	0.054	0.7	1.58	0.47	9.25	3.03	33.1	11.14	48.31	9.16	83.8	15.5	13360	0.871	63.7	131.9	170.5
MAR7_62	616	Ediacaran	12.6	175	b.d	8	727	5.14E+05	3.5	0.048	16.88	0.07	1.11	2.55	0.26	15.61	5.31	66.4	23.48	107.3	21.65	203.8	38.6	12230	1.49	74.9	104.7	196.2
MAR7_5	625	Ediacaran	50	199	b.d	12.2	1295	5.01E+05	3.14	0.23	17.88	0.406	4.99	7.2	0.94	35.4	11.13	128.6	43.3	188.2	35.8	322	60.3	11670	1.401	87.9	138.2	230
MAR7_42	632	Ediacaran	5.1	54	b.d	1	157	4.91E+05	1.76	0.102	2.2	0.14	1.17	0.49	0.21	1.39	0.47	7.6	4.25	31.3	10.12	135.4	33.9	12630	0.85	23.3	7.4	57.9
MAR7_81	652	Cryogenian	51	69	b.d	3.1	562	4.81E+05	1.44	0.082	13.61	0.102	1.07	1.63	0.903	8.5	2.61	35.8	15.22	82.9	20.98	248	65.6	11380	0.193	127.2	83.8	317
MAR7_1	661	Cryogenian	87	227	b.d	20.9	803	5.19E+05	2.25	0.224	25.8	0.31	1.97	3.6	0.815	17.51	5.53	71	24.74	119.1	25.31	248.1	51.1	11550	1.015	53.3	112	131.5
MAR7_21	683	Cryogenian	21.6	105	b.d	3.02	57.3	5.07E+05	0.713	0.045	2.31	0.0261	0.25	0.44	0.245	1.52	0.423	5.11	1.774	8.5	1.79	20.7	4.76	8560	0.373	140	49.5	326
MAR7_74	718	Cryogenian	188	160	4.00E+03	16	1480	4.73E+05	2.23	1.07	25.4	0.44	4.7	9.8	2.81	33.7	11.7	131.5	45.9	212	43.5	411	72.6	11120	0.93	106.3	235	222
MAR7_66	789	Tonian	61	681	b.d	12.1	1705	4.77E+05	1.204	0.043	1.168	0.067	1.28	4.72	0.107	36.1	13.82	172.3	57.1	242.4	44.9	388	69.6	13070	0.528	144.3	51.8	296
MAR7_22	810	Tonian	27	285	900	3.9	1158	5.15E+05	1.44	0.355	22.1	0.5	6.18	8.9	3.64	38	10.78	113.7	37.5	162	35.8	340	70.7	11270	0.42	101	152	202
MAR7_43	1674	Statherian	10	151	b.d	13.7	593	5.11E+05	3.1	0.051	9.89	0.114	1.22	2.7	0.254	14.66	4.7	55.7	19.66	88.7	17.72	169	31.3	11880	1.069	104.7	51.1	93
MAR7_24	1693	Statherian	b.d	81	b.d	5.52	340	5.03E+05	3.02	0.05	10.33	0.037	0.55	1.18	0.12	5.95	2.13	26.6	10.38	54.6	12.26	121.8	25	13210	1.53	227.2	64.2	201.8
MAR7_57	1707	Statherian	4.1	157	b.d	10.9	881	4.89E+05	3.99	0.032	18.65	0.121	1.4	3.99	0.196	21.8	6.75	81.9	29.41	132.9	25.53	240.5	43.9	12570	1.467	197.6	116	171.9
MAR7_15	1727	Statherian	10.3	92	b.d	13.7	492	5.06E+05	3.98	0.118	7.54	0.104	1.31	3.02	0.293	13.4	4.26	46.9	16.22	72.6	14.45	137.5	26.3	12260	1.529	104.3	37.7	90.7
MAR7_2	1742	Statherian	238	191	b.d	25.5	1131	4.98E+05	2.46	0.31	11.41	0.53	7.78	9.52	0.689	39.2	10.98	120.9	39.7	168.7	31.5	287	53.1	9710	0.752	79	64.4	67.6
MAR7_40	1748	Statherian	b.d	171	b.d	15.1	594	5.07E+05	2.49	0.04	9.36	0.079	1.5	2.85	0.247	14.62	4.38	54.7	19.48	87.9	17.69	168.4	32.1	11230	0.701	97.5	52.7	83.1
MAR7_30	1778	Statherian	4.4	101	b.d	10.3	796	5.00E+05	2.84	0.087	17.6	0.209	3.42	5.49	0.34	22.8	6.9	78.7	26.8	116.3	22.64	204.3	37.7	12290	0.974	172.6	92	144.1
MAR7_27	1945	Orosinian	21	379	340	10.7	1263	4.85E+05	6.22	0.26	20.1	0.31	4.2	5.7	0.69	29.8	9.82	121.5	42.6	192.6	37.1	338	61.5	11610	1.81	125.5	50.7	87.7

MAR7_9	2024	Orosinian	55.3	157	b.d	9.7	231	4.87E+05	1.011	0.052	3.76	0.16	2.89	5.29	0.323	16.7	3.65	30.9	7.87	28.6	5.19	43.4	7.36	11990	0.261	190.8	61	148.7
MAR7_33	2104	Rhyacian	51	214	b.d	18.5	975	4.87E+05	2.14	0.71	60	0.95	7.4	7.6	2.18	23.7	7.49	88.5	28.8	136.8	29.3	284	53.4	11050	0.764	155	124	117.8
MAR7_58	2111	Rhyacian	9.4	187	b.d	14.3	804	5.05E+05	1.304	0.052	14.15	0.112	2.53	4.46	0.712	22.9	6.41	74.2	26	114.5	22.7	219	41.7	10430	0.535	206	107.1	142.8
MAR7_51	2123	Rhyacian	29.9	181	b.d	5.46	1105	5.06E+05	9.14	0.036	15.95	0.075	1.45	3.91	0.329	23.46	7.96	98.2	37.5	171.4	33.9	310.6	58.4	13490	3.33	530	115.1	342
MAR7_36	2206	Rhyacian	18.1	176	b.d	10.8	886	4.91E+05	1.9	0.115	11.89	0.133	1.62	2.98	0.606	18.4	5.79	71.5	26.8	132.2	28.9	281	56.4	10740	0.697	208.2	82.6	141
MAR7_61	2233	Rhyacian	103	146	b.d	23.5	1241	5.01E+05	1.96	0.063	13.96	0.254	3.73	6.41	1.97	29.7	8.7	102.2	39.4	184	38.9	381	75.3	9280	0.529	259.4	120.8	190.9
MAR7_64	2285	Rhyacian	38.2	241	b.d	8.3	982	5.04E+05	2.28	0.42	18.41	0.194	1.74	3.31	0.571	17.1	5.99	78.3	30.5	149.4	31.1	305	61.7	13250	1.351	518	167.8	345
MAR7_49	2514	Neoarchean	36	197	b.d	8.1	926	5.03E+05	3.24	0.079	11.8	0.132	1.42	2.48	0.8	15.8	5.74	73.5	29.4	138.8	28.74	272.5	51	12910	1.69	471	99.5	263
MAR7_18	2605	Neoarchean	23.1	245	b.d	7.9	959	5.07E+05	9.28	0.229	14.88	0.108	1.16	2.23	0.234	15.6	6.14	76.6	29.53	146.1	30.5	294	54.8	12010	4.24	550	111.7	278
MAR7_52	2616	Neoarchean	11.2	203	b.d	10	862	5.10E+05	3.11	0.082	13.51	0.1	1.49	3.07	0.462	18.1	5.66	74.3	26.8	124.1	25.6	240	45.6	11950	1.032	93.3	42.3	45.4
MAR7_69	2731	Neoarchean	b.d	264	b.d	17.6	820	5.02E+05	2.51	0.044	48.5	0.148	2.64	5.21	1.139	24.2	6.76	77.6	26.6	118.7	23.6	229.6	43.4	10790	0.648	125.8	98.3	66.9
MAR7_41	2776	Neoarchean	8.6	194	b.d	6.55	422	5.06E+05	1.593	0.057	18.16	0.08	0.89	2.02	0.441	9.35	3.11	37.6	13.58	66.4	13.81	137.3	27.7	11440	0.758	208	29.2	104.3
MAR7_55	3055	Mesoarchean	340	130	610	28	900	4.85E+05	2.59	1.8	19.9	1.53	8.8	6.36	3.43	22.9	6.96	77.3	27	125.6	26.8	292	60.1	13560	1.56	902	101	426
MAR7_75	3371	Paleoarchean	42.7	331	b.d	7.32	1790	5.18E+05	2.24	0.128	19.6	0.347	5.16	8.9	2.78	48.3	14.1	157	55.6	260	51	510	103	10910	0.55	860	197	350
Discordant																												
MAR7_10			510	290	165	54	1002	4.74E+05	4.73	0.95	81.5	0.65	6.72	8.24	2.05	35.1	9.39	100.1	32.5	139.7	27	252.1	47.2	10510	1.721	373	288	256.9
MAR7_20			152	162	260	14.2	536	5.04E+05	5.74	1.75	37.7	3.77	31.6	23	6.4	34.4	7.16	60.5	17.04	68.2	14.5	152.6	32.2	11160	3.46	350	304	770
MAR7_23			330	229	610	10.8	849	4.93E+05	6.97	0.268	7.71	0.192	1.27	1.92	0.321	13.1	5.13	68.5	26.04	130	27.77	264.8	52.2	12070	2.97	20.18	45.6	52.7
MAR7_25			175	206	130	35.8	1030	5.24E+05	9	1.1	30	2.18	14.3	12.1	5.8	39	11.1	116	34.3	145	31.3	255	47.8	13180	2.82	218.9	124	226
MAR7_28			750	187	177	25.1	550	4.99E+05	4.17	0.9	30.8	1.04	7.1	5.8	1.71	11.9	3.79	45.9	16.4	81.8	19.08	205	41.1	13560	3.02	911	252	755
MAR7_34			1380	219	100	18.7	861	4.86E+05	3.5	0.24	16.5	0.266	2.64	4.31	0.61	20.9	6.82	79.4	28.7	125.9	25.6	233	43.5	10580	1.25	70.9	111.6	188

MAR7_53			130	230	2.30E+03	15.4	606	4.93E+05	2.99	0.32	8	0.31	2.64	2.7	0.51	14.7	4.28	53.9	18.7	89.2	17.2	170	35.2	1.16E+04	0.93	171	51.1	186
MAR7_54			43	122	23	9.6	650	5.16E+05	1.85	0.051	14.31	0.164	2.81	4.71	0.903	20	5.81	64.5	21.34	91.2	18	168	32.8	9800	0.463	22.2	58.9	58.7
MAR7_67			22.8	157	140	12.4	1345	5.03E+05	4.02	0.064	11.55	0.383	6.38	10.4	0.78	46.9	12.81	140.9	46.7	196.5	36.8	322	61.4	11520	1.199	119.7	89.2	112.6
MAR7_76			15.8	143	20	16.5	578	5.00E+05	1.44	0.062	14.63	0.124	1.5	2.49	0.568	13.64	4.17	53	18.87	87	18.16	172	34.7	11400	0.605	212.6	91.5	152.2
MAR7_78			160	109	420	22.6	429	5.03E+05	4.24	0.148	8.88	0.141	1.11	2.21	0.18	9.1	2.92	37	13.63	67.5	15	150.9	29.6	13520	1.72	163.3	49.5	167
MAR7_80			20.1	156	68	7.83	741	4.66E+05	7.83	0.051	16.58	0.097	1.52	2.53	0.134	13.19	4.54	60.5	22.38	119.1	26.4	273	52.9	13840	4.23	539	218.9	515
MAR7_82			9	189	34	16.6	554	4.89E+05	1.78	0.051	7.15	0.141	2.32	3.84	0.289	17.77	4.78	54.9	18.64	80.6	15.86	147.8	28.2	11250	0.561	186.2	114.2	132.6
MAR7_84			19.9	193	126	8.5	2326	4.88E+05	5.12	0.092	22.92	0.719	12.64	19.4	0.603	76.7	21.14	249.2	85.7	363.3	69.2	614	108.9	12100	2.53	301	232.2	252.9
MAR7_85			148	280	250	26.5	1319	4.79E+05	2.99	1.78	22.8	2.72	17.8	13.9	5	40.6	11.9	129.3	43.1	188.6	38	353	66	10250	1.174	520	209.4	391
MAR7_87			4.4	58	11	2.72	276.4	4.89E+05	1.3	0.041	17.44	0.04	0.57	1.06	0.495	5.85	1.671	21.13	8.12	42.2	9.8	114.4	25.6	13090	0.493	272	59.7	141.1
MAR7_90			114	158	168	21	855	5.04E+05	3.2	1.18	24.2	1.98	12	9.38	3.5	27.5	8.05	85.2	26.5	113	22.46	221.8	40.6	13300	1.312	263	145.6	253.2
MAR7_93			37.8	107	92	7.74	932	4.98E+05	2.32	0.378	16.22	0.36	4.17	4.87	1.47	21	6.31	74.9	28.5	137	29.5	309	62.6	11040	0.676	366	86.7	242
MAR7_94			146	50	130	28.5	958	4.84E+05	2.85	0.32	9.05	0.28	4.01	6.6	0.84	31.5	9	100.9	33.4	139.7	27.1	246	47.1	9980	1.03	45.2	73.9	117.3
MAR7_97			190	118	119	41	759	4.99E+05	1.95	0.41	18.7	0.28	2.16	3.2	0.74	14.09	4.42	56.3	21.69	109.2	24.1	246	50.6	12700	0.927	466	134.2	332
MAR7_98			100	116	160	12.5	561	4.92E+05	4.06	0.69	10.6	0.64	5	4.36	0.89	12.5	3.97	48.1	17.03	82.5	17.78	183.8	36.9	13560	1.52	260.5	68.7	522
MAR7_99			48	22	530	3.2	690	5.05E+05	5.46	0.3	38.1	0.3	2.18	2.66	1.29	11.4	3.62	49.5	21.3	102	24	275	62	12400	1.33	140	166	358
MAR7_100			10.4	117	120	15.3	533	4.93E+05	1.61	0.057	16.16	0.079	1.12	2.18	0.41	12.45	3.82	46.9	17.27	79.9	16.55	162	31.84	11250	0.642	239.7	94.5	157.7
MAR7_101			23	70	-20	3.82	397	4.89E+05	1.432	0.091	27.7	0.137	1.37	1.98	0.85	9.07	2.61	29.64	11.48	58	13.13	147.4	31.5	11450	0.735	94.2	137.9	248
MAR7_102			10.9	194	-44	17	703	5.01E+05	2.01	0.183	31.7	0.302	2.66	4.06	1.27	17.7	5.08	60.5	21.39	100.3	21.47	212.9	43.5	10740	0.714	186.7	108.9	136.9
MAR7_103			64	86	-50	8.6	637	4.63E+05	6.1	0.054	12.37	0.133	1.72	3.66	0.209	17.09	5.11	60.5	21.47	95.7	19.09	178.7	33.1	11310	2.18	128.7	73	124.8
MAR7_105			1990	171	580	50	1660	4.69E+05	18.8	1.84	83	2.32	17.4	17.6	7.02	49	14.6	176	55.3	246	49.5	457	82.8	10790	3.01	181	104	353

MAR7_106			75	63	170	6.7	481	5.00E+05	5.51	0.318	6.99	0.35	2.45	2.36	0.68	8.17	2.93	37.9	14.22	74	17.56	193.6	39.6	14910	3.22	168.9	107.3	444
MAR7_111			2	429	-104	12.1	1488	4.91E+05	3.01	0.048	6.12	0.106	1.99	4.82	0.241	29.2	10.29	131.8	49.7	233.7	45.9	441	80.8	12960	1.364	221.7	127.5	304
MAR7_113			362	180	410	36	701	4.98E+05	3.18	1.37	21.7	2.18	17.4	11.2	3.6	28	7.1	74	22.9	105	22.2	236	47.3	13250	1.57	683	153	498
MAR7_114			880	182	80	15.9	1080	4.72E+05	1.82	0.061	20.8	0.194	2.31	5.03	1.5	26.6	7.9	100	36.2	166	36.7	374	72.1	10570	0.591	45.5	44.2	67.4
MAR7_115			118	197	150	14.5	1163	4.90E+05	16.8	0.84	19.5	0.98	7.2	6.6	1.59	25.3	7.91	98.2	36.4	175.8	37.2	364	72	13140	9.5	1085	164.1	759
MAR7_118			221	591	250	22.6	1790	4.93E+05	1.51	0.47	5.5	0.75	7.7	9.6	1.49	41.9	14.26	172.4	58.7	251	48.6	445	79.7	12740	0.48	61.3	69.5	167
MAR7_120			9.1	110	0	13.1	1177	4.80E+05	2.9	0.062	11.4	0.155	2.76	6.56	0.399	32.9	9.56	109.7	39.5	169.3	31.8	297	53	11360	1.017	174.3	103.2	144
MAR7_121			-1.8	128	40	16.7	1333	4.75E+05	2.12	0.048	7.24	0.374	6.68	11.45	1.18	49.4	12.61	139.1	45.3	188	34	305	53.9	10090	0.691	81.8	61	67
MAR7_122			370	106	170	5	547	4.82E+05	5.56	0.118	12.46	0.112	1.12	2.09	0.18	8.86	3.11	41.3	16.12	82.2	18.69	195.7	40	13230	2.58	207	215	553
MAR7_123			44	85	-40	4.68	324	4.77E+05	5.9	0.114	8.02	0.104	1.05	1.41	0.106	7.8	2.54	31.1	11.14	50.3	10.2	90.6	17.4	14700	2.01	138	44.3	179
MAR7_126			151	260	450	13.8	1167	4.86E+05	3.2	0.99	18.25	1.06	7.5	7.33	2.75	24.6	7.75	94.9	35.02	176	38.6	407	86.3	9820	0.83	282.4	120.4	279
Detection Limit			Al [ppm]	P [ppm]	Ca [ppm]	Ti [ppm]	Y [ppm]	Zr [ppm]	Nb [ppm]	La [ppm]	Ce [ppm]	Pr [ppm]	Nd [ppm]	Sm [ppm]	Eu [ppm]	Gd [ppm]	Tb [ppm]	Dy [ppm]	Ho [ppm]	Er [ppm]	Tm [ppm]	Yb [ppm]	Lu [ppm]	Hf [ppm]	Ta [ppm]	Pb [ppm]	Th [ppm]	U [ppm]
Minimum Detection Limit			2.163	7.1833	157.55	0.95592	0.10601	2.3661	0.022859	0.014625	0.016551	0.01	0.01	0.01	0.01	0.10252	0.01	0.01	0.01	0.01	0.01	0.01	0.01	0.01	0.01	0.012458	0.0090053	0.068755
Maximum Detection Limit			22.989	64.349	1026.3	8.5124	11.251	561.21	0.26233	0.42819	3.3973	0.31782	1.4131	0.57515	0.54711	1.1469	0.42858	3.9349	0.32817	0.93168	0.24444	2.1198	0.25608	22.779	0.11377	0.68086	1457.9	1234.7
Mean Detection Limit			6.5182582	23.244305	347.02494	2.1343673	0.6462827	103.07711	0.0718702	0.0631497	0.1041798	0.0385825	0.1975921	0.1282703	0.0617051	0.3567833	0.0285516	0.1602602	0.0281104	0.1236991	0.0244775	0.1490744	0.0261515	2.6645643	0.0280919	0.1031435	61.109981	64.388772
Median Detection Limit			6.0579	21.423	331.56	1.9396	0.26704	9.4259	0.065414	0.046518	0.052043	0.028568	0.169	0.11437	0.052095	0.31306	0.020478	0.10948	0.0203	0.095077	0.018185	0.098136	0.020699	0.16026	0.02407	0.032561	10.07	18.397
Associated Error			Al [ppm]	P [ppm]	Ca [ppm]	Ti [ppm]	Y [ppm]	Zr [ppm]	Nb [ppm]	La [ppm]	Ce [ppm]	Pr [ppm]	Nd [ppm]	Sm [ppm]	Eu [ppm]	Gd [ppm]	Tb [ppm]	Dy [ppm]	Ho [ppm]	Er [ppm]	Tm [ppm]	Yb [ppm]	Lu [ppm]	Hf [ppm]	Ta [ppm]	Pb [ppm]	Th [ppm]	U [ppm]

Minimum Absolute Error		1.5	16	59	0.58	3.8	9200	0.057	0.011	0.099	0.0096	0.1	0.14	0.021	0.28	0.054	0.52	0.073	0.45	0.1	1.1	0.19	270	0.026	0.67	0.012	0.024
Maximum Absolute Error		550	590	3800	22	250	24000	2.5	0.6	13	0.95	6.5	5.1	3.1	12	3.1	26	8.5	37	6.7	67	12	1100	1	120	29	34
Mean Absolute Error (±2σ)		47.998734	40.582278	207.49367	3.2629114	44.802532	15072.152	0.2716456	0.1048861	1.4150506	0.1208304	0.8618987	0.8151899	0.2591139	1.9835443	0.505443	4.968481	1.4929494	6.2759494	1.3483544	12.632911	2.295443	435.31646	0.1121519	11.052025	8.6927551	11.330837
Median Absolute Error (±2σ)		11	24	100	1.5	34	15000	0.19	0.049	0.8	0.046	0.4	0.43	0.1	1.3	0.34	3.4	1	4.6	1	10	1.9	420	0.078	6.8	5.9	9

M2AR 7-2 - Zircon compositional data (LA-ICP-MS, n = 74, b.d. = below detection limit)

Analysis ID	Best age (Ma)	Geological time	Al [ppm]	P [ppm]	Ca [ppm]	Ti [ppm]	Y [ppm]	Zr [ppm]	Nb [ppm]	La [ppm]	Ce [ppm]	Pr [ppm]	Nd [ppm]	Sm [ppm]	Eu [ppm]	Gd [ppm]	Tb [ppm]	Dy [ppm]	Ho [ppm]	Er [ppm]	Tm [ppm]	Yb [ppm]	Lu [ppm]	Hf [ppm]	Ta [ppm]	Pb [ppm]	Th [ppm]	U [ppm]
X7_2_84	505	Cambrian	n.m	n.m	b.d	19.2	1002	5.33E+05	n.m	0.19	24	0.413	5.65	7.49	1.465	31.1	8.99	96	32.3	145	30.61	310.1	62	14040	n.m	334	393	1106
X7_2_19	517	Cambrian	n.m	n.m	360	18.3	2260	5.03E+05	n.m	1.73	29.4	1.5	13.5	15.1	4.8	61.8	19.1	218	76.9	338	67.1	626	113.3	11170	n.m	130.1	269	418
X7_2_49	539	Cambrian	n.m	n.m	b.d	16.8	1307	4.96E+05	n.m	0.33	26.65	0.234	3.7	6.45	2.25	34.2	10.49	123.2	44.2	205.8	42.4	409	77.2	10070	n.m	29.93	96.9	93.9
X7_2_129	555	Ediacaran	n.m	n.m	b.d	18.5	3550	5.28E+05	n.m	0.72	14.86	0.37	3.88	8.97	1.34	57.9	22.72	306.8	122.2	579	121.9	1179	217.2	12470	n.m	44	78.6	126.1
X7_2_69	559	Ediacaran	n.m	n.m	b.d	19.5	3300	5.11E+05	n.m	0.64	45.7	0.8	9.7	14.51	4.73	75	25.11	309.3	117	524	107.3	1010	190.9	11960	n.m	68.4	246	208
X7_2_2	560	Ediacaran	n.m	n.m	b.d	10.43	1093	5.00E+05	n.m	0.042	13.37	0.172	2.67	5.32	1.24	27.5	8.3	101.1	37	166	34.1	323	59.3	10190	n.m	55.6	105.5	159.1
X7_2_5	563	Ediacaran	n.m	n.m	b.d	11.15	4190	5.09E+05	n.m	0.02	22.6	0.248	5.46	15.74	5.93	112.6	36.6	431	149.7	608	109	940	163.9	11450	n.m	27.2	133	79.2
X7_2_6	566	Ediacaran	n.m	n.m	b.d	20.1	1590	5.29E+05	n.m	0.93	29.1	1.68	15.1	18.2	4.8	56.2	15.3	162.4	57.1	256	51.6	473	91.2	10840	n.m	187.2	415	543
X7_2_61	567	Ediacaran	n.m	n.m	b.d	23.8	479	5.18E+05	n.m	0.079	10.11	0.053	0.459	0.89	0.482	6.5	2.74	43.2	18.28	94.6	21.74	206.3	34.1	10180	n.m	12.37	35	36.1
X7_2_52	572	Ediacaran	n.m	n.m	b.d	15.3	2890	4.93E+05	n.m	0.105	2.93	0.384	6.07	12.33	1.045	69.7	22.7	285	101.2	447	84.7	759	129.1	10730	n.m	57.5	115.3	169.1
X7_2_64	583	Ediacaran	n.m	n.m	b.d	20.4	745	5.15E+05	n.m	0.392	41.9	0.931	11.57	13.56	4.67	42.6	9.79	88.4	25.5	95	16.9	147.9	26.7	9920	n.m	47.1	238	134.7
X7_2_87	583	Ediacaran	n.m	n.m	b.d	48	1173	5.29E+05	n.m	0.289	7.54	0.387	4.84	8.46	0.91	39.6	11.32	127.1	40.5	172.3	32	285	52.6	10040	n.m	29.3	61	86.1
X7_2_9	584	Ediacaran	n.m	n.m	235	20.5	1130	4.92E+05	n.m	1.35	14.4	1.49	11.9	15	4.56	54.9	14.1	128	34.5	134	26.8	263	50.6	11680	n.m	140	205	413
X7_2_91	590	Ediacaran	n.m	n.m	b.d	18.5	741	5.40E+05	n.m	1.26	60.3	1.51	11.7	8.22	1.9	23.2	6.5	68.9	22.9	106.5	22.28	217.8	43.3	12120	n.m	148.7	369	431
X7_2_94	591	Ediacaran	n.m	n.m	b.d	26.2	694	5.22E+05	n.m	1.17	23.4	1.66	12.5	8.5	2.28	25.2	7.27	76.1	22.7	89.6	17.99	157.9	27.5	12900	n.m	100.4	121.2	287.2
X7_2_30	594	Ediacaran	n.m	n.m	b.d	8.5	1114	5.14E+05	n.m	0.62	27.8	0.613	5.94	7.15	1.33	31.2	9.51	110.5	38.1	170.1	32.64	295	51.2	11580	n.m	104.4	133.4	300.1
X7_2_112	599	Ediacaran	n.m	n.m	b.d	16.6	1031	5.58E+05	n.m	0.058	12.75	0.24	3.58	5.93	0.823	27.6	8.44	97.4	35.26	152.1	28.56	257.3	49.8	11110	n.m	47.07	82.1	124.6
X7_2_45	607	Ediacaran	n.m	n.m	b.d	19.9	665	5.37E+05	n.m	0.524	89.9	0.577	5.08	5.18	1.59	19.59	5.75	64.2	21.14	94	19.14	182.1	35.1	12390	n.m	62.1	109.8	169.4

X7_2_38	608	Ediacaran	n.m	n.m	b.d	21	2770	5.13E+05	n.m	0.424	40.5	0.618	7.21	13.13	5.1	69.3	21.7	257	86.2	386	76	724	136.8	13020	n.m	93.6	300	261
X7_2_53	613	Ediacaran	n.m	n.m	b.d	6.7	870	5.13E+05	n.m	0.102	12.5	0.165	2.98	4.6	1.11	22.9	7.1	84	28.4	129	25.5	238	43.8	11990	n.m	64.2	156	178
X7_2_1	613	Ediacaran	n.m	n.m	b.d	18.6	473	4.88E+05	n.m	0.57	5.64	0.222	1.71	2.06	0.423	11.32	3.7	43.2	16.35	69.9	14.34	137	25.7	8870	n.m	21.2	24.9	56.2
X7_2_63	623	Ediacaran	n.m	n.m	b.d	21.5	813	4.96E+05	n.m	0.084	23.4	0.677	10.04	12.49	5.16	35.3	8.69	86.3	26.7	108.2	22.09	205.8	36.1	9550	n.m	184.9	376	478
X7_2_39	630	Ediacaran	n.m	n.m	b.d	12.63	832	4.93E+05	n.m	0.151	39.6	0.143	2.28	4.17	1.38	20.5	6.21	75.1	27.5	129.6	28.1	284	55	8550	n.m	28.1	84.3	73.8
X7_2_116	634	Ediacaran	n.m	n.m	b.d	6.76	1175	5.46E+05	n.m	0.109	67.7	0.434	6.75	10.75	2.02	39.8	10.78	115.7	39.2	165.2	32.6	303.4	57.7	10380	n.m	89	330	223.6
X7_2_104	641	Cryogenian	n.m	n.m	b.d	3.79	323	4.90E+05	n.m	0.028	5.73	0.023	0.225	0.6	0.327	4.77	1.68	23.1	9.81	53.8	13.08	149.9	34.2	10890	n.m	39.5	43.1	102
X7_2_18	646	Cryogenian	n.m	n.m	b.d	21.9	495	5.16E+05	n.m	0.109	2.82	0.154	1.75	2.72	1.88	14.74	4.55	50.4	17.66	76	14.84	136.8	27.79	6560	n.m	8.39	12	21.82
X7_2_65	647	Cryogenian	n.m	n.m	b.d	11.3	938	5.34E+05	n.m	0.114	13.26	0.129	1.28	2.7	0.767	15.09	5.44	72.9	30	152.7	35.8	387	83.6	12130	n.m	52.2	72.5	131.4
X7_2_44	656	Cryogenian	n.m	n.m	270	9.89	795	5.17E+05	n.m	1.38	19.8	0.51	4.7	5.22	1.61	21.8	6.4	75.5	26	118.7	25	237	43	12040	n.m	121.1	211	313
X7_2_26	666	Cryogenian	n.m	n.m	b.d	13	1200	5.08E+05	n.m	0.32	19.6	0.42	3.38	4.76	0.84	25.3	8.8	112	39.6	177	37.4	349	65.5	11330	n.m	86.6	104	217
X7_2_114	678	Cryogenian	n.m	n.m	251	24.8	2109	5.66E+05	n.m	0.88	12.7	1.51	12.2	13.1	4.67	45.9	16.08	194.1	73	327	66.4	613	115.5	13910	n.m	128.8	136.9	296
X7_2_108	681	Cryogenian	n.m	n.m	b.d	18.3	317	5.54E+05	n.m	0.052	20.62	0.122	1.53	2.89	0.91	9.6	2.72	29.3	10.22	44.4	9.54	91	17.96	12140	n.m	47.2	67.4	112.4
X7_2_55	693	Cryogenian	n.m	n.m	b.d	15.3	922	4.85E+05	n.m	0.035	13.46	0.206	3.4	5.07	1.67	22.4	7.03	82.6	29.4	130.7	26.7	252.7	46.1	7560	n.m	173.2	187	414
X7_2_54	738	Tonian	n.m	n.m	520	16.9	2092	4.82E+05	n.m	0.66	116.5	0.85	11.9	17.65	2.73	81.4	20.88	227.8	74.7	311.5	57.9	517	97.3	8220	n.m	51.9	217.3	108.8
X7_2_128	746	Tonian	n.m	n.m	b.d	17.5	2932	5.52E+05	n.m	0.499	25.5	1.43	15.5	23.2	4.91	91.9	27.1	304.1	105.2	450	86.5	744	139.4	11560	n.m	139.4	376	292.9
X7_2_11	855	Tonian	n.m	n.m	b.d	17.4	2850	5.34E+05	n.m	1.04	20.2	1.69	14.1	16.3	4.42	65.4	21.6	277	99	445	88.7	814	149.4	12250	n.m	128.2	120.3	243
X7_2_50	906	Tonian	n.m	n.m	b.d	26.9	628	5.13E+05	n.m	0.3	47.6	0.578	6.49	7.21	1.8	23.2	6.16	66	20.8	88.6	17.55	169.2	31.3	10810	n.m	25.9	136.9	46.8
X7_2_75	919	Tonian	n.m	n.m	450	11.8	1750	5.24E+05	n.m	1.65	56.1	0.94	8.7	11	3.61	47.4	13.75	163	59.9	268	56.2	537	106.8	10010	n.m	105.3	346	176.8
X7_2_28	936	Tonian	n.m	n.m	b.d	8.3	1183	5.08E+05	n.m	0.015	30.9	0.08	1.26	2.9	0.55	20.64	7.42	98.5	38.7	190.7	43.3	436	80.2	13730	n.m	53.7	126.8	92.7
X7_2_92	949	Tonian	n.m	n.m	b.d	31	1316	5.32E+05	n.m	0.56	12.3	0.82	8.9	10.9	2.85	46.4	13.6	147	46.2	196	38.5	333	60.1	11630	n.m	132.6	140	228.5
X7_2_59	967	Tonian	n.m	n.m	b.d	10.08	775	5.03E+05	n.m	0.038	12.13	0.086	1.17	2.98	0.201	17.5	5.82	73.1	26	118.8	24.8	232	41.5	11930	n.m	144.8	125.6	242.2
X7_2_110	976	Tonian	n.m	n.m	225	16.6	2461	5.61E+05	n.m	0.89	72	1.33	10.9	11	3.99	47.5	17.8	224.4	84.8	389	80.1	744	139.5	14590	n.m	419.3	226.5	668
X7_2_123	1042	Stenian	n.m	n.m	320	19.9	956	5.42E+05	n.m	1.5	33.9	0.55	4.7	4.39	1.02	21.4	6.79	82.5	31.9	145.3	30.91	304.4	59	10620	n.m	89.9	145.2	133
X7_2_103	1045	Stenian	n.m	n.m	301	50	759	5.39E+05	n.m	0.221	26.68	0.219	2.1	2.96	0.461	13.5	4.6	60.9	23.08	117.7	26.9	276.3	57.5	14240	n.m	133.7	143.9	211.6
X7_2_122	1070	Stenian	n.m	n.m	b.d	29.5	628	5.33E+05	n.m	0.29	22.97	0.069	0.94	1.8	0.356	10.01	3.67	47.2	20.08	97.4	22.17	227.9	47.8	13070	n.m	166.9	102	234.6
X7_2_29	1216	Ectasian	n.m	n.m	b.d	32.7	1440	5.33E+05	n.m	0.47	48.4	0.329	3.2	5.15	1.03	25.3	9.31	119.9	46.6	229.5	50.3	487	93.3	12500	n.m	441	403	587
X7_2_33	1691	Statherian	n.m	n.m	b.d	10.2	1004	5.08E+05	n.m	0.302	17.49	0.297	2.82	3.98	0.533	18.7	6.73	85.4	32.5	154.4	34.87	349.2	63	15400	n.m	679	290	624
X7_2_25	1707	Statherian	n.m	n.m	b.d	12.56	1063	5.16E+05	n.m	0.13	11.1	0.187	2.05	3.47	0.523	19.42	6.83	89.1	35	166.5	35.3	337	65.1	12350	n.m	248.2	97.7	215.6
X7_2_14	1733	Statherian	n.m	n.m	b.d	13.5	596	5.12E+05	n.m	0.023	12.65	0.106	1.93	3.5	0.245	15.8	4.88	57	20.96	93.5	18.69	177	32.9	12050	n.m	152	70.7	128.1
X7_2_10	1734	Statherian	n.m	n.m	b.d	12.08	2770	5.13E+05	n.m	0.311	25.44	0.98	13.77	20.4	1.23	88.4	25.9	290	99.2	417	76.8	656	111.1	11840	n.m	412	311	352.2
X7_2_24	1752	Statherian	n.m	n.m	b.d	16.9	1417	5.22E+05	n.m	0.258	11.91	0.484	7.07	10.86	0.775	46	12.85	143.8	49.9	209.5	38.9	341.4	62.3	11530	n.m	145.9	111.4	137.4

X7_2_100	1771	Statherian	n.m	n.m	b.d	12.94	588	5.09E+05	n.m	0.0107	6.05	0.067	1.36	2.77	0.235	14.7	4.41	54.5	18.7	85.3	16.85	154.7	28.41	10280	n.m	60.8	31.7	52.1
X7_2_43	1784	Statherian	n.m	n.m	b.d	9.35	1334	5.06E+05	n.m	0.065	18.41	0.172	3.04	5.66	0.301	31.7	10.51	130	45	205.7	39.1	365	60.8	12130	n.m	421	194	359
X7_2_60	1799	Statherian	n.m	n.m	b.d	4.13	595	5.26E+05	n.m	0.06	6.18	0.1	1	2	0.399	10.74	3.87	51.7	19.34	95	20.45	198	38.4	14930	n.m	306.3	84.9	261.5
X7_2_41	1873	Orosinian	n.m	n.m	b.d	18	577	4.86E+05	n.m	0.67	21.02	0.25	1.89	2.77	0.77	13	3.98	50.1	18.02	88.2	19.03	188.3	36.8	10380	n.m	152.7	91.5	122.3
X7_2_12	2003	Orosinian	n.m	n.m	b.d	18.4	320.4	5.40E+05	n.m	0.122	19.62	0.187	1.64	1.71	0.392	7	2.19	26.6	10.09	47.1	10.45	104.4	21.64	12700	n.m	285.1	106.7	202.9
X7_2_62	2027	Orosinian	n.m	n.m	b.d	7	1080	5.27E+05	n.m	0.063	18.88	0.054	0.62	1.98	0.313	12.89	5.77	86	35.2	171.4	36.6	342	63.8	13450	n.m	201.8	79.8	164.8
X7_2_102	2072	Rhyacian	n.m	n.m	b.d	11	396	5.34E+05	n.m	0.218	15.67	0.383	3.21	3.22	1.21	9.94	2.93	33.7	11.91	59.3	13.89	144.1	31.6	13520	n.m	369	151.5	284
X7_2_97	2091	Rhyacian	n.m	n.m	b.d	16	510	5.46E+05	n.m	0.174	11.78	0.367	3.25	3.97	0.677	16.25	4.32	50.4	16.46	74.7	14.79	137.1	25.85	11200	n.m	187.9	79.9	131.1
X7_2_101	2167	Rhyacian	n.m	n.m	b.d	10.5	942	5.13E+05	n.m	0.132	21.5	0.469	7.68	11.63	1.78	38.2	9.45	95.2	30.6	130.5	26.2	242.2	45.5	10680	n.m	204.3	101.6	143.5
X7_2_120	2242	Rhyacian	n.m	n.m	b.d	7.74	800	5.52E+05	n.m	0.188	16.4	0.311	2.84	3.62	0.737	17.7	5.78	70.3	27	121.1	24.8	228.9	44.4	11220	n.m	367	158	225.4
X7_2_121	2527	Neoarchean	n.m	n.m	b.d	5.6	1164	5.19E+05	n.m	0.117	25.93	0.136	1.74	3.38	0.268	21.5	7.27	96.4	40.3	182.4	37.8	352	62.9	12030	n.m	810	196.3	451
X7_2_27	2589	Neoarchean	n.m	n.m	b.d	10.7	794	5.13E+05	n.m	0.04	10.11	0.107	1.2	2.58	0.357	14.7	5.18	68.9	26.58	125	26.46	257.1	47	10610	n.m	222.5	54.1	121.7
X7_2_93	2622	Neoarchean	n.m	n.m	b.d	33	482	5.21E+05	n.m	0.205	23	0.286	3.38	3.33	0.604	14	3.91	44	14.48	69.1	15.28	160.4	34.5	12960	n.m	305	61.7	167
X7_2_90	3066	Mesoarchean	n.m	n.m	b.d	6.38	1318	5.02E+05	n.m	0.0139	16.9	0.167	3.24	6.29	1.53	33.8	10.44	122.9	43.2	195.5	40.4	379	70.3	10170	n.m	206	89.3	89.5
Discordant																												
X7_2_98			n.m	n.m	-26	19.6	1462	5.27E+05	n.m	0.055	9.56	0.173	2.44	4.92	1.093	29.4	9.96	125.3	46.7	227.7	49.2	477	93	11600	n.m	85.7	177	346
X7_2_13			n.m	n.m	70	14.93	2111	5.55E+05	n.m	0.612	13.02	0.903	7.82	12.49	4.25	59.5	18.95	211.7	73.7	314.8	60.5	549.2	103.5	12490	n.m	69.8	194.8	243.8
X7_2_82			n.m	n.m	180	15.4	1406	5.23E+05	n.m	0.484	27.74	0.505	4.16	5.11	1.54	23.7	8.9	117.2	44.3	214.7	45.4	439	82.6	14390	n.m	63.4	275	212.7
X7_2_15			n.m	n.m	72	6	700	5.31E+05	n.m	0.13	24.2	0.207	2.27	3.53	0.67	15.6	5.26	62	23.2	105.7	22.7	219.3	41.5	12730	n.m	102.1	200	337
X7_2_106			n.m	n.m	240	23.9	2150	5.41E+05	n.m	1.06	104	1.26	11	11.5	4.66	49	15.9	195	72.3	328	69	647	123	12630	n.m	193.6	263	312
X7_2_21			n.m	n.m	128	28.5	833	5.24E+05	n.m	0.595	34.7	0.84	6.86	7.35	2.44	25.9	7.58	83.8	27.34	118.6	23.37	222.6	42.4	11700	n.m	161.2	155	136.7
X7_2_79			n.m	n.m	70	4.05	347	5.27E+05	n.m	0.191	4.42	0.243	1.73	1.82	0.402	6.94	2.32	28.9	11	53.1	11.61	116.1	24.25	14030	n.m	428	73	421
X7_2_32			n.m	n.m	128	34.4	2710	5.17E+05	n.m	1.8	22.9	1.75	13.3	15.9	6.13	62	20.3	248	87.3	410	86.1	842	153.2	13340	n.m	218.3	136	359
X7_2_74			n.m	n.m	564	59.7	3020	5.28E+05	n.m	1.94	129.5	2.56	24.1	31.8	12.55	120.3	34.2	348	107	406	76.7	708	129.5	12540	n.m	120.7	596	342
X7_2_96			n.m	n.m	104	9.6	446	5.21E+05	n.m	0.74	20.8	1.02	7.1	6	1.92	14.5	4.14	45.7	13.7	61	12.65	127	23.9	12390	n.m	165.9	25.1	334

M2AR 8-1 - Zircon compositional data (LA-ICP-MS, n = 92, b.d. = below detection limit)

Analysis ID	Best age	Geological time	Al [ppm]	P [ppm]	Ca [ppm]	Ti [ppm]	Y [ppm]	Zr [ppm]	Nb [ppm]	La [ppm]	Ce [ppm]	Pr [ppm]	Nd [ppm]	Sm [ppm]	Eu [ppm]	Gd [ppm]	Tb [ppm]	Dy [ppm]	Ho [ppm]	Er [ppm]	Tm [ppm]	Yb [ppm]	Lu [ppm]	Hf [ppm]	Ta [ppm]	Pb [ppm]	Th [ppm]	U [ppm]

	(Ma)																											
MAR_8_59	481	Cambrian	0	208	-50	9.5	631	4.71E+05	1.54	0.038	4.81	0.097	1.79	3.82	0.165	17.6	5.25	58.8	20.72	89.6	17.24	166	30.1	9790	0.477	67.3	33	44.9
MAR_8_34	551	Ediacaran	32.5	206	-47	8.2	707	4.87E+05	1.86	0.235	22.6	0.185	1.72	2.8	0.567	14.6	4.73	59.3	22.42	106.6	22.18	223	42.5	11590	0.811	91.6	192	274
MAR_8_3	561	Ediacaran	45.5	616	55	5.27	2720	5.02E+05	3.19	0.072	34.3	0.128	2.65	8.05	4.49	58.1	18.3	246	90.9	441	94.3	943	193	10460	0.622	38.7	199	114.2
MAR_8_2	571	Ediacaran	29	570	-38	6.9	1990	4.93E+05	3.78	0.149	8.85	0.203	2.12	5.32	0.88	36.7	12.84	175.5	67.3	333	71	673	129	11670	1.41	131.5	144	377
MAR_8_22	574	Ediacaran	13.3	241	-50	33	1480	5.04E+05	1.61	0.139	14.44	0.66	9.92	11.58	3.52	49.2	14.33	157.4	50.7	219.8	42.3	389	69.7	9040	0.702	36.7	109.5	104.7
MAR_8_48	579	Ediacaran	13.7	446	83	3.8	1509	5.01E+05	2.03	0.051	28.2	0.173	2.98	6.27	1.88	33.1	10.32	125.9	49.5	242	53.6	569	115.2	10000	0.472	42.6	158	121.9
MAR_8_44	586	Ediacaran	2.6	226	27	6.2	903	4.86E+05	3.35	0.138	29.8	0.427	5.48	8.3	1.4	32.8	8.9	91.7	29.3	120.5	22.4	194	34	9810	1.119	117.1	203	333
MAR_8_7	601	Ediacaran	250	218	60	22.2	671	4.83E+05	2	0.139	8.55	0.114	2.05	2.81	0.594	14.92	4.69	57.5	20.96	101.7	22.18	222.3	44	11490	0.657	65.2	57	174.1
MAR_8_65	602	Ediacaran	3.9	201	50	17	1450	4.94E+05	2.06	0.196	38.4	0.83	11.68	16.2	6.67	56.6	14.2	145	47.4	203	41.1	417	78.1	8490	0.568	54.6	296	162
MAR_8_31	609	Ediacaran	133	720	600	10.5	2668	5.14E+05	5.66	1.7	35.6	1.03	5.7	6.48	1.08	43	15.51	218.9	90	459	100	998	202.7	12550	1.91	138.4	202.7	368
MAR_8_62	615	Ediacaran	47	155	31	14	589	4.82E+05	1.86	0.25	46	0.62	5.2	5	2.36	18.3	5.5	55	17.4	77	16.6	163	30.1	11100	0.728	229	94.7	175
MAR_8_12	626	Ediacaran	125.2	234	66	12.2	185	4.95E+05	0.865	0.054	2.69	0.088	1.45	3.71	0.325	15.2	3.37	26.2	5.7	18.53	2.74	20.2	2.9	1.32E+04	0.367	69.1	47	181
MAR_8_43	645	Cryogenian	2.8	101	-14	5.6	272	4.87E+05	1.131	0.05	6.82	0.047	0.45	0.69	0.305	4.08	1.43	19.3	8.27	42.5	10.8	124.4	28.6	13750	0.67	108.9	36.4	276
MAR_8_45	648	Cryogenian	29.8	192	58	12.5	1005	4.99E+05	2.25	0.071	25.3	0.145	2.18	3.39	1.23	15.6	5.39	73.9	29.7	156	36.7	395	82.5	9650	0.925	106.9	240	270
MAR_8_57	648	Cryogenian	31	432	170	10.9	1990	4.91E+05	2.93	0.57	45.9	0.64	8.27	13.11	3.66	59.4	17.32	195.1	70	309	61.6	564	106.7	10360	0.91	267	227.3	195
MAR_8_56	688	Cryogenian	88	185	-54	14.4	555	4.86E+05	1.78	0.103	12.87	0.141	1.71	3.14	1.08	14.1	4.35	50.7	17.87	82	17.1	173	32.5	8760	0.626	28.8	53.8	75.9
MAR_8_38	706	Cryogenian	19.3	312	-49	5.9	3220	4.81E+05	5.49	0.129	10.27	0.595	9.96	18.8	5.64	102	30.7	351	119	517	99.1	916	163	8830	1.68	67.8	148	155
MAR_8_49	707	Cryogenian	6.3	248	150	7.1	618	4.79E+05	2.41	0.4	41	0.31	2.8	5.07	1.71	17.9	5.2	56.4	20.16	89.5	18.59	186	35.3	10140	0.603	49.2	115.8	113.7
MAR_8_37	718	Cryogenian	2	34	71	3.25	136	4.81E+05	4.22	0.03	12.9	0.0256	0.285	0.57	0.217	2.29	0.7	9.2	4.08	20.9	5.37	61.6	15.4	10250	1.63	30	18.6	69
MAR_8_47	958	Tonian	271	222	36	19.3	1120	4.77E+05	2.49	0.218	8.35	0.263	3.9	7.53	1.1	34.8	10.16	114.1	38.8	158.4	30.3	270	48.5	9910	0.763	51.7	42.1	85.1
MAR_8_9	988	Tonian	121	152	-20	21.1	402	5.10E+05	0.906	0.3	16.8	0.148	1.5	1.95	0.8	9.12	2.84	32.8	12.67	60.7	13.97	148.5	32.5	12030	0.269	59.5	37.3	93.8
MAR_8_27	1050	Stenian	2.8	170	-39	13	549	4.73E+05	2.18	0.032	8.37	0.08	1.23	3.26	0.203	15.7	4.64	52.2	18.09	83.3	15.82	147.2	25.9	11380	0.801	96.1	43.9	140.3
MAR_8_35	1076	Stenian	31	263	-20	8.5	1200	5.00E+05	2.26	0.28	13.07	0.406	5.33	8.78	1.84	38.1	11.01	121.1	40.6	173.4	33.3	304	55.5	10570	0.863	59.8	41.9	87.5
MAR_8_26	1261	Ectasian	13.7	247	24	19	903	5.00E+05	2.09	0.087	7.1	0.126	1.4	3.29	0.368	19.5	6.59	77.6	28.3	129.7	25.7	239	42.9	11490	0.806	117	39.4	139
MAR_8_11	1540	Calymmian	6.40E+03	220	160	33	527	4.20E+05	2.46	0.39	25	0.174	1.42	2.36	0.73	10.4	3.55	44.8	16.7	80.7	17.4	168	34.3	9440	0.76	28.2	28.2	28.4
MAR_8_23	1582	Calymmian	6.5	256	20	12.7	971	4.78E+05	3.1	0.108	15.9	0.124	2.1	3.57	0.53	19.1	6.86	82.7	31	148	32.1	317	61.1	10370	0.997	148.5	64.5	145
MAR_8_58	1974	Orosinian	94	1155	-8	16.1	3080	4.92E+05	2.12	0.267	5.45	0.16	1.69	4.78	0.784	36.5	16.4	241	101.2	517	113.5	1106	210	13880	1.263	82.5	78.1	286
MAR_8_8	1982	Orosinian	93	176	51	11.4	641	4.85E+05	4.91	0.4	43	0.249	2.21	3.24	0.87	14.3	4.7	55.7	20.34	98.5	21.64	219.9	44.1	12350	1.55	259.1	122.9	200.4
MAR_8_36	2022	Orosinian	59	267	2	20.6	790	4.76E+05	2.55	0.94	16.4	1.47	9.8	12.5	4.6	37	8.3	85	24.8	106	18.1	177	30.3	9130	0.646	212	71.6	172
MAR_8_21	2115	Rhyacian	53	348	48	13.6	1430	4.87E+05	2.85	0.365	33.4	0.81	6.9	8	1.62	38.5	11.88	139.8	47.7	210	41.2	371	64.6	11870	3.17	485	85.6	375
MAR_8_64	2144	Rhyacian	79	640	41	53	1540	4.94E+05	1.1	0.5	17	0.68	7.3	11.5	5.6	62	20.8	160	45	146	26.1	189	31.1	11660	0.296	71.3	106	194

MAR_8_61	2155	Rhyacian	12.8	183	-91	4.2	436	4.97E+05	3.35	0.034	13.77	0.042	0.51	1.42	0.472	7.57	2.79	35.9	14.3	66.6	14.1	145	28.3	12630	2.08	44.4	48.2	122
MAR_8_53	2155	Rhyacian	0.8	251	59	24	1095	4.68E+05	2.84	0.037	55	0.274	3.96	6.66	2.96	28.9	8.64	99.9	36.4	167	33.6	327	60.3	8200	0.849	35.4	222	135
MAR_8_17	2156	Rhyacian	9.5	129	-19	11.1	433	4.83E+05	1.03	0.048	26.9	0.096	1.52	2.77	0.89	11.49	3.3	37.7	12.95	60.1	13.16	134.6	27.1	10260	0.288	159.9	53.7	106.4
MAR_8_5	2174	Rhyacian	51.8	344	40	19.8	1399	5.01E+05	3.99	0.107	39.5	0.201	3.08	6	1.5	31	10.07	125.2	47.3	219.3	44.7	429	83.9	10560	1.93	560	274.7	385
MAR_8_60	2178	Rhyacian	3.9	144	-11	11.6	452	4.84E+05	1.031	0.031	24	0.088	1.38	3.24	0.722	12.87	3.62	41	14.61	65.7	13.8	134.4	26	10020	0.382	172.6	69.9	117
MAR_8_42	2199	Rhyacian	137	203	53	10.4	1348	5.03E+05	2.21	0.226	18.17	0.318	4.87	7.79	1.223	34.7	10.45	122.7	43.8	196.8	39.9	369	71.2	10790	1.001	510	173.6	340
MAR_8_41	2573	Neoarchean	22.7	135	88	23	434	4.88E+05	1.73	0.049	11.61	0.098	1.31	2.51	0.405	12.15	3.77	41.4	14.71	64.2	12.69	117.8	22.2	10680	0.635	242	61.1	126.6
MAR8_121	130	Early Cretaceous	-0.7	239	230	22.6	1725	4.98E+05	14.03	0.063	145.3	0.409	7.47	12.98	2.31	58.3	17.63	207.5	63.7	257.3	46.1	384	65.6	6690	4.73	6.58	136.3	89.5
MAR8_67	367	Devonian	2	180	-63	8.4	1306	4.65E+05	9.55	0.069	14.78	0.262	4.28	8.42	0.574	44.2	13.53	148.9	48.3	198.8	35.1	297	50.2	8700	3.22	20.02	71.8	92.7
MAR8_95	535	Cambrian	15.8	170	129	37.8	1050	4.63E+05	2.49	0.231	64.3	0.95	11.2	12.9	3.18	46.7	12.1	114	34.9	143	27.2	240	41.3	9140	0.9	32.8	175	100
MAR8_92	538	Cambrian	164	1307	-27	11.1	3190	4.63E+05	2.71	0.191	8.19	0.219	2.19	5.69	0.87	38.3	17.54	263.2	107.2	559	131.2	1325	248	12410	1.572	142.8	70.4	440
MAR8_66	571	Ediacaran	2.8	203	56	14	837	4.74E+05	4.88	0.88	17.5	0.26	3	4.73	0.279	20.8	6.61	77.8	26.6	122.2	23.7	227	41.9	10900	1.93	59.6	105.2	170.3
MAR8_80	576	Ediacaran	18	141	100	30	806	4.86E+05	1.04	0.102	9.5	0.121	1.11	2.61	0.91	14.2	5.12	64.6	24.9	120.6	25.83	253.7	50.8	14750	0.371	113	284.8	315
MAR8_72	578	Ediacaran	109	508	20	15.2	1487	5.08E+05	1.61	0.63	12.1	0.94	7.8	9.7	3.39	38.3	13.92	158.4	47.2	196	37.7	341	64.1	15100	0.867	164	30.5	469
MAR8_128	606	Ediacaran	7.3	104	60	6	561	5.15E+05	3.13	0.041	47.1	0.121	1.73	2.71	1.04	14.78	4.07	49.1	16.84	78.6	16.87	174.1	34.4	11650	1.156	86.1	194.4	242
MAR8_101	616	Ediacaran	650	384	520	24.7	949	4.68E+05	1.57	1.45	16.2	0.51	3.7	3.78	1.02	20.1	6.64	84.4	29.7	136.3	27.7	272	49.5	8180	0.412	19.76	48.9	53.8
MAR8_84	620	Ediacaran	10	180	-38	12.4	554	4.79E+05	2.35	0.06	30.4	0.177	1.79	2.51	0.46	12.79	4.06	49	17.16	78.8	16.67	162.8	30.6	13940	1.205	100.6	130.4	254
MAR8_87	629	Ediacaran	59	204	290	16.8	635	5.06E+05	1.335	0.37	6.51	0.275	3.28	3.91	0.77	18.7	5.36	59.8	20	90.4	17.9	163	30.4	9410	0.503	67	51.3	116.5
MAR8_70	633	Ediacaran	177	203	-10	18.9	149	4.71E+05	1.34	0.052	9.17	0.113	1.77	5.72	1.21	24.3	4.83	27.9	4.79	12.8	1.59	11.1	1.75	13130	0.524	41.5	18.5	106.8
MAR8_88	663	Cryogenian	161	202	16	12.7	242	5.02E+05	1.157	0.062	3.73	0.052	1.03	3.2	0.239	16.32	3.98	31.6	7.9	28.5	5.17	45	8.5	14440	0.321	101.6	29.5	244
MAR8_118	666	Cryogenian	7.20E+03	257	4.30E+03	15.1	2070	5.04E+05	1.95	0.9	13.9	0.524	6.62	11.5	2.29	56.4	18	213	72.7	309	58.5	546	96.7	9940	0.771	72.9	147.6	184.4
MAR8_112	669	Cryogenian	-1.2	134	40	4.4	465	5.10E+05	4.51	0.044	13.76	0.055	0.71	1.68	0.608	7.95	2.85	36.1	13.68	69.4	15.64	168	33.6	11660	2.2	113.4	79.6	280
MAR8_75	675	Cryogenian	38.8	224	147	11.6	909	4.74E+05	2.73	0.065	7.31	0.153	2.55	4.87	0.509	23.5	7.35	86.3	30.08	132.1	26.37	251	49.3	9600	0.997	38	43	94.1
MAR8_99	678	Cryogenian	14	205	27	28.7	909	4.85E+05	1.93	0.12	5	0.39	3.7	7.6	2.1	21.3	6.2	73	26.6	130.2	29.4	292	60.2	11390	0.915	137.4	81.8	338
MAR8_123	705	Cryogenian	20	103	48	3.3	95	5.09E+05	0.65	0.171	5.7	0.28	1.7	1.46	0.89	5.9	1.49	12.8	3	10.5	2	18.8	3.6	13760	0.169	135.5	3.3	333
MAR8_73	707	Cryogenian	-0.8	151	13	14.5	494	4.68E+05	1.49	0.04	45.8	0.13	2.02	3.81	1.47	17.06	4.67	49.7	16.94	72.3	14.81	139.6	28.5	9370	0.498	30.4	80.8	69.9
MAR8_96	707	Cryogenian	13.3	236	-62	17.9	756	4.97E+05	2.08	0.063	5.78	0.072	1.4	3.27	0.324	17.85	5.81	70.4	24.7	110.7	21.5	204	38.4	10960	0.752	47	45.7	104.7
MAR8_113	786	Tonian	2.5	61	-160	2.37	216	5.33E+05	0.641	0.065	3.63	0.042	0.52	0.6	0.311	2.81	0.99	14.2	5.85	34.6	9.4	127.3	32.4	11960	0.162	47.6	28.4	98.2
MAR8_114	808	Tonian	19.6	192	-139	6.8	768	4.99E+05	4.14	0.069	15.2	0.101	1.39	2.64	0.41	14.53	5.09	67	24.6	114	24.7	240	44.9	11420	1.54	91.7	83.8	187
MAR8_119	945	Tonian	49	227	40	26.2	808	5.22E+05	4.4	1.01	17.6	0.45	4.2	4.68	0.75	19.9	6.32	76	26.1	121.7	24.4	244.8	46	11890	1.44	62.4	56.9	107
MAR8_91	975	Tonian	3.8	255	-124	12.79	588	4.90E+05	2.3	0.037	20.09	0.058	0.88	2.43	0.45	12.08	3.86	48.3	18.33	87.3	18.78	184.2	35.7	11800	0.747	55.9	59	90.8

MAR8_71	1014	Stenian	26	195	-55	6.3	1242	4.75E+05	2.93	0.066	13.1	0.08	1.54	3.33	0.64	20.14	7.34	99.2	39.3	200.1	43.4	438	88.5	11100	1.024	210.3	79.2	329
MAR8_125	1049	Stenian	41	212	-25	19.3	1068	5.20E+05	2.92	0.86	19.7	0.66	5.2	5.58	1.69	22.6	7.69	90.4	32.5	147.2	31.5	302	56.5	11910	1.45	187.8	184	291
MAR8_104	1059	Stenian	250	311	100	46	1204	5.14E+05	3.41	0.71	43	1.07	10.8	12	5.4	36.9	10.4	111.7	36.4	153.7	30.9	303	53.4	12730	1.332	226	262	331
MAR8_117	1227	Ectasian	0.6	235	-34	13.4	1000	4.89E+05	3.05	0.032	9.68	0.067	1.29	2.75	0.277	18.42	6.47	87.5	31.3	148	30.5	295	56.5	10560	0.853	81.9	31	105.6
MAR8_68	1254	Ectasian	172	283	-68	21.8	1300	4.95E+05	2.47	1.5	106	3.1	21	23	8	60	16.9	166	45	187	39	374	66	11430	0.982	290	308	378
MAR8_90	1543	Calymian	1070	247	200	39	900	4.70E+05	3.33	0.84	47	0.77	5.7	6.9	2.4	21.9	7.1	81	28	130	26.4	259	50	11260	1.13	208	53.8	219
MAR8_97	1989	Orosinian	9.1	171	-46	6.7	969	5.20E+05	2.14	0.049	25.2	0.231	3.61	5.27	2.19	23.6	6.6	78.2	29.5	139.6	31.4	334	71	10840	0.654	260	144	201
MAR8_130	2078	Rhyacian	154	564	189	13.7	1850	5.03E+05	2.11	0.73	12.4	1.32	11.3	14.3	3.04	54.7	17	187	62	266	50.9	473	86.7	12710	0.928	624	135.4	481
MAR8_85	2131	Rhyacian	8.5	116	92	6	308	5.04E+05	0.938	0.041	13.76	0.053	0.61	1.43	0.533	6.91	1.85	22.7	9.23	47.4	12.02	131.8	30.8	12400	0.318	166.2	41	112.1
MAR8_77	2136	Rhyacian	9.1	157	151	18.2	386	4.72E+05	1.14	0.036	24.8	0.095	1.45	2.91	1.05	12.43	3.5	36.2	11.98	54.2	10.86	110.6	20.6	9630	0.329	104.4	41.8	69.1
MAR8_93	2194	Rhyacian	123	70	37	7.5	174.1	4.89E+05	0.671	0.047	2.96	0.0258	0.375	0.74	0.303	3.5	1.2	14.5	5.59	29.1	6.43	74.9	16.8	9620	0.16	56.3	9.08	37
MAR8_78	2194	Rhyacian	473	248	125	35.7	1028	4.94E+05	1.69	1.07	31	1.12	9	9.6	3.66	31.1	9	103	33.3	145	28.2	273	56.3	11990	0.361	147.5	51.5	106.5
MAR8_86	2203	Rhyacian	228	252	89	18.1	788	5.01E+05	2.59	0.178	31.09	0.164	1.67	3.05	0.644	15.69	5.48	65.7	24.33	113	22.68	213.7	41.42	14600	1.317	374	127.5	246.6
MAR8_122	2471	Siderian	30	173	110	38.3	723	5.11E+05	2.01	0.18	21	0.37	3.8	4.91	1.05	18.7	5.69	68.8	23.1	103.3	20.61	201.6	37.7	10370	0.722	439	204.2	264
MAR8_83	2694	Neoarchean	23	143	101	4.2	461	4.81E+05	0.709	0.077	4.39	0.069	1.03	1.98	0.67	8.57	3.12	38.5	14.38	72.3	15.53	163.4	34.7	11530	0.182	128	17.1	69
Discordant																												
MAR_8_16			20.4	187	-62	3.7	658	4.82E+05	2.88	0.049	3.16	0.045	0.55	1.24	0.163	9.58	3.8	49.7	20.43	101.8	22.4	231	44.2	13070	1.274	182	95	397
MAR_8_18			339	1067	133	31.5	3450	4.67E+05	2.82	1.24	36.6	2.63	25.5	34.5	12.6	118	34.7	381	119.3	515	99.8	907	156.1	12130	1.13	148.6	295	499
MAR_8_39			25	946	196	11.9	2760	4.87E+05	6.36	0.168	18.2	0.253	3.99	9.8	0.643	58.6	21.2	255	96.3	435	85.5	780	138.3	14270	2.31	187.7	117.6	209
MAR_8_46			8.5	325	-28	13.6	1127	4.88E+05	5.17	0.069	46.7	0.132	1.91	4.52	1.27	23.3	7.88	99.9	37.4	175.4	36.5	360	69.4	10200	1.71	21.69	92.8	116.4
MAR_8_50			13.8	670	2.10E+03	5.97	663	5.07E+05	3.12	1.2	28.7	0.73	5.2	4.8	0.92	16.2	5.02	59.9	20.83	95.3	19.58	192	35.4	10510	1.198	165.7	90.2	149
MAR_8_54			110	286	50	9.5	1352	4.95E+05	5.32	0.64	66.3	0.64	5.03	6.35	1.86	27.9	9.11	112.4	41	201	43.1	445	84.1	11320	2.21	142.8	287	330
MAR8_79			35.6	196	238	29.5	1258	4.90E+05	6.01	0.181	36.9	0.686	9.34	11.7	4.47	43.8	11.51	125.8	41.4	185.3	37.1	347	68	9010	2.48	7.53	98.9	89.6
MAR8_94			88	245	68	12.7	940	4.72E+05	1.89	0.8	52.3	1.7	14.3	12.9	6	39.2	10.1	99	29.6	123	25.5	245	45.4	10180	0.704	102.3	287	275
MAR8_100			340	238	288	23.1	990	5.01E+05	2.09	1.3	43.9	2.77	23	19.5	8.7	41.7	11.2	112	31.6	124	22	210	34.4	13010	0.384	114.8	44.9	107
MAR8_103			156	194	18	14.8	1088	5.17E+05	3.82	0.99	86.9	1.7	14.2	15.1	5.84	41.9	11.15	112.5	34	142.1	27.4	267	54.6	11890	0.573	91	467	281
MAR8_106			1180	111	-60	46	416	5.11E+05	0.95	0.253	10.95	0.15	1.72	2.52	1.004	10.35	2.98	36.6	12.89	60.6	12.65	127.2	24.93	10170	0.282	23.52	50.5	59.7
MAR8_107			136	406	-69	23.6	2270	4.97E+05	6.52	1.54	62.4	3.06	24.2	25.4	9.3	75.9	23	252	77.4	318	64.8	609	105.9	10720	1.86	140.4	271	393
MAR8_115			990	310	80	19.1	859	5.18E+05	4.51	1.71	73	2.09	14.7	10.1	4.1	30.9	8.3	79.6	26.6	109	21.4	215	41.4	13960	1.58	133.3	51	186
MAR8_124			64	204	140	13.8	1023	5.33E+05	2.15	0.249	24	0.341	3.95	5.44	2.08	22.4	7.13	87.9	31.3	145	30.5	305	61.2	11310	0.602	60.3	105	157
MAR8_129			82	161	110	16.4	699	5.13E+05	1.4	0.409	42.8	0.636	8.11	11.1	4.48	32.8	8.19	84.3	23.7	92.9	17.5	162	29.1	10530	0.285	34.6	107	108.7

Detection Limit		Al [ppm]	P [ppm]	Ca [ppm]	Ti [ppm]	Y [ppm]	Zr [ppm]	Nb [ppm]	La [ppm]	Ce [ppm]	Pr [ppm]	Nd [ppm]	Sm [ppm]	Eu [ppm]	Gd [ppm]	Tb [ppm]	Dy [ppm]	Ho [ppm]	Er [ppm]	Tm [ppm]	Yb [ppm]	Lu [ppm]	Hf [ppm]	Ta [ppm]	Pb [ppm]	Th [ppm]	U [ppm]
Minimum Detection Limit		2.8833	10.054	65.867	0.6881	0.071351	2.6667	0.027192	0.0192	0	0	0	0	0	0.088777	0	0	0	0	0	0	0	0	0.012285	0	0.027673
Maximum Detection Limit		9.8815	53.154	571.24	3.4039	0.45389	296	0.1137	0.10223	0.088333	0.064051	0.43368	0.36857	0.1132	0.5675	0.050161	0.26596	0.049548	0.24698	2.8491	0.26935	0.048038	11.679	0.0571	0.10341	0.054724	0.18722
Mean Detection Limit		5.9590365	22.505635	289.04487	1.7596589	0.1825599	10.725932	0.0626062	0.0439583	0.0406126	0.0266837	0.1543735	0.1013675	0.0505104	0.2831823	0.0189752	0.0661558	0.0158798	0.0704063	0.0605757	0.0720815	0.0175568	0.3307226	0.024692	0.0309807	0.0104747	0.0621383
Median Detection Limit		6.0888	22.502	278.01	1.7026	0.18377	6.1588	0.061988	0.040919	0.040412	0.027262	0.13138	0.074222	0.047203	0.27913	0.017586	0.053472	0.015879	0.069321	0.012682	0.062162	0.01883	0.088876	0.023362	0.028595	0.010775	0.058582
Associated Error		Al [ppm]	P [ppm]	Ca [ppm]	Ti [ppm]	Y [ppm]	Zr [ppm]	Nb [ppm]	La [ppm]	Ce [ppm]	Pr [ppm]	Nd [ppm]	Sm [ppm]	Eu [ppm]	Gd [ppm]	Tb [ppm]	Dy [ppm]	Ho [ppm]	Er [ppm]	Tm [ppm]	Yb [ppm]	Lu [ppm]	Hf [ppm]	Ta [ppm]	Pb [ppm]	Th [ppm]	U [ppm]
Minimum Absolute Error		1.7	18	56	0.91	9.4	11000	0.061	0.011	0.16	0.0097	0.091	0.15	0.05	0.34	0.11	1.2	0.31	1.4	0.19	1.5	0.24	250	0.024	0.29	0.48	2
Maximum Absolute Error		2300	180	1400	140	380	26000	0.73	13	40	4.5	17	13	5.6	33	7.4	57	13	44	8.4	76	12	680	0.31	38	66	48
Mean Absolute Error (±2σ)		82.598413	34.857143	120.33333	5.9093651	70.974603	17968.254	0.2201587	0.4082063	4.6420635	0.2562651	1.6555714	1.5304762	0.5996825	3.714127	0.947619	8.8634921	2.4009524	9.5301587	1.8655556	17.706349	3.0992063	471.74603	0.0791111	7.1365079	8.244127	12.592063
Median Absolute Error (±2σ)		13	27	88	2.5	46	18000	0.17	0.06	2	0.061	0.56	0.59	0.14	2	0.46	5	1.4	6.4	1.2	12	2.3	480	0.07	4.7	3.9	8.9

M2AR 10I - Zircon compositional data (LA-ICP-MS, n = 49, b.d. = below detection limit)

Analysis ID	Best age (Ma)	Geological time	Al [ppm]	P [ppm]	Ca [ppm]	Ti [ppm]	Y [ppm]	Zr [ppm]	Nb [ppm]	La [ppm]	Ce [ppm]	Pr [ppm]	Nd [ppm]	Sm [ppm]	Eu [ppm]	Gd [ppm]	Tb [ppm]	Dy [ppm]	Ho [ppm]	Er [ppm]	Tm [ppm]	Yb [ppm]	Lu [ppm]	Hf [ppm]	Ta [ppm]	Pb206 [ppm]	Th232 [ppm]	U238 [ppm]
10I_85	577	Ediacaran	n.m	n.m	b.d	15.9	571	5.36E+05	n.m	0.445	14.9	0.292	3.06	3.58	0.719	15.73	4.76	52.5	18.26	80.7	16.53	154.6	31.06	10620	n.m	32.7	49.8	89.8
10I_13	585	Ediacaran	n.m	n.m	b.d	5.8	583	5.39E+05	n.m	0.078	43.2	0.126	1.91	3.03	0.946	12.34	3.88	46.6	17.64	86.5	19.76	209.6	43.2	12710	n.m	125.6	222.9	343
10I_28	592	Ediacaran	n.m	n.m	b.d	10.7	1011	5.37E+05	n.m	0.096	21.5	0.311	5.44	8.62	0.404	34.5	9.79	109.9	37.3	159.2	30.6	280	53	11810	n.m	80.4	172.3	217.8
10I_45	609	Ediacaran	n.m	n.m	259	25.8	3160	5.23E+05	n.m	0.86	44.5	1.7	14.7	17.03	6.2	70.4	22.58	279	105.9	502	104	1043	202.8	11200	n.m	110.9	264	294
10I_37	610	Ediacaran	n.m	n.m	510	43	1089	4.84E+05	n.m	0.97	51.4	0.847	10.63	14.56	6.25	48.6	11.91	116	37.2	152.6	28.9	269.9	51	8430	n.m	51.4	176.9	135
10I_14	627	Ediacaran	n.m	n.m	b.d	20.6	2560	5.12E+05	n.m	0.48	23.4	0.79	9.8	13.4	3.29	65.1	22.1	257	90	391	75.9	667	119.7	11060	n.m	67.6	199	173
10I_119	635	Ediacaran	n.m	n.m	b.d	12.4	5150	4.99E+05	n.m	0.275	32.9	0.787	11.64	23.54	3.98	123.3	40.3	502	187	817	158.8	1462	266	10100	n.m	200.9	541	520
10I_108	749	Tonian	n.m	n.m	b.d	17.8	404	5.15E+05	n.m	0.078	3.9	0.142	2.03	2.84	0.356	11.93	3.33	38.6	13.48	61	12.82	130.6	26.45	10990	n.m	50.8	14.3	101.3
10I_109	902	Tonian	n.m	n.m	b.d	12	1007	5.24E+05	n.m	0.343	10.65	0.78	6.3	6.97	2.17	24.3	7.74	90.9	32.6	146.5	30.5	293.1	57.4	12790	n.m	175.9	80.4	313.9
10I_54	1651	Statherian	n.m	n.m	b.d	16	552	5.27E+05	n.m	0.078	5.24	0.12	1.37	2.7	0.19	13.51	4.25	50.2	18.59	84.1	17.55	179.2	37.7	12460	n.m	151.3	49.5	170.2
10I_60	1654	Statherian	n.m	n.m	b.d	35	623	5.07E+05	n.m	0.074	12.25	0.193	2.25	4.14	0.406	19.3	5.64	63.7	21.86	91.3	18.23	171.7	29.81	11040	n.m	131.3	80.3	119.7

10I_79	1673	Statherian	n.m	n.m	b.d	43.1	734	5.30E+05	n.m	0.64	16.3	1.07	7.4	7.4	1.51	23.6	6.96	74.2	25	108.5	21.7	204.6	38.5	13070	n.m	156.3	94.3	170.2
10I_36	1685	Statherian	n.m	n.m	b.d	15.8	1542	5.20E+05	n.m	0.156	9.87	0.585	8.57	12.37	1.15	55.1	14.93	162.3	54.5	228	41.5	367	66.5	10610	n.m	131.4	100.5	128.4
10I_89	1694	Statherian	n.m	n.m	b.d	18.9	1706	5.32E+05	n.m	0.53	14.22	0.421	4.81	7.21	0.494	38.4	12.47	151	55.9	259	51.4	482	88.5	13950	n.m	381	149.3	368
10I_98	1697	Statherian	n.m	n.m	b.d	26	1048	5.31E+05	n.m	0.245	18.11	0.31	3.49	5.12	0.497	24.74	8.01	95.5	34.6	153.4	31	281	52.7	13050	n.m	427	186	385
10I_68	1703	Statherian	n.m	n.m	214	29.3	986	5.27E+05	n.m	0.3	18.1	0.67	6.8	8.7	0.87	31.2	9.55	99.4	33.7	146.3	28.6	258.4	47.4	12940	n.m	329.1	264	311
10I_78	1715	Statherian	n.m	n.m	1080	46	930	5.24E+05	n.m	1.99	39.6	2.64	19.3	13.2	4.5	32	10.1	105	32.2	137	28.3	263	49.8	13490	n.m	271.5	180	288
10I_59	1729	Statherian	n.m	n.m	b.d	20.9	792	5.26E+05	n.m	0.391	20.8	0.64	5.11	6.31	1.24	21	6.47	75.7	27	120.8	25.62	246.8	47	12870	n.m	232.7	87.7	252
10I_48	1740	Statherian	n.m	n.m	b.d	12.2	730	5.35E+05	n.m	0.025	7.99	0.141	2.12	3.88	0.299	19.73	5.99	68.8	24.46	110	21.22	197.1	36.4	12230	n.m	122.7	60.3	103.7
10I_111	1748	Statherian	n.m	n.m	b.d	16.4	1430	5.13E+05	n.m	0.08	13.46	0.494	7.86	11.6	0.538	47.8	13.6	151	51.3	214	40.4	361	64.6	11580	n.m	173	135	142.7
10I_100	1752	Statherian	n.m	n.m	b.d	18.9	1274	5.35E+05	n.m	0.209	12.38	0.505	7.76	10.86	1.16	45.7	12.74	135.6	44.5	185	35	309.4	57.6	11930	n.m	194.9	114.2	173.8
10I_105	1761	Statherian	n.m	n.m	b.d	14.6	949	5.29E+05	n.m	0.5	21.5	0.82	7.5	7.2	1.27	27.7	8.21	95.7	34.2	150.9	29.9	277	50.2	13150	n.m	210.4	121.9	189
10I_127	1763	Statherian	n.m	n.m	b.d	7.01	1015	4.89E+05	n.m	0.015	20.36	0.057	1.34	3.71	0.137	19.7	6.56	92.1	36.69	167.8	34.9	334.3	58.5	16430	n.m	436	169.5	357.8
10I_6	1774	Statherian	n.m	n.m	b.d	12.67	682	5.03E+05	n.m	0.032	10	0.1	1.4	3.01	0.214	16	5.14	61	22.93	103.7	20.81	192.9	34.7	10880	n.m	119.6	57.2	97
10I_66	1780	Statherian	n.m	n.m	b.d	39.9	1757	4.90E+05	n.m	0.211	12.3	1.131	15.75	19.83	1.138	76.1	19.57	196.4	61.9	243.5	44.6	380	63.9	10250	n.m	116.2	102.1	100.7
10I_42	1801	Orosinian	n.m	n.m	930	27	1391	5.20E+05	n.m	1	17.7	0.7	6.1	10.4	1.08	42.1	13.16	139.2	48	206	39.2	340	60.3	11330	n.m	145	101.1	129
10I_40	1809	Orosinian	n.m	n.m	b.d	41.9	644	5.30E+05	n.m	0.048	8.19	0.147	2.11	3.88	0.437	18.87	5.6	64.9	22.47	97.5	18.47	175.3	32.4	11540	n.m	64.9	47.4	53.7
10I_71	1830	Orosinian	n.m	n.m	280	48.9	777	5.21E+05	n.m	0.234	6.9	0.223	2.16	4.64	0.574	22.2	6.72	74.4	26.3	111.2	21.85	198.7	38.1	10470	n.m	72.9	46.1	61.2
10I_81	1915	Orosinian	n.m	n.m	b.d	16.5	568	4.99E+05	n.m	0.144	8.94	0.307	2.71	2.97	0.75	13.26	4.24	47.3	17.41	81.4	18.27	193.4	42.6	10920	n.m	487	56.5	418
10I_24	1957	Orosinian	n.m	n.m	244	14.1	840	5.06E+05	n.m	1.26	57	2.47	17.6	12.2	6	33.3	8.4	88	27.6	111	21.8	195	35	12090	n.m	323	285	255
10I_130	2045	Orosinian	n.m	n.m	330	58	702	4.97E+05	n.m	0.62	13.2	1.02	10.2	11.5	1.29	28.8	7.64	81.5	24.5	93.1	18.5	168	28.6	17220	n.m	566	182	414
10I_58	2090	Rhyacian	n.m	n.m	337	25.7	550	5.03E+05	n.m	1.62	17.8	1.82	13.4	8.5	3.11	19.9	5.3	54.6	17.46	79.6	16.53	165.9	32.5	11390	n.m	398	130.2	354
10I_46	2123	Rhyacian	n.m	n.m	320	22.7	1433	5.26E+05	n.m	1.82	13.2	0.97	7.63	8.9	1.39	40	11.6	137.1	49.2	221.7	43.4	416	80.7	10950	n.m	623	210.1	478
10I_15	2126	Rhyacian	n.m	n.m	b.d	8.7	641	5.10E+05	n.m	0.82	26.8	1.18	7.5	6.2	3.02	17.9	4.99	56.6	20.9	102.8	22.53	237	48.5	12460	n.m	508	134.9	353
10I_39	2131	Rhyacian	n.m	n.m	b.d	36	831	4.71E+05	n.m	1.05	47.8	1.47	11.6	8.4	2.83	27	7.43	73.3	27	118.6	24.2	238	45.4	11080	n.m	313	154	280
10I_51	2139	Rhyacian	n.m	n.m	271	54	836	5.16E+05	n.m	1.45	25.05	0.85	6.07	4.26	1.34	15.66	5.18	64.2	24.89	126.1	28.51	299.1	57.8	14740	n.m	1808	399	1180
10I_33	2156	Rhyacian	n.m	n.m	233	10.7	538	5.22E+05	n.m	0.9	24.3	1.36	9.8	6.4	2.9	14.8	4.4	48.1	16.4	80.1	18.2	195	41	13030	n.m	354	44	265
10I_23	2187	Rhyacian	n.m	n.m	112	12.4	1441	4.95E+05	n.m	0.014	14.98	0.322	4.92	8.53	1.43	39.6	11.79	140.1	49.1	216.1	42.4	389.6	69.7	10380	n.m	299.8	164.3	189.7
10I_99	2199	Rhyacian	n.m	n.m	440	66	1365	5.26E+05	n.m	1.77	86.2	3.24	21.7	16.9	6.9	40.6	12	128.5	42.9	196	40.4	387	74.8	11640	n.m	508	312	367
10I_112	2204	Rhyacian	n.m	n.m	220	8.1	711	5.52E+05	n.m	1.03	11.44	0.578	3.27	2.26	0.718	10.06	4.12	57.5	23.26	116	26.77	290.7	61	15320	n.m	559	52.2	424
10I_19	2341	Siderian	n.m	n.m	b.d	39	1039	5.27E+05	n.m	0.52	45.5	0.78	6.9	7.5	2.2	27.3	7.87	90.4	32.9	155.2	32.93	335.2	69	11310	n.m	502	246.5	300.2
10I_47	2390	Siderian	n.m	n.m	280	36	837	5.12E+05	n.m	0.79	20.1	1.16	9	7.3	3.6	24.9	7.27	79.6	28	125.3	26.1	261	47.3	10600	n.m	377	177	252
10I_87	2412	Siderian	n.m	n.m	b.d	7.6	418	5.24E+05	n.m	0.143	11.1	0.212	1.71	2.08	0.664	9.4	3.4	39.2	13.56	61.3	13.03	131.3	28.08	11630	n.m	640	88.8	373.8

10I_21	2605	Neoarchean	n.m	n.m	b.d	59	2540	5.01E+05	n.m	0.209	22.95	0.643	7.74	12.6	1.98	66.2	20.55	244	87.3	381	72.9	664	118.2	11030	n.m	472	331	254
10I_20	2685	Neoarchean	n.m	n.m	b.d	21.5	1390	4.96E+05	n.m	0.274	15.2	0.313	3.92	6.4	0.99	34.3	11.1	132	47.4	207	41	381	67.8	10940	n.m	254	143	131
Discordant																												
10I_7			n.m	n.m	280	14.1	707	5.43E+05	n.m	0.402	14.4	0.319	2.97	3.67	0.97	14.56	4.4	53.4	21.2	106.9	24.8	259.3	64	11780	n.m	135.2	149.9	292
10I_16			n.m	n.m	450	12.4	613	5.20E+05	n.m	1.56	20.7	1.31	9.3	6.6	2.19	15.5	4.7	55.2	19.92	96.8	21.6	229.6	50	12010	n.m	353.1	65.6	400
10I_97			n.m	n.m	18	46	991	5.16E+05	n.m	0.125	14.56	0.3	3.54	5.85	0.963	28	8.24	91.2	32.5	144.2	28.76	278.1	56.6	11310	n.m	143	66	153.2
10I_124			n.m	n.m	750	47	1242	4.91E+05	n.m	1.74	59.4	2.43	17.6	12.1	3.75	32	9.51	110.7	40.5	185.7	38.5	389	73.9	12740	n.m	455	325	418

M2AR 11-1- Zircon compositional data (LA-ICP-MS, n = 52, b.d. = below detection limit)

Analysis ID	Best age (Ma)	Geological time	Al [ppm]	P [ppm]	Ca [ppm]	Ti [ppm]	Y [ppm]	Zr [ppm]	Nb [ppm]	La [ppm]	Ce [ppm]	Pr [ppm]	Nd [ppm]	Sm [ppm]	Eu [ppm]	Gd [ppm]	Tb [ppm]	Dy [ppm]	Ho [ppm]	Er [ppm]	Tm [ppm]	Yb [ppm]	Lu [ppm]	Hf [ppm]	Ta [ppm]	Pb [ppm]	Th [ppm]	U [ppm]
X11_1_66	530	Cambrian	n.m	n.m	b.d	22.5	747	5.09E+05	n.m	0.258	9.52	0.47	5.36	7.1	1.12	26.8	7.43	79.7	25.4	100.3	19.68	175.9	30.7	10450	n.m	42.4	85.3	127
X11_1_107	533	Cambrian	n.m	n.m	b.d	2.91	1810	5.05E+05	n.m	0.115	30.3	0.604	10.9	16.6	2.14	69.2	19.7	206	66.9	270	51	457	80.2	10060	n.m	70	262	214.2
X11_1_62	567	Ediacaran	n.m	n.m	b.d	8.95	665	5.19E+05	n.m	0.011	17.57	0.0489	0.98	2.39	0.249	15.12	4.88	61.8	22.67	101	21.76	206.5	36.9	11650	n.m	69.5	99.6	199.2
X11_1_127	586	Ediacaran	n.m	n.m	b.d	7.95	816	4.90E+05	n.m	1.65	22.8	0.504	3.61	3.57	0.348	19.19	6.58	78.9	28.1	123.3	25.43	234.9	42.9	10760	n.m	92.8	141.8	262
X11_1_50	599	Ediacaran	n.m	n.m	b.d	6.77	552	5.33E+05	n.m	0.061	17.54	0.105	1.34	3.12	1.159	14.66	4.14	48.2	17.04	76.8	16.57	167.7	33.6	10860	n.m	123.5	131.1	327
X11_1_124	644	Cryogenian	n.m	n.m	b.d	3.83	891	4.88E+05	n.m	0.04	17.9	0.069	0.95	2.22	0.628	13.45	4.95	66.6	28.5	142.6	34.6	364	75.4	11550	n.m	120.2	149.3	304
X11_1_116	650	Cryogenian	n.m	n.m	b.d	8.4	1562	4.95E+05	n.m	0.052	19.3	0.121	1.44	3.05	1.13	22.1	7.82	108.8	46	233	53	538	113.1	9640	n.m	78	124.6	193.2
X11_1_82	665	Cryogenian	n.m	n.m	b.d	39.4	1243	5.41E+05	n.m	0.35	25.3	0.269	4.13	7.55	1.197	35.1	10.16	117.7	40.2	174.9	35.5	330	62.2	11210	n.m	86.3	229	220.9
X11_1_34	682	Cryogenian	n.m	n.m	b.d	12.7	299	5.36E+05	n.m	0.05	10.48	0.079	0.94	1.65	0.523	8.18	2.51	27.8	9.78	42.6	8.57	81.5	15.48	12150	n.m	31.88	21.21	76.1
X11_1_109	943	Tonian	n.m	n.m	b.d	6.54	3020	4.96E+05	n.m	0.101	18.45	0.556	7.98	15.6	4.01	90.7	28.8	319	110.8	459	86.5	763	136.3	9060	n.m	181.3	466	306
X11_1_117	1689	Statherian	n.m	n.m	b.d	18.1	1124	4.91E+05	n.m	0.276	9.71	0.342	3.62	6.72	0.51	29.6	9	104.6	36.4	155.8	31.1	275	52.6	10450	n.m	195	95.1	160
X11_1_28	1706	Statherian	n.m	n.m	b.d	10.49	635	5.38E+05	n.m	0.046	18.06	0.108	1.41	2.77	0.145	13.95	4.64	59	22.27	103.2	23.17	228.3	39.9	13930	n.m	302	128.4	262
X11_1_10	1713	Statherian	n.m	n.m	b.d	7.3	1829	5.04E+05	n.m	0.031	17.71	0.456	7.98	14.15	0.437	57.1	17.46	194.1	65.4	280.9	55.5	505	83.1	11910	n.m	283	170.2	256.9
X11_1_87	1720	Statherian	n.m	n.m	b.d	5.77	790	5.53E+05	n.m	0.43	18.8	0.671	6.86	6.59	0.966	22.3	6.54	76.2	27.11	123.7	26.67	259.6	47.7	15890	n.m	505	217.6	492
X11_1_36	1721	Statherian	n.m	n.m	b.d	13.5	838	5.20E+05	n.m	0.3	18.9	0.62	3.7	3.88	0.218	20.47	6.2	77.3	28.3	126.1	25.47	240.6	43	11310	n.m	214.8	101.8	194
X11_1_126	1726	Statherian	n.m	n.m	b.d	15.9	504	4.84E+05	n.m	0.039	5.53	0.103	1.62	3.02	0.315	14.21	4.21	49.3	17.01	72.7	14.74	139.6	25.52	10000	n.m	61.4	26.36	55.2
X11_1_54	1736	Statherian	n.m	n.m	b.d	25.6	837	5.01E+05	n.m	0.61	16.1	0.388	4.32	6.36	0.643	26	7.3	79.2	27.5	115.4	22.66	208.2	37.9	9290	n.m	74.2	49.6	60.6
X11_1_125	1737	Statherian	n.m	n.m	205	25	1550	4.95E+05	n.m	1.33	33.2	2.8	19.8	16	4.2	46.1	14.7	162	53.6	236	47.7	428	76.2	11960	n.m	519	290	537
X11_1_40	1738	Statherian	n.m	n.m	210	19.7	877	4.88E+05	n.m	0.157	9.1	0.238	3.63	5.87	0.72	23.1	6.95	78.1	27.3	116.5	23.15	205.4	40.7	9420	n.m	104.7	57.6	97.3
X11_1_86	1742	Statherian	n.m	n.m	b.d	50.2	1035	5.66E+05	n.m	0.104	17.63	0.164	2.55	5.05	0.304	25.1	8.14	96.5	35.8	162	33.31	308.9	57.6	14040	n.m	304.4	153.9	279.6

X11_1_25	1745	Statherian	n.m	n.m	b.d	21	693	5.37E+05	n.m	0.028	11.16	0.146	2.3	4.21	0.349	19.26	5.74	66.1	23.48	99.6	20.99	195	34.3	11620	n.m	149	117	135.1
X11_1_106	1748	Statherian	n.m	n.m	b.d	50	741	5.15E+05	n.m	0.142	10.29	0.163	2.07	4.11	0.419	20.25	6.34	74.7	26.51	115.8	22.64	209.2	37.8	10570	n.m	108.9	64.8	93.1
X11_1_110	1751	Statherian	n.m	n.m	b.d	10.7	658	5.45E+05	n.m	0.042	10.36	0.07	1.38	2.38	0.185	12.94	4.39	56.9	21.93	101	21.64	204.6	38.9	13330	n.m	200.2	61.8	166.5
X11_1_96	1752	Statherian	n.m	n.m	b.d	5.22	779	4.46E+05	n.m	0.015	14.47	0.062	1.18	2.71	0.101	15.18	5.24	66.6	24.76	116	25.04	237.4	42.4	10630	n.m	315	103.7	279
X11_1_55	1755	Statherian	n.m	n.m	b.d	28	1303	5.13E+05	n.m	0.389	49.5	0.4	4.06	5.95	1.33	27.2	8.43	106.8	41.3	196.3	43.2	433	85.2	10120	n.m	184.7	145.1	146.7
X11_1_123	1760	Statherian	n.m	n.m	3.10E+03	11.1	1267	4.53E+05	n.m	0.047	11.14	0.283	5.23	9.94	0.688	44.3	12.01	128.9	43.7	176.5	33.7	290.3	50	8950	n.m	108.8	92.6	93.8
X11_1_102	1761	Statherian	n.m	n.m	b.d	17.1	1673	5.21E+05	n.m	0.102	9.81	0.691	11.55	16.6	0.649	65.1	17.66	182.6	60.6	238.7	44.8	380	66.2	10370	n.m	189.5	142.5	165.4
X11_1_44	1782	Statherian	n.m	n.m	b.d	16.5	712	4.65E+05	n.m	0.067	5.74	0.206	3.31	4.5	0.518	20.2	5.71	63.9	21.75	94.1	18.73	166.7	30.14	8850	n.m	125.7	48.9	100
X11_1_104	1784	Statherian	n.m	n.m	b.d	17.5	1408	5.23E+05	n.m	0.095	7.88	0.424	7.64	12.6	1.29	51.1	13.95	146.5	49.5	202	37.1	331	59.2	10670	n.m	128.1	94.3	115.1
X11_1_129	1784	Statherian	n.m	n.m	b.d	31.1	1261	4.82E+05	n.m	0.34	10.46	0.365	5.12	8.33	1.07	35.2	10.43	115.9	40.8	172.8	33.2	292	53.9	9980	n.m	140	70.8	110
X11_1_11	1836	Orosinian	n.m	n.m	b.d	26.2	1422	5.34E+05	n.m	0.54	11.15	0.489	6.98	10.9	0.872	47.7	13.45	150	51.3	211	40.2	360	63	11400	n.m	138	99.3	114
X11_1_8	1848	Orosinian	n.m	n.m	b.d	26.5	939	4.98E+05	n.m	0.09	3.71	0.376	5.96	8.5	1.6	34.9	9.06	95.5	31.4	126.8	24.1	220.1	38.6	8870	n.m	29.6	22.1	23.8
X11_1_12	1896	Orosinian	n.m	n.m	460	38	244	5.39E+05	n.m	0.29	2.18	0.201	1.74	2.66	0.52	9.1	2.49	24.8	7.85	33.2	6.48	64.5	13.2	14370	n.m	278	26.4	224
X11_1_59	1913	Orosinian	n.m	n.m	238	63	1135	4.81E+05	n.m	0.73	8.83	0.97	10.4	11.4	2.05	41.9	11.27	118.2	39.8	162.8	31	279	49.6	9490	n.m	66.7	54.5	62.3
X11_1_37	2058	Rhyacian	n.m	n.m	b.d	17.9	263	4.98E+05	n.m	0.226	11.9	0.513	5.98	6.94	2.21	18.75	4.14	33.4	9	30.3	5.03	44.5	7.28	9680	n.m	284	136.3	203.3
X11_1_120	2069	Rhyacian	n.m	n.m	b.d	9	1176	5.17E+05	n.m	0.96	21.4	0.93	9.2	8.8	2.51	35.9	9.7	105.6	36.8	170.1	37.5	360	71.4	11870	n.m	756	125.3	578
X11_1_42	2104	Rhyacian	n.m	n.m	b.d	5.03	508	4.99E+05	n.m	0.045	7.35	0.063	0.96	2.01	0.458	9.74	3.44	41.7	14.99	63.8	13.46	129.2	24.4	10130	n.m	413	64.2	290
X11_1_15	2137	Rhyacian	n.m	n.m	b.d	10.5	1804	5.43E+05	n.m	0.66	8	0.69	6.5	7.9	1.01	35.3	12.21	158.3	60.2	285.8	61.5	611	116.1	13460	n.m	1379	247	1039
X11_1_130	2158	Rhyacian	n.m	n.m	b.d	7.91	1144	4.86E+05	n.m	0.434	31.6	0.524	4.51	5.72	1	26.1	8.24	102.2	37.7	170.3	35.8	326	58.4	10840	n.m	619	244	449
Discordant			n.m	n.m					n.m																n.m			
X11_1_56			n.m	n.m	11	17.4	786	5.45E+05	n.m	0.27	12.95	0.264	2.14	3.04	0.986	13.47	4.86	59.6	23.06	113.9	27.43	291	61.09	12040	n.m	113.1	133.2	302.6
X11_1_2			n.m	n.m	-19	10.29	649	5.36E+05	n.m	0.011	15.99	0.084	1.43	3.32	0.183	15.9	5.06	59.9	22.01	96.5	20.7	190.3	35	12550	n.m	181.2	96.1	155.2
X11_1_78			n.m	n.m	260	6.7	506	5.00E+05	n.m	0.41	19.7	0.52	5.7	6.3	1.49	19.1	4.96	50.8	16.2	67.7	13.3	128	23.2	10270	n.m	54.2	99	140.2
X11_1_58			n.m	n.m	790	50.2	1044	5.22E+05	n.m	1.1	11.54	0.698	4.99	4.05	1.49	15.2	5.89	79.2	31.9	173	44	484	99.7	13620	n.m	374	82.1	412
X11_1_26			n.m	n.m	196	4.56	652	5.25E+05	n.m	0.18	4.67	0.13	1.61	2.22	0.259	12.46	4.12	55.5	21.6	108	23.9	240	45.3	14100	n.m	208.8	59.6	229.3
X11_1_61			n.m	n.m	22	4.55	346	5.04E+05	n.m	0.178	10.83	0.139	0.92	1.22	0.337	5.4	1.8	23.9	10.36	52.7	13.36	153.3	32.4	11970	n.m	422	127	352
X11_1_23			n.m	n.m	52	12.3	1025	5.36E+05	n.m	0.77	5.7	0.74	5	4.78	1.4	21.6	7.67	94.9	36.4	170.3	38.2	382	71.6	16190	n.m	731	115.3	592
X11_1_24			n.m	n.m	1180	35.6	642	5.22E+05	n.m	1.58	30.8	0.88	6.6	4.13	1.23	15.28	4.49	54.7	20.58	95.9	21.53	213.4	40.6	12260	n.m	320	149.7	263
X11_1_119			n.m	n.m	10	37	1100	4.74E+05	n.m	1.59	210	2.4	16.6	9	4.3	27.9	8.1	101	34.6	170	37.6	366	70.1	10000	n.m	322	178	331
X11_1_83			n.m	n.m	107	25.1	245	5.50E+05	n.m	0.095	2.57	0.076	0.72	0.86	0.303	3.95	1.37	17.34	7.51	39.3	10.08	117.3	29.1	13050	n.m	103	89.7	80.8
X11_1_17			n.m	n.m	1110	13.3	467	5.39E+05	n.m	1.33	27.6	1.04	5.9	4.7	1.71	13.7	3.63	39.7	14.1	68.6	16.79	185.6	42.6	12920	n.m	166.7	201	348
X11_1_41			n.m	n.m	72	46.4	635	5.00E+05	n.m	0.611	37.2	1.296	10.78	10.91	3.88	23.7	6.27	62.6	19.62	82.4	17.74	173.4	32.6	9510	n.m	79.4	187	179.9

X11_1_92			n.m	n.m	53	38.3	523	5.42E+05	n.m	0.47	8.43	0.173	1.61	2.73	0.354	13.87	4.28	50.1	18.36	79.1	16.45	153.7	29.8	11170	n.m	35.4	43.2	90.9